APPENDIX K:
CSIRO NUMERICAL MODELLING REPORT

EARTH SCIENCE AND RESOURCE ENGINEERING
www.csiro.au

Angus Place and Springvale Colliery Operations Groundwater Assessment

D P Adhikary and A Wilkins
Report No EP132799
May 2013

Angus Place Colliery and Springvale Colliery

Citation

Adhikary, DP and Wilkins, A (2013) Angus Place and Springvale Colliery Operations – Groundwater Assessment. Report No EP132799, CSIRO, Australia.

Copyright and disclaimer

Important disclaimer

Executive Summary

Centennial Coal is seeking consent to extend their underground operations in the Angus Place (AP) and neighbouring Springvale (SV) Collieries. The proposed extensions involve 19 new longwall panels at Angus place, and 20 new longwall panels at Springvale; each mining the Lithgow seam. The extensions are proposed to begin in mid 2013 and complete by 2033.

A numerical model has been created and analysed to assess the effect of these proposed extensions upon groundwater in order to understand the likely magnitude and extent of strata depressurization and the impacts on certain swamps and streams within the region. The model covers the 30km x 30km area of hilly terrain centred on the collieries. There has been extensive mining within the region already, and the model includes forty historical and active mines. The model also contains 21 swamps and river reaches that are believed to be almost permanently waterlogged. The model uses all currently available geological information and extends previous studies to define 6 water-bearing aquifers. The model is built and run in CSIRO's finite-element solver called COSFLOW.

Model calibration and validation

Calibration and validation of the model is performed in 2 stages.

1. Calibration. Here the model parameters are varied iteratively (using trial-and-error and the PEST: Parameter Estimation software) so that maximal agreement between simulation results and observations is achieved. The model parameters to vary are: the permeabilities of each material layer; the rainfall recharge; the riverbed conductance; and, the mining-induced permeability-change ramp function. Each calibration iteration has three stages:
    a. Steady-State Calibration. The 'Model' is run to steady-state before any mining activity with particular model parameters. This involves running an 'Extended Model' (covering a 60km x 40km area completely covering the 'Model' area) to steady-state, interpolating the porepressures onto the 'Model' to obtain realistic boundary conditions, and then running the 'Model' to steady-state. The strata permeabilities and the rainfall recharge rate are varied iteratively to achieve maximal agreement between simulated elevation heads and the measured elevation heads at 85 piezometers (see Appendix A).
    b. Transient Calibration. Starting from steady-state, the 'Model' is run in transient mode from 1950 to 20 December 2006. Varying stress periods are used to match the mining schedule. The mining-induced permeability-change ramp function, the riverbed conductance and the rainfall recharge rate are varied to obtain maximal agreement between the simulation and the following observations: the elevation heads at 125 piezometers; the median baseflow at Sunnyside swamp; and, the mine-water inflow rates for Springvale and Angus Place Collieries (see Appendix A).
    c. (a) and (b) above are repeated iteratively until maximal agreement between simulation results and observations is achieved.

2. Validation. Using the model parameters obtained in the Calibration stage, the calibrated 'Model' is run from 20 December 2006 to 1 Jan 2012 in transient mode using three-monthly stress periods with mining schedule discussed in Section 2.3 and transient rainfall discussed in Section 2.9. The 'Model' results are validated against the following observations from 2006 to 2012: 142 vibrating wire piezometer pressure readings; median baseflow at Sunnyside swamp; mine-water inflow rates for Springvale and Angus Place Collieries; and, water heads at shallow depths in several swamps.

Once the model parameters are validated the model is run in predictive mode. A summary of the results of the numerical simulations are as follows:

Drawdown of water levels

- The drawdown of saturated water heads at the ground surface over the proposed extensions is very similar to that already experienced above the currently-mined longwall panels. The maximum saturated drawdown experienced is of the order of centimetres.
- The drawdown of saturated water heads at the ground surface above the Angus Place mine is not significantly affected by the Springvale mine, and vice-versa.
- During recovery after mining completes, the time taken for pressure heads at the ground surface to reach virtual steady-state is less than 50 years in all mining scenarios.
- The maximum drawdown of 160m occurs in the Lithgow seam in the proposed extension to Springvale. At 5.5km from the mines, the drawdown in the Lithgow Seam is approximately 10m. At 7km from the mines the drawdown in the Lithgow seam is approximately 5m.
- The drawdown within the Lithgow seam in and around the Angus Place mine is not significantly affected by Springvale mining. The drawdown within the Lithgow seam in and around Springvale mine is slightly affected by mining of the proposed Angus Place extensions.

Impact on swamps/streams/

- The discharge/recharge to/from most of the streams and swamps modelled does change when undermined.
- The YS6 layer is found to be the most important aquitard. The swamps and streams lying above the YS6 layer are much less impacted by mining than the swamps and creeks that are unsupported by the YS6 layer underneath.
- Due to the lack of mine observational data to enable accurate estimate of magnitude and extent of cracking at shallow depths, three scenarios concerning the mining-induced permeability changes are investigated (Base case, Truncated-ramp 1 and Truncated-ramp 2). The differences in the calibration statistics (i.e. RMS errors) between these three scenarios are statistically insignificant. The actual impact of mining is expected to lie within the bounds predicted by these three models. The following observations can be made from these three models:
    - "Base case" predicts an increase in baseflow to a number of swamps and creeks following mining. This may be attributed to mining induced delamination of near surface strata causing increase in horizontal permeability (which consequently causes faster dissipation of water from 'water-mounds' distributed over the mining region causing higher baseflow) and recovery of water levels to higher elevations with respect to pre-mining levels causing higher baseflow during recovery period.
    - "Truncated-ramp1" predicts the least impact on baseflow among the three models; this ramp function is similar to the ones commonly adopted in groundwater impact assessment using MODFLOW.
    - "Truncated-ramp2" predicts intermediate impact on baseflow with respect to "Base case" and "Truncated-ramp1"; some of the predicted impacts on baseflow from this model are identical to those obtained from "Truncated-ramp1" while some are similar to those predicted by the "Base case".
- The simulation results are presented in Tables S1 and S2 below. In the Base case, undermining of streams/swamps causes an average water head change of few centimetres; a projected maximum water head drop of 0.36m is predicted for the Gang Gang South East Swamp.
- The effect of future climate change has been studied simply. Increasing rainfall recharge by 15% increases median baseflow by 11.2%, while decreasing rainfall recharge by 15% decreases median baseflow by 10.0%. Increasing/decreasing evapotranspiration by 15% decreases/increases median baseflow by 2.5%.
- Since Cox's River was not explicitly included in the model, two proxies have been explored for assessing the impact of the proposed Angus Place and Springvale extensions on the Cox's River:
    - The changes in baseflow for Long Swamp, which lies along Cox's river. No change in baseflow to Long Swamp is predicted.

- The drop in pressure heads at the surface of the model along Cox's river. The model predicts that the proposed extensions will cause a maximum head drop of 0.01m.

Table S1 Maximum predicted loss in baseflow to the simulated swamps and streams with respect to baseflow at 2012

Swamps and streams simulated in this study	Maximum loss in groundwater discharge (ML/day)						Comment
	Base case		Truncated ramp1		Truncated ramp2		
	ML/day	%	ML/day	%	ML/day	%	
CA2 (includes Carne Central Swamp)	0.268	23.550	0.249	21.861	0.288	25.308	21.9 – 25% drop
Carne West Swamp	Increase in baseflow		0.000	0.000	0.000	0.000	Very small volume
Carne Creek Total	Slight decrease during mining		Slight decrease during mining		Slight decrease during mining		Small increase during recovery
Gang Gang South East	0.175	307.018	0.002	4.211	0.025	43.860	Leaky swamp (increase in leakage 4 to 300%)
Gang Gang Swamp South	0.022	36.667	0.000	0.000	0.032	57.143	Leaky swamp (increase in leakage 0 to 57%); very small volume
Kangaroo Swamp	0.004	24.667	0.000	0.000	0.002	50.000	0 to 50% drop; very small volume
Kangaroo Creek (KC1)	0.129	Division by a small number	0.074	86.047	0.122	64.894	Very small volume, simulated discharge to the creek was almost nil at 2012 in 'Base case'
Kangaroo Creek (KC2)	0.035	32.407	0	0	Slight increase		Increase in baseflow
Lamb Creek	0.078	46.118	0.010	12.312	0.036	30.252	12 - 46% drop; very small volume
Long Swamp	0.000	0.000	0.000	0.000	0.000	0.000	No change
Marrangaroo Creek	0.126	17.500	0.070	9.655	0.118	16.389	9 – 17.5% drop
Nine Mile Swamp	Increase in baseflow		Increase in baseflow		Increase in baseflow		Increase, very small volume
Paddy's Creek	0.002	1.227	0.001	0.617	0.004	2.454	Very small change
Pine Swamp	0.000	0.349	Increase in baseflow		Increase in baseflow		Increase
Tri-Star Swamp	0.041	93.182	0.006	13.182	0.040	90.909	13 to 90% drop, very small volume
Twin Gully Swamp	0.030	41.096	0.002	2.740	0.021	28.375	2 to 41% drop, very small volume
Sunnyside Swamp	0.007	7.292	Increase in baseflow		Increase in baseflow		Small increase
Wolgan River Total	0.359	27.765	0.120	10.195	0.216	18.321	10 to 27% drop

Table S2 Predicted maximum drop in the average standing groundwater levels in the simulated swamps with respect to the groundwater levels in December 2012

Swamps and streams simulated in this study	Base case (m)	Truncated ramp 1 (m)	Truncated ramp 2 (m)
CA2 (includes Carne Central Swamp)	0.103	0.095	0.110
Carne West Swamp	Small head increase	0.000	0.000
Gang Gang Swamp South East	0.364	0.005	0.052
Gang Gang Swamp South	0.030	0.000	0.043
Kangaroo Swamp	0.095	0.000	0.051
Long Swamp	0.017	0.000	0.000
Nine Mile Swamp	Small head increase	Small head increase	Small head increase
Pine Swamp	Small head increase	No change	No change
Tri-Star Swamp	0.081	0.011	0.079

Twin Gully Swamp	0.051	0.003	0.035
Sunnyside Swamp	0.013	Small head increase	Small head increase

Impact on private bores

- The effect of mining on private bores within 10km of AP and SV is tabulated. For the 79 private bores of depth less than 50m, the proposed extensions cause an average saturated head drop of less than a centimetre by year 2033 when mining completes. The drawdown in some deeper bores is large.

Mine water inflow

- The average life of mine water inflow rates for the Angus Place and Springvale Collieries is predicted to increase from about 26ML/day currently and average around 35ML/day to 43ML/day between 2020 to 2032.
- The mine water-inflow rates into the Springvale longwall panels are not affected by mining Angus Place, and vice-versa.

Water Balance

- The water balance within the groundwater system seems to remain fairly consistent throughout the validation and predictive periods except for the mine inflows which increase from about 30 ML/day (2006 to 2012) to 35 ML/day (2013 to 2018), 47 ML/day (2019-2024) and 50 ML/day (2024-2032). The groundwater recharge fluctuates around 131 ML/day and evapotranspiration fluctuates around low to mid 90 ML/day. The discharge to swamps/stream remains virtually steady at around 15 ML/day and leakage from streams/swamps averages around 6 ML/day.

Recovery

- Mining causes the aquifer containing the Lithgow seam to become unsaturated above the longwall panels in all scenarios. This unsaturated region fills with water by around 50 years after mine completion.
- The Mt York claystone is the main aquitard in the region. Based on current geological information, this layer is continuous and thick over the entire region. Mining causes a 15-70m thick unsaturated region to develop in the aquifer below the Mt York claystone layer. This aquifer partially fills after mine completion and, in all scenarios, reaches virtual steady-state after 350 years. In the Base case, the water content of this aquifer is then approximately 96% of its pre-mining water content.
- Depending on the geology, the aquifers above the Mt York claystone also slightly de-saturate. In the Base case, these aquifers suffer a loss of approximately 3% of their water content above the longwall mines, and this loss remains during recovery.

Recommendations

- It is recommended that the mining induced water pressure changes in AQ3 (the aquifer directly below the Mt York claystone) and above be properly studied by installing additional piezometers in a number of targeted boreholes at various depths in these aquifers.
- It is recommended that monitoring of baseflow to swamps and streams be intensified.
- It is recommended that the numerical model developed in this study be routinely updated/improved by validating the simulated results against additional monitoring data as mining progresses to assist with the better prediction and assessment of mining impact on the groundwater system within the APE and SV Colliery region.

Contents

Figures

Tables

Acknowledgments

This work is conducted at the request of Mr Peter Corbett (Regional Technical Services Manager, Centennial Coal West) and is jointly funded by Angus Place and Springvale Collieries.

1 Background

Centennial Coal Pty Limited operates Springvale and Angus Place Collieries, which is located in the Western Coalfield of New South Wales. Centennial is seeking approvals to extract the proposed Longwalls 416 to 432 and 501 to 503 within Springvale Colliery and Longwalls 1001 to 1019 within Angus Place Colliery in the Lithgow Seam.

This study is conducted at the request of Mr Peter Corbett (Regional Technical Services Manager, Centennial Coal West). The report provides a hydrogeological assessment of proposed longwall mining at Springvale and Angus Place Collieries based on numerical simulation. Mine data are used to define a conceptual hydrogeological model of the region of interest and the major hydrostratigraphic units identified in the conceptual hydrogeological model are used to define the structure of the finite element mesh in the numerical model. The properties of the major hydrostratigraphic units are either specified directly from the mine data or calibrated by matching calibration runs of a numerical model with mine data.

All together forty historical and active mines (open pits, bord and pillar mines, and longwall mines) located in close proximity have been included in the numerical simulation in order to assess the cumulative impact of extensive network of past, present and proposed mining operations on the groundwater system.

Chapter 2 describes the conceptual hydrogeological model developed in this study and the numerical models that are used in the calibration process, final predictions and impact assessments. It provides descriptions of model extent, hydrogeological setting (including the existing groundwater system), simulated mines, simulated swamps and streams, mine monitoring data, and rainfall recharge and evapotranspiration (ET) discharge.

Chapter 3 provides a description of model calibration and validation procedures used in this study along with the calibration and validation results.

Chapter 4 provides predictions and impact assessments.

Chapter 5 provides a description of recovery scenarios simulated in this study.

Chapter 6 provides a brief description of model limitations.

Chapter 7 provides recommendations for future monitoring and modelling work.

The six accompanying appendices to this report provide the following information:

- Appendix A – Analysis of mine data (piezometer monitoring, mine inflow measurement, baseflow measurement)
- Appendix B – Comparison of measured and simulated piezometric heads (piezometric heads vs. time and piezometric heads vs. depth)
- Appendix C – Simulated discharge/recharge to/from swamps and streams
- Appendix D – Simulated drawdown
- Appendix E – Simulated discharge/recharge to/from swamps and streams with seepage boundary
- Appendix F - A brief theoretical background on COSFLOW, the numerical code used in this study

2 Conceptual Model and Numerical Models

A conceptual model is a simplified presentation of the groundwater flow system including major hydrostratigraphic units, their flow properties and boundary conditions. Such a conceptual hydrogeological model for Angus Place and Springvale Collieries is described in this chapter. This model is used to develop a number of different finite element meshes of various regions of interest and these meshes are used to calibrate parameters used to describe properties of the hydrostratigraphic units in numerical simulations in cases where these parameters cannot be estimated directly, but are inferred by matching mine data and simulation results. Numerical simulations are conducted using CSIRO's in-house software called "COSFLOW". COSFLOW is briefly described in Appendix F.

COSFLOW solves non-isothermal, multi-component, multi-phase fluid and heat flow coupled with Cosserat elasto-plasticity. For this project, COSFLOW is used with a single liquid phase – water – in isothermal conditions with no coupling with mechanical deformation. The strata fracturing induced by the mechanical deformations caused by mining are included by altering permeability of the rock around the mined region as described in Section 2.13.

The groundwater modelling work presented in this report has been conducted in accordance with the Murray-Darling Basin Commission Groundwater Flow Guideline (MDBC, 20001) and the Australian Groundwater Modelling Guideline (AGMG, 2012). This model type falls in a Moderate Complexity Model (MDBC, 2001) and Class 2 Confidence Level (AGMG, 2012) category, requiring more data and a better understanding of the groundwater system dynamics, and suitable for providing estimates of dewatering requirements for mines and excavations and the associated impacts.

2.1 Model extents

In plan view, the 'Model' area lies within the 30km x 30km region defined by the geographic coordinates 221000E - 251000E and 6288000N - 6318000N (shown by a square in Figure 1). The mining region is characterised by hilly terrain. The model area, as shown in Figure 2 can be seen to be intersected by river gorges and stream channels, and valleys.

The topography dips dramatically to the east of the mining region and the surface topography in the model area varies significantly from 550 m to 1260m AHD as shown in Figure 2. It is expected that the groundwater from the mining region seeps out of the hills to the east as well as through the river/stream channels within the mining region. Further east of the model region, the surface topography reduces to almost sea-level in places.

In order to prescribe realistic boundary conditions on the eastern boundary of the 'Model', an 'Extended model' is also used (shown by a rectangle in Figure 1). The 'Extended model' lies within the 60 x 40 km rectangle defined by the geographic coordinates 220000E – 280000E and 6285000N – 6325000N. The extent of the 'Model' and 'Extended model' in relation to other regions in New South Wales is shown in Figure 1 and Figure 2.

Figure 1 'Model' and 'Extended model' domains shown by the square and rectangle, respectively

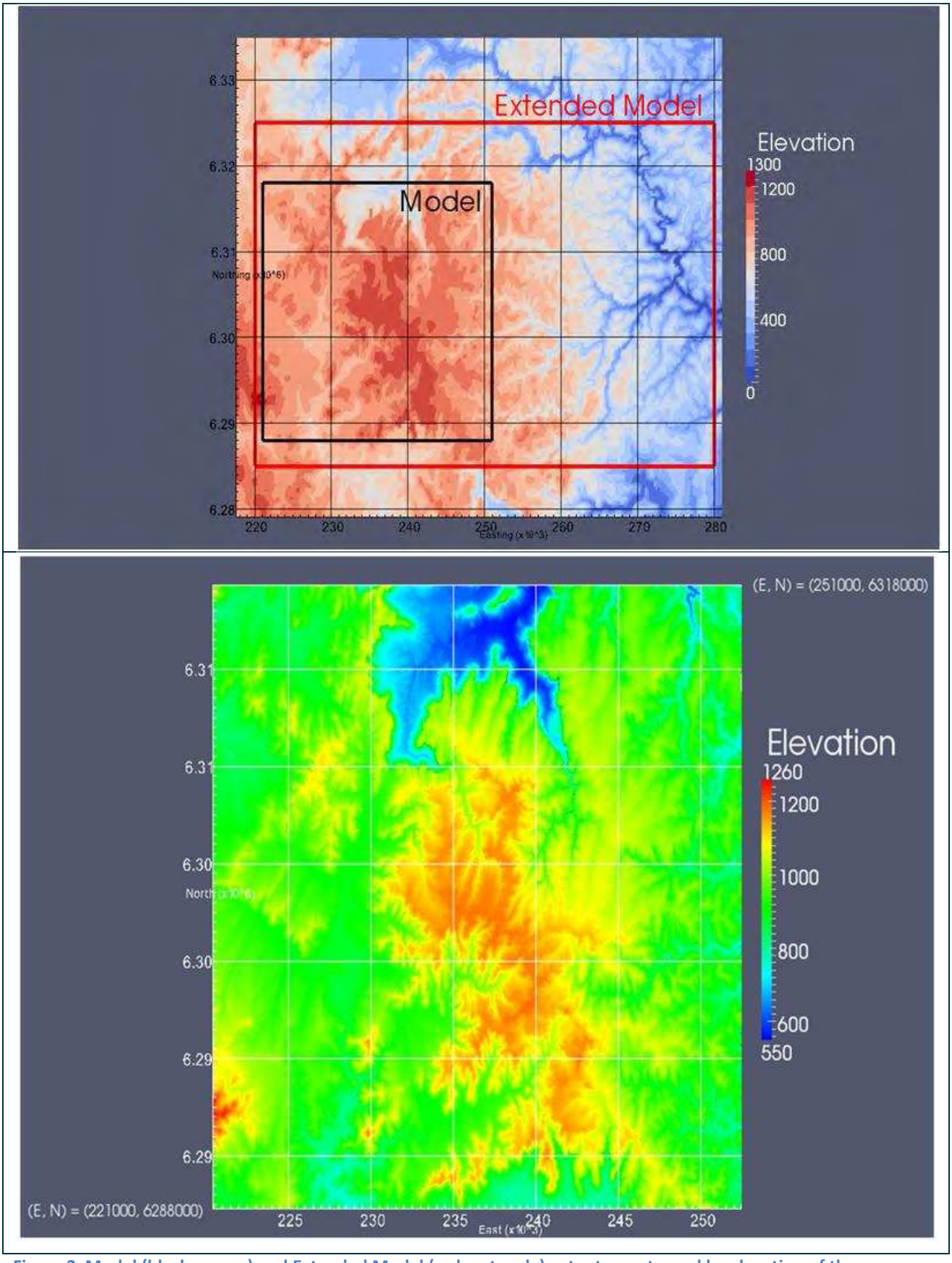

Figure 2 Model (black square) and Extended Model (red rectangle) extents, contoured by elevation of the topography

2.2 Mines simulated in the study

The mines located in the vicinity of Springvale and Angus Place Collieries as listed in Table 1 are included in the study. The outlines of the mines simulated are shown in Figure 3.

Table 1 Mines simulated in the model

Abbreviation	Full Name	Abbreviation	Full Name
APBP	Angus Place Bord and Pillar	FLY	Folly open cut
APE	Angus Place, East	INV	Invincible
APLW1	Angus Place longwalls 1 and 2	JHN	Johnsdale open cut
APLW2	Angus Place longwall s 3 to 10	KER1	Kerosene vale open cut 1
APLW3	Angus Place longwalls 11 to 13	KER2	Kerosene vale open cut 2
APLW4	Angus Place longwalls 25 to 26N	KER3	Kerosene vale open cut 3
APLW5	Angus Place longwall 17 to 24	LGS	Lithgow State
APLW6	Angus Place longwalls 910 to 980	LGS_1	Lithgow State
BBN	Baal Bone	NEW1	Newport open cut 1
CAL	CAL Colliery	NEW2	Newport open cut 2
CLR_1	Clarence Bord and Pillar region 1	OPK	Oakey Park
CLR_2_3	Clarence Bord and Pillar regions 2 and 3	PDL1	Pinedale open cut 1
CLR_4_5	Clarence Bord and Pillar regions 4 and 5	PDL2	Pinedale open cut 2
CLR_LW	Clarence longwall cluster	RWN	Renown
CLR_7	Clarence longwall 7	SPR_1	Springvale longwalls 1 to 423
COL1	Commonwealth opencut 1	SPR_2	Springvale longwalls 424 to 431
COL2	Commonwealth opencut 2	SPR_3	Springvale longwalls 501 to 503
COM	Commonwealth Colliery	STW	Steel works
EAS	Eastern Main	WWG	Wallerwang
FBK	Fernbrook – Hermitage	VAL	Vale of Clwydd

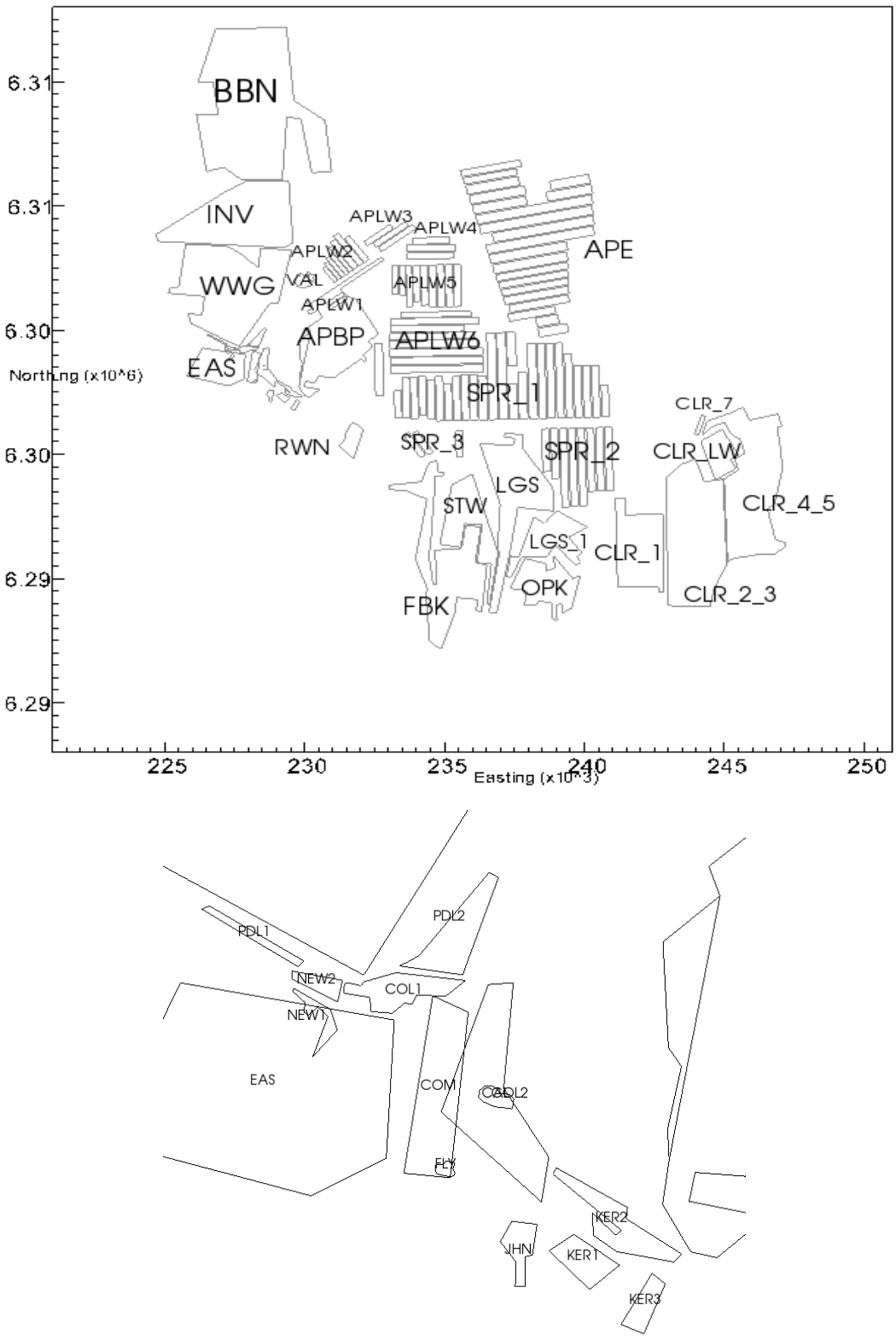

Figure 3 Outline view of mine-plans supplied by Centennial Coal including area around the small opencut mines which lie between Eastern Main mine and Angus Place Bord and Pillar

2.3 Mining schedule

Table 2 lists all the mining panels and areas used in the model. It refers to mining regions by labels which are defined in Figure 4 to Figure 6.

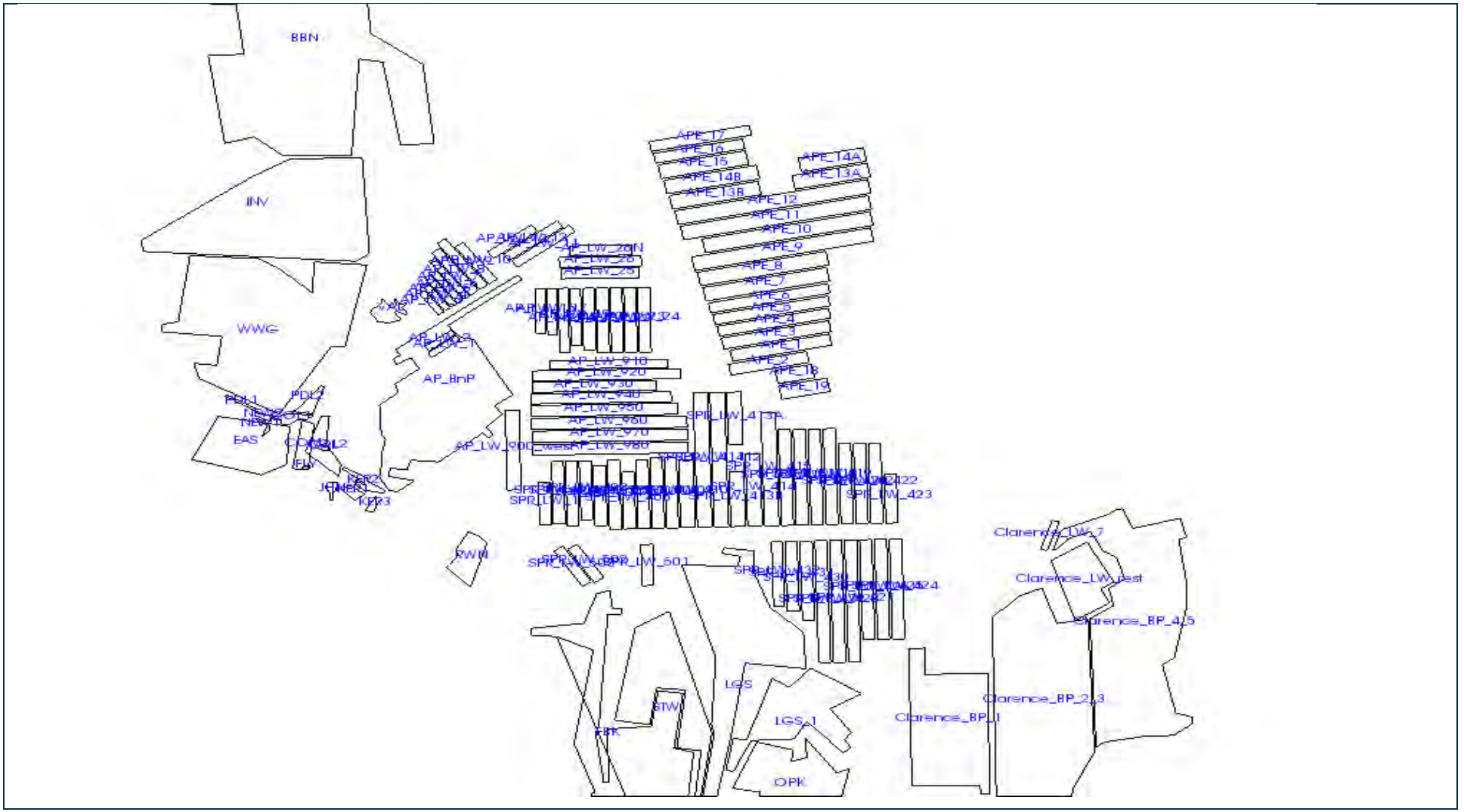

Figure 4 View of the mining regions with labels for each region

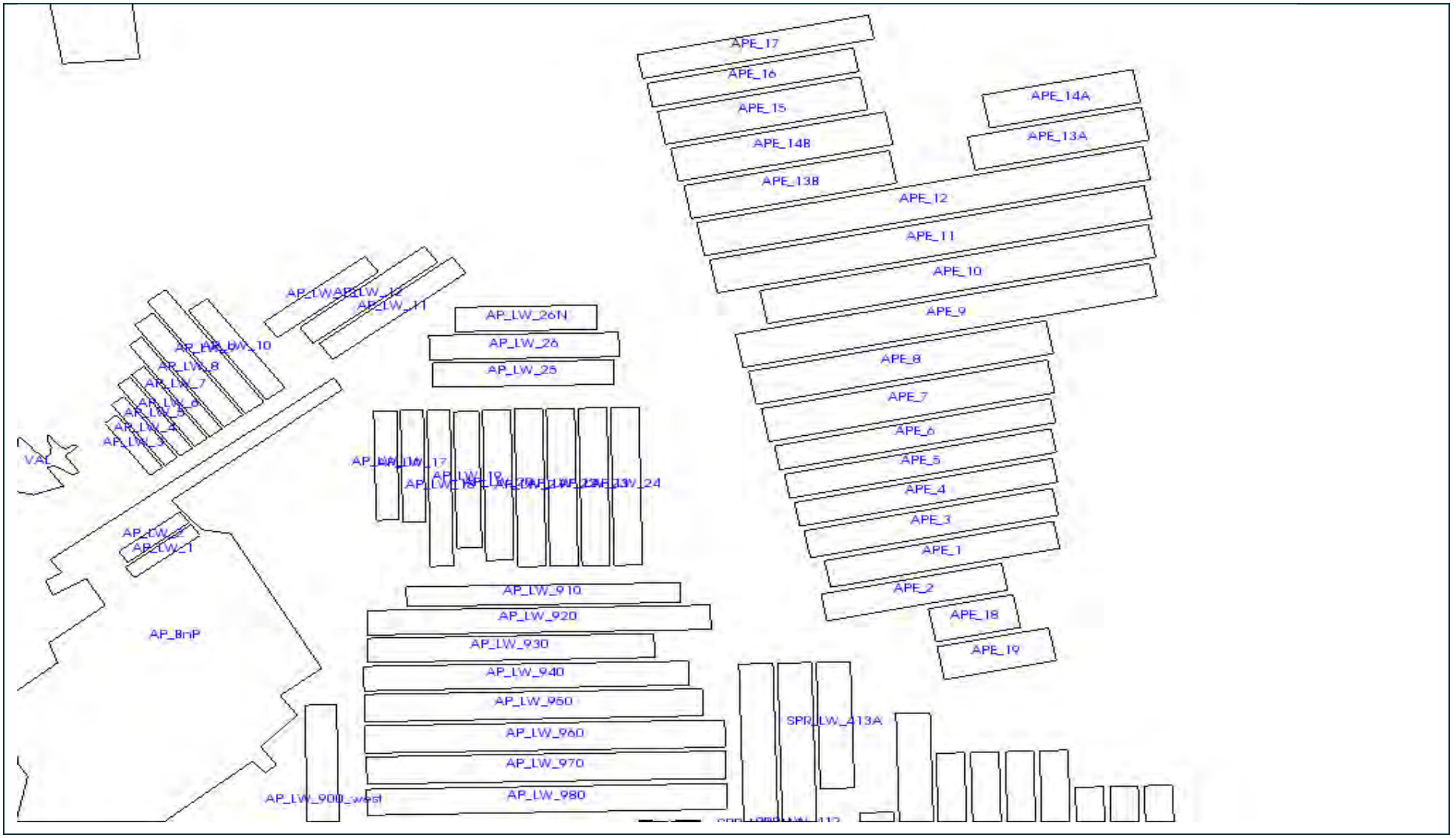

Figure 5 View of the mining regions of Angus Place mine, with labels

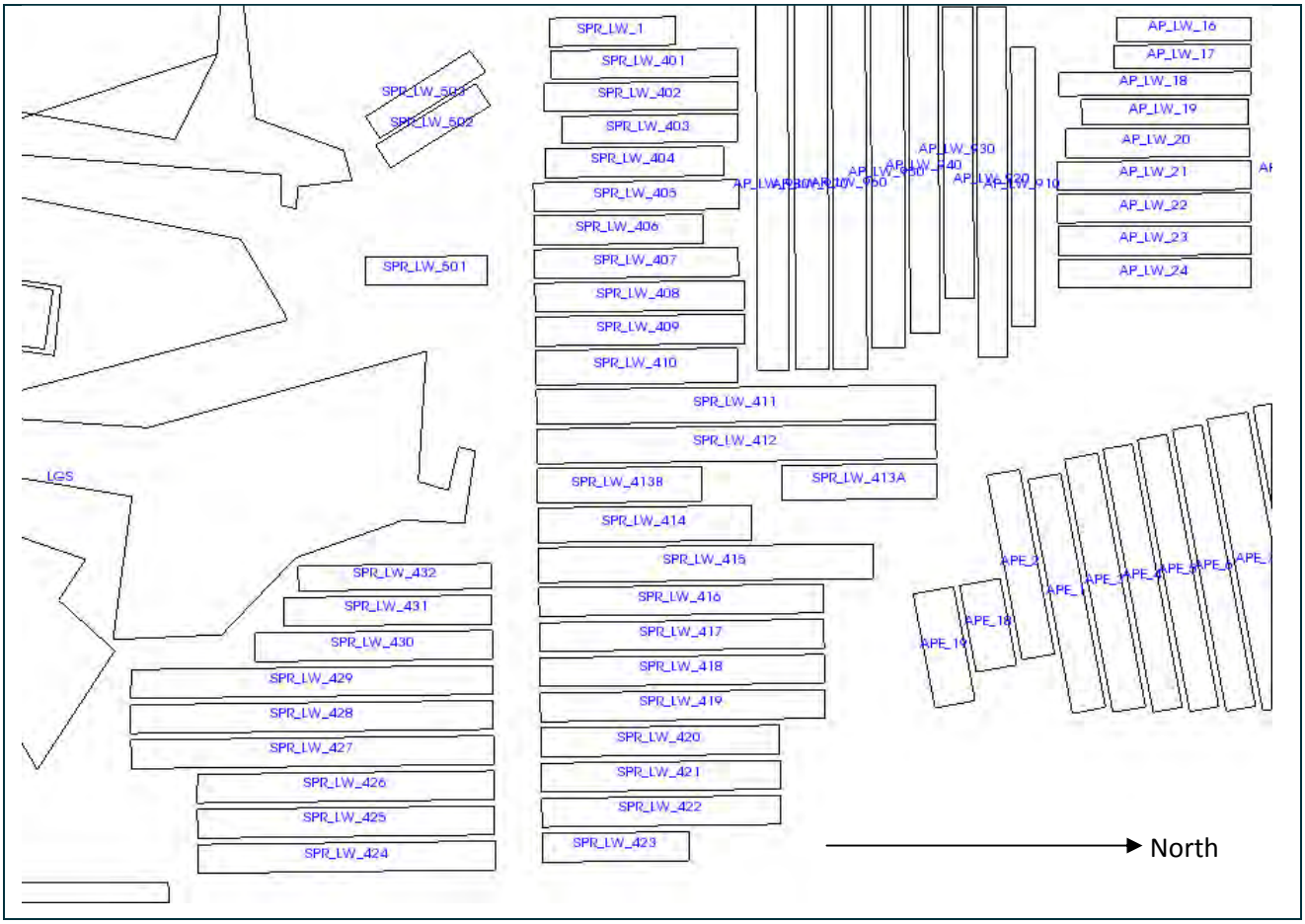

Figure 6 View of the mining regions of Springvale mine, with each region labelled. Note that the orientation is such that north is rotated

Transient calibration commences from 1950, transient validation commences from 20 December 2006 and transient prediction commences from 1 January 2012. The stress period used in the current study varies as described below. The columns in Table 2 are:

- The Name column lists the name of the panel or area to be mined.
- The Start Date and End Date columns list the relevant dates. These are approximately what are used in the model, subject to the following conditions:
    - If the start date is before 1950, the entire region is excavated in the year 1950
    - If the start date is between 1950 and 1980, the entire region is excavated at the average of the start and end, rounded to the nearest 10 years.
    - If the start date is between 1980 and 2000, the entire region is excavated at the average of the start and end, rounded to the nearest 5 years. (The first six year's-worth of Clarence_BP_2_3 are excavated in 1995.)
    - If the start date is between 2000 and 2006, the entire region is excavated at the start date.
    - If the start date is between 2006 and 2012, the region is excavated in chunks appropriate to the 3-monthly stress periods used in the transient validation part of the model. The number of chunks is indicated by the Step column of the table. (The central 6 years of Clarence_BP_2_3 are excavated in 3-monthly chunks. Only the first 6 years of Clarence_BP_4_5 is excavated in this fashion.)
    - If the start date is after 2012, the region is excavated in one step at the start date. (The last 3 years of Clarence_BP_2_3 and the last 15 years of Clarence_BP_4_5 are excavated in yearly sections.)

- The Type column indicates either a Longwall (LW), Bord and Pillar (BP) or Opencut mine. This is important because the permeability changes induced by these mines differ. This is described more fully in Section 2.13.4.
- The Pressure column indicates the porepressure on the walls of the excavated region. This is described more fully in Section 2.12.
- The Direction column indicates the mining direction. This is only relevant for subdividing the region into a number of subregions corresponding to 3-monthly, that is, for regions excavated during the 2006-2012 period (or yearly periods for Clarence_BP_2_3 and Clarence_BP_4_5).
- The Step column indicates the number of steps used to excavate the region. This is only relevant for regions excavated during the transient validation, that is, during the 2006-2012 period.

Table 2 Mining sequence and other information (see text for explanation) for the mines in the model

Name	Start_Date	End_Date	Type	Pressure (Pa)	Direction	Seam	Step
AP_LW_1	31/08/1979	25/05/1980	LW	0	EtoW	LTH	3
AP_LW_2	26/08/1980	8/12/1980	LW	0	EtoW	LTH	2
AP_LW_3	16/02/1981	6/07/1981	LW	0	NtoS	LTH	2
AP_LW_4	11/08/1981	13/11/1981	LW	0	NtoS	LTH	2
AP_LW_5	16/02/1982	15/06/1982	LW	0	NtoS	LTH	2
AP_LW_6	13/07/1982	18/11/1982	LW	0	NtoS	LTH	2
AP_LW_7	17/01/1983	1/08/1983	LW	0	NtoS	LTH	3
AP_LW_8	10/08/1983	14/12/1984	LW	0	NtoS	LTH	6
AP_LW_9	28/03/1985	8/07/1986	LW	0	NtoS	LTH	6
AP_LW_10	18/08/1986	27/08/1987	LW	0	NtoS	LTH	5
AP_LW_11	10/11/1987	24/10/1988	LW	0	EtoW	LTH	4
AP_LW_12	8/12/1988	2/09/1989	LW	0	EtoW	LTH	3
AP_LW_13	28/09/1989	25/06/1990	LW	0	EtoW	LTH	3
AP_LW_16	24/10/1990	9/09/1991	LW	0	StoN	LTH	4
AP_LW_17	4/11/1991	28/10/1992	LW	0	StoN	LTH	4
AP_LW_18	4/01/1993	13/12/1993	LW	0	StoN	LTH	4
AP_LW_19	19/03/1994	5/03/1995	LW	0	StoN	LTH	4
AP_LW_20	25/04/1995	7/05/1996	LW	0	StoN	LTH	5
AP_LW_21	17/06/1996	17/10/1997	LW	0	StoN	LTH	6
AP_LW_22	2/12/1997	11/12/1998	LW	0	StoN	LTH	5
AP_LW_23	4/01/1999	26/11/1999	LW	0	StoN	LTH	4
AP_LW_24	20/12/1999	29/12/2000	LW	0	StoN	LTH	5
AP_LW_25	21/02/2001	19/12/2001	LW	0	EtoW	LTH	4
AP_LW_26	14/02/2002	11/12/2002	LW	0	EtoW	LTH	4
AP_LW_26N	20/02/2003	30/09/2003	LW	0	EtoW	LTH	3
AP_LW_920	2/03/2004	18/10/2005	LW	0	EtoW	LTH	7
AP_LW_930	19/12/2005	11/02/2007	LW	0	EtoW	LTH	5
AP_LW_940	27/03/2007	23/06/2008	LW	0	EtoW	LTH	6
AP_LW_950	8/08/2008	15/02/2010	LW	0	EtoW	LTH	7
AP_LW_960	7/04/2010	5/07/2011	LW	0	EtoW	LTH	6
AP_LW_970	24/08/2011	8/10/2012	LW	0	EtoW	LTH	5
AP_LW_980	27/11/2012	28/04/2014	LW	0	EtoW	LTH	6
AP_LW_900_west	9/06/2014	5/05/2015	LW	0	StoN	LTH	4

APE_1	16/06/2015	9/03/2016	LW	0	EtoW	LTH	3
APE_2	20/04/2016	15/11/2016	LW	0	EtoW	LTH	3
APE_3	5/01/2017	20/10/2017	LW	0	EtoW	LTH	4
APE_4	20/10/2017	1/06/2018	LW	0	EtoW	LTH	3
APE_5	13/07/2018	15/02/2019	LW	0	EtoW	LTH	3
APE_6	8/03/2019	14/10/2019	LW	0	EtoW	LTH	3
APE_7	25/11/2019	1/10/2020	LW	0	EtoW	LTH	4
APE_8	12/11/2020	1/10/2021	LW	0	EtoW	LTH	4
APE_9	29/11/2021	2/03/2023	LW	0	EtoW	LTH	6
APE_10	13/04/2023	10/06/2024	LW	0	EtoW	LTH	5
APE_11	22/07/2024	3/11/2025	LW	0	EtoW	LTH	6
APE_12	15/12/2025	11/05/2027	LW	0	EtoW	LTH	6
APE_13A	22/06/2027	10/01/2028	LW	0	EtoW	LTH	3
APE_13B	21/02/2028	2/10/2028	LW	0	EtoW	LTH	3
APE_14A	13/11/2028	17/05/2029	LW	0	EtoW	LTH	3
APE_14B	28/06/2029	26/02/2030	LW	0	EtoW	LTH	3
APE_15	15/04/2030	15/11/2030	LW	0	EtoW	LTH	3
APE_16	6/01/2031	16/06/2031	LW	0	EtoW	LTH	2
APE_17	28/07/2031	4/02/2032	LW	0	EtoW	LTH	3
APE_18	17/03/2032	1/07/2032	LW	0	EtoW	LTH	2
APE_19	12/08/2032	21/12/2032	LW	0	EtoW	LTH	2
AP_LW_910	2/04/2030	16/09/2030	LW	0	EtoW	LTH	2
SPR_LW_1	10/02/1995	1/1/1996	LW	0	NtoS	LTH	4
SPR_LW_401	1/3/1996	1/1/1997	LW	0	NtoS	LTH	4
SPR_LW_402	1/2/1997	1/11/1997	LW	0	NtoS	LTH	4
SPR_LW_403	1/1/1998	1/11/1998	LW	0	NtoS	LTH	4
SPR_LW_404	1/1/1999	1/2/2000	LW	0	NtoS	LTH	5
SPR_LW_405	10/04/2000	26/03/2001	LW	0	NtoS	LTH	4
SPR_LW_406	27/05/2001	23/01/2002	LW	0	NtoS	LTH	3
SPR_LW_407	28/03/2002	9/01/2003	LW	0	NtoS	LTH	4
SPR_LW_408	20/02/2003	18/12/2003	LW	0	NtoS	LTH	4
SPR_LW_409	18/02/2004	10/12/2004	LW	0	NtoS	LTH	4
SPR_LW_410	9/02/2005	19/01/2006	LW	0	NtoS	LTH	4
SPR_LW_411	10/03/2006	26/10/2007	LW	0	NtoS	LTH	7
SPR_LW_412	14/12/2007	22/06/2009	LW	0	NtoS	LTH	7
SPR_LW_413A	7/08/2009	1/04/2010	LW	0	NtoS	LTH	3
SPR_LW_413B	20/05/2010	29/12/2010	LW	0	NtoS	LTH	3
SPR_LW_414	11/02/2011	21/11/2011	LW	0	NtoS	LTH	4
SPR_LW_415	15/03/2012	1/7/2013	LW	0	NtoS	LTH	6
SPR_LW_416	1/7/2013	1/4/2014	LW	0	NtoS	LTH	4
SPR_LW_417	1/6/2014	1/1/2015	LW	0	NtoS	LTH	3
SPR_LW_418	1/3/2015	1/9/2015	LW	0	NtoS	LTH	3
SPR_LW_419	1/11/2015	1/4/2016	LW	0	NtoS	LTH	2
SPR_LW_420	1/6/2016	1/11/2016	LW	0	NtoS	LTH	2
SPR_LW_421	1/1/2017	1/6/2017	LW	0	NtoS	LTH	2
SPR_LW_422	1/8/2017	1/12/2017	LW	0	NtoS	LTH	2

SPR_LW_423	1/2/2018	1/5/2018	LW	0	NtoS	LTH	1
SPR_LW_424	1/7/2018	1/1/2019	LW	0	StoN	LTH	3
SPR_LW_425	1/3/2019	1/9/2019	LW	0	StoN	LTH	3
SPR_LW_426	1/11/2019	1/5/2020	LW	0	StoN	LTH	3
SPR_LW_427	1/7/2020	1/3/2021	LW	0	StoN	LTH	3
SPR_LW_428	1/5/2021	1/12/2021	LW	0	StoN	LTH	3
SPR_LW_429	1/2/2022	1/9/2022	LW	0	StoN	LTH	3
SPR_LW_430	1/11/2022	1/5/2023	LW	0	StoN	LTH	3
SPR_LW_431	1/7/2023	1/12/2023	LW	0	StoN	LTH	2
SPR_LW_432	1/2/2024	1/7/2024	LW	0	StoN	LTH	2
SPR_LW_501	1/1/2024	1/5/2024	LW	0	StoN	LTH	2
SPR_LW_502	1/6/2024	1/9/2024	LW	0	StoN	LTH	2
SPR_LW_503	1/10/2024	1/2/2025	LW	0	StoN	LTH	2
Clarence_LW_rest	1/10/1993	1/3/1998	LW	0	StoN	KAT	18
Clarence_LW_7	1/6/1997	1/9/1997	LW	0	StoN	KAT	2
OPK	1/1/1887	1/1/1948	BP	1.30E+06	EtoW	LTH	1
FBK	1/1/1886	1/1/1986	BP	1.30E+06	EtoW	LTH	1
LGS	1/1/1916	1/1/1964	BP	1.30E+06	EtoW	LTH	1
STW	1/1/1921	1/1/1957	BP	1.30E+06	EtoW	LTH	1
COM	1/1/1904	1/1/1943	BP	Flooded	EtoW	LTH	1
CAL	1/1/1925	1/1/1939	BP	Flooded	EtoW	LTH	1
WWG	1/1/1925	1/1/1979	BP	Flooded	EtoW	LTH	1
RWN	1/1/1921	1/1/1956	BP	Flooded	EtoW	LTH	1
INV	1/1/1906	1/1/1998	BP	Flooded	EtoW	LTH	1
VAL	1/1/1926	1/1/1934	BP	Flooded	EtoW	LTH	1
LGS_1	1/1/1916	1/1/1964	BP	1.30E+06	EtoW	LTH	1
EAS	1/1/1960	1/1/1992	BP	Flooded	EtoW	LTH	1
BBN	1/1/1985	1/1/2010	LW	Flooded	StoN	LTH	25
JHN	1/1/1949	1/1/1952	Opencut	Flooded	EtoW	LTH	1
KER1	1/1/1950	1/1/1954	Opencut	Flooded	EtoW	LTH	1
KER2	1/1/1950	1/1/1954	Opencut	Flooded	EtoW	LTH	1
KER3	1/1/1950	1/1/1954	Opencut	Flooded	EtoW	LTH	1
COL1	1/1/1948	1/1/1954	Opencut	Flooded	EtoW	LTH	1
COL2	1/1/1948	1/1/1954	Opencut	Flooded	EtoW	LTH	1
NEW1	1/1/1952	1/1/1954	Opencut	Flooded	EtoW	LTH	1
NEW2	1/1/1952	1/1/1954	Opencut	Flooded	EtoW	LTH	1
FLY	1/1/1888	1/1/1926	Opencut	Flooded	EtoW	LTH	1
PDL1	1/01/2006	10/10/2030	Opencut	0	EtoW	LTH	1
PDL2	1/01/2006	10/10/2030	Opencut	0	EtoW	LTH	1
Clarence_BP_1	9/07/2006	9/07/2027	BP	0	EtoW	KAT	8
Clarence_BP_2_3	21/07/1994	21/07/2015	BP	0	StoN	KAT	21
Clarence_BP_4_5	20/12/2006	20/12/2027	BP	0	StoN	KAT	21
AP_BnP	1/01/1980	2/07/2015	BP	0	NtoS	LTH	1

2.4 Geology and hydrogeology

2.4.1 Overview

Springvale and Angus Place Collieries are located in the western margins of the Sydney Basin and extract coal from the Lithgow Seam, which lies in the upper Permian Illawarra Coal Measures. These coal measures are dominated by fluvial sandstones and floodplain siltstones with some claystone (probably volcanic in origin) and coal.

The region consists of a sequence of sedimentary rocks of Triassic and Permian age. There are five main geological groups within the region: Narrabeen Group, Illawarra Coal Measures, Shoalhaven Group, Lambie Group, and basement rocks. There are also a few small areas of shallow unconsolidated Quaternary sediments in creek lines which consist of sands and silts.

Palaris (2013a, 20013b) compiled the available borehole information and examined the lithological sequence within the mining region. The Narrabeen Group correlated by Palaris (2013a) consists predominantly of sandstones and can be subdivided into the following five formations from top to bottom:

- Burralow Formation;
- Banks Wall Sandstone;
- Mt York Claystone;
- Burra-Moko Head Sandstone; and
- Caley Formation.

Similarly, the units correlated in the Illawarra Coal Measures by Palaris (2012a, 2013b) are:

- Katoomba Seam
- Middle River Coal Member (upper)
- Denman Formation
- Irondale Coal
- Lithgow/Lidsdale Coal

In addition to these units, the Permian sequence consists largely of interbedded sandstones and shales, mudstones, relatively thin sandstone units, thin tuffaceous claystones, and rare conglomerates. The Marangaroo Formation consists predominantly of sandstone in the Angus Place/Springvale lease. The Denman Formation (known locally as the Baal Bone Formation) is a significant unit in the area as it has been correlated throughout the Sydney Basin. The Denman Formation gradationally underlies the regionally correlated Watts (Waratah) Sandstone.

Figure 7 presents a typical stratigraphic section within Springvale and Angus Place Collieries.

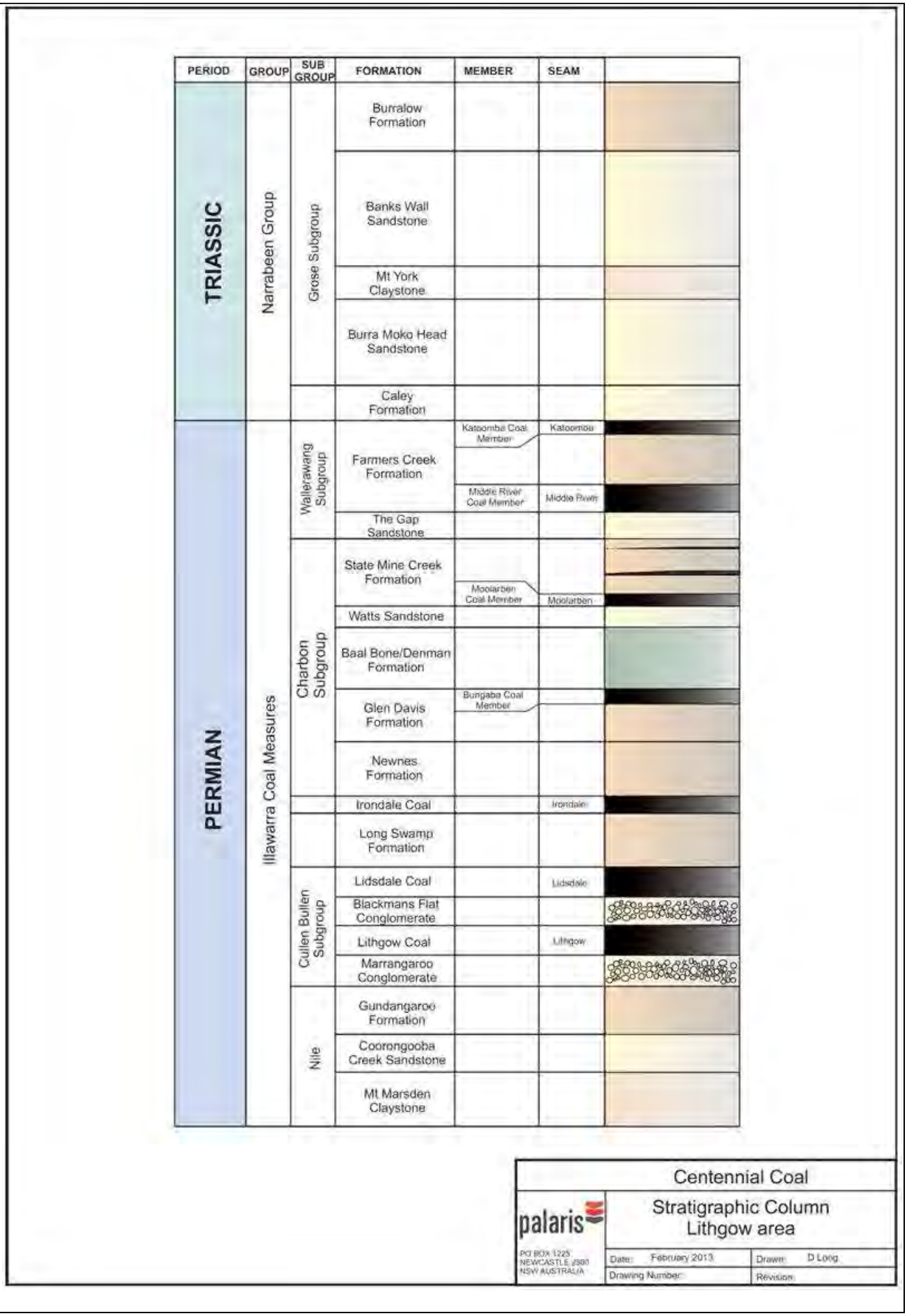

Figure 7 Typical stratigraphy at Springvale and Angus Place Collieries (Palaris, 2013a)

2.4.2 Hydrogeology – previous studies

The hydrogeology in the Springvale and Angus Place Colliery region was investigated between 2003 and 2008 and is described in ACARP reports C14033 and C18016. In those studies, the distribution of pore-water pressures within the Springvale region was investigated using more than 100 vibrating wire piezometers installed at Springvale Colliery.

In that study, the Mt York Claystone, consisting of a sequence of interbedded claystone and sandstone, was identified as a major aquiclude separating the shallow and the deeper (regional) groundwater systems. The Mt York Claystone occurs as a continuous layer and averages 22m in thickness in the Angus Place and Springvale Colliery region. Typically, the unit consists of two or three discrete claystone bands, up to 4m thick, separated by sandstone/siltstone bands, up to 8m thick. This layer is reasonably consistent in nature within the Angus Place and Springvale region (Palaris, 2013b).

In ACARP reports C14033 and C18016 the following five aquifers[†] and four semi-permeable layers were identified on the basis of lithological interpretation available at that time, detailed analysis of initial piezometric heads and observed piezometric responses to mining:

- Aquifer1 – sandstone with laminated siltstone (Berry Siltstone), Sandstone (Marrangaroo Formation), Lidsdale/Lithgow Coal Seams and Long Swamp Formation (Sandstone and Siltstone);
- Semi-permeable layer (SP1) – sandstone and siltstone (Baal Bone/Denman Formation);
- Aquifer2– sandstone with laminated siltstone;
- Semi-permeable layer (SP2) – siltstone with sandstone laminations located just below the Katoomba Seam;
- Aquifer3 - sandstone with laminated siltstone, Katoomba Seam;
- Semi-permeable layer (SP3) – siltstone/sandstone, mudstone (Mt York Claystone);
- Aquifer4 – sandstone;
- Semi-permeable layer (SP4) – siltstone, mudstone, Claystone
- Aquifer5 - sandstone

2.4.3 Updated hydrogeology – further division of AQ4

Centennial Coal has subsequently identified a number of continuous claystone layers YS1 to YS6 (see Figure 8) within the Burralow Formation consisting of medium- to coarse grained sandstones interbedded with fine-grained sandstone/siltstone/claystone units (Palaris, 2013a).

As will be discussed in Section 2.5, the bottommost claystone layer called YS6 identified within the Burralow Formation is explicitly incorporated in the model thus dividing the Aquifer4 into two separate aquifers. The semi-permeable layer SP4 identified in the ACARP reports C14033 and C18016 is found to almost coincide with the YS4 layer. Thus the floor of the SP4 layer as described in the ACARP reports has been slightly modified to match exactly with the floor of the YS4 layer. Other claystone layers lying within the Burralow Formation are considered implicitly in the model by assigning aggregate (equivalent) flow properties; these flow properties are considered as model parameters and are derived during model calibration and validation process by matching numerical model results with the observed/monitored data.

[†] It is important to emphasize that the term aquifer used in this report may not be considered as 'Aquifers' used commonly to describe a rock layer with readily extractable ground water resource. In this report the term 'aquifer' is used to describe water bearing rock layers with relatively higher permeability than the layers that prohibit vertical flow.

The updated hydrogeological sequence (layering) incorporated in the model from top to bottom is described in Section 2.5.

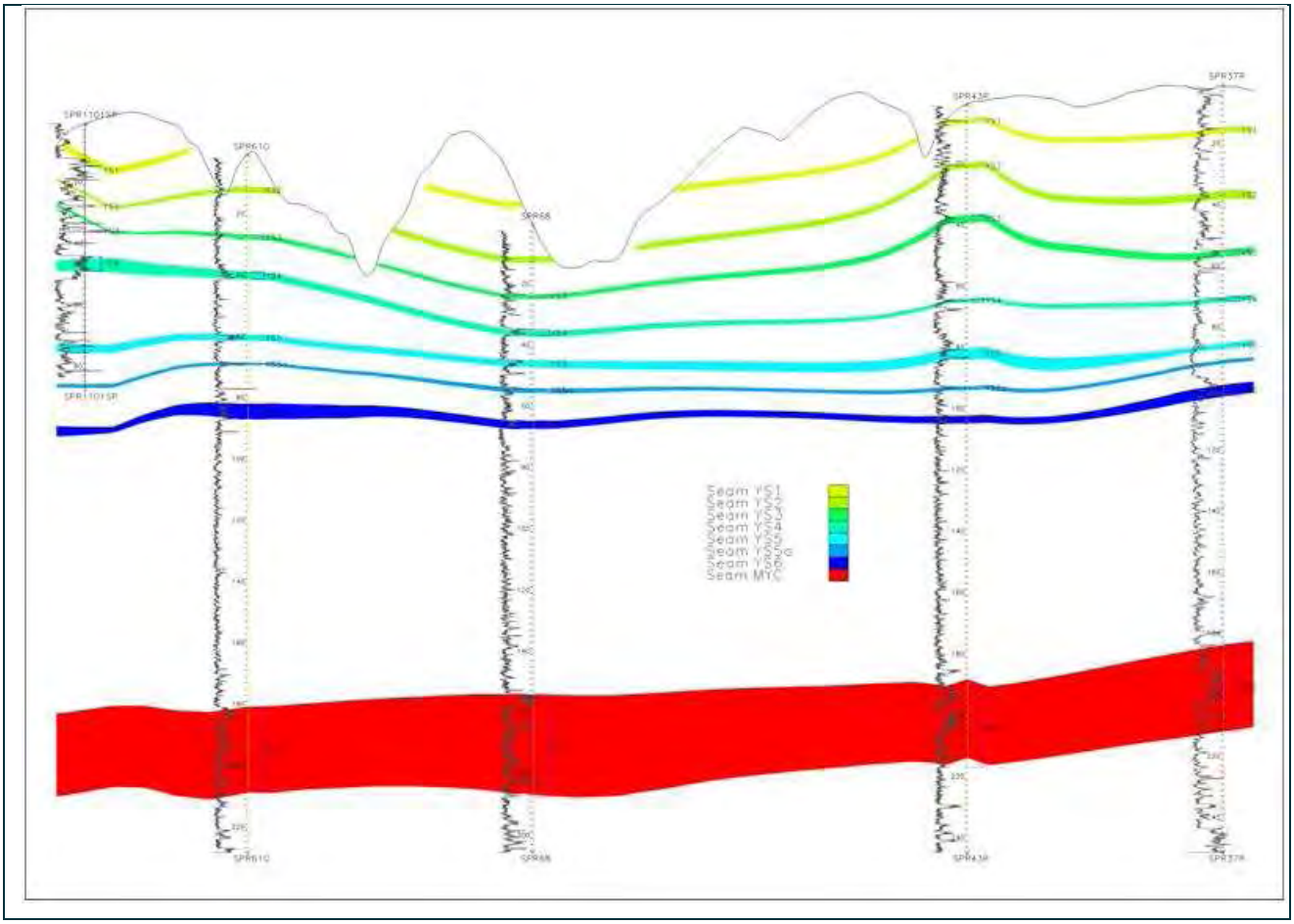

Figure 8 Correlated units in the Narrabeen Group (Palaris, 2013a)

2.4.4 High-level geological model

Palaris (2013b) recently developed a high-level geological model spanning approximately 15,000 km2 of the Western Coalfield for Centennial Coal. Figure 9 shows the area covered in the study with the location of boreholes that provided stratigraphic data. The report provided a general indication of the thickness, depth, dip direction and outcrop locations of key stratigraphic horizons (i.e. the Mount York Claystone, the Katoomba seam, the Denman Formation and the Lithgow seam) within the geological sequence. The high-level geological model helped better define the extended model described in Section 2.1.

The outcrop lines for the four stratigraphic layers and a typical cross-section WE2 (marked in Figure 10) are presented in Figure 10 and Figure 11 respectively.

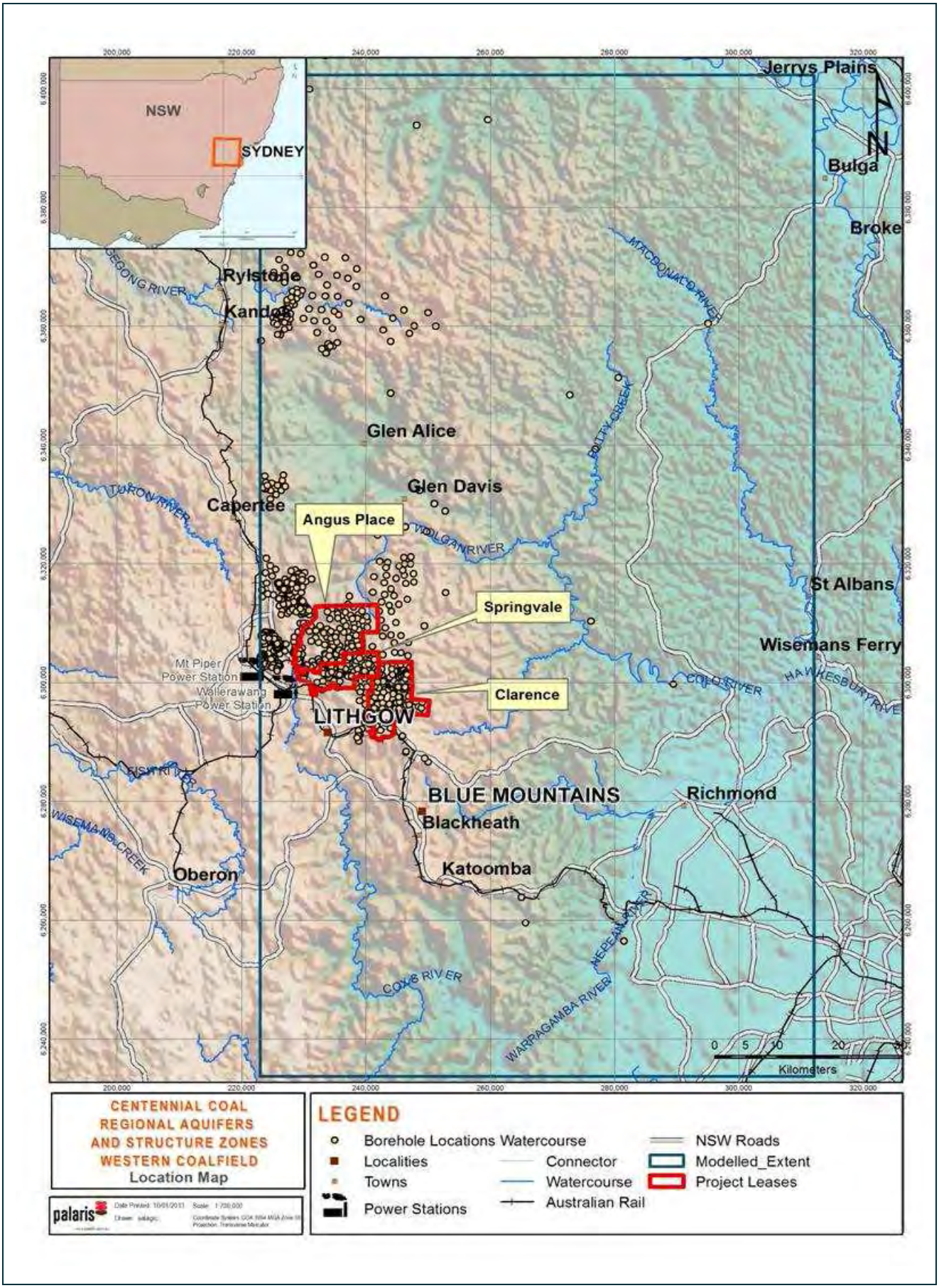

Figure 9 Location plan showing the data coverage used by Palaris (2013b)

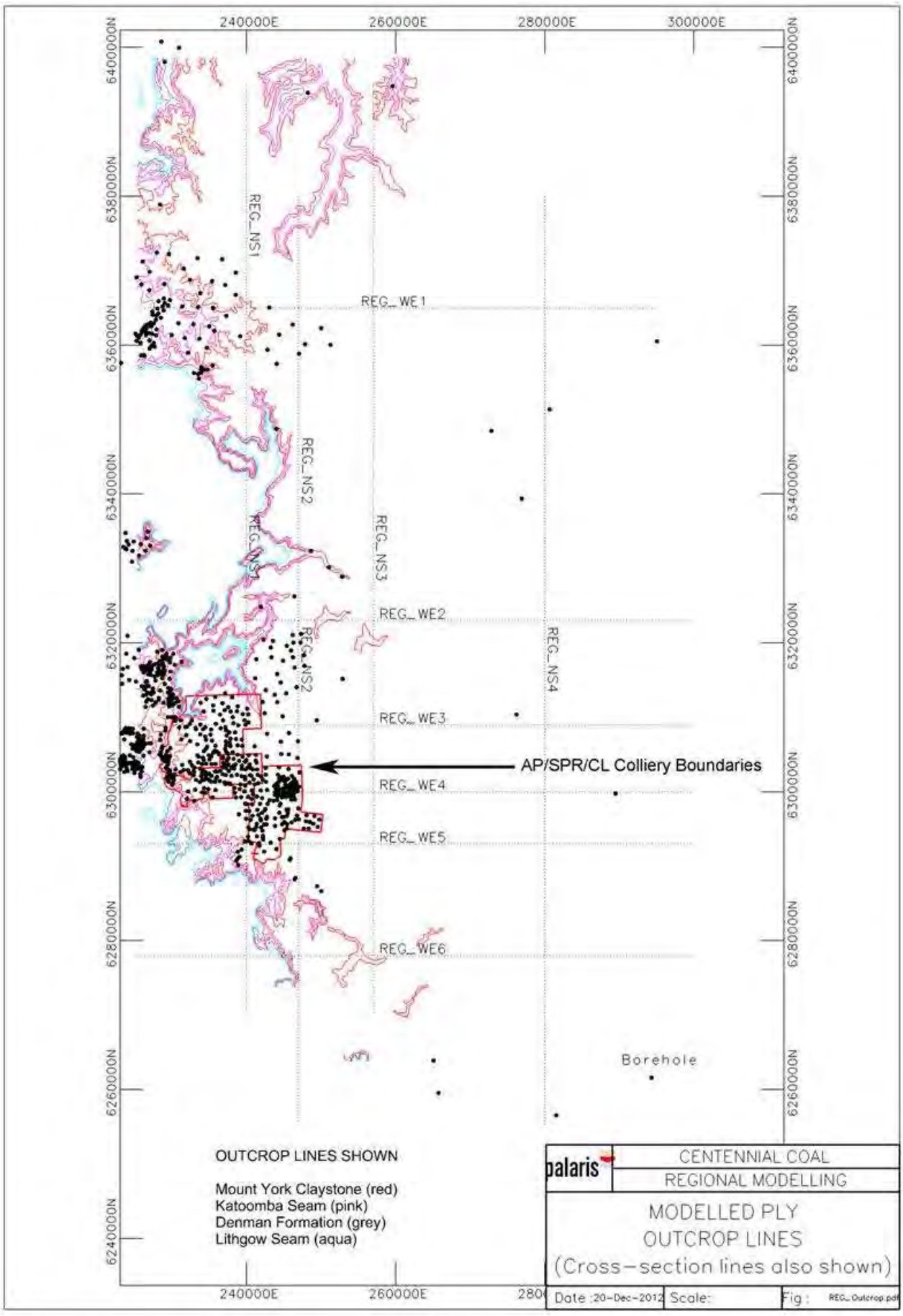

Figure 10 Key Stratigraphic horizon outcrop and cross-section locations (Palaris, 2013b)

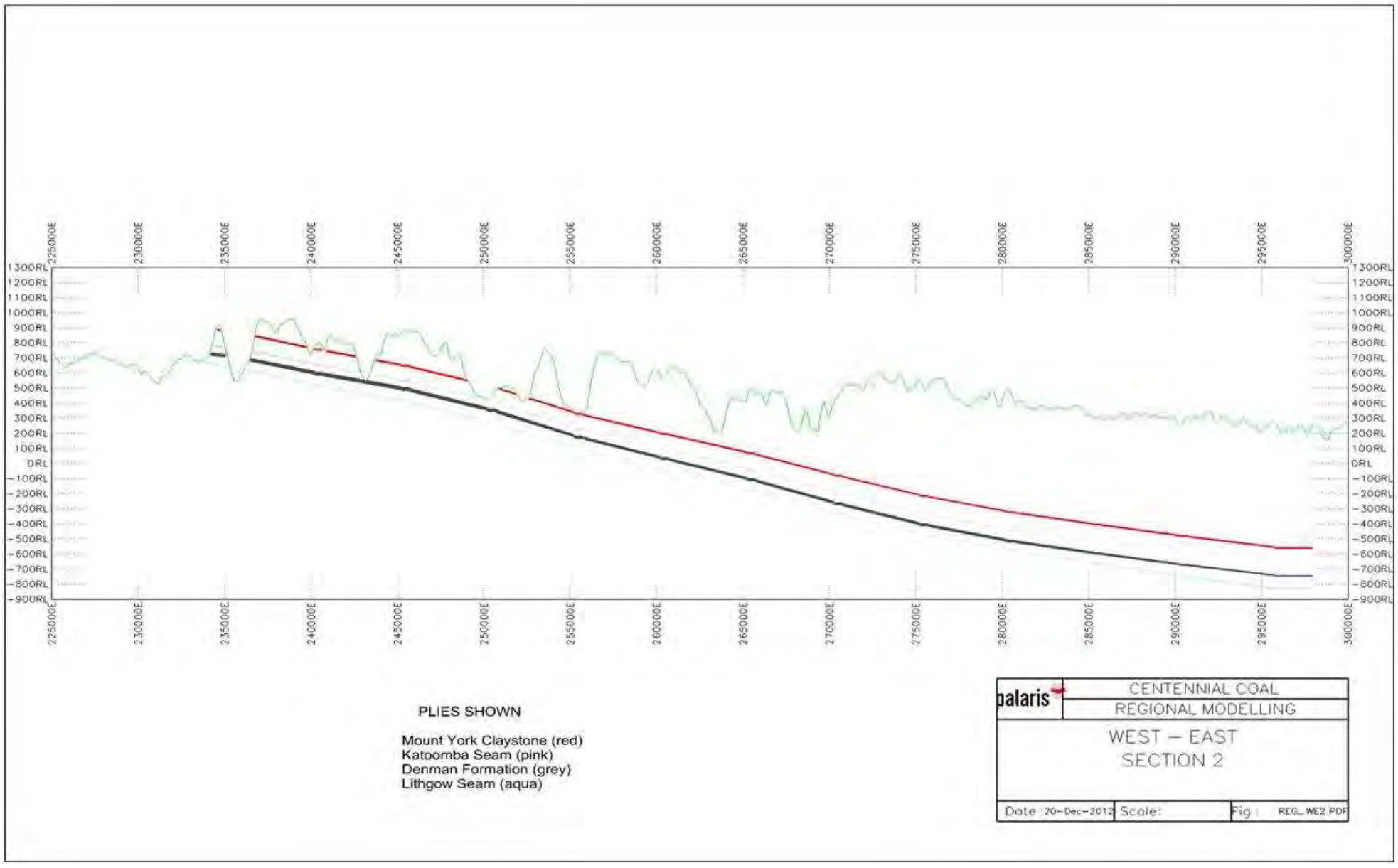

Figure 11 Cross-section WE2 (high level geological model; Palaris, 2013b)

Figure 12 to Figure 15 present four stratigraphic cross-sections (marked in Figure 10) within the Angus Place and Springvale Colliery region. These cross-sections show that the aquicludes considered in the model are fairly continuous and consistent with the regional geological setting.

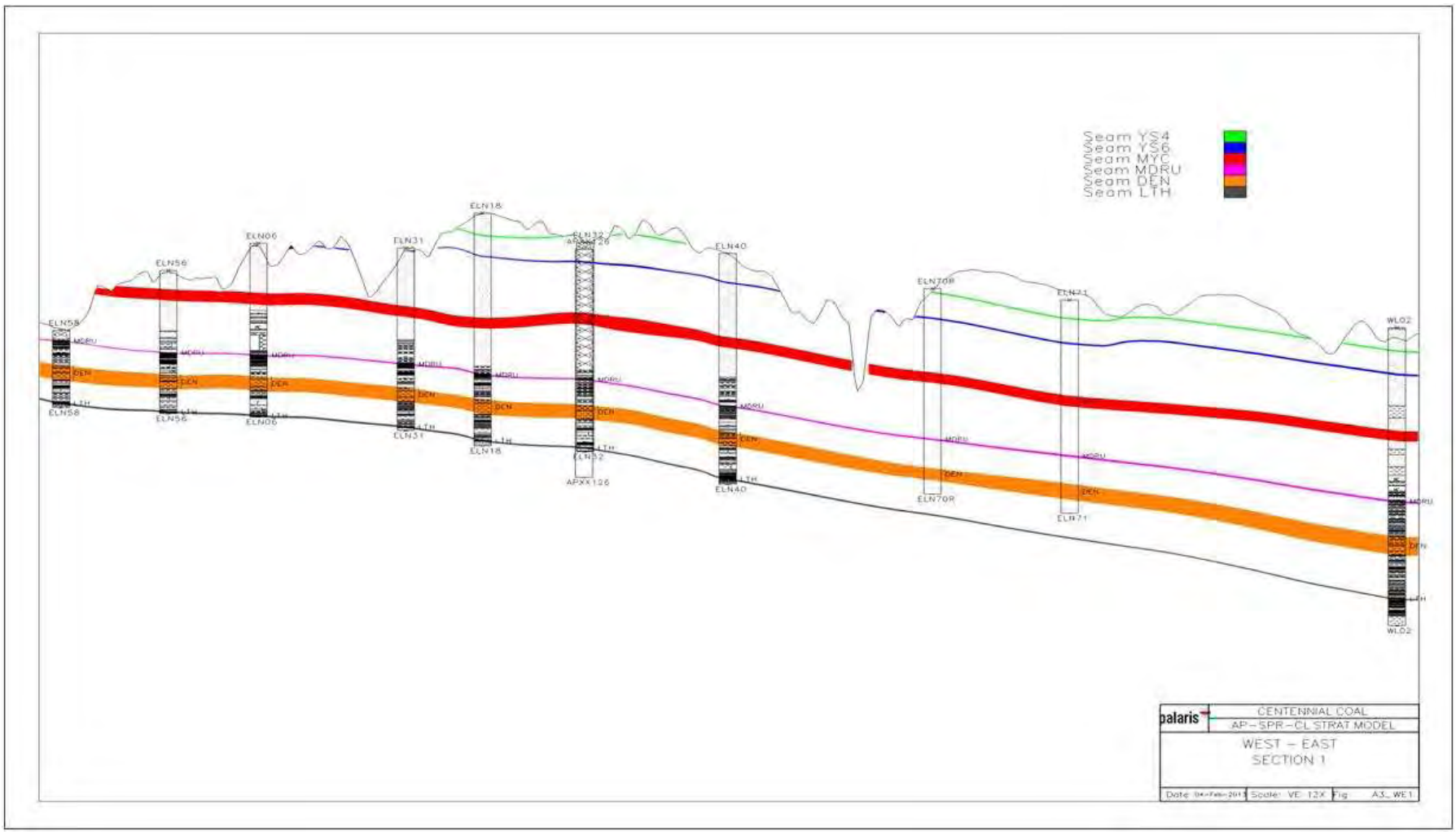

Figure 12 Geological cross-section WE1 showing Lithgow Seam (aqua), Denman Formation (grey), Katoomba Seam (pink), Mt York Claystone (red), YS6 (blue) and YS4 (Green) (detailed geological model; Palaris, 2013a)

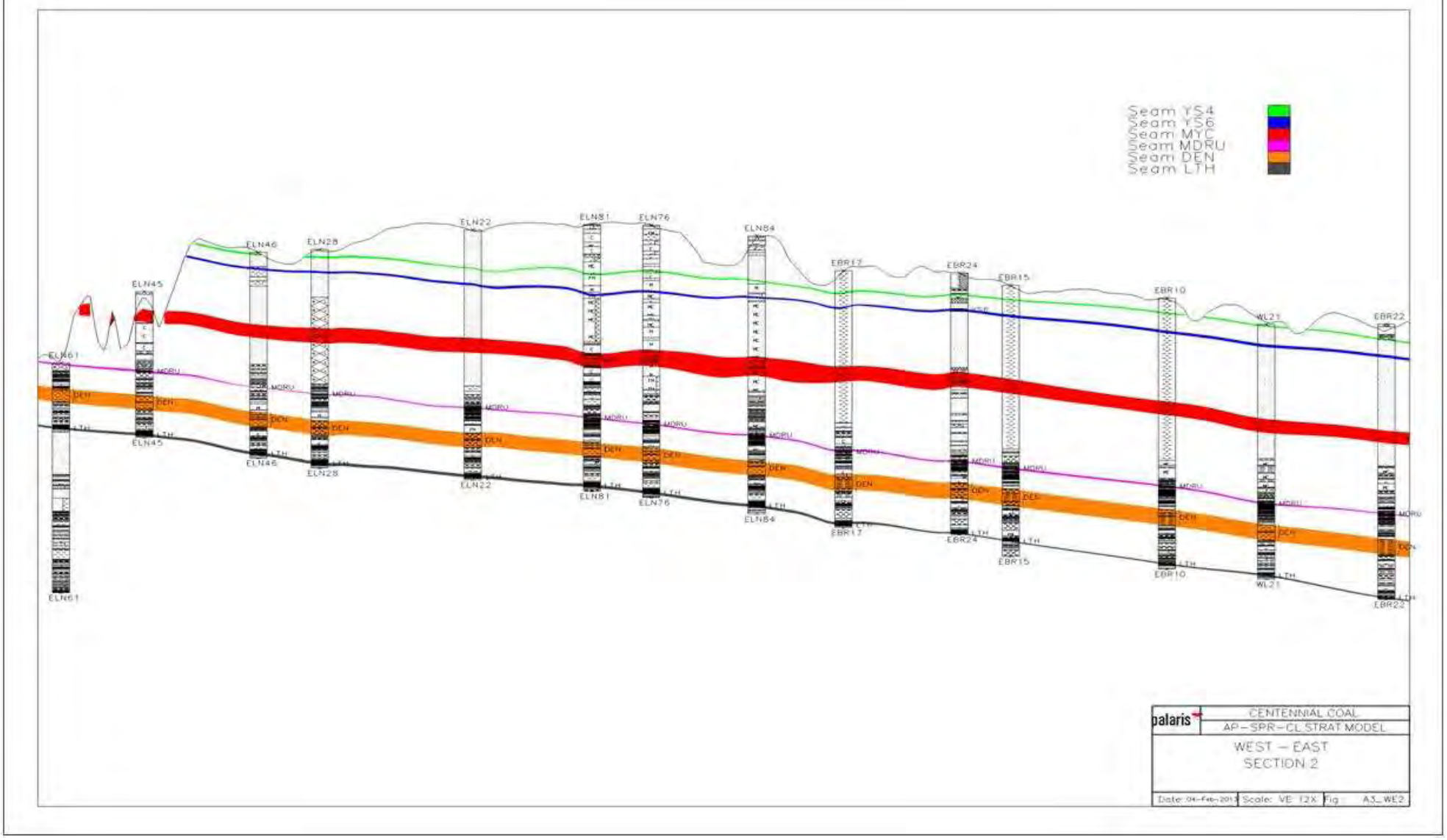

Figure 13 Geological cross-section WE2 showing Lithgow Seam (aqua), Denman Formation (grey), Katoomba Seam (pink), Mt York Claystone (red), YS6 (blue) and YS4 (Green) (detailed geological model;Palaris, 2013a)

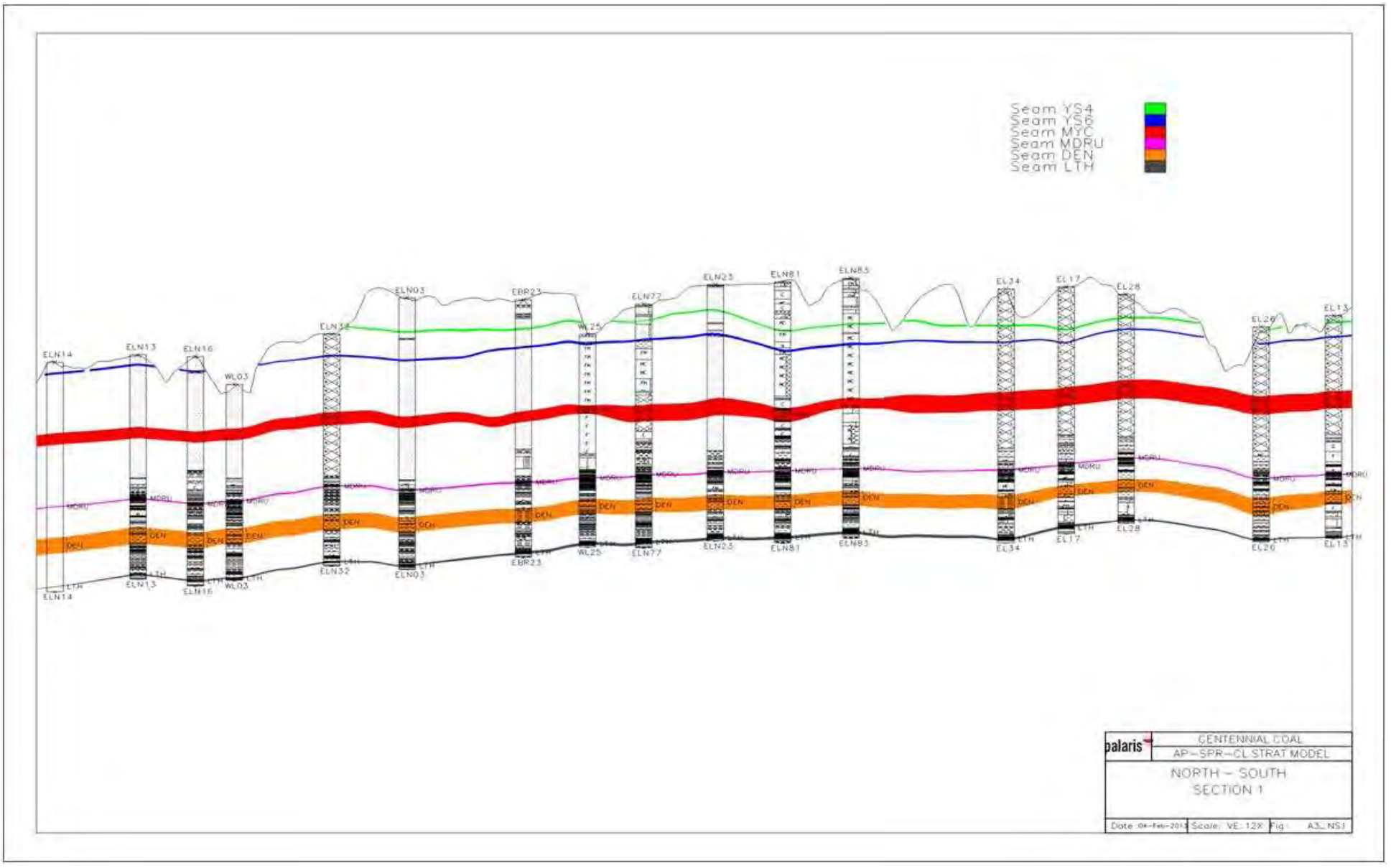

Figure 14 Geological cross-section NS1 showing Lithgow Seam (aqua), Denman Formation (grey), Katoomba Seam (pink), Mt York Claystone (red), YS6 (blue) and YS4 (Green) (detailed geological model; Palaris, 2013a)

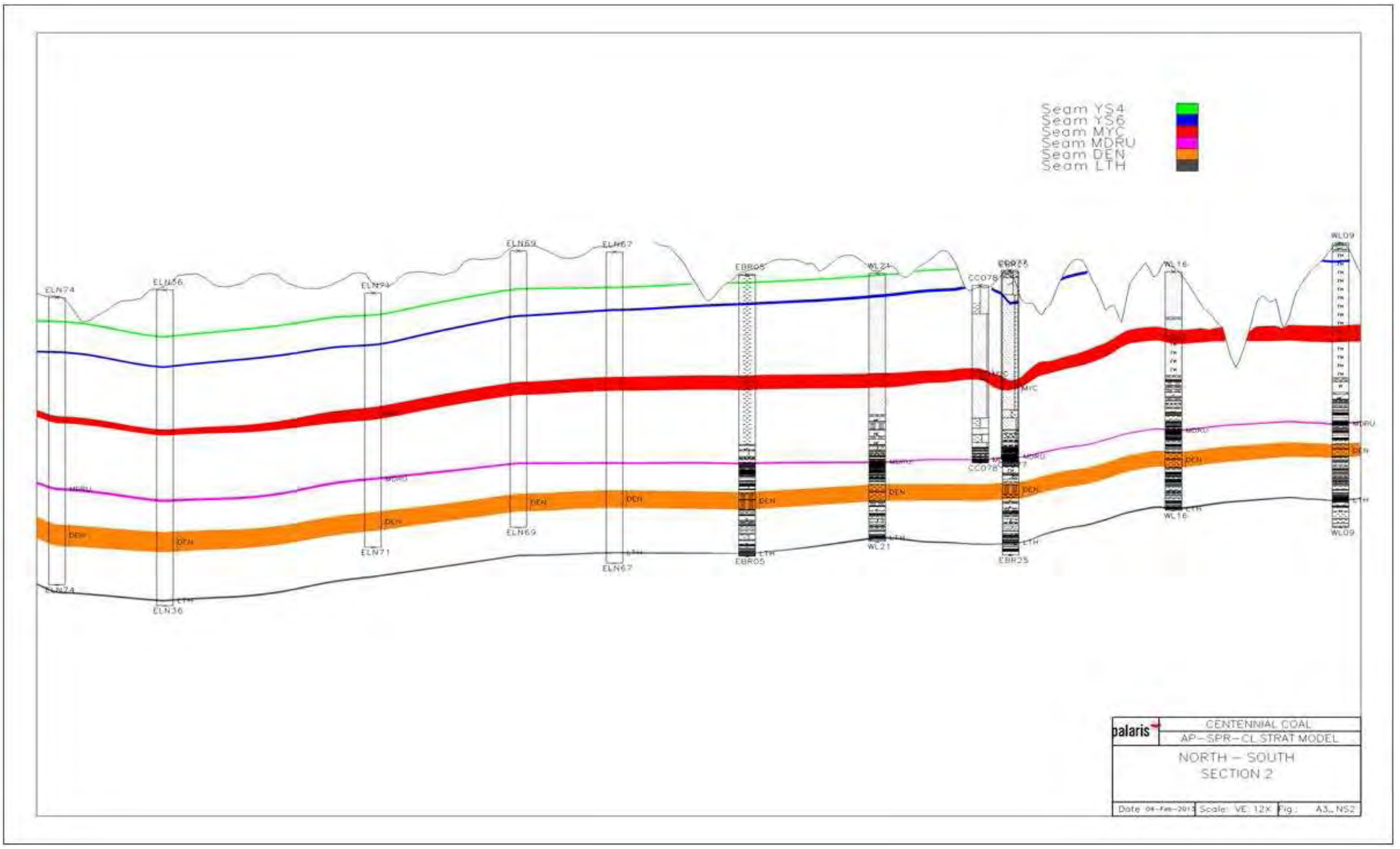

Figure 15 Geological cross-section NS2 showing Lithgow Seam (aqua), Denman Formation (grey), Katoomba Seam (pink), Mt York Claystone (red), YS6 (blue) and YS4 (Green) (detailed geological model; Palaris, 2013a)

2.5 Hydrogeological layers used in the model

Based on the above information, the hydrogeological model is defined conceptually in terms of six water bearing layers (Aquifer1 to Aquifer6) separated by five low-permeability layers (SP0 to SP4, which includes YS4 and YS5) as shown in Figure 16. The shorthand notations used in the figures are listed in Table 3.

SP0 – This is the base of the model and located at about 5m below the floor of the Lithgow seam (represented by one elemental layer in the finite-element mesh).

Aquifer1 – This aquifer is found to include Lidsdale/Lithgow Coal Seam which is hydraulically connected with the laminated siltstone (Berry Siltstone) and sandstone of Marrangaroo Formation underneath and the sandstone and siltstone of Long Swamp Formation (AQ1) and Irondale Coal Seam above (represented by 4 elemental layers).

SP1 - Aquifer1 is separated from Aquifer2 by a semi-permeable layer (SP1) located within the Baal Bone/Denman Formation and comprises mudstone, siltstone and claystone (represented by one elemental layer).

Aquifer2 – This aquifer contains sandstone with laminated siltstone and Middle River Coal Member AQ2 (represented by one elemental layer).

SP2 -A semi-permeable layer with coal, siltstone and mudstone is the boundary between Aquifer2 and Aquifer3. This semi-permeable layer is assumed to occur just below the Katoomba Seam (represented by one elemental layer).

Aquifer3 – This aquifer can be identified in the sandstone (AQ3) of the Burra Moko Head Formation and the Caley Formation and located below the Mt York Claystone. It is hydraulically connected with the Katoomba Seam (represented by 4 elemental layers)

SP3 - A semi-permeable claystone layer (Mt York Claystone) separates Aquifer3 and Aquifer4 (represented by one elemental layer).

Aquifer4 – This aquifer is located in the Banks Wall Sandstone (AQ4, Narrabeen Group) (represented by two elemental layers).

YS6 – A thin semi-permeable claystone layer separates Aquifer4 and Aquifer5 (represented by one elemental layer).

Aquifer5 – This aquifer is located in the Burralow Formation (AQ5, represented by one elemental layer).

SP4 – A thin semi-permeable layer located in the Burralow Formation and comprises claystone (YS4) and sandstone/ siltstone (represented by one elemental layer).

Aquifer6 – This aquifer is located in the upper part of the Narrabeen Group sandstone (AQ6). This is an unconfined aquifer and only appears near the top of the Newnes plateau (represented by one elemental layer).

Weath – This is a 10m thick layer of weathered material which is assumed to cover the top surface of the model (represented by one elemental layer).

Thus all together there are 17 material layers (i.e. base, floor, Lithgow Seam (mined section), Lithgow Seam (roof), AQ1, SP1, AQ2, SP2, Katoomba Seam, AQ3, SP3, AQ4, YS6, AQ5, SP4, AQ6, and Weath) which are discretised into 20 elemental layers in the finite-element mesh.

Table 3 Shorthand notations

AQ	Sandstone/Siltstone		IRD	Irondale coal seam
MYC	Mt York Clay aquitard		KAT	Katoomba coal seam
SP	Low permeability layer		LTH	Lithgow coal seam
Weath	Weathered alluvium		MRD	Middle River coal seam

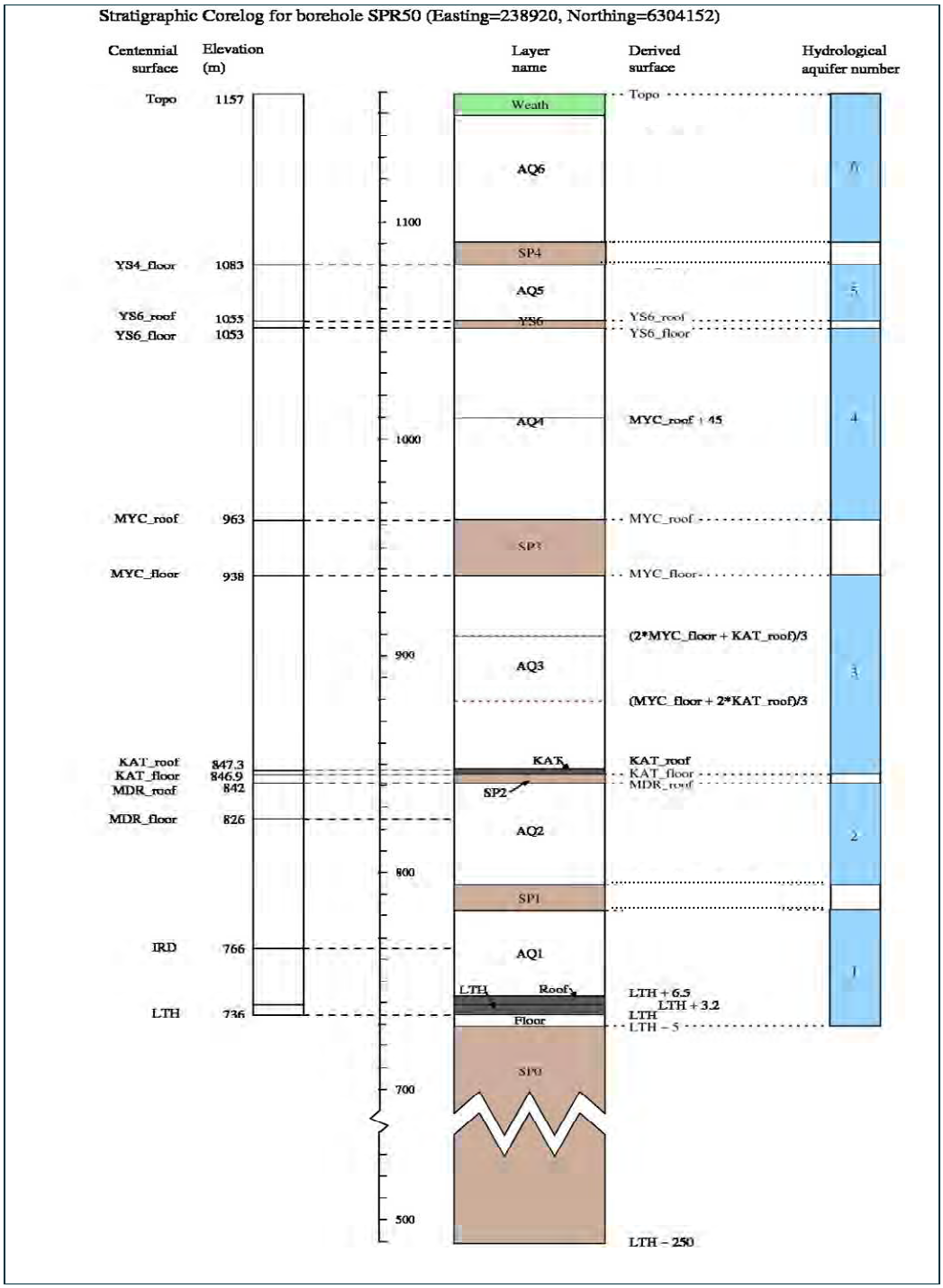

Figure 16 Model stratigraphy (right) and corelog showing elevation of geological surfaces supplied by Centennial Coal (left) at piezometer borehole SPR50 (238290E, 6304152N). Red dotted lines indicate subdivision of a single material layer into a number of finite element layers to improve vertical resolution

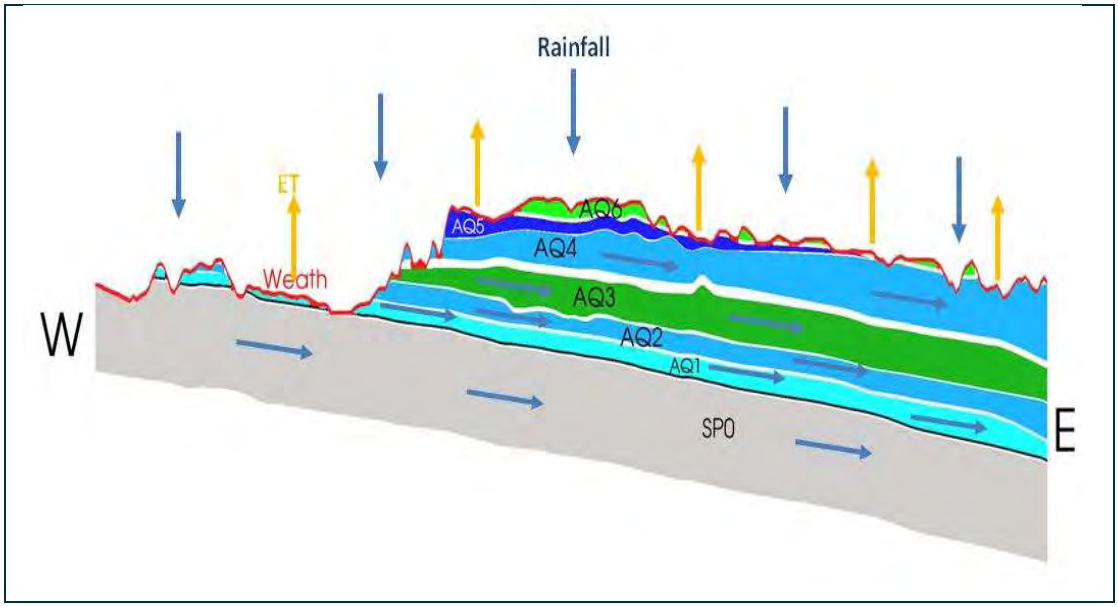

Figure 17 Stratigrapy, rainfall and ET as conceptualised in the model

Figure 17 illustrates the six groundwater systems as conceptualised in the model; AQ1 to AQ6 in the figure represents the sandstone/siltstone layers within the aquifers Aquifer1 to Aquifer6 respectively.

Without the Weathered layer, the geology at the surface of the model is shown in Figure 18.

Aquifer recharge is presumed to occur from the top and at the west side of the model where the aquifer layers outcrop and natural flow occurs towards the northeast where it is discharged from the model boundary.

Figure 19 shows two cross-sections developed from the numerical mini-regional scale model.

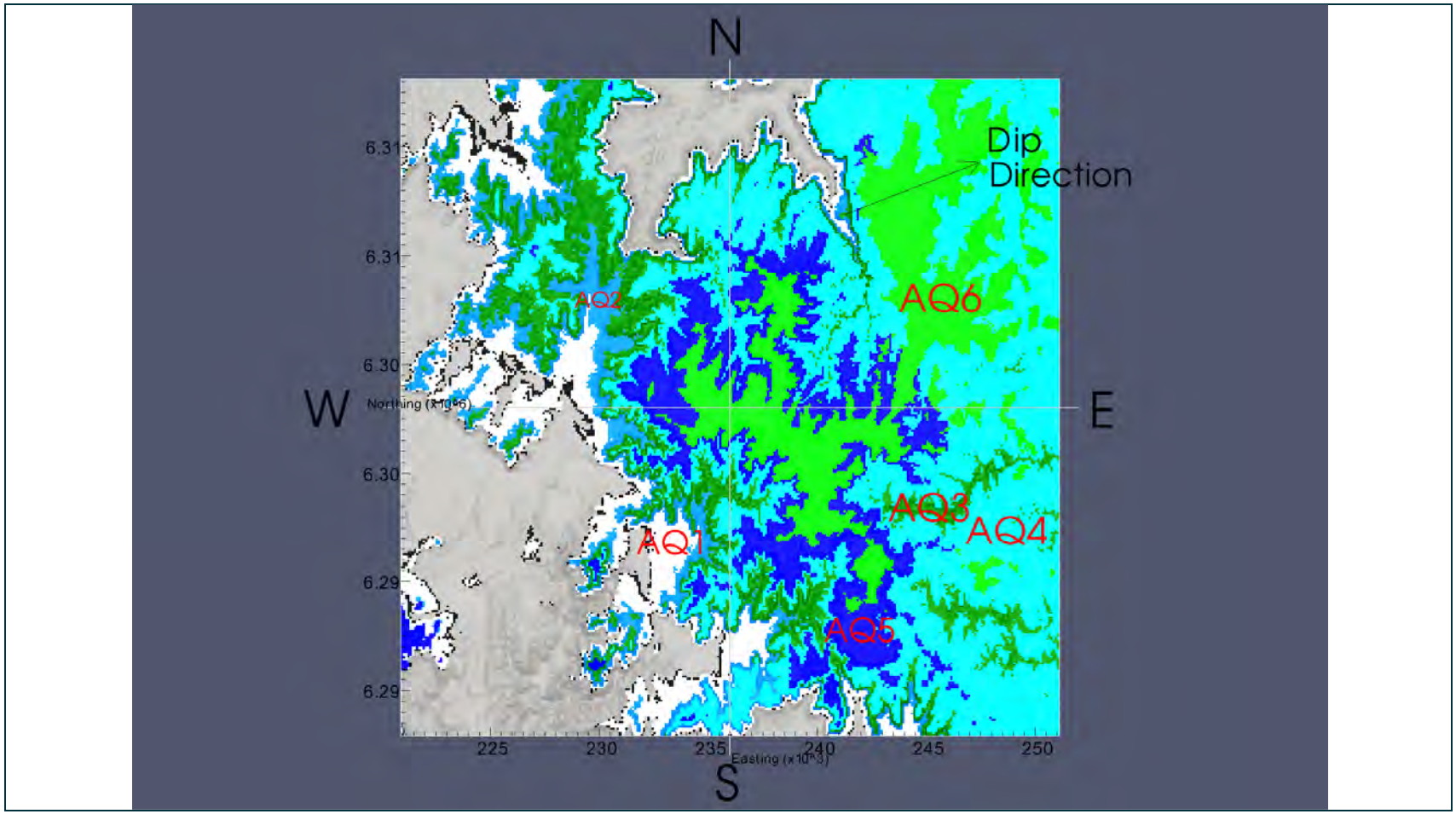

Figure 18 Surface geology generated within the model, with the weathered layer stripped away. The aquifers are coloured with different shades of blue and green, while the coal seam is black, and the basement (SP0) is grey. The layers are quite close to planar, and parallel, and their dip direction is 19 degrees north of east, as shown. The dip angle is 0.87 degrees, or 15m/1km. Finally, the position of two cross-sectional slices – WE and NS – is shown

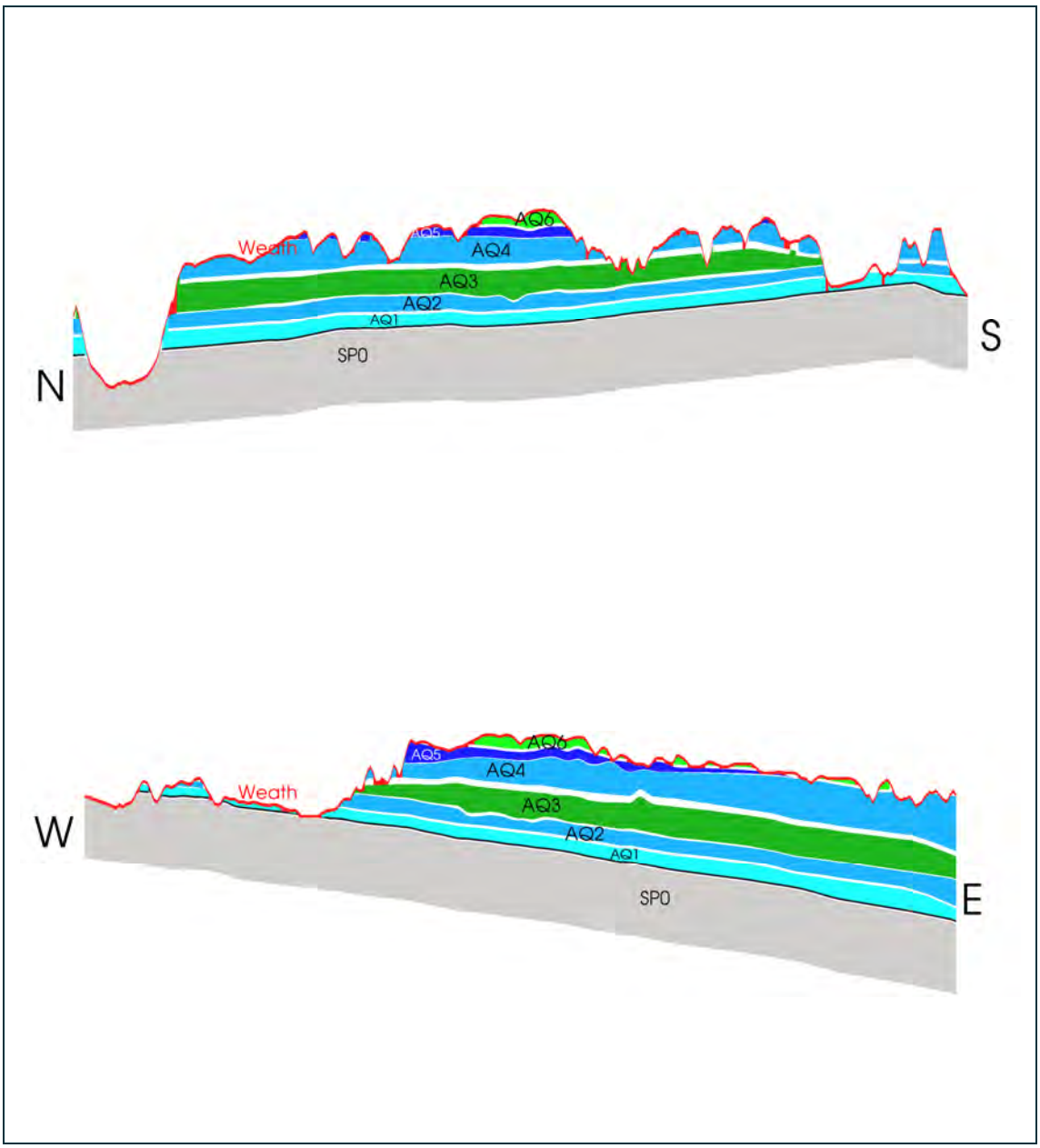

Figure 19 Two vertical cross-sections through the centre of the model. Colours indicate the material, and the topmost "Weath" layer is shown in red. The vertical exaggeration is 10

2.6 Hydrogeologic parameters

The movement of groundwater is largely controlled by hydraulic conductivity and storage capacity (porosity) of the hydrogeologic layers. In general, both hydraulic conductivity and storage capacity vary both laterally and vertically. However, in this study the hydraulic conductivity and storage capacity are assumed to remain constant within the hydrogeologic units. The model layers are grouped into six hydrogeologic units as listed in Table 4. The input parameters for each unit are estimated by matching results from a sequence of calibration numerical models to mine data varying the parameters from initial estimates, ensuring that they lie within defined bounds. The initial estimate and defined bounds are listed in Table 4.

Table 4 Hydrogeologic property variations used in the model calibration

Hydrogeologic Units	Horizontal permeability (K_{hor}, md)	Initial estimate (K_{hor}, md)	Horizontal to vertical permeability ratio (K_{ratio})	Initial estimate (K_{ratio})	Porosity
Weath	20 to 200	160	1 to 8	6	0.15 to 0.2
Sandstone/Siltstone (AQ)	2 to 100	16	5 to 20	16	0.05 to 0.2
Semi-permeable (SP)	0.1 to 5e-6	SP0 = 5e-2 SP1 = 1e-3 SP2 = 1e-3 SP3 = 1e-2 SP4 = 1e-2 YS6 = 1e-2	1 to 5	1	0.05 to 0.15
Katoomba Seam	1 to 200	5	2 to 10	2	0.05 to 0.10
Lithgow Seam	1 to 50	10	2 to 10	2	0.05 to 0.10
Lithgow_floor	0.5 to 10	5	1 to 10	5	0.05 to 0.15
Basement (SP0)	0.1 to 0.01	0.01	1 to 10	2	0.05 to 0.1

*Permeability of 1 md (= 1E-15 m^2) is equivalent to hydraulic conductivity of 9.71E-09 m/sec (≈1E-8 m/sec)

2.7 Deep piezometers

Measurements from 182 piezometers in 31 boreholes are used to compare with model heads and calculate RMS/SRMS statistics during steady-state calibration, transient calibration, and validation. There are substantial data which have been analysed in a separate report (Adhikary and Morla, 2013). Appendix A shows the positions of all piezometer boreholes, and explores each piezometer in turn, defining when each piezometer is used for comparison with the model.

2.8 Rivers and swamps

Natural discharge and recharge of ground water occurs at rivers and swamps. The rivers and swamps which are considered in this study and mapped to the numerical models are shown in Figure 20 and listed in Table 5. Nodes (which are corner points of finite elements in the numerical models) lying along the streams, rivers and swamps are assigned initially a reference stream-node-pressure boundary condition as described in Section 2.8.

Depending upon whether a swamp/stream is permanently water-logged or not, the swamp/stream node is either assigned a constant staging height (perennial condition) or a drain (ephemeral) condition as shown in Table 5 as described in Section 2.8. Perennial nodes will allow exchange of water in either direction between the stream and aquifer, whereas ephemeral node will record discharge when the groundwater pressure at the node is positive, but will allow groundwater level to drop below the node elevation without inducing leakage. The conductance of swamp/stream nodes is a calibration parameter. An initial hydraulic conductance value of 0.1 day^{-1} per unit riverbed area is assigned to these nodes.

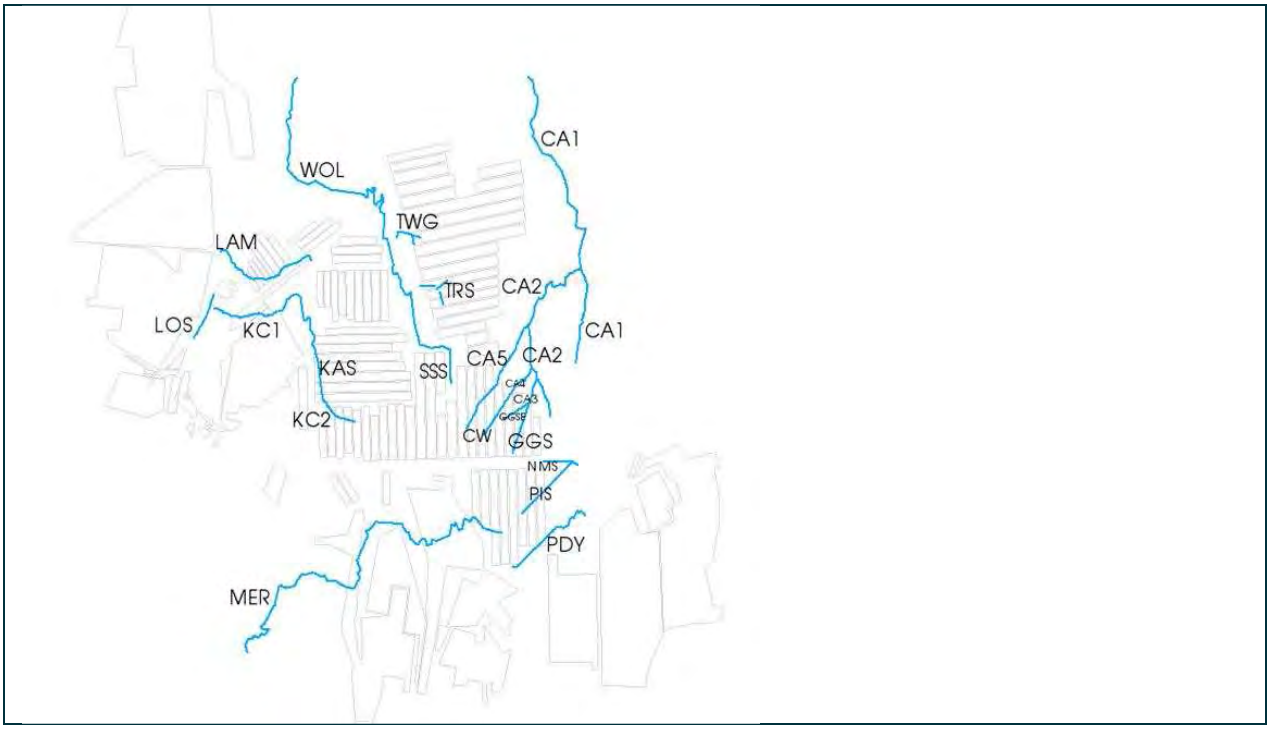

Figure 20 River reaches and swamps of interest in the model

Table 5 Swamps and River reaches considered in the model

Notation	Rivers and swamps	Boundary conditions		Notation	Rivers and swamps	Boundary conditions
CA1	Carne Creek, main branch which flows north	Perennial		LAM	Lamb Creek	Ephemeral
CA2	Carne Creek, central branch which flows from east of LW431 and into CA1	Perennial		LOS	Long Swamp	Perennial
CA3	Carne Creek, branch which flows from GGSE and GGS to CA2	Perennial		MER	Marangaroo Creek	Perennial
CA4	Carne Creek, branch flows from CW to CA2	Perennial		NMS	Nine-Mile Swamp	Perennial
CA5	Carne Creek, western branch which flows from above LW415 to CA2	Perennial		PDY	Paddy's Creek	Ephemeral
CW	Carne West Swamp, which flows to CA4	Ephemeral		PIS	Pine Swamp	Perennial
GGSE	Gang-Gang Swamp east which flows to CA3	Perennial		TRS	Tri-Star Swamp	Ephemeral
GGS	Gang-Gang Swamp south, which flows to CA3	Perennial		TWG	Twin-Gully Swamp	Ephemeral
KC1	Kangaroo Creek, downstream of KAS	Perennial		SSS	Sunnyside Swamp, which flows into WOL	Perennial
KC2	Kangaroo Creek, upstream of KAS	Ephemeral		WOL	Wolgan River	Perennial
KAS	Kangaroo Swamp	Ephemeral				

2.9 Rainfall recharge, evapotranspiration and baseflow

2.9.1 Rainfall in the area

The model is run from steady-state through calibration (1950 to 12 Dec 2006), validation (12 Dec 2006 to 1 Jan 2012) and then prediction (1 Jan 2012 onwards). For most of this time average rainfall is applied to the model, but during the years 2006-2012 (inclusive) 3-montyly average rainfall is used in the model.

Rainfall is recorded at Newnes Plateau weather station, which is owned by Centennial Coal and operated by Aurecon. It is also recorded at the nearby Lithgow Cooerwull BOM station 063226. Relevant data are listed in Table 6.

Table 6 Quarterly and average rainfall (mm/day) for Springvale and BOM weather stations

Time period	Newnes Plateau rainfall (mm/day)	Lithgow Cooerwull BOM station 063226 rainfall (mm/day)
1st 2006	1.81	2.76
2nd 2006	0.84	0.57
3rd 2006	1.77	1.37
4th 2006	1.39	1.18
1st 2007	3.12	3.39
2nd 2007	3.96	3.55
3rd 2007	1.10	1.09
4th 2007	4.06	2.60
1st 2008	3.29	2.60
2nd 2008	1.90	1.45
3rd 2008	1.93	1.85
4th 2008	3.12	2.88
1st 2009	2.34	2.37
2nd 2009	2.91	2.19
3rd 2009	1.45	1.62
4th 2009	2.02	1.91
1st 2010	3.40	3.08
2nd 2010	2.42	1.43
3rd 2010	2.63	2.19
4th 2010	4.87	3.93
1st 2011	3.29	2.72
2nd 2011	2.42	1.80
3rd 2011	1.84	1.77
4th 2011	3.92	3.40
1st 2012	5.62	4.38
2nd 2012	2.28	1.72
3rd 2012	1.33	1.31
Average May 2002 to July 2012	2.47 mm/day (900 mm/year)	2.10 mm/day (765 mm/year)
Average rainfall	2.63mm/day (2006 to 2012) 2.78mm/day (2007 to 2010)	2.17 mm/day (1878 to 1973,) (793mm/year)

In addition, during 1938 to 1999, Lithgow Newnes Forest Centre (BOM station 063062) recorded an average daily rainfall of 2.99 mm/day (1092 mm/year). This station was closed in 1999, but its recordings are most pertinent to this study. Therefore, during steady-state, and most of transient calibration and prediction, a rainfall rate of 3 mm/day is used. During 2006 to the third quarter of 2012, the quarterly data from the Newnes Plateau station is used.

2.9.2 Evapotranspiration in the model

The nearest weather station to record evaporation is the Bathurst station (063005). Mean daily evaporation for the four quarters of the year are shown in Table 7. These data guide rates of evapotranspiration in the model.

Table 7 Quarterly and yearly average rates of evaporation (mm/day) from the Bathurst weather station

1st quarter	2nd quarter	3rd quarter	4th quarter	Yearly average
5.7 mm/day	1.9 mm/day	1.9 mm/day	5.2 mm/day	3.7 mm/day

Groundwater is lost through Evapotranspiration (ET). In the model, ET is applied using the following exponential function:

$$ET = ET_{max} e^{-\alpha d^2} \quad (1)$$

Where,

d – depth to groundwater level

ET_{max} – maximum value at d=0

α - a parameter controlling the extinction depth

An extinction depth of 5m is assumed in the model, and during steady-state calibration and transient calibration ET_{max} is taken as equal to the average evaporation rate of 3.7mm/day. Figure 21 shows the ET function used in the model. During transient validation, ET_{max} is taken equal to the pan evaporation given in the above table.

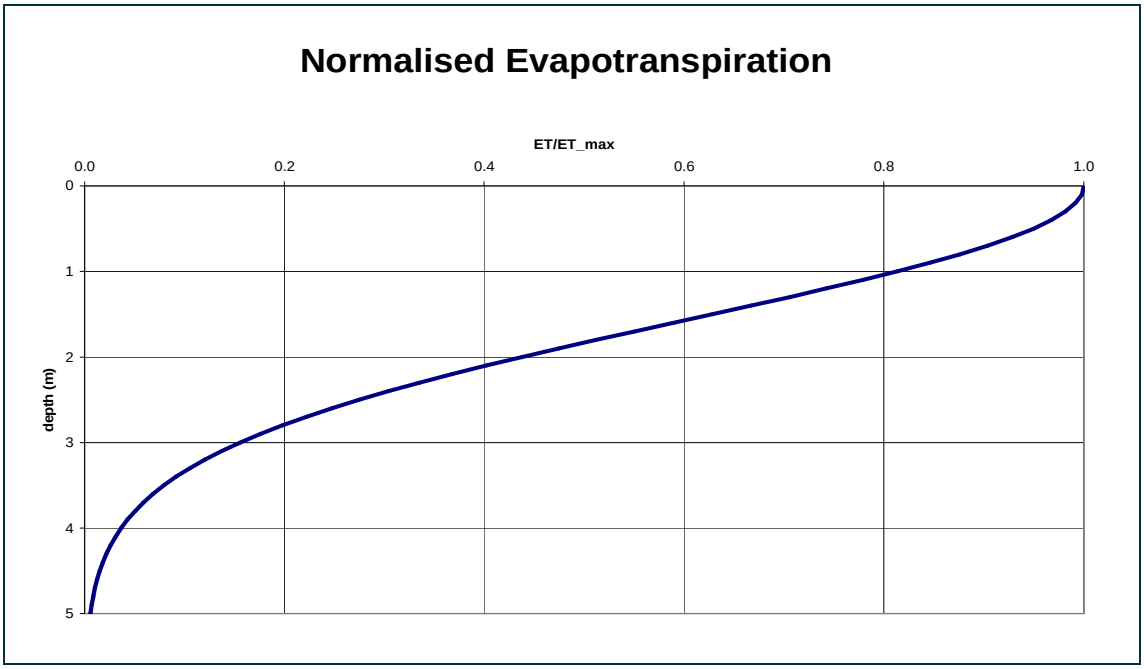

Figure 21 ET/Emax as a function of depth used in the model

2.9.3 Geometry, streamflow and baseflow of Sunnyside Swamp

Sunnyside Swamp lies above Springvale mine, to the east of LW413 and to the west of LW415, as shown in Figure 22 and Figure 23. Its catchment (shown in pink in Figure 22 and Figure 23) has an area approximately 2.9km^2. Sunnyside Swamp itself has an approximate width of 40m and area of 0.08km^2.

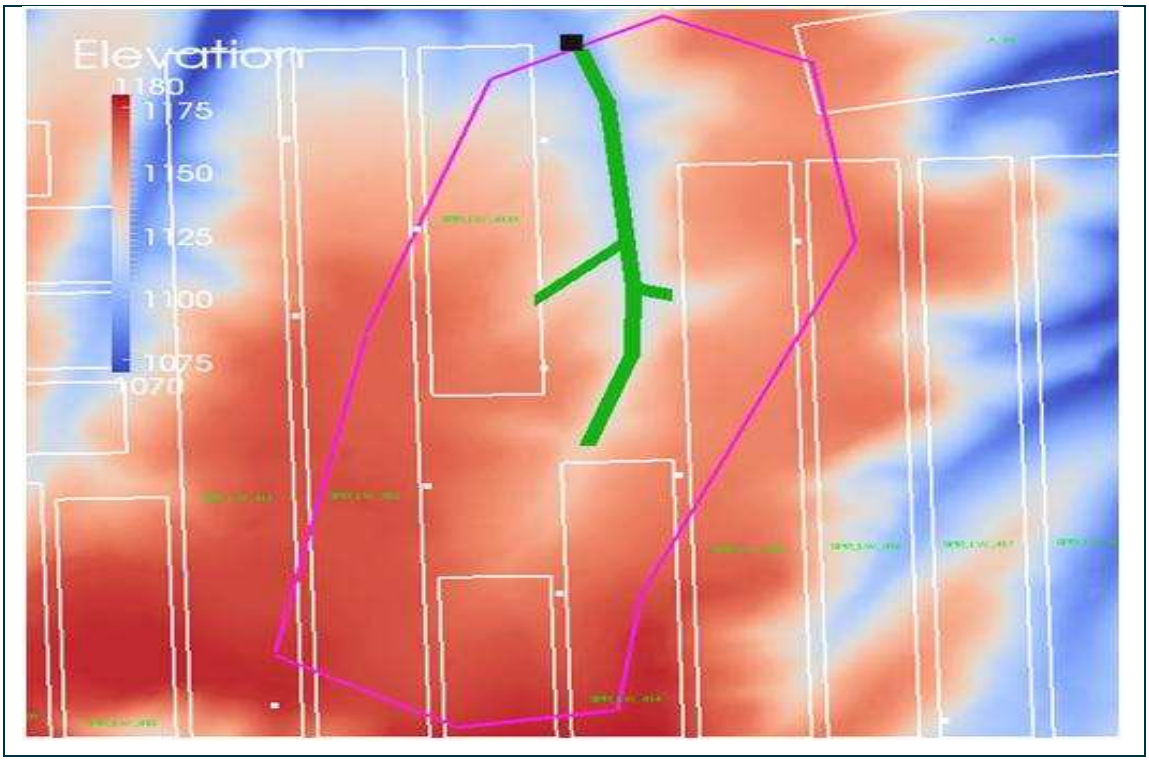

Figure 22 Sunnyside Swamp in green. Its approximate catchment area is shown by the pink polygon. Mining panels are shown by white rectangles and borehole positions by white points. The flow-monitoring station at Sunnyside's northern end is a black square

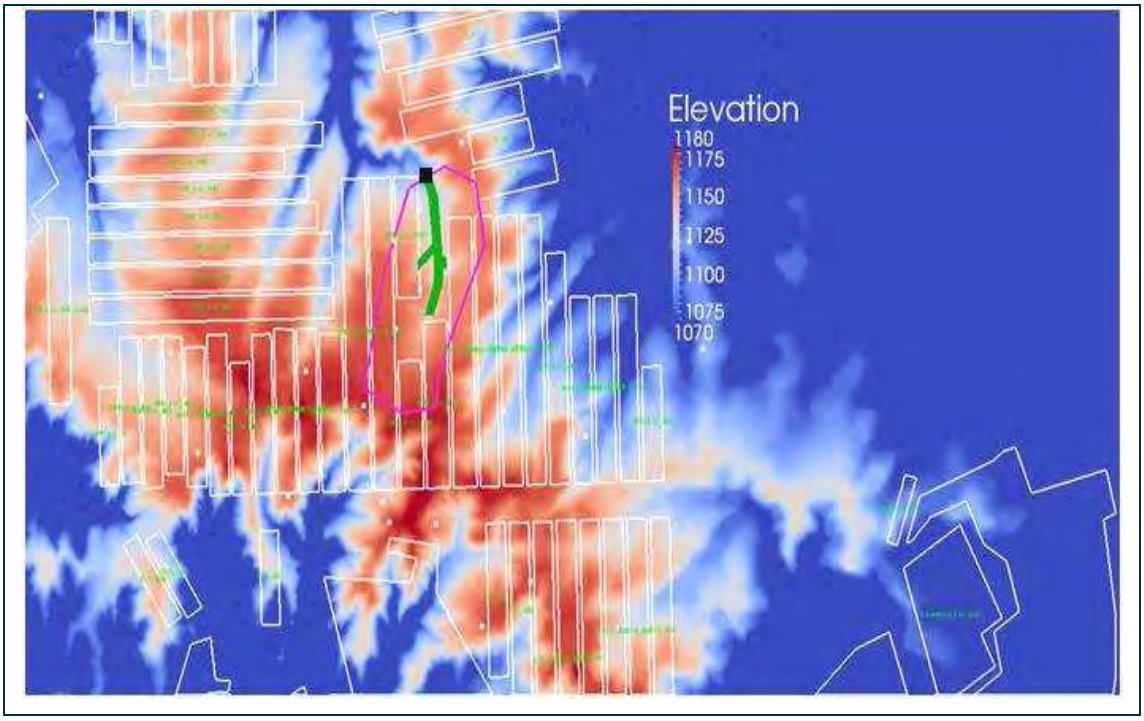

Figure 23 Similar to Figure 22, but showing a larger region. Sunnyside Swamp lies near the highest point of the model as shown by the pink polygon

Two gauging stations are installed in the swamp to monitor the flow: one in the middle of the swamp and one at a downstream location. The downstream station, SS-DS, is situated at the swamp's northern end, where measurements were taken twice a month between January 2010 and April 2012 (except for October 2011). In addition, daily measurements of flow were made in the period from April 2010 to November 2010. The summary of mean daily flow per month is given in Table 8.

The data show that the highest flows occur in the period from October to December, and that the flow is sustained all year round.

Table 8 Sunnyside Swamp mean daily flow per month

Month	Jan	Feb	Mar	Apr	May	Jun	Jul	Aug	Sept	Oct	Nov	Dec	Annual Mean	Min	Max
Sunnyside Swamp D/S (kL/day)	205.3	104.7	723	477.3	592.5	612.2	431.7	440.6	433.5	715	1055	1699	604	104.7	1698.8

Daily flow exceedance for the swamp has been calculated by RPS Aquaterra (2012b). The results given in Table 9 below indicate that there is flow in the swamp around 90% of the time. The data indicate that water levels have not fallen below 18 mm above the crest weir level during the analysed time period indicating that when no flow occurs, there is most likely ponding within the swamp.

Table 9 Sunnyside Swamp- daily flow exceedance

Percentile	5	10	20	30	40	50	60	70	80	90	95
Sunnyside Swamp D/S(kL/day)	0	0	27.8	59	87.2	148.5	269.6	474	667.2	1176	2215

RPS Aquaterra (2012b) has calculated the baseflow contribution to the swamp by using daily streamflow data for Sunnyside Swamp (April to November 2010). These data are considered consistent, reliable and suitable for baseflow separation analysis. The analysis was performed using the Lyne and Hollick Filter (Nathan and McMahon, 1990). The results are shown in Table 10.

Table 10 Sunnyside Swamp - Calculated base flow and Base Flow Index (BFI) exceedance

	Baseflow (kL/d)	BFI (%)
Percentile 5	0.0	0%
Percentile 10	0.2	6%
Percentile 20	0.3	25%
Percentile 30	7.4	42%
Percentile 40	30.6	60%
Percentile 50	93.4	81%
Percentile 60	140.5	100%
Percentile 70	171.7	100%
Percentile 80	262.2	100%
Percentile 90	337.0	100%
Percentile95	385.1	100%

Sunnyside Swamp preserves flow throughout the year, and half of the time (50 percentile) a significant fraction (81%) of the flow in the swamp is provided by baseflow. More than half of the time, the flow is 100% sustained by baseflow. This indicates that the baseflow contribution to the swamp is important for its sustainability.

During the observation period April 2010 to November 2010, the average rainfall on the Newnes Plateau was 3.3 mm/day, meaning that Sunnyside's catchment received 9.6ML/day on average. Mean annual flow, as measured at the gauging station, is about 0.6ML/day (see Table 8), or 6% of the rainfall recharge. The remaining 94% is transferred to groundwater or lost to evapotranspiration. This is consistent with the typical forested catchment evapotranspiration losses as measured during a series of experiments and modelling studies (Zhang *et al,* 1999).

2.9.4 Rainfall recharge and evapotranspiration in the model

The above analyses suggest that around 95% of rainfall in the catchment is transferred to groundwater or lost to evapotranspiration. Groundwater recharge does not generally exceed 10% of rainfall and evapotranspiration is the biggest output component of the water balance, and varies in the range from 80-90% of rainfall. This understanding is supported by over 250 field experimental studies in Australia and in the world in forested catchments. These studies have found that there is a strong relationship between long term average evapotranspiration and rainfall (Holmes and Sinclair, 1986; Turner, 1999, Zhang *et al*, 1999). Figure 24shows the least squares fitted function for forested catchments (Zhang *et al*, 1999), which indicates the relationship between rainfall and annual evapotranspiration from forested catchments.

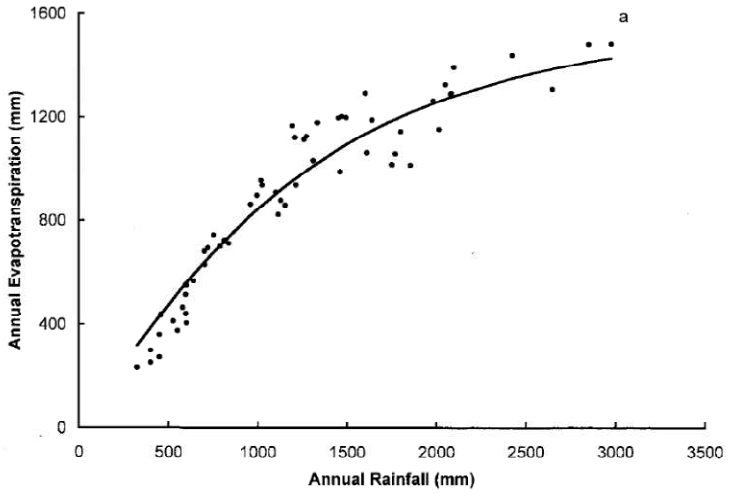

Figure 24 Fitted function for forested catchment (after Zhang et al, 1999)

These results indicate that for 1.1m annual rainfall, the observed evapotranspiration varies between 900-1000 mm/year (80-90%).

Given these considerations, in the model, we apply recharge using the following rules:

- A recharge rate of 3.7mm/day, which is 3.7/3 = 123% of the rainfall rate, is applied to finite-element nodes which lie in creeks or swamps. This exactly balances ET at these nodes, so without groundwater flow, the standing water level would be at the ground surface at these nodes. This is motivated by the comment made earlier that while 10% of time the Sunnyside swamp is not flowing , during that time the water level in the swamp does not fall below 18mm above the crest weir level (during April to November 2010) indicating ponding, and with similar anecdotal evidence provided verbally by Aurecon. The high value of recharge is meant to model surface runoff and storage of surface water in the swamps and creeks. A much higher recharge rate would be rejected by the model and in reality lead to higher streamflow values than observed at Sunnyside Swamp and Kangaroo Creek. In practise, both ET and rainfall recharge are therefore turned off at these swamp nodes of the model.

- Rainfall recharge is applied to all other nodes at the ground surface in the model using 5% of the actual rainfall.

For instance during steady-state, the 10 ML/day received at Sunnyside Swamp goes to, approximately: 0.4 ML/day of streamflow; approximately 0.4 ML/day of ET from groundwater; and approximately 0.5 ML/day of recharge to groundwater. This leaves 8.7ML/day, which includes all other ET components such as rainfall interception by vegetation (Gash, 1979), transpiration from wet and dry canopy (Langford and O'Shaughness, 1978), net radiation (Monteith, and Unsworth, 1992), advection (McNaughton and Jarvis,1983; Calder, 1996), vapour pressure deficit, turbulent transport , leaf area (Greenwood et al. 1982) and plant available water capacity (Greacen and Williams, 1983), but these processes are not captured by the model.

2.10 Initial pore water pressures and saturations

The 'Extended model' is initialised with hydrostatic head distributions with the phreatic surface at elevation 1000m. Since the main purpose of the extended model is to compute the distribution of porepressures within the mini-regional scale model, impermeable boundary conditions are used on the sides and bottom of the model. Rainfall and evapotranspiration is applied and the numerical model is run to steady-state.

The porepressures and saturations thus achieved are interpolated onto the 'Model (mini-regional scale model)' yielding the distribution depicted in Figure 25

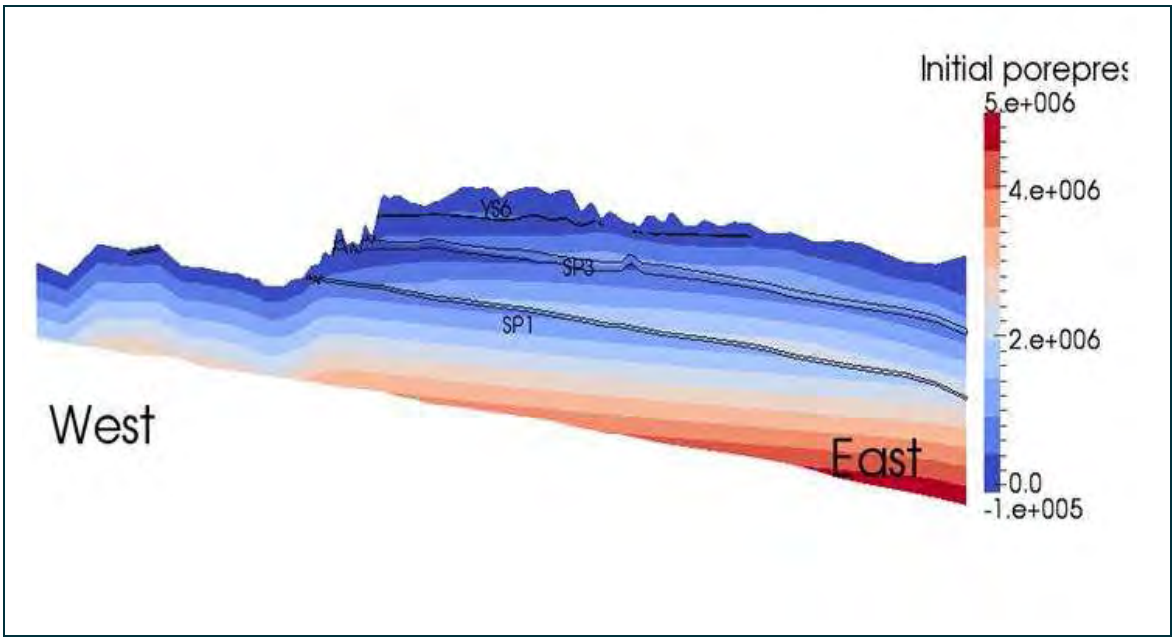

Figure 25 Initial porepressure on a vertical west-east slice through the model. The positions of semi-permeable layers SP1, SP3 and YS6 are shown. This cross section is the same as that of Figure 19

2.11 Boundary conditions

Numerical groundwater models require the specification of some conditions on the model boundary. Figure 26 shows the boundary conditions used in the model.

Once the porepressures and saturations obtained from the extended model are interpolated onto the mini-regional scale model, the model is run to steady-state with porepressures fixed on the sides (see Figure 26, but not the bottom or top) to remove any discrepancies which might have occurred during interpolation. During this, rainfall, ET and seepage boundary conditions are applied to the top surface. This prepares the numerical model for transient calibration. A typical result is shown in Figure 25.

During transient calibration, and validation, the porepressures remained fixed on the sides, but not the bottom or the top of the model. The top surface has rainfall, ET and seepage boundary conditions applied.

Specification of the BC1 and BC2 parts of the boundaries allows investigation during prediction. Mainly the basement layer is exposed on BC1 boundary.

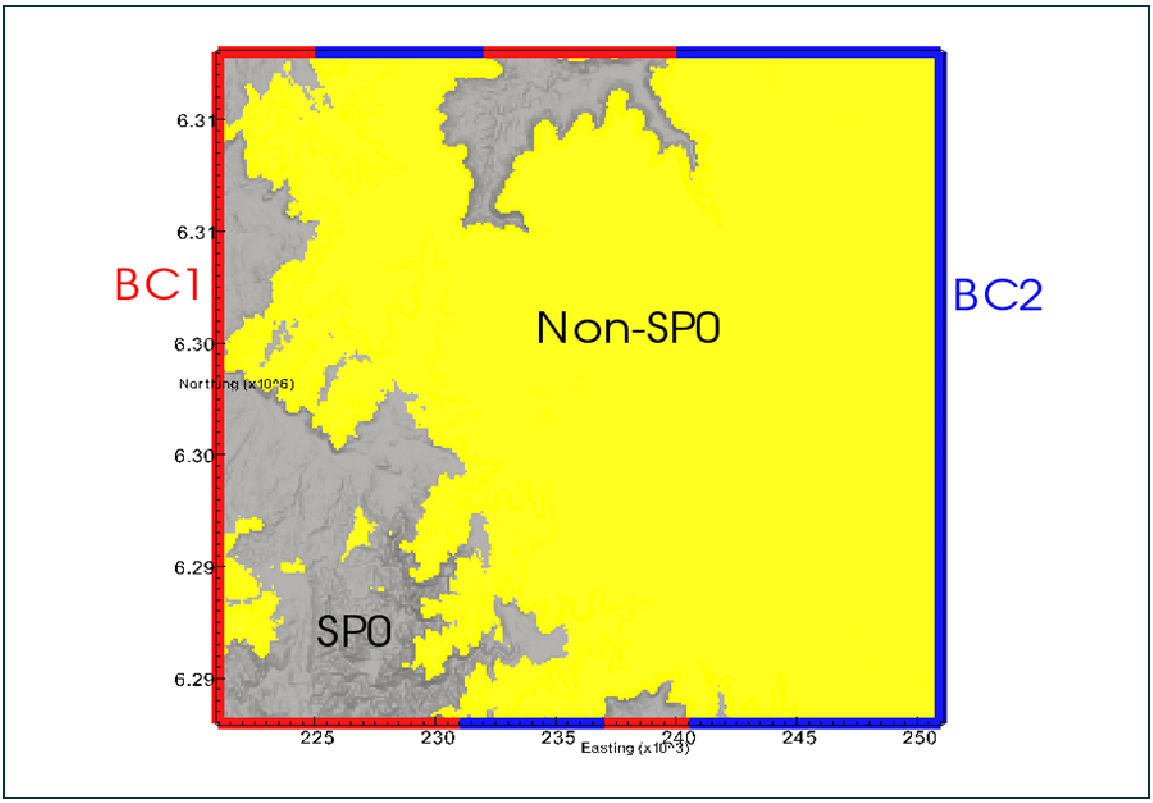

Figure 26 Two types of boundary conditions (BC1 or BC2) can be applied to the edges of the model. The colouring of the central region shows the model geology

At all stages of the modelling, all nodes on the top of the numerical model are subjected to rainfall recharge, as explained in Section 2.9. In addition, all nodes on the top of the model are drained by ET, as quantified in Section 2.9.2. Finally, all nodes except those lying along creeks and rivers listed in Table 5 are prescribed with seepage conditions; that is, water is removed from them to ensure their porepressure never exceeds zero. However, given the magnitude of the ET used in the model, this is a rare occurrence.

The nodes along the creeks and swamps listed in Table 5 were treated as either (i) perennial nodes to allow direct estimates for groundwater recharge from these rivers and swamps or vice-versa (discharge/baseflow) to these rivers and swamps; or (ii) ephemeral nodes to allow direct estimates of discharge/baseflow. The stream node formulation is given in Appendix F. These nodes also have a different applied rainfall, as explained in Section 2.9.2.

2.12 Boundary conditions on mines

In the numerical model, mine workings can be simulated by either deleting the Finite Elements (Cells) that lie within the excavation region in the model or by assigning drain node properties to the Finite Element Nodes that lie within the excavation region in the model. In the case of open-pits, finite elements are deleted from the ground surface to the floor of the mined seam, whereas the underground workings are simulated by assigning the drain nodes within the elements lying in the coal seam being mined and the mine boundaries.

In the model, the mines are categorised into the following four groups:

1. Old workings that are flooded with water – do not use drain nodes, mining induced permeability values are assigned to the elements lying within the excavation boundaries and in the surrounding

strata. The nodal pressures on the excavation boundaries are not constrained; i.e. these excavations and surrounding strata are treated simply as highly fractured media filled with water.

2. Old Lithgow State mine and surrounding mines (OPK, FBK, LGS, LGS_1, STW) that are flooded with water – these mines are treated slightly differently from other old flooded mines. Based on piezometric data obtained from piezometers located in SPR31 and the observation of Springvale geologist Andrew Knight (2003) who indicated that water was exiting from the old state mine from about 130m above the Lithgow Seam level, porepressure on the Lithgow Seam within the old state mine is computed by assuming a water head of 130m in the Lithgow Seam. A seep constraint is prescribed (so that porepressure is not allowed to exceed 1.3 MPa) to the nodes lying within the Old Lithgow State Mine boundary. Mining induced permeability values are assigned to the finite elements within the excavation boundary and in the surrounding strata. Thus the Old State mine region and the surrounding strata are treated again simply as highly fractured media filled with water but with porepressure constraint ($P_w \leq 1.3$MPa) assigned at the Lithgow seam level.
3. Old workings that are being pumped out – these mines have drain-node properties assigned to the Finite Element Nodes lying within the excavation region and mining induced permeability values assigned to surrounding strata. The drain property means the porepressures are less than zero within the excavated region (i.e. $P_w \leq 0$).
4. Current and future Springvale, Angus Place and Clarence longwalls panels (being pumped out)-
    - Finite Element Nodes lying within these longwalls panels are assigned with drain node properties. Porepressure is restricted to be equal to or less than zero (i.e. $P_w \leq 0$) on these drain nodes.
    - Mining induced permeability values are assigned to the Finite Elements lying within the mining regions and the surrounding strata as the longwall excavation is simulated.

2.13 Hydrogeological response model

2.13.1 Deformations and permeability changes due to longwall mining

Hua et al (2008) in their ACARP report C14033 have provided a comprehensive review of the hydrogeological impacts of mining and have supplied an extensive list of published papers/reports on the subject.

On the basis of the literature review, Hua et al (2008) came to a conclusion that, in general, (although terminology is not precise) the researchers tended to divide the overburden strata into three to four zones with distinctive deformation characteristics (in order of increasing height above the mining seam, see for example Figure 27) as:

- A caving zone with broken blocks of rock detached from the roof (less than 10 times the extraction height, probably about 5 times the extraction height);
- A disturbed or fractured zone where the rocks have sagged downwards and consequently suffered bending, fracturing, joint opening and bed separation (about 15-40 times the extraction height);
- A constrained zone where the strata have sagged slightly over the panel without suffering significant fracturing or alteration to the original geomechanical properties (variable thickness); and
- A surface zone with tensile fracturing (to a depth of 20m).

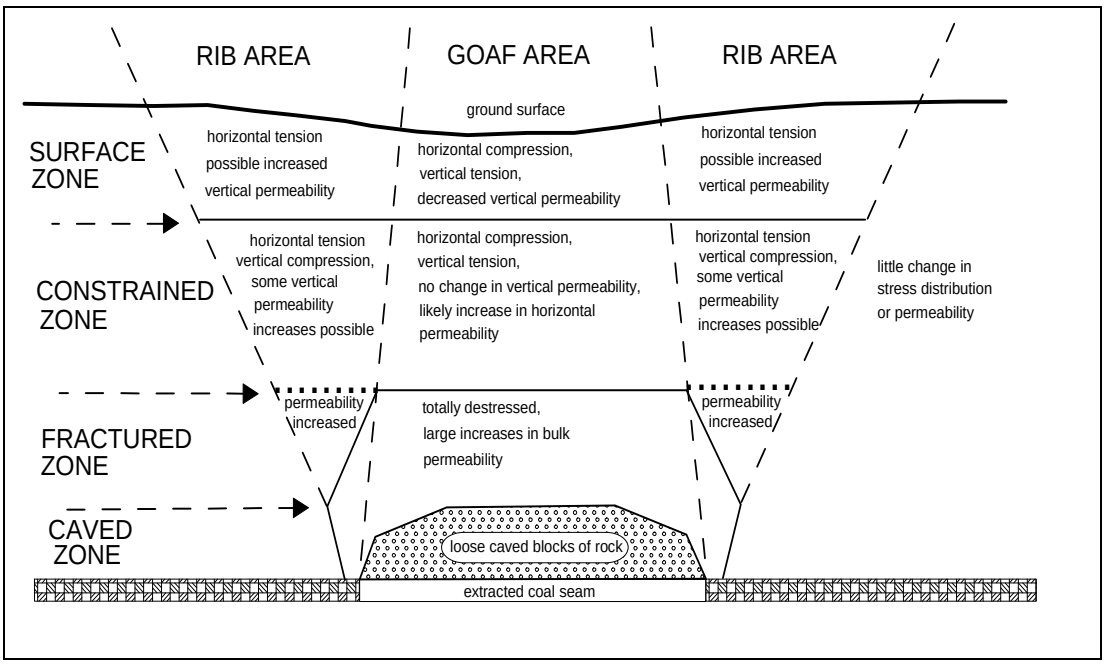

Figure 27 A hydrogeological model proposed for the Central Coast by Forster and Enever (1992)

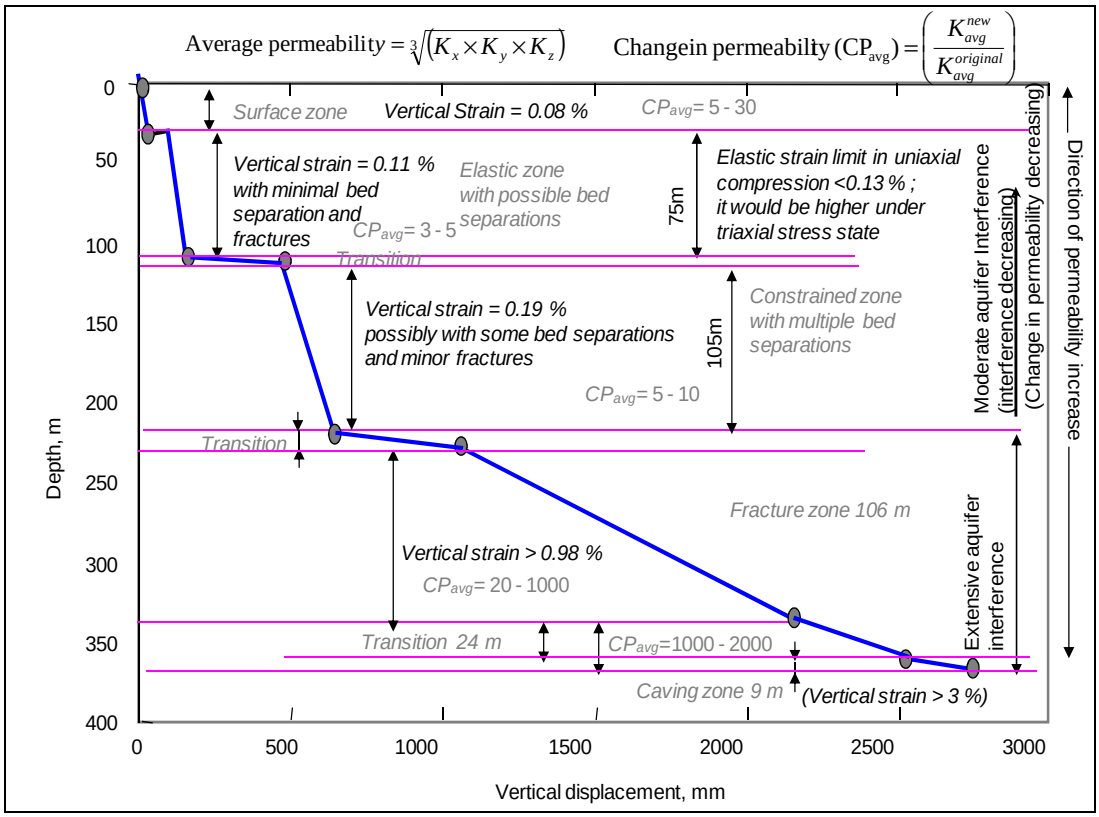

Figure 28 Hydrogeological response model for Springvale Colliery (ACARP C18016)

In ACARP report (C18016), the overburden strata were divided into separate deformation zones with distinctive hydrogeological response characteristics. Figure 28 presents a hydrogeological response model developed for Springvale Colliery. This model clearly shows the following deformation zones within the overburden above the consolidated goaf:

- Caving zone with broken blocks of strata (to about 3 times the extraction height);
- Transition zone where the rock strata is going through gradual transition from caving zone to fracture zone (up to 7 times the extraction height);

- Fracture zone where the strata have sagged downwards and have suffered bending, fracturing, and bed separation (about 33 to 44 times the extraction height);
- Constrained zone where the strata may have some bed separations and fracturing without causing significant alterations to the original strata properties (about 32 to 35 times the mining height and 5 to 10 fold increase in average permeability);
- Elastic zone with minimal bed separations (about 20 to 23 times the mining height and 3 to 5 fold increase in average permeability); and
- Surface zone with some bed separations and tensile fracturing up to 20m to 30m thick (5 to 30 fold increase in average permeability)

2.13.2 Theory of mining-induced permeability changes used in COSFLOW's coupled mechanical-fluid simulations

The flow of fluid is controlled by the permeability of the porous medium, which is either estimated by field measurements or through theoretical/empirical formulations. There are different formulae proposed in the literature for estimating the permeability of a porous medium depending upon whether the porous medium is intact or contains a network of fractures. The permeability of a porous rock remains a highly non-linear dynamic function of mining induced stress and subsequent fractures. Thus, it is not only important to estimate the initial permeability correctly, but equally important to compute its possible variation induced by mining.

Kozeny and Ber (1927), Hubbert (1940), Krumbein and Monk (1943), De Wiest (1969) attempted to establish a relationship between stress and permeability through a definition of hydraulic radius which is a function of grain diameter, porosity, grain shape and packing. As rock masses usually contain natural fractures which predominantly control the fluid movements, there is a distinctive advantage in formulating a numerical model on the basis of equivalent fracture network. In that framework, fluid flow through a single fracture can be expressed using a flow through parallel plate analogue, where a fracture is idealized as a planar opening with a constant aperture (Bai and Elsworth 1994 and see references cited in that report).

Such an approach to describe the rock mass permeability through equivalent fracture idealization is well suited to coal measure rocks (i.e. rock masses in a coal mining environment). Seedsman (1996) discussed hydrogeological aspects of Australian longwalls and pointed out that water flow in coal measure rocks in New South Wales and Queensland in Australia is dominated by defects, cleats, joints, bedding and faults rather than via pores in the rock mass.

For a laminar flow within the fracture network, the hydraulic conductivity of a set of parallel fractures with a spacing, s, and aperture, a, is given by (e.g. Louis, 1969):

$$k = \frac{\rho g a^3}{12 s \mu} \qquad (2)$$

where ρ is the fluid density, g is the gravitational acceleration and μ is the dynamic viscosity of the fluid.

By assuming a fractured rock mass consisting of many interconnected fractures, it may be further idealised as an equivalent porous continuum where the rock mass is represented by an equivalent anisotropic hydraulic conductivity matrix defined in terms of mean fracture spacing and mean aperture. Here it is assumed that the principal directions of this matrix are aligned with the coordinate axes. For a fractured rock with fracture spacing F_{si} (i = 1, 2, 3) and fracture apertures F_{ai} (i = 1, 2, 3), the relationships between the absolute initial (pre-mining) permeability components (k_{11}, k_{22}, and k_{33}) and the fracture parameters can be expressed as:

$$k_{11}^{ini} = \frac{F a_2^3}{12 F s_2} + \frac{F a_3^3}{12 F s_3} \qquad (3)$$

$$k_{22}^{ini} = \frac{Fa_3^3}{12Fs_3} + \frac{Fa_1^3}{12Fs_1} \quad (4)$$

$$k_{33}^{ini} = \frac{Fa_1^3}{12Fs_1} + \frac{Fa_2^3}{12Fs_2} \quad (5)$$

This formulation is amenable to easy evaluation of modifications to the hydraulic conductivities as a function of stress induced changes in fracture aperture. In this study, change in rock mass permeability is formulated on the basis of the mine induced strain (Elsworth, 1989, Bai and Elsworth 1994, Liu and Elsworth 1997), as follows.

$$k_{11} = \frac{1}{2} k_{11}^{ini} \left[\left(1 + \beta_2 \Delta\varepsilon_{22}\right)^3 + \left(1 + \beta_3 \Delta\varepsilon_{33}\right)^3 \right] \quad (6)$$

$$k_{22} = \frac{1}{2} k_{22}^{ini} \left[\left(1 + \beta_1 \Delta\varepsilon_{11}\right)^3 + \left(1 + \beta_3 \Delta\varepsilon_{33}\right)^3 \right] \quad (7)$$

$$k_{33} = \frac{1}{2} k_{33}^{ini} \left[\left(1 + \beta_1 \Delta\varepsilon_{11}\right)^3 + \left(1 + \beta_2 \Delta\varepsilon_{22}\right)^3 \right] \quad (8)$$

where $\Delta\varepsilon_{ii}$ are the normal strain components and β_i are expressed as:

$$\beta_i = 1 + \frac{1 - R_m}{\left(\frac{Fa_i}{Fs_i}\right)^n} \quad , \text{i=1,2,3} \quad (9)$$

Here, R_m is the modulus reduction ratio (ratio of rock mass modulus to rock matrix modulus), the term F_{ai}/F_{si} may be defined as a function of equivalent fracture porosity and n is a constant (in Liu and Elsworth (1997), n is assumed to be equal to 1.0). Both R_m and n are considered to be fitting parameters and hence need to be calibrated properly against well-documented field data. If R_m equals 1.0 then β_i equals 1.0, resulting in minimal strain induced permeability changes. When R_m tends to 0.0 (i.e. the case of highly fractured rock), β_i will attain the maximum value and hence will induce large changes in permeability.

The major shortcoming identified in the Liu and Elsworth (1997) formulation is difficulty in estimating R_m for each rock unit (Eq 9). Liu and Elsworth (1997) suggested that R_m should lie between 0.0 and 1.0; R_m equals to 1.0 implying the least change in permeability and Rm equals to 0.0 implying the highest change in permeability. If the value of R_m were kept the same (say 0.4) everywhere, it would result in a very high value of permeability almost everywhere in the model. Thus there is a need to vary the value of R_m throughout the model; i.e. have a lower value for R_m near the excavated regions and increase it gradually away from the excavated regions. This introduces a dilemma; how to choose the value of R_m?

To resolve this issue, CSIRO based on the past experience incorporated the flowing expression linking R_m with the plastic strain:

$$R_m = \frac{\beta_p}{1 + \alpha_p \varepsilon_p} \quad (10)$$

Here α_p and β_p are the model input parameters and εp is the rock plastic strain resulting in reduced Rm with higher plastic strains. In the COSFLOW simulations described in ACARP C18016, α=100 to 170 and β=1.0 were assumed. This resulted in a high confidence in the numerical predictions.

2.13.3 Permeability changes from coupled hydro-mechanical models of Springvale mine

A number of mine scale coupled hydro-mechanical numerical models incorporating the theory in Section 2.13.2 have been run to generate the mining induced permeability values. This guides the approach used in the mini-regional scale model.

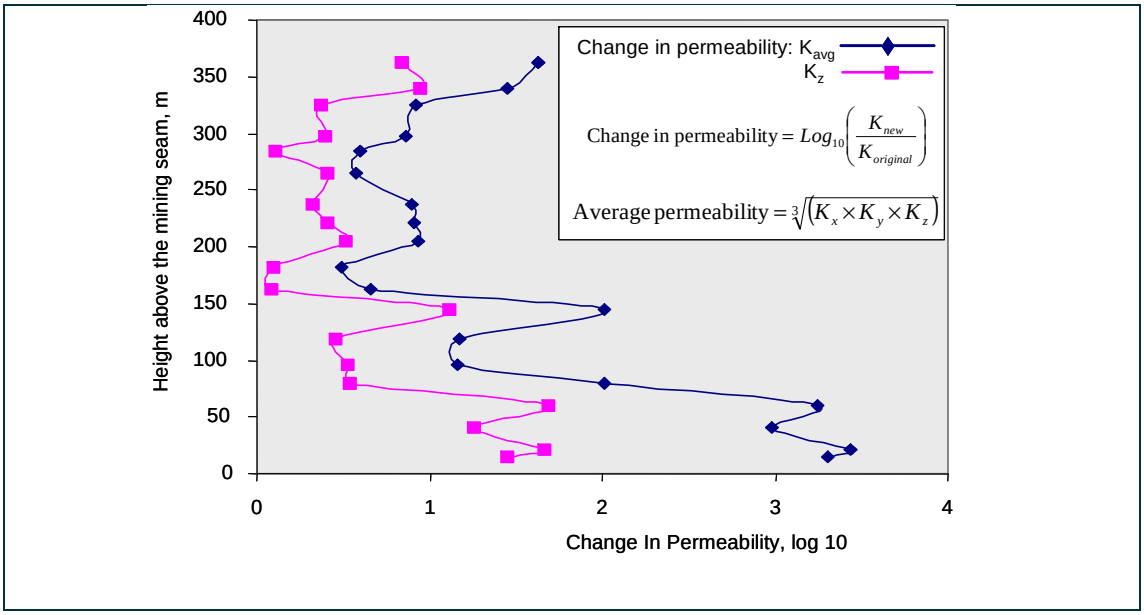

Figure 29 Overall change in permeability over the consolidated goaf area across longwall 411, (K_z – vertical permeability, K_{avg} – average permeability)

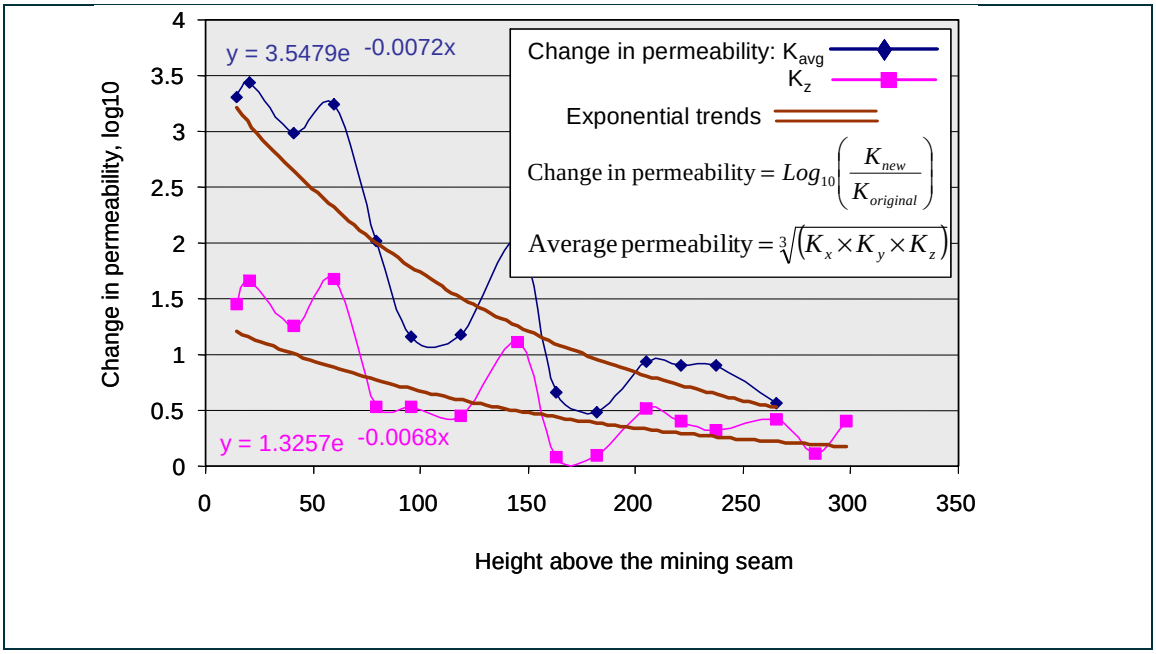

Figure 30 Exponential fit to the overall change in permeability over the consolidated goaf area across longwall 411, (K_z – vertical permeability, K_{avg} – average permeability, up to 300m above the mining)

Figure 29 and Figure 30 show the predicted changes in the average (overall) permeability (i.e. $\sqrt[3]{(k_x k_y k_z)}$) over the consolidated goaf area as obtained for Springvale Colliery. The overall change in permeability at any specific height above the mining seam is computed by averaging the changes in permeability reported by all the finite elements lying at that specific height within the entire longwall panel. Thus the data presented in Figure 29 and Figure 30 is expected to represent an average value of permeability change over the consolidated goaf region. The permeability near the active longwall face could be seen to change by up

to seven orders of magnitude along the chain pillar edges and along the active longwall face. This high permeability region could be seen to extend up to a few hundred meters behind the longwall face.

2.13.4 Permeability changes used in the model

Figure 29 and Figure 30 show a typical result from a coupled hydro-mechanical model of Springvale or Angus place mines. In the model of this report, the permeabilities of finite elements lying above and below a mined section are changed as soon as the section is mined.

The change of permeability depends on the distance of the element above the mined section. The above figures demonstrate that the vertical permeability component over the consolidated goaf area away from the active longwall face may change by roughly 1 order of magnitude just above the mine, while the horizontal components may change by about 3 orders of magnitude.

The above figures also show that the semi-permeable layers (at 60m and 150m) have a higher change of permeability than the aquifers. This is expected from the theory in Section 2.13.2 since the aperture of micro-cracks is smaller for these layers.

The results from the coupled models (presented above) cannot be used directly due to the following:

- The coupled models have much higher resolution in the plan. This means that permeability changes over the pillar edges (where there are large shearing and expansion) can be distinctly different from changes over the centre of the goaf (where there can be compaction). The finite-element sizes used in this mini-regional scale model do not allow these details to be captured.
- The coupled models have much higher resolution vertically. For instance, the element size in the vertical direction was only 5m, compared with this model where they are about 30m.

On the basis of CSIRO's experience, we define the permeability change, ΔK, by

$$\Delta K = log_{10}\left(\frac{K_{final}}{K_{initial}}\right) \quad (11)$$

where K is a permeability component (Figure 31). In the model, Δk, is defined by a ramp function.

As a function of x, the height above the seam,

$\Delta K = 0$ for $x<-h$

$\Delta K = m$ for $-h<=x<=0$

$\Delta K = M - (M - m)x/H$ for $0<x<H$

$\Delta K = m$ for $h>=H$

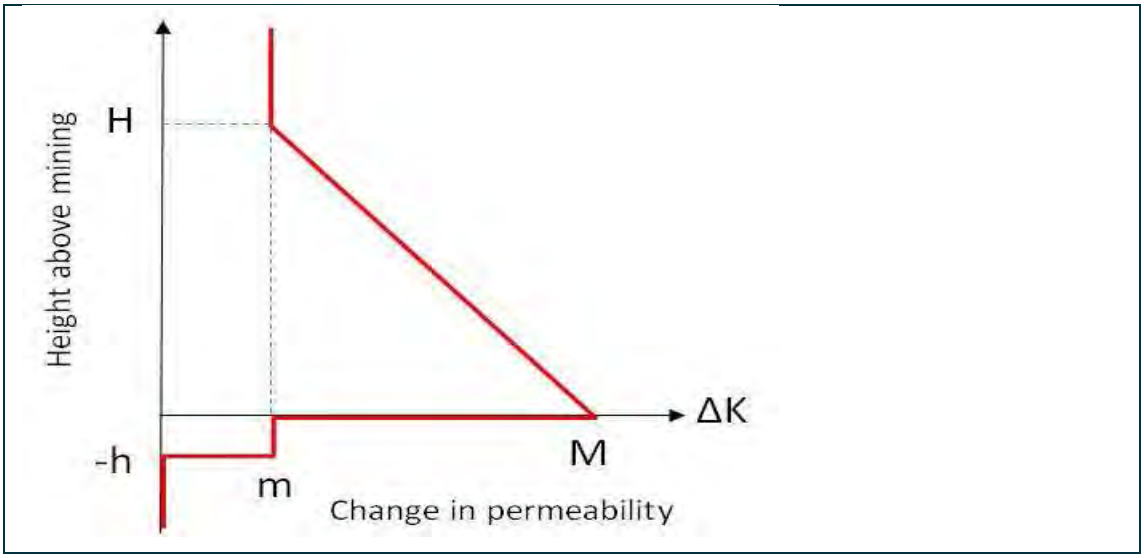

Figure 31 Ramp function used for permeability change P as a function of height above the seam

The parameters M, m, H and h are determined during calibration, and Table 11 to Table 13 list their initial values on entering the calibration procedure.

The conductivity of the nodes used to model excavated areas is derived from the permeability of the surrounding fractured rock, so it is not a free parameter.

It is well-known that the water make from thin longwall panels will be smaller than from wider panels. To model this, both H and M are made functions of panel width, w. For w<315m:

$$M = (1 + a(w-315)/315)M\_315 \quad (12)$$

$$H = (1 + a(w-315)/315)H\_315 \quad (13)$$

where, M_315 and H_315 are, respectively, the maximum (M) and height (H) of the ramp function for panels of width 315m as obtained from the coupled models. For panels of width $w>315$, the M_315 and H_315 parameters are used. When the parameter a=0 there is no dependence on panel width, while increasing a leads to an increasing dependence, and a is a calibration parameter, and its initial value upon entering the calibration procedure is 0.5.

The change in permeability of the uncompacted strata near the longwall face will be higher than the change in permeability above the goaf region of a longwall panel. Therefore, an additional expression is used to compute M in the region closer to the longwall face and that above the consolidated goaf:

$$M = M\_goaf / b \quad (14)$$

where b is a calibration parameter. In the model, an element is converted to a "goaf" element 80 days after it becomes a "face" element (that is, 80 days after the coal is mined). The initial value of b upon entering the calibration procedure is 0.5.

Finally, in the goaf region, the roof is compressed against the floor, making it more difficult for water to enter the mine. Hence, the conductivity of the seep nodes used to model the excavated areas is not just derived from the surrounding goaf permeability, but is instead derived as follows:

$$C\_goaf = 10\text{^}c\ C\_face \quad (15)$$

Here c is a calibration parameter, and C_face is the conductivity of the material. c accounts for both reduction in permeability, and also reduction in surface area available for water to enter the mine. Based on CSIRO's experience, the initial value of c upon entering the calibration procedure is -4.

Table 11 Initial values of permeability change parameters entering the calibration procedure for longwall mines

Material		H_315	h	M_315	m
AQ	$P_{vertical}$	230	50	1 to 3	0.25
	$P_{horizontal}$	230	50	3 to 7	0.75
SP	$P_{vertical}$	230	50	2.5 to 4	0.25
	$P_{horizontal}$	230	50	8 to 12	0.75

Table 12 Initial values of permeability change parameters entering the calibration procedure for bord and pillar mines

Material		H	h	M	m
AQ	$P_{vertical}$	10	2	0.1	0
	$P_{horizontal}$	10	2	0.3	0
SP	$P_{vertical}$	10	2	1.5	0
	$P_{horizontal}$	10	2	5	0

Table 13 Initial values of permeability change parameters on entering the calibration procedure for opencut mines

Material		H	h	M	m
AQ	$P_{vertical}$	0	0	0	0
	$P_{horizontal}$	0	0	0	0
SP	$P_{vertical}$	0	0	0	0
	$P_{horizontal}$	0	0	0	0

2.13.5 Process of strata deformation during longwall extraction

Coal measure rocks are essentially bedded in nature. When coal is extracted at depths, the immediate roof deforms and bends into the mining void. This induces shearing along the bedding planes, delamination/separation along the bedding planes, and deformation and bending of overlying strata. The process of rock deformation starts from the mining seam and propagates upward with substantial time lag as mining progresses: there is substantial lag between the time of coal extraction and the time the ground surface above the extraction point subsides. During this process, first the rock layers closer to the mining seam delaminate from the upper-lying rock layers, bend towards the mining voids and then fracture or break. The extent of fracturing depends on its position relative to the mining horizon. As the mining face moves further away, the rock layer lying further above subsequently undergoes a similar process of shearing, delamination, bending and fracturing (and possible breaking). This process continues all the way from the mining level to the surface with some delays.

In this process, delamination of the rock layers creates voids within the rock mass at specific locations and time. Delamination and bending of overlying strata tend to fill (close) these voids to some extent, but the rock mass never returns to its in situ condition due to rock block rotations and asperity mismatch, i.e. the rock mass undergoes the process of delamination (opening of cracks) followed by only partial closing of the opened cracks (Shen et al., 2010). This results in a dilated rock mass with unrecovered plastic deformation, and a net increase in horizontal permeability in the overburden rocks with respect to pre-mining condition.

The past studies conducted at CSIRO (e.g. Hua et al., 2007) suggest that in coal mining environments represented by stratified rocks, fractures tend to reach all the way to the surface when the longwall width to depth ratio is greater than about 0.75; obviously the extent and connectivity of fracturing varies from site to site depending upon the site specific geological conditions. Similar conclusions can be drawn:

- from Gale (2009) who presented the results of a study representing a number of different mine sites in Australia, and
- indirectly from Walker (1988) who conducted a four year field study to assess the impact of longwall mining on shallow groundwater sources by monitoring fluctuations in groundwater levels in 10 shallow observation wells above a series of longwall panels in southwestern Pennsylvania. He noted that out of ten groundwater monitoring wells, water levels in six wells returned to their pre-mining levels or higher.

Using the “Base case” ramp function described above causes rock permeability to change all the way to the ground surface. However, a constrained ramp function that truncates at a certain height above mining and never reaches the ground surface is commonly adopted in hydrogeological modelling in Australia. Due to the lack of adequate mine observational data at the Springvale and Angus Place Collieries needed for accurately estimating the extent of fracturing (specifically the extent of connective cracking at shallow depths), two additional models with the following ramp functions were run:

(1) Truncated-ramp1 – the ramp function is truncated to zero for heights above 230m so that there are no permeability changes in the upper strata (this is commonly used in groundwater impact assessments using MODFLOW). The magnitude of changes in horizontal and vertical permeability for heights below 230m is assumed to be the same as in the “Base case”.

(2) Truncated-ramp2 – for heights above 230m the ramp function acts only on the vertical permeability component, while the horizontal component is maintained at the in situ value. The magnitude of changes in horizontal and vertical permeability for heights below 230m is assumed to be the same as in the "Base case". The magnitude of change in vertical permeability for heights above 230m is assumed to be the same as in the "Base case".

The actual mining condition is expected to lie within the bounds predicted by these three models.

2.14 Model discretisation

Simulation of groundwater flow using COSFLOW requires both spatial and temporal discretisation. Spatial discretisation is achieved through the finite element method. A plan mesh containing quadrilateral elements is swept vertically, honouring layer-boundaries to create a 3D mesh with hexahedral elements. Temporal discretisation is achieved through using the fully implicit method to solve the Darcy-Richards equation.

The plan mesh is constructed so that it has elements of side length approximately 50m in the central region of the model around the Springvale and Angus Place mining region, and around the swamps and streams that lie above these panels. This is the region that is of most importance to this study, and it is also the region where the stratigraphy and hydrogeology are most well-defined. Finite-element nodes are placed at each piezometer-hole location as well as along line segments which define the rivers and swamps, so that no interpolation is required to obtain results at those points. The mesh size is then graded to 1000m at the edges of the model. The final result is a plan mesh that contains approximately 45000 quadrilateral elements (Figure 32 and Figure 33).

During the vertical sweeping procedure, one layer of 3D elements is placed in each of the 20 elemental layers (2 of the 17 material layers are subdivided into finer elements to yield better vertical resolution as indicated in Figure 16). The final 3D mesh has approximately 900000 finite elements. Figure 34 shows the west-east vertical cross section through the centre of the model.

The 3D mesh for the extended model is constructed using the same method; however, the plan mesh is significantly coarser, with square elements of side length 1000m everywhere.

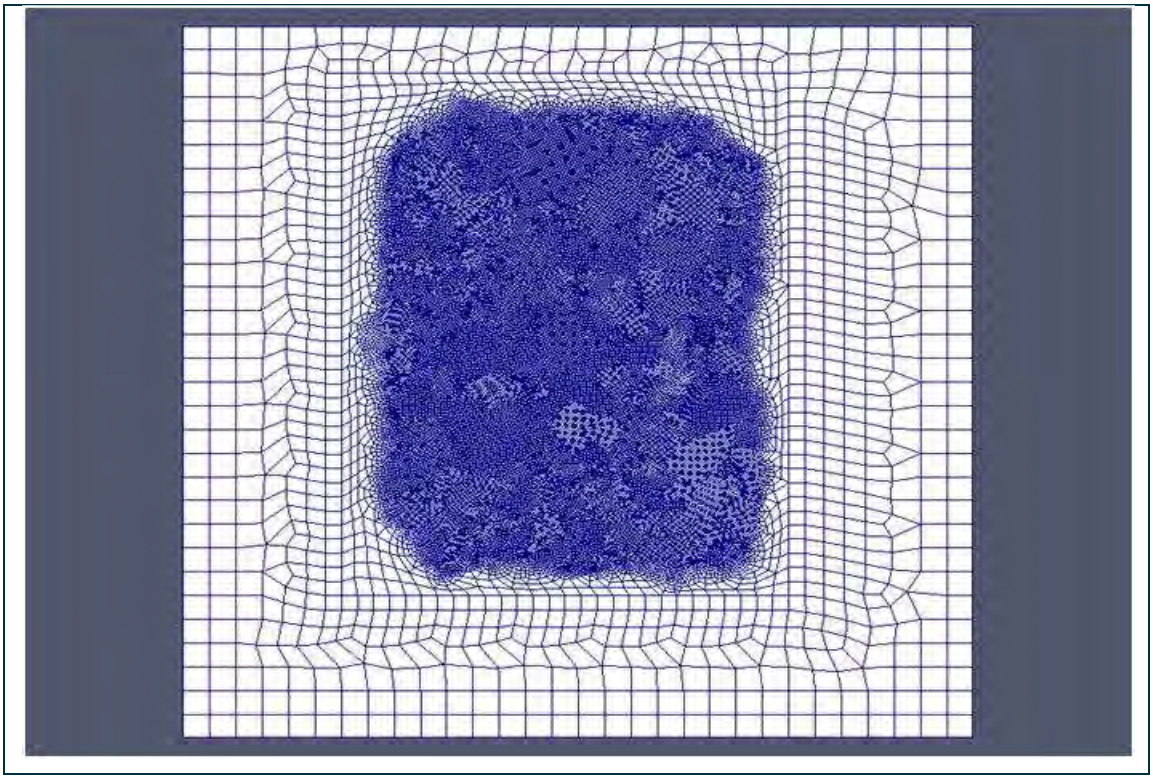

Figure 32 Plan mesh of the model

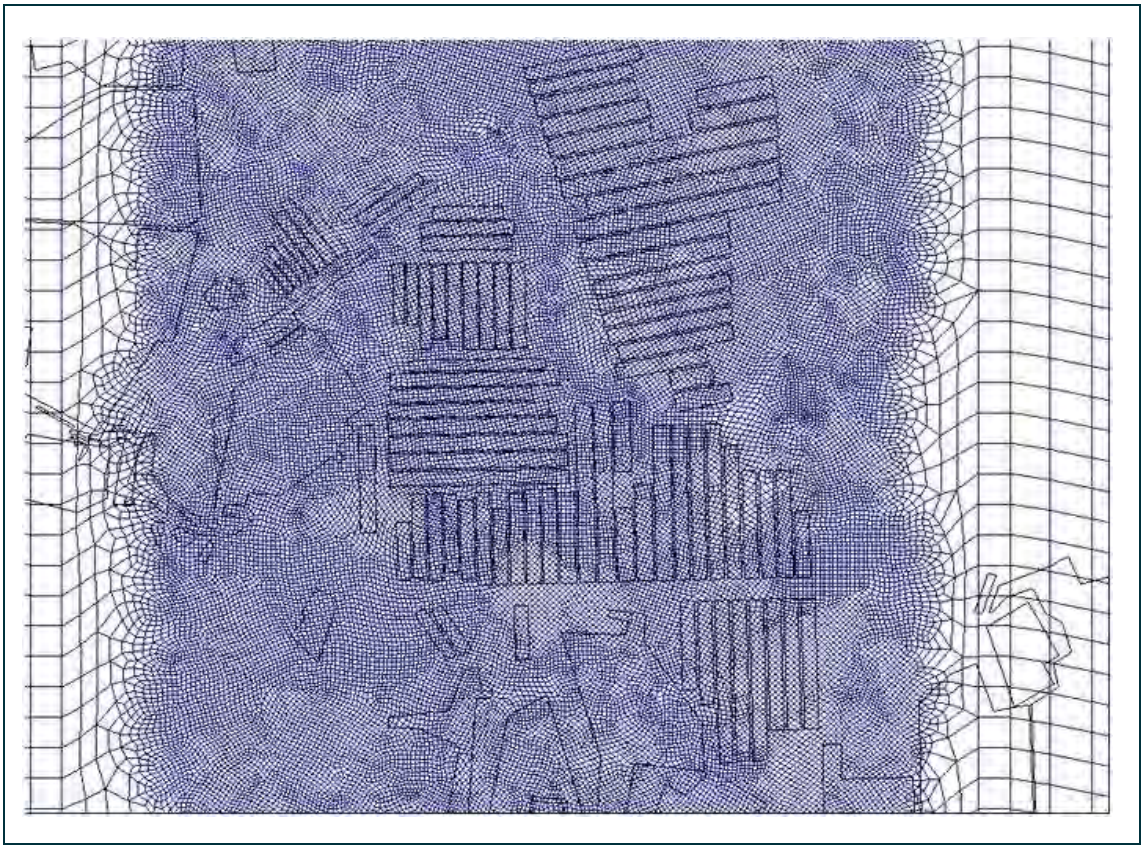

Figure 33 Closeup view of the fine mesh over the Springvale and Angus Place region

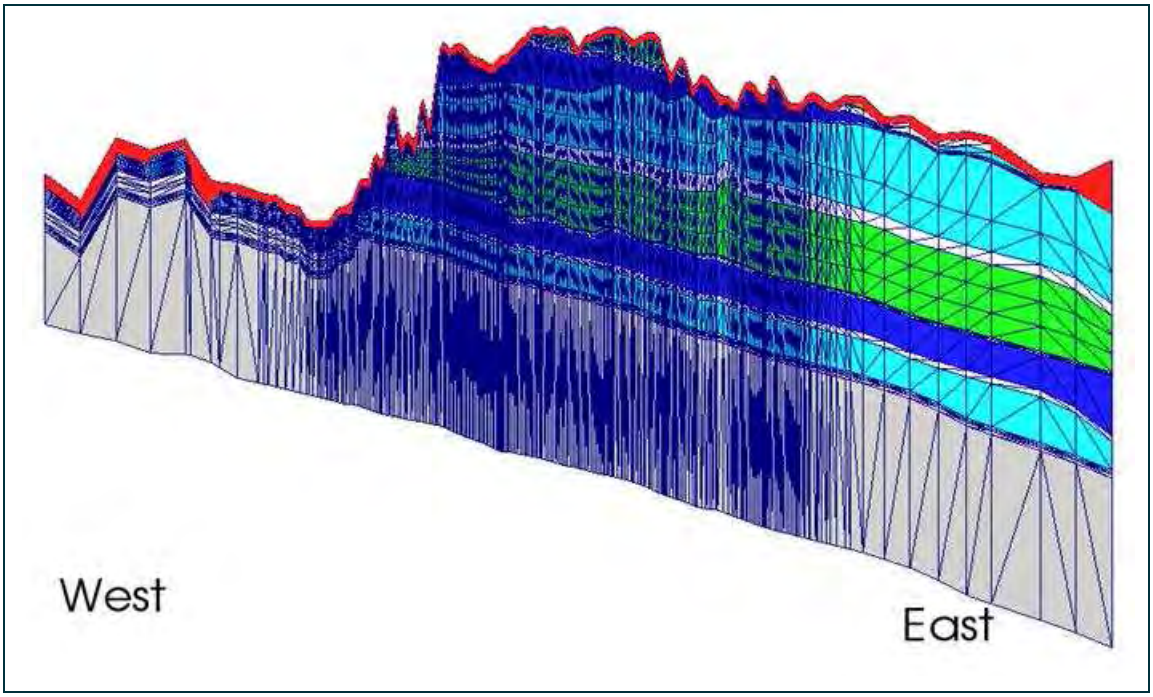

Figure 34 West-East vertical cross section through the centre of the model showing the vertical mesh. Coloured by material layer. This picture is similar to Figure 19, however here the vertical exaggeration is 20

3 Model Calibration and Validation

3.1 Hydrogeological parameters

The objective of the model calibration was to first obtain a set of water pressures within the model region that would represent pre-mining groundwater conditions and then perform simulations of historic and current mine workings to arrive at water pressures that represent recent groundwater levels. Thus, a numerical model was set up and first run in steady-state mode to arrive at pre-mining long-term average groundwater conditions and then run in transient mode to arrive at recent groundwater conditions.

Table 14 and Table 15 list the values thus obtained by using trial-and-error, and then by using the PEST software. Figure 35 shows the calibrated ramp function representing the mining induced change in permeabilities.

Table 14 Calibrated model parameters

Hydrogeologic Units	Horizontal permeability (md)	Vertical permeability (md)	Porosity
Weath	200	25	0.15
AQ1	2	0.5	0.05
AQ2	80	8	0.1
AQ3	80	8	0.1
AQ4	30	2	0.1
AQ5	30	2	0.1
AQ6	25	2.5	0.1
SP0	5e-2	5e-2	0.05
SP1	5e-6	5e-6	0.1
SP2	5e-5	5e-5	0.1
SP3	1e-2	1e-2	0.1
SP4	1e-3	1e-3	0.1
YS6	1e-3	1e-3	0.1
KAT	2.5	2.5	0.1
LTH	2.5	2.5	0.1

*Permeability of 1 md (= 1E-15 m^2) is equivalent to hydraulic conductivity of 9.71E-09 m/sec (≈ 1E-8 m/sec)

Table 15 Calibrated permeability change parameters for Longwall mines

Material		H_315	h	M_315	m
AQ	$P_{vertical}$	230	50	2.1	0.25
	$P_{horizontal}$	230	50	6.2	0.75
SP	$P_{vertical}$	230	50	3.7	0.25
	$P_{horizontal}$	230	50	11.2	0.75

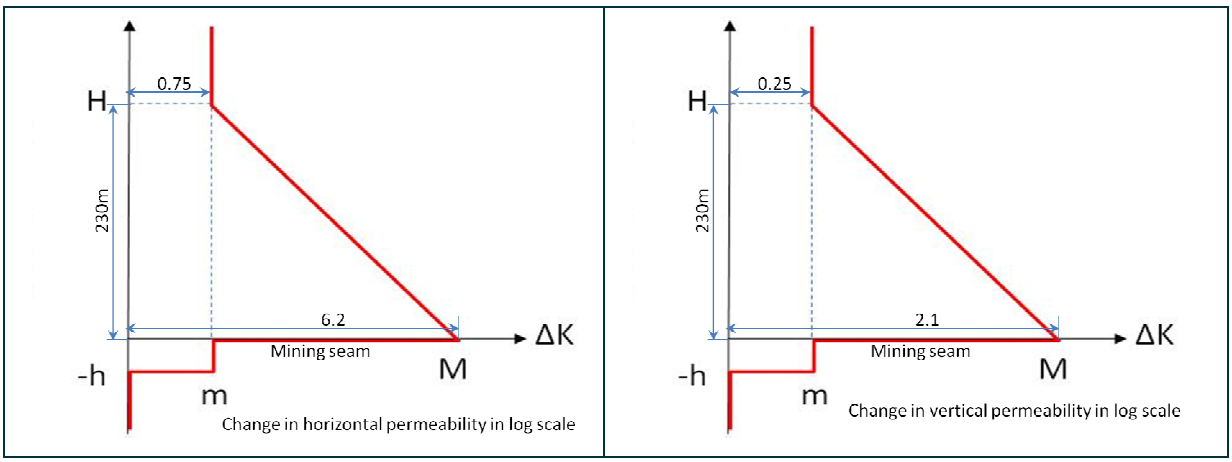

Figure 35 Calibrated ramp function representing change in permeability (log scale)

The steady-state calibration is conducted by running a number of simulations in parallel with different combinations of horizontal and vertical permeabilities and recharge values until a reasonably good agreement between the observed water levels and the simulated water levels is achieved. The model input parameters thus obtained is refined using PEST software. Further refinement of the input parameters is undertaken during the transient calibration. Here, the objective is to minimise the weighted sum of: the root mean square (RMS) difference between measured piezometric heads and model predictions of piezometric heads during steady-state and transient calibration; the RMS difference of the mine inflow values during transient calibration; and the difference in baseflow from Sunnyside swamp.

The riverbed conductance of 1e-10 m/s/Pa per unit area (or, in more conventional units, the conductivity is 0.085 day^{-1} for a 1m thick riverbed per unit area) is found to yield the desired baseflow to Sunnyside Swamp.

RPS Aquaterra (2012b) provided the ramp function (the permeability-change functions) for the Bord and Pillar mines and the Opencut mines as shown in Table 12 and Table 13. The calibrated values for the Longwall mines are shown in Table 14, along with a=0.75 (modification of ramp function for different panel widths), b=0.5 (modification of ramp function in goaf region), and c=-4 (modification of wall conductance in goaf region).

The calibration procedures used in this study are described in detail in Sections 3.2 to 3.5.

3.2 Model calibration procedure

The parameter calibration relies on the quality of measured data e.g. piezometric heads, mine water inflows and baseflows. A comprehensive study of the groundwater system in the Angus Place (AP) and Springvale (SV) mine region was started only in early 2000. Thus only relatively short span of piezometric monitoring data are available for calibration in comparison to much longer period of mining activity in the region.

Here the model parameters are varied iteratively (using trial-and-error and the PEST software) so that maximal agreement between simulation results and observations is achieved. The model parameters to vary are: the permeabilities and porosities of each material layer; the rainfall recharge; the riverbed conductance; and, the mining-induced permeability-change ramp function. Different values of rainfall rates (from 1% to 7%) are used in the calibration process.

Calibration of the model is performed in 2 stages:

- Steady-state calibration: The 'Model' is run to steady-state before any mining activity with particular model parameters. As described in Section 2.1, the 'Extended model' is first run to steady-state, with particular permeabilities for the model layers, riverbed conductance, rainfall and ET. Once the porepressures and saturations obtained from the 'Extended model' are interpolated onto the mini-regional scale 'Model', the 'Model' is run to steady-state with the boundary

conditions as shown in Figure 26 . The strata permeabilities and the rainfall recharge rate are varied iteratively to achieve maximal agreement between simulated elevation heads and the measured elevation heads at about 85 piezometers (see Appendix A and Appendix B).

- Transient calibration: Starting from the steady-state, the model is run in transient mode from 1950 to 20 December 2006 (roughly the middle of Springvale LW411, and the end of Angus Place LW930) in transient mode. Varying stress periods are used to match the mining schedule. The mining-induced permeability-change ramp function, the riverbed conductance and the rainfall recharge rate are varied to obtain maximal agreement between the simulation and the following observations: the elevation heads at about 125 piezometers; the median baseflow at Sunnyside swamp; and, the mine-water inflow rates for Springvale and Angus Place Collieries (see Appendix A and Appendix B).
- The above calibration process is repeated iteratively until maximal agreement between simulation results and observations is achieved.

3.3 Steady-state calibration

During steady-state calibration, rainfall is assumed to be constant at 3mm/day. A calibrated recharge rate of 5% is applied to nodes that do not lie on modelled rivers and swamps, and are not fully saturated. The maximum value of ET is assumed to be constant at 3.7mm/day. The extinction depth is kept at 5m throughout calibration.

3.3.1 Steady-state calibration performance

The comparison of the simulated elevation heads with the measured elevation heads at the piezometers listed in Appendix A is shown in Figure 36. The RMS difference is 23.1m, and the SRMS difference is 5.5%.

The comparison has been made for the layers above Mt York clay (SP3 layer) (blue dots in the figure); Mt York Clay, AQ3 and Katoomba layers (pink dots); SP2 and AQ2 layers (yellow dots), and layers below AQ2 (light-blue dots). Exploring the graph, the scatter is slightly larger in the SP2 and AQ2 layers. There is also a slight bias towards higher pressures in the layers below AQ2, potentially suggesting there could be some other unidentified semi-permeable layers within AQ1 region.

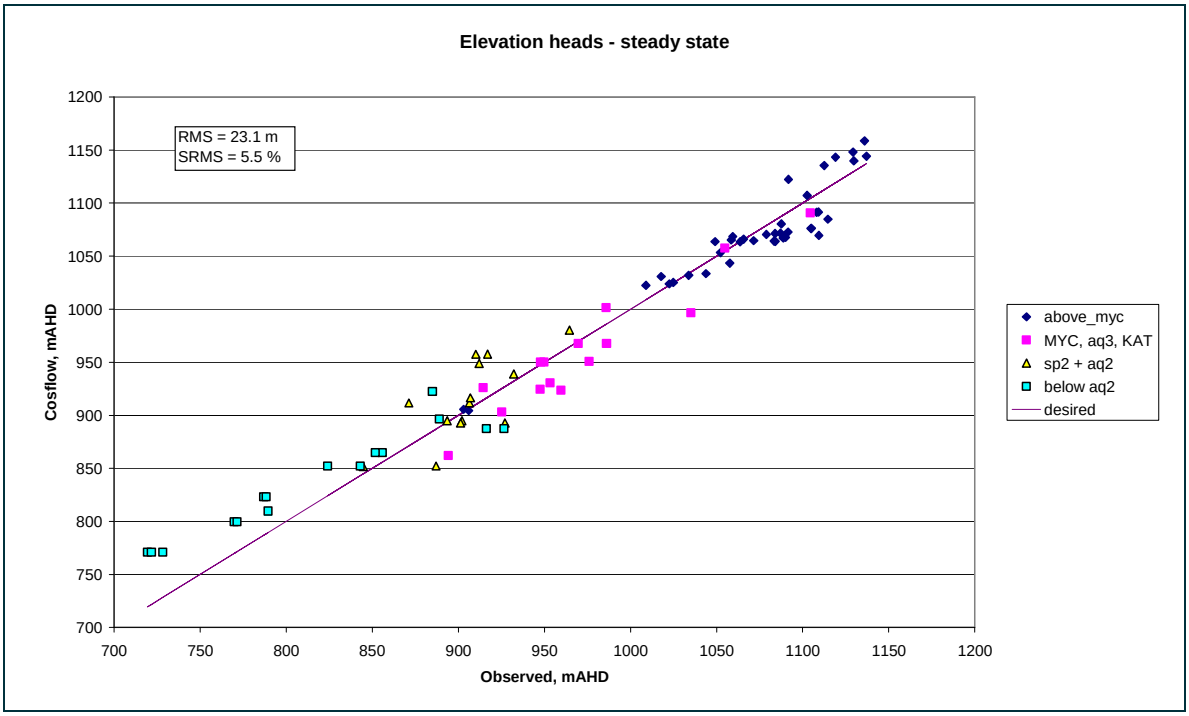

Figure 36 Scatter plot for steady-state calibration

3.3.2 Steady-state water balance

The steady-state water balance across the entire model area is summarised in Table 16. The total recharge to the groundwater system is 132 ML/day, comprising mainly rainfall recharge (126.8 ML/day) and leakage from swamps and streams into the groundwater system (5.2 ML/day).

The groundwater in the model region discharges through various means such as ET, seepage through model boundaries, baseflow to streams and swamps etc. The total groundwater discharge across the model is 131.9 ML/day. ET represents the major source of discharge (96.7 ML/day). Baseflow to the swamps and streams is 14.5 ML/day.

A net loss of groundwater across the model boundaries is 20.7 ML/day.

Table 16 Simulated water balance for the steady-state calibration model

Component	Groundwater Inflow (Recharge) (ML/day)	Groundwater Outflow (Discharge) (ML/day)
Rainfall recharge	126.8	
Evapotranspiration		96.7
Swamps and rivers	5.2	14.5
Seepage through top of the model		0.0
Net outflow through model boundary (ML/day)		20.7 .
Total (ML/day)	132.0	131.9
Discrepancy	0.14%	

3.4 Sensitivity analysis

Sensitivity analysis is conducted to study model input parameter sensitivity to model results. The sensitivity analysis is carried out by varying (either decreasing or increasing) one parameter at a time and evaluating the effects of these parameters on the calibration objectives. The RMS values and the baseflow quantity to Sunnyside Swamp are recorded for every sensitivity study scenario and then compared with each other. Such a comparison assists in the identification of sensitive model parameters that would yield a significant change in the RMS difference or the baseflow.

The sensitivity analysis is conducted on the following model input parameters:

- Horizontal and vertical permeability of the model layers;
- Rainfall and ET; and
- River-bed conductance.

Sensitivity of the model result to the permeability variation is assessed by multiplying:

- the horizontal permeability by factors of 0.5 (decrease) and 2 (increase), and
- the vertical permeability by factors of 0.1 (decrease) and 10 (increase).

Sensitivity to rainfall recharge and ET is studied by multiplying:

- the rainfall recharge by 0.85 (decrease) and 1.15 (increase),
- the extinction depth by 0.5 (decrease) and 2 (increase), and
- ETmax by 0.5 (decrease) and 2 (increase).

Table 17 presents the results of the sensitivity study.

Table 17 Sensitivity study results

Variation and multiplier		Steady-state RMS difference (m)	Sunnyside baseflow (ML/day)
Base model, no variation		23.09	0.099
Weath	0.5 hor	23.68	0.079
	2.0 hor	22.68	0.115
	0.1 vert	23.42	0.075
	10 vert	23.22	0.107
AQ6	0.5 hor	23.36	0.095
	2.0 hor	22.75	0.103
	0.1 vert	22.72	0.095
	10 vert	23.22	0.102
SP4	0.5 hor	23.09	0.099
	2.0 hor	23.09	0.099
	0.1 vert	23.22	0.101
	10 vert	22.09	0.085
AQ5	0.5 hor	23.41	0.102
	2.0 hor	22.77	0.095
	0.1 vert	24.20	0.101
	10 vert	22.62	0.099
YS6	0.5 hor	23.09	0.099
	2.0 hor	23.09	0.099
	0.1 vert	23.19	0.100
	10 vert	22.83	0.097
AQ4	0.5 hor	23.08	0.100
	2.0 hor	23.76	0.099
	0.1 vert	25.79	0.100
	10 vert	22.96	0.099
SP3	0.5 hor	23.09	0.099
	2.0 hor	23.09	0.099
	0.1 vert	24.20	0.100
	10 vert	33.59	0.099
AQ3 and KAT	0.5 hor	23.33	0.099
	2.0 hor	23.82	0.099
	0.1 vert	23.02	0.099
	10 vert	23.54	0.099
SP2	0.5 hor	23.09	0.099
	2.0 hor	23.09	0.099
	0.1 vert	23.09	0.099
	10 vert	23.14	0.099
AQ2	0.5 hor	23.82	0.099
	2.0 hor	23.87	0.099
	0.1 vert	21.53	0.099
	10 vert	24.23	0.099
SP1	0.5 hor	23.09	0.099
	2.0 hor	23.09	0.099
	0.1 vert	22.85	0.099
	10 vert	28.02	0.099
AQ1, floor and LTH	0.5 hor	23.95	0.099
	2.0 hor	22.44	0.099
	0.1 vert	21.69	0.099
	10 vert	23.54	0.099
SP0	0.5 hor	23.16	0.099
	2.0 hor	22.93	0.099
	0.1 vert	23.05	0.099
	10 vert	23.86	0.099
Riverbed conductance	0.1	23.36	0.063
	10	23.02	0.107
Rain recharge	0.85	23.08	0.087
	1.15	23.14	0.111
ET extinction depth	0.5	23.11	0.122
	2.0	22.93	0.089
ET max	0.5	23.42	0.111
	2.0	22.93	0.089

It can be seen that the variations in the model input parameters listed in Table 17 do not have statistically significant effects on model RMS difference except that the case with ten time increase in vertical permeability of SP1 layer yielded 21% increase in RMS difference.

Baseflow to Sunnyside Swamp is found to be very sensitive to some of the model input parameters e.g. riverbed conductance, rainfall recharge, ET extinction depth and ETmax and permeability of the topmost weathered layer. Baseflow to Sunnyside Swamp is predicted to decrease by 36% if the riverbed conductance is reduced by a factor of ten and increase by only 13% if the conductance is increased by a factor of ten. However, it is worthwhile to note that if the model input parameters were changed, the model could be easily calibrated to match the monitored baseflow value by changing the riverbed conductance without having any significant impact on the RMS.

3.5 Transient calibration

From 1950 to 1 Jan 2006, varying stress periods are used to match the mining schedule, rainfall is assumed to be constant at 3mm/day, and during 2006, 3-monthly stress periods are used with rainfall given by the Newnes Plateau rainfall gauge listed in Table 6. A recharge rate of 5% is applied to nodes that do not lie on modelled rivers and swamps, and are not fully saturated.

From 1950 to 1 Jan 2006, the maximum value of ET is assumed to be constant at 3.7mm/day, and during 2006, 3-monthly stress periods are used with ET's maximum value given in Table 7. The extinction depth is kept at 5m throughout calibration.

The simulated mine panels and their extraction dates are listed in Table 18. The extraction dates are derived using the method described in Section 2.3 where the columns of Table 18 are also described.

Table 18 Mines simulated in the model during transient calibration

Name	Start_Date	End_Date	Type	Pressure	Direction	Seam	Step
AP_LW_1	1/1/1980	1/1/1980	LW	0	EtoW	LTH	1
AP_LW_2	1/1/1980	1/1/1980	LW	0	EtoW	LTH	1
AP_LW_3	1/1/1980	1/1/1980	LW	0	NtoS	LTH	1
AP_LW_4	1/1/1980	1/1/1980	LW	0	NtoS	LTH	1
AP_LW_5	1/1/1980	1/1/1980	LW	0	NtoS	LTH	1
AP_LW_6	1/1/1980	1/1/1980	LW	0	NtoS	LTH	1
AP_LW_7	1/1/1985	1/1/1985	LW	0	NtoS	LTH	1
AP_LW_8	1/1/1985	1/1/1985	LW	0	NtoS	LTH	1
AP_LW_9	1/1/1985	1/1/1985	LW	0	NtoS	LTH	1
AP_LW_10	1/1/1985	1/1/1985	LW	0	NtoS	LTH	1
AP_LW_11	1/1/1990	1/1/1990	LW	0	EtoW	LTH	1
AP_LW_12	1/1/1990	1/1/1990	LW	0	EtoW	LTH	1
AP_LW_13	1/1/1990	1/1/1990	LW	0	EtoW	LTH	1
AP_LW_16	1/1/1990	1/1/1990	LW	0	StoN	LTH	1
AP_LW_17	1/1/1990	1/1/1990	LW	0	StoN	LTH	1
AP_LW_18	4/01/1993	13/12/1993	LW	0	StoN	LTH	1
AP_LW_19	19/03/1994	5/03/1995	LW	0	StoN	LTH	1
AP_LW_20	25/04/1995	7/05/1996	LW	0	StoN	LTH	1
AP_LW_21	17/06/1996	17/10/1997	LW	0	StoN	LTH	1
AP_LW_22	2/12/1997	11/12/1998	LW	0	StoN	LTH	1
AP_LW_23	4/01/1999	26/11/1999	LW	0	StoN	LTH	1

AP_LW_24	20/12/1999	29/12/2000	LW	0	StoN	LTH	1
AP_LW_25	21/02/2001	19/12/2001	LW	0	EtoW	LTH	1
AP_LW_26	14/02/2002	11/12/2002	LW	0	EtoW	LTH	1
AP_LW_26N	20/02/2003	30/09/2003	LW	0	EtoW	LTH	1
AP_LW_920	2/03/2004	18/10/2005	LW	0	EtoW	LTH	1
AP_LW_930	19/12/2005	11/02/2007	LW	0	EtoW	LTH	5
SPR_LW_1	1/1/1995	1/1/1995	LW	0	NtoS	LTH	1
SPR_LW_401	1/3/1996	1/1/1997	LW	0	NtoS	LTH	1
SPR_LW_402	1/2/1997	1/11/1997	LW	0	NtoS	LTH	1
SPR_LW_403	1/1/1998	1/11/1998	LW	0	NtoS	LTH	1
SPR_LW_404	1/1/1999	1/2/2000	LW	0	NtoS	LTH	1
SPR_LW_405	10/04/2000	26/03/2001	LW	0	NtoS	LTH	1
SPR_LW_406	27/05/2001	23/01/2002	LW	0	NtoS	LTH	1
SPR_LW_407	28/03/2002	9/01/2003	LW	0	NtoS	LTH	1
SPR_LW_408	20/02/2003	18/12/2003	LW	0	NtoS	LTH	1
SPR_LW_409	18/02/2004	10/12/2004	LW	0	NtoS	LTH	1
SPR_LW_410	9/02/2005	19/01/2006	LW	0	NtoS	LTH	1
SPR_LW_411	10/03/2006	26/10/2007	LW	0	NtoS	LTH	7
Clarence_LW_rest	1/1/1996	1/1/1996	LW	0	StoN	kat	1
Clarence_LW_7	1/6/1997	1/9/1997	LW	0	StoN	kat	1
OPK	1/1/1950	1/1/1950	BP	1.30E+06	EtoW	LTH	1
FBK	1/1/1950	1/1/1950	BP	1.30E+06	EtoW	LTH	1
LGS	1/1/1950	1/1/1950	BP	1.30E+06	EtoW	LTH	1
STW	1/1/1950	1/1/1950	BP	1.30E+06	EtoW	LTH	1
COM	1/1/1950	1/1/1950	BP	Flooded	EtoW	LTH	1
CAL	1/1/1950	1/1/1950	BP	Flooded	EtoW	LTH	1
WWG	1/1/1950	1/1/1950	BP	Flooded	EtoW	LTH	1
RWN	1/1/1950	1/1/1950	BP	Flooded	EtoW	LTH	1
INV	1/1/1950	1/1/1950	BP	Flooded	EtoW	LTH	1
VAL	1/1/1950	1/1/1950	BP	Flooded	EtoW	LTH	1
LGS_1	1/1/1950	1/1/1950	BP	1.30E+06	EtoW	LTH	1
EAS	1/1/1980	1/1/1980	BP	Flooded	EtoW	LTH	1
BBN	1/1/1985	1/1/2010	LW	Flooded	StoN	LTH	25
JHN	1/1/1950	1/1/1950	Opencut	Flooded	EtoW	LTH	1
KER1	1/1/1950	1/1/1950	Opencut	Flooded	EtoW	LTH	1
KER2	1/1/1950	1/1/1950	Opencut	Flooded	EtoW	LTH	1
KER3	1/1/1950	1/1/1950	Opencut	Flooded	EtoW	LTH	1
COL1	1/1/1950	1/1/1950	Opencut	Flooded	EtoW	LTH	1
COL2	1/1/1950	1/1/1950	Opencut	Flooded	EtoW	LTH	1
NEW1	1/1/1950	1/1/1950	Opencut	Flooded	EtoW	LTH	1
NEW2	1/1/1950	1/1/1950	Opencut	Flooded	EtoW	LTH	1
FLY	1/1/1950	1/1/1950	Opencut	Flooded	EtoW	LTH	1
PDL1	1/01/2006	10/10/2030	Opencut	0	EtoW	LTH	1
PDL2	1/01/2006	10/10/2030	Opencut	0	EtoW	LTH	1

Clarence_BP_1	9/07/2006	9/07/2027	BP	0	EtoW	kat	8
Clarence_BP_2_3	21/07/1994	21/07/2015	BP	0	StoN	kat	21
Clarence_BP_4_5	20/12/2006	20/12/2027	BP	0	StoN	kat	21
AP_BnP	1/01/1998	1/1/1998	BP	0	NtoS	LTH	1

3.5.1 Transient calibration performance

The comparison of the simulated elevation heads with the measured elevation heads at the piezometers listed in Appendix A is shown in Figure 37. The RMS difference is 28.8m, and the SRMS difference is 6.9%. Comparisons of observed and simulated hydrographs provided in Appendix B demonstrate good agreements between simulation results and observations.

Comparisons of measured and simulated piezometric heads

The comparison has been made for the layers above Mt York clay (SP3 layer) (blue dots in the figure); Mt York Clay, AQ3 and Katoomba layers (pink dots); SP2 and AQ2 layers (yellow dots), and layers below AQ2 (light-blue dots). Exploring the graph, the scatter is larger in the SP2 and AQ2 layers. Again, there is also a slight bias towards higher pressures in the layers below AQ2.

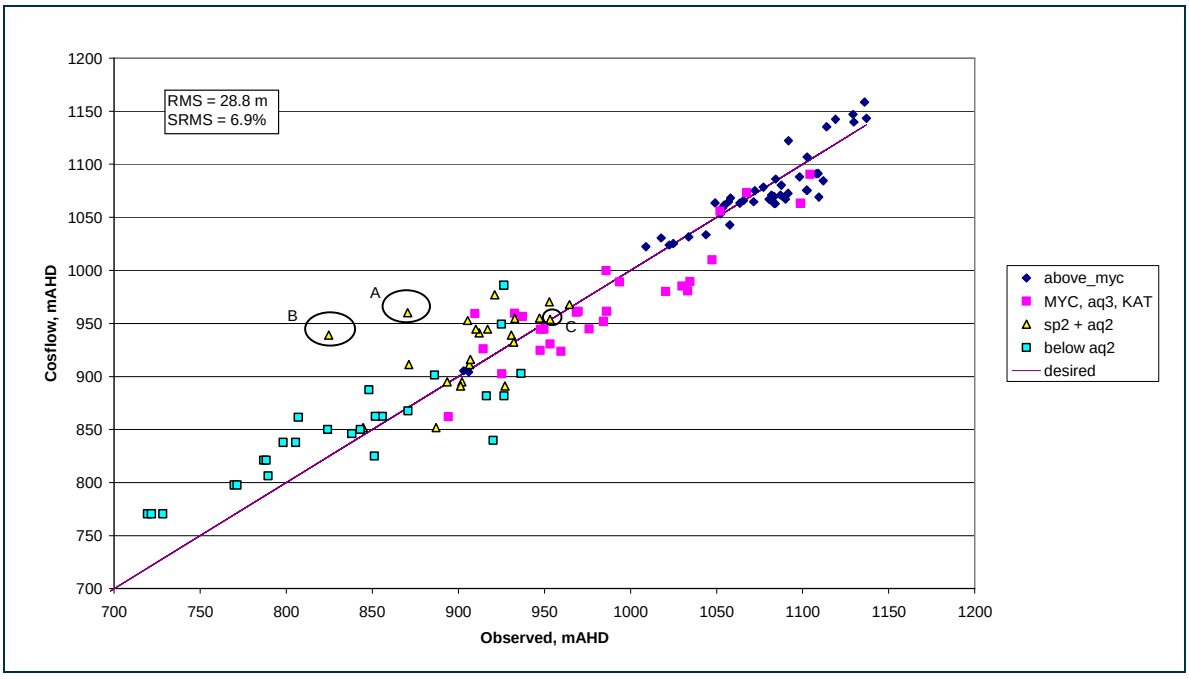

Figure 37 Scatter plot for transient calibration

Two outliers in AQ2 deserve special mention (see Figure 37).

- Piezo2 of SPR35. The model predicts elevation head of 960m, while the piezometer measures 871m. On the other hand, the nearby P3 of SPR33, labelled "C" in the Figure, also located in AQ2, reads 953m and the model yields 954m. In the model, there is very little to distinguish these two piezometers: they are at similar depths in the same material and should be similarly affected by mining. Perhaps Piezo2 of SPR35 is not reading reliably. However, in Section 3.6.1 it is shown that during validation, the model predicts a head drop of 41m while in reality Piezo2 exhibits a drop of 40m. Therefore, even though the absolute value in the model is too high by about 90m, the model's response to mining is reasonable. Barnett et al. (2012) present similar view "analysis of uncertainty should recognise that there is more uncertainty when reporting confidence intervals around an absolute model output, and less uncertainty when a prediction can be formulated as a subtraction of two model results".

- Piezo3 of AP1104. The model predicts elevation head of 939m, while the piezometer measures 824m. On the other hand, Piezo4 of the same borehole is also in AQ2 according to the model, and reads 931m, while the model predicts 939m. This is expected of the model since the piezometers are in the same aquifer. Piezo4 is located about 23m above Piezo3, but the difference in measured water head is around 80m. It indicates a possibility of the existence of a semi-permeable layer locally between these piezometers causing the loss in water heads. The regional scale model does not incorporate such a localised variation in the geology and hence this could be a possible reason for the observed discrepancy.

Comparison of observed and simulated piezometric vertical head profiles

Before 2006, only a small number of piezometers were installed at the Springvale Colliery. Figure 38 shows comparisons of observed and simulated head profiles in monitoring bores SPR26 at different times. It can be seen that the trend between the observed and simulated piezometric head profiles remain more or less unchanged during the calibration period indicating a good and consistent calibration statistics. More vertical head profile comparison plots are provided in Section 3.6.2 and Appendix B indicating a good calibration.

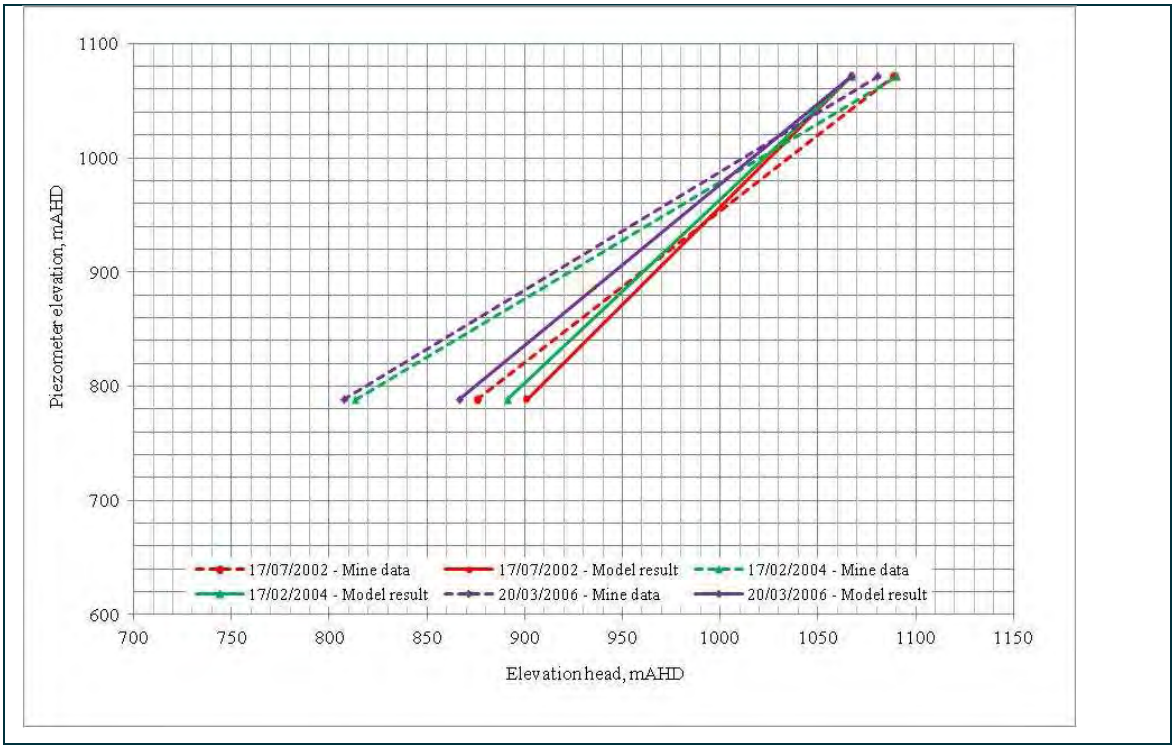

Figure 38 Comparison of observed and simulated head profile SPR26

Comparison with mine inflow rates

The comparison between the model results and observed mine inflows is shown in Figure 39. Table 19 enumerates the comparison with the calibration objectives. Evidently, in the model both Springvale and Angus Place are producing slightly less water than was measured. The ramp function could be altered to address this (with a greater M_315, for instance), however, this also will increase the Springvale's rate of increase (slope of the mine inflow curve) which is already too high at 20 l/s/year. At this stage, the calibrated model inputs parameters are accepted as giving reasonable model outputs, however their performance will be checked again during model validation.

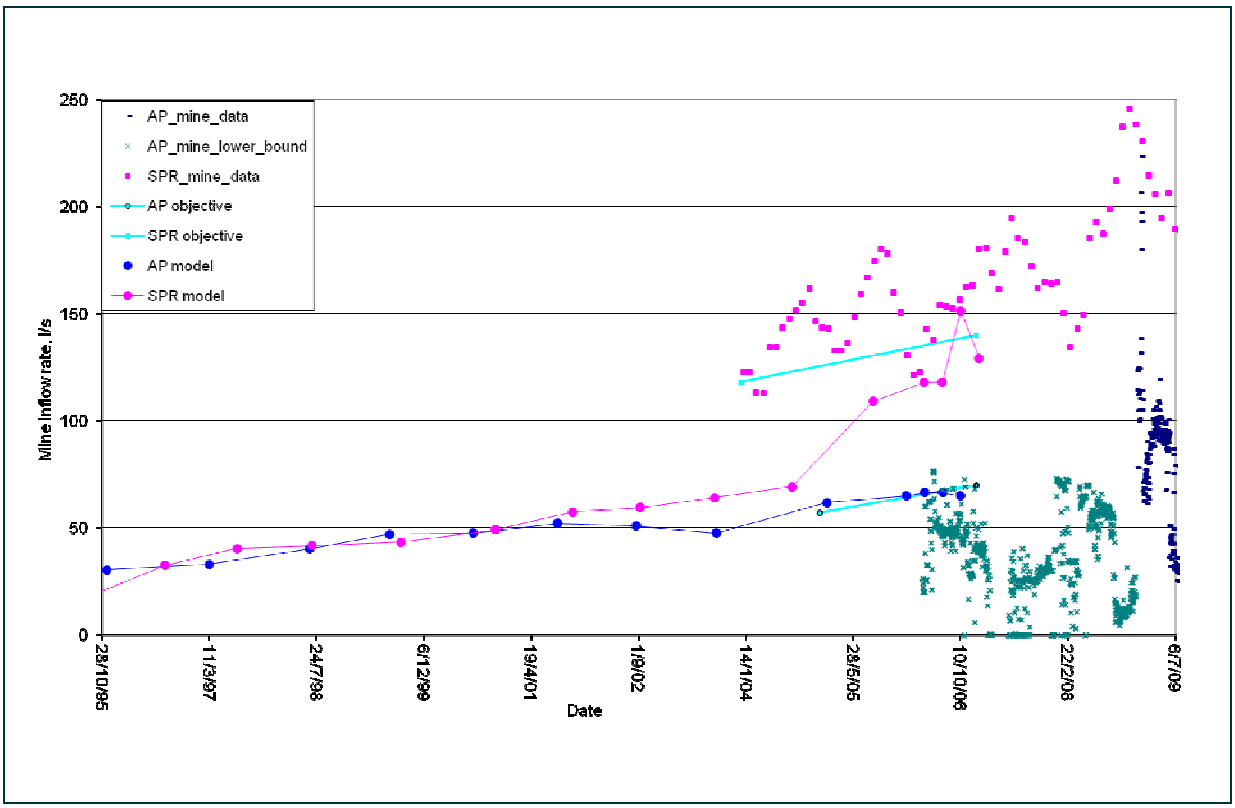

Figure 39 Comparison between model results with monitored mine inflow rates (the objective functions shown by the light blue lines are discussed in Appendix A)

Table 19 Comparison of model results with monitored mine inflow rates

	Springvale Measured value	Springvale Model	Angus Place Measured value	Angus Place Model
Final flow rate (l/s)	140	129	70 - 100	65
Rate of increase (l/s/year)[2]	7.3	20	6.5	5.8

Comparison with baseflow into Sunnyside Swamp

Figure 40 shows the simulated baseflow to Sunnyside Swamp as a function of time, and Table 20 enumerates the comparison with the median value. The simulated baseflow value is in good agreement with the observation (as displayed in Table 10). Evident is the fluctuation in baseflow due to seasonal rainfall and ET during the year 2006.

[2] The rates of increase are calculated over 2004-2007 and 2005-2007 for Springvale Colliery and Angus Place Colliery respectively.

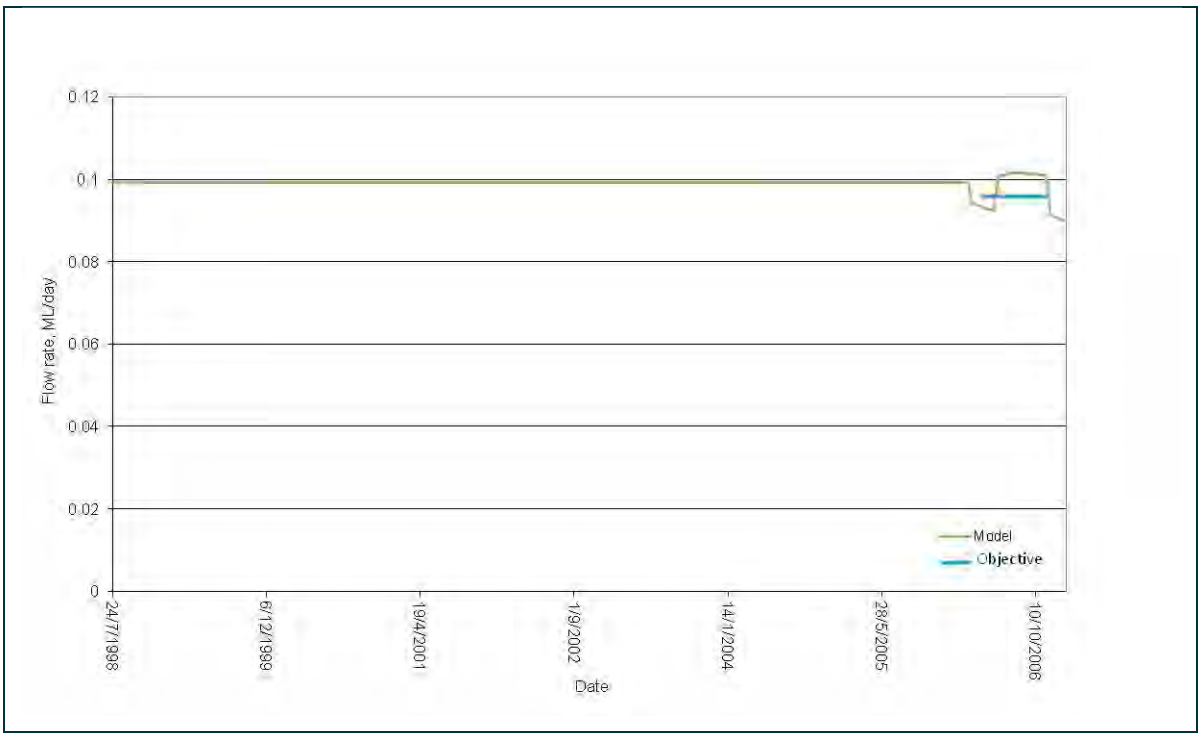

Figure 40 Simulated baseflow balance to Sunnyside Swamp

Table 20 Comparison of baseflow to Sunnyside Swamp

	Median value	Model
Baseflow to Sunnyside swamp (ML/day)	0.093 (0.003 to 0.26 for 20% to 80%)	~0.095

3.5.2 Water balance during transient calibration

The average rates of recharge and discharge throughout the calibration period are given in Table 21. The average recharge to the groundwater system is 131 ML/day, comprising mainly rainfall recharge (126 ML/day) and leakage from swamps and streams into the groundwater system (5 ML/day).

Table 21 Average rates of recharge and discharge throughout the transient calibration period from 1950 to 2006

Component	Transient calibration period from 1950 to 2006		Steady-state calibration	
	Groundwater Inflow (Recharge) (ML/day)	Groundwater Outflow (Discharge) (ML/day)	Groundwater Inflow (Recharge) (ML/day)	Groundwater Outflow (Discharge) (ML/day)
Rainfall recharge	125.8		126.8	
Evapotranspiration		98.3		96.7
Swamps and rivers	5.2	14.6	5.2	14.5
Net outflow through model boundary (ML/day)	20.6		20.7	
Mine inflow (ML/day)		3.74		0
Total (ML/day)	131.0	137.3	132.0	131.9
Net Outflow (ML/day)	6.24		0	
Change in fluid volume contained (storage) in the model (ML/day)	6.24		0	
Discrepancy	0.01 %		0.14%	

The average groundwater discharge across the model is 137 ML/day. ET represents the major source of discharge (98.3 ML/day). Baseflow to swamps and streams is 15 ML/day.

A net loss of groundwater across the model boundary is 21 ML/day. The loss in fluid storage in the groundwater system is 6 ML/day. Mine inflow during the transient calibration is 4 ML/day, which accounts for about half of the net loss in the fluid storage.

3.5.3 Sensitivity to the permeability-change ramp function parameters

The effect of the ramp function on mine inflow rates during calibration is shown in Table 23. Around the calibrated value of M_315, the dependence on this parameter is virtually linear. The dependence on "a", the panel-width multiplier, is obviously greater for narrow panels than it is for wide panels, and the effect on the Springvale group of panels (LW1 to LW411) is enumerated as an example. The dependence on "b", the goaf permeability multiplier is nonlinear. Reducing b below the base value of 0.5 has a much smaller effect than increasing b. The dependence on "c", the goaf conductance multiplier is also nonlinear. Lowering c below -5 has limited effect: conversely, raising c above -2 has greater effect on the flow rates. Most important, however, is that increasing b or c has an additional unwanted effect: for such scenarios the inflow rates for mined panels remain unrealistically high for many years after the panel has been completed.

Table 22 Sensitivity to ramp function and the conductance of the goaf region

Variation compared with Base case (M_315=6.2, a=0.75, b=0.5, c=-4)	Effect on flow rates
M_315 = 6.3	All inflow rates increase by 7%
M_315 = 6.1	All inflow rates decrease by 7%
a=0.5	Springvale inflow increases by 4%
a=1.0	Springvale inflow decreases by 5%
b=0.8	All inflow rates increase by 43%
b=0.6	All inflow rates increase by 7%
b=0.4	All inflow rates decrease by 2%
c=-5	All inflow rates decrease by 2%
c=-3	All inflow rates increase by 10%
c=-2	All inflow rates increase by 46%

3.6 Transient validation

The model is run from the end of the calibration period (20 Dec 2006) through to 1 Jan 2012 (roughly the end of Springvale LW414, and the first part of Angus Place LW970). The model's elevation heads at about 142 piezometers (see Appendix A) are compared with the measured elevation heads. The simulated baseflow in Sunnyside Swamp is compared with the median value. The simulated water inflow rates for Springvale and Angus Place mines are compared with the measured values.

During the validation period 3-monthly stress periods are used with rainfall given by the Newnes Plateau rainfall gauge listed in Table 6. A recharge rate of 5% is applied to nodes that do not lie on modelled rivers and swamps, as discussed in Section 2.9.

ET's values used within the validation period are given in Table 7. The extinction depth is kept at 5m throughout calibration.

In addition to the mining panels listed in Table 18, the following mining panels as shown in Table 23 are excavated during validation.

Table 23 Additional mines simulated in the model during transient validation

Name	Start_Date	End_Date	Type	Pressure	Direction	Seam	Step
AP_LW_940	27/03/2007	23/06/2008	0	LW	EtoW	LTH	6
AP_LW_950	8/08/2008	15/02/2010	0	LW	EtoW	LTH	7
AP_LW_960	7/04/2010	5/07/2011	0	LW	EtoW	LTH	6
AP_LW_970	24/08/2011	8/10/2012	0	LW	EtoW	LTH	5
SPR_LW_411	10/03/2006	26/10/2007	0	LW	NtoS	LTH	7
SPR_LW_412	14/12/2007	22/06/2009	0	LW	NtoS	LTH	7
SPR_LW_413A	7/08/2009	1/04/2010	0	LW	NtoS	LTH	3
SPR_LW_413B	20/05/2010	29/12/2010	0	LW	NtoS	LTH	3
SPR_LW_414	11/02/2011	21/11/2011	0	LW	NtoS	LTH	4

3.6.1 Water balance during transient validation

The average rates of recharge and discharge throughout the transient validation period are given in Table 24. The average recharge to the groundwater system is 122 ML/day, comprising mainly rainfall recharge (116.3 ML/day) and leakage from swamps and streams into the groundwater system (5.5 ML/day).

The average groundwater discharge across the model is 156 ML/day. ET represents the major source of discharge (92.3 ML/day). Baseflow to swamps and streams is 15 ML/day.

A net loss of groundwater across the model boundary is 18 ML/day. The loss in fluid storage in the groundwater system is 34 ML/day. Mine inflow during the transient validation is 31 ML/day, which accounts for about 92% of the net loss in the fluid storage.

Table 24 Average rates of recharge and discharge throughout the transient validation period

Component	Transient validation performance from 2007 to 2012		Transient calibration period from 1950 to 2006	
	Groundwater Inflow (Recharge) (ML/day)	Groundwater Outflow (Discharge) (ML/day)	Groundwater Inflow (Recharge) (ML/day)	Groundwater Outflow (Discharge) (ML/day)
Rainfall recharge	116.3		125.8	
Evapotranspiration		92.3		98.3
Swamps and rivers	5.5	14.6	5.2	14.6
Net outflow through model boundary (ML/day)	17.9 .		20.6	
Mine inflow (ML/day)		30.9		3.74
Total	121.8	155.7	131.0	137.3
Net Outflow (ML/day)	33.9		6.24	
Change in fluid volume contained in model (ML/day)	-33.9		6.24	
Discrepancy	0.09 %		0.01 %	

3.6.2 Transient validation performance

The comparison of the model's elevation heads with the measured elevation heads at the piezometers listed in Appendix A is shown in Figure 41. The RMS difference is 32.1m, and the SRMS difference is 7.6%.

The comparison has been made for the layers above Mt York clay (SP3 layer) (blue dots in the figure); Mt York Clay, AQ3 and Katoomba layers (pink dots); SP2 and AQ2 layers (yellow dots), and layers below AQ2 (light-blue dots). Exploring the graph, again the scatter is significantly larger in the SP2 and AQ2 layers. There is also a slight bias towards higher pressures in the layers below AQ2.

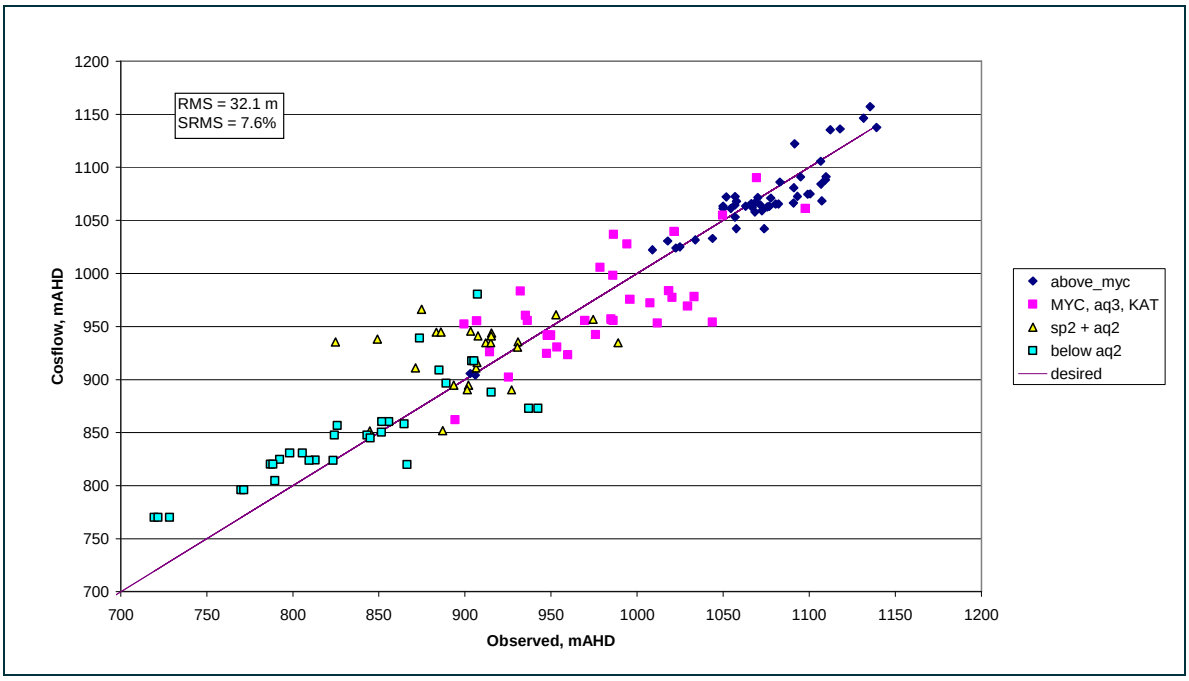

Figure 41 Scatter plot for transient validation

Comparisons of measured and simulated piezometric heads

Comparisons of measured and simulated piezometric heads versus time for all the piezometer holes are provided in Appendix B. Appendix B also provides comparisons of simulated and measured vertical head profiles. Typical comparisons of simulated and measured heads are presented in Figure 42 to Figure 47. From these figures, it can be seen that the simulated water heads generally agrees well with the measurements. However, there are some differences between the measured heads and simulated heads which are largely reflected through the RMS difference of 32.1m. Adhikary and Morla (2013) have conducted a qualitative assessment of the monitored piezometric data. Understanding the changes in piezometric heads is not always easy as a number of factors may affect the piezometer readings as discussed in that report. Thus the level of agreement between the observed piezometric heads and the simulated piezometric heads obtained using an uncoupled fluid flow (groundwater flow) only code can be considered excellent.

By studying the piezometer data presented in Appendix A, one can conclude that piezometers situated within and above YS6 are only marginally affected by mining. An example of P6 (AQ5) and P8 (AQ6) in SPR48 which sits above the chain pillar between LW412 and LW413A is shown in Figure 42.

In the model, the top two piezometers display a slow decline of 5m over the period 1/1/2008 to 1/1/2012. Since real (varying) rainfall data are used in the transient validation period it is difficult to distinguish between climate and mining effects. However, from Table 24 it can be seen that the simulated rainfall recharge deficit is 9.5 ML/Day during the transient validation period in comparison to the transient calibration period (i.e. from 1950 to 2006). The rainfall deficiency may well explain the reason for slow decline in the simulated piezometric heads at shallow depths.

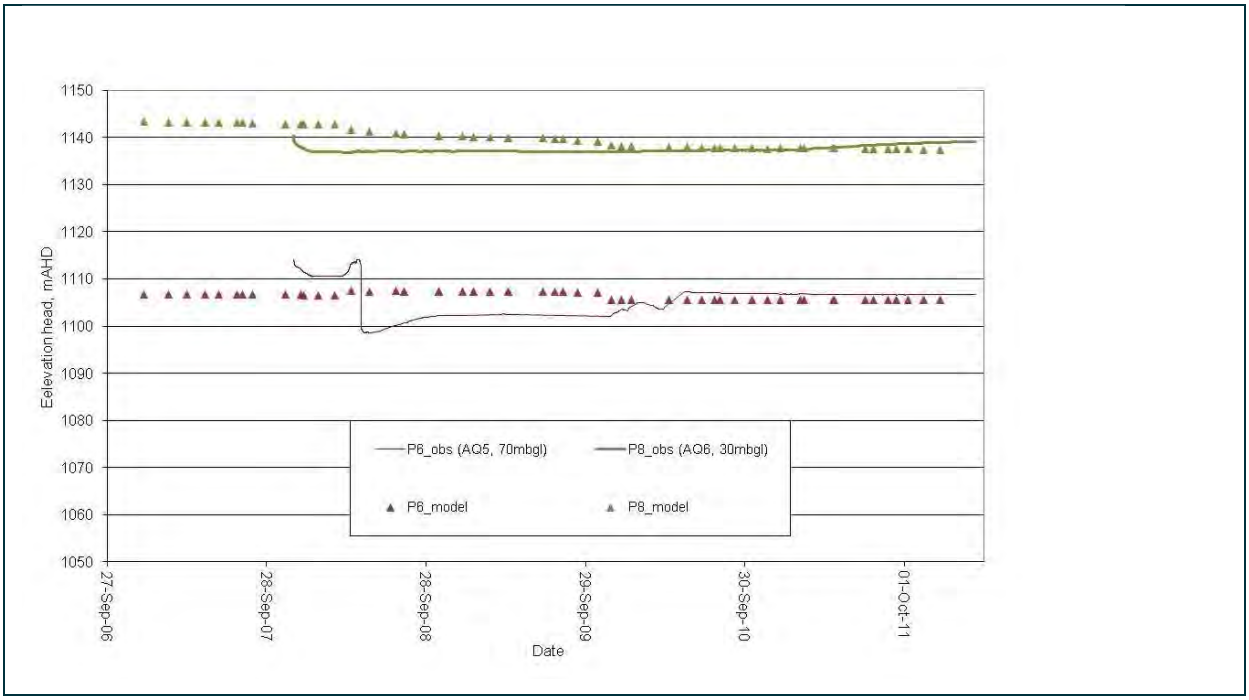

Figure 42 P6 and P8 of SPR48 lie above layer YS6 show very little response to mining over random fluctuations.

Some of the piezometers situated in AQ4 which are above or beside panels mined during validation are damaged by mining, and some exhibit head increases due to rock deformation, and it is difficult to compare the response of the model with observations. P3 to P8 of SPR49 (in the pillar east of LW412) lie in MYC and above, and are either steady or exhibit quite small head drops (Figure 43). Piezometers (P4, P5 and P6) are located within one aquifer (AQ4) in the model thus there is hardly any difference in their simulated elevation heads.

The situation is different below AQ3: all the heads measured by all piezometers above or beside panels mined during validation are affected by mining. For instance, P2 of SPR35 (above the chain pillar between LW413B and LW414, Figure B14 Appendix B) sits in AQ2 and exhibits a head drop of 40m during the measurement period, while the model's head drop is 41m over the same time frame. This piezometer was mentioned in the Section 3.5.1 above as an outlier: here we see that even though its absolute reading is too high by about 90m, its response is reasonable. Figure 44 shows the comparison for SPR34 which lies in the pillar to the east of LW413B.

Finally, a number of piezometers record steady values during the validation period because they are situated well away from mining. Figure 45 presents comparisons of measured and simulated piezometric heads in SPR1102. P6 exhibits a head increase of about 25m over two months for no obvious reason; it could have been affected by any of the factors discussed in Adhikary and Morla (2013). Similar comparisons of measured and simulated piezometric heads in AP10PR are shown in Figure 46.

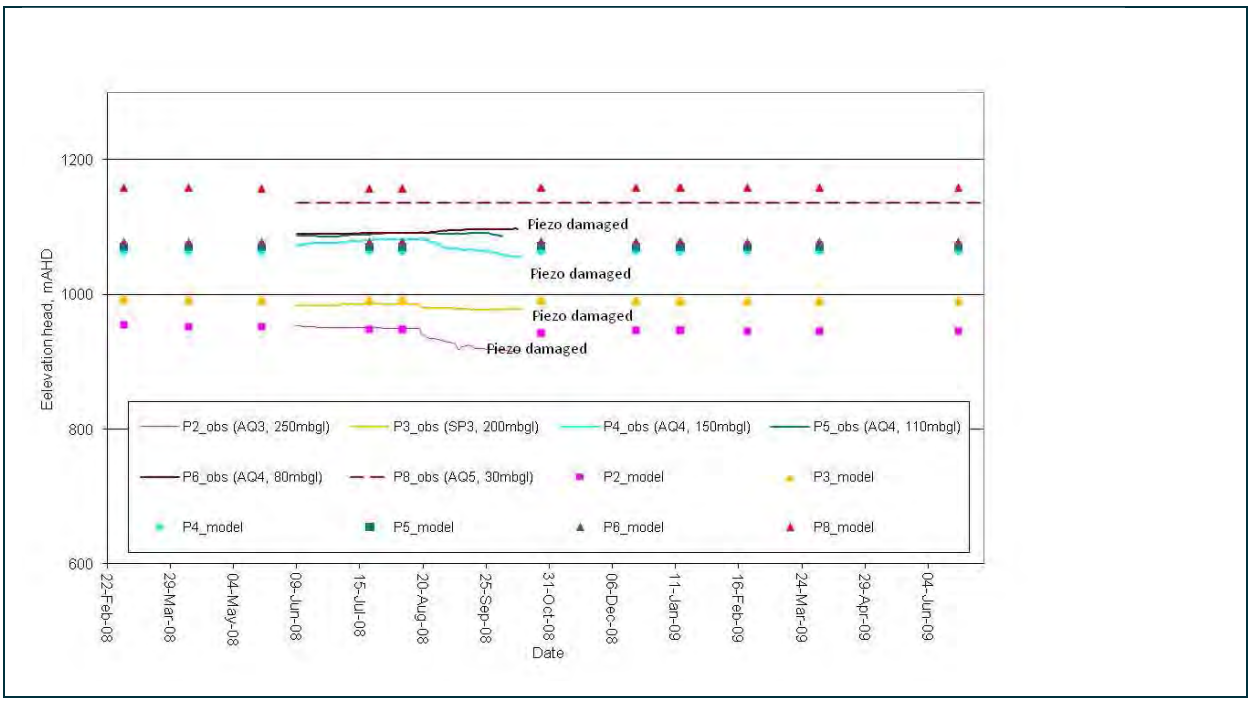

Figure 43 Comparison of model results and observations for SPR49 located in the chain pillar between SPR LW-412 and LW-413, piezo depths range from 30mbgl to 250mbgl – most of the piezometers were damaged once the longwall retreated past the piezo-hole location

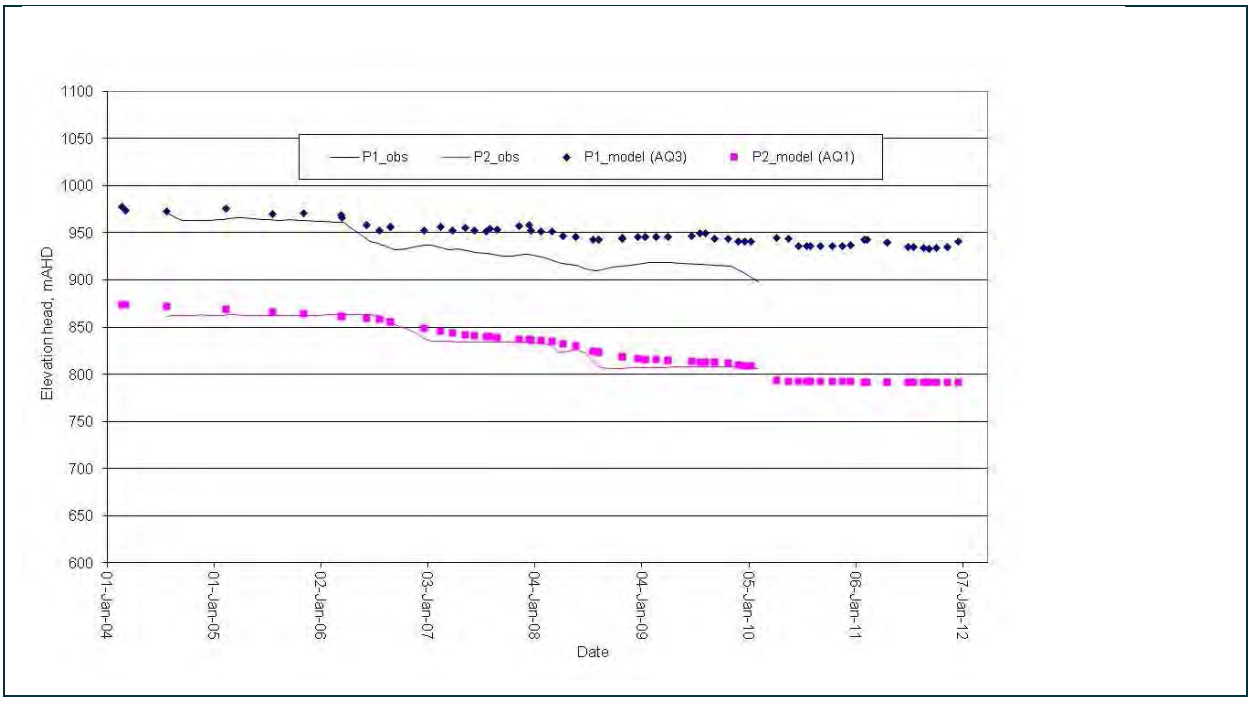

Figure 44 Comparison of model results and observations for SPR34 located at the edge of SPR LW-413A at 270mbgl (P1) and 359mbgl (P2) within the sandstone/siltstone layers in Aquifer3 and Aquifer1 respectively

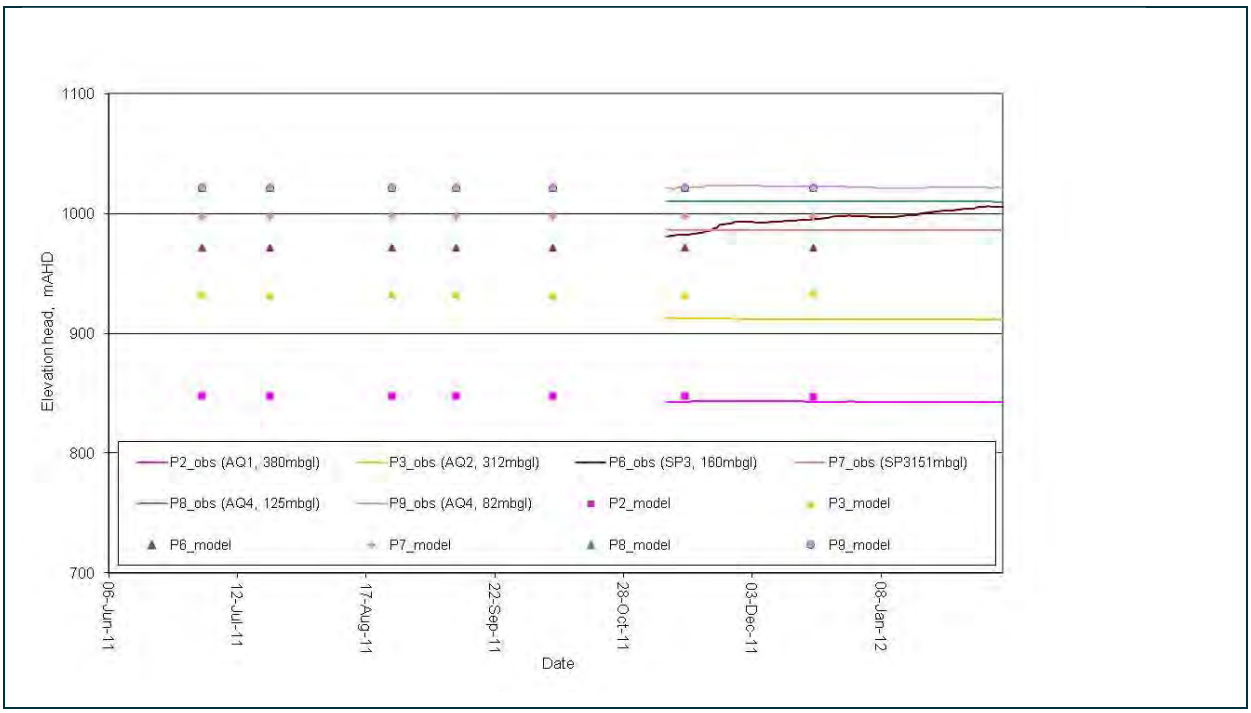

Figure 45 Comparison of observed and simulated piezometer elevation heads for SPR1102 located at the eastern margin of the proposed longwall panels at Springvale Colliery well away from the current mining activites, piezo depths range from 82mbgl to 380mbgl

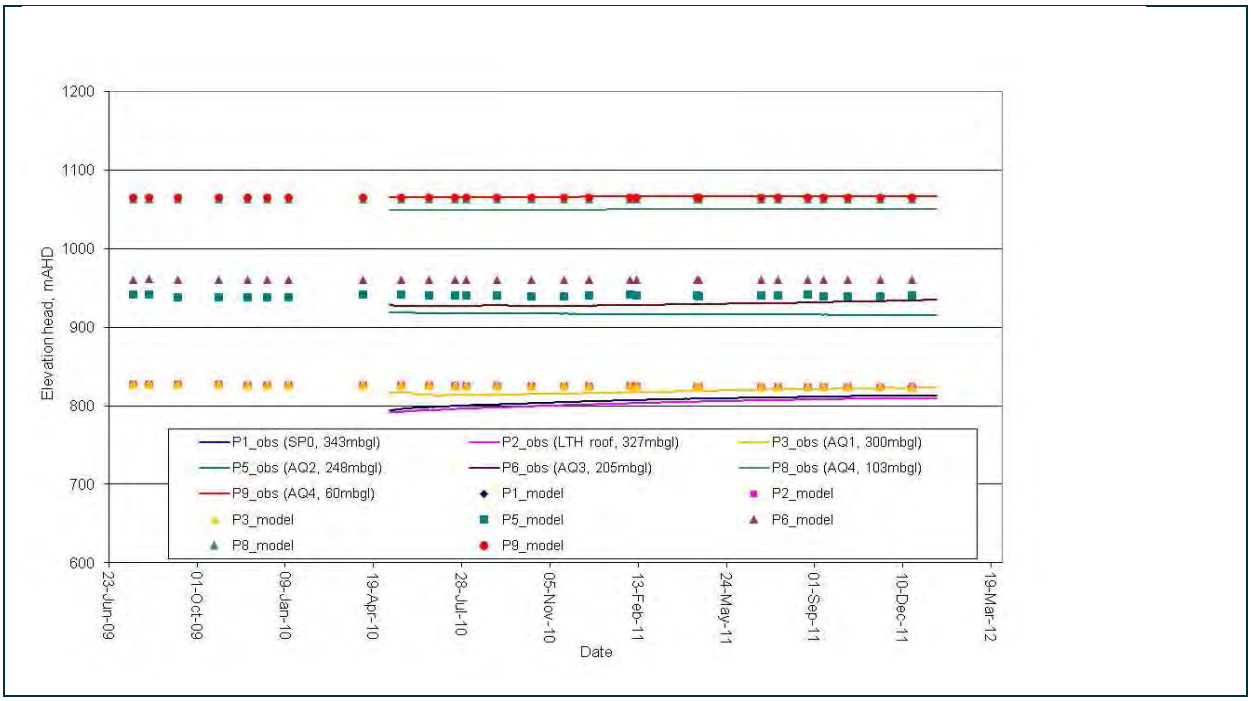

Figure 46 Comparison of observed and simulated piezometer elevation heads for AP10PR located in the chain pillar between APE-4 and APE-5 longwall panels away from the current mining activities, piezo depths range from 103mbgl to 343mbgl

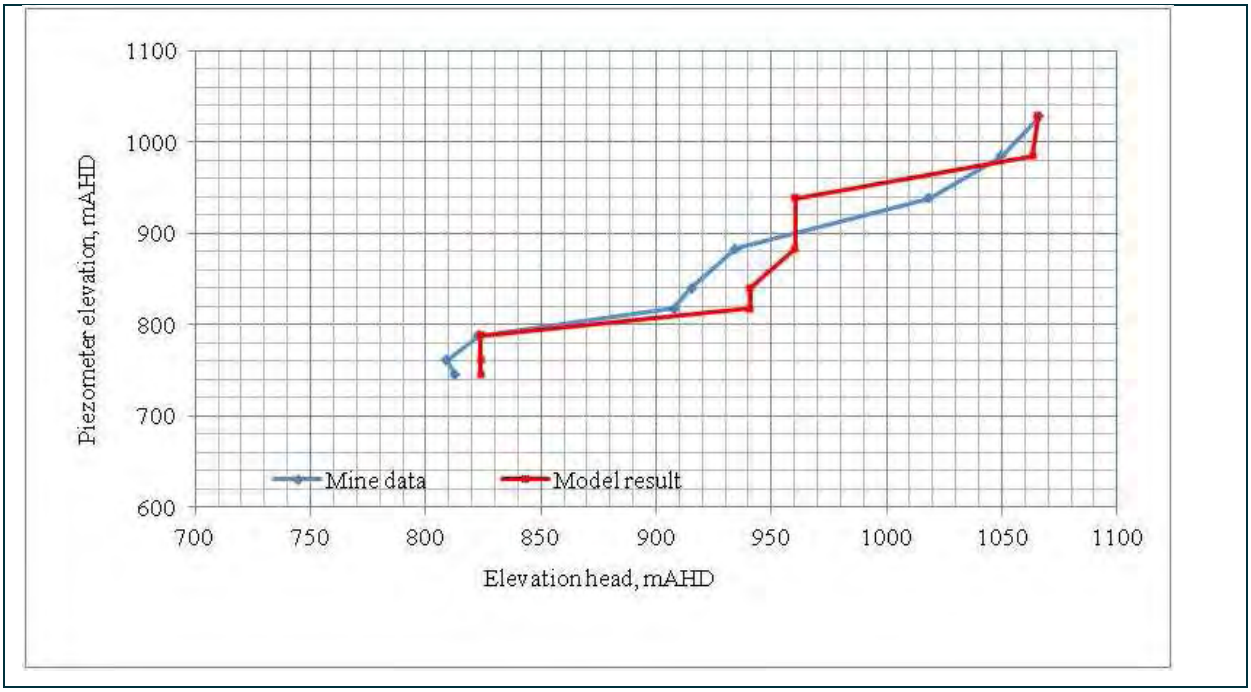

Figure 47 Comparison of observed and simulated piezometer elevation head profiles AP10PR (Date 01/01/2012)

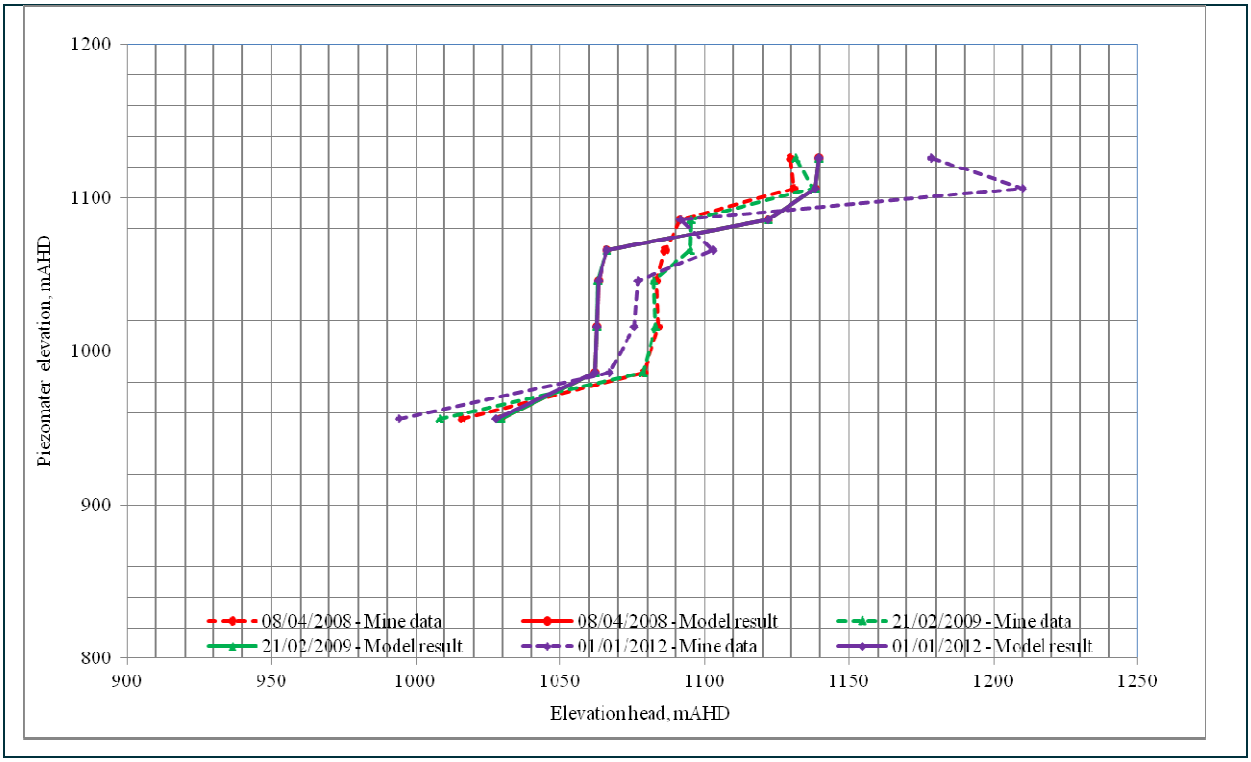

Figure 48 Comparison of observed and simulated piezometer elevation head profiles SPR50

Figure 47 and Figure 48 (and other plots in Appendix B) show that the agreements between the measured and simulated vertical head profiles at different times are excellent indicating a good calibration of model parameters.

Comparison with swamp groundwater levels

The measured groundwater levels within the modelled Type-C swamps are enumerated In Appendix A. Table 25 lists a comparison between the observations and simulated groundwater levels at the end of the validation period (1/1/2012).

Based on the 6 observations where groundwater depths can be estimated, the RMS difference is 0.4m. Because this is based on only 6 observations, the confidence interval for this RMS difference may be quite large: we can be 95% sure that the true RMS difference for groundwater depths in the modelled Type-C swamps is between 0.25m and 0.98m. This is much smaller than the RMS difference for heads throughout the entire model.

Table 25 Comparison between observed and simulated groundwater levels

Site	Swamp	Observed groundwater depth (mbgl) at 1/1/2012	Simulated groundwater depth (mbgl) at 1/1/2012
SS-SV8 (SS1)	Sunnyside (SSS)	0.1	-0.33
SS-SV9 (SS2)	Sunnyside (SSS)	0.2	-0.33
SS 03	Sunnyside (SSS)	<0	-0.21
SS-04	Sunnyside (SSS)	<0	-0.20
SS-05	Sunnyside (SSS)	<0	-0.37
SSE2-SV13	Sunnyside East (CA5)	-0.05	0.23
SSE3-SV14	Sunnyside East (CA5)	0.0	0.0
CW1-SV10	Carne West (CW)	0.05	0.47
CW2-SV11	Carne West (CW)	0.2	0.57

Comparison with mine inflow rates

The comparison between the model results and observed mine inflow rates is shown in Figure 49 and the comparison with the objective is shown in Table 26. As can be seen, the simulated mine inflow rates compare well with the mine data.

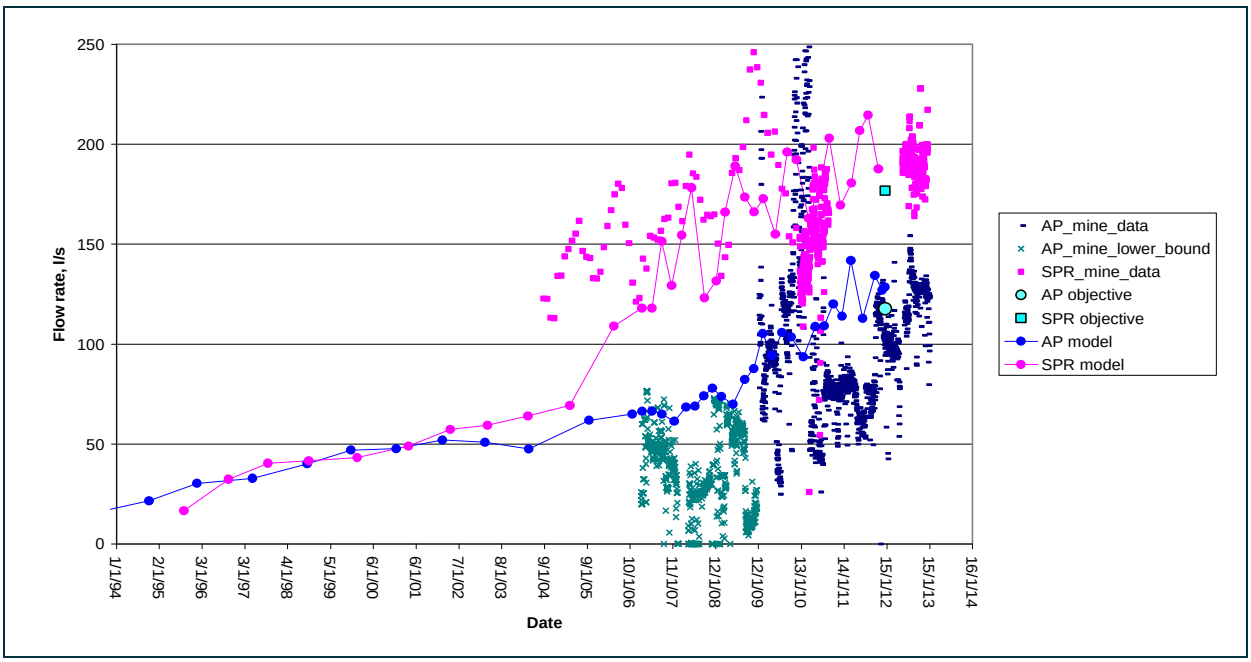

Figure 49 Comparison between model results with monitored mine inflow rates

Table 26 Comparison of model results with monitored mine inflow rates

	Springvale Measured value	Springvale Model	Angus Place Measured value	Angus Place Model
Final flow rate (l/s)	177	188	118	129

Comparison with baseflow to Sunnyside Swamp

Figure 50 shows the simulated baseflow balance to Sunnyside Swamp as a function of time. Evident is the fluctuation in baseflow due to seasonal rainfall and ET during the years 2006 - 2012. Table 27 enumerates the comparison of simulated baseflow balance to Sunnyside Swamp with the mine observation. The simulated baseflow balance value is in good agreement with the observation (as calculated in Table 10). From Figure 50, it can be seen that the baseflow to the Sunnyside Swamp remained steady implying no effects of the mining activities to 2012.

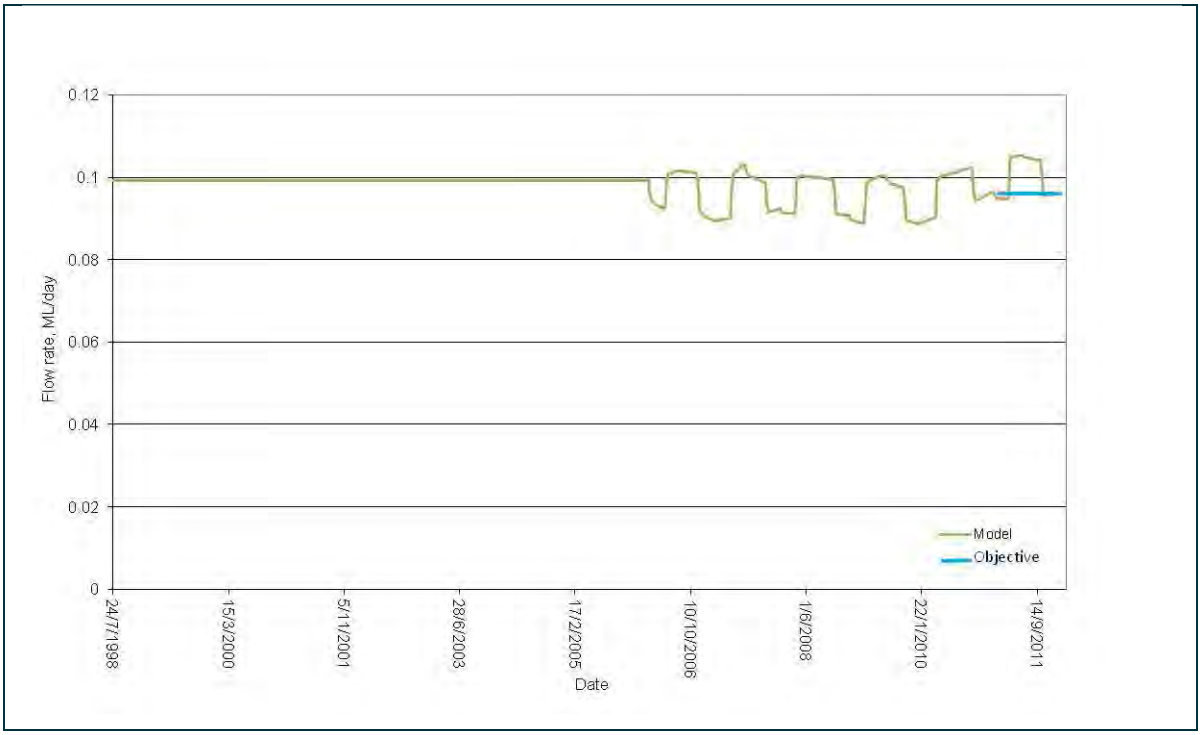

Figure 50 Simulated baseflow balance to Sunnyside Swamp

Table 27 Comparison of baseflow to Sunnyside Swamp

	Median value	Model
Baseflow to Sunnyside Swamp (ML/day)	0.093 (0.003 to 0.26 for 20% to 80%)	~0.095

3.6.3 Relative water content within the model region

Figure 51 shows the estimated volume of water contained in each layer within the model, Figure 52 shows the volume of water lost from each layer and Figure 53 shows the fraction of water remaining in each layers in the model region in January 2012 compared with pre-mining steady-state condition. Maximum storage losses can be seen to occur in AQ1 (2.25%).

The simulated loss of water within the weathered zone can be attributed partially to climate effects as discussed in Section 3.6.2, where the reference is made to Table 24 in explaining the deficit in rainfall recharge during the transient validation period.

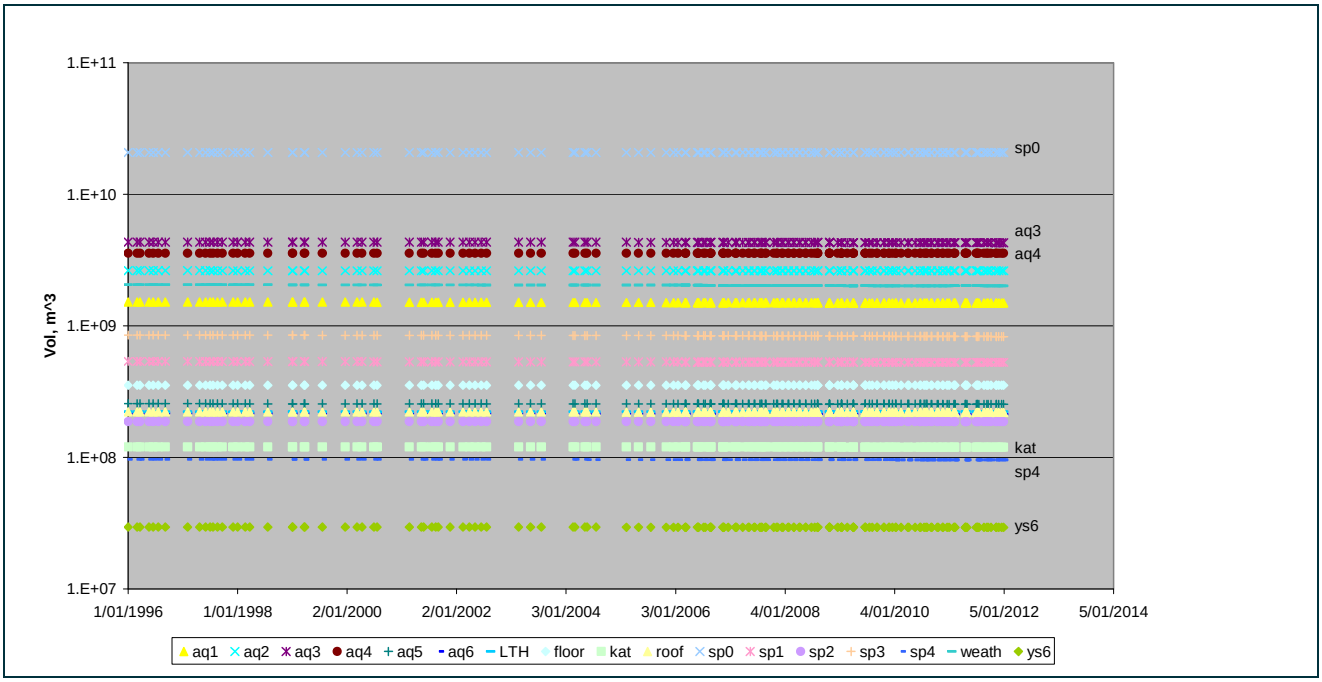

Figure 51 Volume of water content in each layer within the model

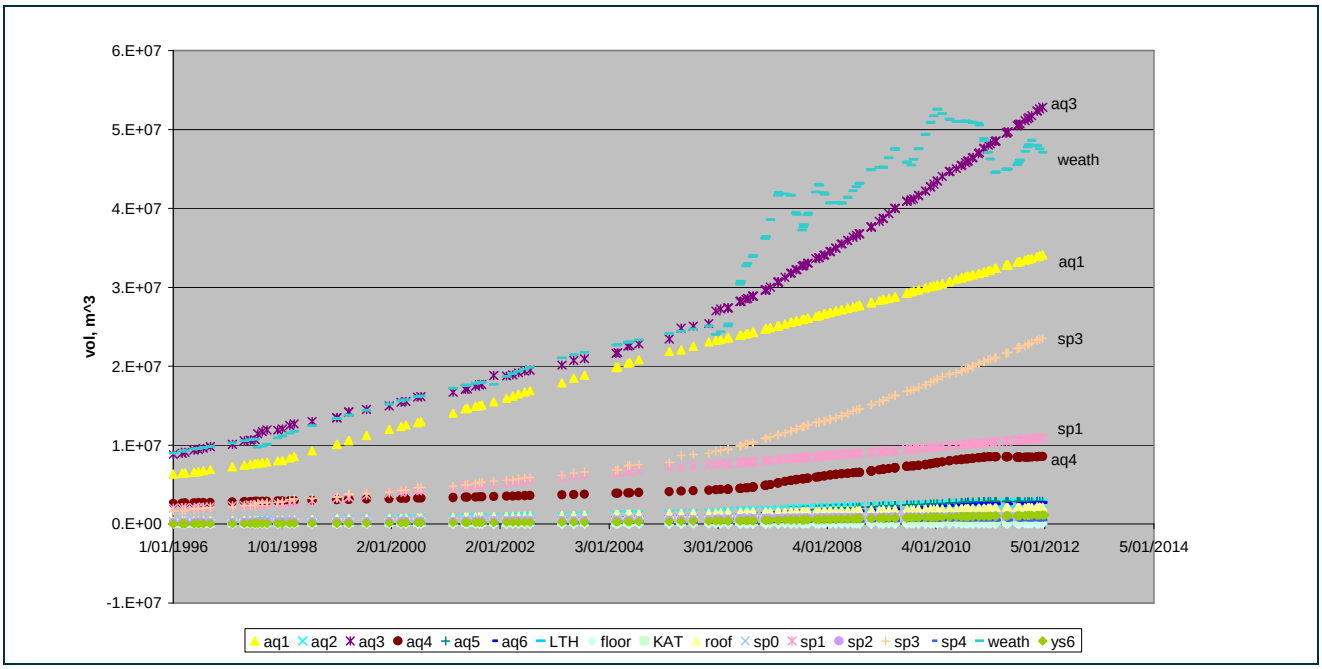

Figure 52 Volume of water lost from each layer compared with steady-state pre-mining conditions

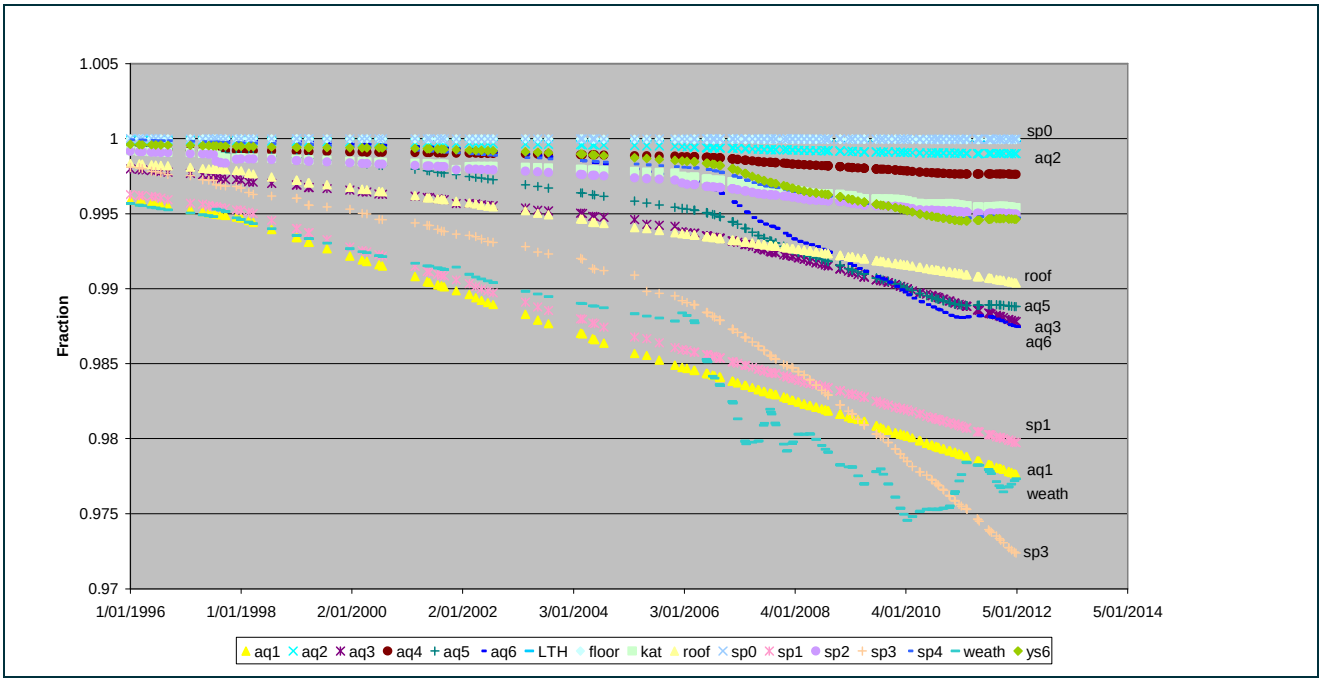

Figure 53 Fraction of fluid volume content in each layer compared with steady-state pre-mining conditions

3.6.4 Drawdown after validation period at 1 January 2012

Figure 54 to Figure 59 present plots of simulated drawdown in different layers at the end of the validation period (1 January 2012) compared with the steady-state virgin condition[3]. As can be seen from these figures the largest simulated drawdown (about 100m) occurs in Lithgow Seam, and 5m of drawdown is experienced approximately 4km from the mining region. The simulated drawdown can be seen to decrease gradually with height above the Lithgow Seam. The drawdown in layers above AQ2 is also influenced by Clarence Colliery and climatic variation.

In these figures and elsewhere, we define saturated drawdown between times A and B as:

Saturated drawdown between times A and B = max(headA, 0) – max(headB, 0) (16)

The "max" is needed because COSFLOW solves saturated-unsaturated fluid-flow problems (like MODFLOW-SURFACT) and so the pressure heads can be negative (indicating unsaturated flow).

The simulated drawdown within the shallow groundwater aquifers are shown in Figure 58 to Figure 60[4]. It is worthwhile to reiterate that the simulated drawdown show mixed climate and mining effects as discussed earlier.

[3] It must be emphasized that the drawdown reported here show mixed climate and mining effects since actual variable rainfall recharge and ET rates are applied during the validation period. The simulated drawdown can be attributed partially to climate effects as discussed in Section 3.6.2, where the reference is made to Table 24 in explaining the deficit in rainfall recharge during the transient validation period.

[4] It is to be noted that the water head can never go lower than -10m in the model since the immobile saturation has been set to 0.1, and the capillary suction curve is approximately -10m at that point. The physical assumption here is that water meniscus would not be able to sustain the tension beyond 100 kPa and would burst beyond that point.

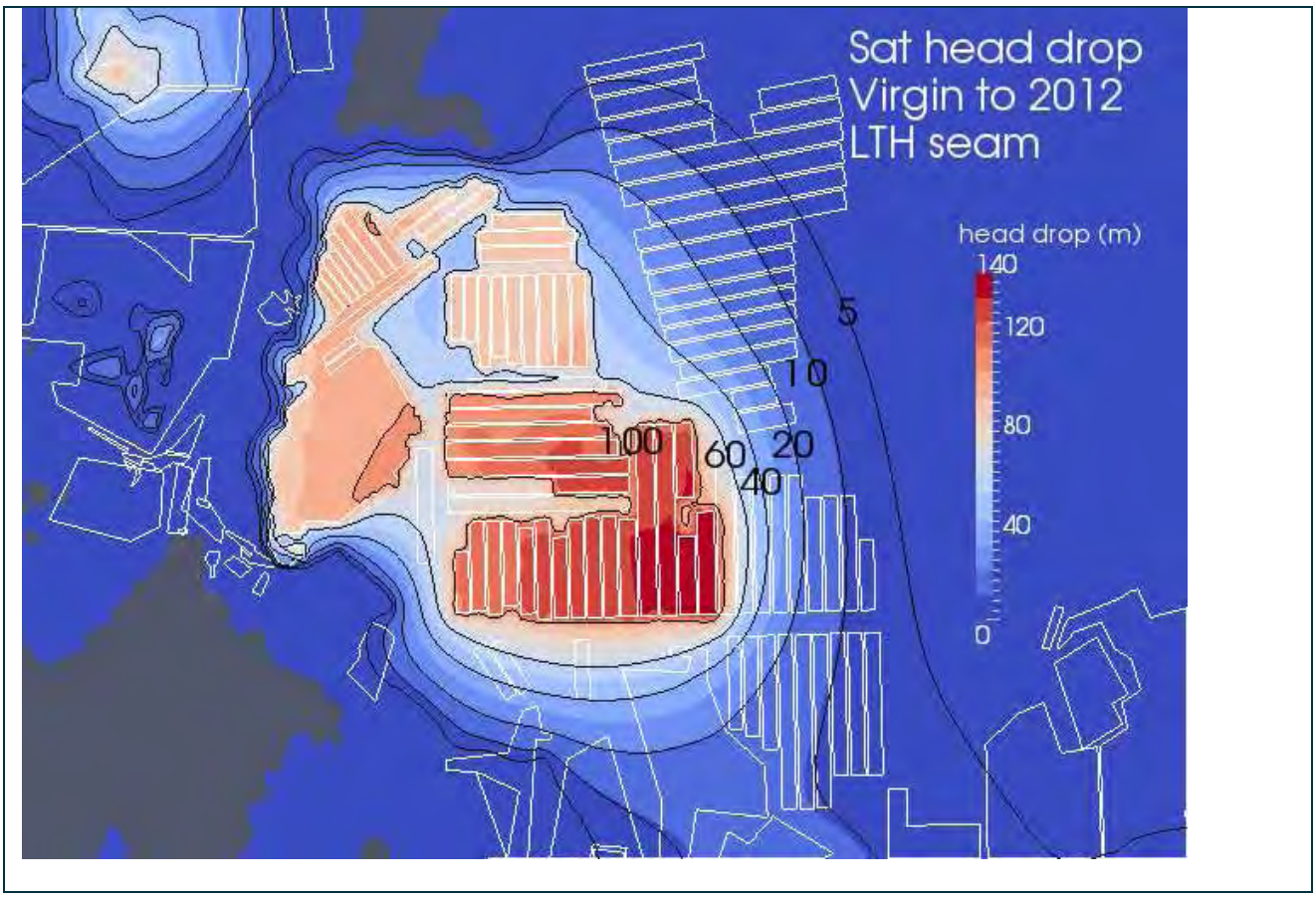

Figure 54 Distribution of drawdown in the Lithgow Seam at the end of validation period

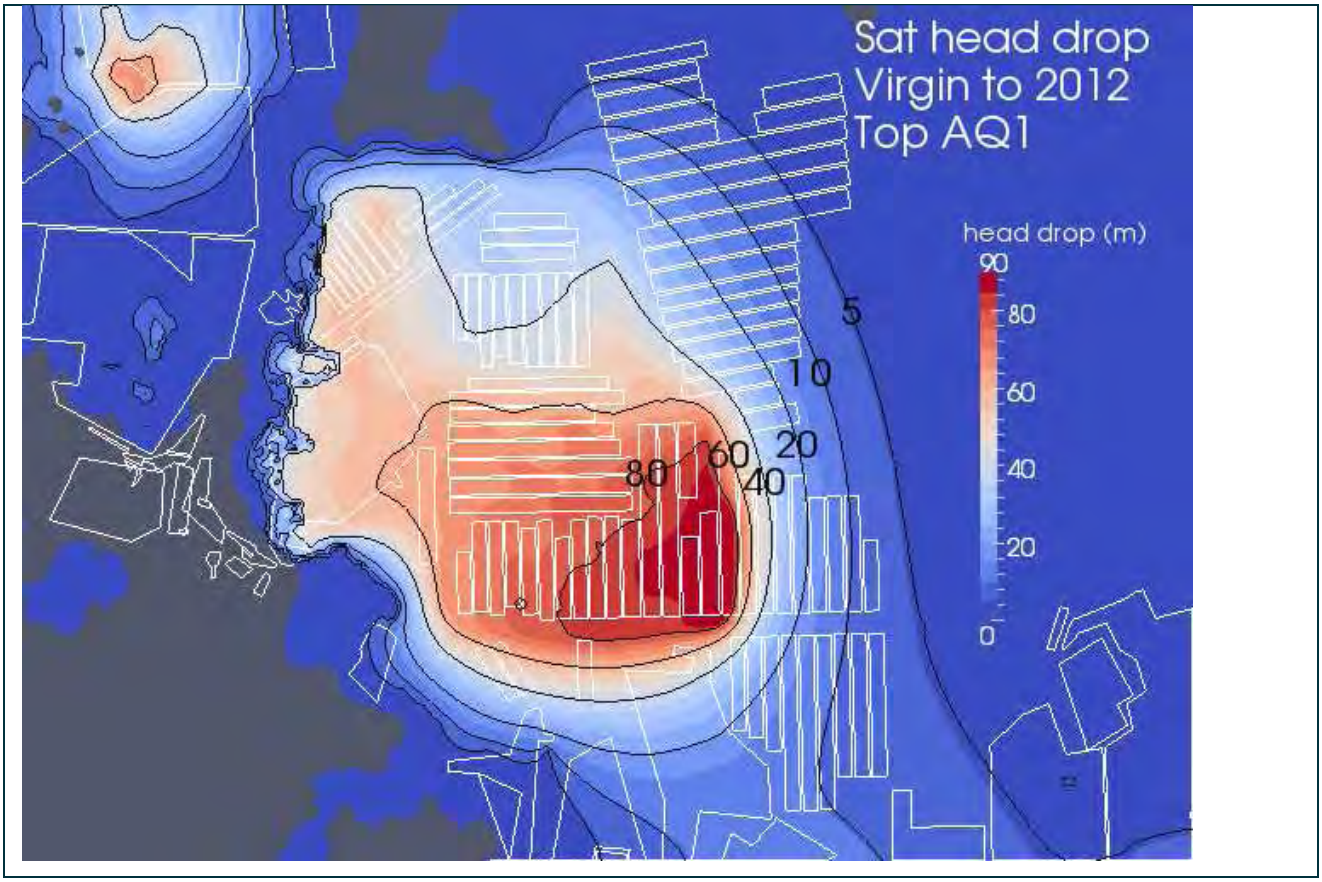

Figure 55 Distribution of drawdown at the top of AQ1 at the end of validation period

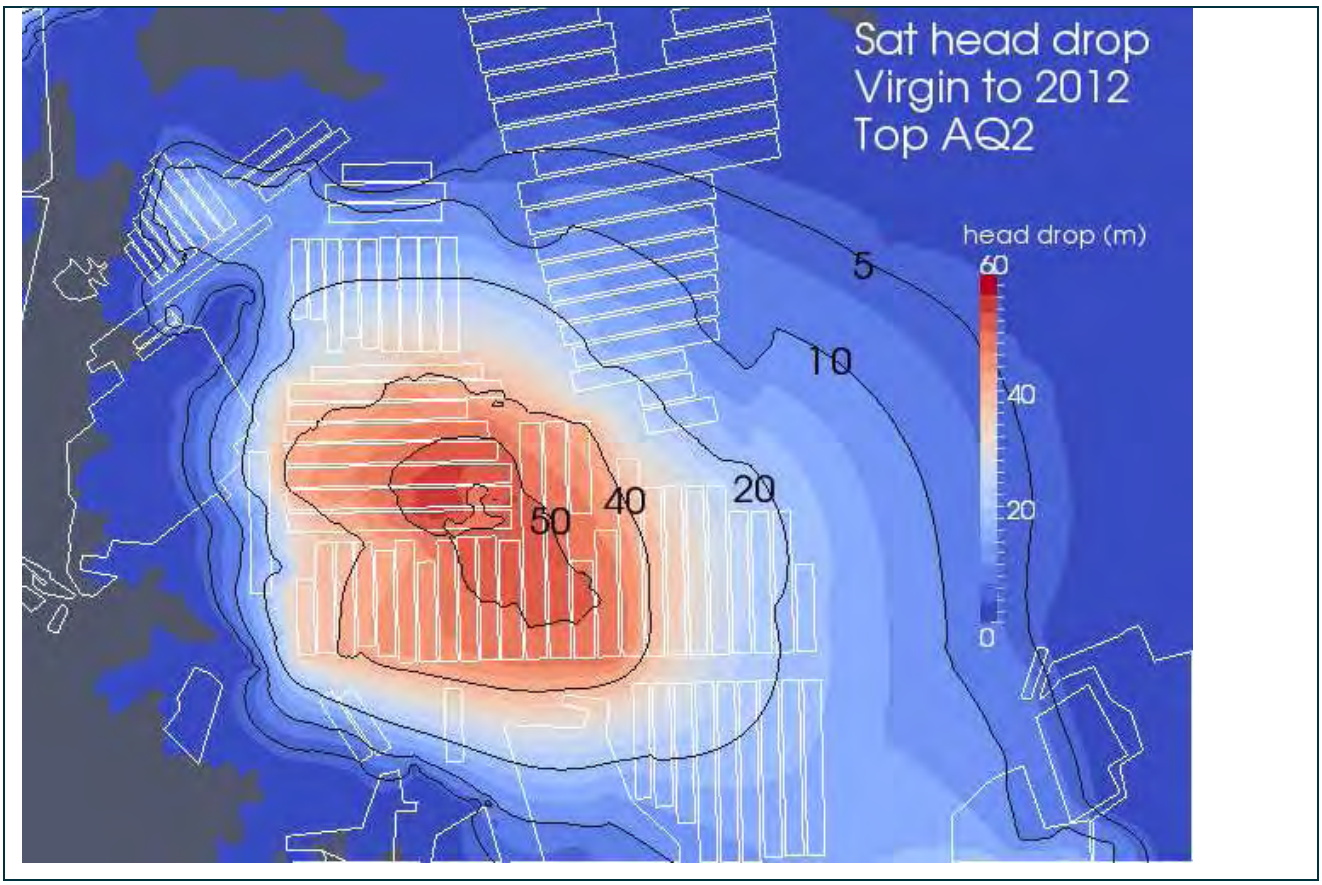

Figure 56 Distribution of drawdown at the top of AQ2 at the end of validation period

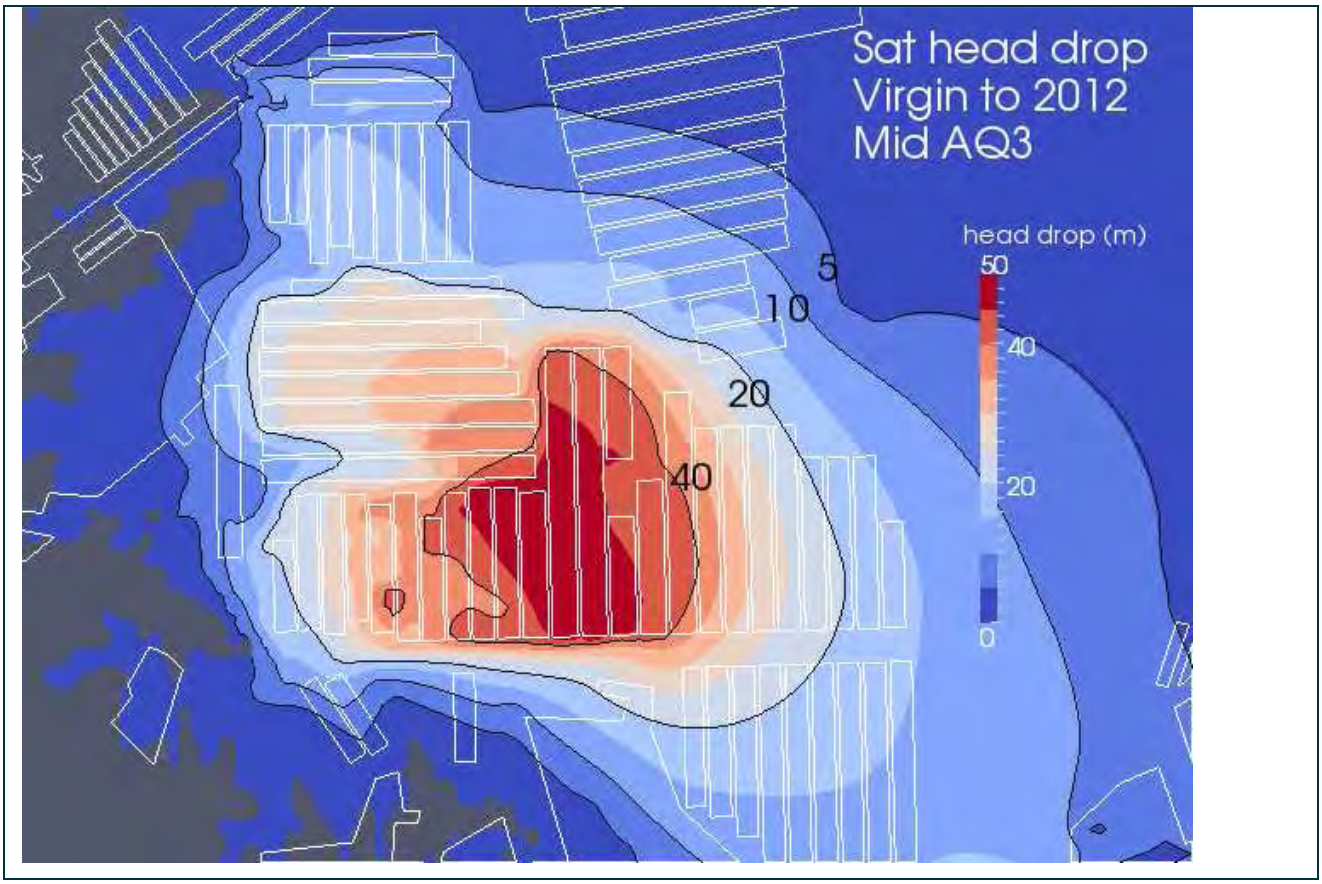

Figure 57 Distribution of drawdown at the middle of AQ3 at the end of validation period

Figure 58 Distribution of drawdown at the middle of AQ4 at the end of validation period

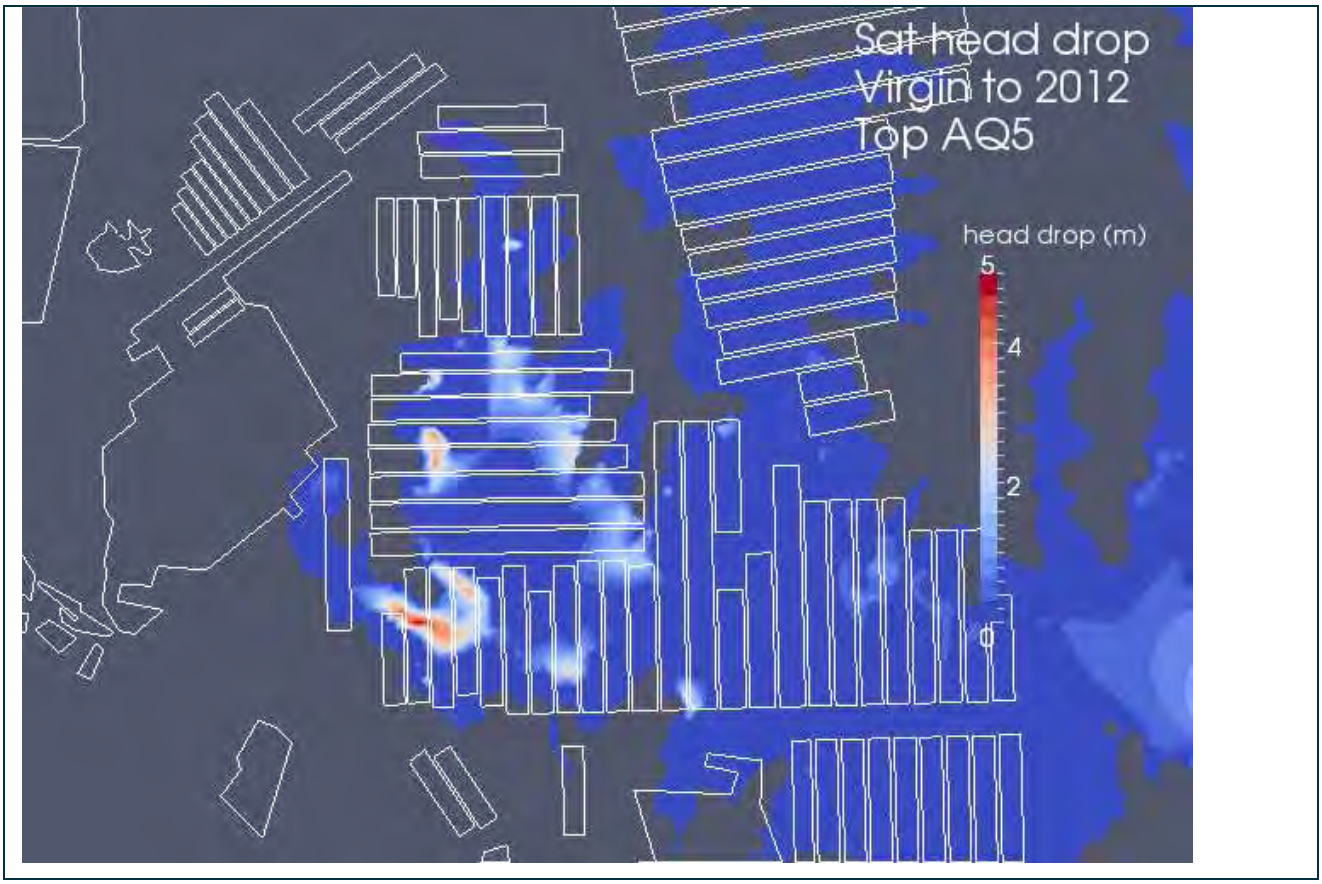

Figure 59 Distribution of drawdown at the top of AQ5 at the end of validation period

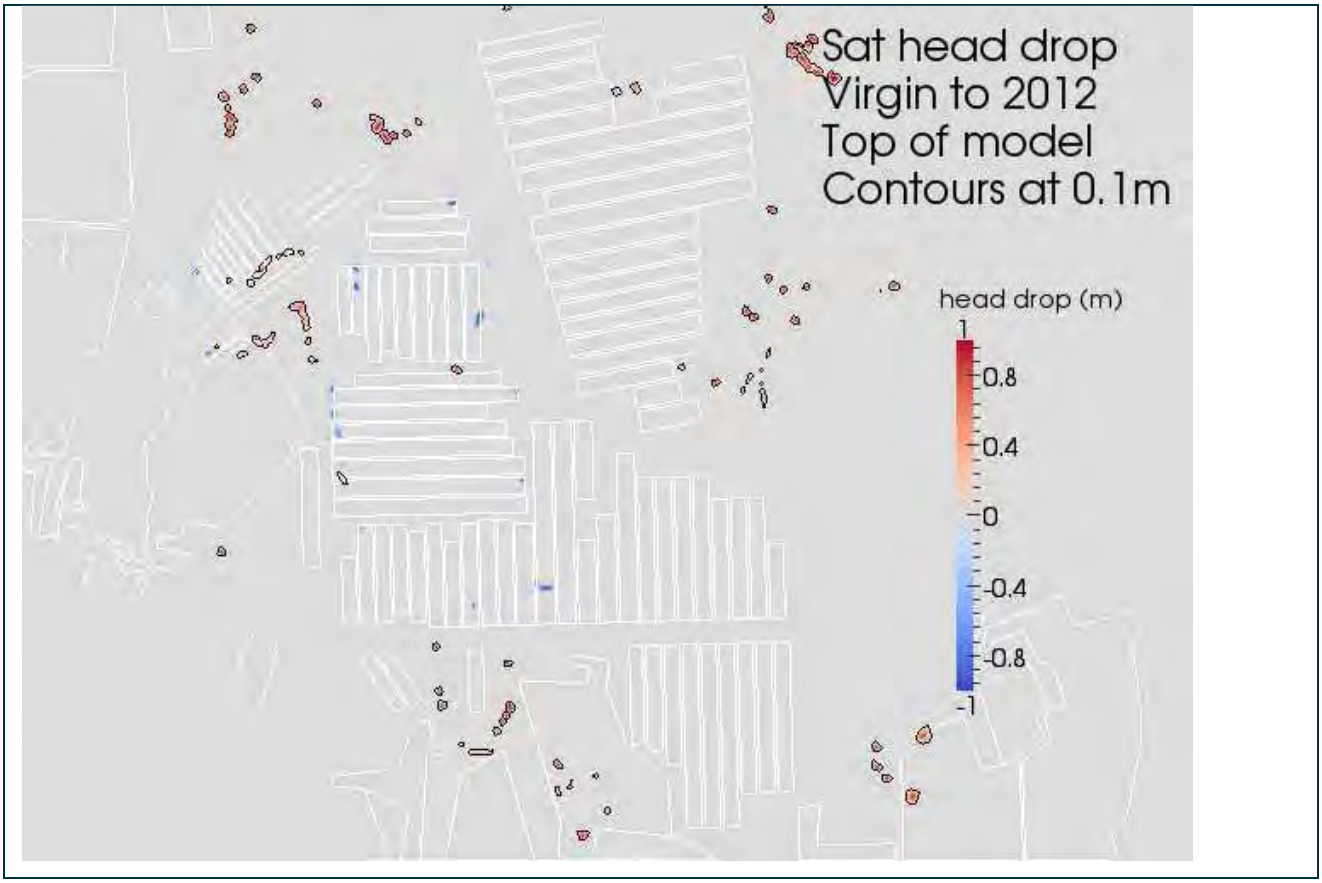

Figure 60 Distribution of saturated head drop at the ground surface at the end of validation period

Figure 61 shows the position of 6 vertical cross sections which are used in this report to study aspects of porepressure drawdown.

- NS, running from (235200E, 6309900N) to (235200E, 6303700N) across the currently-mined Angus Place panels.
- WE, running from (232000E, 6301700N) to (238800E, 6301700N) across the currently-mined Springvale panels.
- AB, running from (236000E, 6300000N) to (242500E, 6300000N) across the future Springvale panels.

The phreatic surfaces on vertical sections WE and NS before and after mining are shown in Figure 62 and Figure 63. Developments of unsaturated regions are evident in AQ1 and AQ3. The following observations can be made from Figure 62 and Figure 63:

- extensive desaturation occurs in AQ1,
- though porepressures do drop in AQ2 and AQ4 they remain virtually fully saturated,
- desaturation of the top of AQ3 starts from the hill sides and propagates inwards slowly (see Figure 62),
- although the upper aquifers, AQ4, AQ5 and AQ6 do become slightly desaturated, the upper aquitards, MYC, YS6 and SP4 are shielding them, and
- the magnitude of desaturation of the topmost strata varies depending upon whether it is a valley or a ridge
    - desaturation along the valley floors are negligible, and
    - desaturation under the ridges is larger.

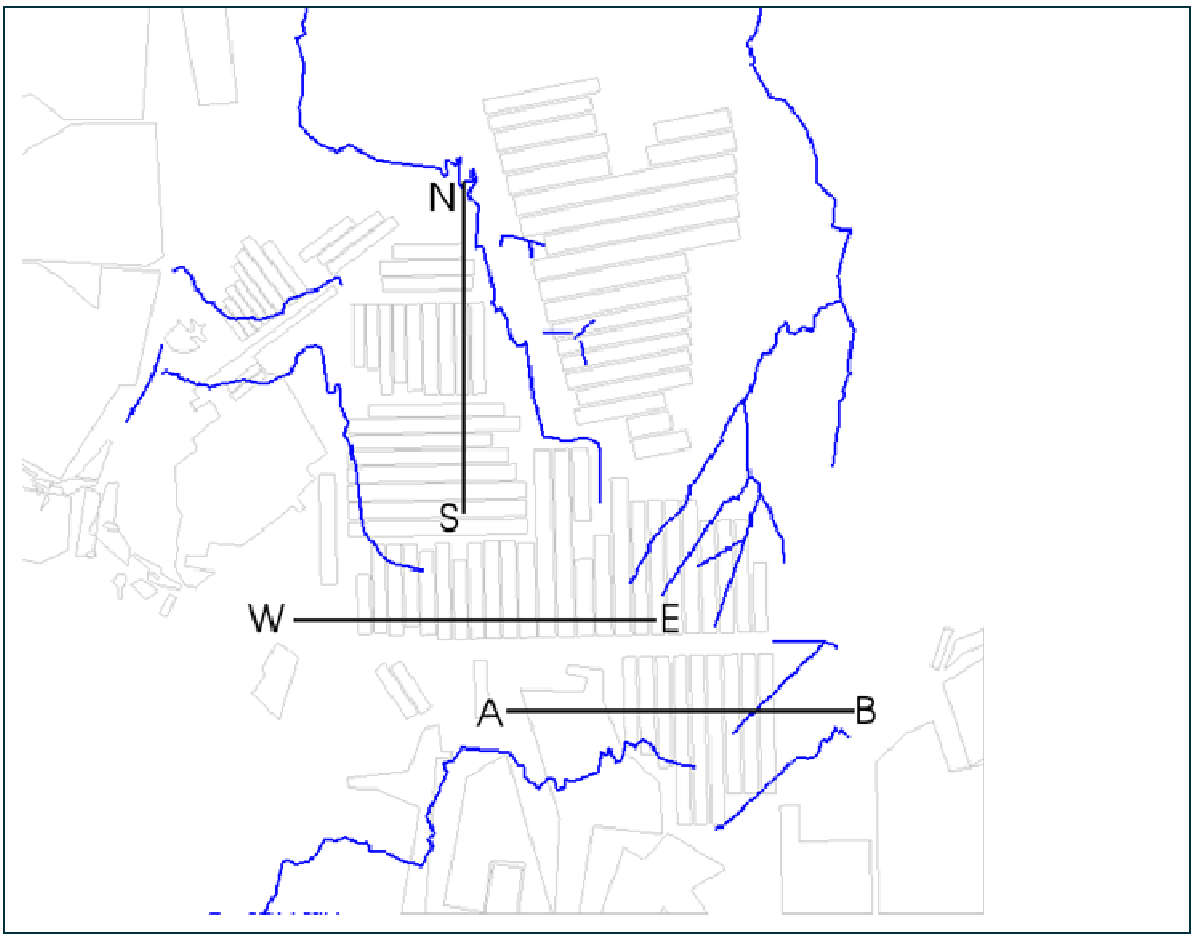

Figure 61 Location of cross-sections used for showing drawdown

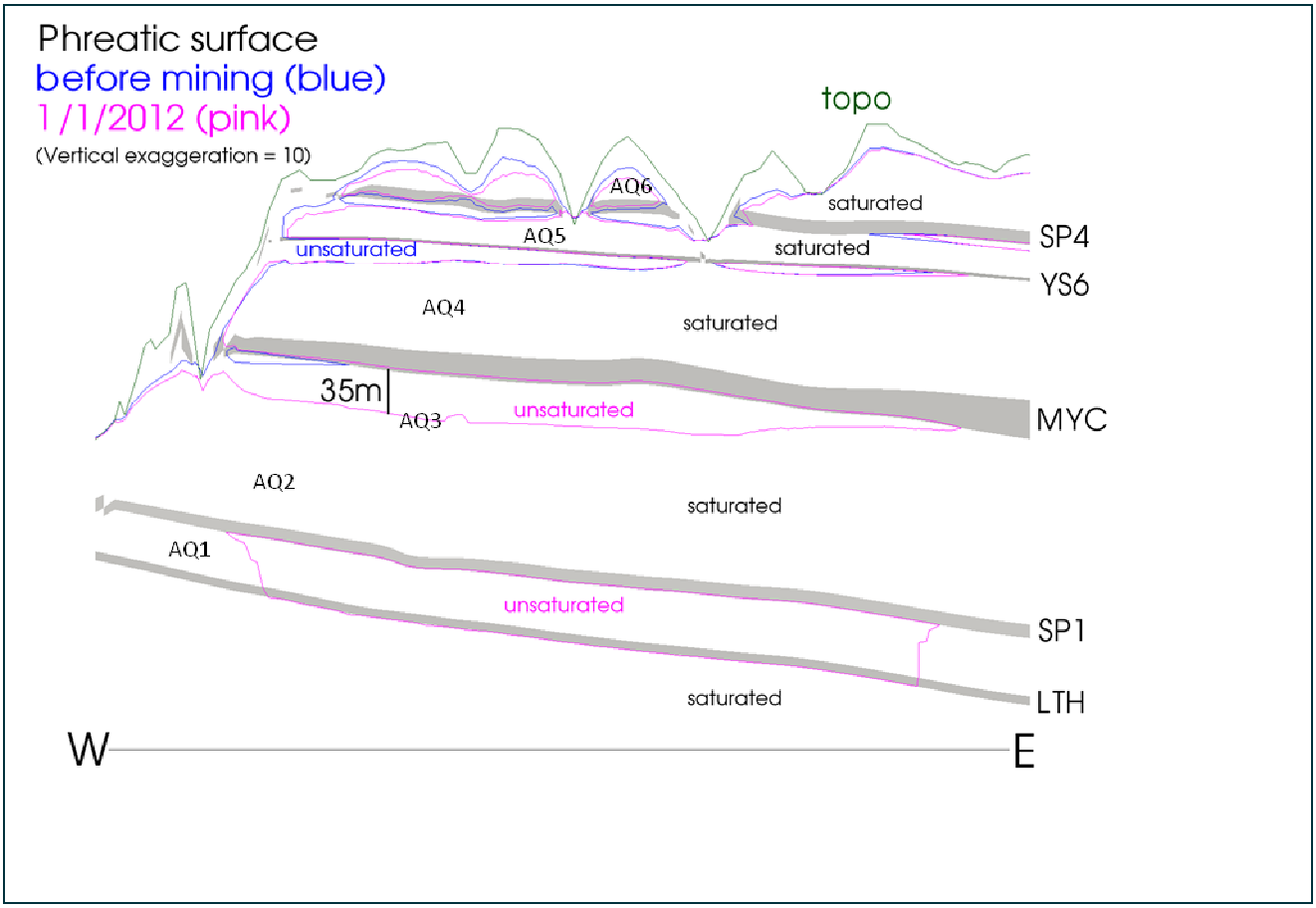

Figure 62 Phreatic surface before mining (blue lines) and after validation (pink lines) along W-E section

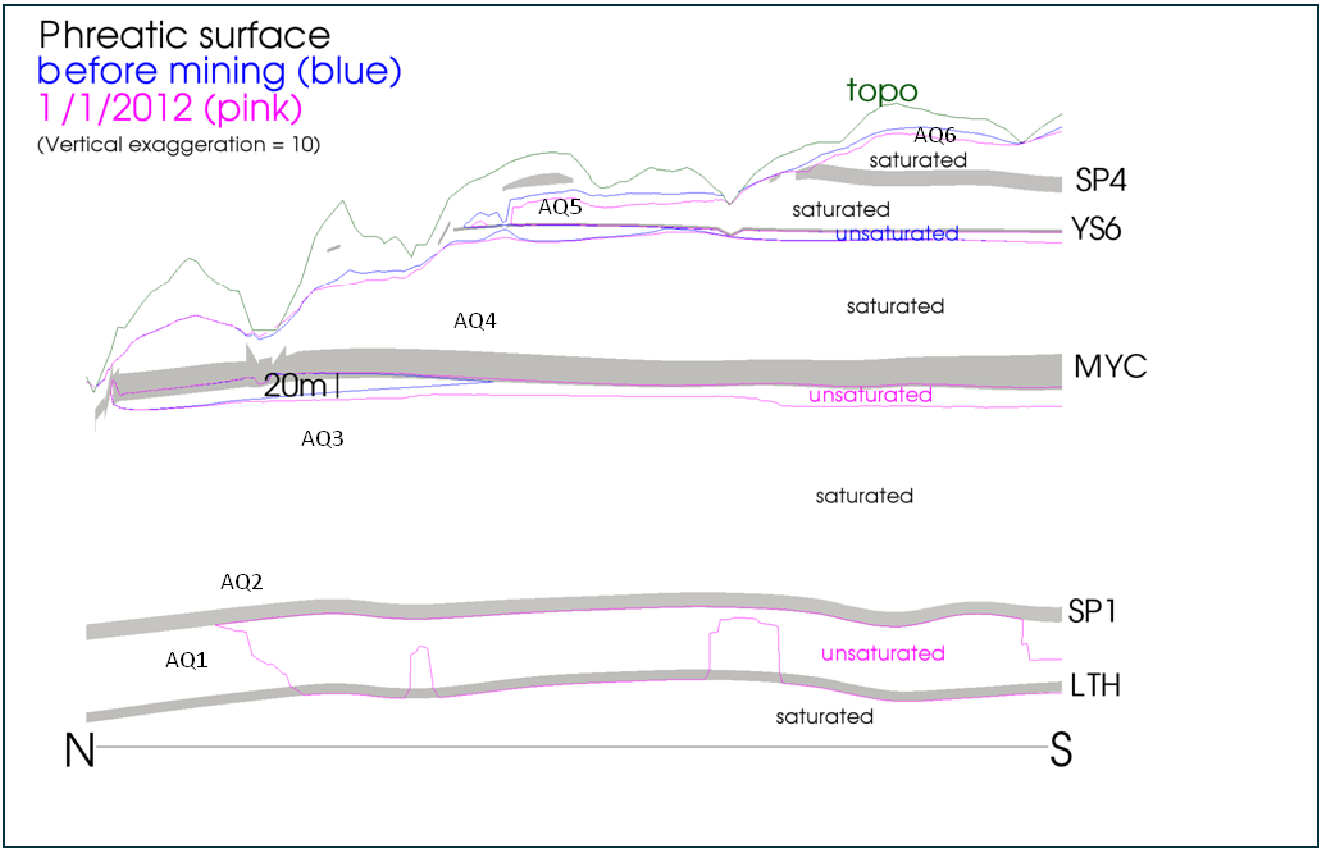

Figure 63 Phreatic surface before mining (blue lines) and after validation (pink lines) along N-S section

4 Prediction and Groundwater Impact Assessment

4.1 Scenarios simulated

Sections 3.6.4 describes the depressurisation of the strata due to climatic variation and past and present mining activities in the region until 2012. The proposed Angus Place Extension (APE) and SV longwall panels will result in further depressurisation of the strata in the region. The magnitude of depressurisation will vary from place to place depending upon the relative position and distance from the mining voids, the extent of mining induced strata fracturing, and the relative position of the aquitard layers. The extraction of APE and SV panels may induce:

- loss of pressures in the strata,
- potential change in baseflow to swamps and streams, and
- potential loss on pressures on private bores.

Table 28 Scenarios simulated in predictive and recovery modes

Scenarios	Description
Base case	This case continues from the calibration-validation model. The model was run using the actual rainfall data to October 2012 and then run with a constant rainfall recharge rate of 0.15mm/day. The Angus Place mine is completed: the remainder of AP_LW_970 is mined, AP_LW_980, and so on through to APE_19 which completes on 21 Dec 2032. The Springvale mine is completed: SPR_LW_415 is mined, and so on through to SPR_LW_503. The Clarence mine is also completed. The detailed mining schedule is given in Table 2. On 1 Jan 2033, all mine-water pumping is turned off and the mine voids are allowed to flood with water. Results are extracted at years 2083, 2133 and 2233, and then the model is allowed to reach a steady-state.
High rain	This case is identical to the Base case except that rainfall recharge is increased by 15% to 0.1725mm/day. This case is designed to address aspects of climate change.
Low rain	This case is identical to the Base case except that rainfall recharge is decreased by 15% to 0.1275mm/day.
High ET	This case is identical to the base except that ET_max is increased by 15% to 4.255mm/day. This case is designed to address aspects of climate change.
Low ET	This case is identical to “base” except that ET_max is decreased by 15% to 3.145mm/day.
No new	This case uses the same rainfall, ET and ramp function as the Base case. However, mining and mine-water pumping of Angus Place ceases at the end of AP_LW_900_west; and the mining and mine-water pumping of Springvale ceases at the end of SPR_LW_415 (see Figure 5 and Figure 6 and Table 2 for mine schedule). Clarence mine is still completed, and mine-water pumping is turned off upon completion. The mine voids are then allowed to flood with water. Results are extracted at years 2033, 2083, 2133 and 2233
No new APE	This case uses the same rainfall, ET and ramp function as the Base case. However, mining and mine-water pumping of Angus Place ceases at the end of AP_LW_900_west. Springvale and Clarence mine are completed as in the Base case, and mine-water pumping is turned off upon completion. Results are extracted at years 2033, 2083, 2133 and 2233.
No new SV	This case uses the same rainfall, ET and ramp function as the Base case. However, mining and mine-water pumping of Springvale mine ceases at the end of SPR_LW_415. Angus Place and Clarence mine are completed as in the Base case, and mine-water pumping is turned off upon completion. Results are extracted at years 2033, 2083, 2133 and 2233.

In order to assess the potential impacts of proposed extraction of APE and SV longwalls, a number of transient predictive numerical simulations are conducted from 1 January 2012. Extraction of the proposed APE and SV longwall panels is conducted as per the mine development schedule shown in Table 2; SPR_LW415 starts at March 2012 and APE_1 starts at June 2015. The extractions of the proposed SV and APE longwalls are completed in February 2025 and December 2032 respectively. Once the APE extraction is completed in December 2032, all the mines are assumed to be flooded and groundwater recovery was

simulated. The results of recovery simulations are extracted at 2083, 2133, 2233 and 2383 corresponding to 50 years, 100 years, 200 years and 350 years after completion of APE extraction respectively.

Eight different scenarios as shown in Table 28 are simulated; results described in this section refer to the Base case unless otherwise stated. In addition, further two scenarios as presented in Table 29 are simulated to study the effect of mining on the shallow groundwater using truncated permeability change ramp functions as described in Section 2.13.4.

Table 29 Scenarios simulated with Truncated-ramp functions to study the impacts on baseflow

Scenarios	Description
Truncated-ramp1	This case continues from the steady-state model. This case is identical to the base except the ramp function representing the mining induced changes in permeability is truncated to zero for heights above 230m above the mining seam so that there are no permeability changes in the upper strata.
Truncated-ramp2	This case continues from the steady-state model. This case is identical to the Base case except that the ramp function acts only on the vertical permeability component, while the horizontal component is maintained at the in situ value; the magnitude of change in vertical permeability is assumed to be the same as in the Base case.

4.2 Predictive simulation

4.2.1 Water balance during the predictive period

The average rates of recharge and discharge throughout the predictive period from 2012 to 2018 are given in Table 30. The average recharge to the groundwater system is 131 ML/day, comprising mainly rainfall recharge (125 ML/day) and leakage from swamps and streams into the groundwater system (6 ML/day).

The average groundwater discharge across the model is 163 ML/day. ET represents the major source of discharge (95 ML/day). Baseflow to swamps and streams is 15 ML/day.

A net loss of groundwater across the model boundary is 18 ML/day. The loss in fluid storage in the groundwater system is 32 ML/day. Mine inflow during the predictive period is 35 ML/day, which accounts for about 111% of the net loss in the fluid storage.

Table 30 Average rates of recharge and discharge 2012 to 2018

Component	Groundwater Inflow (Recharge) (ML/day)	Groundwater Outflow (Discharge) (ML/day)
Rainfall recharge	125.2	
Evapotranspiration		94.6
Swamps and rivers	5.7	14.6
Net outflow through model boundary (ML/day)	18.4 .	
Mine inflow (ML/day)		35.4
Total (ML/day)	130.9	163.1
Net Outflow (ML/day)	32.2	
Change in fluid volume contained (storage) in the model (ML/day)	-31.9	
Discrepancy	1.7x10-1 %	

The average rates of recharge and discharge throughout the predictive period from 2019 to 2024 are given in Table 31.

Table 31 Average rates of recharge and discharge 2019 to 2024

Component	Groundwater Inflow (Recharge) (ML/day)	Groundwater Outflow (Discharge) (ML/day)
Rainfall recharge	126.5	
Evapotranspiration		93.9
Swamps and rivers	6.24	14.8
Net outflow through model boundary (ML/day)	17.9	
Mine inflow (ML/day)		47.1
Total (ML/day)	132.7	173.7
Net Outflow (ML/day)	41.0	
Change in fluid volume contained (storage) in the model (ML/day)	-41.0	
Discrepancy	2.0x10-3 %	

The average recharge to the groundwater system is 133 ML/day, comprising mainly rainfall recharge (126 ML/day) and leakage from swamps and streams into the groundwater system (6ML/day).

The average groundwater discharge across the model is 174 ML/day. ET represents the major source of discharge (94 ML/day). Baseflow to the swamps and streams is 15 ML/day.

A net loss of groundwater across the model boundary is 18 ML/day. The loss in fluid storage in the groundwater system is 41 ML/day. Mine inflow during the predictive period is 47 ML/day, which accounts for about 115% of the net loss in the fluid storage.

Table 32 Average rates of recharge and discharge 2025 to 2032

Component	Groundwater Inflow (Recharge) (ML/day)	Groundwater Outflow (Discharge) (ML/day)
Rainfall recharge	126.5	
Evapotranspiration		91.8
Swamps and rivers	6.6	14.7
Net outflow through model boundary (ML/day)	17.7 .	
Mine inflow (ML/day)		50.5
Total (ML/day)	133.1	174.7
Net Outflow (ML/day)	41.6	
Change in fluid volume contained (storage) in the model (ML/day)	-41.6	
Discrepancy	1.4x10-3 %	

The average rates of recharge and discharge throughout the predictive period from 2025 to 2032 are given in Table 32. The average recharge to the groundwater system is 133 ML/day, comprising mainly rainfall recharge (126 ML/day) and leakage from swamps and streams into the groundwater system (7 ML/day). The average groundwater discharge across the model is 175 ML/day. ET represents the major source of discharge (95 ML/day). Baseflow to swamps and streams is 15 ML/day.

A net loss of groundwater across the model boundary is 18 ML/day. The loss in fluid storage in the groundwater system is 42 ML/day. Mine inflow during the predictive period is 50 ML/day, which accounts for about 121% of the net loss in the fluid storage.

Table 33 Comparison between the simulated rates of recharge and discharge during predictive period

Component	2012 to 2018		2018 to 2024		2025 to 2032	
	Groundwater Inflow (Recharge) (ML/day)	Groundwater Outflow (Discharge) (ML/day)	Groundwater Inflow (Recharge) (ML/day)	Groundwater Outflow (Discharge) (ML/day)	Groundwater Inflow (Recharge) (ML/day)	Groundwater Outflow (Discharge) (ML/day)
Rainfall recharge	125.2		126.5		126.5	
Evapotranspiration		94.6		93.9		91.8
Swamps and rivers	5.7	14.6	6.24	14.8	6.6	14.7
Net outflow through model boundary (ML/day)	18.4		17.9		17.7	
Mine inflow (ML/day)		35.4		47.1		50.5
Total (ML/day)	130.9	163.1	132.7	173.7	133.1	174.7
Net Outflow (ML/day)	32.2		41.0		41.6	
Change in fluid volume contained (storage) in the model (ML/day)	-31.9		-41.0		-41.6	
Discrepancy	1.7x10-1 %		2.0x10-3 %		1.4x10-3 %	

Table 33 presents a comparison between the simulated water balances at different times during the predictive period. The water balance within the groundwater system seems to remain fairly consistent throughout the validation (see Table 24) and predictive periods except for the mine inflows which increase from about 30 ML/day (2006 to 2012) to 35 ML/day (2013 to 2018), 47 ML/day (2019-2024) and 50 ML/day (2024-2032). The groundwater recharge fluctuates around 131 ML/day and evapotranspiration fluctuates around low to mid 90 ML/day. The discharge to swamps/stream remains virtually steady at around 15 ML/day and leakage from streams/swamps averages around 6 ML/day.

4.2.2 Mine water inflow prediction

Figure 64 to Figure 66 show the predicted mine water inflow for the Angus Place and Springvale longwall operations to 2032. The average life of mine water inflow is predicted to increase from about 300 l/s currently and average out around 400 l/s to 500 l/s between 2020 to 2032 (Figure 64). Figure 65 and Figure 66 present predicted mine water inflows into the Springvale mine (with and without APE longwalls) and into Angus Place mine (with and without the future SV longwalls) respectively. It can be seen that the extraction of APE has no effect on the mine water inflow into SV panels and vice versa i.e. for mine water-make, extractions of APE and SV panels have a negligible effect on each other.

In 2012, CSIRO conducted coupled deformation and groundwater flow simulations for both Angus Place and Springvale Collieries to provide estimates of water inflows into the mines (Adhikary and Khanal, 2012). Figure 67 presents a comparison between the results obtained in this study and those obtained from the coupled simulations. The mine water inflow predicted in this study can be seen to agree generally well with the coupled simulations results. In the coupled simulations two values of mine inflows were produced encompassing two possible value of strata plasticity dependent permeability change function (see Adhikary and Khanal, 2012). The coupled model seems to over predict the mine inflow between 2023 and 2027 compared to the results obtained in this study.

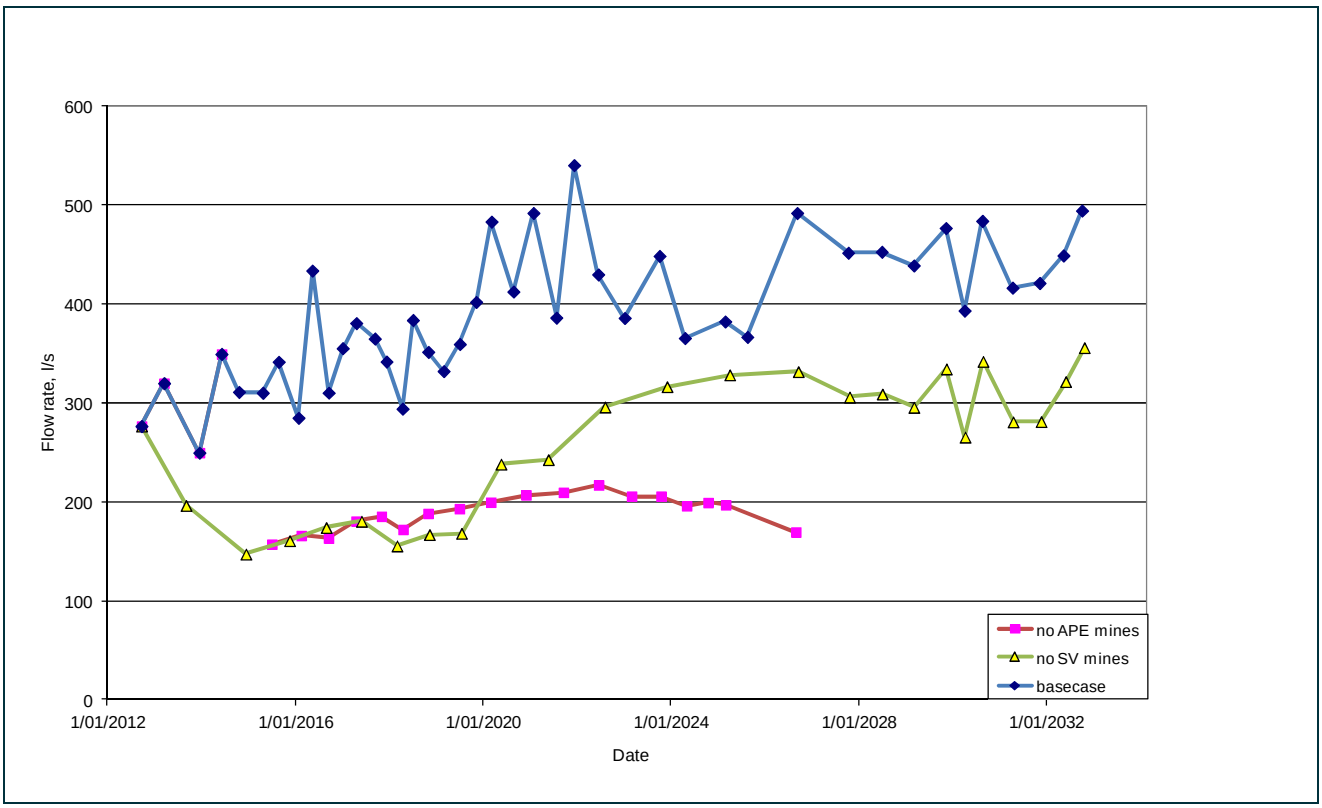

Figure 64 Predicted mine water inflow for the entire AP and SV Collieries combined: (i) blue dots (Base case) - all AP and SV panels mined, (ii) red dots - only new SV panels mined (APE is not mined) and (iii) yellow dots only APE panels mined (no new SV panels mined)

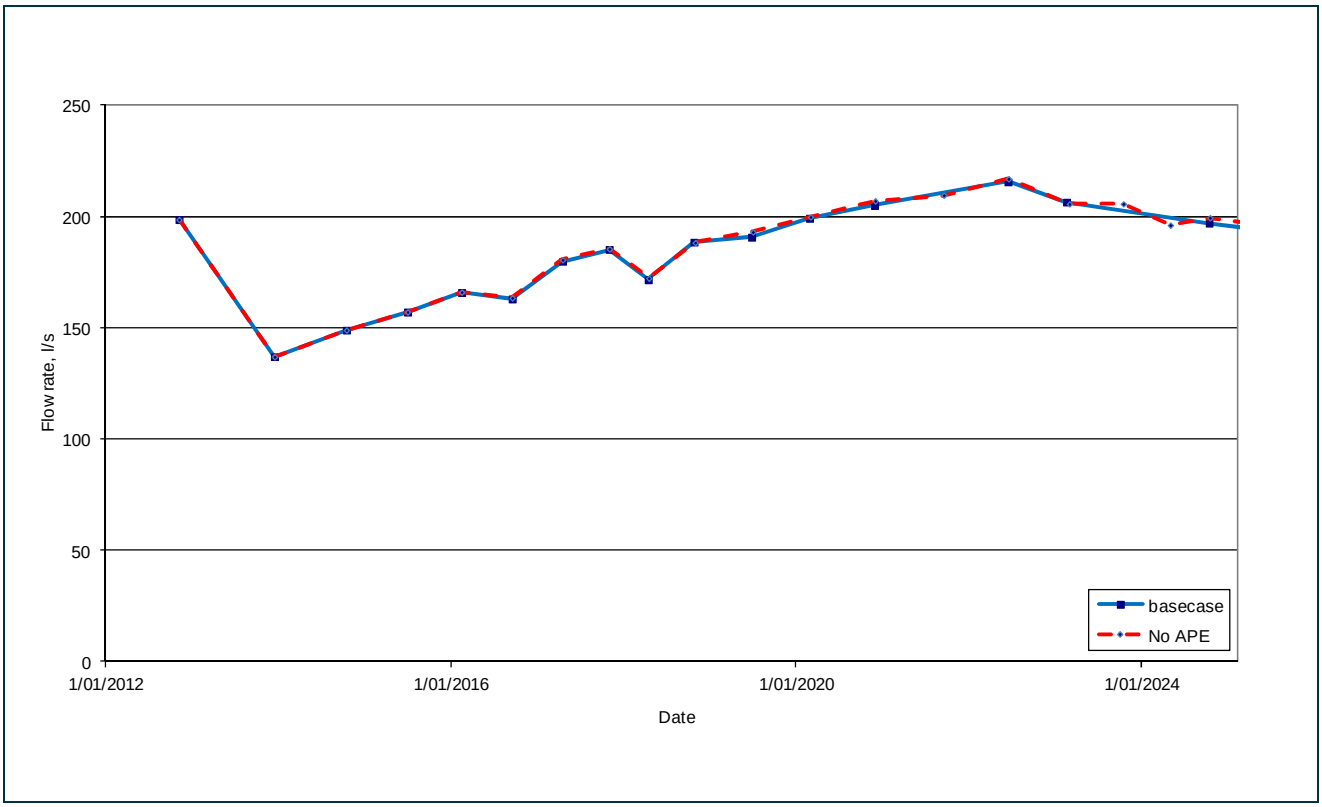

Figure 65 Predicted mine water inflow into the Springvale operations only

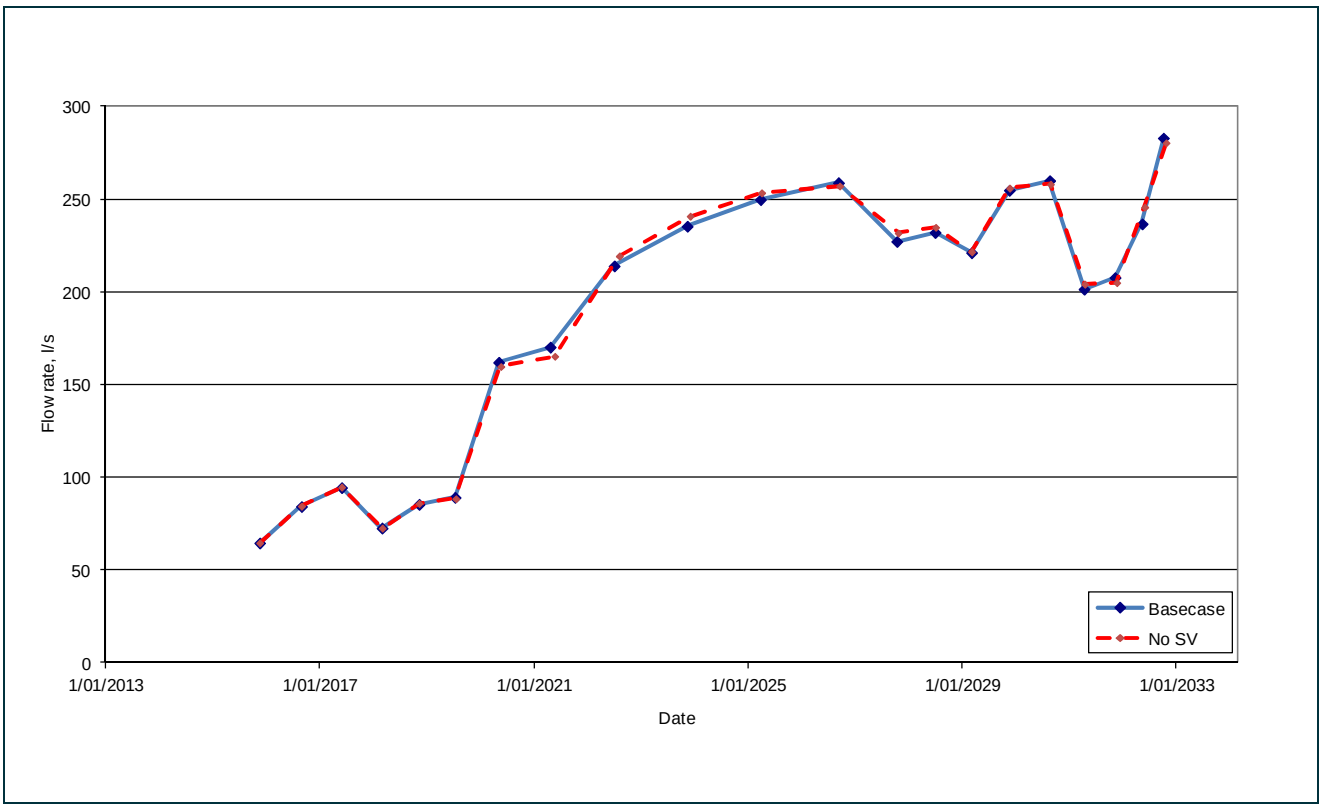

Figure 66 Predicted mine water inflow into APE only

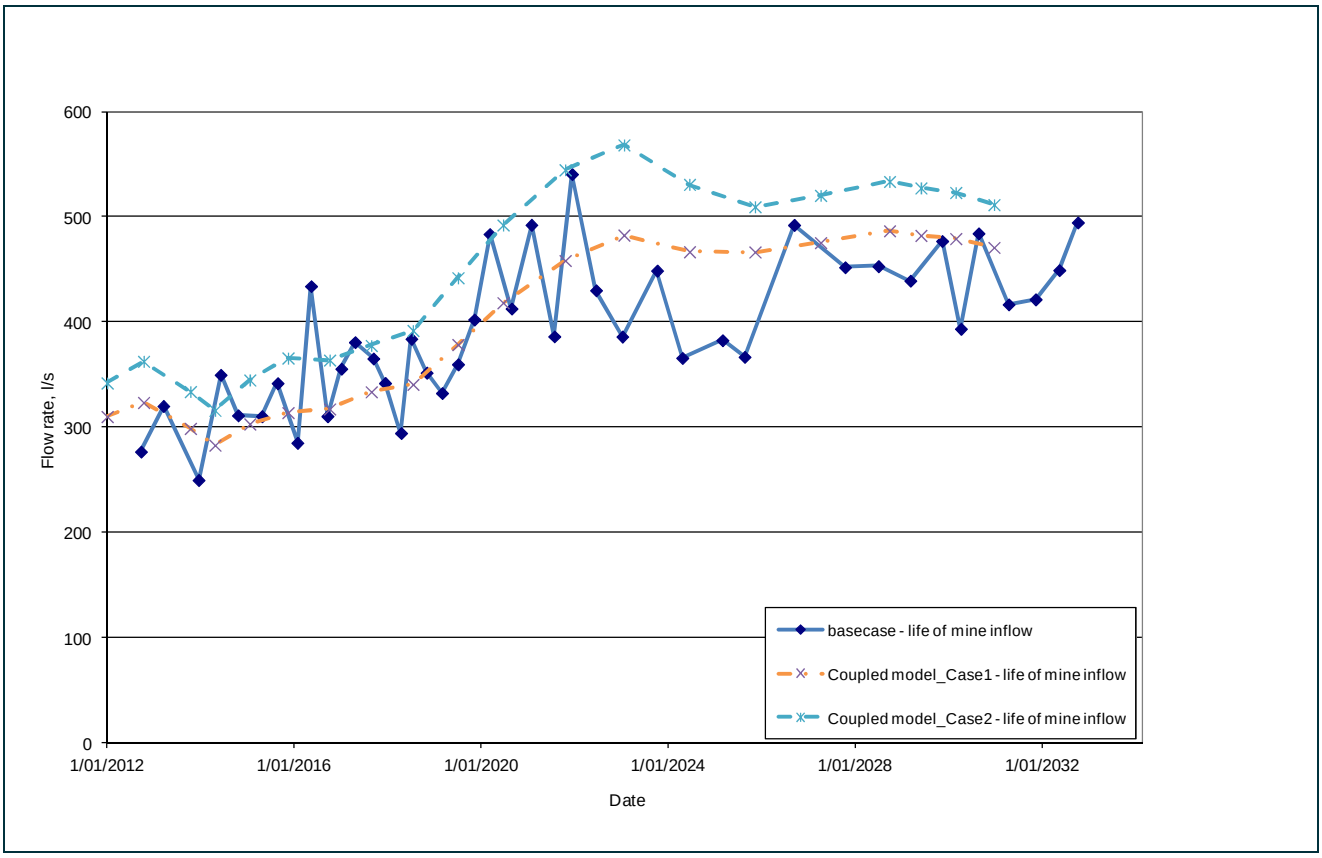

Figure 67 A comparison of mine water inflow predictions obtained from the coupled deformation-groundwater flow modelling and the uncoupled groundwater flow only modelling

4.2.3 Predicted changes in baseflow to swamps and streams

Appendix C provides simulated groundwater discharge plots for the twenty-one swamps and streams modelled explicitly in this study (Figures C2 to C22 in Appendix C). The swamps and streams simulated are

represented by a number of finite element nodes in the model. Naturally, the number of nodes used to represent one swamp/stream will vary from the number of nodes used to represent another swamp/stream depending on the size of the swamps/streams.

It is worthwhile to note that the simulated baseflow will be sensitive to assumed ramp function representing the mining induced permeability changes at shallow depths. As described in Section 2.13.4, two additional scenarios (i.e. truncated-ramp1 and truncated-ramp2) representing the possible variations in magnitude and extent of cracking at shallow depths are simulated. The following observations can be made from these three models:

- Base case model – predicts an increase in baseflow to a number of swamps and creeks following mining. This may be attributed to mining induced delamination of near surface strata and recovery of water levels to higher elevations with respect to pre-mining levels.
- Truncated-ramp1 model – as expected, this model generally predicts the least impact on baseflow among the three models.
- Truncated-ramp2 model – it generally predicts intermediate impact on baseflow with respect to the Base case and truncated-ramp1 models; some of the predicted impacts on baseflow from this model are similar to those obtained from the truncated-ramp1 model while some are similar to those predicted by the Base case model.

The actual mining impact on baseflow is expected to lie within the bounds predicted by these three models.

Figure 68 and Figure 69 show the baseflow balance to Carne Creek and Wolgan River. The simulated discharge from the Base model to Carne Creek is about 6.4 ML/day at the pre-mining condition, which then drops to 6 ML/day in 2032. After the completion of mining the baseflow discharge to the river increase again; in 2232 the simulated discharge is 6.7 ML/day. The increase in baseflow discharge is mainly due to the increase in water levels during the recovery period. Both the 'Truncated-ramp1' and 'Truncated-ramp2' models are predicting similar trend in baseflow decrease immediately after mining and then gradually increasing during recovery period. The 'Truncated-ramp1' model generally predicts the least increase in baseflow by 2380.

The simulated discharge to Wolgan River is about 1.3 ML/day at the pre-mining condition, which then increases to 1.7 ML/day in mid 2012. The increase in baseflow discharge is mainly due to the mining induced delamination of strata lying above the mining voids resulting in increase in horizontal conductivity. The discharge is predicted to subsequently decrease to 1.4 ML/day, 1.2 ML/day and 1 ML/day in 2022, 2032 and 2064 respectively. All three models (i.e. Base case, Truncated-ramp1 and Truncated-ramp2) show similar trends of decrease in baseflow with time. The Base case model predicts slightly larger decrease in baseflow followed by the truncated-ramp2 model (intermediate) and the truncated-ramp1 model (least decrease).

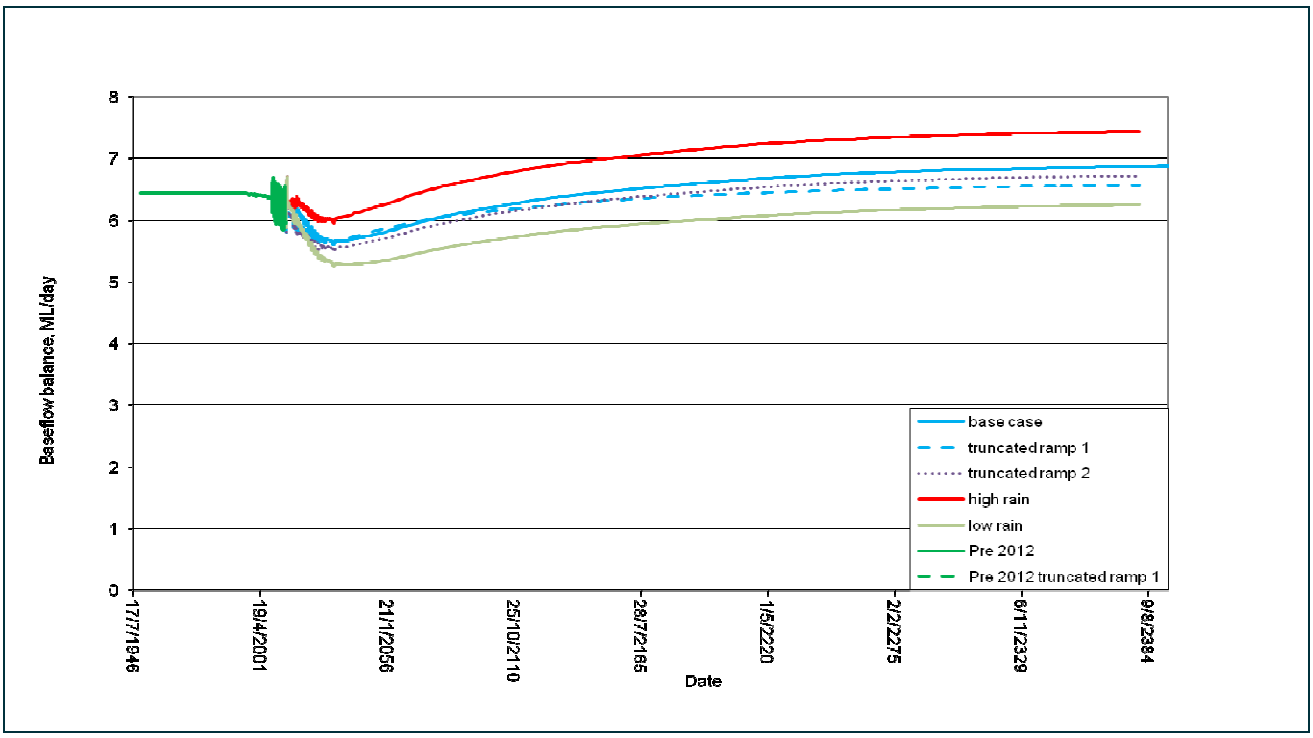

Figure 68 Simulated total baseflow balance to Carne Creek reach included in the model (CA1+CA2+CA3+CA4+CA5+CW5+CW+GGS+GGSE, see Table 5 for notation)

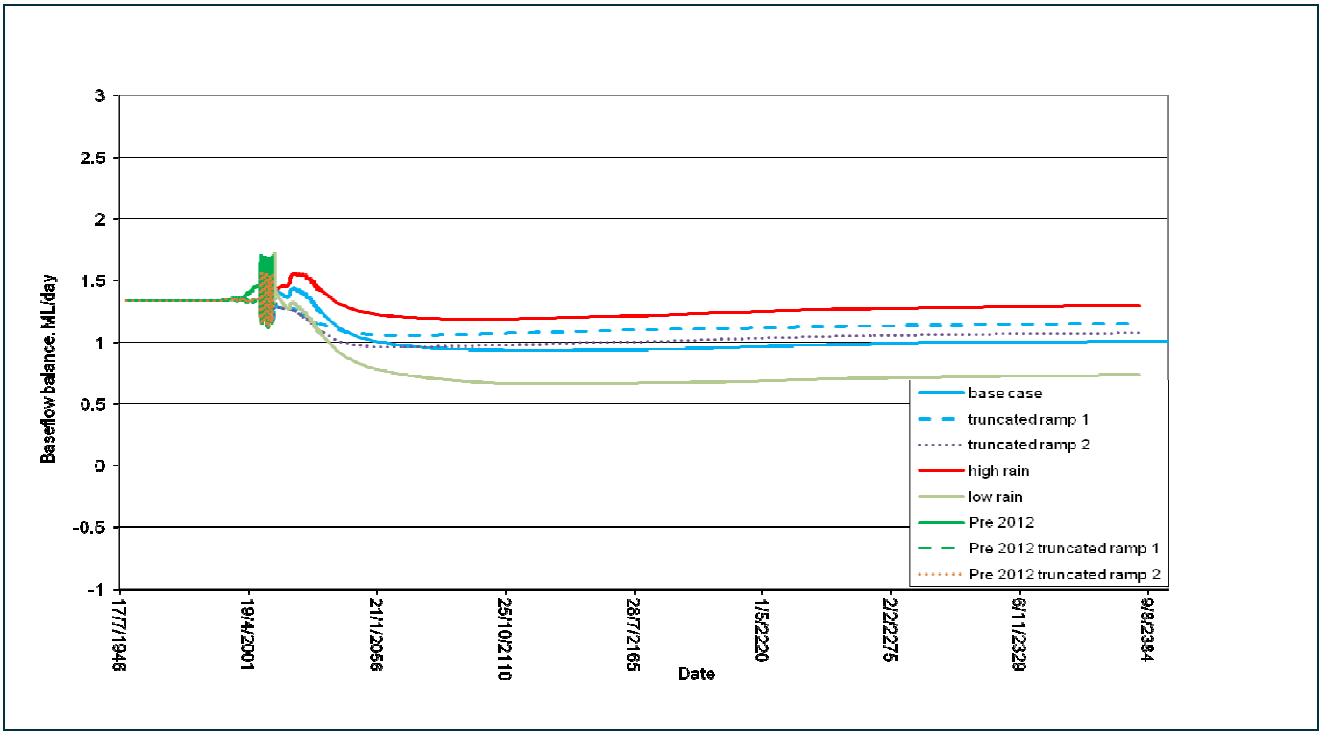

Figure 69 Simulated total baseflow balance to Wolgan River reach included in the model (WOL+TWG+TRS+SSS, see Table 5 for notation)

Table 34 to Table 36 enumerates the changes in the groundwater discharge to the swamps/streams before, during and after mining for the Base case, Truncated-ramp1 and Truncated-ramp2 models. Table 37 enumerates the simulated maximum change (loss or gain) in baseflow.

Table 34 Predicted groundwater discharge to swamps and streams simulated in this study (Base case)

Swamps and streams simulated in this study	Groundwater discharge (ML/day)						
	Pre-mining	Dec 2012	Seasonal variation	2022	2032	2064	Minimum
CA2 (includes Carne Central Swamp)	1.30	1.14	0.14	1.14	0.99	0.89	0.90
Carne West Swamp	0.02	0.02	0.01	0.02	0.05	0.05	0.04
Carne Creek Total	6.44	5.91	0.96	5.91	5.89	5.62	5.90
Gang Gang South East	-0.05	-0.06	0.02	-0.06	-0.22	-0.23	-0.23
Gang Gang Swamp South	-0.05	-0.06	0.02	-0.06	-0.01	-0.08	-0.08
Kangaroo Swamp	0.01	0.02	0.00	0.02	0.02	0.01	0.01
Kangaroo Creek (KC1)	0.30	0.00	0.24	-0.07	-0.13	-0.07	-0.13
Kangaroo Creek (KC2)	0.07	0.11	0.24	0.12	0.10	0.08	0.07
Lamb Creek	0.17	0.17	0.02	0.17	0.11	0.10	0.13
Long Swamp	-0.07	-0.07	0.01	-0.07	-0.07	-0.07	-0.07
Marrangaroo Creek	0.93	0.72	0.30	0.72	0.71	0.65	0.60
Nine Mile Swamp	0.02	0.01	0.01	0.01	0.02	0.02	0.02
Paddy's Creek	0.17	0.16	0.01	0.16	0.16	0.16	0.17
Pine Swamp	0.09	0.09	0.01	0.09	0.21	0.17	0.15
Tri-Star Swamp	0.05	0.04	0.01	0.04	0.14	0.11	0.06
Twin Gully Swamp	0.08	0.07	0.01	0.07	0.07	0.09	0.06
Sunnyside Swamp	0.10	0.10	0.01	0.10	0.11	0.10	0.09
Wolgan River Total	1.34	1.29	0.55	1.42	1.24	0.98	0.93

Table 35 Predicted groundwater discharge to swamps and streams simulated in this study (Truncated ramp1)

Swamps and streams simulated in this study	Groundwater discharge (ML/day)					
	Pre-mining	Dec 2012	2022	2032	2064	Minimum
CA2 (includes Carne Central Swamp)	1.30	1.14	0.99	0.90	0.93	0.89
Carne West Swamp	0.02	0.02	0.02	0.02	0.02	0.02
Carne Creek Total	6.44	5.91	5.79	5.63	5.95	5.60
Gang Gang South East	-0.05	-0.06	-0.06	-0.06	-0.06	-0.06
Gang Gang Swamp South	-0.05	-0.06	-0.06	-0.06	-0.06	-0.06
Kangaroo Swamp	0.01	0.01	0.01	0.01	0.01	0.01
Kangaroo Creek (KC1)	0.30	-0.09	-0.11	-0.16	-0.09	-0.16
Kangaroo Creek (KC2)	0.07	0.06	0.07	0.07	0.07	0.06
Lamb Creek	0.17	0.08	0.08	0.07	0.08	0.07
Long Swamp	-0.07	-0.08	-0.07	-0.07	-0.07	-0.07
Marrangaroo Creek	0.93	0.73	0.72	0.68	0.67	0.66
Nine Mile Swamp	0.02	0.01	0.02	0.02	0.02	0.02
Paddy's Creek	0.17	0.16	0.16	0.16	0.16	0.16
Pine Swamp	0.09	0.09	0.09	0.09	0.09	0.09
Tri-Star Swamp	0.05	0.04	0.04	0.04	0.04	0.04
Twin Gully Swamp	0.08	0.07	0.07	0.07	0.07	0.07
Sunnyside Swamp	0.10	0.09	0.10	0.10	0.10	0.10
Wolgan River Total	1.34	1.18	1.25	1.15	1.06	1.06

Table 36 Predicted groundwater discharge to swamps and streams simulated in this study (Truncated ramp2)

Swamps and streams simulated in this study	Groundwater discharge (ML/day)					
	Pre-mining	Dec 2012	2022	2032	2064	Minimum
CA2 (includes Carne Central Swamp)	1.30	1.14	0.98	0.87	0.87	0.85
Carne West Swamp	0.02	0.02	0.02	0.02	0.02	0.02
Carne Creek Total	6.44	5.91	5.71	5.52	5.80	5.50
Gang Gang South East	-0.05	-0.06	-0.08	-0.08	-0.08	-0.08
Gang Gang Swamp South	-0.05	-0.06	-0.08	-0.09	-0.09	-0.09
Kangaroo Swamp	0.01	0.00	0.00	0.00	0.00	0.00
Kangaroo Creek (KC1)	0.30	-0.19	-0.26	-0.31	-0.23	-0.31
Kangaroo Creek (KC2)	0.07	0.06	0.07	0.07	0.07	0.07
Lamb Creek	0.17	0.12	0.10	0.09	0.12	0.08
Long Swamp	-0.07	-0.08	-0.07	-0.07	-0.07	-0.07
Marrangaroo Creek	0.93	0.72	0.70	0.63	0.61	0.60
Nine Mile Swamp	0.02	0.01	0.02	0.02	0.02	0.02
Paddy's Creek	0.17	0.16	0.16	0.16	0.16	0.16
Pine Swamp	0.09	0.09	0.09	0.09	0.09	0.09
Tri-Star Swamp	0.05	0.04	0.04	0.03	0.02	0.00
Twin Gully Swamp	0.08	0.07	0.07	0.07	0.06	0.05
Sunnyside Swamp	0.10	0.10	0.10	0.10	0.10	0.10
Wolgan River Total	1.34	1.18	1.24	1.09	0.96	0.96

Table 37 Maximum loss in baseflow

Swamps and streams simulated in this study	Maximum loss in groundwater discharge (ML/day)						Comment
	Base case		Truncated ramp1		Truncated ramp2		
	ML/day	%	ML/day	%	ML/day	%	
CA2 (includes Carne Central Swamp)	0.27	24	0.25	22	0.29	25	22 – 25% drop
Carne West Swamp	Increase in baseflow		0.000	0.000	0.000	0.000	Very small volume
Carne Creek Total	Increase in baseflow		Increase in baseflow		Increase in baseflow		Small increase
Gang Gang South East	0.17	307	0.002	4	0.025	44	Leaky swamp (increase in leakage 4 to 307%)
Gang Gang Swamp South	0.02	37	0.000	0.000	0.032	57	Leaky swamp (increase in leakage 0 to 57%); very small volume
Kangaroo Swamp	0.004	25	0.000	0.000	0.002	50.000	0 to 50% drop; very small volume
Kangaroo Creek (KC1)	0.13	Division by a small number	0.07	86	0.12	65	65 to 86% drop, very small volume
Kangaroo Creek (KC2)	0.03	32	0.000	0.000	Increase in baseflow		0 to 32% drop, very small volume
Lamb Creek	0.08	46	0.010	12	0.04	30	12 - 46% drop; very small volume
Long Swamp	0.000	0.000	0.000	0.000	0.000	0.000	No change
Marrangaroo Creek	0.13	17	0.07	10	0.12	16	9 – 17% drop

Nine Mile Swamp	Increase in baseflow		Increase in baseflow		Increase in baseflow		Increase, very small volume
Paddy's Creek	0.002	1	0.001	0.6	0.004	2	Very small change
Pine Swamp	0.000	0.3	Increase in baseflow		Increase in baseflow		Increase
Tri-Star Swamp	0.04	93	0.006	13	0.040	91	13 to 91% drop, very small volume
Twin Gully Swamp	0.030	41	0.002	3	0.021	28	3 to 41% drop, very small volume
Sunnyside Swamp	0.007	7	Increase in baseflow		Increase in baseflow		Small increase
Wolgan River Total	0.36	28	0.120	10	0.22	18	10 to 27% drop

Figure 70 shows YS6 outcrops in the Angus Place and Springvale mining region. The YS6 layer is found to be the most important aquitard. The swamps and streams lying above the YS6 layer are much less impacted by mining than the swamps and creeks that are unsupported by the YS6 layer underneath.

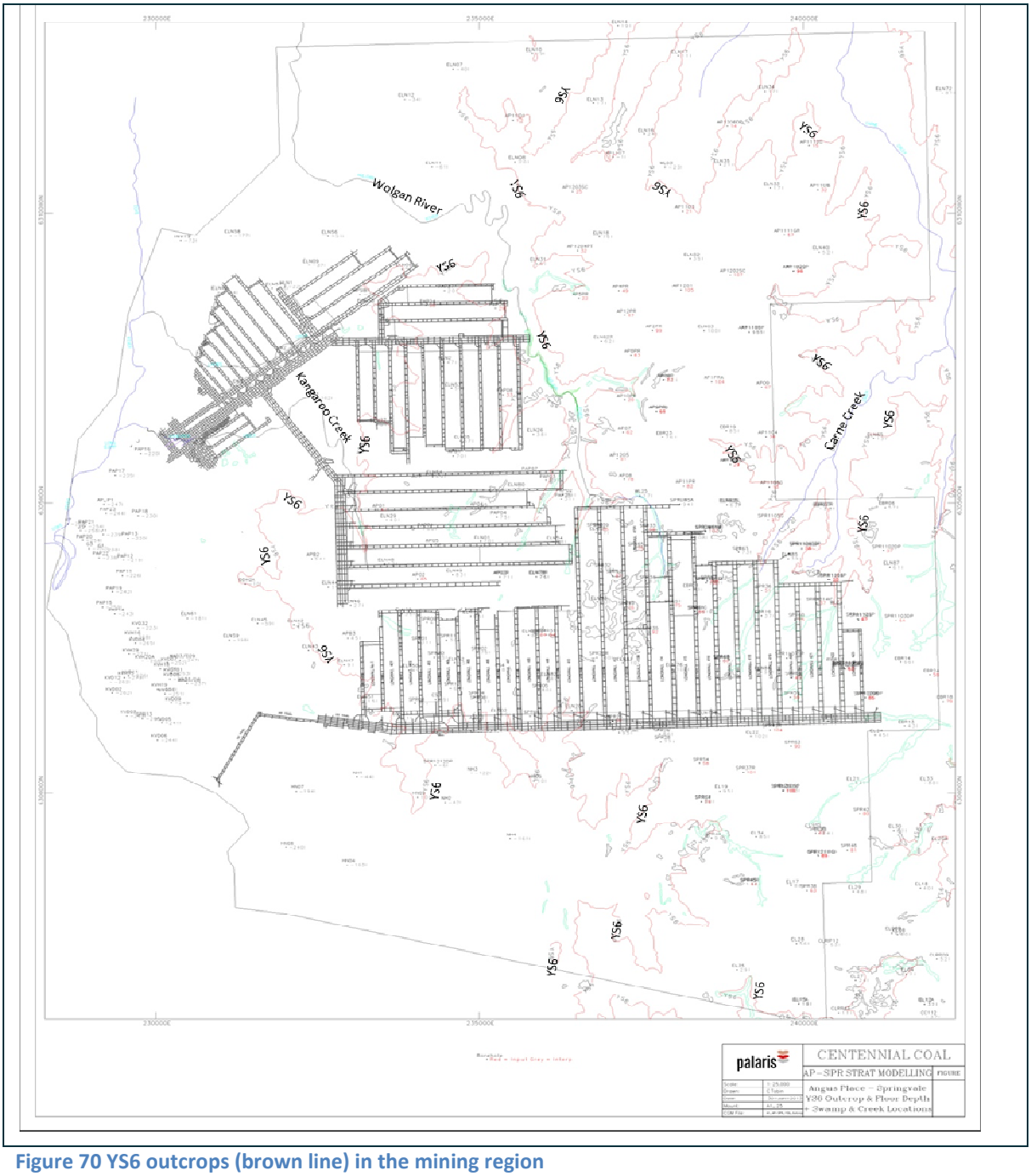

Figure 70 YS6 outcrops (brown line) in the mining region

As described earlier, a conductance of 0.085 day-1 per unit area of riverbed was assumed for all the streams and swamps. The discharge/recharge to/from streams/swamps is computed as described in Section Appendix F. Using the expression given in Appendix F, and the simulated stream/swamp area and the simulated discharge values, estimates are made for average standing water levels with respect to the ground surface and shown in Table 38 to Table 40. In reality, relative to the ground surface the groundwater could lie above the predicted standing groundwater level in one part of a swamp/stream and could lie below in another part.

As can be seen from Table 38 to Table 40 the simulated mining induced changes in the groundwater levels in the swamps/streams are of the order of centimetres; a maximum groundwater level drop of 0.36 m is estimated for the Gang Gang Southeast Swamp in 2022 for the Base case. On the other hand, the Truncated-ramp1 and Truncated-ramp2 models predict only about 5mm drop in water levels for this Swamp.

As baseflow magnitude is almost linearly dependent upon the standing water level above the ground surface, the results presented here must be viewed with caution when the baseflow values are small. For example, let us say the standing groundwater level is just barely below/above the ground surface, then a change of a few millimetres in the standing water level may entirely change the groundwater and surface water interaction process within the model; a leaky swamp/stream may suddenly become a discharging swamp/stream or vice versa.

Table 41 presents the maximum predicted drop in the average standing water levels in the swamps and streams simulated using the Base case, Truncated-ramp1 and Truncated-ramp2 models.

Table 38 Predicted average change in the standing groundwater levels in swamps/streams before, during and after mining (Base case)

Swamps and streams simulated in this study	Predicted average head above the ground surface (m)					Predicted average head drop from pre-mining (m)				Predicted average head drop since 2012 (m)		
	Pre-mining	2012	2022	2032	2064	2012	2022	2032	2064	2022	2032	2064
CA2 (includes Carne Central Swamp)	0.499	0.436	0.379	0.340	0.345	0.063	0.120	0.159	0.154	0.057	0.096	0.091
Carne West Swamp	0.027	0.025	0.074	0.063	0.056	0.002	-0.046	-0.035	-0.029	-0.048	-0.037	-0.030
Carne Creek Total	0.558	0.512	0.510	0.487	0.511	0.046	0.047	0.071	0.047	0.002	0.025	0.001
Gang Gang Swamp South East	-0.106	-0.119	-0.458	-0.479	-0.477	0.012	0.352	0.373	0.371	0.339	0.360	0.358
Gang Gang Swamp South	-0.065	-0.081	-0.007	-0.101	-0.108	0.016	-0.058	0.036	0.043	-0.074	0.020	0.027
Kangaroo Swamp	0.179	0.384	0.384	0.361	0.333	-0.205	-0.205	-0.182	-0.153	0.000	0.023	0.051
Kangaroo Creek (KC1)	0.116	-0.001	-0.025	-0.051	-0.029	0.117	0.141	0.167	0.144	0.024	0.050	0.027
Kangaroo Creek (KC2)	0.067	0.103	0.114	0.096	0.077	-0.036	-0.047	-0.029	-0.010	-0.011	0.008	0.027
Lamb Creek	0.102	0.102	0.068	0.057	0.076	0.000	0.034	0.045	0.026	0.034	0.045	0.026
Long Swamp	-0.101	-0.101	-0.101	-0.101	-0.101	0.000	0.000	0.000	0.000	0.000	0.000	0.000
Marrangaroo Creek	0.148	0.115	0.113	0.104	0.095	0.033	0.035	0.045	0.053	0.002	0.012	0.020
Nine Mile Swamp	0.037	0.025	0.039	0.037	0.037	0.011	-0.002	0.000	0.000	-0.014	-0.011	-0.011
Paddy's Creek	0.120	0.115	0.114	0.115	0.117	0.006	0.006	0.006	0.003	0.001	0.000	-0.003
Pine Swamp	0.087	0.084	0.203	0.167	0.148	0.004	-0.116	-0.080	-0.060	-0.120	-0.084	-0.064
Tri-Star Swamp	0.097	0.087	0.266	0.211	0.116	0.010	-0.170	-0.114	-0.020	-0.179	-0.124	-0.030
Twin Gully Swamp	0.130	0.125	0.125	0.153	0.105	0.005	0.005	-0.022	0.026	0.000	-0.027	0.021
Sunnyside Swamp	0.181	0.176	0.194	0.185	0.168	0.005	-0.013	-0.004	0.014	-0.018	-0.009	0.008
Wolgan River Total	0.187	0.181	0.199	0.173	0.137	0.006	-0.012	0.014	0.050	-0.018	0.008	0.044

Note: Positive values indicate head drops and negative value indicate head increases.

Table 39 Predicted average change in the standing groundwater levels in swamps/streams before, during and after mining (Truncated-ramp1)

Swamps and streams simulated in this study	Predicted average head above the ground surface (m)					Predicted average head drop from pre-mining (m)				Predicted average head drop since 2012 (m)		
	Pre-mining	2012	2022	2032	2064	2012	2022	2032	2064	2022	2032	2064
CA2 (includes Carne Central Swamp)	0.499	0.436	0.378	0.345	0.354	0.062	0.121	0.154	0.144	0.058	0.091	0.082
Carne West Swamp	0.027	0.025	0.027	0.027	0.027	0.002	0.000	0.000	0.000	-0.002	-0.002	-0.002
Carne Creek Total	0.558	0.512	0.501	0.488	0.515	0.046	0.057	0.070	0.043	0.011	0.024	-0.003
Gang Gang Swamp South East	-0.106	-0.119	-0.123	-0.123	-0.121	0.012	0.017	0.017	0.015	0.004	0.004	0.002
Gang Gang Swamp South	-0.065	-0.081	-0.079	-0.081	-0.078	0.016	0.015	0.016	0.013	-0.001	0.000	-0.003
Kangaroo Swamp	0.179	0.153	0.179	0.179	0.153	0.026	0.000	0.000	0.026	-0.026	-0.026	0.000
Kangaroo Creek (KC1)	0.116	-0.033	-0.044	-0.062	-0.034	0.149	0.159	0.178	0.150	0.010	0.029	0.001
Kangaroo Creek (KC2)	0.067	0.060	0.066	0.066	0.066	0.007	0.001	0.001	0.001	-0.006	-0.006	-0.006
Lamb Creek	0.102	0.048	0.046	0.042	0.047	0.054	0.056	0.060	0.055	0.002	0.006	0.000
Long Swamp	-0.101	-0.118	-0.101	-0.101	-0.101	0.017	0.000	0.000	0.000	-0.017	-0.017	-0.017
Marrangaroo Creek	0.148	0.116	0.115	0.108	0.107	0.032	0.033	0.040	0.042	0.001	0.008	0.009
Nine Mile Swamp	0.037	0.025	0.034	0.034	0.034	0.011	0.003	0.002	0.002	-0.009	-0.009	-0.009
Paddy's Creek	0.120	0.114	0.114	0.113	0.115	0.006	0.006	0.007	0.006	0.000	0.001	-0.001
Pine Swamp	0.087	0.084	0.870	0.087	0.087	0.004	0.000	0.000	0.000	-0.003	-0.003	-0.004
Tri-Star Swamp	0.097	0.087	0.085	0.083	0.081	0.010	0.012	0.014	0.016	0.002	0.004	0.006
Twin Gully Swamp	0.130	0.125	0.125	0.123	0.123	0.005	0.005	0.007	0.007	0.000	0.002	0.002
Sunnyside Swamp	0.181	0.173	0.180	0.180	0.181	0.009	0.001	0.001	0.000	-0.008	-0.007	-0.009
Wolgan River Total	0.187	0.165	0.174	0.160	0.148	0.023	0.013	0.027	0.039	-0.010	0.004	0.017

Note: Positive values indicate head drops and negative value indicate head increases.

Table 40 Predicted average change in the standing groundwater levels in swamps/streams before, during and after mining (Truncated-ramp2)

Swamps and streams simulated in this study	Predicted average head above the ground surface (m)					Predicted average head drop from pre-mining (m)				Predicted average head drop since 2012 (m)		
	Pre-mining	2012	2022	2032	2064	2012	2022	2032	2064	2022	2032	2064
CA2 (includes Carne Central Swamp)	0.499	0.436	0.375	0.335	0.335	0.063	0.124	0.164	0.164	0.061	0.101	0.102
Carne West Swamp	0.027	0.025	0.027	0.026	0.026	0.002	0.000	0.001	0.001	-0.001	-0.001	-0.001
Carne Creek Total	0.558	0.512	0.495	0.478	0.503	0.046	0.063	0.080	0.055	0.017	0.034	0.009
Gang Gang Swamp South East	-0.106	-0.119	-0.164	-0.169	-0.169	0.012	0.058	0.063	0.062	0.046	0.050	0.050
Gang Gang Swamp South	-0.065	-0.075	-0.112	-0.117	-0.117	0.011	0.047	0.052	0.052	0.036	0.042	0.042
Kangaroo Swamp	0.179	0.102	0.102	0.102	0.090	0.077	0.077	0.077	0.090	0.000	0.000	0.013
Kangaroo Creek (KC1)	0.116	-0.073	-0.099	-0.120	-0.088	0.188	0.215	0.236	0.203	0.026	0.047	0.015
Kangaroo Creek (KC2)	0.067	0.060	0.064	0.063	0.063	0.007	0.003	0.004	0.004	-0.004	-0.003	-0.003
Lamb Creek	0.102	0.071	0.062	0.051	0.072	0.031	0.040	0.051	0.030	0.009	0.020	-0.001
Long Swamp	-0.101	-0.118	-0.101	-0.101	-0.101	0.017	0.000	0.000	0.000	-0.017	-0.017	-0.017
Marrangaroo Creek	0.148	0.115	0.112	0.100	0.097	0.033	0.037	0.048	0.051	0.004	0.015	0.018
Nine Mile Swamp	0.037	0.026	0.034	0.034	0.034	0.011	0.002	0.002	0.002	-0.009	-0.009	-0.009
Paddy's Creek	0.120	0.115	0.113	0.113	0.113	0.006	0.007	0.007	0.007	0.001	0.001	0.001
Pine Swamp	0.087	0.083	0.087	0.086	0.086	0.004	0.001	0.001	0.001	-0.003	-0.003	-0.003
Tri-Star Swamp	0.097	0.087	0.085	0.059	0.038	0.010	0.012	0.037	0.059	0.002	0.028	0.049
Twin Gully Swamp	0.130	0.124	0.125	0.122	0.106	0.006	0.005	0.009	0.024	-0.001	0.003	0.018
Sunnyside Swamp	0.181	0.174	0.180	0.180	0.180	0.008	0.001	0.001	0.002	-0.007	-0.007	-0.006
Wolgan River Total	0.187	0.165	0.174	0.152	0.135	0.022	0.014	0.035	0.053	-0.009	0.013	0.030

Note: Positive values indicate head drops and negative value indicate head increases.

Table 41 Predicted maximum drop in the average standing groundwater levels in swamps/streams with respect to the groundwater levels in December 2012

Swamps and streams simulated in this study	Base case (m)	Truncated-ramp1 (m)	Truncated-ramp2 (m)
CA2 (includes Carne Central Swamp)	0.103	0.095	0.110
Carne West Swamp	Small head increase	0.000	0.000
Carne Creek Total	Small head increase	Small head increase	Small head increase
Gang Gang Swamp South East	0.364	0.005	0.052
Gang Gang Swamp South	0.030	0.000	0.043
Kangaroo Swamp	0.095	0.000	0.051
Kangaroo Creek (KC1)	0.129	0.074	0.122
Kangaroo Creek (KC2)	0.035	0.000	-0.003
Lamb Creek	0.047	0.006	0.022
Long Swamp	0.017	0.000	0.000
Marrangaroo Creek	0.020	0.011	0.019
Nine Mile Swamp	Small head increase	Small head increase	Small head increase
Paddy's Creek	Small head increase	0.002	0.004
Pine Swamp	Small head increase	No change	No change
Tri-Star Swamp	0.081	0.011	0.079
Twin Gully Swamp	0.051	0.003	0.035
Sunnyside Swamp	0.013	Small head increase	Small head increase
Wolgan River Total	0.050	0.017	0.030

**As discussed earlier, the actual mining impact on baseflow is expected to lie within the bounds predicted by the three models.*

4.2.4 Predicted drawdown

Appendix D provides the simulated drawdown for the Lithgow Seam, AQ1, AQ2, AQ3, AQ4, AQ5, AQ6 and the top of the model (i.e. the ground surface) following 5, 11 and 18 years of mining of APE longwalls within the predictive simulation period.

Figures D1 to D21 in Appendix D show the simulated drawdown with respect to the pre-mining groundwater conditions and Figures D22 to D42 show the simulated drawdown with respect to groundwater levels at 2013.

Figure 71 and Figure 72 show two typical drawdown plots in the Lithgow Seam after mining the APE longwalls. Figure 71 shows the drawdown with respect to the pre-mining groundwater condition while Figure 72 shows the drawdown with respect to the groundwater level at 2013. A maximum drawdown of 120m is predicted around the SV longwalls. The maximum depressurization seems to occur within the SPR_LW423 region with respect to the groundwater level at 2013 (Figure 72). The magnitude of depressurization gradually decreases away from the SPR_LW423 region; 5m drawdown contour can be seen to extend about 5km from SV (just outside the eastern boundary of the Clarence Colliery).

The depressurization of the strata can be seen to decrease with the vertical distance away from the Lithgow Seam (Figures D25 to D30). However, the drawdown patterns in AQ2 and AQ3 are similar to those in AQ1.

The depressurization of AQ3 occurs in a different manner (Figures D31 to D33). In 2033, maximum drawdown in AQ3 (with respect to the groundwater levels in 2013) can be seen to concentrate over the APE longwalls. Depressurization in AQ4 can also be seen to concentrate more over the APE longwalls (Figure D36).

The average saturated head drop at the ground surface is generally of the order of centimetres (see Figure 73).

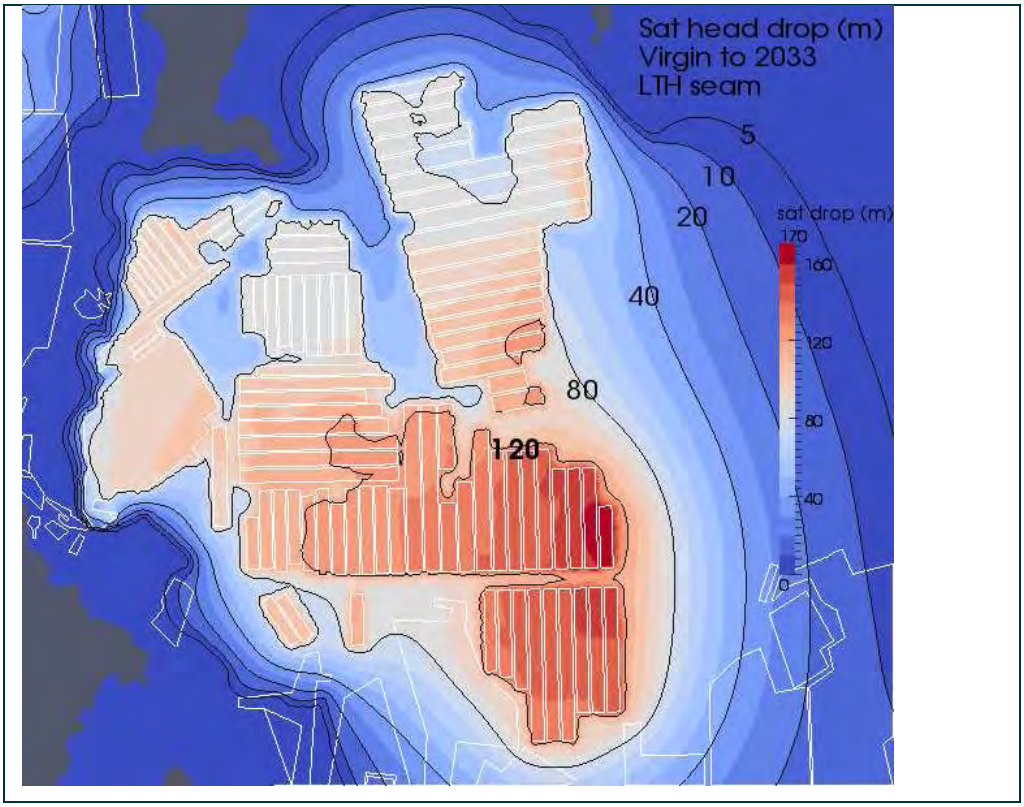

Figure 71 Distribution of drawdown in the Lithgow Seam in January 2033 with respect to pre-mining groundwater condition

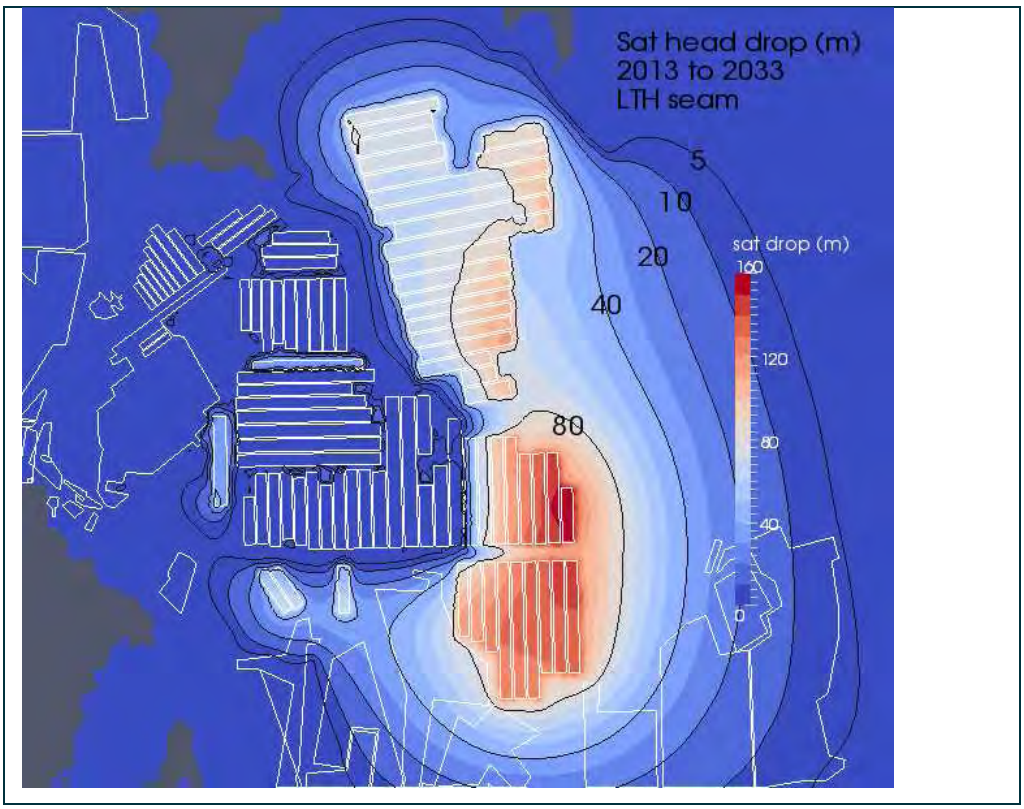

Figure 72 Distribution of drawdown in the Lithgow Seam in January 2033 with respect to groundwater levels in January 2013

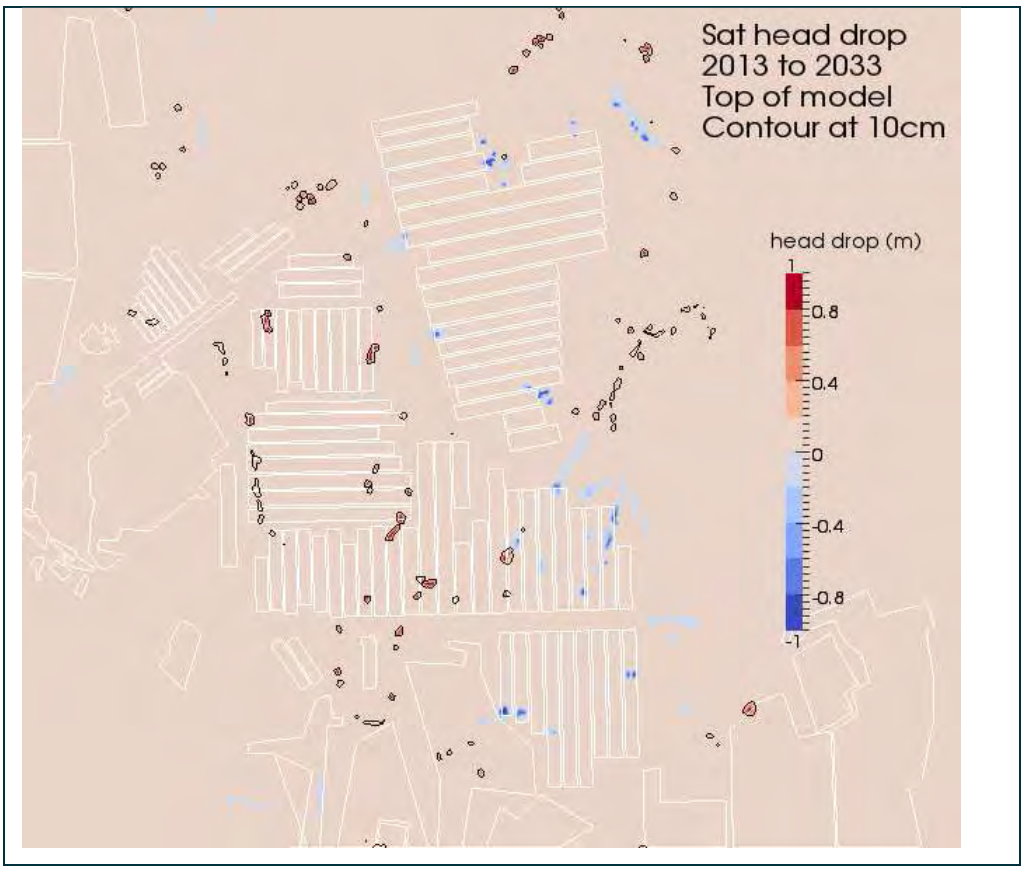

Figure 73 Distribution of head drops at the ground surface in January 2033 with respect to groundwater levels in January 2013

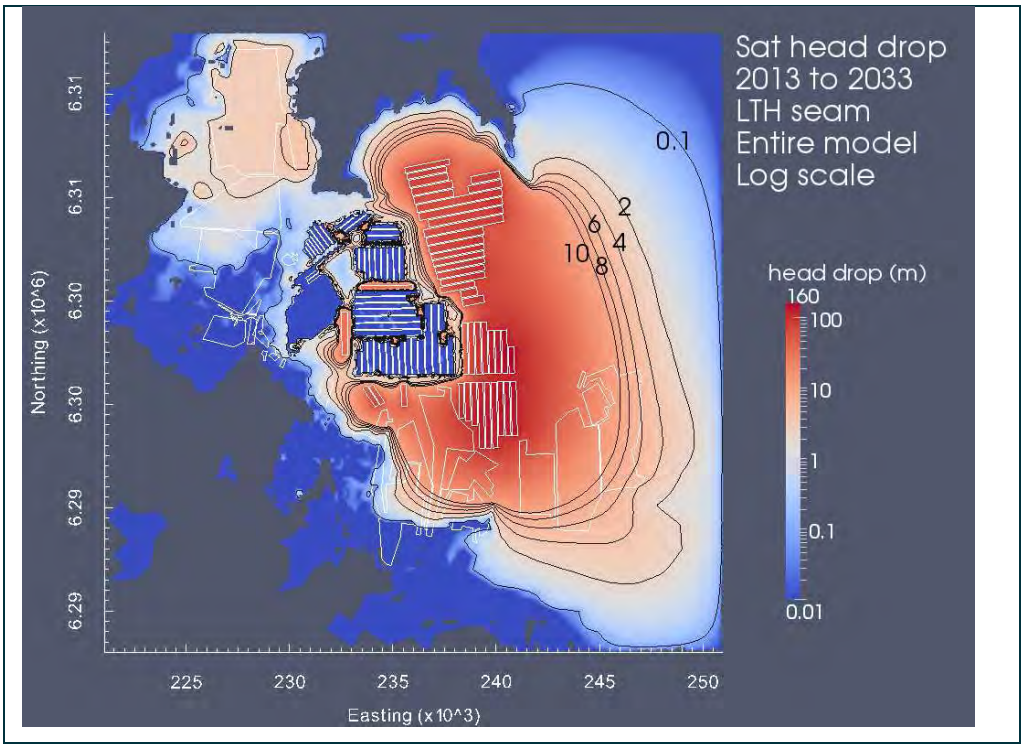

Figure 74 Drawdown in 2033 with respect to groundwater levels in January 2013 (entire model)

Figure 74 shows the drawdown in the Lithgow Seam with respect to groundwater levels in January 2013 for the entire model. Water heads on the eastern side of the model boundary can be seen to drop by up to 10m at a distance of 5 to 10km from mining operations. Further away, the magnitude of head drop seems to decrease rapidly; the drop in water heads seems to decrease from 10m to 2m within 2 to 3 km distance.

In order to study the effect of model boundary on the simulated results, additional model with a seepage boundary (MODFLOW equivalent general head boundary) condition is also run with a very high conductance at the boundary nodes. The model parameters are kept the same as those in the Base model. The seepage boundary conditions would (a) not allow any water inflow at the boundary thus it permits pressure drop along the boundary and (b) not allow the pressure on the boundary to exceed the prescribed reference pressure values by allowing water to seep out of the boundary should pressure tend to increase beyond the prescribed pressure value. Thus this is the most stringent boundary condition as it would not allow any influx from the outer boundary. The real/natural condition should lie between the modelled seepage boundary and the fixed pressure boundary.

Figure 75 shows the simulated saturated drawdowns in the Lithgow Seam with respect to the groundwater levels at the pre-mining condition for the entire model. The drawdowns are plotted for both the fixed head as well as the seepage boundary conditions. As can be seen there is only a marginal difference between the 10m drawdown contour obtained from the fixed head boundary model and the seepage boundary model in the Lithgow seam; this demonstrates that the effect of the fixed boundary condition in the model result is minimal. Similarly, the baseflow to streams and swamps obtained from the seepage boundary model is found to be almost identical to those obtained from the base case (see Appendix E).

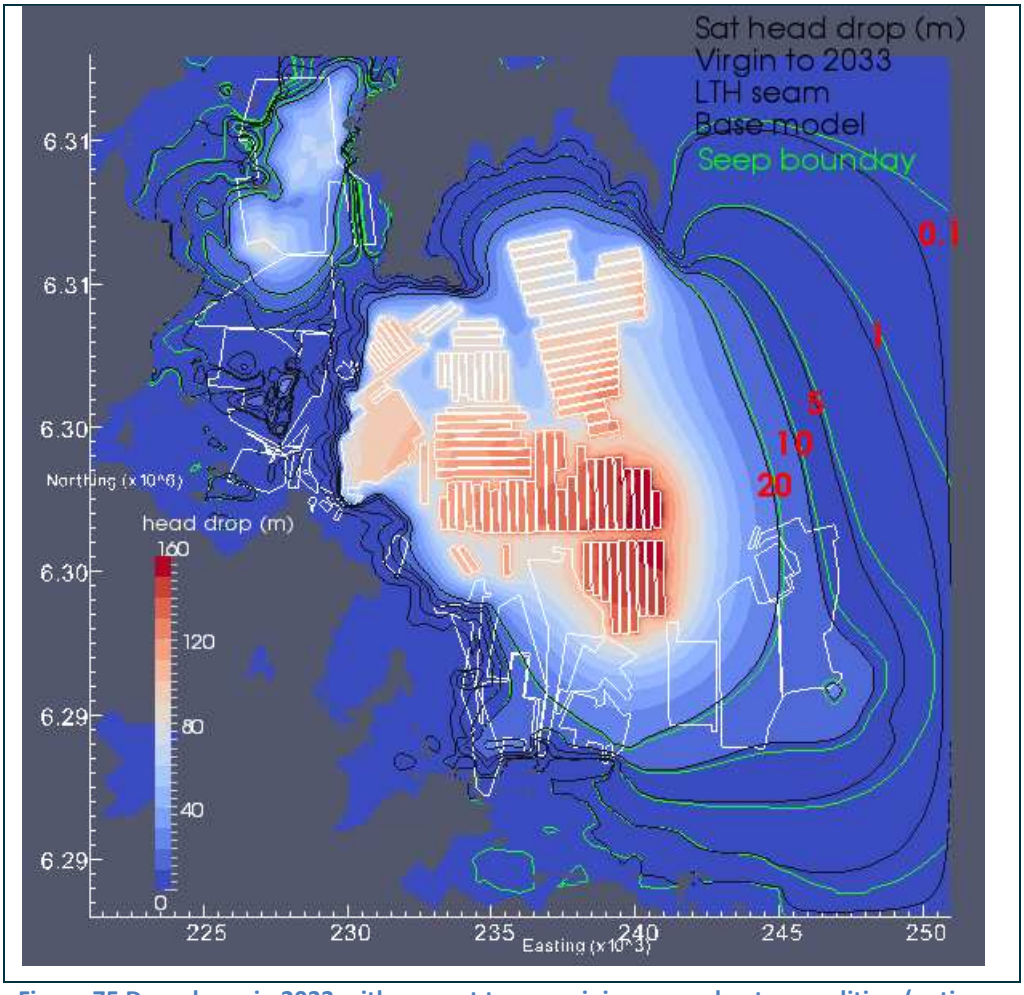

Figure 75 Drawdown in 2033 with respect to pre-mining groundwater condition (entire model)

4.2.5 Changes in the groundwater phreatic surface

The phreatic surfaces on the vertical sections shown in Figure 61 before mining (1949), at the end of the validation period (2012) and at the end of the predictive period (2033) after mining are shown in Figure 76 to Figure 78.

These figures contain a lot of information and give a good qualitative understanding of water redistribution by mining. However, while the phreatic-surface lines delineate regions of full saturation from regions of partial saturation, the figures do not give any information about the porepressures within each region. Scanning downwards along a vertical line from the top of the model determines whether an area is saturated or unsaturated. For example, in Figure 76, to determine the saturated regions for the virgin configuration, the following procedure can be used. The region directly below the word "topo" is unsaturated. Moving downwards by about 5m a blue line is encountered which separates the unsaturated from the saturated region, meaning that the region below this blue line is saturated. Moving further downwards the lower part of SP4 another blue line is encountered, meaning the region below this line is unsaturated. Moving further downwards still, another blue line is encountered below YS6, meaning the region below this line is saturated. No more blue lines are encountered to the bottom of the model, so the lower part is all fully saturated.

The following observations can be made from Figure 76 to Figure 78.

- Extensive desaturation occurs in AQ1 wherever mining has occurred in the Lithgow seam,
- Though porepressures do drop in AQ2, as evidenced by the drawdown pictures in Appendix D, the aquifer remains fully saturated,
- Much of AQ3 becomes desaturated above the mining panels and beyond them to the hillsides.
- AQ4 remains almost fully saturated, only in section NS desaturation is observed. AQ4 is shielded by the MYC layer,
- A slight drop of the phreatic surface in AQ5 is evident in section WE, but mostly AQ5 appears to be shielded by MYC and YS6, and
- Underneath the topographic ridges at the top of the model, the phreatic surface drops by a few metres, while the drops near the valley regions are significantly less.

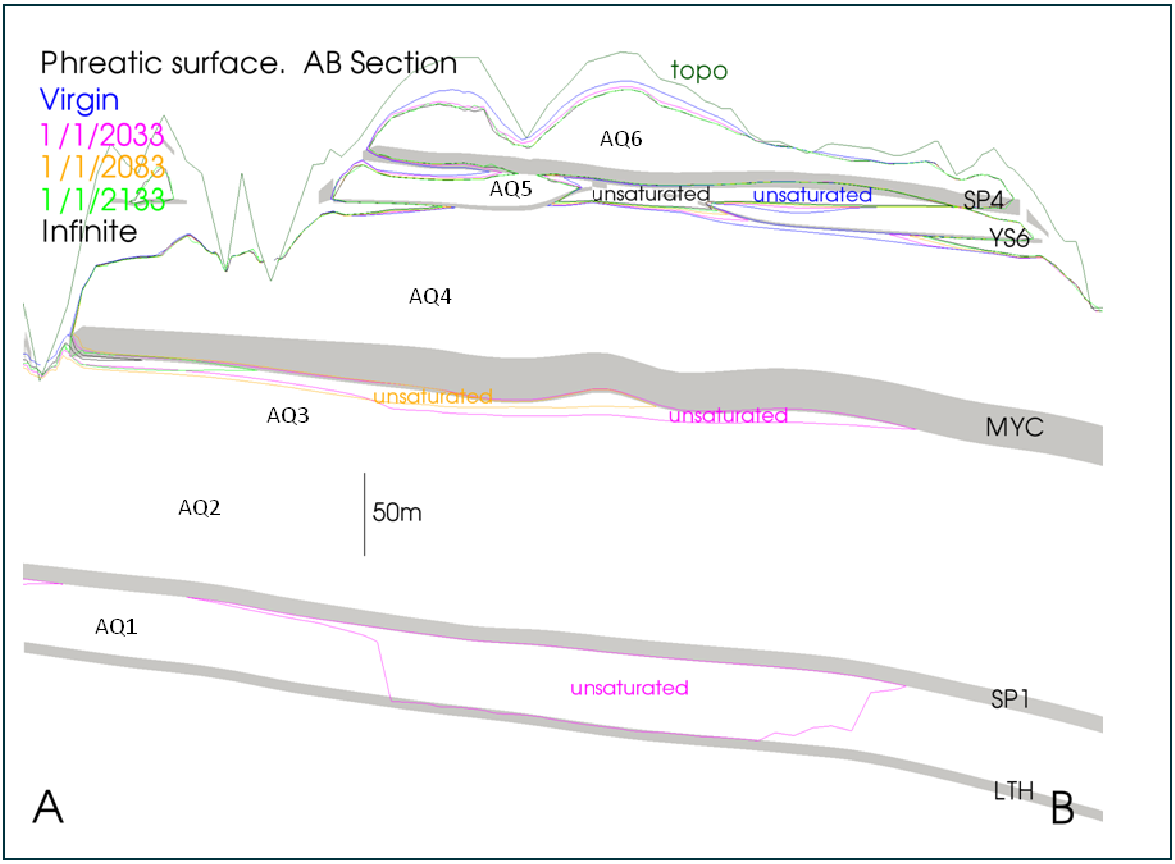

Figure 76 Phreatic surface before mining (blue lines), after mining (pink lines), 50 years after mining (yellow lines), 100 years after mining (green lines) and steady-state after mining (black lines) along A-B section

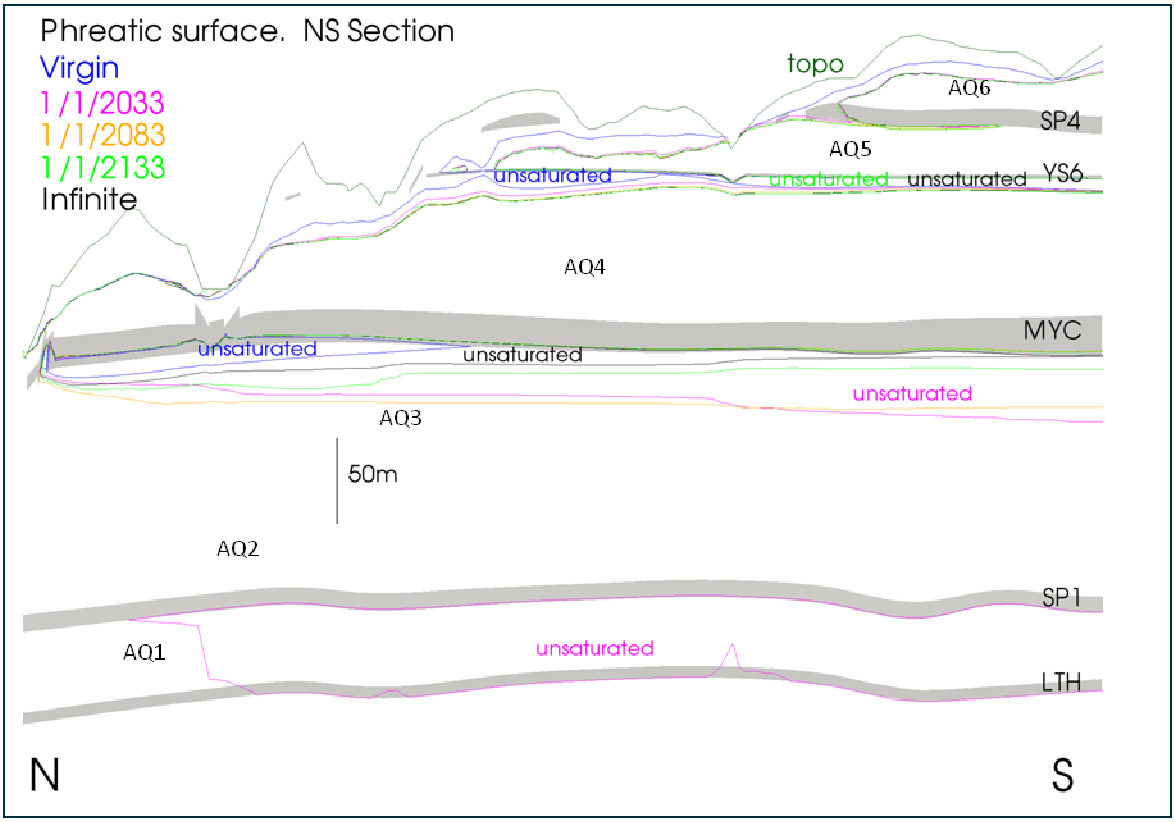

Figure 77 Phreatic surface before mining (blue lines), after mining (pink lines), 50 years after mining (yellow lines), 100 years after mining (green lines) and steady-state after mining (black lines) along N-S section

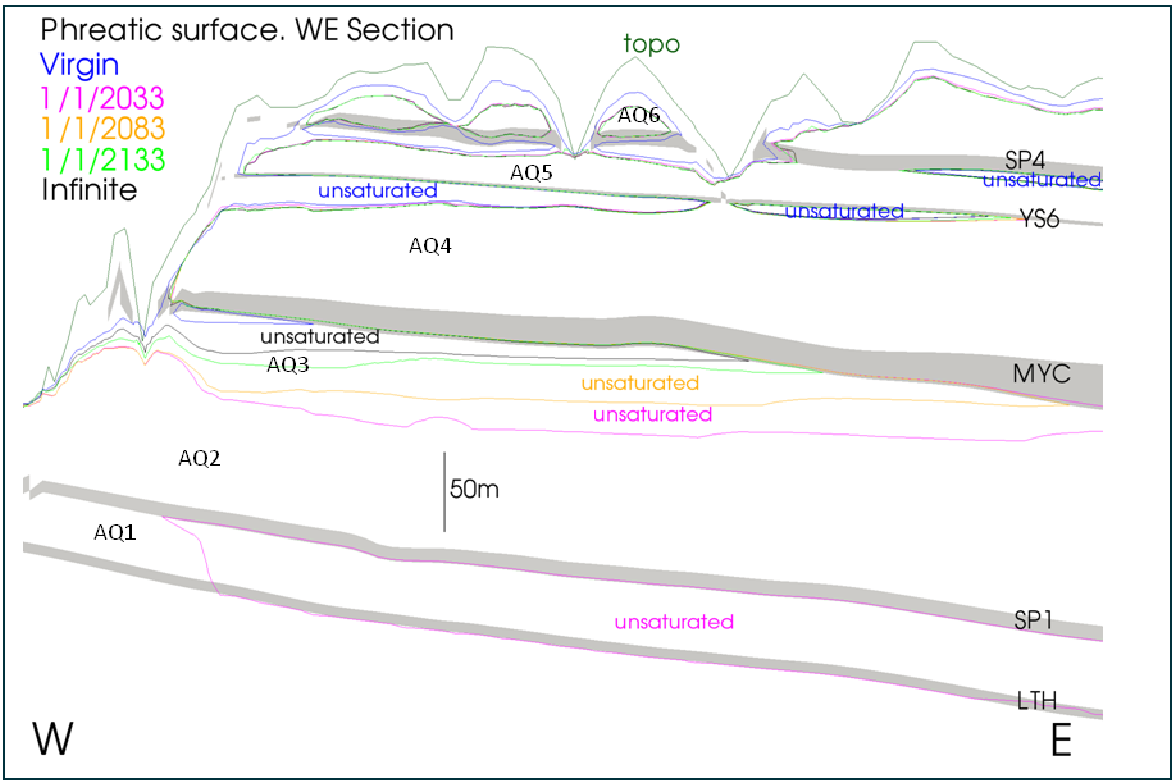

Figure 78 Phreatic surface before mining (blue lines), after mining (pink lines), 50 years after mining (yellow lines), 100 years after mining (green lines) and steady-state after mining (black lines) along E-W section

4.2.6 Head drops along the Cox's River

Cox's river was not explicitly included in the model, and so the model cannot directly yield the changes in baseflow due to mining. However, two proxies for these changes have been explored:

1. The changes in baseflow for Long Swamp, which lies along Cox's river. These changes have been presented in Appendix C, and are negligible.
2. The drop in saturated heads at the surface of the model along Cox's river.

These pressure heads along Cox's river are explored further in this section.

Firstly, the model predicts that the phreatic surface generally lies below Cox's river, as shown in Figure 79. Since Cox's river was not included explicitly, the depth of the water table must be obtained using interpolation. There are two ways of doing this: interpolating the depth values, which typically yield lower water tables than the true situation; interpolating the phreatic elevation values, which typically yield higher water tables than the true situation. These interpolation schemes are described in Figure 80.

In Figure 80 COSFLOW nodes are at the black dots, where the phreatic surface is correctly simulated. The interpolation using the phreatic surface's depth is shown as a red line. Typically this yields a lower phreatic surface in valleys and a higher surface in ridges when compared with the real phreatic surface. The interpolation using the phreatic surface's elevation is shown as a black dashed line. Typically this yields a higher phreatic surface in valleys and a lower surface in ridges when compared with the real phreatic surface.

At the southern end of the river, the Elevation Interpolation suggests that the depth is negative (the water table is above the ground surface). While this may be true, this is the region where the interpolation of COSFLOW's results is less accurate due to large finite-element mesh sizes, as shown in Figure 81.

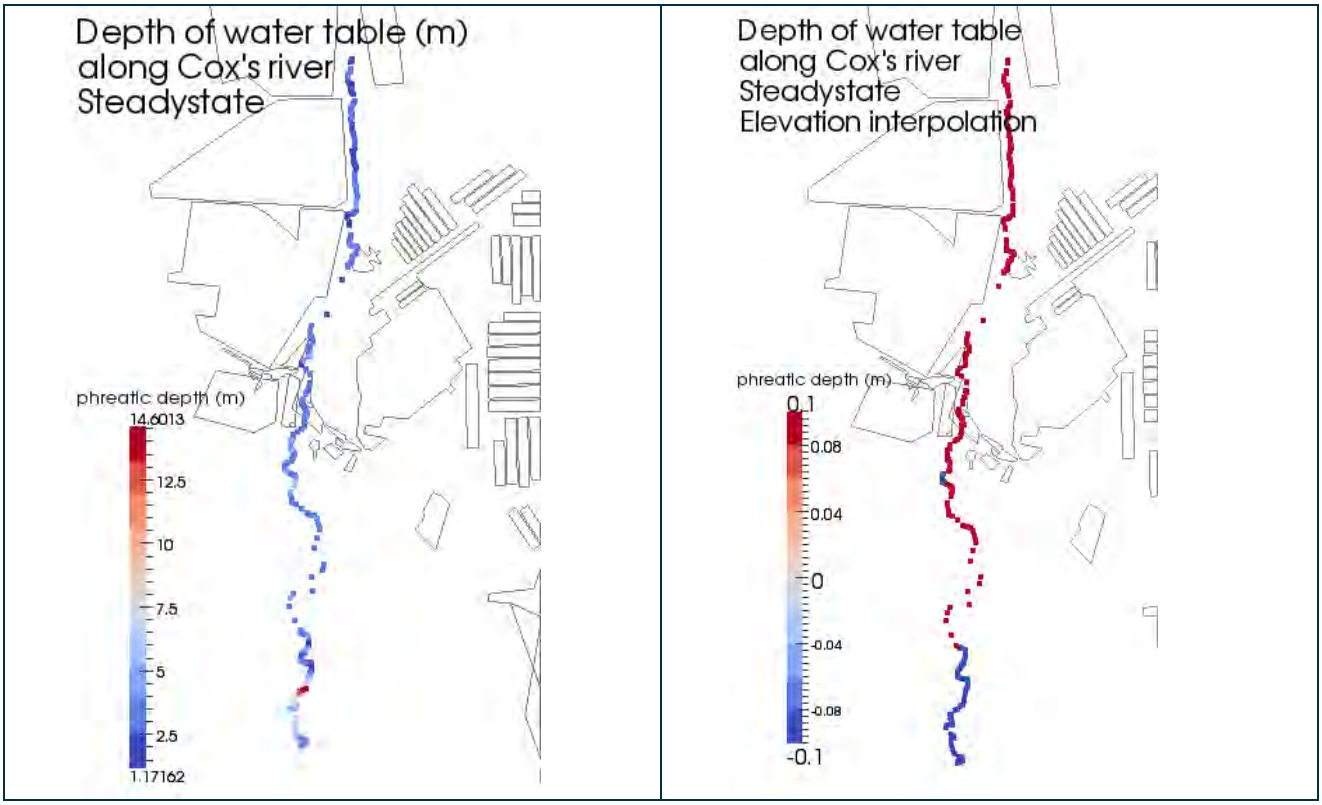

Figure 79 Depth of the watertable along Cox's river before any mining. Left picture: interpolation using the phreatic depth. Right picture: interpolation using the phreatic elevation. Notice that the depth is positive along most of Cox's river regardless of the interpolation used.

The drop in the phreatic surface along Cox's river is between steady-state, year 2013 and year 2033 is shown in Figure 82. Note that a logarithmic scale has been used and that most of the drops are of the

order of centimetres. The largest effects are at the north of the modelled region, and are not due to mining Angus Place or Springvale mines, as shall be seen in Figure 83[5].

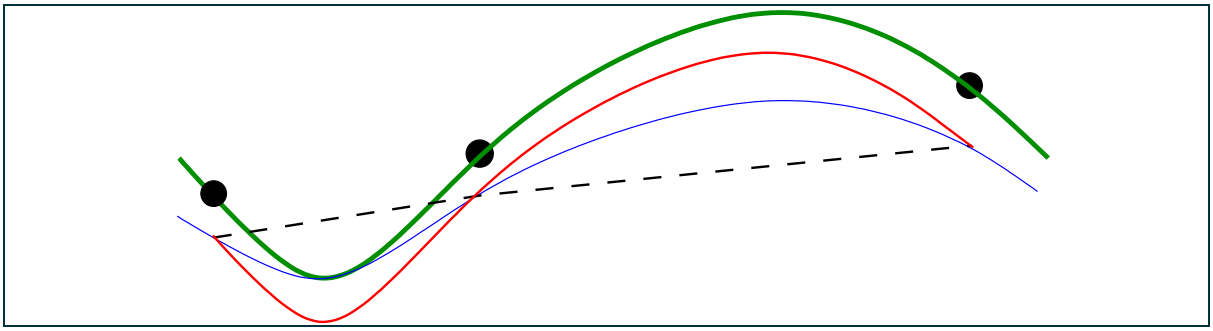

Figure 80 The phreatic surface (blue line) below the topography (green line)

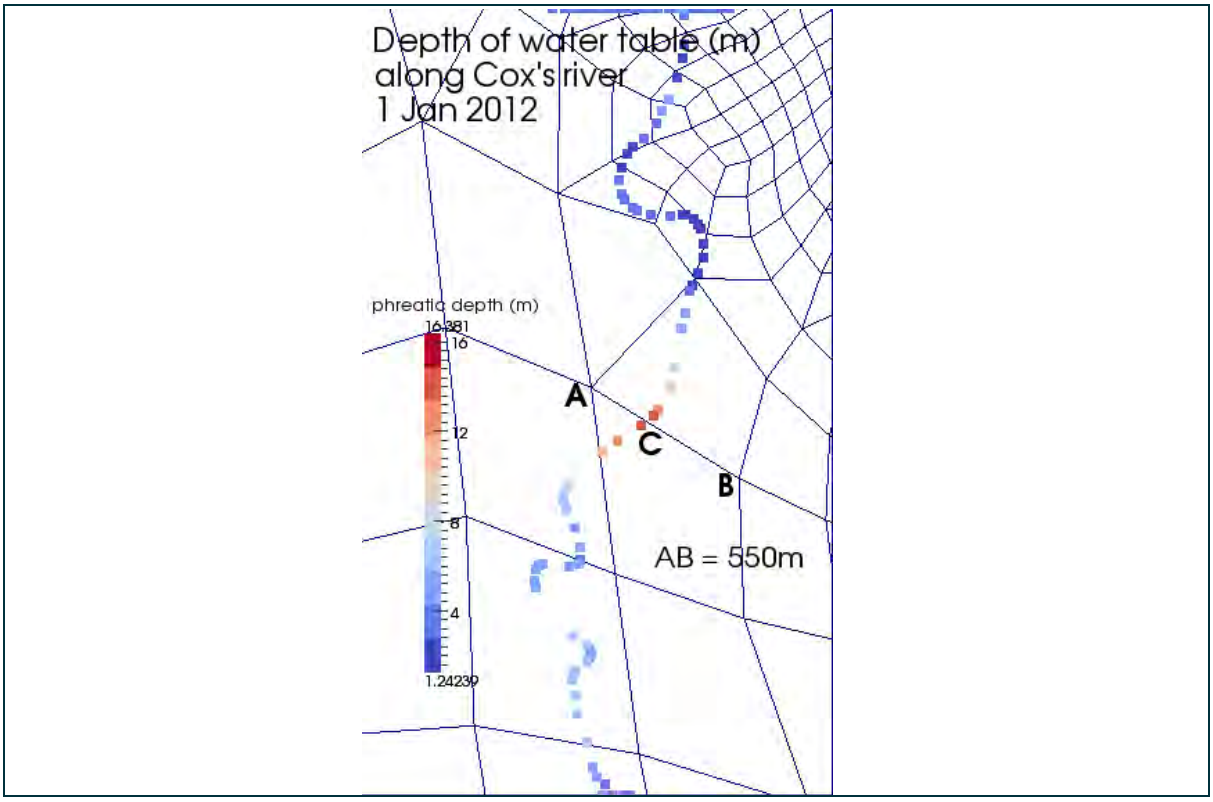

Figure 81 The finite element mesh is overlayed upon results from Figure 79. At the southern end of Cox's river, the interpolation is much less accurate since the element side-length is around 500m. By inspecting Figure 2, it is easy to imagine the interpolation from results at "A" and "B" to point "C" has significant error.

Figure 83 shows the drop in phreatic surface along Cox's river between year 2013 and year 2033 due to mining the Angus Place Extension, and new Springvale panels (LW416 onwards). This picture was obtained by comparing the drops in the "base" and "no new" scenarios. Again a logarithmic scale has been used, and this time the maximum drop is 1cm, and most head drops are less than 1mm.

Thus the Cox's river could be categorised as a leaking river. Assuming the same riverbed conductance as the Sunnyside Swamp, this drop in the water table would account for a maximum extra leakage of 0.01 ML/day per unit width of the river.

[5] Indeed, these effects may not be entirely accurate since: (1) the mesh density in that region is low; and (2) are largely due to mines to the west whose mine schedules and geometries are not represented as accurately as the mines to the east.

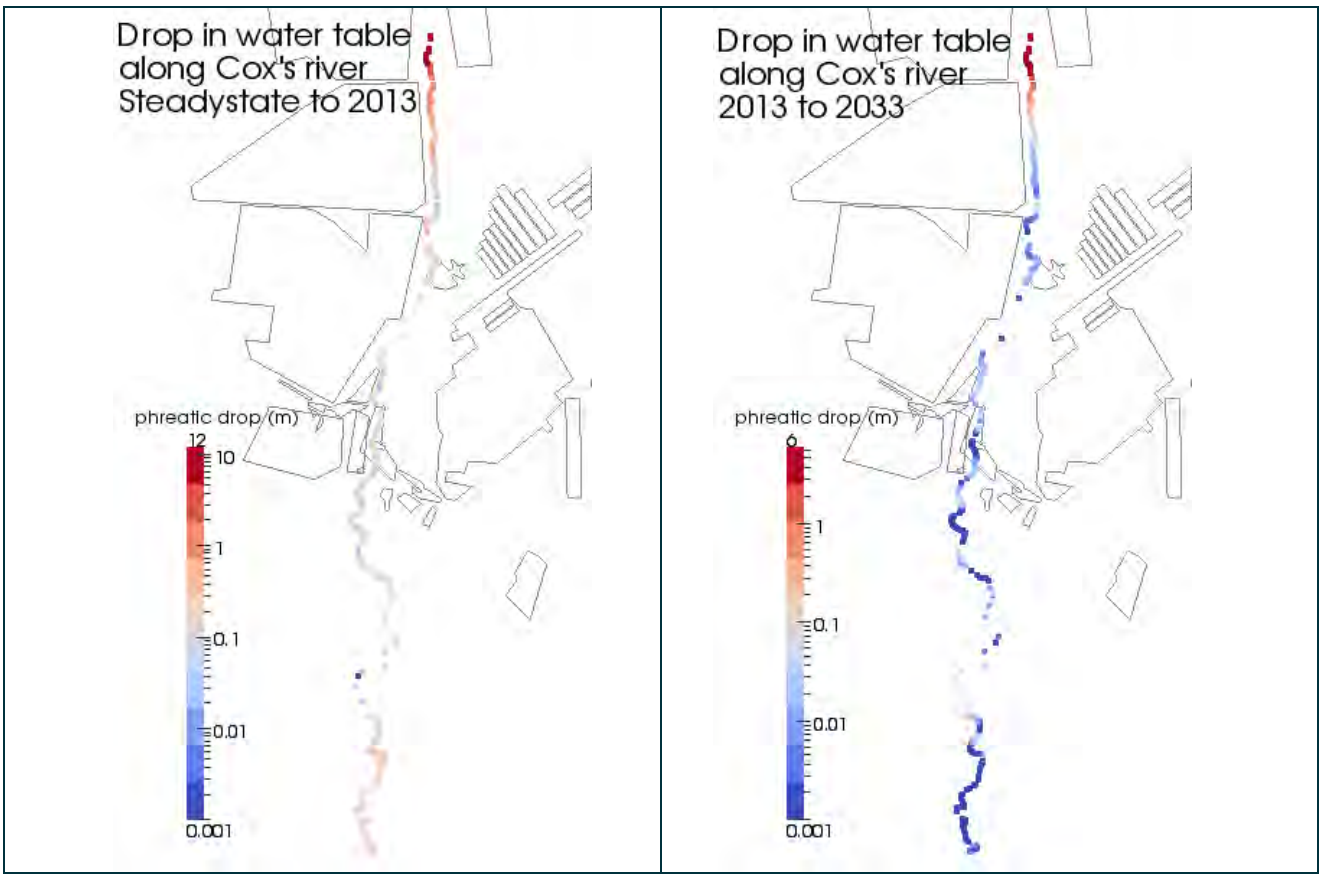

Figure 82 Drop in the phreatic surface along Cox's river between steady-state and 2013 (left), and 2013 and 2033 (right. A logarithmic scale has been used

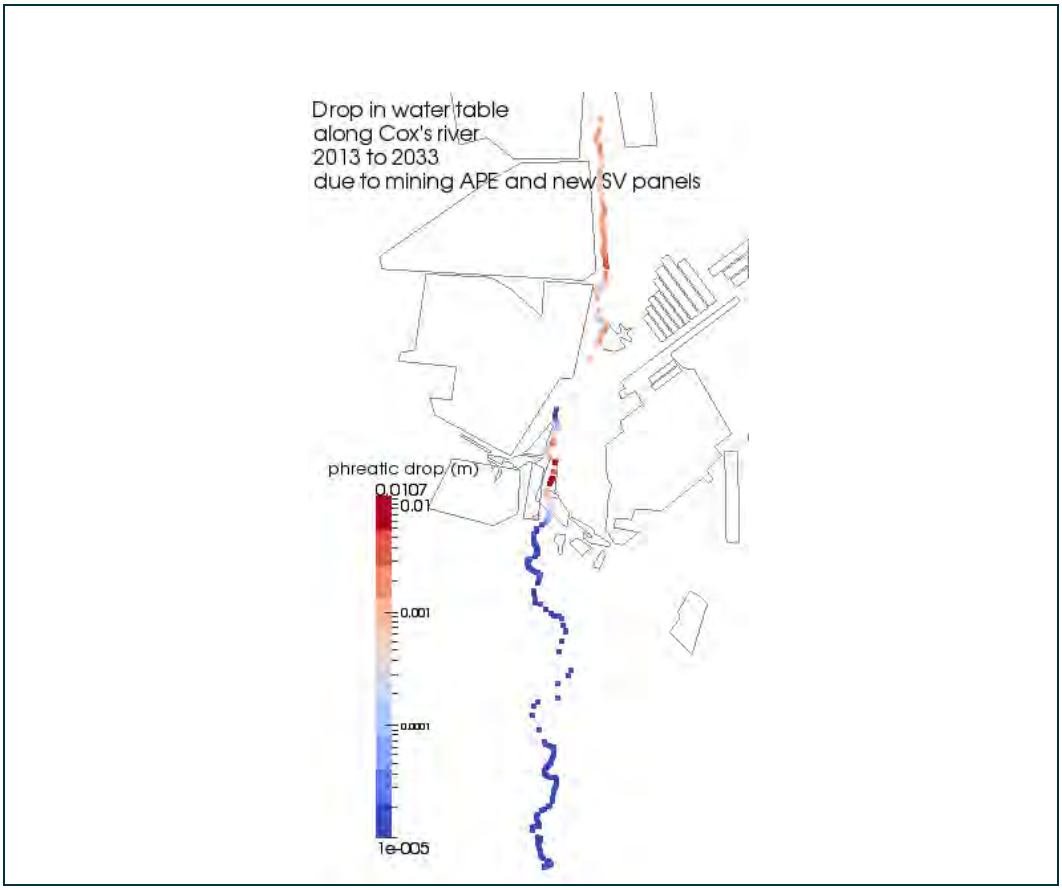

Figure 83 Drop in the phreatic surface along Cox's river between 2013 and 2033 due to mining APE and the new SV panels. A logarithmic scale has been used

4.2.7 Saturated head drops on private bores

Table 42 shows the positions of 108 private bores within 10km of the Springvale and Angus Place mines. The simulated head drops at the bottom of each of these private bores compared with the initial heads at year 2013 are produced. The data is tabulated for the years 2033, 2083 and 2233. A negative value indicates the head has risen compared with 2013. Clearly, for most private bores of depth less than 50m the head drops are very small, and the median head drop is 0.0 in 2033. This is depicted graphically in Figure 84 where private bores have been categorised by their depths in order to highlight the drawdown quantities. These data were obtained by interpolation from cosflow results in a similar way as was done for Cox's river in Section 4.2.6

Table 42 also contains a column which tabulates the effect due to mining APE and SV LW416 onwards. These data were obtained by comparing the "base" case with the "no new" case. The effect of these mines on most of the bores is very small: the median effect of these mines is an extra drawdown of 1cm in 2033.

Column 8 in Table 42 shows water recovery by 2033 if no new SV and APE panels were extracted. Column 5 is the simulated drawdown at 2033 (Base case) with respect to the groundwater levels at 2013; a positive value denotes drawdown and a negative value denotes recovery.

Column 9 is the net effect of mining the proposed SV and APE panels; *however one should be careful while reading the data in Column 9. For example for bore 'GW110484' the actual simulated saturated drawdown in 2033 is 1m (Column 5, Base case); if the proposed APE and SV panels are not extracted then the water levels would have risen by 13m (Column 8). Thus the net effect of mining of proposed APE and SV panels is 13.75m (1.06m (column5)+12.69m (column 8)) as shown in Column 9. Thus if the proposed APE and SV panels are extracted water level would drop by only 1m compared to the present water levels but not by 13.75m*.

Table 42 Private bore data and simulated head drops at the bottom of each bore

Name	Depth (m)	Easting (m)	Northing (m)	**Base case saturated drawdown 2033 (cm)**	Base case saturated drawdown 2083 (cm)	Base case saturated drawdown 2233 (cm)	No new APE and SV mines saturated drawdown by 2033	Saturated drawdown due to new APE and SV mining, 2033 (cm)
GW110706	1.1	242423.9781	6295518.565	**0.00**	0.00	0.00	0.00	0.00
GW110707	1.4	242589.9818	6295588.561	**0.00**	0.00	0.00	0.00	0.00
GW110704	1.55	241549.9799	6296991.556	**0.00**	0.00	0.00	0.00	0.00
GW110705	1.7	241838.9793	6297075.554	**0.00**	0.00	0.00	0.00	0.00
GW101299	3.75	233678.8713	6294345.323	**-0.08**	-0.19	-0.19	-0.14	0.06
GW100625	4.1	236219.0107	6297108.796	**0.00**	0.00	0.00	0.00	0.00
GW101294	4.25	233679.0855	6294345.328	**-0.08**	-0.19	-0.19	-0.14	0.06
GW067397	4.5	237222.3253	6292575.023	**0.00**	0.00	0.00	0.00	0.00
GW067395	5	237152.5896	6292818.885	**-0.06**	-0.14	-0.15	-0.09	0.02
GW011892	5.4	232547.2939	6296341.407	**-0.02**	-0.02	-0.02	-0.02	0.00
GW067398	5.5	237283.343	6292514.694	**-0.06**	-0.11	-0.12	-0.07	0.02
GW101293	5.9	233679.0912	6294345.122	**-0.08**	-0.19	-0.19	-0.14	0.06
GW109263	6	230187.9797	6302354.436	**0.46**	-3.67	-3.82	-3.52	3.98
GW101297	6	233678.8713	6294345.323	**-0.08**	-0.19	-0.19	-0.14	0.06
GW100627	6	236218.5822	6297108.785	**0.00**	0.00	0.00	0.00	0.00
GW100629	6	236218.5822	6297108.785	**0.00**	0.00	0.00	0.00	0.00
GW100628	6	236218.5934	6297108.373	**0.00**	0.00	0.00	0.00	0.00
GW100638	6	236218.8021	6297108.585	**0.00**	0.00	0.00	0.00	0.00

GW067396	6	237158.1676	6292750.4	**-0.06**	-0.14	-0.15	-0.09	0.02
GW101301	6.8	233678.8713	6294345.323	**-0.08**	-0.19	-0.19	-0.14	0.06
GW067399	7	237309.9943	6292626.122	**-0.06**	-0.13	-0.14	-0.08	0.02
GW101292	7.2	233678.8827	6294344.911	**-0.08**	-0.19	-0.20	-0.14	0.06
GW103224	7.6	238274.7953	6293737.768	**0.00**	-0.30	-0.44	-0.22	0.22
GW109260	9	231948.9767	6301451.453	**0.00**	0.00	0.00	0.00	0.00
GW101302	9	233679.0912	6294345.122	**-0.08**	-0.19	-0.20	-0.14	0.06
GW100632	9	236218.8021	6297108.585	**0.00**	0.00	0.00	0.00	0.00
GW100633	9	236218.8021	6297108.585	**0.00**	0.00	0.00	0.00	0.00
GW100639	10.5	236218.5878	6297108.579	**0.00**	0.00	0.00	0.00	0.00
GW100631	10.5	236218.8021	6297108.585	**0.00**	0.00	0.00	0.00	0.00
GW103223	10.5	238308.8795	6293687.65	**0.00**	-0.26	-0.37	-0.19	0.19
GW101303	11	233678.877	6294345.117	**-0.08**	-0.19	-0.20	-0.14	0.06
GW100636	11	236218.7965	6297108.791	**0.00**	0.00	0.00	0.00	0.00
GW101300	11.8	233678.8827	6294344.911	**-0.08**	-0.19	-0.19	-0.13	0.06
GW110162	12	228444.977	6304250.408	**0.02**	0.01	0.01	0.02	0.00
GW101295	12	233679.0912	6294345.122	**-0.08**	-0.19	-0.20	-0.14	0.06
GW100626	12	236218.3623	6297108.985	**0.00**	0.00	0.00	0.00	0.00
GW100637	12	236218.5878	6297108.579	**0.00**	0.00	0.00	0.00	0.00
GW110480	13	229530.0858	6301968.354	**0.03**	0.02	0.02	0.02	0.01
GW100634	13.8	236218.8021	6297108.585	**0.00**	0.00	0.00	0.00	0.00
GW109264	14.3	229630.9758	6302170.427	**0.07**	-0.07	-0.07	-0.07	0.14
GW109265	14.9	229379.974	6301983.427	**0.00**	0.00	0.00	0.00	0.00
GW060428	15	231161.8846	6296888.799	**-0.02**	-0.03	-0.03	-0.02	0.00
GW055053	15.2	232063.158	6295156.214	**0.01**	0.01	0.01	0.01	0.00
GW100718	15.2	236218.8077	6297108.379	**0.00**	0.00	0.00	0.00	0.00
GW110481	15.8	229165.9717	6301605.418	**-0.13**	-0.13	-0.13	-0.13	0.00
GW105295	16	230238.8218	6307853.102	**0.10**	0.03	-0.01	0.06	0.04
GW105294	16	230336.5413	6307810.719	**0.14**	0.01	-0.05	0.07	0.06
GW100635	16	236218.8021	6297108.585	**0.00**	0.00	0.00	0.00	0.00
GW104218	17.3	234133.6385	6292824	**-0.43**	-0.98	-0.99	-0.79	0.35
GW109262	17.45	230233.9737	6301697.431	**0.03**	0.02	0.02	0.02	0.00
GW101304	18	233679.2998	6294345.334	**-0.08**	-0.19	-0.19	-0.14	0.06
GW109261	18.03	229803.9774	6301348.424	**-0.10**	-0.10	-0.11	-0.10	0.00
GW057399	18.3	231849.8257	6296322.052	**0.06**	0.06	0.06	0.06	0.00
GW054416	18.3	237937.4211	6293005.006	**0.00**	-0.01	-0.01	0.00	-0.01
GW053081	18.6	232055.4583	6295433.524	**0.06**	0.06	0.06	0.06	0.00
GW110483	21	229148.9736	6303041.421	**0.08**	-0.13	-0.13	-0.11	0.20
GW100630	21	236218.5822	6297108.785	**0.00**	0.00	0.00	0.00	0.00
GW055055	21.3	232064.1806	6296050.483	**0.05**	0.05	0.05	0.05	0.00
GW104220	21.3	234172.6387	6292798	**-0.47**	-1.05	-1.06	-0.85	0.38
GW072713	21.336	228517.0702	6302704.19	**0.05**	0.05	0.05	0.05	0.00
GW047900	21.9	236485.7628	6292225.397	**-0.01**	-0.02	-0.02	-0.01	0.00
GW101296	23.2	233678.877	6294345.117	**-0.08**	-0.19	-0.20	-0.14	0.06

GW110161	27.5	228449.9786	6304254.411	**0.04**	0.04	0.04	0.04	0.00
GW101985	30	242016.9328	6296553.982	**-0.07**	-0.09	-0.10	-0.07	0.00
GW106646	30	243457.972	6294097.611	**-0.05**	-0.20	-0.45	-0.06	0.01
GW058108	30.5	232569.7116	6296465.371	**0.01**	0.01	0.01	0.01	0.00
GW057365	30.5	232726.4125	6296408.04	**0.03**	0.03	0.03	0.03	0.00
GW060112	31.4	232057.8654	6294416.004	**-0.03**	-0.04	-0.04	-0.03	-0.01
GW110482	33	229153.0534	6303045.399	**0.08**	-0.13	-0.14	-0.12	0.20
GW058554	33.5	232464.674	6296524.131	**-0.04**	-0.04	-0.04	-0.04	0.00
GW102428	38.1	232195.5546	6294111.469	**-0.05**	-0.06	-0.06	-0.05	-0.01
GW054781	38.1	232468.0896	6296400.883	**-0.06**	-0.06	-0.06	-0.06	0.00
GW104221	38.6	234132.6385	6292824	**-0.44**	-1.00	-1.01	-0.81	0.37
GW072919	40	238297.7325	6293735.083	**0.03**	-0.47	-0.60	-0.39	0.41
GW109845	42	243779.9802	6293855.571	**-0.02**	-0.27	-0.44	-0.09	0.07
GW101461	45	228707.9521	6301414.808	**0.04**	0.04	0.04	0.04	0.00
GW050996	45.7	230231.93	6299638.118	**-0.04**	-0.04	-0.04	-0.04	0.00
GW107329	48	230019.9774	6307333.426	**0.22**	-2.68	-3.54	-0.94	1.16
GW068505	48.8	237289.6462	6292088.028	**-0.05**	-0.08	-0.08	-0.06	0.01
GW100967	50	232630.9179	6294135.888	**-0.04**	-0.05	-0.05	-0.04	0.00
GW109307	55	237496.2689	6292947.912	**-0.03**	0.28	0.28	0.30	-0.33
GW062815	56.7	228909.621	6302101.026	**-0.10**	-0.11	-0.11	-0.11	0.01
GW053046	58.5	229845.5293	6306997.161	**0.20**	-1.50	-1.91	-0.65	0.85
GW110484	59	229721.9713	6302884.423	**1.06**	-13.10	-13.28	-12.69	13.75
GW109844	60	243656.9777	6293782.574	**-0.05**	-0.36	-0.58	-0.13	0.08
GW110485	66.6	229731.9803	6301994.423	**0.05**	-0.30	-0.31	-0.28	0.33
GW103238	68.45	231462.8253	6299285.72	**0.19**	0.19	0.18	0.19	0.00
GW102427	68.45	231520.5745	6299797.356	**0.01**	0.01	-0.15	-0.05	0.06
GW102426	70	231545.5603	6299828.886	**0.02**	0.01	-0.18	-0.06	0.08
GW039443	70	231951.6138	6297311.627	**0.17**	0.17	0.17	0.17	0.00
GW105433	72	238302.6406	6293824.033	**0.04**	-3.13	-3.35	-2.95	2.99
GW105435	72	238312.6408	6293760.033	**0.04**	-2.54	-2.72	-2.40	2.44
GW105434	72	238318.6408	6293795.033	**0.04**	-2.73	-2.93	-2.57	2.61
GW109842	72	243604.9783	6293744.574	**-0.06**	-0.41	-0.65	-0.15	0.09
GW109843	72	243683.9837	6293871.568	**-0.03**	-0.36	-0.59	-0.11	0.08
GW109022	78	241743.9821	6293079.554	**0.24**	-1.13	-1.64	-0.21	0.44
GW058348	99.3	236477.3396	6292533.514	**0.25**	0.30	0.29	0.32	-0.07
GW105064	104	230353.585	6307749.755	**0.36**	-10.00	-12.76	-3.61	3.97
GW105734	120	244008.659	6294415.318	**3.61**	-21.30	-28.47	-5.66	9.27
GW030862	146	232011.306	6305423.047	**0.69**	-1.22	-9.46	-5.30	5.99
GW102728	156.5	244489.3773	6294414.206	**3.10**	-24.84	-30.71	-12.35	15.45
GW108187	197	245529.1095	6295851.426	**3.76**	-33.27	-37.01	-21.31	25.07
GW109766	258	246342.9774	6299272.603	**15.50**	-1.55	-2.31	-0.33	15.82
GW109783	271.9	242072.278	6293481.244	**3.93**	-7.22	-14.48	-0.23	4.17
GW109767	273.6	242637.9752	6296367.56	**13.11**	-20.27	-29.53	-4.48	17.59
GW108185	295	246570.1041	6301610.434	**6.94**	-1.92	-24.25	2.07	4.88

GW109336	319.5	237341.9351	6296561.646	**22.56**	-17.63	-27.56	1.10	21.46
GW109337	400	237488.9801	6300777.513	**24.61**	-101.53	-124.42	-85.40	110.02

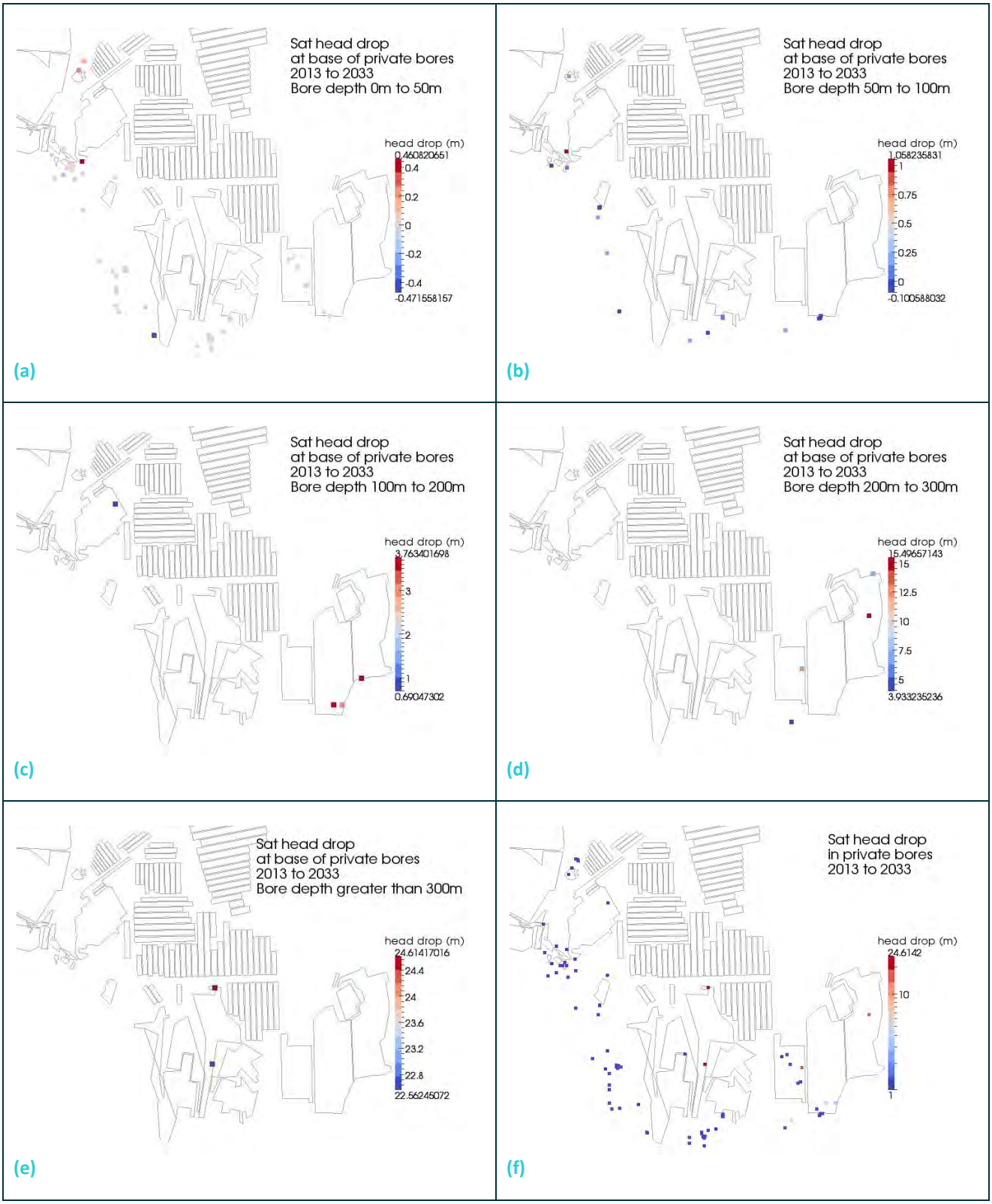

Figure 84 Head drops in private bores due to mining of the proposed APE and SV longwalls (Base case)

4.2.8 Comparison of different mining scenarios

In Section 4.1 (Table 28) three different scenarios simulated in this study were discussed: (i) No new mining, (ii) No APE and (iii) No new SV. The relative impact of each scenario with respect to the Base case is discussed here.

Impact on Cox's River - Section 4.2.5 the drawdown in Cox's River was discussed. It was shown that mining APE and SV LW416 onwards induce a net drawdown at Cox's River of less than 1cm, and most drawdown quantities are much less than 1mm.

Impact on Private bores - Section 4.2.6 the drawdown at the bottom of private bores was discussed. The net effect of the APE and the new SV LW416 onwards on private bores was tabulated. In 2033, the median effect of these mines on private bores of depth less than 50m was 1.1cm, however, some deeper bores suffer substantial drawdown.

Impact of baseflow to swamps and streams - baseflow to the swamps and streams remained fairly steady after 2015 when no new longwalls were extracted beyond 2015 (Appendix C).

Impacts on near-surface groundwater - comparisons are made between the Base case and the "No new mining", "No APE" and "No new SV" scenarios. A comparison of these cases is not entirely straightforward, as recall that pumping and subsequent flooding occurs at different times for different regions in these different scenarios. For instance, pumping of SV in the "No new mining" and "No new SV" scenarios ceases after excavation of LW415, while it ceases after LW503 in the "No APE" scenario, and at 1/1/2033 in the "base" case. Nevertheless, some very important conclusions can be made.

Figure 85 compares the porepressure changes at the top of the model for the four scenarios. The following conclusions can be drawn.

- By comparing "Base case" with "No new SV" in the regions above the entire Angus Place mine (including APE), the new Springvale mining has negligible effect on porepressure change above Angus Place.
- By comparing "base" with "No APE" in the regions above the entire Springvale mine (including the new proposed panels), the APE mining has negligible effect on the porepressure change above the Springvale.
- By comparing "base" with "No new mining", and noting how the drawdown over the AP Bord-and-Pillar region change with time by comparing "base2033" with "base2083", the mining of APE and the new Springvale panels can be seen to have very little effect on the porepressure change over the currently-mined region.

In summary: in the model, the porepressure change at the ground surface above a mine is directly influenced by the underlying panels and hardly influenced at all by other mining activity. Furthermore:

- By comparing all pictures in Figure 85, the porepressure change above the new proposed mines is no greater than that above the currently-existing mines; and,
- By comparing "base2012" with "base2033", continued pumping of an excavated longwall does not significantly change the maximum porepressure change above it, but causes those regions with small amounts of drawdown to slowly shrink in size.

Figure 86 shows the simulated porepressure changes on the ground surface by comparing "Base case" with "No new SV" and "No APE" at 2025 and 2033 which shows negligible effect of SV mines on drawdowns above Angus Place and vice versa.

Therefore an important conclusion is that the impacts on the near-surface groundwater above the newly-proposed mines are likely to be very similar to those already experienced above the currently-mined panels. The maximum drawdown encountered will be of similar size, but the extent of the regions of large drawdown will be smaller because the panels below will not have been pumped for as many years.

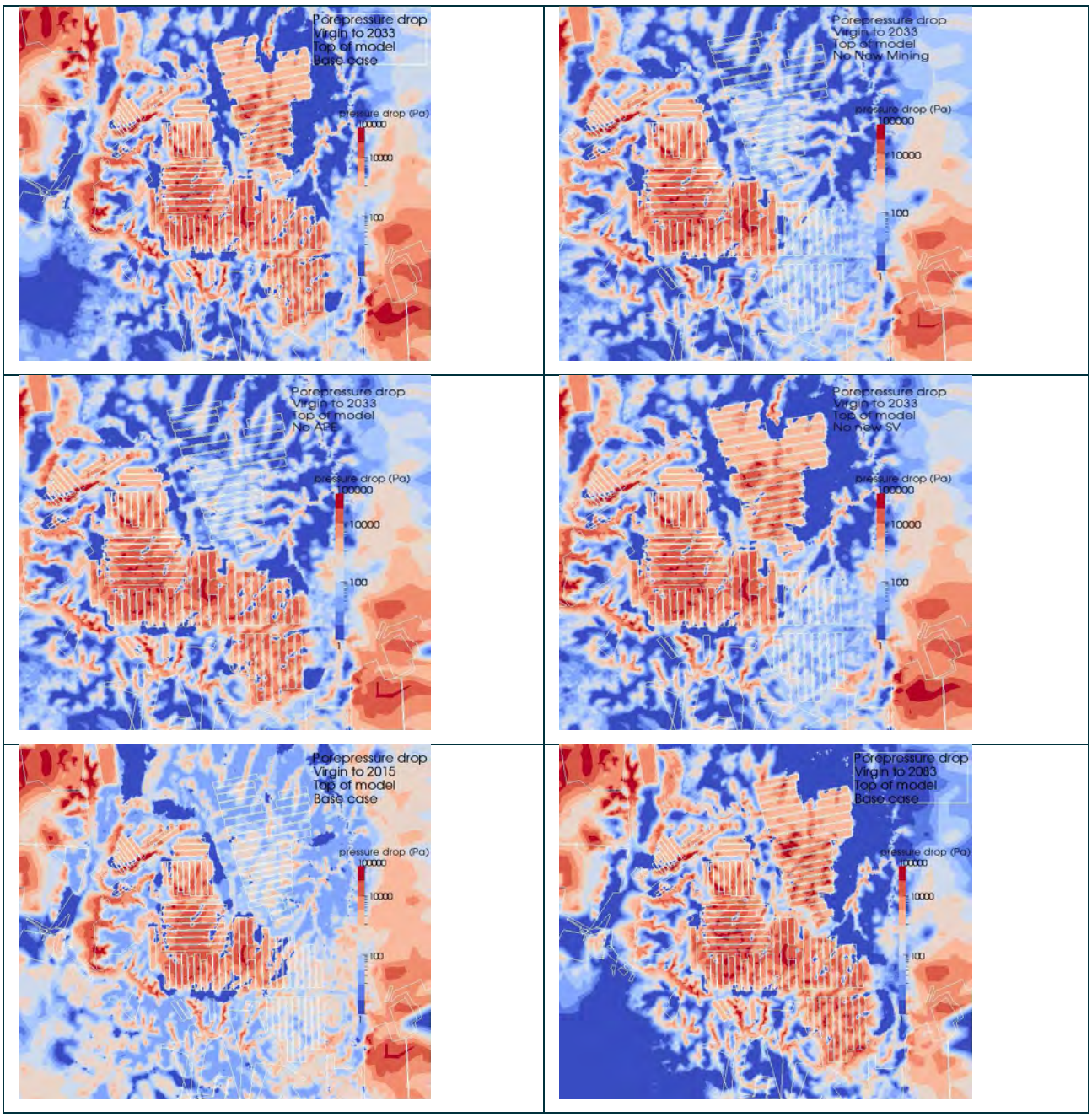

Figure 85 Porepressure change at the top of the model for 4 scenarios. Top left: Base model. Top right: No new mining. Middle left: No APE. Middle right: No new SV. Bottom left: Base model at 2015. Bottom right: Base model at 2083

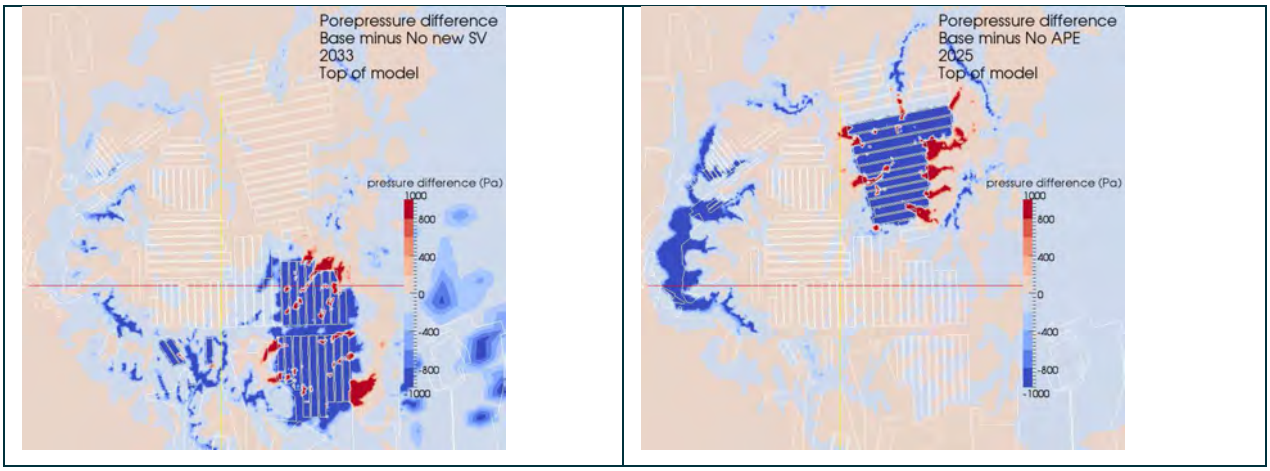

Figure 86 Porepressure change at the top of the model for two scenarios with respect to the Base case

Drawdown in the Lithgow seam - Figure 87 shows the Lithgow seam. Contoured is the head of the Base model minus the head of the "No New SV" scenario. Naturally, this is nonzero in the Springvale mine for two reasons: (1) in the "No New SV" scenario LW416 onwards is not mined; (2) in the "No New SV" scenario, pumping of Springvale mine ceases after extraction of LW415. What is more important is that excavating Springvale has negligible effect on the heads in and around the Angus Place mine and vice versa.

Figure 88 shows the Lithgow seam, and contoured is the head difference between the Base model and the "No New" scenario. At 2033 the Base model has just ceased pumping, while the "No New" model has been flooded for about 20 years. By 2083 the head difference between these two scenarios in the currently excavated regions (up to AP LW980 and SV LW415) is around 20m. Further pictures may be found in Appendix D.

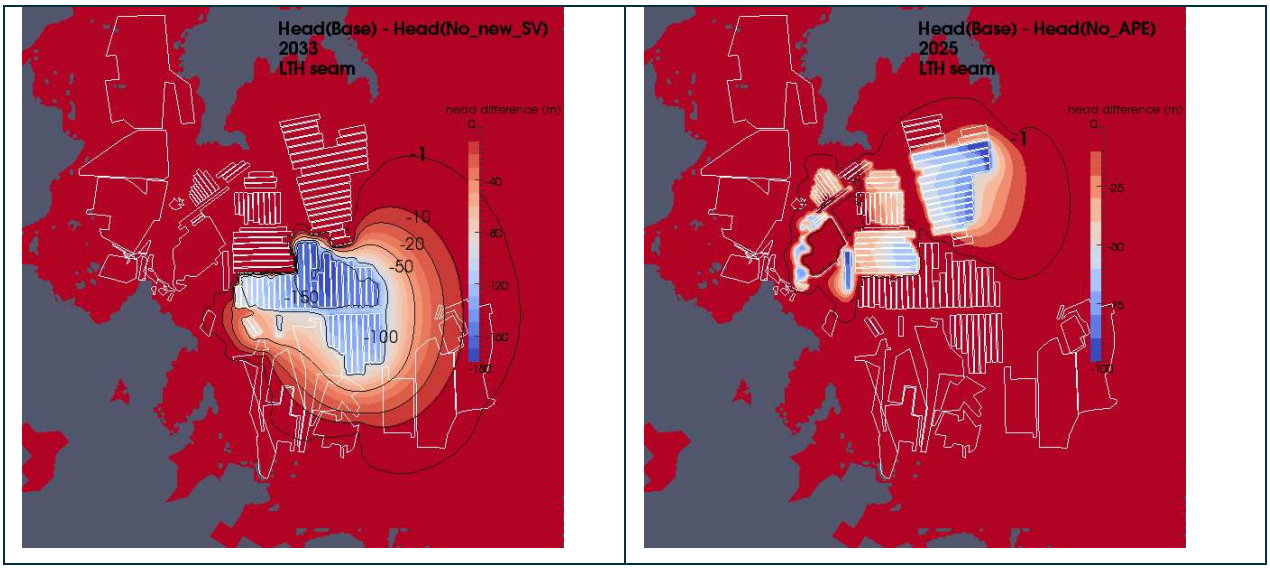

Figure 87 In the Lithgow seam at year 2033 (left) and year (right): the head of the Base model minus the Head of the "No new SV" and "No New APE" models

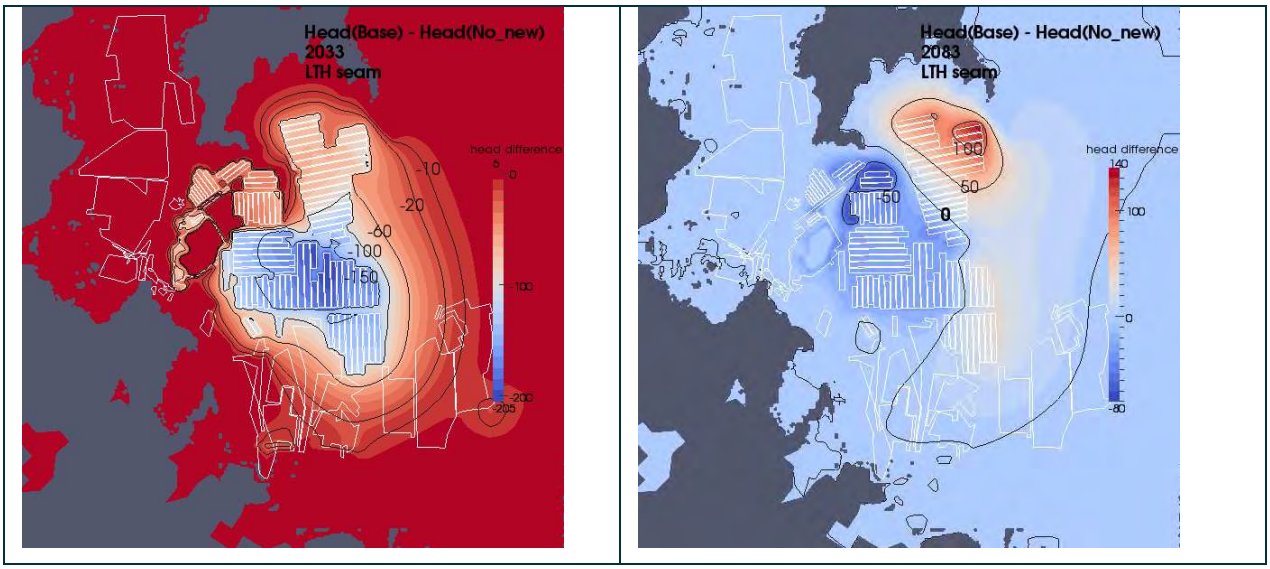

Figure 88. In the Lithgow seam at times 2033 (left) and 2083 (right). Contoured is the head of the base model minus the head of the "No New" scenario.

4.2.9 Climate Change Scenarios

Due to a drier climate over the last few decades, the groundwater resources in Australia are experiencing increasing pressures. Thus, a climate-change impact assessment has become an integral part of groundwater modelling studies in recent years. However, there is still a lack of well defined procedures for properly deriving the climate change parameters. The Australian Groundwater Modelling Guidelines (2012) briefly discusses this aspect in Section 6.4; however, no specific guidance on this topic is provided.

In 2004 Council of Australian Governments formed a National Water Initiative (NWI) to concentrate effort on assessing the risks associated with climate change. The National Water Commission produced a report entitled "Climate Change Impact on Groundwater Resources in Australia", which identified the annual rainfall as the most important climate parameter, and stated that the groundwater recharge and the rainfall ratio are related non-linearly due to variability in rainfall intensity or the number of consecutive rain days.

A detailed investigation of probable future climate conditions (rainfall and temperature) and how the change in rainfall intensity or consecutive rain days may impact on the groundwater recharge rate in the present model region is naturally beyond the scope of this study. Thus four different simplistic scenarios shown in Table 43 are simulated.

Table 43 Climate change parameters

Parameter	Change %
Rainfall	± 15
ETmax	± 15

The rainfall data given in Table 6 yields an average rainfall of 2.47 mm/day in the AP and SV mining region between 2002 and 2012 and an average rainfall of 2.78mm/day between 2007 and 2010, which is about 13% increase over the 2002 to 2012 period. Figure 89 shows the projected rainfall for wet, medium and dry climate scenarios for 2030 and 2050 over the entire country (Barron, OV et al, 2011). The change in rainfall is projected to vary spatially in magnitude. Based on the available rainfall data and the projected rainfall diagram (Figure 89), rainfall recharge is varied by ± 15% in this study.

Table 44 and Table 45 shows the predicted discharge to streams/swamps for 15% increase and 15% decrease of the rainfall recharge respectively. 15% increase in rainfall recharge is projected to increase the median discharge to streams/swamps by 11.2%. Baseflow to swamps and streams with negligible baseflows (e.g. Gang Gang South East Swamp) is predicted to almost double.

Similarly, 15% decrease in rainfall recharge is projected to decrease the median discharge to streams/swamps by 10%. The swamps and streams with small baseflows may cease to yield any discharge (e.g. Kangaroo Creek).

The change in pan-evaporation rate (ET_{max}) seems to have no appreciable effect on the discharge to streams/swamps. Increasing ET_{max} by 15% decreases baseflow by 2.5% on average. Decreasing ET_{max} by 15% has the opposite effect

Rainfall and Evapotranspiration have some effects to the drawdown in the private bores. The effect of these parameters on the deep bores is small, but the effect on those of depth less than 50m is shown in Table 46. For instance, in the high-rainfall scenario, the drawdown in these shallow bores is, on average, 13cm less than the Base case scenario.

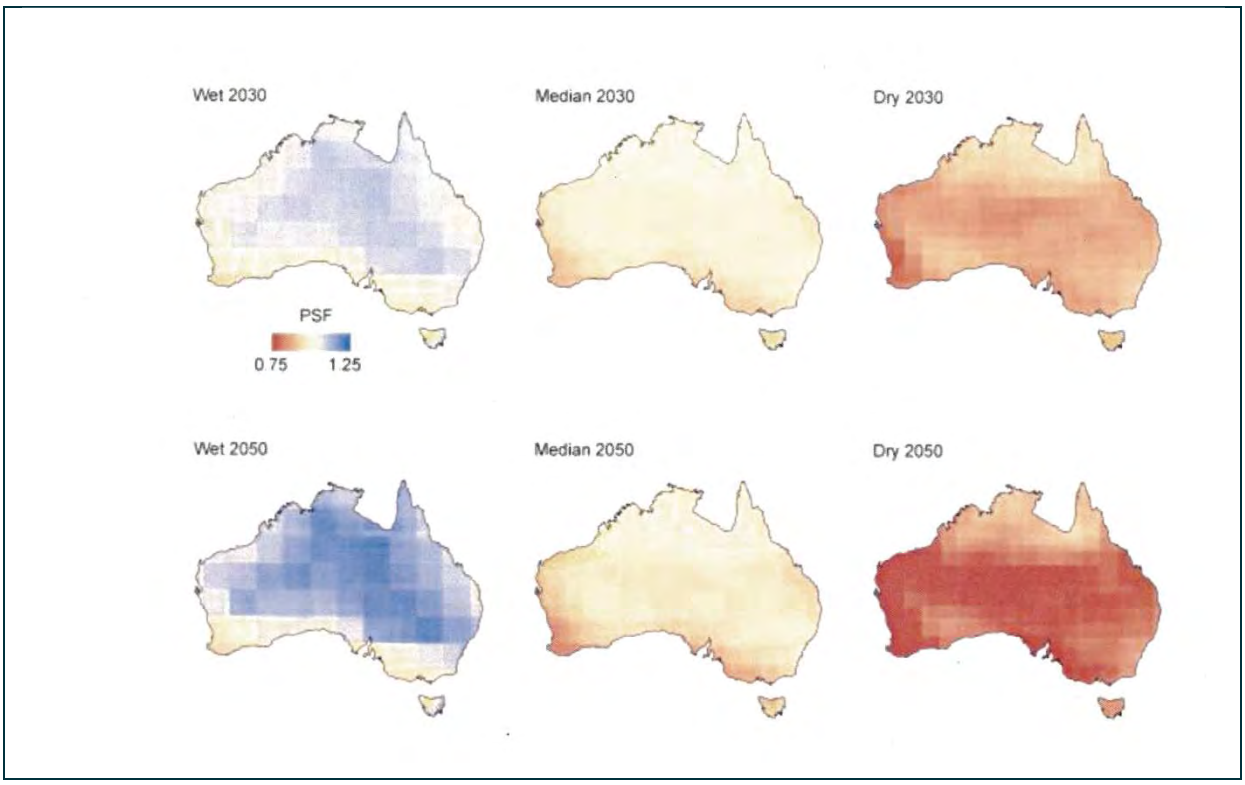

Figure 89 Precipitation scaling factors (PSF): change in annual average rainfall projected for wet, median and dry future climate scenarios for 2030 (top row) and 2050 (bottom row) relative to base (Barron, OV et al, 2011)

Table 44 Projected increase in baseflow due to 15% increase in rainfall recharge

Swamps and streams	Discharge in 2022 (ML/day)	Increase in discharge (%)	Discharge in 2032 (ML/day)	Increase in discharge (%)	Discharge in 2064 (ML/day)	Increase in discharge (%)
CA2 (includes Carne Central Swamp)	1.052	19.5	0.974	8.2	1.014	12.7
Carne West Swamp	0.056	3.7	0.051	10.9	0.047	13.7
Carne Creek Total	6.420	4.1	6.270	5.7	6.690	7.4
Gang Gang Swamp South East	0.005	105.0	0.003	103.0	0.006	106.0
Gang Gang Swamp South	-0.018	50.0	-0.038	36.7	-0.039	39.4
Kangaroo Swamp	0.016	5.3	0.015	8.6	0.014	10.8
Kangaroo Creek Total	0.146	21.7	0.086	115.0	0.145	61.1
Lamb Creek	0.127	11.4	0.116	22.1	0.158	22.5
Long Swamp	0.033	4.7	0.034	8.4	0.034	13.0
Marrangaroo Creek	0.928	9.2	0.933	12.4	0.918	16.1
Nine Mile Swamp	0.030	30.4	0.030	30.4	0.031	34.8
Paddy's Creek	0.173	6.1	0.173	6.1	0.180	10.4
Pine Swamp	0.220	4.8	0.187	0.5	0.175	1.7
Tri-Star Swamp	0.146	8.1	0.125	16.8	0.080	37.9
Twin Gully Swamp	0.078	6.8	0.099	11.2	0.073	21.7
Sunnyside Swamp	0.113	6.3	0.109	8.0	0.102	11.4
Wolgan River Total	1.371	9.7	1.236	13.4	1.108	20.4

Table 45 Projected decrease in baseflow due to 15% decrease in rainfall recharge

Swamps and streams	Discharge in 2022 (ML/day)	Increase in discharge (%)	Discharge in 2032 (ML/day)	Increase in discharge (%)	Discharge in 2064 (ML/day)	Increase in discharge (%)
CA2 (includes Carne Central Swamp)	0.870	-1.1	0.810	-10.0	0.797	-11.4
Carne West Swamp	0.050	-7.2	0.042	-9.6	0.036	-13.4
Carne Creek Total	5.930	-3.9	5.580	-5.9	5.740	-7.9
Gang Gang Swamp South East	-0.100	0.0	-0.100	0.0	-0.100	0.0
Gang Gang Swamp South	-0.054	-50.8	-0.083	-39.0	-0.094	-44.5
Kangaroo Swamp	0.014	-6.7	0.013	-8.6	0.010	-23.1
Kangaroo Creek Total	-0.006	-105.0	-0.117	-392.5	-0.106	-217.8
Lamb Creek	0.101	-11.1	0.077	-19.4	0.094	-27.1
Long Swamp	0.030	-5.0	0.030	-3.9	0.030	-0.7
Marrangaroo Creek	0.763	-10.2	0.726	-12.5	0.650	-17.8
Nine Mile Swamp	0.017	-24.3	0.016	-31.7	0.014	-38.3
Paddy's Creek	0.154	-5.5	0.152	-6.7	0.152	-6.7
Pine Swamp	0.198	-5.7	0.156	-16.1	0.138	-19.8
Tri-Star Swamp	0.124	-8.1	0.093	-13.1	0.034	-41.4
Twin Gully Swamp	0.068	-6.8	0.081	-9.0	0.050	-16.7
Sunnyside Swamp	0.100	-5.9	0.093	-8.3	0.081	-11.9
Wolgan River Total	1.163	-7.0	0.971	-10.9	0.758	-17.6

Table 46 Effect of rainfall and ET on the head drops measured in private bores of less than 50m depth

Scenario	Average effect on drawdown for bores of depth less than 50m
High rain	-13 cm
Low rain	+15 cm
High ET	+2 cm
Low ET	-2 cm

5 Recovery Simulation

Once the APE extraction was completed in December 2032, all the mines were assumed to be flooded and groundwater recovery was simulated in transient mode to 2383 and then the model is allowed to attain a steady-state. The scenarios simulated are described in Table 28.

5.1.1 Water balance during the recovery period

The average rates of recharge and discharge throughout the recovery period from 2033 to 2083 are given in Table 47. The average recharge to the groundwater system is 133 ML/day, comprising mainly rainfall recharge (126.5 ML/day) and leakage from swamps and streams into the groundwater system (7 ML/day).

The average groundwater discharge across the model is 127 ML/day. ET represents the major source of discharge (94 ML/day). Baseflow to swamps and streams is 15 ML/day.

A net loss of groundwater across the model boundary is 18 ML/day. The gain in fluid storage in the groundwater system is 6 ML/day.

Table 47 Average rates of recharge and discharge 2033 to 2083

Component	Groundwater Inflow (Recharge) (ML/day)	Groundwater Outflow (Discharge) (ML/day)
Rainfall recharge	126.5	
Evapotranspiration		94.3
Swamps and rivers	6.8	14.7
Net outflow through model boundary (ML/day)	18.0 .	
Mine inflow (ML/day)		0
Total (ML/day)	133.3	127.0
Net Outflow (ML/day)	-6.3	
Change in fluid volume contained (storage) in the model (ML/day)	+6.3	
Discrepancy	3.4x10-4 %	

The average rates of recharge and discharge throughout the recovery period from 2083 to 2183 are given in Table 48.

The average recharge to the groundwater system is 133 ML/day, comprising mainly rainfall recharge (126 ML/day) and leakage from swamps and streams into the groundwater system (7 ML/day).

The average groundwater discharge across the model is 130 ML/day. ET represents the major source of discharge (97 ML/day). Baseflow to swamps and streams is 15 ML/day.

A net loss of groundwater across the model boundary is 18 ML/day. The gain in fluid storage in the groundwater system is 3 ML/day.

Table 48 Average rates of recharge and discharge 2083 to 2183

Component	Groundwater Inflow (Recharge) (ML/day)	Groundwater Outflow (Discharge) (ML/day)
Rainfall recharge	126.5	
Evapotranspiration		96.8
Swamps and rivers	6.7	15.2
Net outflow through model boundary (ML/day)	18.2 .	
Mine inflow (ML/day)		0
Total (ML/day)	133.2	130.2
Net Outflow (ML/day)	-3.02	
Change in fluid volume contained (storage) in the model (ML/day)	+3.02	
Discrepancy	1.3x10-4 %	

The average rates of recharge and discharge throughout the recovery period from 2183 to 2383 are given in Table 49. The average recharge to the groundwater system is 133 ML/day, comprising mainly rainfall recharge (126 ML/day) and leakage from swamps and streams into the groundwater system (6.5 ML/day).

The average groundwater discharge across the model is 130 ML/day. ET represents the major source of discharge (98.2 ML/day). Baseflow to swamps and streams is 15 ML/day.

A net loss of groundwater across the model boundary is 18 ML/day. The gain in fluid storage in the groundwater system is less than 1 ML/day.

Table 49 Average rates of recharge and discharge 2183 to 2383

Component	Groundwater Inflow (Recharge) (ML/day)	Groundwater Outflow (Discharge) (ML/day)
Rainfall recharge	126.4	
Evapotranspiration		98.2
Swamps and rivers	6.5	15.7
Net outflow through model boundary (ML/day)	18.2 .	
Mine inflow (ML/day)		0
Total (ML/day)	132.9	132.1
Net Outflow (ML/day)	-0.84	
Change in fluid volume contained (storage) in the model (ML/day)	+0.84	
Discrepancy	4.3x10-5 %	

Table 50 Average rates of recharge and discharge 2033 to 2383

Component	Recovery from 2033 to 2083		Recovery from 2083 to 2183		Recovery from 2183 to 2383	
	Groundwater Inflow (Recharge) (ML/day)	Groundwater Outflow (Discharge) (ML/day)	Groundwater Inflow (Recharge) (ML/day)	Groundwater Outflow (Discharge) (ML/day)	Groundwater Inflow (Recharge) (ML/day)	Groundwater Outflow (Discharge) (ML/day)
Rainfall recharge	126.5		126.5		126.4	
Evapotranspiration		94.3		96.8		98.2
Swamps and rivers	6.8	14.7	6.7	15.2	6.5	15.7
Net outflow through model boundary (ML/day)	18.0		18.2		18.2	
Mine inflow (ML/day)	0		0		0	
Total (ML/day)	133.3	127.0	133.2	130.2	132.9	132.1
Net Outflow (ML/day)	-6.3		-3.02			-0.84
Change in fluid volume contained (storage) in the model (ML/day)	+6.3			+3.02		+0.84
Discrepancy	3.4x10-4 %		1.3x10-4 %		4.3x10-5 %	

From Table 50, it can be seen that the model is close to a steady-state after 350 years; the changes in the groundwater balance between 2183 and 2383 is very small. The rate of change in groundwater storage account for only around 0.6% of the total recharge in this period.

5.1.2 Water content within the model

Figure 90 and Figure 91 depict the water content changes in each layer throughout mining and recovery. In absolute terms, AQ3 loses most water and it takes around 350 years to achieve effective steady-state. The topmost layers, Weath and AQ6, also lose 3% and 8% of their water content respectively, but take only around 50 years to achieve steady-state. As discussed earlier, the loss of water in the upper strata during the period from 2006 to 2012 may also be attributed to the climatic variation.

AQ1 loses around 5% of its water content and also takes around 50 years to achieve steady-state. Because the model has a 30km x 30km extent, only approximately 25% of AQ3 is undermined. This is the region that loses water. The figures below pertain to the whole model, so that a loss of 4.5% from AQ3 over the whole model means the part of AQ3 directly over mining panels loses approximately 18% of its water (4.5/25%). Similarly, many years after mine completion, the whole of AQ3 has 1% less water than initially, and the parts over mining panels contain approximately 4% less than the pre-mining state. This is illustrated qualitatively in the phreatic-surface cross sections.

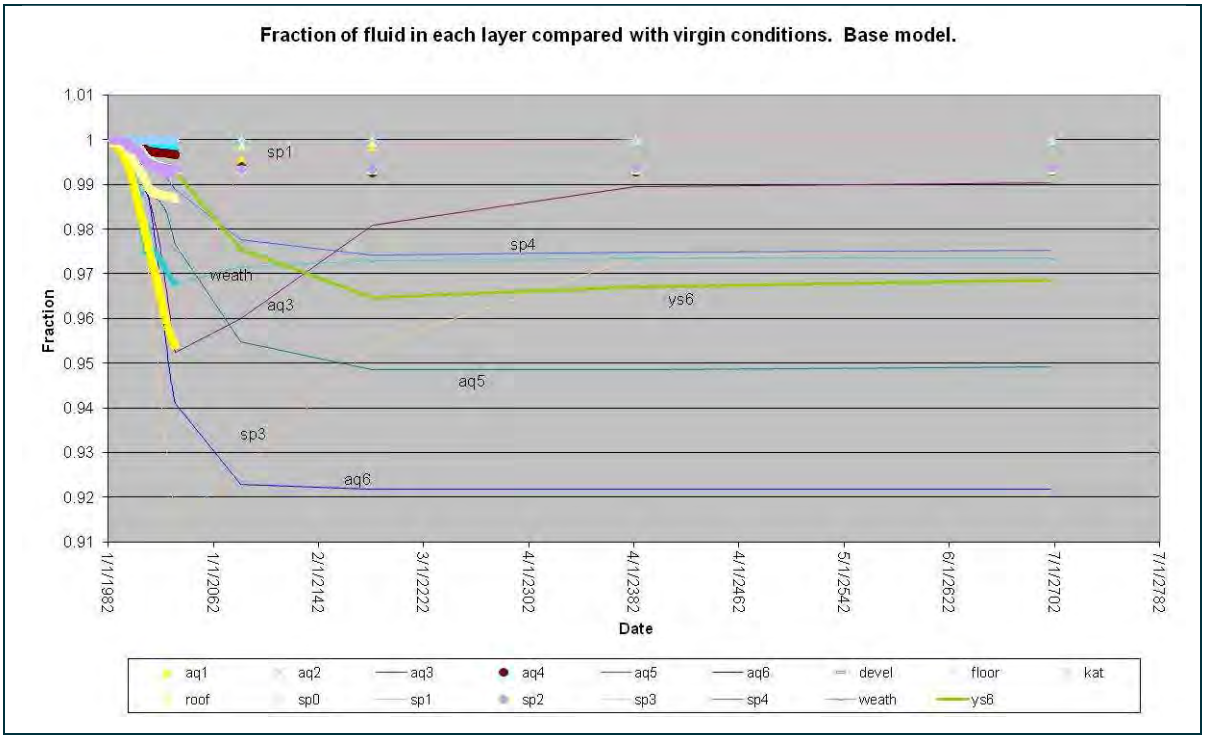

Figure 90 Fraction of fluid in each layer compared with virgin conditions during recovery

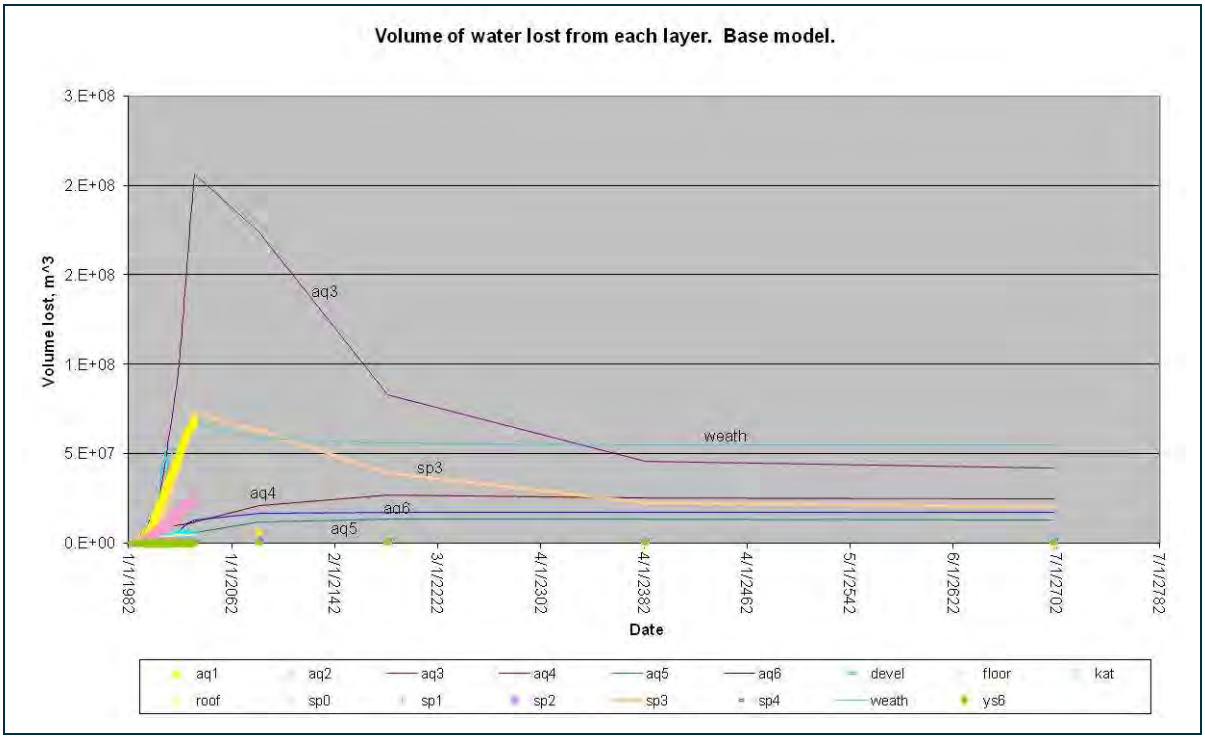

Figure 91 Volume of water lost from each layer between virgin conditions and year 2683

5.1.3 Recovery of water levels

Appendix D provides the simulated recovery of water levels in the Lithgow Seam, AQ1, AQ2, AQ3, AQ4, AQ5, AQ6 and the top of the model (i.e. the ground surface) following 50 and 100 years of recovery after completion of mining.

Figures D43 to D56 in Appendix D show the simulated recovery of water levels with respect to the pre-mining groundwater conditions and Figures D57 to D70 show the simulated recovery of water levels with respect to groundwater levels at the end of the validation period (1 Jan 2012).

Figure 92 and Figure 93 show two typical recovery plots (recovery-negative and drawdown-positive) with respect to the pre-mining groundwater condition in the Lithgow Seam following 50 years and 100 years of completion of mining respectively. Figure 92 shows the recovery 50 years following completion of mining while Figure 93 shows the recovery 150 years following completion of mining. The groundwater levels in the Lithgow seam have increased by up to 100m above the pre-mining groundwater levels. The groundwater recharge zone seems to develop first in the APE_12 and APE_13A mine voids the deepest point within the Lithgow Seam and then gradually expand laterally in the south westerly direction filling up more mining voids. The area with 40m drawdown (west of the AP and SV mines, Figure 92) can be seen to be gradually being recharged from 2083 to 2183 (Figure 93). The drawdown quantities are typically negative, indicating an increase in porepressure compared with pre-mining conditions. This is due to mining-induced permeability enhancements allowing water to enter lower strata at a faster rate than before mining.

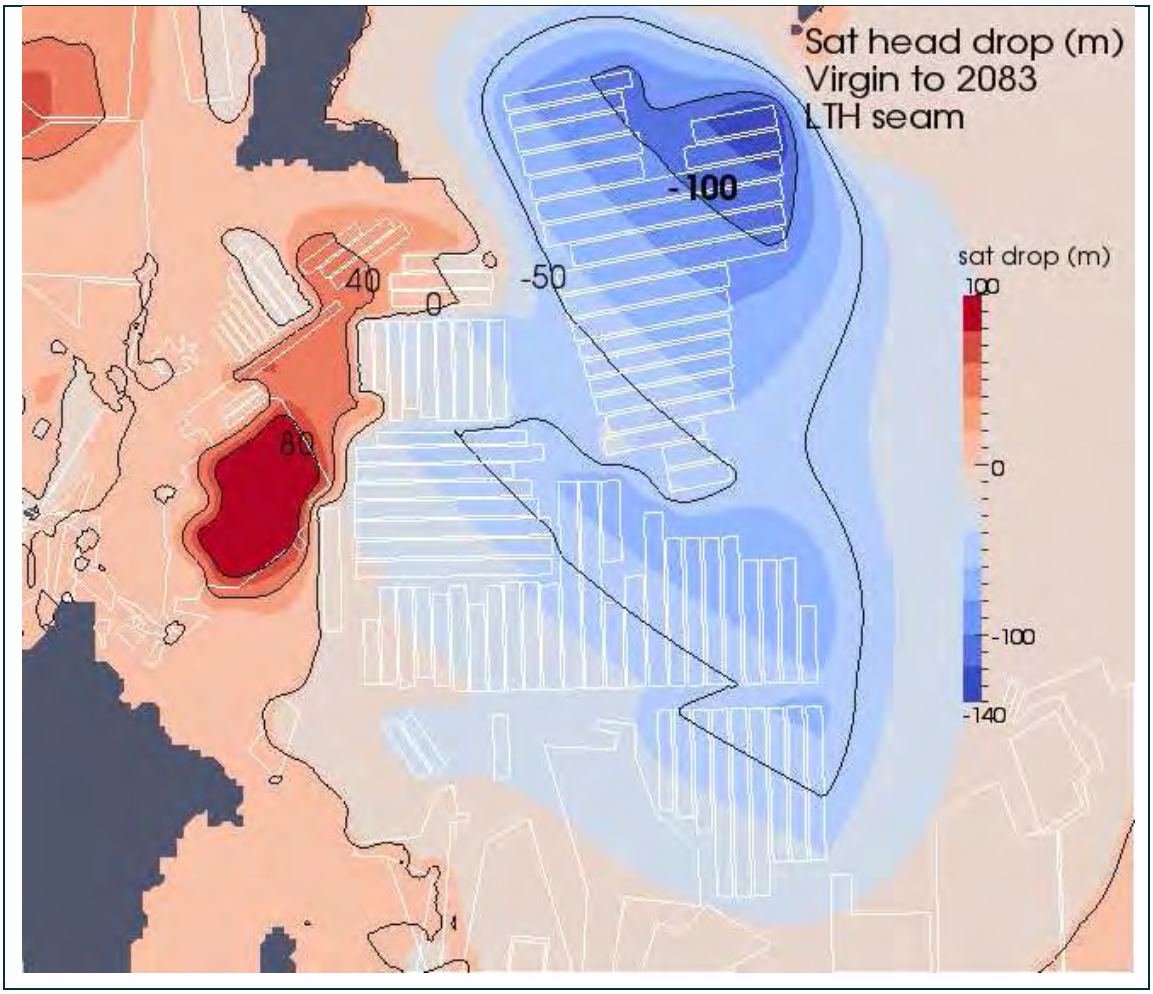

Figure 92 Distribution of head drops in the Lithgow Seam at 2083 with respect to pre-mining groundwater condition

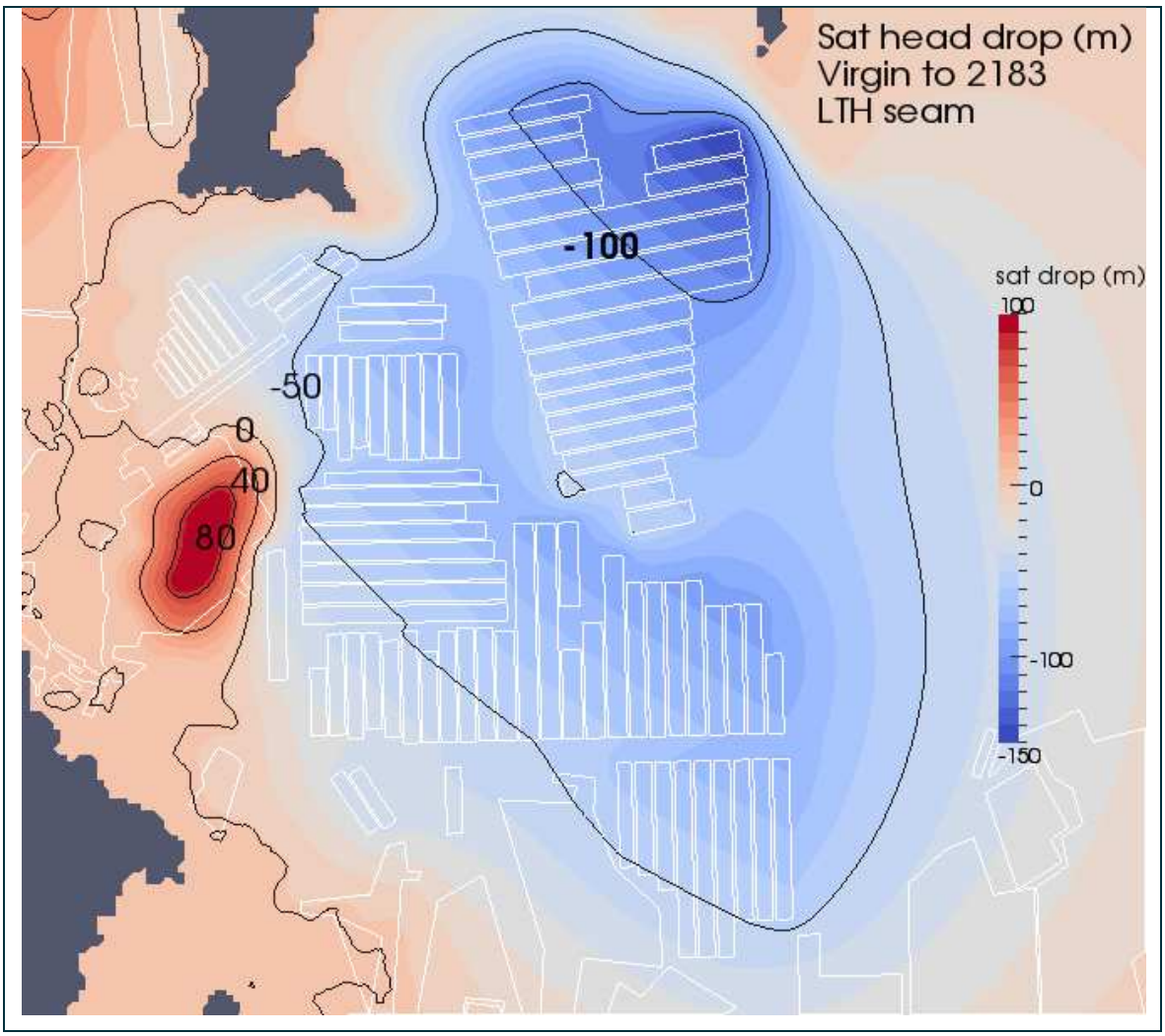

Figure 93 Distribution of head drops in the Lithgow Seam at 2183 with respect to pre-mining groundwater condition

Recovery of water levels within AQ1, AQ2 and AQ3 can be seen in Figures D45 to D50. The groundwater recharge zone again seems to develop first in the APE_12 and APE_13A regions and then gradually expand laterally in the south westerly direction filling up more strata.

Figure 94 and Figure 95 show the head drops at the ground surface of the model compared with the virgin conditions at 2083 and 2183. Head drops are similar in magnitude over the new APE and Springvale panels than those over the already-mined regions (compare with Figure 60 for instance). Figure 94 and Figure 95 are quite similar, demonstrating that for the model's topmost layer, steady-state is effectively achieved by 2083, which is also supported by graphs in Section 5.1.2.

The following observations can be made.

- The extensive desaturation occurring in AQ1 above the mining panels completely disappears within 50 years.
- The unsaturated zones in AQ3 below MYC slowly fill over the 100 years after mining, but in most cases there remains a small unsaturated zone even after the model has been run to steady-state.
- The strata above MYC effectively reach steady-state within 50 years after mining ceases.
- Some regions in AQ4 below YS6 which were initially saturated remain unsaturated after mining, while some regions which were initially unsaturated become saturated after mining.
- The regions above SP4 experience a phreatic-surface drop of a few metres below the topographic ridges, and less than this in the valleys, and the phreatic surface in this region typically falls very slightly during the 50 years after mining ceases before reaching steady-state.

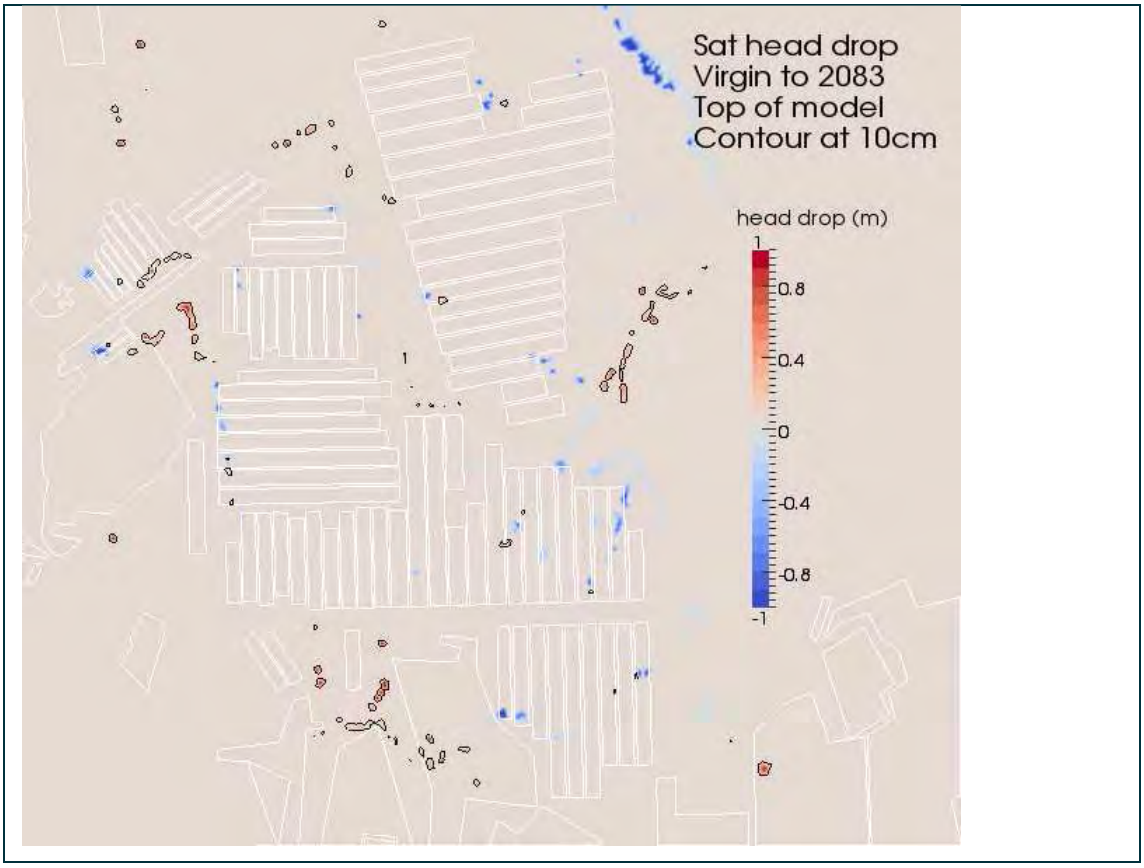

Figure 94 Distribution of saturated head drops at the ground surface in 2083 with respect to pre-mining groundwater condition.

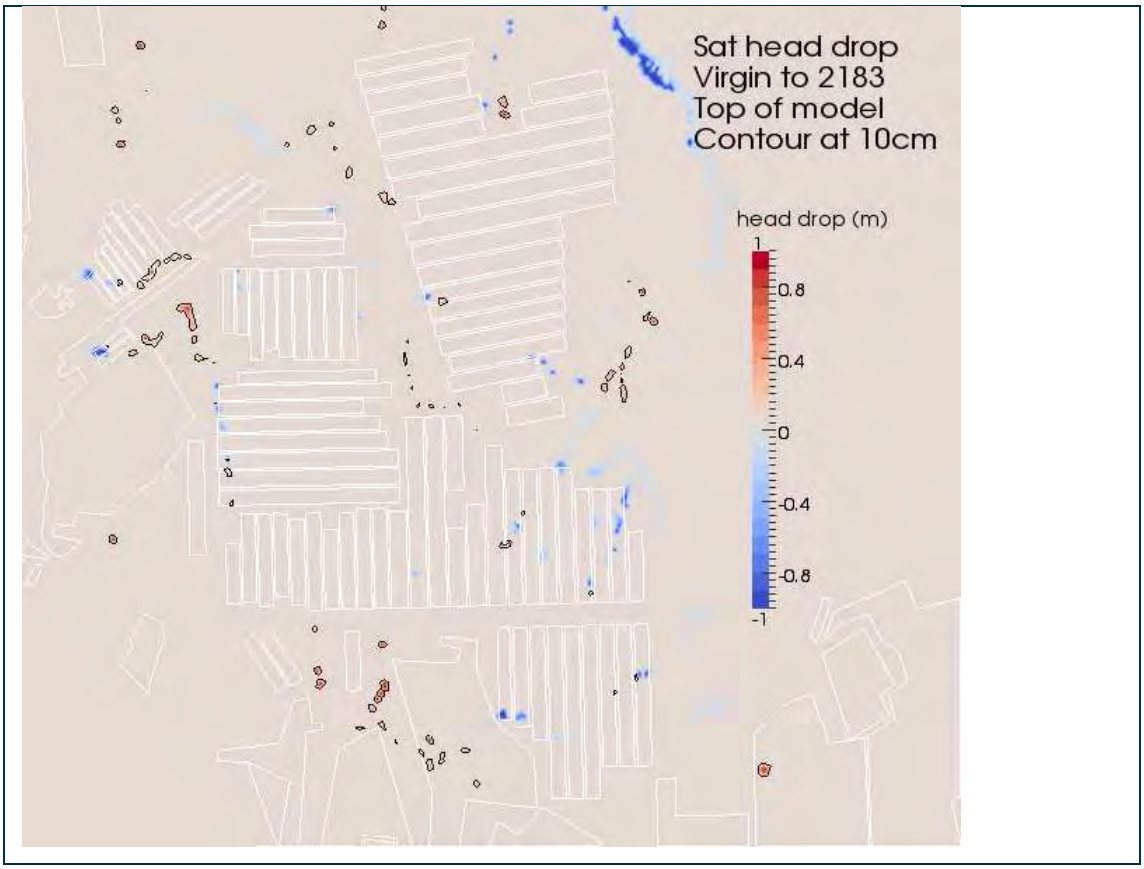

Figure 95 Distribution of saturated head drops at the ground surface in 2183 with respect to pre-mining groundwater condition

6 Model Limitations

A numerical groundwater model is necessarily a simplified representation of complex hydrogeological system. It is not possible to represent the natural groundwater system accurately using numerical models mainly due to the complexities associated with natural systems, our inability to adequately understand the hydrogeological variation both temporally and spatially, and the limitations imposed by numerical methods. Thus it needs to be recognised that a groundwater model is a simplified version of a real groundwater flow system, and therefore cannot replicate groundwater behaviour with 100% accuracy. Rojstaczer (1994) and the references cited there discuss the limitations of numerical groundwater models in great detail. However, a numerical groundwater model may serve as a tool to help understand declining ground-water levels due to mine dewatering and assess the effects of possible management scenarios.

The main limitations of the groundwater model considered in this study are:

- **Short span of observational data** – the parameter calibration relies on the quality of observation data, but only relatively short span of piezometric monitoring data are available for calibration in comparison to much longer period of mining activity in the region. This could have potentially impacted on the accuracy of simulated pre-mining water heads.
- **Non-uniqueness** – this is a well recognised problem in groundwater modelling and is the main issue faced during the model calibration process. The Australian Groundwater Modelling Guidelines notes “One challenge in model calibration is commonly described as the non-uniqueness problem, the possibility that multiple combinations of parameters may be equally good at fitting historical measurements.” The sensitivity studies of Sections 3.4 and 0 enumerate the differences in the model results obtained by varying permeability of model layers, rainfall recharge and ET, and the permeability-change parameters. .
- **Error and uncertainty** - there could be many sources of error and uncertainty in models. The model error may stem from practical limitations of mesh size (resolution), time discretisation, uncertainty in model input parameters, limited calibration data, and the possible significant effects of some of the processes not simulated by the model. These factors, along with unavoidable error in observations, result in uncertainty in model predictions. The numerical groundwater model is constructed with the aim of simulating the process of regional scale depressurization due to mine dewatering. The mesh size of 60m is used to discretise the AP and SV mining region and the much coarser mesh is used away from the AP and SV mining region. Thus the model mesh is not suitable to simulate the processes that occur at much finer scales e.g. development of subsidence induced compression and extension zones at the near surface strata, near-surface tensile cracking, valley closure and upsidence, river bed cracking etc. In addition, surface cracking occurs in a generally unpredictable fashion, which adds further difficulty in simulating such processes using a model designed for a regional scale groundwater impact assessment.
- **Model resolution issues** – the mesh size used in this study may not be suitable for reliably predicting the behaviour of swamps that are being supported by perched groundwater systems. The model reliability could be improved by simulating the behaviour of the perched groundwater fed swamps/streams using fine scale micro models.
- **Coupled strata deformation and groundwater flow process** - the model does not simulate the dynamic interaction between mining induced deformation and strata fracturing and flow of groundwater directly. As discussed in Adhikary and Wilkins (2012), the processes to be modelled are complex and coupled. Mining excavation leads to relief of in situ stresses. The stress relief leads to rock deformation and fracture, which in turn leads to changes in rock permeability and water pore pressures. Pore pressure changes lead to water flow. Flow of water into the mining voids causes further reduction in reservoir pressure leading to desorption of previously trapped methane in coal seams. These processes lead to further changes in effective stress and deformation and the

cycle continues. This is a dynamic process and all of the factors must be considered simultaneously to achieve accurate predictions. Any attempt to simulate such a process in isolation is undesirable.

- **Mining induced permeability change** - though, the numerical model considers the change in strata permeability induced by mining and assigns different values of permeabilities to the model elements using a ramp function as discussed in Section 2.13.4, the mining induced fractures are assumed to be smeared across the model mesh as opposed to the actual fractures within the strata which tend to be more localized and discrete. The model has assumed two distinct zones of fracturing above a longwall panel i.e. an unconsolidated zone closer to an active longwall face and a zone above a well consolidated goaf; however, the model ignores possible local variations of permeability changes, e.g. ignores the role of chain-pillars and assigns the same permeability values across the width of the longwall panel.
- **Uniform model parameters** – the model input parameters are assumed to be uniform i.e. rainfall recharge and ET do not vary spatially and hydraulic properties within each layer are assumed to remain constant. Due to a lack of data, any possible local variations on these parameters are not considered.
- **Baseflow estimates** - A constant riverbed conductance of 0.085 day^{-1} per unit riverbed area is assumed in the model. The computed baseflow is validated only against the monitored baseflow to Sunnyside Swamp. There were no data to calibrate baseflow values into other streams and swamps.
- **Geological structural features** - they are not included in the model due to a lack of adequate data on their characteristics e.g. exact location, exact orientation, exact extent both laterally and vertically, persistency and hydraulic properties. A number of piezometers installed at the AP and SV mining region can be seen to be exhibiting an anomalous behaviour (i.e. rising or falling water heads with time) that cannot be attributed solely to the effect of mine dewatering, but could possibly be attributed to the mining induced deformations along geological structures (Adhikary and Morla, 2013). Depending upon the hydraulic characteristics a geological structure either can act as a flow barrier or can act as a medium with excessively high conductivity providing a direct link between water bodies located at greater distance.
- **Surface water-groundwater interrelation** – A simplistic formulation has been incorporated in the model using River and Swamp formulation described in Section 0. The limitations in this approach are:
    - river conductance is assumed to remain constant throughout the modelling process. The possibility of change in the conductance of a losing stream with time is not considered explicitly. Since COSFLOW solves a fully non-linear saturated-unsaturated flow, it is expected that this is being taken care indirectly by the change in relative permeability as a function of node saturation; relative permeability at 0.1 saturation reduces to zero. The Australian Groundwater Modelling Guidelines notes “the rate at which losing streams lose water to groundwater varies as the conditions beneath the streambed change from saturated to unsaturated to almost dry”. Thus the model has a potential to over predict leakages from swamps and streams. At the time of modelling, the only reliable field data available were the flow measurements at Sunnyside Swamp. Thus the river node conductance was calibrated to match the baseflow to Sunnyside Swamp. The same value of conductance has been assigned for every stream/swamp nodes throughout the model.
    - the model does not consider the dynamic interaction between the surface water and the groundwater. Groundwater discharge to streams or loss of water from streams due to leakage is not considered in the calculation of change in staging heights.

7 Recommendations for Future Work

7.1 Monitoring

Springvale and Angus Place Collieries have installed an extensive network of shallow and deep piezometers to monitor the possible fluctuation in both:

- near surface groundwater levels that may impact on the baseflow to swamps and streams in the mining region, and
- regional groundwater levels.

Both collieries conduct mine water balances to account for all monitored volumes of water entering and leaving the workings.

Both collieries monitor stream flows at a number of gauging stations as described in Aurecon (2012).

7.1.1 Piezometric monitoring

It is suggested that both collieries continue collecting and analysing data from the existing network of piezometers and expand the existing monitoring programme with additional piezometers to help enhance our current knowledge of groundwater systems in the mining region. The model results indicate that AQ3 will undergo substantial depressurisation during mining. This may adversely impact the perched groundwater system lying above AQ3 (i.e. above the Mt York Claystone). Thus it is suggested that Springvale and Angus Place Collieries put emphasis on monitoring the porepressures above the proposed mining operations within AQ3, AQ4, AQ5 and AQ6 using grouted-in multi-level piezometers in order to better calibrate/validate the numerical model and provide better modelling predictions throughout the life of mine.

In locating of the multi-level piezometric holes consideration should be given to their placements relative to mine plan as well as site access. Water level measurements should be automated with hourly recordings throughout the life of mine.

7.1.2 Swamp/Stream monitoring

The model results suggest that the swamps/streams may be affected to some degree as they are undermined. However, the model suffers from a lack of calibration in this regard: the only Type-C swamp which has been undermined and has baseflow and piezometric data available is Kangaroo Creek Swamp, and comparing the model results with observations has proved difficult due to a lack of knowledge about the upstream Kangaroo Creek which feeds the swamp, and the complicated nature of the swamp and its nearby spring and pool (see Appendix A, Section 5). Therefore, it is suggested that both collieries monitor flows and groundwater levels in the important swamps.

To accurately monitor baseflow and streamflow from a swamp, regular measurements of flow due to rainfall events need to be made. It is recommended that V-notch weirs be constructed at kilometre intervals within each swamp of importance. Piezometers at the base of these weirs should record pressure heads (which can be translated into flow rates) with high frequency since most flows due to high rainfall events will dissipate within 24 hours.

In addition, piezometers should be located at similar intervals within the swamps to measure groundwater levels.

It is most important to install these monitoring stations well before mining underneath the swamp in order to establish a baseline flow and groundwater level data.

It would be more useful if the length of the monitoring bores could be increased to 3 m; some of the current monitoring bores at the mines seem to be too shallow (about 1 m long) prohibiting a proper assessment of the mining impact beyond 1 m depth.

7.2 Detailed mapping of aquitard layers

A more detailed understanding of the nature (continuity and thickness) of semi-permeable layers underlying the important swamps would be useful for understanding these swamps' response to undermining. There is enough evidence to suggest that the underlying semi-permeable layers largely dictate a swamp's response to mining. This can be seen in the response of Kangaroo Swamp to undermining by Angus Place LW940 and LW950, as described in Appendix A, Section 5. Geological investigation conducted by the mine indicated that YS6 outcrops just above the swamp, but below the spring. Hence the swamp is not supported by YS6, but the spring is, which could be the reason the swamp is affected by the extraction of LW940, but the spring is not. Thus it is important to better understand the structure of semi-permeable layers underlying the important swamps. In the current model, the YS layer has been assumed to be continuous, extending over the whole domain. If this is not so, the response of the groundwater systems lying above the YS6 layer could differ.

7.3 Modelling

The current numerical model, being designed for the assessment of the cumulative impact of multiple mines on groundwater systems at a regional scale, has been discretised using a rather coarser mesh. The mesh size in the AP and SV mining region are about 50 to 60 m, which becomes coarser away from the AP and SV mining regions. It is recommended that:

- the model developed in this study be used as one of the management tools for the prediction of impact of mining on the groundwater system throughout the life of mine,
- fine scale micro-models of critical groundwater fed swamps/streams be developed on the basis of the knowledge gained from the model developed in this study and used in detailed assessment of the impact of mining on swamps and streams. Boundary conditions for the micro swamp/stream models could be interpolated from the updated regional scale model, and
- the proposed hydrogeological investigation, groundwater and swamp monitoring be used to further improve the model accuracy by fine tuning the model input parameters on an ongoing basis.

References

Adhikary, DP and Morla, R (2013a) Qualitative assessment of possible effects of geological structures and seepage faces on water heads at Springvale and Angus Place Collieries. CSIRO Report No. EP13588.

Adhikary, DP and Morla, R (2013b) Deep hole piezometric data analysis – Springvale and Angus Place Collieries. CSIRO Report

Adhikary, DP and Wilkins, A (2012) Reducing the Impact of longwall extraction on groundwater system. ACARP Report C18016.

Aurecon (2012) Groundwater monitoring report for June – July 2012, Angus Place and Springvale groundwater monitoring programme. Report No 208362/208354, pp. 54.

Barnett, B, Townley, LR, Post, V Evans, RE, Hunt, RJ, Peeters, L, Richardson, S, Werner, AD, Knapton, A and Boronkay, A (2012) Australian groundwater modelling guidelines. Waterlines report, National Water Commission, Canberra. pp. 191

Bai, M, and Elsworth, D (1994) Modeling of subsistence and stress-dependent hydraulic conductivity for intact rock and fractured porous media. Rock Mech. Rock Engng,. **Vol. 27(4)**, 209-234.

Bish, S (1999) Hydrogeological assessment for Coxs River catchment. Consultant Report, Department of Land and Water Conservation, Sydney South Coast Region, Australia

Cosserat, E and Cosserat, F (1909) *Theorie des corps deformables*. Hermann, Paris.

De Wiest (ed.) (1969): *Flow through porous media*. Academic Press, London, pages 530.

Elsworth, D (1989) Thermal permeability enhancement of blocky rocks: one dimensional flows. *Int. J. Rock Mech. Min. Sci. Geomech*. Abstr., **Vol. 26 (3/4)**, 329-339.

Forster, I and Enever, J (1992) Hydrogeological response of overburden strata to underground mining. Office of Energy Report, **Vol. 1**, pages 104.

Greacen, EL, and Williams, J (1983) Physical properties and water relations, In: Soil – an Australian viewpoint. CSIRO/Academic Press, pp.499-530

Greenwood, EAN, Beresford, JD, Bartle, JR and Barron, RJW (1982) Evaporation from vegetation in landscapes developing secondary salinity using the ventilated-chamber technique. IV. Evaporation from a regenerating forest of Eucalyptus wandoo on land formerly cleared for agriculture. J. Hydrol., **58**: 357-366.

Gale, W (2009) Aquifer inflow prediction above longwall panels. ACARP Report C13013.

Guo, H, Adhikary, DP and Gabeva, D (2007) Hydrogeological response to longwall mining. ACARP Report C14033.

Holmes, JW and Sinclair, JA (1986) Water yield from some afforested catchments in Victoria.

Hubbert, MK (1940) The theory of ground water motion. *J. Geol.*, **Vol. (48)**, 785-944.

Hydrology and Water Resources Symposium, Griffith University, Brisbane, 25-27 November 1986. The Institution of Engineers, Australia

Kozeny, J and Ber, S (1927) Wiener Akad, Abt. 2a, 136-271.

Krumbein, WC and Monk, GD (1943) Permeability as a function of the size parameters of unconsolidated sand. *Trans. Am. Inst. Min. Metall. Petrol. Engng.*, **Vol. (151)**, 153-163.

Langford, KJ and O'Shaughnessy, PJ (1978) A study of canopy interception in native forests and conifer plantations. Melbourne and Metropolitan Board of Works, Report. No., MMBW-W-0007, pp 88.

Liu, J, and Elsworth, D (1997) Three-dimensional effects of hydraulic conductivity enhancement and desaturation around mined panels. *Int. J. Rock Mech. Min. Sci*. **Vol. 34, (8)**, 1139-1155.

Louis, C (1969) Groundwater flow in rock masses and its influence on stability. Rock Mech. Res. Report 10, Imperial College, UK.Palaris (2013a) Stratigraphic setting – Angus Place and Springvale Collieries. Doc No CEY1504-02, pp 75.

McNaughton, KG and Jarvis, PG (1983) Predicting the effects of vegetation changes on transpiration and evaporation. In "Water Deficits and Plant Growth" (T.T. Kozowski, Ed.). **Vol. VII**. Academic Press, New York, Calder, 1996, 1-47.

Monteith, JL and Unsworth, MH (1990) Principles of Environmental Physics. 2nd. edn. Routledge, Chapman and Hall, New York, pp 291.

Murray-Darling Basin Commission (2001) Groundwater flow modelling guideline. Canberra. August 2001, pp. 125.

Nathan, RJ and McMahon, TA (1990) Evaluation of Automated Techniques for Base Flow and Recession Analyses. Water Resources Research, **Vol 26 (7)**, 1465-1473.

Barron, OV et al (2011) Climate change impact on groundwater resources in Australia. Waterlines report, National Water Commission, Canberra, pp. 222.

Palaris (2013a) Stratigraphic setting, Angus Place and Springvale Collieries. Doc NO. CEY1535-01, pp 88.

Palaris (2013b) Regional geological modelling in the southern part of the Western Coalfield. Doc No CEY1504-02, pp 28.

Rojstaczer, SA (1994) The limitations of groundwater models. Journal of Geological Education, Vol. 42, 362-368.

RPS Aquaterra (2012a) Swamp groundwater impact case study. Memorandum, Doc No **002a**, pp. 20.

RPS Aquaterra (2012b) Personal communication.

Seedsman, R (1996) A review of the hydrogeological aspects of Australian longwalls. Symposium on geology in longwall mining, Eds. G.H. McNally and C.R. Ward, 269-272.

Shen, B, Alehossein, H, Poulsen, B and Waddington, A (2010) Subsidence Control Using Coal Washery Waste, ACARP Report C16023.

Turner, KM (1991) Annual evapotranspiration of native vegetation in a Mediterranean-type climate. Water Resour. Bull., **27**, 1-6.

Walker, JS (1988) Case study of the effects of longwall mining induced subsidence on shallow groundwater sources in the Northern Appalachian coalfield. US Bureau of Mines Report No 9198, pp 17.

Zhan Lg, Dawes W.R. and Walker G.R. (1999) Predicting the effect of vegetation on changes on catchment average water balance, Cooperative Research Centre for Catchment Hydrology, Technical report 99/12.

CONTACT US

t 1300 363 400
+61 3 9545 2176
e enquiries@csiro.au
w www.csiro.au

YOUR CSIRO

Australia is founding its future on science and innovation. Its national science agency, CSIRO, is a powerhouse of ideas, technologies and skills for building prosperity, growth, health and sustainability. It serves governments, industries, business and communities across the nation.

FOR FURTHER INFORMATION

CSIRO Earth Science and Resource Engineering
Deepak Adhikary
t +61 7 3327 4496
e Deepak.adhikary@csiro.au

EARTH SCIENCE AND RESOURCE ENGINEERING
www.csiro.au

Appendix A
Observation, Calibration and Validation Objective

Angus Place and Springvale Colliery Operations

Groundwater Assessment

D P Adhikary and A Wilkins
Report No EP132799
May 2013

Springvale Colliery and Angus Place Colliery

Citation

Adhikary, DP and Wilkins, A (2013) Angus Place and Springvale Colliery operations groundwater assessment. Appendix A – Observation, calibration and validation objective. Report No EP132799.

Copyright and disclaimer

Important disclaimer

Contents

Figures

1 Selection of Piezometers

In this Appendix, available piezometer data are described. In total there are 182 piezometers in 31 boreholes. Many of these are used to calculate RMS/SRMS statistics during steady-state calibration, transient calibration, and validation. Which piezometers are used, and the dates that are used for each piezometer are shown in columns 3, 4 and 5 of the following tables. Column 3 corresponds to the date used for steady-state calibration, column 4 for transient calibration, and column 5 for validation. There is no foolproof way of choosing which piezometers to use, and when, and the following guidelines have been used.

- For steady-state calibration. The piezometer should have been reporting fairly steady heads. The piezometer should not be too close to a mined region, especially if it lies in the lower aquifers, as these will be affected more strongly by mining. In total, 85 piezometers are chosen for steady-state calibration.
- For transient calibration. The piezometers should have been reporting fairly steady heads, or have readings at the end of the calibration period (20 Dec 2006). Piezometers which exhibit large increases in measured heads with time, or erratic behaviour, are not used as this phenomenon must be caused by something not considered in this report (such as mechanical deformations: this is discussed in Adhikary and Morla, 2013). In total, 126 piezometers are chosen for transient calibration.
- For transient validation. The piezometers should have been reporting fairly steady heads, or have readings close to the end of the validation period (1 Jan 2012). Piezometers which are damaged by mining are typically not used. Piezometers which have dried out (i.e. reading negative pressures), or those which exhibit large increases in measured heads, or erratic behaviour, are not used as this phenomenon must be caused by something not considered in this report (such as mechanical deformations: this is discussed in Adhikary and Morla, 2013). In total, 142 piezometers are chosen for transient validation.

The positions of the piezometer holes are shown in Figure A1.

Figure A1 Position of boreholes containing piezometers used in this model

SPR1102				
241235E, 6304180N. Elevation of Collar 1091				
P1 (407m, SP0)	Steady	21/4/12	21/4/12	21/4/12
P2 (380m, AQ1)	Steady	21/4/12	21/4/12	21/4/12
P3 (312m, AQ2)	Steady	21/4/12	21/4/12	21/4/12
P4 (300m, AQ2)	Increase from 160m to 200m during first 2 months, possibly "settling-in" period			21/4/12
P5 (292m, AQ2)	Slow increase from 90m to 120m during first 5 months			21/4/12
P6 (160m, SP3)	Slow increase from 50m to 80m during first 5 months			21/4/12
P7 (151m, SP3)	Steady	21/4/12	21/4/12	21/4/12
P8 (125m, AQ4)	Steady	21/4/12	21/4/12	21/4/12
P9 (82m, AQ4)	Slow increase from 11m to 18m during first 5 month	21/4/12	21/4/12	21/4/12

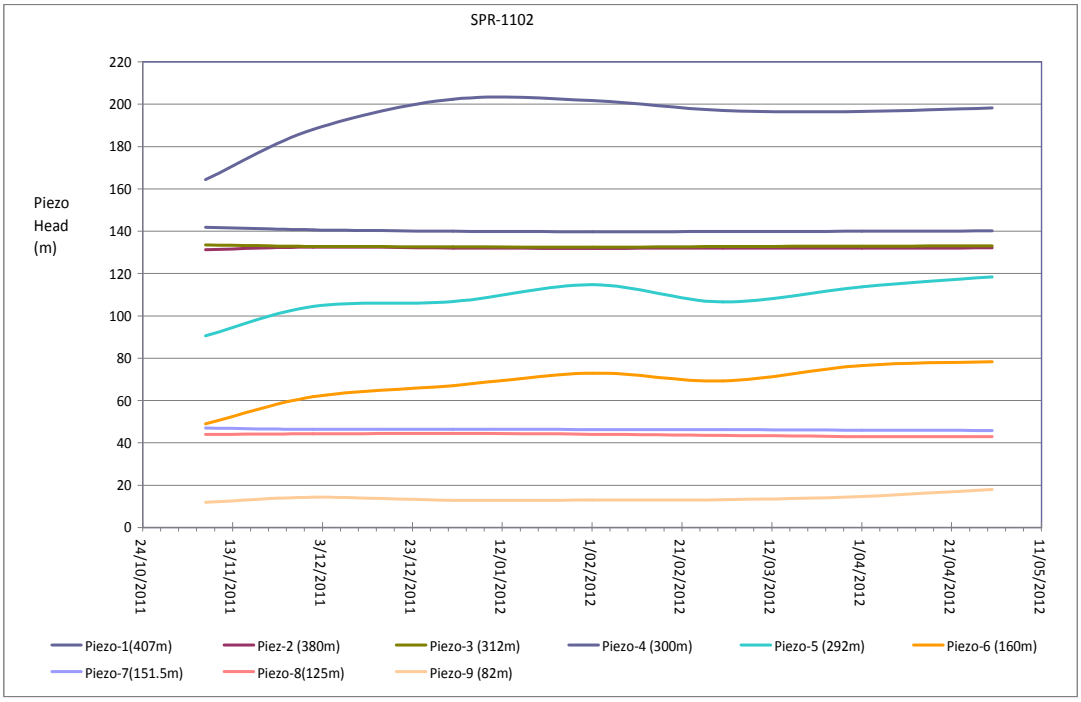

Appears to be largely unaffected by mining. The observed increases in water heads could be due to issues with grouting resulting in increased settling-in periods for some piezometers, or could be due to effects described in Adhikary and Morla, 2013.

Figure A2 Description of piezometer hole SPR1102

SPR1103				
241430E, 6302983N. Elevation of Collar 1062				
P1 (407m, floor)	Steady	21/4/12	21/4/12	21/4/12
P2 (381m, AQ1)	Steady	21/4/12	21/4/12	21/4/12
P3 (326m, AQ2)	Small increase over first month, possibly “settling-in” period			21/4/12
P4 (313m, AQ2)	Increase from 95m to 105m during first 2 months, ,then steady at 100m possibly “settling-in” period			21/4/12
P5 (290m, KAT)	Steady	21/4/12	21/4/12	21/4/12
P6 (258m, AQ3)	Steady	21/4/12	21/4/12	21/4/12
P7 (178m, SP3)	Varying between 90m and 110m			21/4/12
P8 (151m, AQ4)	Varying between 100m and 125m			21/4/12
P9 (138m, AQ4)	Steady	21/4/12	21/4/12	21/4/12

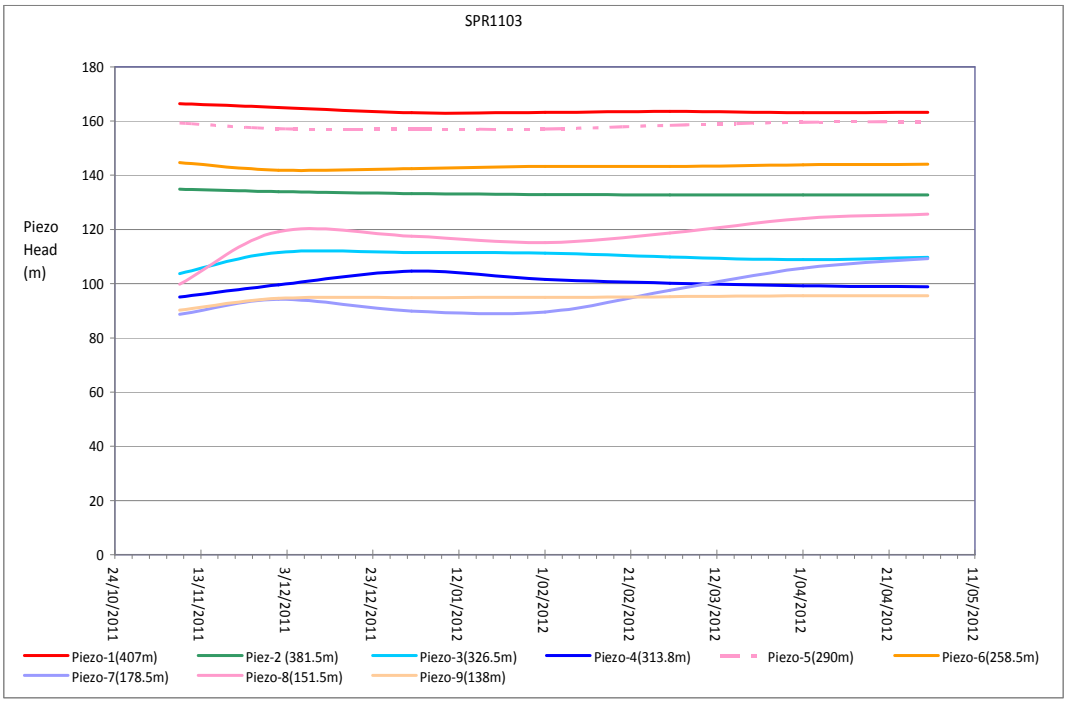

Appears to be largely unaffected by mining.

Figure A3 Description of piezometer hole SPR1103

SPR26				
237061E, 6301251N. Elevation of Collar 1144				
P1 (356m, LTH)	Large decrease from 90m to 25m during LW407 and LW408, then steady decrease to almost zero by end LW412		20/12/06	13/3/10
P2 (73m, AQ4)	Steady decrease from LW409 to zero at end LW412	1/9/02	20/12/06	13/3/10

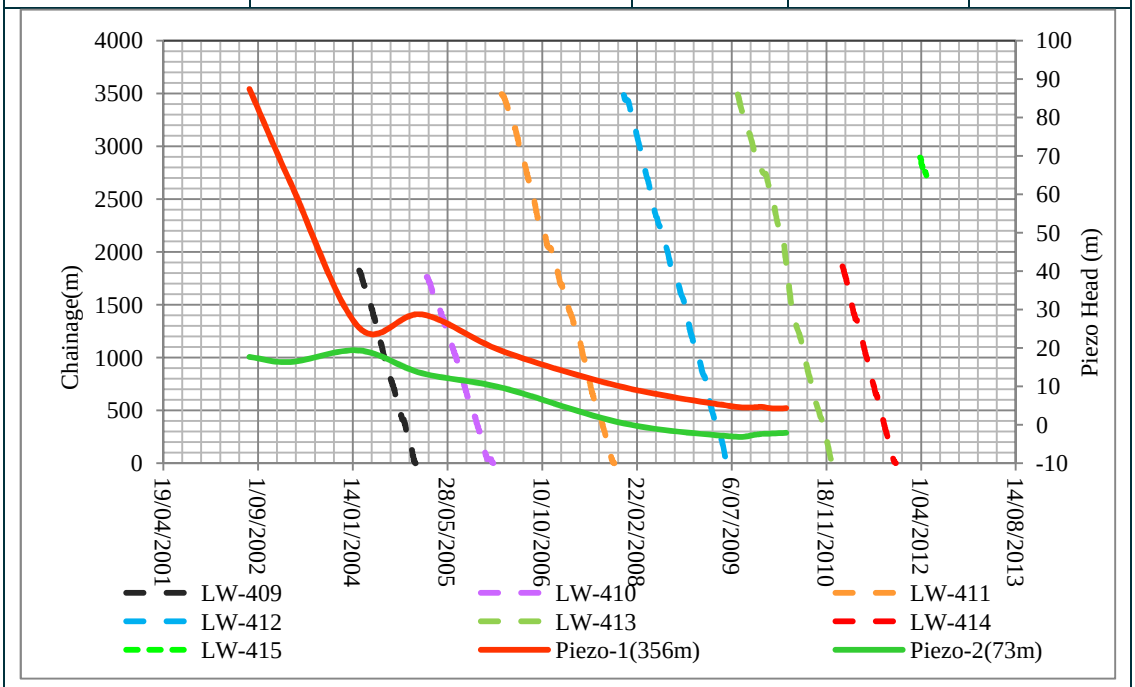

Strongly affected by mining, and, given its location, possibly the main headings located south of Springvale longwall panels could have affected Piezo-1.

Figure A4 Description of piezometer hole SPR26

SPR29				
237791E, 6301016N. Elevation of Collar 1163				
P1 (382m, roof)	Affected by LW408 to 410, and then largely unaffected. Steady		20/12/06	27/7/09

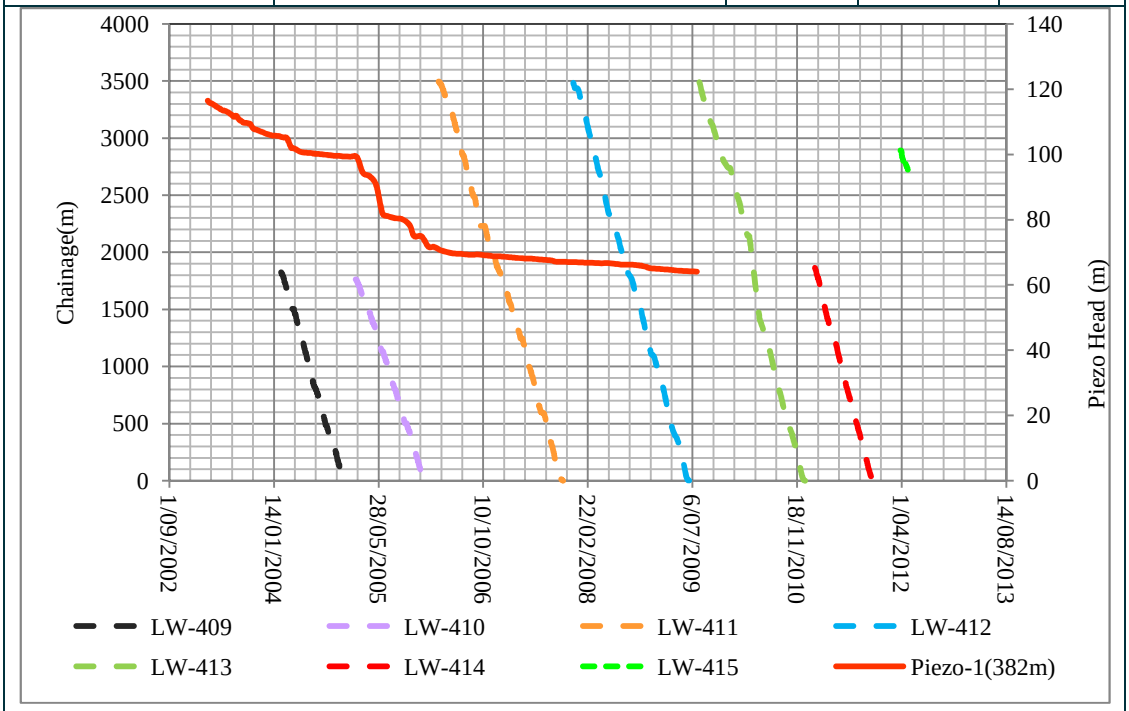

Strongly affected by mining

Figure A5 Description of piezometer hole SPR29

SPR33				
237575E, 6304545N. Elevation of Collar 1125				
P1 (80m, AQ4)	Gradual drop from 40m to 30m over LW409 to 412. Rapid drop to almost zero over LW413A	1/6/07	20/12/06	21/4/12
P2 (160m, SP3)	Gradual drop from 87m to 82m over LW409 and 410. Rapid drop to 40m over LW411 and 412. Rapid drop to 15m over LW413A		20/12/06	21/4/12
P3 (280m, AQ2)	Gradual drop from 113m to 108m over LW409 and 410. Rapid drop to 50m over LW412, then to zero over LW413A		20/12/06	
P4 (336m, AQ1)	Unexplained increase from 113 to 130 during LW409 and 410. Rapid drop to 50m over LW411 and 412, then to zero over LW413A		20/12/06	

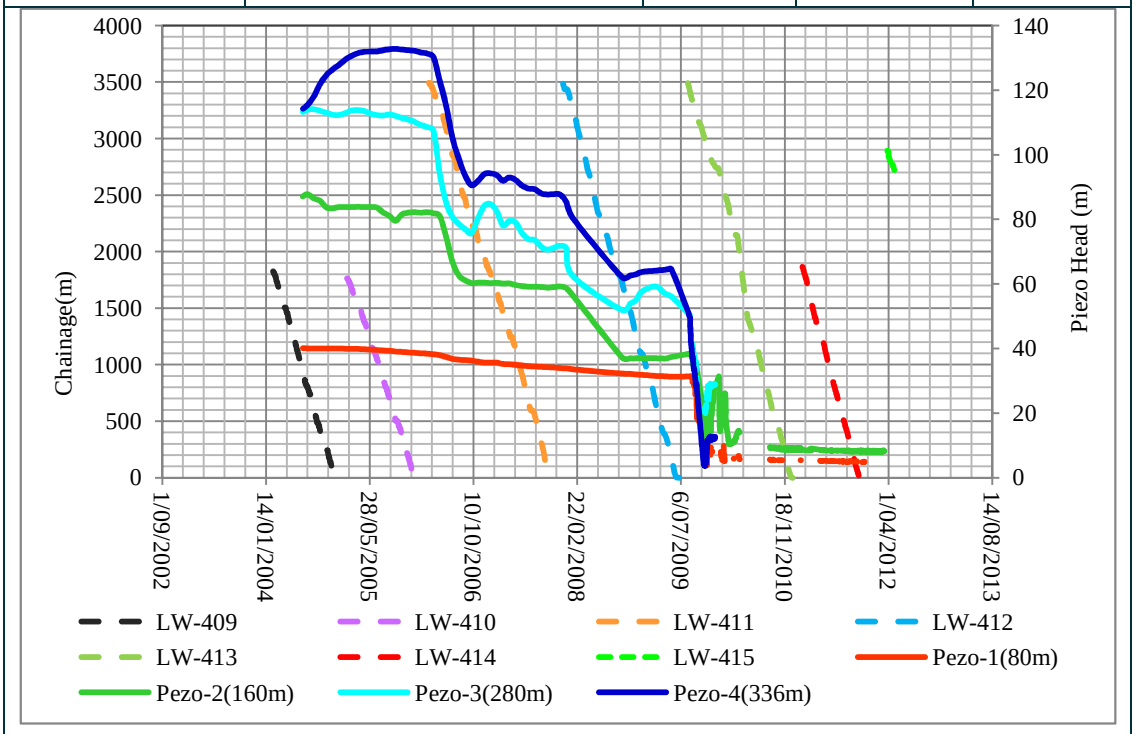

Strongly affected by mining. The initial increase in water head in Piezo-4 could be due to an issue with grouting or an effect described by Adhikary and Morla, 2013.

Figure A6 Description of piezometer hole SPR33

SPR34				
237573E, 6303655N. Elevation of Collar 1157				
P1 (270m, AQ3)	Initial drop from 88 to 77m during LW409, then almost steady. Decrease from 74m to almost zero during LW411 to 413A		20/12/06	
P2 (359m, AQ1)	Steady during LW409 and 410. Drop from 64m to almost zero during LW411 to 413A		20/12/06	

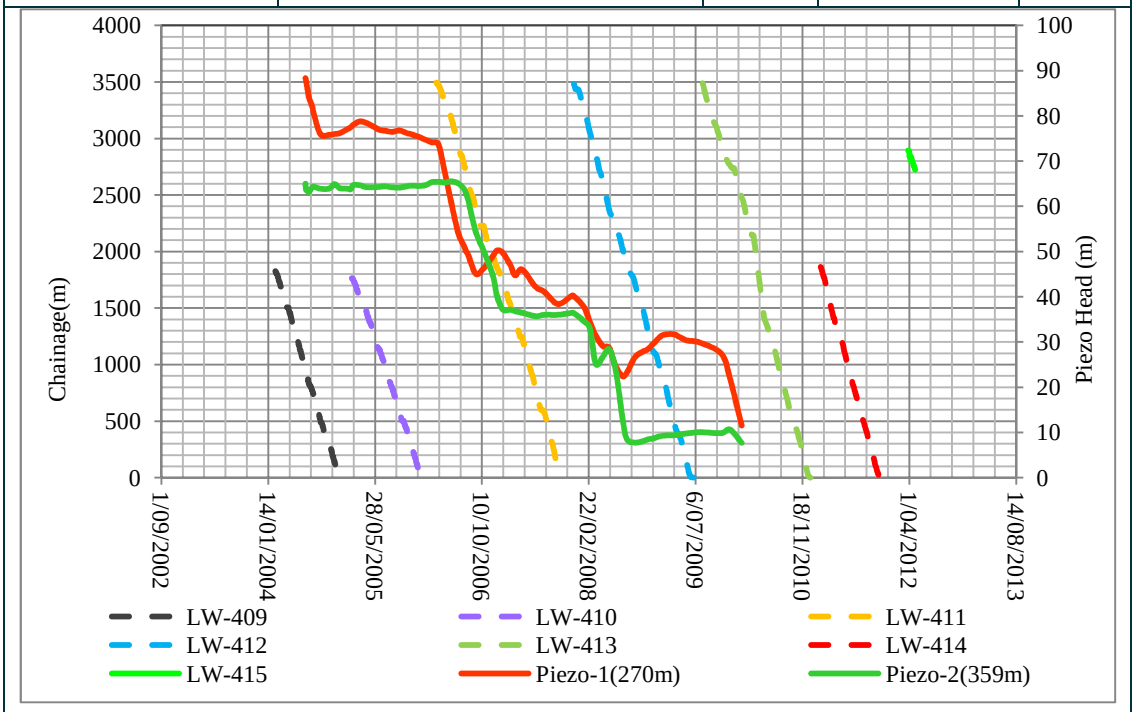

Strongly affected by mining.

Figure A7 Description of piezometer hole SPR34

SPR35				
237618E, 6302778N. Elevation of Collar 1163				
P2 (310m, AQ2)	Almost uniform drop from 35m to almost zero during end LW409 to end LW411. Possibly inaccurate readings after that time.		20/12/06	

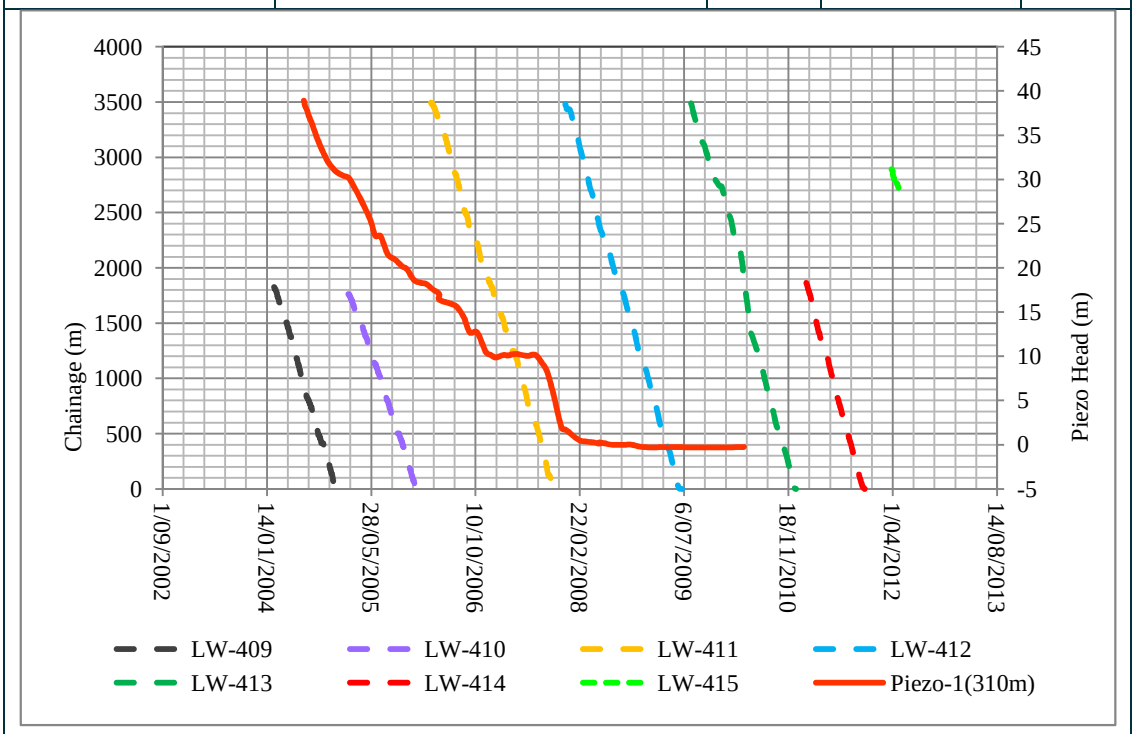

Strongly affected by mining.

Figure A8 Description of piezometer hole SPR35

SPR36				
239358E, 6303496N. Elevation of Collar 1098				
P1 (389m, SP0)	Increase from 80m to 120m from 2006 to 2012			
P2 (376m, floor)	After initial "settling-in" period, decrease from 165m to 120m over course of LW411 and 412. Then increase to 130 by end of LW413B		20/12/06	21/4/12
P3 (320m, SP1)	After initial "settling-in" period, gradual decrease from 160m to 137m during LW411 to end LW414.		20/12/06	21/4/12
P4 (274m, AQ2)	Decrease from 130m to 90m during LW411 to end LW414		20/12/06	21/4/12
P5 (146m, SP3)	Decrease from 104m to 98m during LW411 to end LW414	14/3/06	20/12/06	21/4/12
P6 (130m, AQ4)	Steady	14/3/06	20/12/06	21/4/12
P7 (75m, AQ4)	Steady	14/3/06	20/12/06	21/4/12
P8 (35m, AQ5)	Decrease from 25m to 14m during LW411 to end LW414	14/3/06	20/12/06	21/4/12

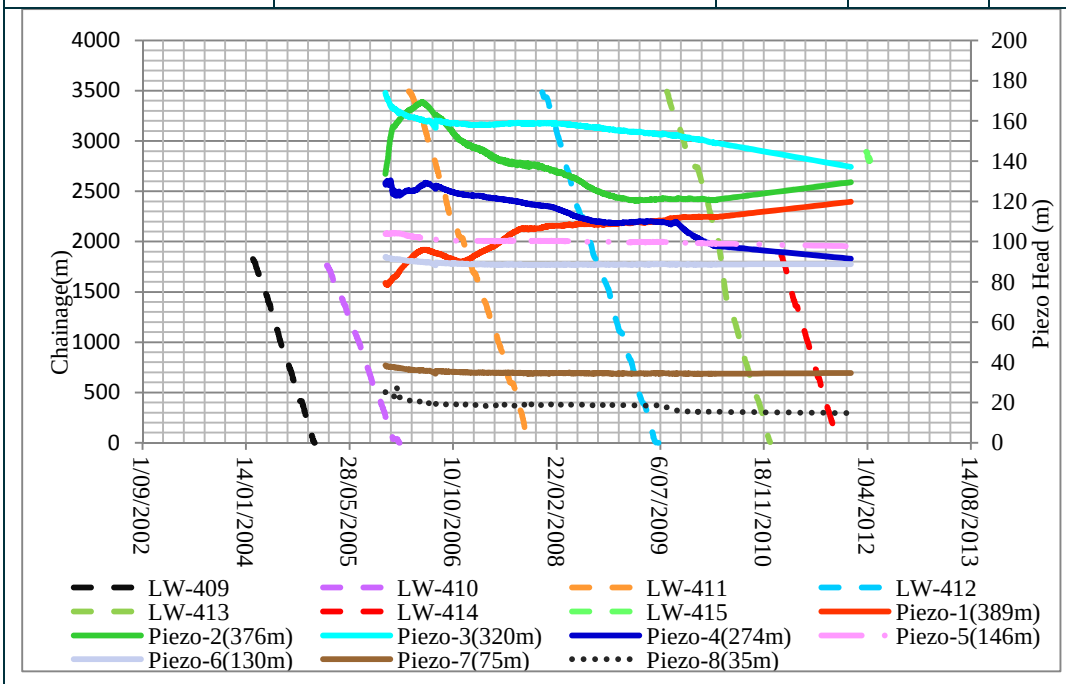

P1 to P5 probably affected by mining. Head increases in some of the piezometers could be due to effects described in Adhikary and Morla, 2013

Figure A9 Description of piezometer hole SPR36

SPR37				
239074E, 6300367N. Elevation of Collar 1171				
P1 (405m, LTH)	After initial "settling-in" period, steady at 120m during LW411. Decrease to 60m during LW412 to 414		20/12/06	21/4/12
P2 (350m, SP1)	After initial "settling-in" period, decrease from 113m to 52m during LW411 to 414		20/12/06	21/4/12
P3 (320m, AQ2)	After initial "settling-in" period, decrease from 80m to 23m during LW411 to 414		20/12/06	21/4/12
P4 (260m, AQ3)	After initial "settling-in" period, decrease from 125m to 84m during LW411 to end LW414		20/12/06	21/4/12
P5 (187m, SP3)	Slight decrease from 118m to 113m during LW411 to LW414	14/3/06	20/12/06	21/4/12
P6 (165m, AQ4)	Slight decrease from 98m to 92m during LW411 to LW414	14/3/06	20/12/06	21/4/12
P7 (135m, AQ4)	Slight decrease from 69m to 64m during LW411 to LW414	14/3/06	20/12/06	21/4/12
P8 (110m, YS6)	Decrease from 43m to 34m during LW411 to end LW414	14/3/06	20/12/06	21/4/12

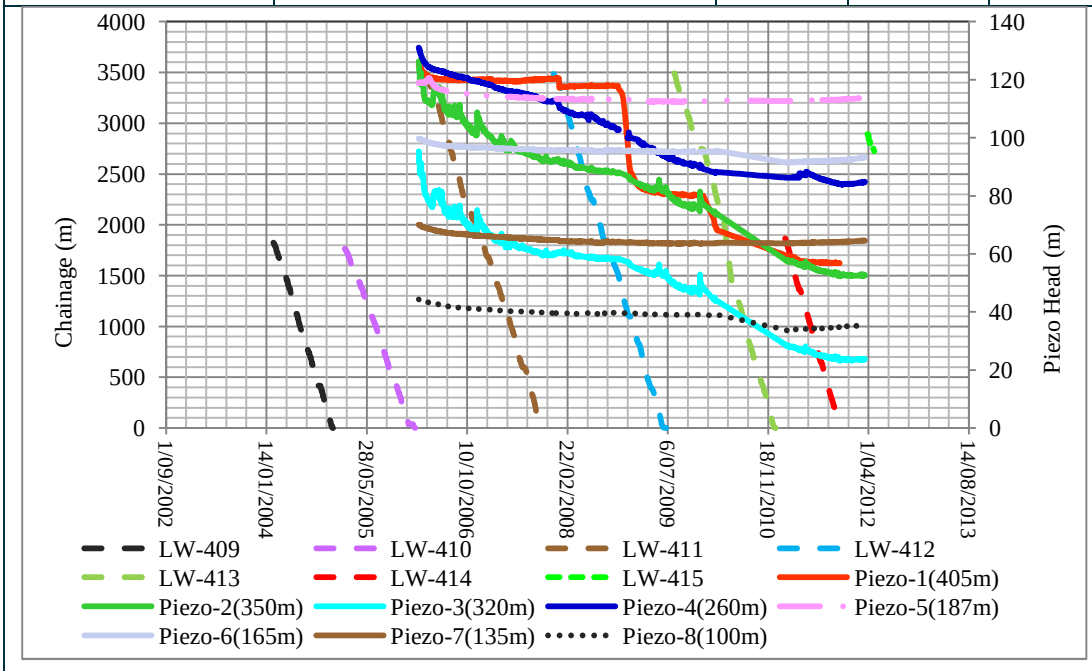

P1 to P4 affected by mining, P5 to P8 much less so.

Figure A10 Description of piezometer hole SPR37R

SPR38				
240062E, 6298330N. Elevation of Collar 1148				
P1 (370m, SP0)	Unexplained rise to 150m, then somewhat constant during LW411, then decrease to 125m during LW412 and 413			21/4/12
P2 (355m, LTH)	Unexplained rise to 135m, then constant during LW411, then decrease to 116m during LW412			21/4/12
P3 (300m, SP1)	Drop to 77m, then rise to 85m during LW411, then decrease to 60m during LW412 and 413		20/12/06	21/4/12
P4 (230m, AQ3)	Decrease from 79m to 14m during LW411 to end 413		20/12/06	21/4/12
P5 (190m, AQ3)	Decrease from 81m to 60m during LW411 to end 413		20/12/06	21/4/12
P6 (135m, SP3)	Moving between 91 and 97m during LW411 and 412	11/7/06	20/12/06	21/4/12
P7 (100m, AQ4)	Steady at 60m during LW411 and 412, then drop to 47m during 413.	11/7/06	20/12/06	21/4/12
P8 (80m, AQ4)	Steady at 42m	11/7/06	20/12/06	21/4/12

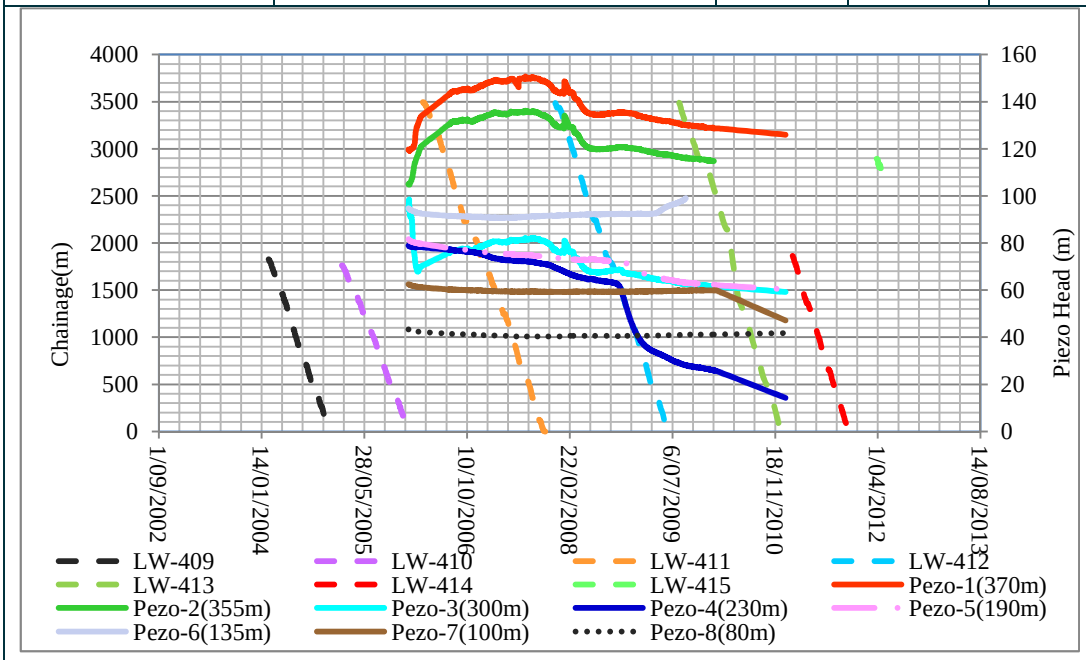

P1 to P5 and P7 possibly affected by mining even though this borehole is some distance from the SV panels: possibly due to effects described in Adhikary and Morla, 2013.

Figure A11 Description of piezometer hole SPR38

SPR39				
226846E, 6304550N. Elevation of Collar 1133				
P1 (380m, SP0)	Damaged			
P2 (374m, floor)	Damaged			
P3 (340m, AQ1)	Damaged			
P4 (270m, AQ2)	Decrease from 80m to 20m during LW411 then damaged.		14/3/06	
P5 (240m, AQ3)	Started to read negative during LW411		14/3/06	
P6 (155m, SP3)	Decrease from 90m to 11m during LW411, then negative readings		14/3/06	
P7 (140m, AQ4)	Decrease from 80m to 7m during LW411, then negative readings		14/3/06	
P8 (80m, AQ4)	After initial "settling in" period, decrease from 24m to 0m during LW411, then negative readings		14/3/06	

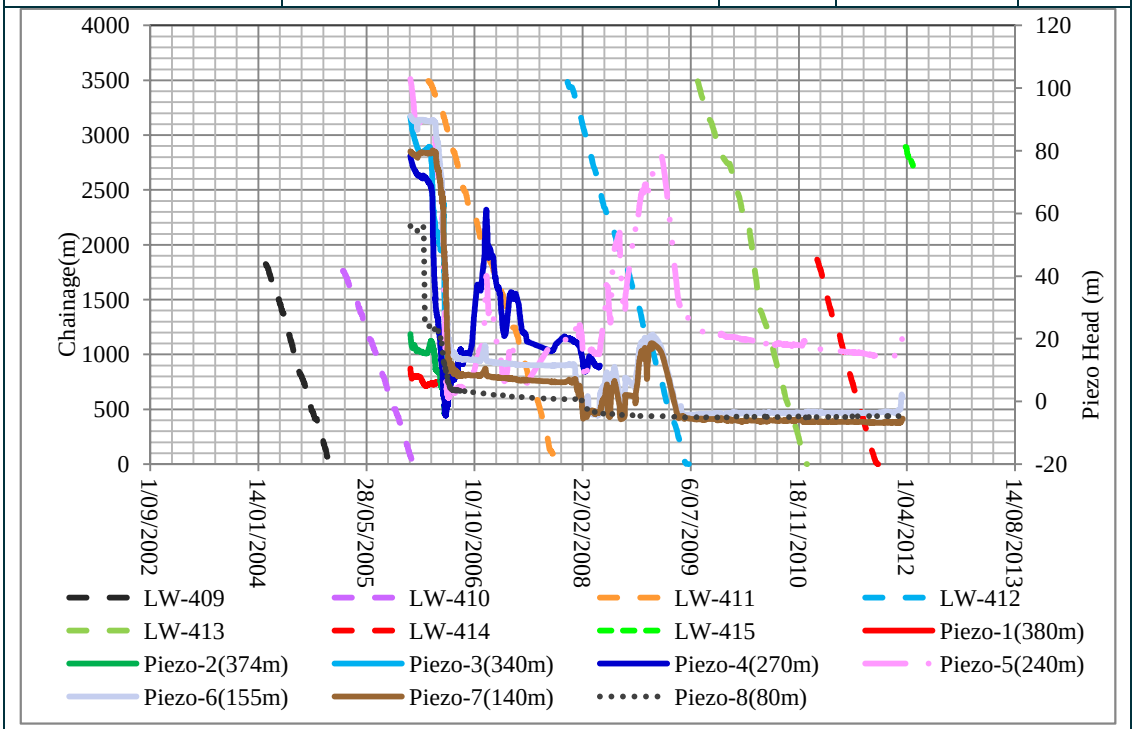

All piezometers affected by mining LW411. The heads in Piezo-4 to Piezo-7 seemed to be increasing and decreasing on a number of occasions, possibly indicating an intermittent link with near surface water bodies (possibly discharged mine water).

Figure A12 Description of piezometer hole SPR39

SPR48				
237217E, 6304198N. Elevation of Collar 1153				
P1 (200m)	Damaged			
P2 (170m, AQ4)	Large initial decrease, then damaged during 413A			
P3 (140m, AQ4)	Decrease from 58m to zero during LW412 and 413A, then negative			
P4 (110m, AQ4)	Decrease from 34m to 6m during LW412 and 413A, then to zero at end 414			21/4/12
P5 (90m, YS6)	Moving between 5 and 24m	1/3/09	1/3/09	21/4/12
P6 (70m, AQ5)	Moving between close to zero and 20m	1/3/09	1/3/09	21/4/12
P7 (50m, SP4)	Steady at close to zero	1/3/09	1/3/09	21/4/12
P8 (30m, AQ6)	Steady at close to zero	1/3/09	1/3/09	21/4/12

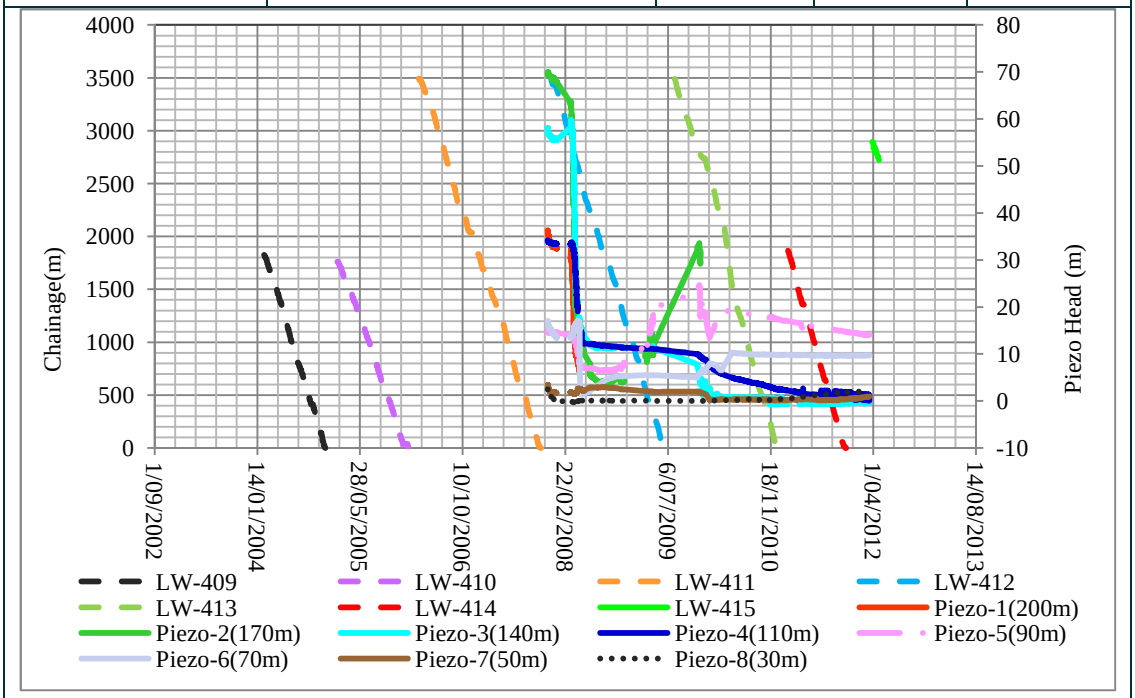

P1 to P6 affected by mining. P7 and P8 probably unaffected by mining. Head increases in some of the piezometers are unusual and may be due to effects described in Adhikary and Morla, 2013.

Figure A13 Description of piezometer hole SPR48

SPR49				
237245E, 6303199N. Elevation of Collar 1166				
P1 (295m, SP2)	Decrease from 45m to 14m during LW412 and 413A, then damaged			
P2 (250m, AQ3)	Decrease from 37m to zero during LW412 and 413A, then damaged			
P3 (200m, SP3)	Decrease from 18m to 12m during LW412 and 413A, then damaged			
P4 (150m, AQ4)	Decrease from 56m to 44m during LW412 and 413A, then damaged			
P5 (110m, AQ4)	Steady at 31m then damaged.	4/7/08	4/7/08	
P6 (80m, AQ4)	Increase from 4m to 11m during LW412 and 413A, then damaged			
P7 (50m, AQ5)	Increase from 12m to 18m during LW412 and LW413A, then unexplained large increase to 60m during 413B and 414			
P8 (30m, AQ5)	Steady at close to zero	4/7/08	4/7/08	21/4/12

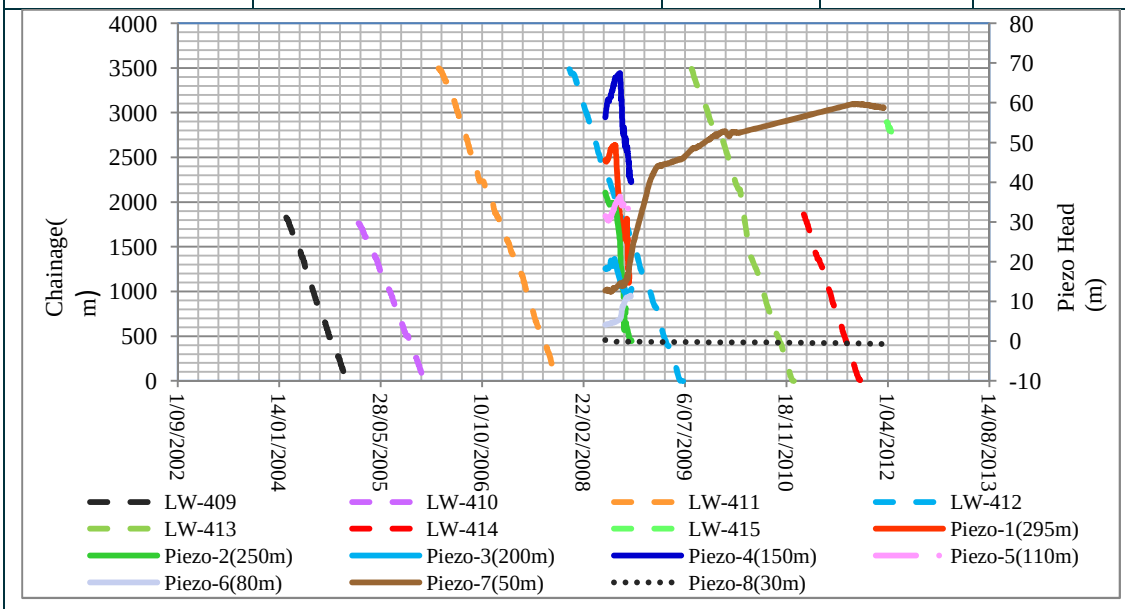

P1 to P4 affected by mining. P7 exhibiting strange behaviour, which may be due to effects described in Adhikary and Morla, 2013.

Figure A14 Description of piezometer hole SPR49

SPR50				
238290E, 6304152N. Elevation of Collar 1156				
P1 (200m, SP3)	Decrease from 63m to 38m during LW412 to end 414			21/4/12
P2 (170m, AQ4)	Decrease from 95m to 80m during LW412 to end 414			21/4/12
P3 (140m, AQ4)	Decrease from 68 to 59m during LW412 to end 414	22/2/08	22/2/08	21/4/12
P4 (110m, AQ4)	Decrease from 38m to 30m during LW412 to end 414	22/2/08	22/2/08	21/4/12
P5 (90m, AQ5)	Unexplained increase from 20m to 43m during LW412, then slow decrease to 36m by end of 414			
P6 (70m, AQ5)	Moving between 2m and 10m	22/2/08	22/2/08	21/4/12
P7 (50m, SP4)	Unexplained increase from 20m to 43m during LW412, then large increase to 113m during 413A, then decrease to 104m by end 414			
P8 (30m, AQ5)	Steady at 4m during LW412, then unexplained increase to 512 by end LW414	22/2/08	22/2/08	

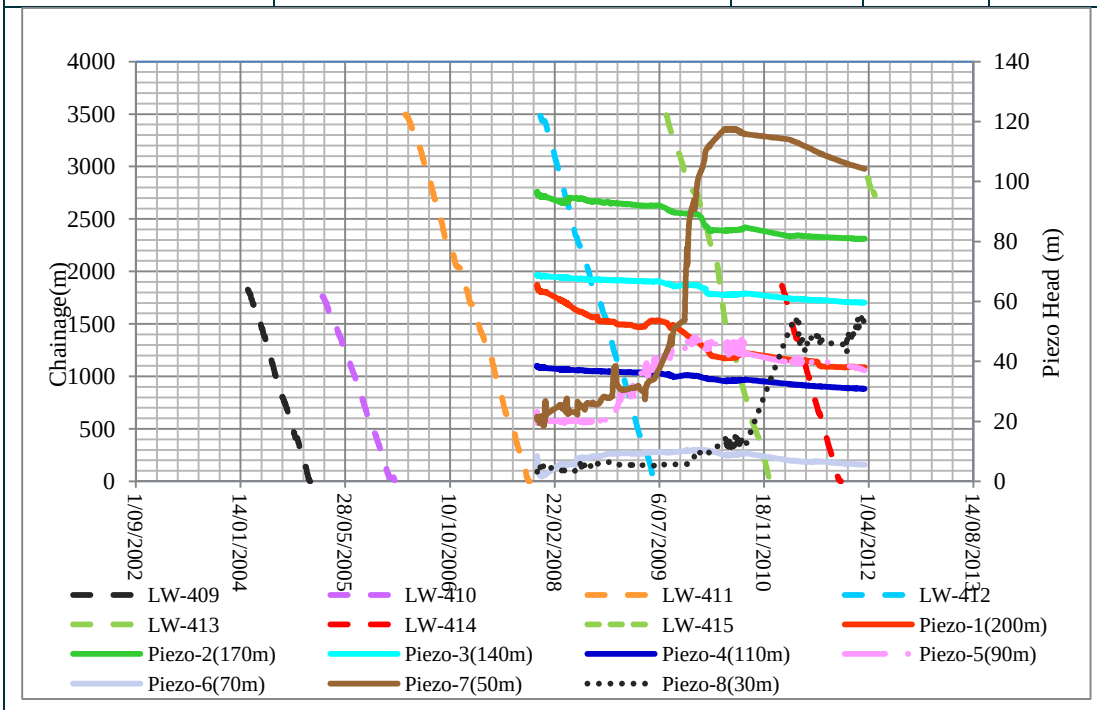

P1 to P4 affected by mining, other piezometers exhibiting unusual behaviour, which could be due to effects described in Adhikary and Morla, 2013.

Figure A15 Description of piezometer hole SPR50

SPR51				
237957E, 6303240N. Elevation of Collar 1158				
P1 (350m, SP1)	Decrease from 92m to negative during LW412 to end 414			
P2 (310m, AQ2)	After initial "settling in", decrease from 62m to zero during LW412 to end 414			21/4/12
P3 (230m, AQ3)	Decrease from 70m to negative during LW412 to end 414.			
P4 (190m, SP3)	Decrease from 70m to 14m during LW412 to end 414			21/4/12
P5 (150m, AQ4)	Decrease from 82m to 42m during LW412 to end 414			21/4/12
P6 (90m, AQ4)	Decrease from 24m to zero during LW412 to end 414			21/4/12
P7 (30m, AQ5)	Increase from zero to 3m	29/10/08	29/10/08	21/4/12

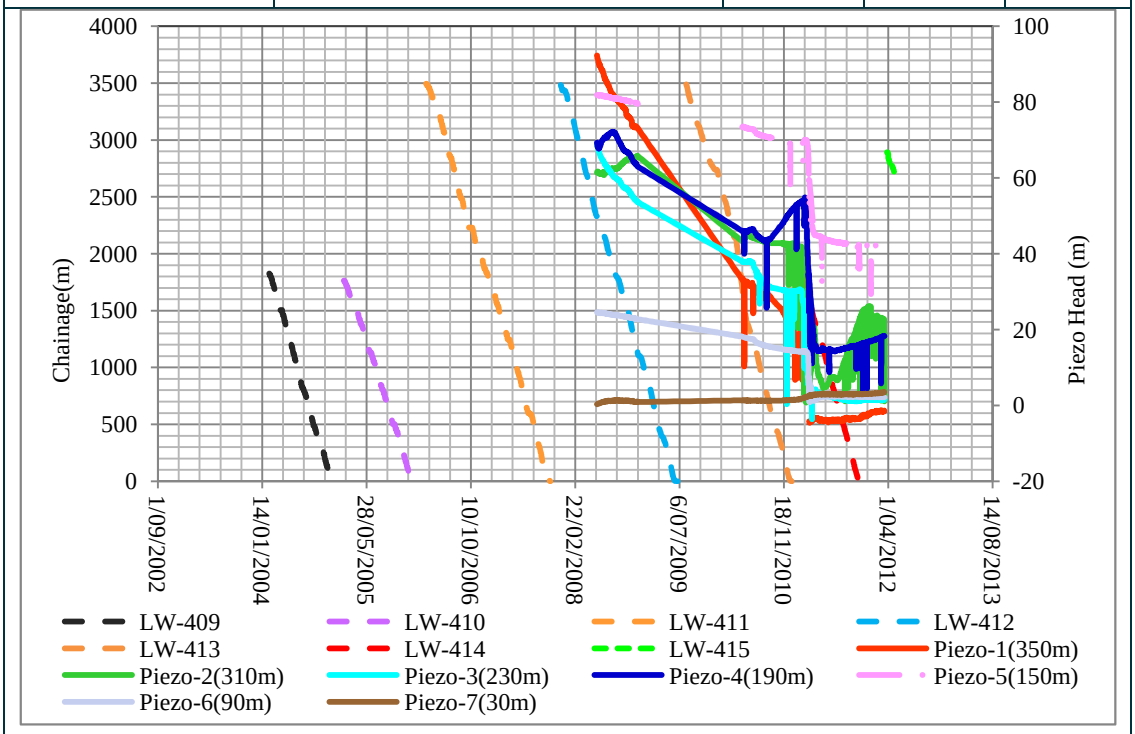

P1 to P6 affected by mining. P7 very low readings. Sudden increase and decrease in heads in some of the piezometers could be due to effects described in Adhikary and Morla, 2013.

Figure A16 Description of piezometer hole SPR51

SPR64				
238420E, 6299864N. Elevation of Collar 1163				
P1 (390m, floor)	After “settling-in”, unexplained rise from 120m to 136m during 413A and 414			
P2 (370m, AQ1)	After “settling-in”, decrease from 84m to 75m			
P3 (310m, AQ2)	After “settling-in”, decrease from 78m to 68m			
P4 (270m, AQ3)	After “settling-in”, decrease from 52m to 45m			
P5 (200m, AQ3)	Unexplained increase from 66m to 128m, perhaps settling in? Then steady.			
P6 (150m, AQ4)	Unexplained increase from 75m to 100m.			
P7 (100m, AQ4)	Unexplained initial increase from 44m to 108m, perhaps settling in? Then gradual increase to 130m			
P8 (30m, SP4)	Unexplained increase from 10m to 50m			

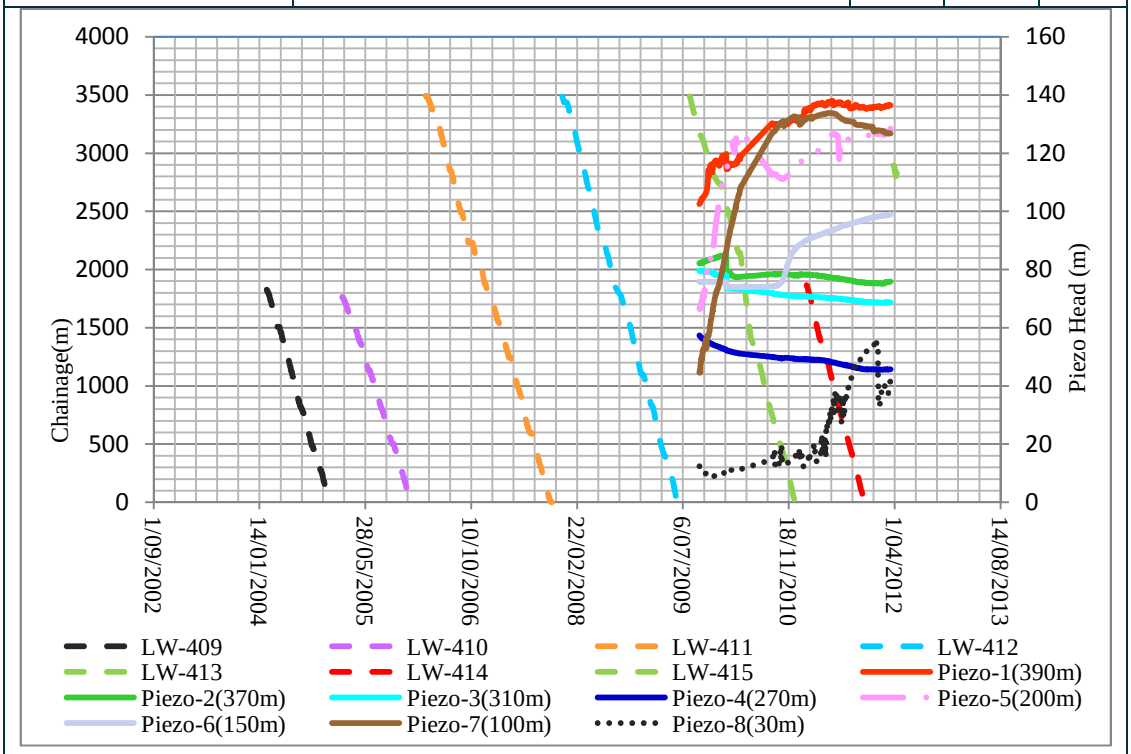

P2, P3 and P4 dropping, which could be due to mining. This is strange considering its distance from SV Panels. However, all other piezometers are exhibiting unusually large increases in pressures, possibly due to effects described in Adhikary and Morla, 2013.

Figure A17 Description of piezometer hole SPR64

SPR66				
239824E, 6301994N. Elevation of Collar 1109				
P1 (372m, LTH)	Increase from 178m to 200m during LW413 and 414	1/1/10	1/1/10	1/4/12
P2 (348m, AQ1)	After "settling-in", increase from 166m to 181m	1/1/10	1/1/10	1/4/12
P3 (290m, AQ2)	After "settling-in", increase from 145m to 155m	1/1/10	1/1/10	1/4/12
P4 (230m, AQ3)	After "settling-in", increase from 92m to 103m	1/1/10	1/1/10	1/4/12
P5 (180m, AQ3)	After large change in"settling-in", decrease from 179m to 169m			
P6 (130m, AQ4)	Steady at 111m	1/1/10	1/1/10	1/4/12
P7 (80m, AQ4)	After "settling-in", steady at 80m	1/1/10	1/1/10	1/4/12
P8 (35m, AQ5)	Steady at 19m	1/1/10	1/1/10	1/4/12

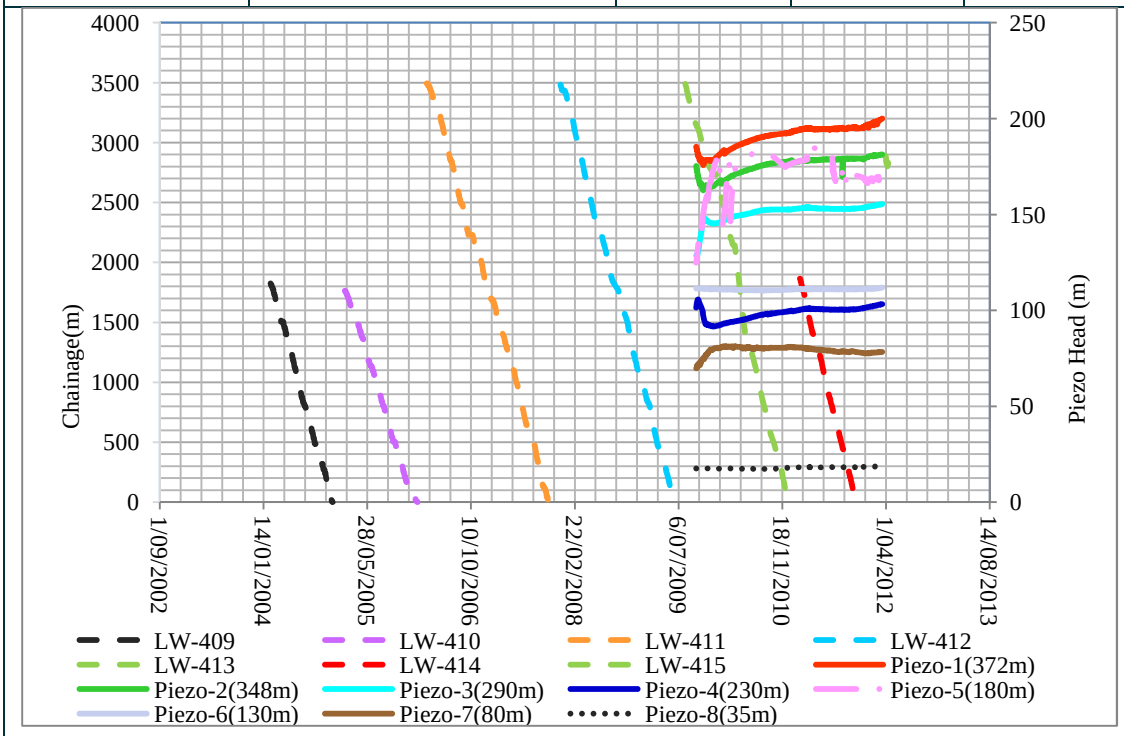

Increases in piezometer pressures could be due to effects described in Adhikary and Morla, 2013. P5 has a very pronounced "settling-in" period.

Figure A18 Description of piezometer hole SPR66

SPR67				
238420E, 6299864N. Elevation of Collar 1124				
P1 (260m, AQ3)	After “settling-in”, decrease from 70m to 30m during LW413 and 414			1/4/12
P2 (200m, AQ3)	Unexplained movement between 84m and 104m			1/4/12
P3 (160m, SP3)	Unexplained movement between 56m and 70m			1/4/12
P4 (110m, AQ4)	Decrease from 78 to 66m			1/4/12
P5 (90m, AQ4)	Decrease from 60m to 44m			1/4/12
P6 (70m)	Damaged			
P7 (50m, AQ5)	Unexplained behaviour between 18m and 40m			
P8 (35m, AQ5)	Unexplained behaviour between 4m and 20m			

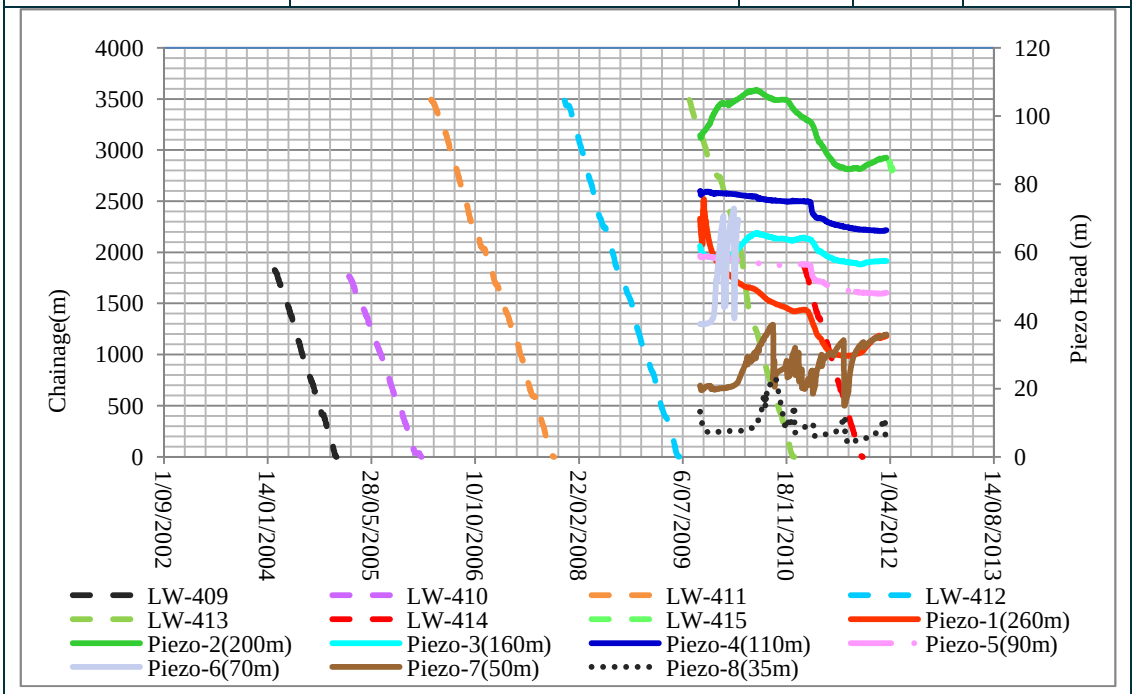

P1 to P5 probably affected by mining. P7 and P8 are exhibiting strange behaviour that could be due to effects described in Adhikary and Morla, 2013

Figure A19 Description of piezometer hole SPR67

AP1101				
235516E, 6311594N. Elevation of Collar 1088				
P1 (327m, AQ1)	Steady at 37m	1/8/12	1/8/12	1/8/12
P2 (300m, AQ1)	Steady at 8m	1/8/12	1/8/12	1/8/12
P3 (248m, AQ2)	Steady at 62m	1/8/12	1/8/12	1/8/12
P4 (235m, AQ2)	Decrease from 56m to 52m	1/8/12	1/8/12	1/8/12
P5 (210m, AQ3)	Stabilised at 44m	1/8/12	1/8/12	1/8/12
P6 (150m, AQ3)	Steady at 23m	1/8/12	1/8/12	1/8/12
P7 (92m, AQ4)	After initial "settling-in" period, stabilised at 55m	1/8/12	1/8/12	1/8/12

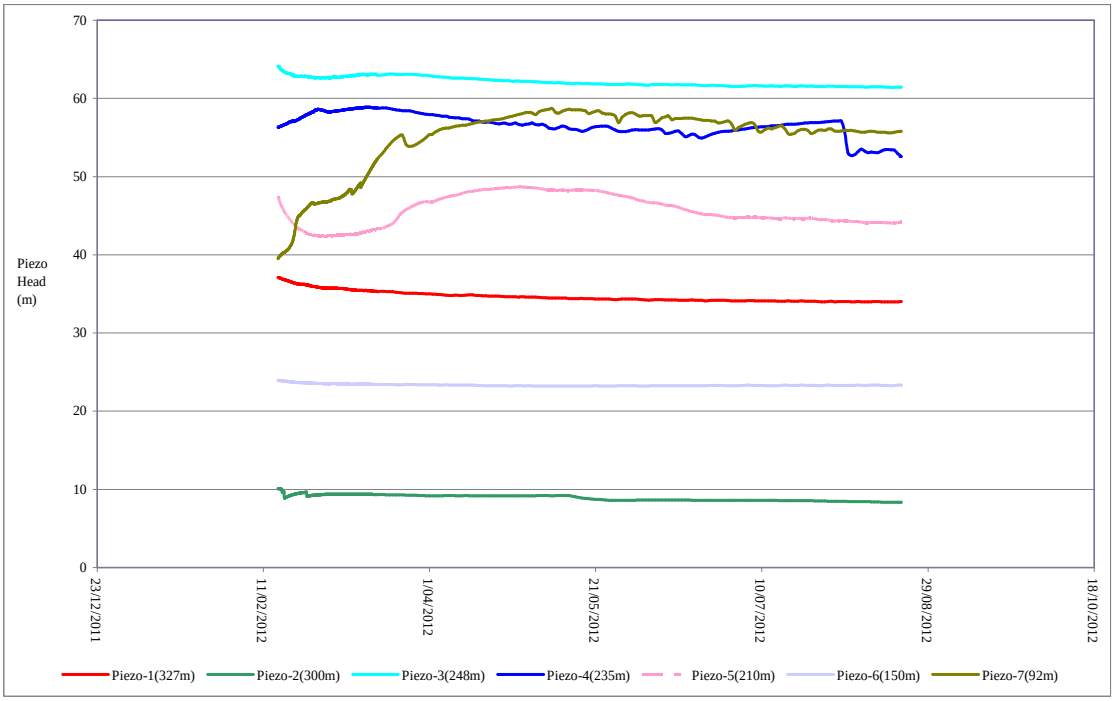

After "settling-in", piezometers are fairly steady.

Figure A20 Description of piezometer hole AP1101

AP1102				
239856E, 6308995N. Elevation of Collar 1135				
P1 (435m, LTH)	After “settling-in”, stabilised at around 70m	21/11/12	21/11/12	21/11/12
P2 (426m, AQ1)	After “settling-in”, stabilised at around 65m	21/11/12	21/11/12	21/11/12
P3 (392m, AQ2)	Stabilised at around 150m	21/11/12	21/11/12	21/11/12
P4 (338m, AQ2)	Stabilised at around 104m	21/11/12	21/11/12	21/11/12
P5 (265m, AQ3)	Stable at 60m	21/11/12	21/11/12	21/11/12
P6 (210m, SP3)	Moving between 8m and 46m	21/11/12	21/11/12	21/11/12
P7 (123m, AQ4)	Stabilised at around 10m	21/11/12	21/11/12	21/11/12

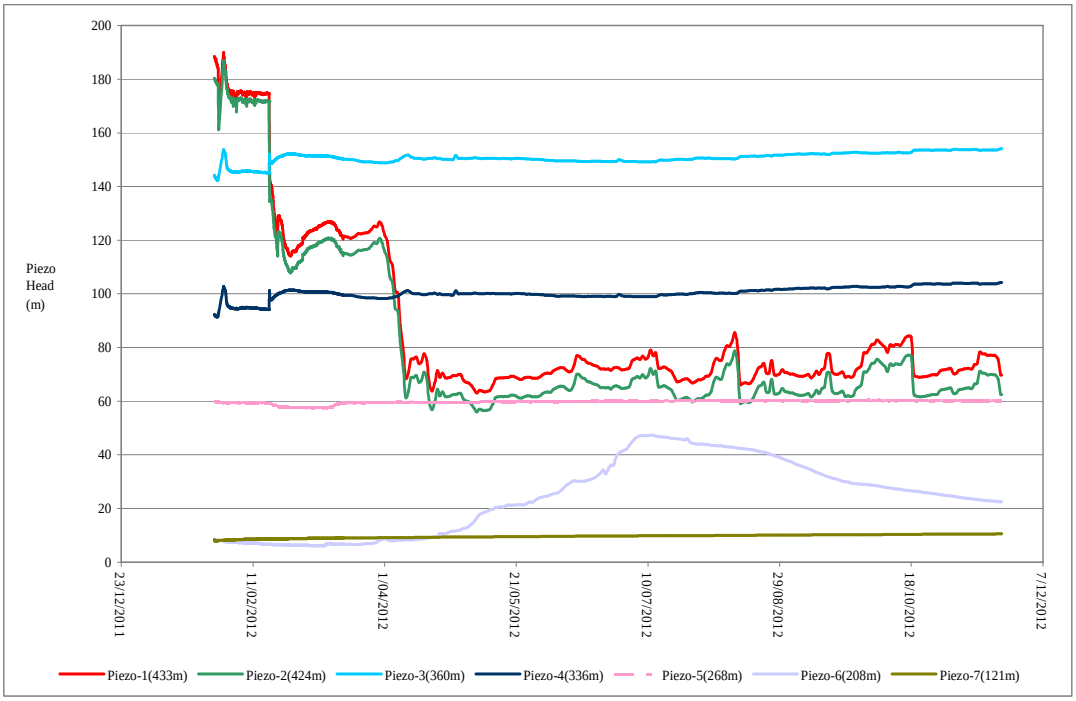

After “settling-in”, piezometers appear to be fairly stable.

Figure A21 Description of piezometer hole AP1102

AP1104				
239426E, 6306145N. Elevation of Collar 1088				
P1 (370m, AQ1)	Stabilised at 80m		16/3/12	16/3/12
P2 (360m, AQ1)	Stabilised at 77m		16/3/12	16/3/12
P3 (300m, AQ2)	Stabilised at 37m		16/3/12	16/3/12
P4 (277m, AQ2)	Stabilised at 120m		16/3/12	16/3/12
P5 (255m, AQ3)	Stabilised at 115m	16/3/12	16/3/12	16/3/12
P6 (240m, AQ3)	Stabilised at 102	16/3/12	16/3/12	16/3/12
P7 (170m, AQ3)	Stabilised at 58m	16/3/12	16/3/12	16/3/12

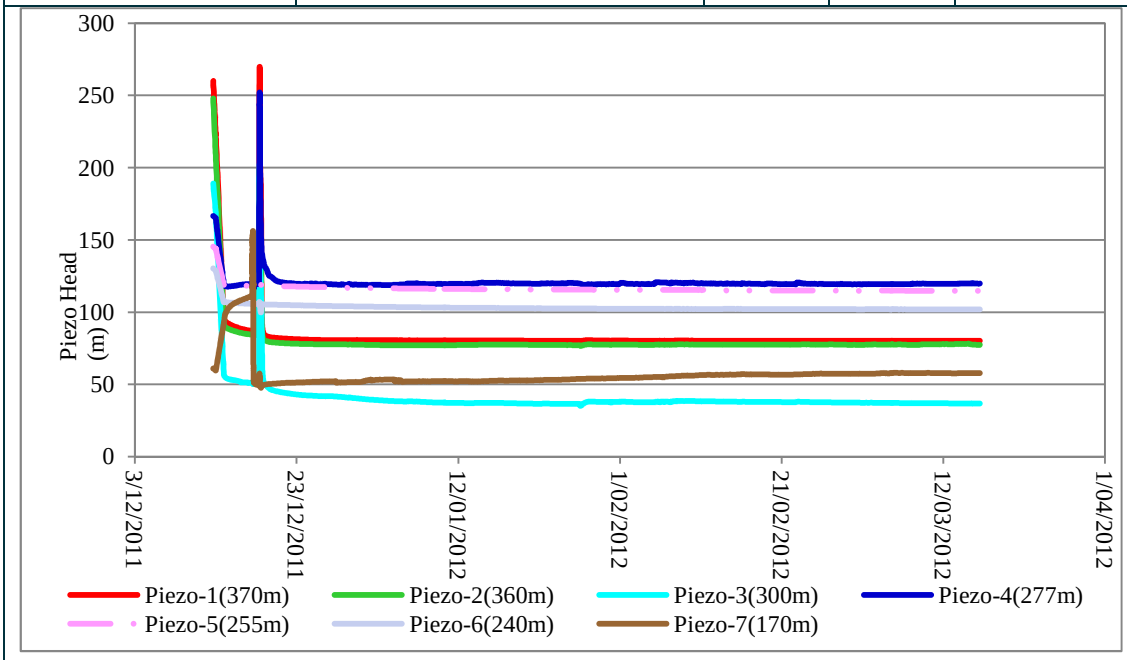

After "settling-in", piezometers appear to be fairly stable.

Figure A22 Description of piezometer hole AP1104

AP1106				
240235E, 6310388N. Elevation of Collar 1044				
P1 (380m, floor)	Stabilised at 55m	21/11/12	21/11/12	21/11/12
P2 (356m, AQ1)	Stabilised at 34m	21/11/12	21/11/12	21/11/12
P3 (335m, AQ1)	Stabilised at 19m	21/11/12	21/11/12	21/11/12
P4 (275m, AQ2)	Stabilised at 76m	21/11/12	21/11/12	21/11/12
P5 (251m, AQ2)	Stabilised at 94m	21/11/12	21/11/12	21/11/12
P6 (174m, AQ3)	Stabilised at 24m	21/11/12	21/11/12	21/11/12

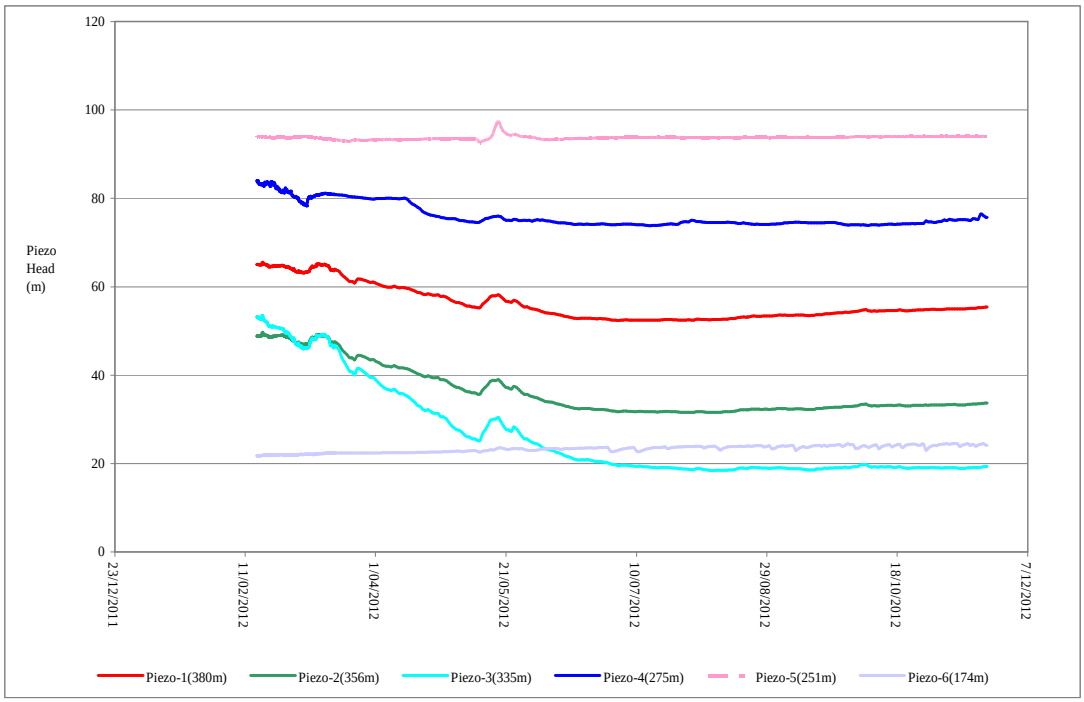

After "settling-in", piezometers appear to be fairly stable.

Figure A23 Description of piezometer hole AP1106

AP1107				
237069E, 6310980N. Elevation of Collar 1048				
P1 (290m, AQ1)	Around 32m	16/3/12	16/3/12	16/3/12
P2 (238m, AQ2)	Around 61m	16/3/12	16/3/12	16/3/12
P3 (212m, AQ2)	Around 70m	16/3/12	16/3/12	16/3/12
P4 (209m, SP2)	Around 68m	16/3/12	16/3/12	16/3/12
P5 (150m, AQ3)	Around 62m	16/3/12	16/3/12	16/3/12
P6 (81m, AQ4)	Around 51m	16/3/12	16/3/12	16/3/12
P7 (54m, AQ4)	Around 47m	16/3/12	16/3/12	16/3/12

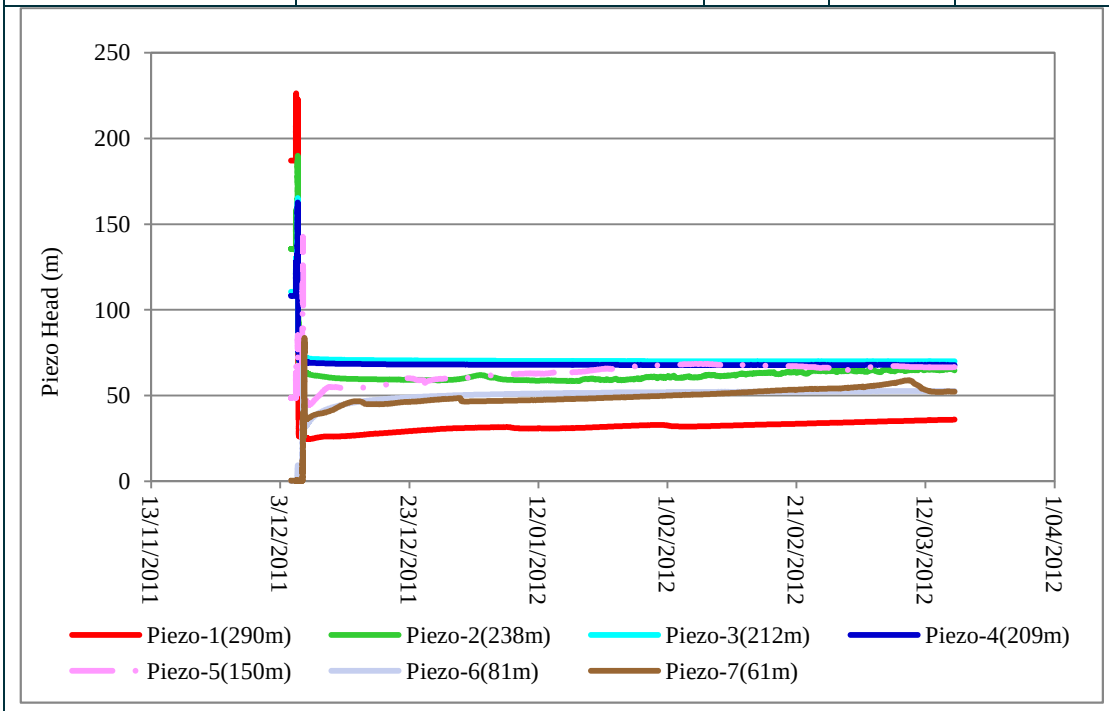

After "settling-in", most piezometers are slowly increasing.

Figure A24 Description of piezometer hole AP1107

AP10PR				
237243E, 6306778N. Elevation of Collar 1088				
P1 (343m, SP0)	Unexplained increase from 49m to 68m			16/3/12
P2 (327m, roof)	Unexplained increase from 30m to 48m			16/3/12
P3 (300m, AQ1)	After "settling-in", increase from 28m to 35m			16/3/12
P4 (270m, AQ2)	Decrease from 94m to 90m	18/11/10	18/11/10	16/3/12
P5 (248m, AQ2)	Decrease from 78m to 75m	18/11/10	18/11/10	16/3/12
P6 (205m, AQ3)	Unexplained increase from 43m to 51m			16/3/12
P7 (150m, AQ3)	Varying between 55m and 80m			
P8 (103m, AQ4)	Stable at around 38m	18/11/10	18/11/10	16/3/12
P9 (60m, AQ4)	Stable at around 64m	18/11/10	18/11/10	16/3/12

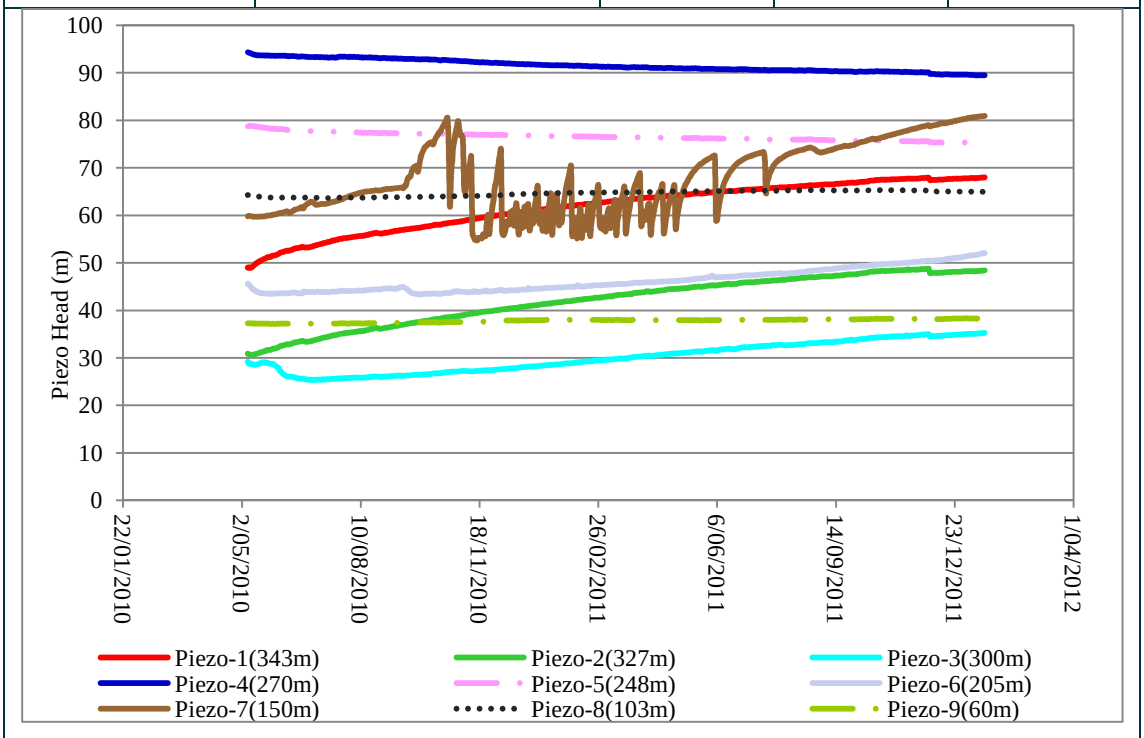

Increases in P1, P2, P3 and P6, possibly due to effects described in Adhikary and Morla, 2013. P7 appears unstable

Figure A25 Description of piezometer hole AP10PR

AP11PR				
238143E, 6305296N. Elevation of Collar 1054				
P1 (320m, AQ2)	After "settling-in", fairly steady at around 70m		10/8/10	23/12/11
P2 (295m, AQ3)	Oscillates around 50m		10/8/10	23/12/11
P3 (263m, AQ3	Small increase from 42 to 46m		10/8/10	23/12/11
P4 (223m, AQ3)	Increases from 38m to 54m somewhat erratically		10/8/10	23/12/11
P5 (167m, AQ4)	Unexplained erratic behaviour, tending to about 80m			23/12/11
P6 (128m, AQ4)	Unexplained sudden jump from 27m to 46m		10/8/10	23/12/11
P7 (93m, AQ4)	Stable at 2m	18/11/10	10/8/10	23/12/11
P8 (72m, AQ5)	Unexplained increase from 10m to 28m		10/8/10	23/12/11
P9 (43m, AQ5)	After "settling-in", decrease to zero	18/11/10	10/8/10	23/12/11

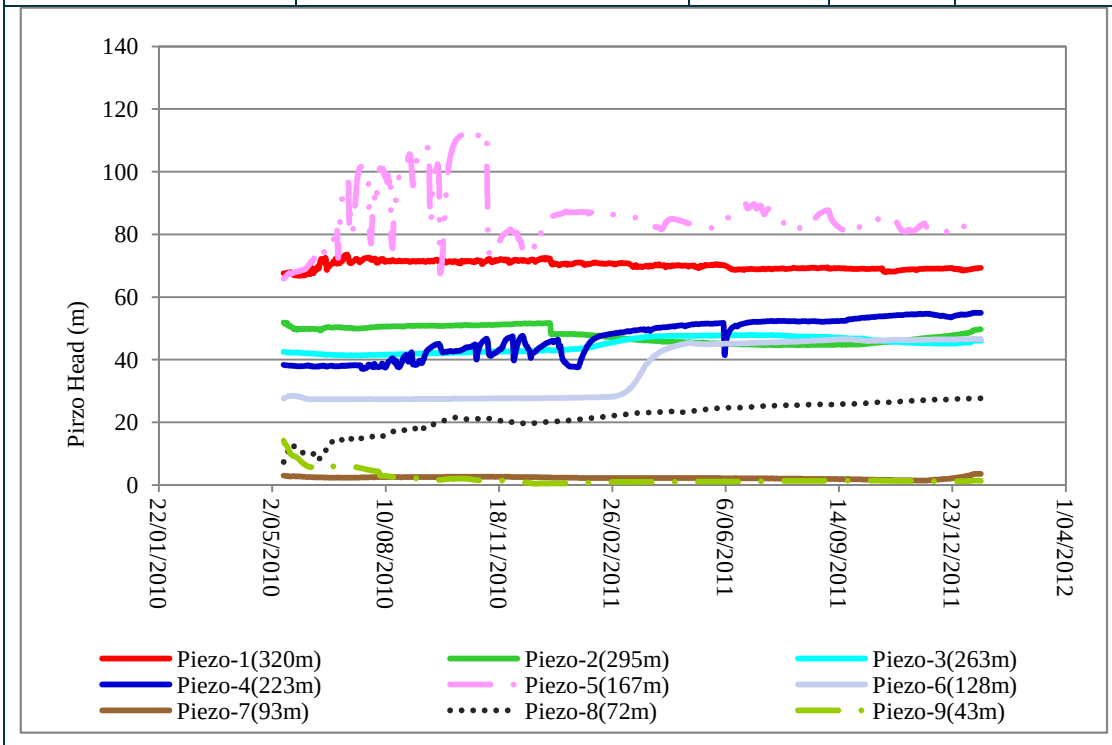

P4, P5, P6 and P8 all exhibit unusual behaviour

Figure A26 Description of piezometer hole AP11PR

AP2PR				
237677E, 6307973N. Elevation of Collar 1054				
P1 (411m, LTH)	Unexplainable increase from 55m to 110m			
P2 (381m, AQ1)	Unexplainable increase from 80m to 94m		2/5/10	23/12/11
P3 (300m, AQ2	Slow decrease from 80 to 76m	2/5/10	2/5/10	23/12/11
P4 (213m, AQ3)	Erratic behaviour between 80m and 110m, ending at 104m			23/12/11
P5 (181m, AQ4)	Unexplainable increase from 76m to 84m	2/5/10	2/5/10	23/12/11
P6 (92m, AQ5)	Erratic behaviour between 5m and 40m, ending at around 20m		2/5/10	23/12/11

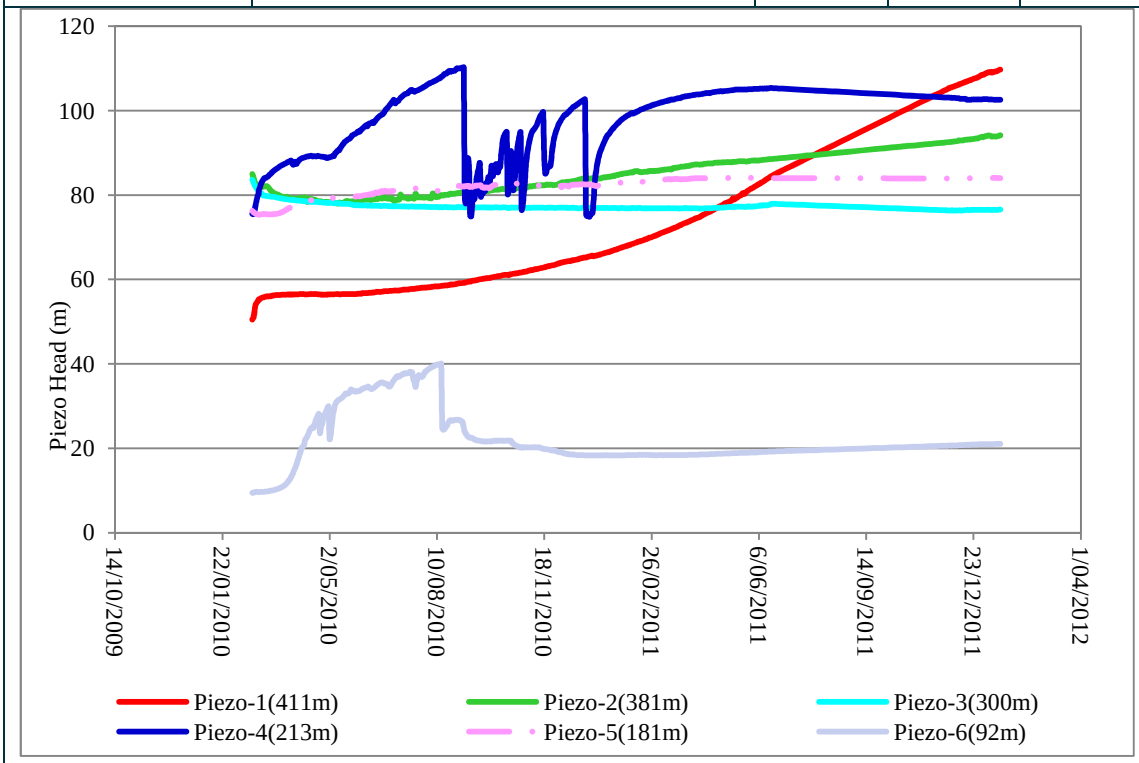

P1 has large increase, P4 and P6 exhibit erratic behaviour. P2 and P5 have small increases. These behaviours may be due to effects described in Adhikary and Morla, 2013.

Figure A27 Description of piezometer hole AP2PR

APB2				
232410E, 6304043N. Elevation of Collar 1140				
P1 (320m, floor)	Steady at 4m		1/2/12	1/2/12
P2 (293m, AQ1)	Steady at 14m		1/2/12	1/2/12
P3 (243m, AQ2)	Steady at 50m		1/2/12	1/2/12
P4 (185m, AQ3)	Steady at 59m		1/2/12	1/2/12
P5 (160m, SP3)	Steady at 52m		1/2/12	1/2/12
P6 (135m, AQ4)	Steady at 50m		1/2/12	1/2/12
P7 (69m, AQ4)	Steady at zero	1/2/12	1/2/12	1/2/12

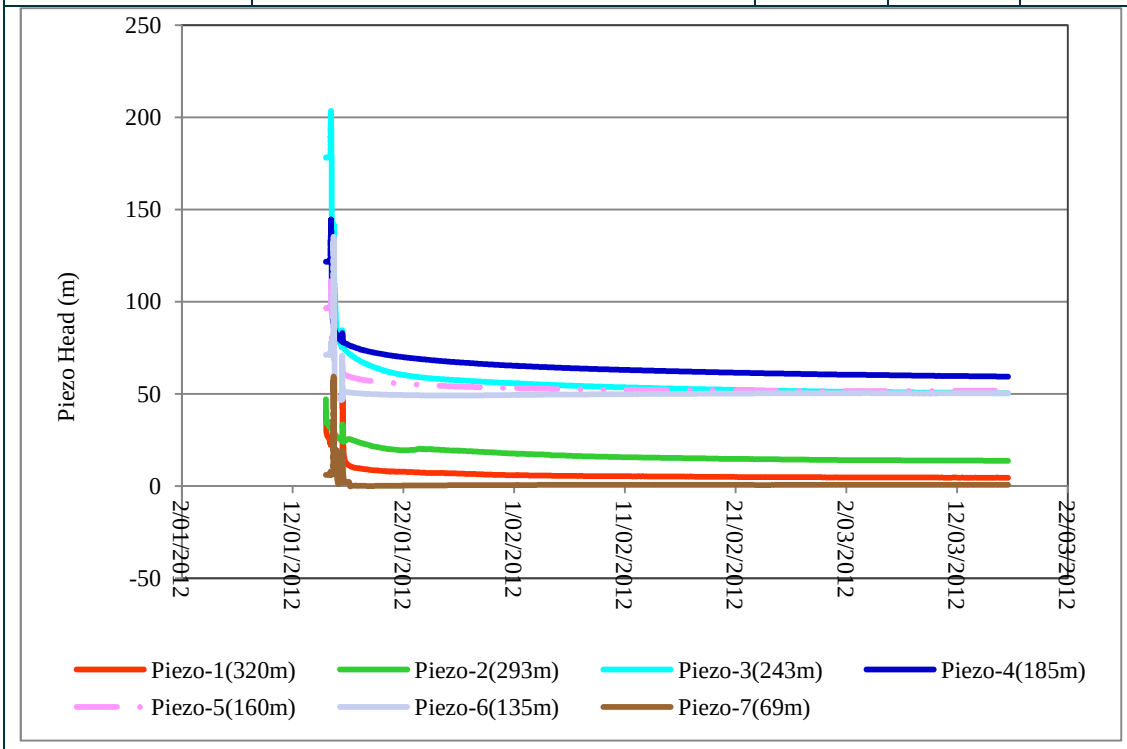

After initial "settling-in" period, piezometers are steady.

Figure A28 Description of piezometer hole APB2

Kerosene Vale Piezometers

There are also data for 4 shallow piezometers in the area of Kerosene mine. The coordinates of these piezometer holes and the standing water levels in each are shown in Table 1.

Table 1 Information on piezometer holes at Kerosene Vale

Name	Easting	Northing	Elevation of standing water (mAHD) on 29/7/2009
MB7A	229531	6301971	903m (3m depth)
MB8A	229166	6301607	904m (6m depth)
MB9A	229149	6303042	889m (15m depth)
MB10B	229730	6302889	885m (53m depth)

All these piezometers at Kerosene Vale are used in the calibration and validation. These boreholes were not incorporated into the mesh, so the model results are obtained via interpolation.

2 Mine Inflow Data

2.1 Springvale Colliery inflow data

The combined total water pump rates from the Springvale series of longwall panels LW1, LW401, etc (collectively called SPR_1 in the model) are available from January 2004 to the present. They are shown in Figure A29. In that figure, three linear fits have been performed. The first fit is to pre 2010 data, which appear to be somewhat correlated with panel extracted (the four peaks correspond to the centres of panels 409, 410, 411 and 412). These data are coloured pink. The second fit is to post 2009 data, which, perhaps, because of their scarcity are not obviously correlated with panel extraction. These data are coloured blue. The third fit is to all the data. Also shown on the graph are the times at the end of transient calibration and validation.

The objective for calibration is to achieve a flow rate of 140 l/s at the end of the calibration period, and an average rate of increase of 7.3 l/s/year (slope of the inflow curve) during the years 2004 to 2007. This objective is also shown in Figure A29.

The flow rate at the end of validation should be 177 l/s which is also shown in Figure A29 by an yellow line and an yellow circle.

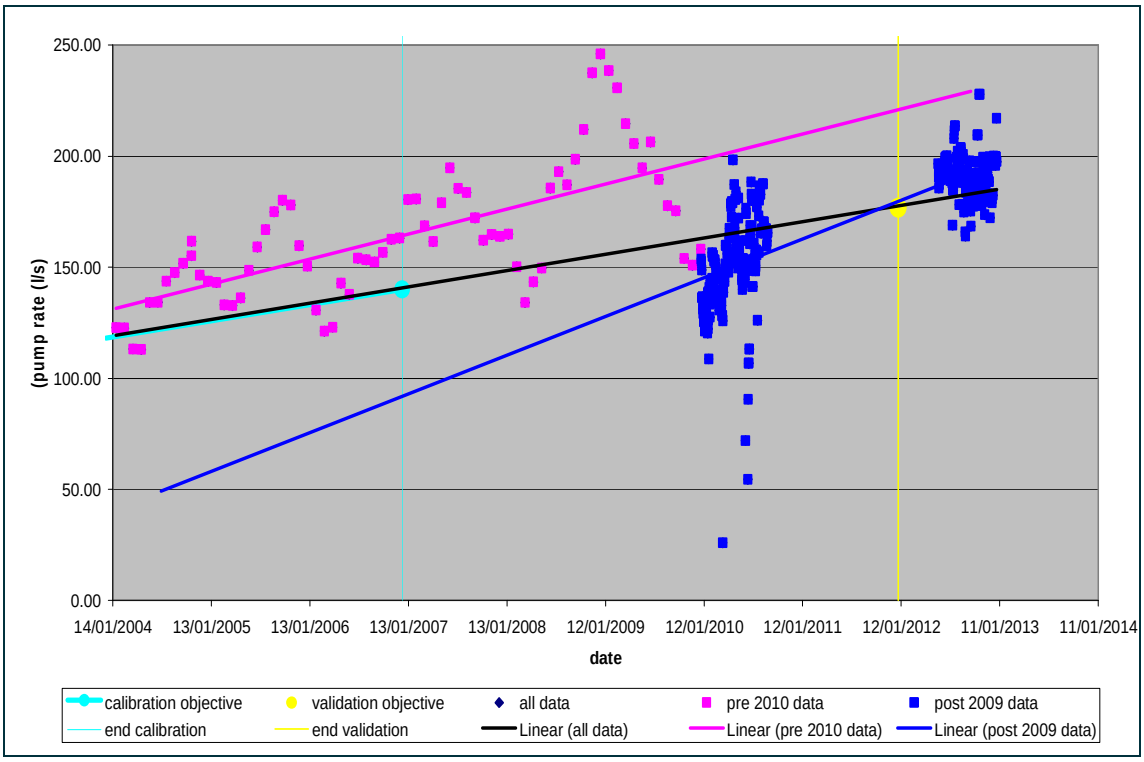

Figure A29 Mine water inflow data Springvale Colliery

2.2 Angus Place Colliery Inflow data

The combined total water pump rates from the Angus Place series of longwall panels LW16 to LW26, LW26N, and LW920 to LW970 (collectively called APLW4, APLW5 and APLW6) are available from January 2009 to the present. There are also pump rates available for the so-called "930" and "940" pumps from April 2006 to December 2008, which drain part of the Angus Place panels, so the total Angus Place pump rate must be greater than these data.

The observed rates are shown in Figure A30. In that graph, three linear fits have been made. The first is to pre October 2010 data, which have a large scatter, and is coloured pink in the graph. The second is to post September 2010 data where some correlation between flow rate and panel extraction can be made: the three clusters of points correspond roughly to panels 950, 960 and 970. These data are coloured blue. The third linear fit is to all the data (excluding the lower bound data), and are coloured black.

The objective for calibration is to achieve a flow rate between 70l/s and 100l/s at the end of calibration (to satisfy the lower bound and to not exceed the linear fit to the observed data), with an average rate of increase of 6.5l/s/year during 2005 and 2006. The year 2005 was included, even though there is no data for that year, because the model only outputs flow rates at a few times during 2005 and 2006, so this reduces the chance of incorrectly estimating the slope from the model results.

The flow rate at the end of validation should be 118 l/s which is also shown in Figure A30 by an yellow line and an yellow circle.

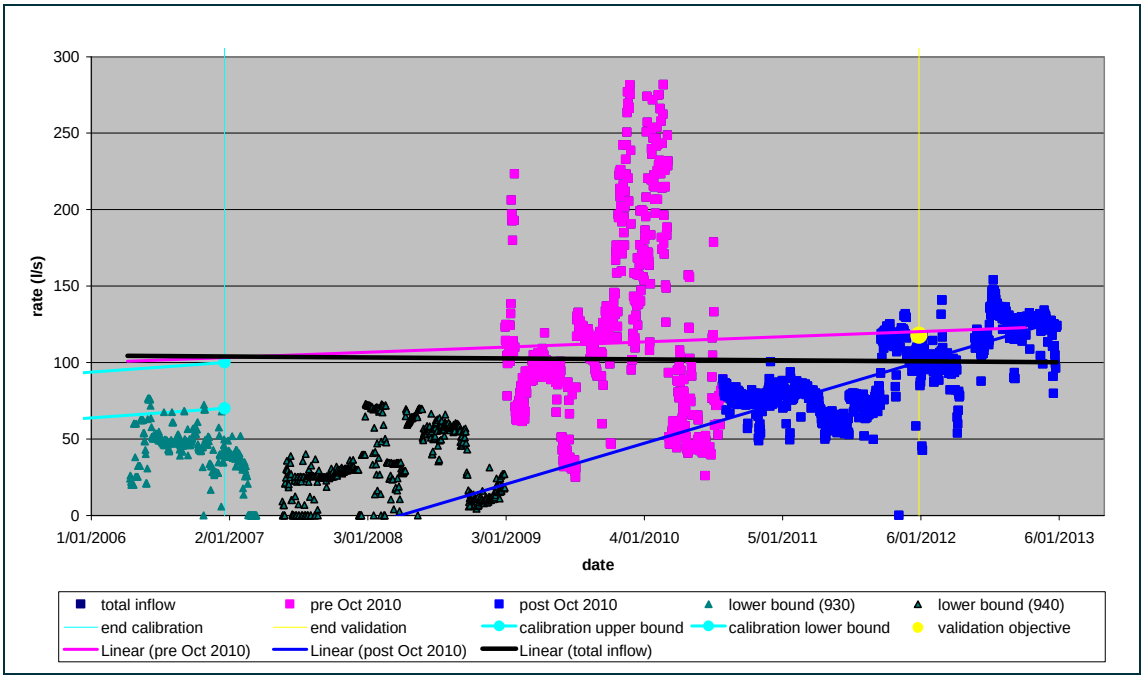

Figure A30 Mine water inflow data Angus Place Colliery

3 Baseflow into Sunnyside Swamp and Kangaroo Creek

The calculation of baseflow values for a number swamps at Angus Place and Springvale Mining region is discussed in Section 2.9. The baseflow values noted in Section 2.9 for Sunnyside Swamp were estimated by Aquaterra. The objective for calibration was to achieve 0.093 ML/day baseflow from Sunnyside Swamp at the end of the calibration period and during the validation period from January 2010 to April 2012.

In Section 2.9 baseflow values were also quoted for Kangaroo Creek. However, these cannot be directly compared with the model, as we do not know which parts of Kangaroo Creek are perennial and which parts are ephemeral, and whether baseflow from one part of the creek ends up at the Kangaroo Creek weir (flow monitoring point), or whether it contributes to leakage in another part of the creek.

4 Observed Groundwater Levels at Type C - Swamps

Aurecon (2012) and RPSAquaterra (2012) present monitoring results at a number of swamps and assess the potential impacts of mining at Angus Place and Springvale region. We are particularly interested in how well the model agrees with observations within the modeled Type-C (assumed to be mostly waterlogged) swamps. In order to monitor fluctuations in the groundwater level, monitoring systems (piezometers and LevelTROLL) have been installed at a number of Type-C swamps that has been simulated in this study (see Table 2). From Aurecon (2012) and RPSAquaterra (2013), it can be seen that the groundwater levels at these swamps do fluctuate in response to rainfall; however, they at least allow a qualitative comparison to be made with the model.

Table 2 Swamps and observed groundwater levels

Site	Swamp	Easting	Northing	Comments	Estimated groundwater depth (mbgl) at 1/1/2012
SS-SV8 (SS1)	Sunnyside (SSS)	237783	6303571	Varies around 0.1m BGL	0.1
SS-SV9 (SS2)	Sunnyside (SSS)	237765	6303509	Varies around 0.2m BGL	0.2
SS 03	Sunnyside (SSS)	237845	6303838	Mostly above surface	<0
SS-04	Sunnyside (SSS)	237791	6304398	Mostly above surface	<0
SS-05	Sunnyside (SSS)	237782	6304627	Mostly above surface	<0
SSE2-SV13	Sunnyside East (CA5)	238850	6303360	Fluctuates between about 0.5m and -0.3m BGL	-0.05
SSE3-SV14	Sunnyside East (CA5)	239058	6303568	Fluctuates between about 0.2m and -0.1m BGL	0.0
CW1-SV10	Carne West (CW)	239382	6303246	Fluctuates between about 0.2m and 0.0m BGL	0.05
CW2-SV11	Carne West (CW)	239351	6303196	Fluctuates between about 0.2m and 0.1m BGL	0.2

5 Observed Groundwater Levels around Kangaroo Creek Swamp

Aurecon (2012) monitor the groundwater levels within Kangaroo Creek Swamp using shallow piezometer KC1. They also monitor the water depth (KWH) in a small pool downstream of a spring which feeds the lower end of the swamp.

As Angus Place LW940 passes under KC1 around May 2008 the groundwater level drops below the base of this borehole, as shown in Figure A31. As Angus Place LW950 passes under KWH in early 2010, its level drops to almost zero, as shown in Figure A32. However, Kangaroo Swamp is illustrative of the complex nature of the swamps in this region. Anecdotal evidence suggests the spring which feeds the small pool has not been greatly affected by mining, and yet both the swamp and pool were affected. The swamp was affected by LW940, and yet the pool seems only affected by LW950. The pool's level suddenly rises in late 2010 which isn't clearly correlated with mining activity or rainfall. Given enough input data, these observations could be explored by a high-resolution model of the swamp region, however, the Model of this report cannot capture such fine-scale effects. The model simply shows a decrease in baseflow to Kangaroo Swamp in response to longwall mining.

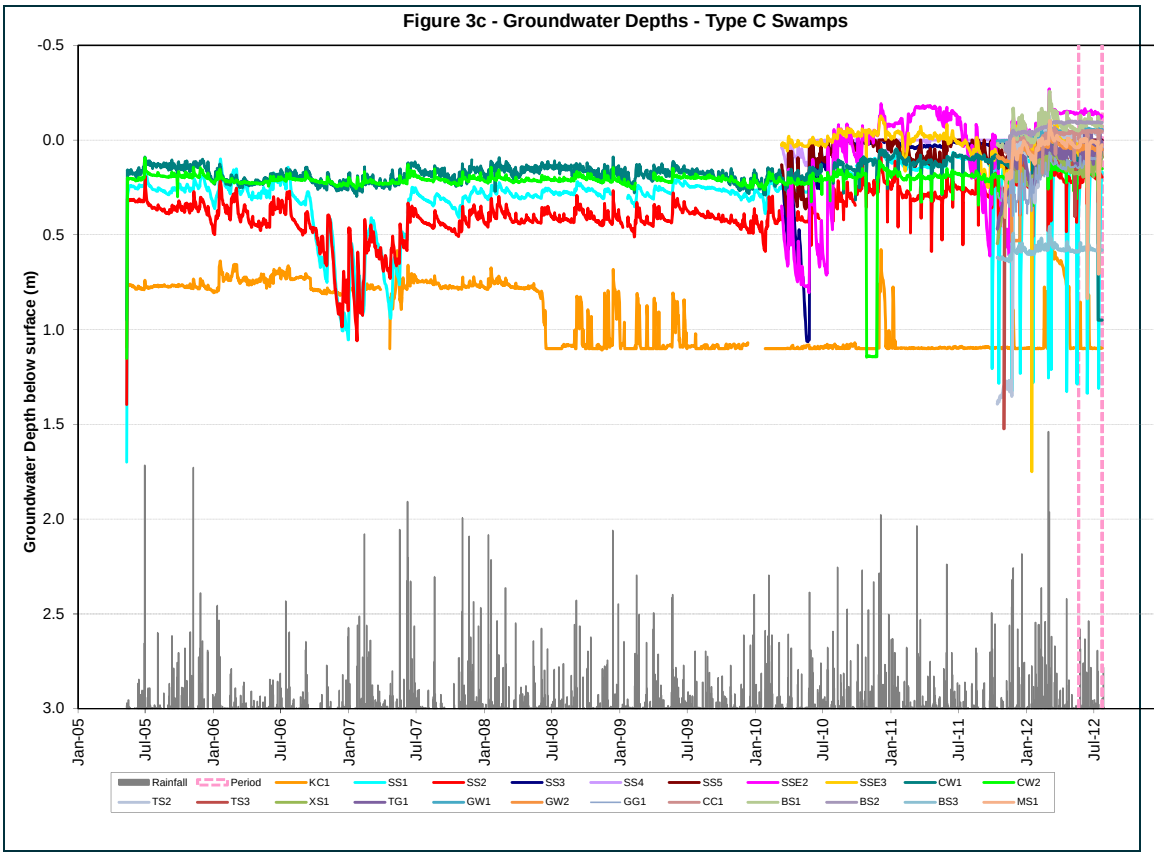

Figure A31 Groundwater depth in Type C swamps. In particular, KC1 is the lower brown line that dips suddenly around April 2008.

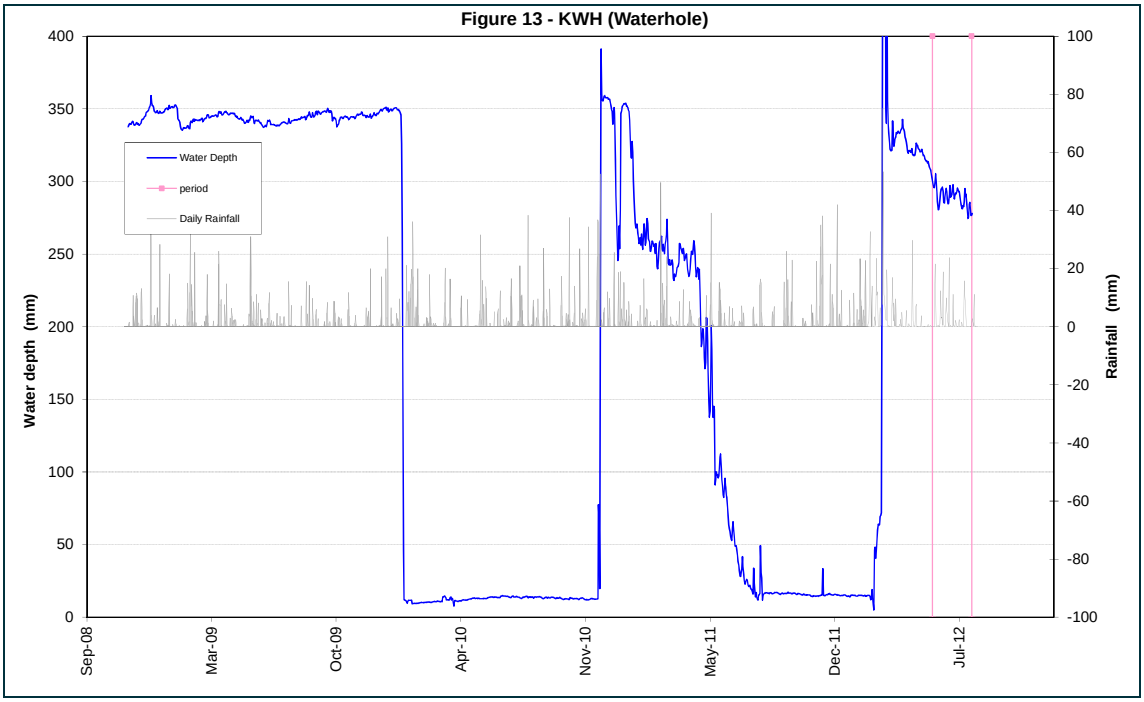

Figure A32 Water depth in the waterhole located close to the lower end of Kangaroo Swamp. As Angus Place LW950 passes under the waterhole in early 2010, its level drops.

EARTH SCIENCE AND RESOURCE ENGINEERING
www.csiro.au

Appendix B
Monitored and Simulated Piezometer Head Profiles

Angus Place and Springvale Colliery Operations

Groundwater Assessment

D P Adhikary and A Wilkins
Report No EP132799
May 2013

Springvale Colliery and Angus Place Colliery

Citation

Adhikary, DP and Wilkins, A (2013) Adhikary, DP and Wilkins, A (2013) Angus Place and Springvale Colliery operations groundwater assessment. Appendix B – Monitored and measured piezometer head profiles. Report No EP132799.

Copyright and disclaimer

Important disclaimer

List of Figures

Comparison of Piezometer Elevation Heads

In Chapter 3 many of the piezometers were used to calculate RMS and SRMS errors for calibration and validation. Here the elevation heads at all piezometers are plotted as a function of time (see Figure B1 to Figure B26), in order to compare the simulated piezometer heads with observations. Figure B27 to Figure B59 provides comparisons of simulated and measured vertical head profiles.

From these figures, it can be seen that the simulated water heads generally agrees well with the measurements. However, there are some differences between the measured heads and simulated heads which are largely reflected through the RMS error of 32.1m. Adhikary and Morla (2013) have conducted a qualitative assessment of the monitored piezometric data. Understanding the changes in piezometric heads is not always easy as a number of factors may affect the piezometer readings as discussed in that report. Thus the level of match between the observed piezometric heads and the simulated piezometric heads obtained using an uncoupled fluid flow (groundwater flow) only code is remarkable.

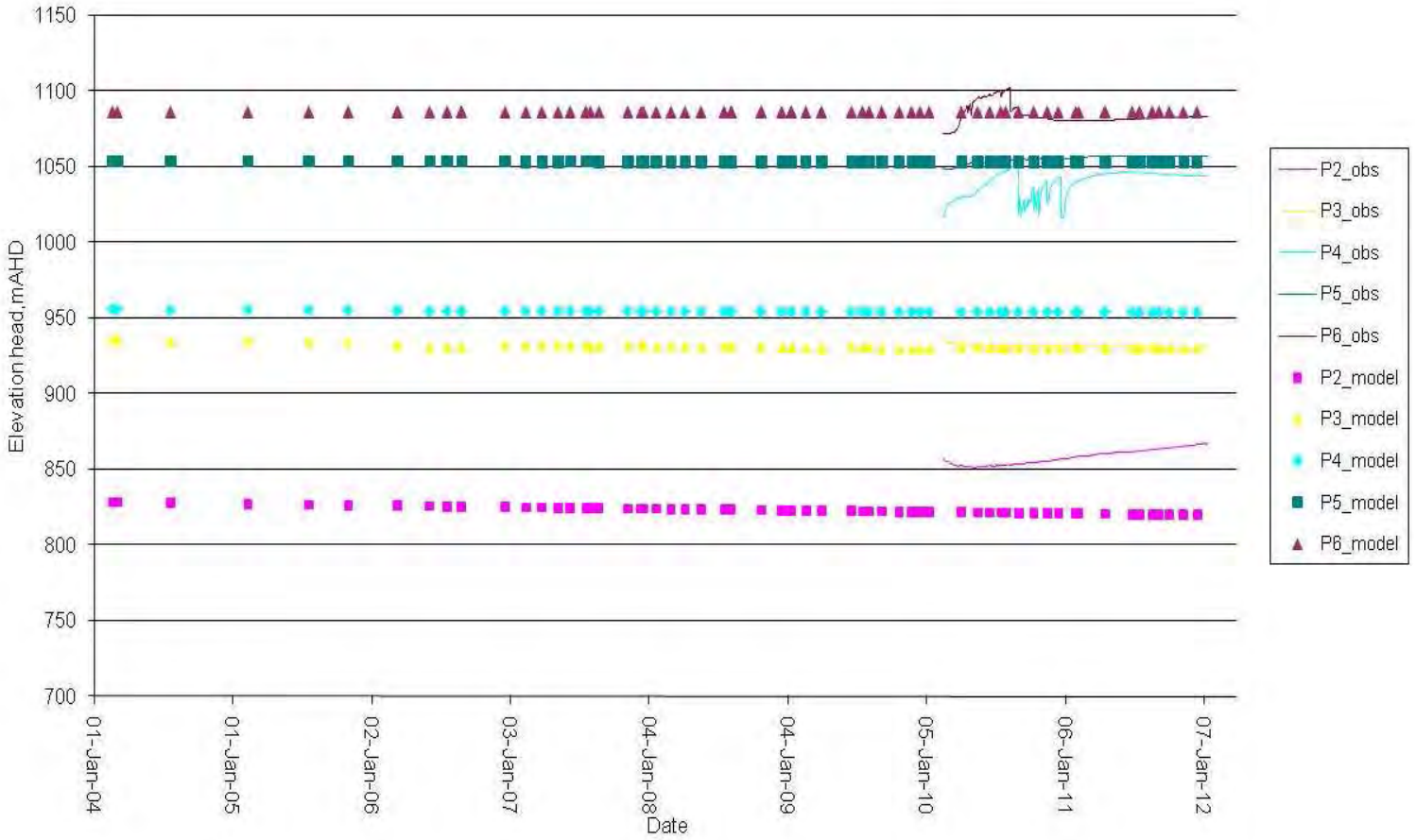

Figure B1 Comparison of observed and simulated piezometer elevation heads (Piezometer hole AP2PR)

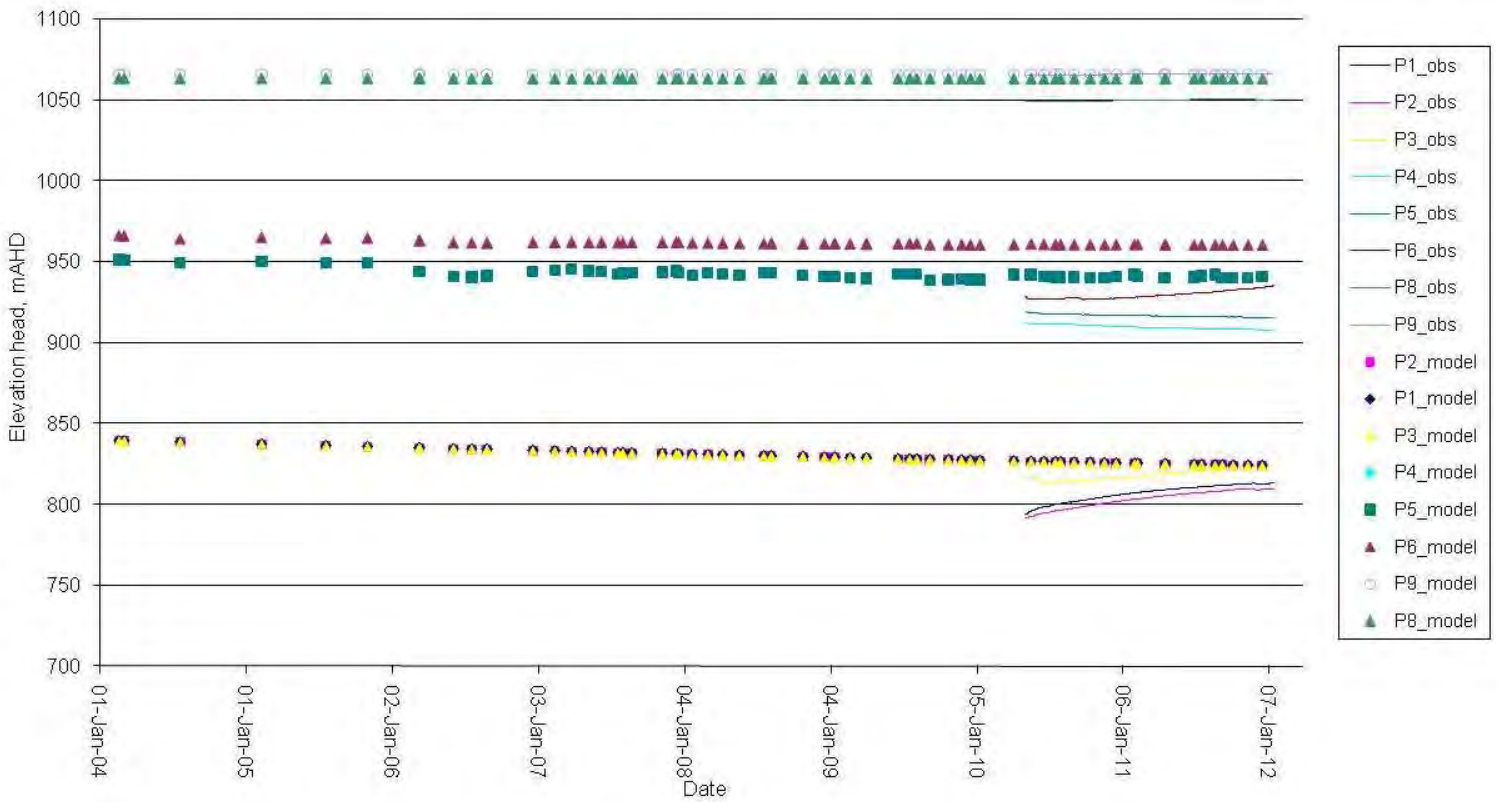

Figure B2 Comparison of observed and simulated piezometer elevation heads (Piezometer hole AP10PR)

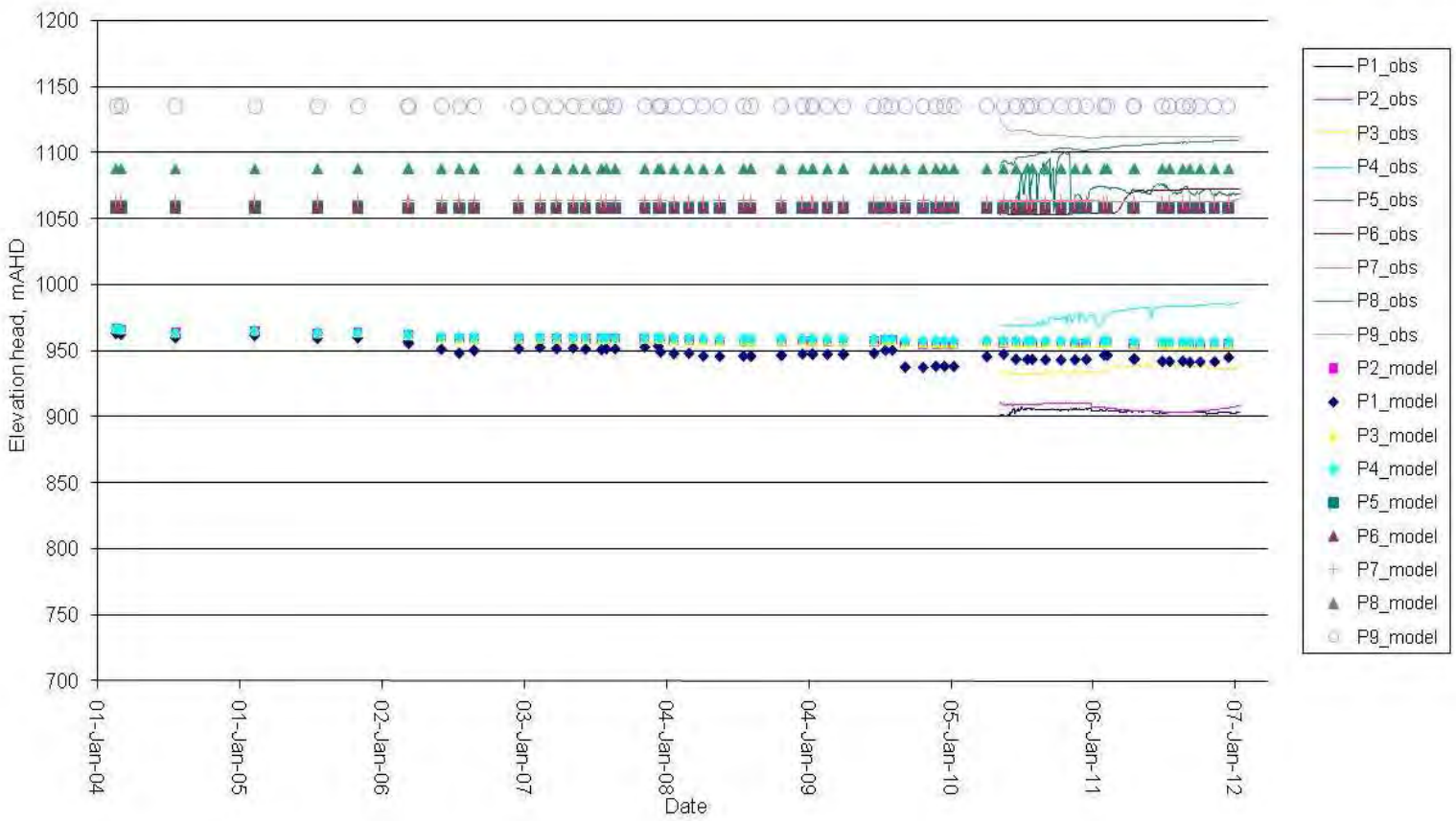

Figure B3 Comparison of observed and simulated piezometer elevation heads (Piezometer hole AP11PR)

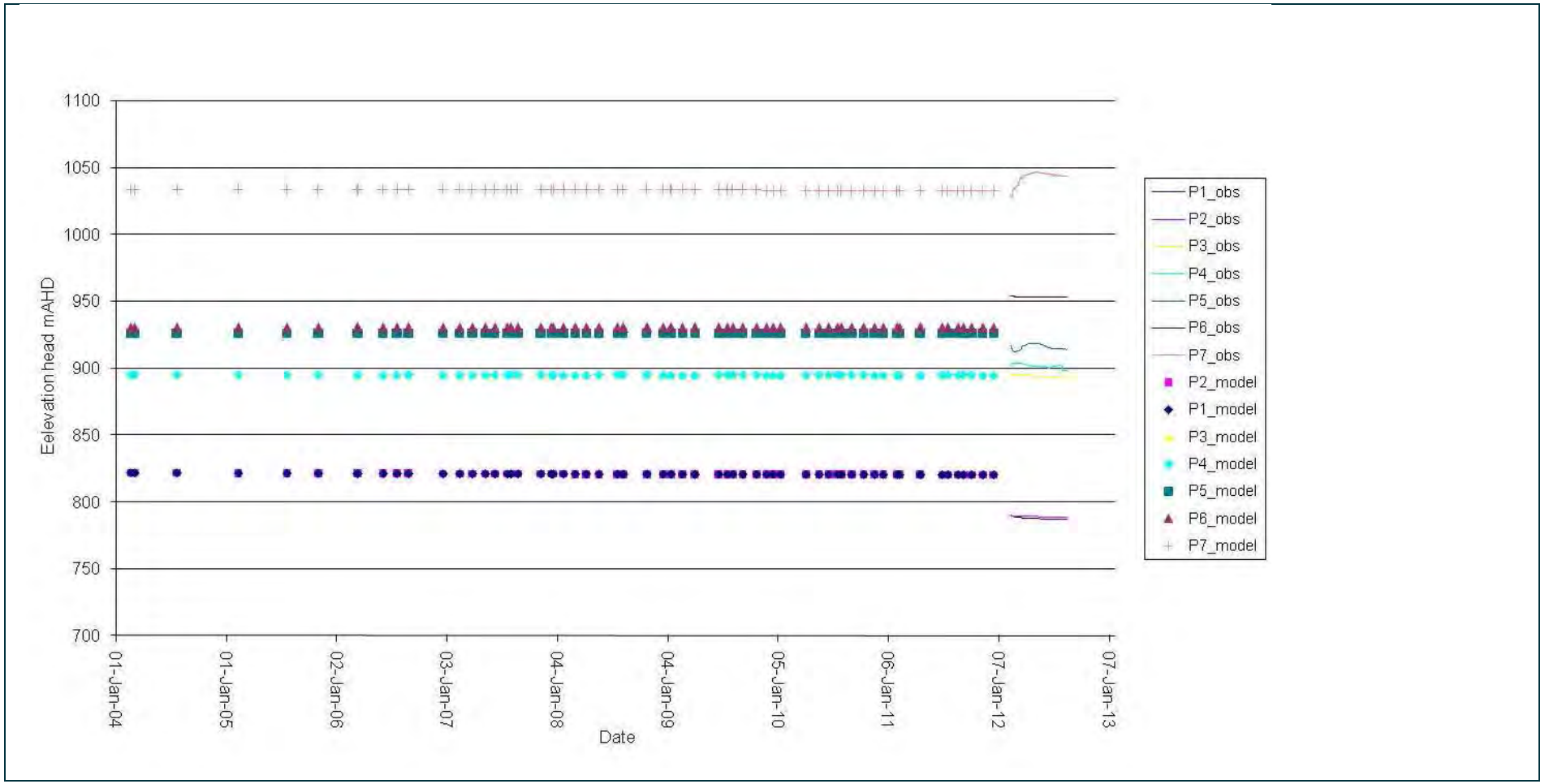

Figure B4 Comparison of observed and simulated piezometer elevation heads (Piezometer hole AP1101)

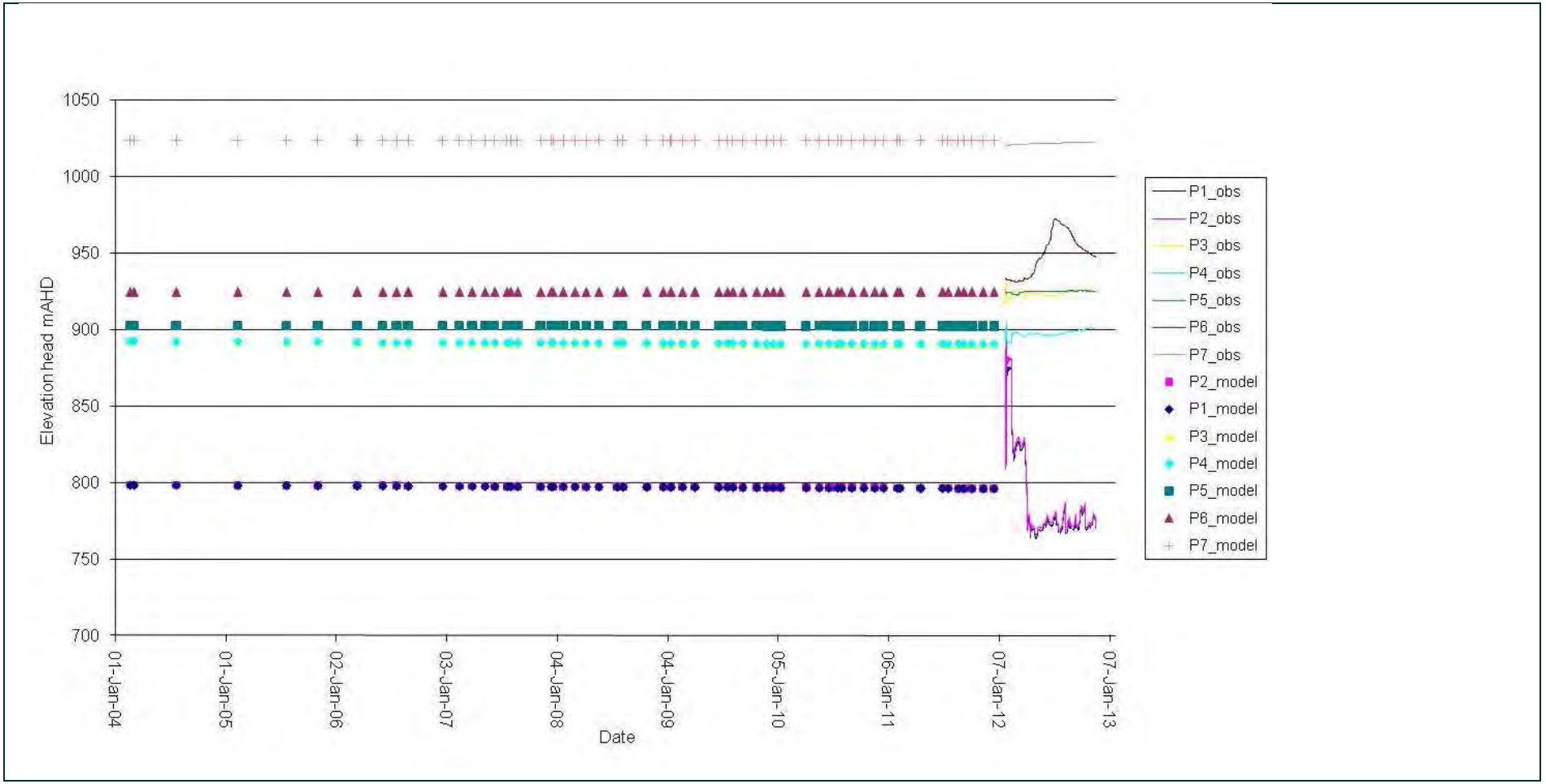

Figure B5 Comparison of observed and simulated piezometer elevation heads (Piezometer hole AP1102)

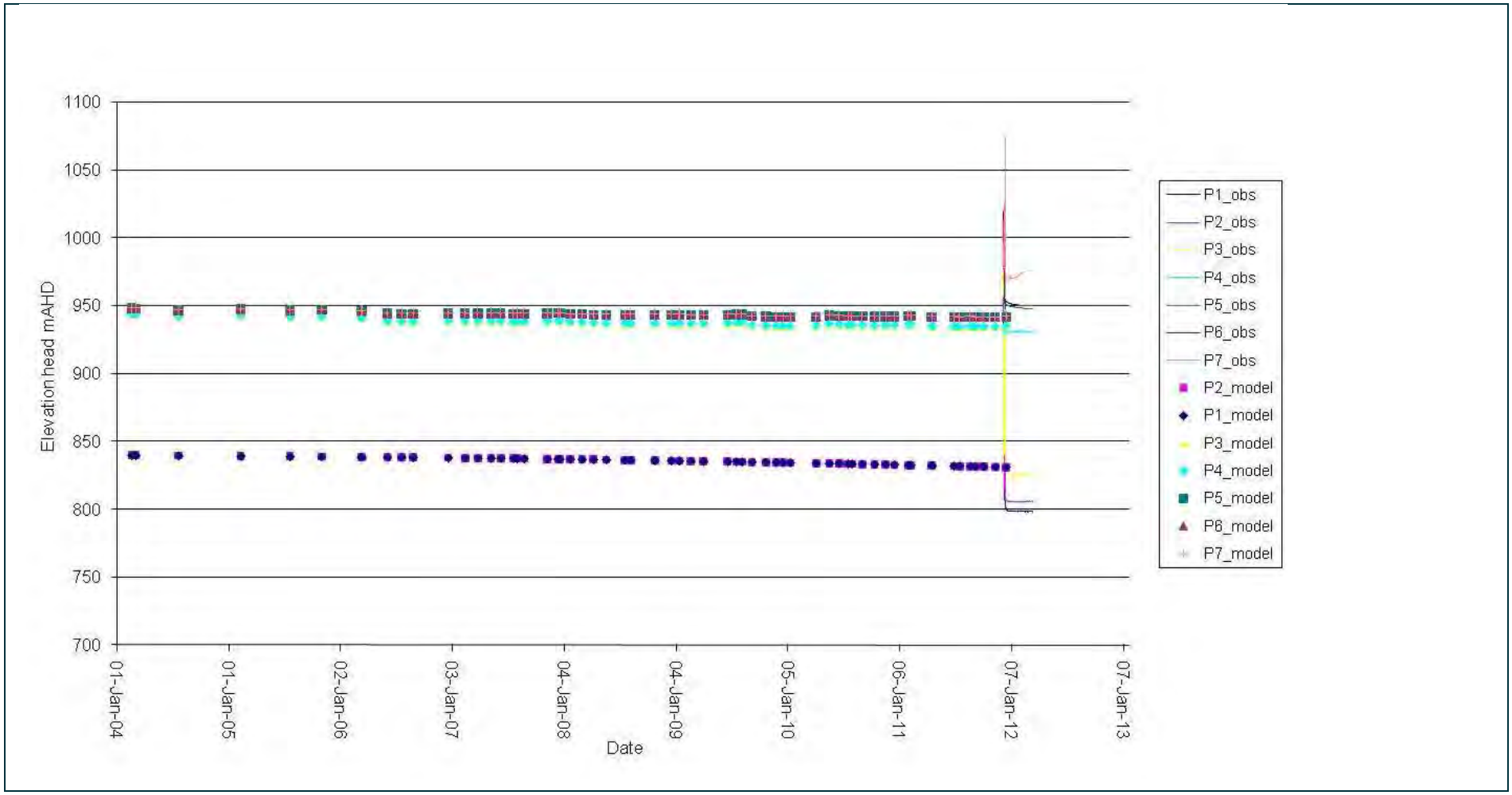

Figure B6 Comparison of observed and simulated piezometer elevation heads (Piezometer hole AP1104)

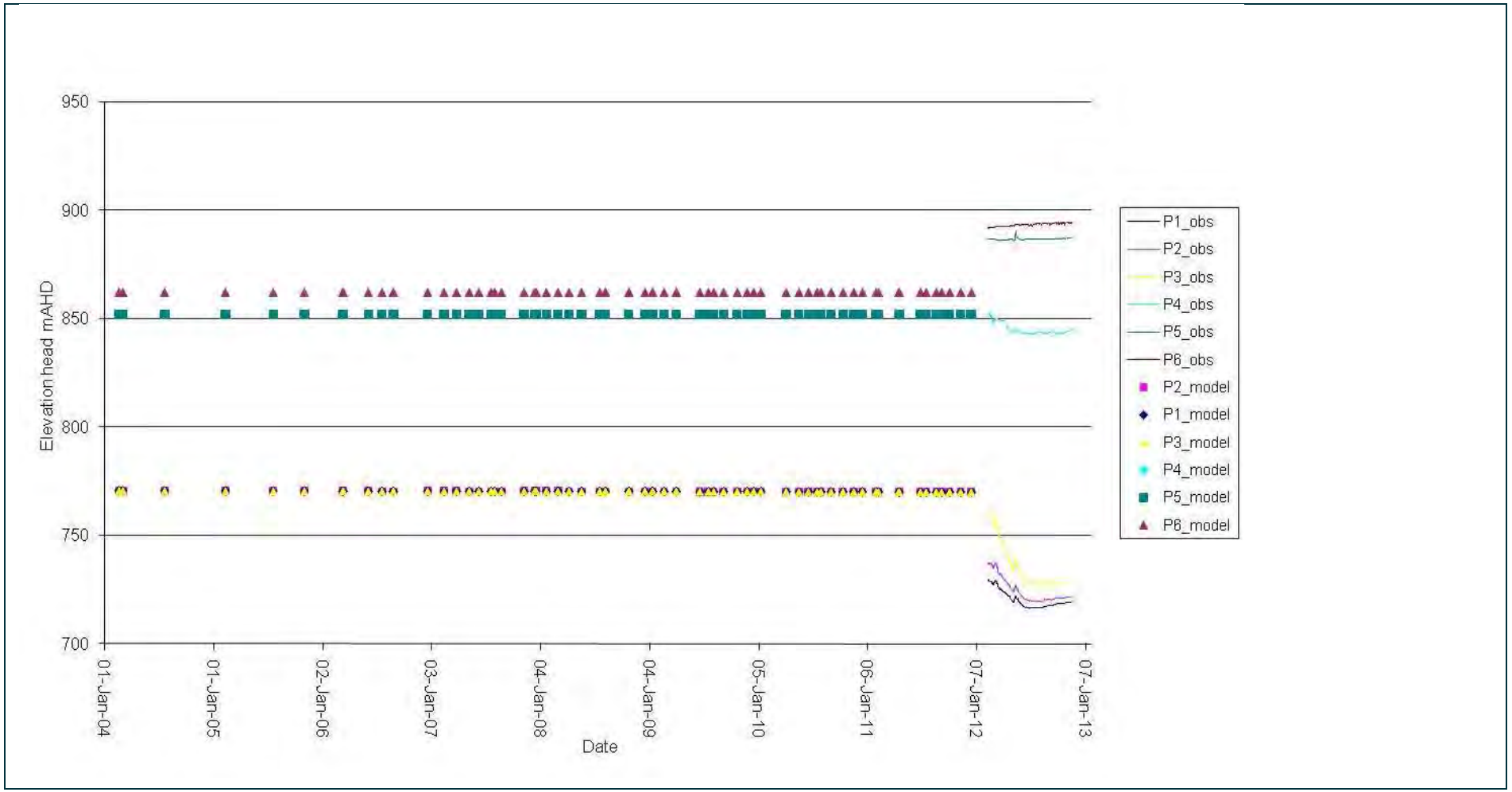

Figure B7 Comparison of observed and simulated piezometer elevation heads (Piezometer hole AP1106)

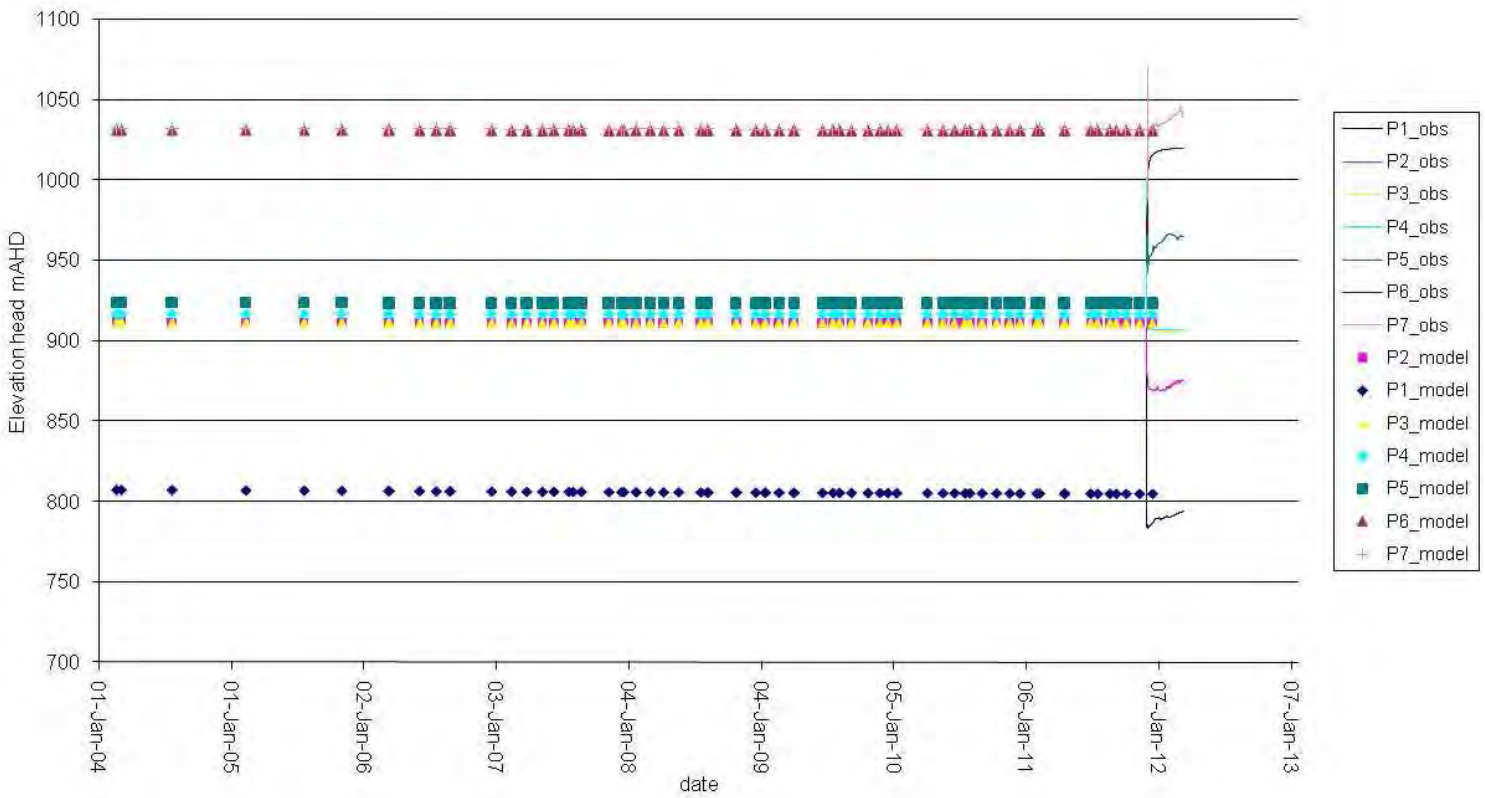

Figure B8 Comparison of observed and simulated piezometer elevation heads (Piezometer hole AP1107)

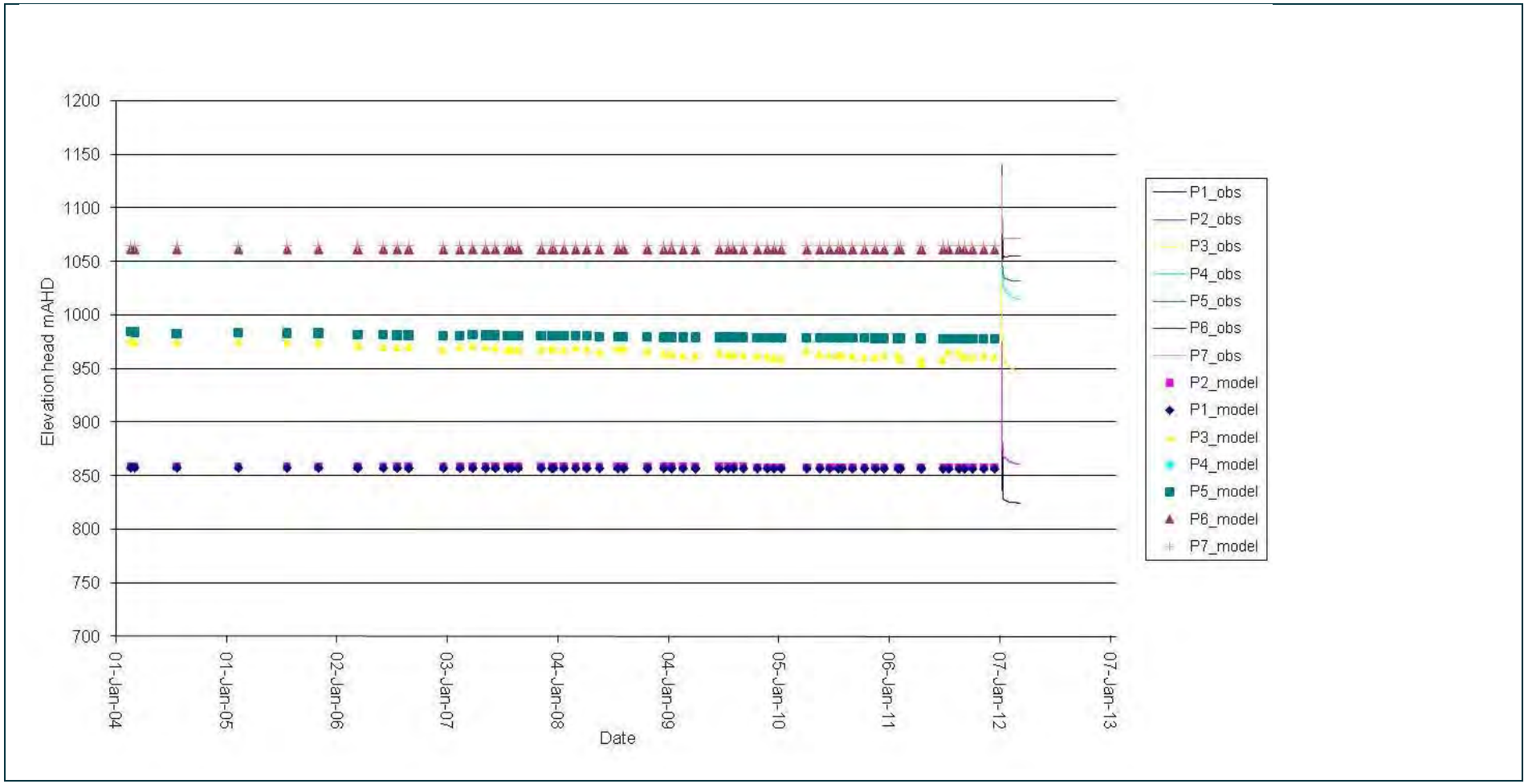

Figure B9 Comparison of observed and simulated piezometer elevation heads (Piezometer hole APB2)

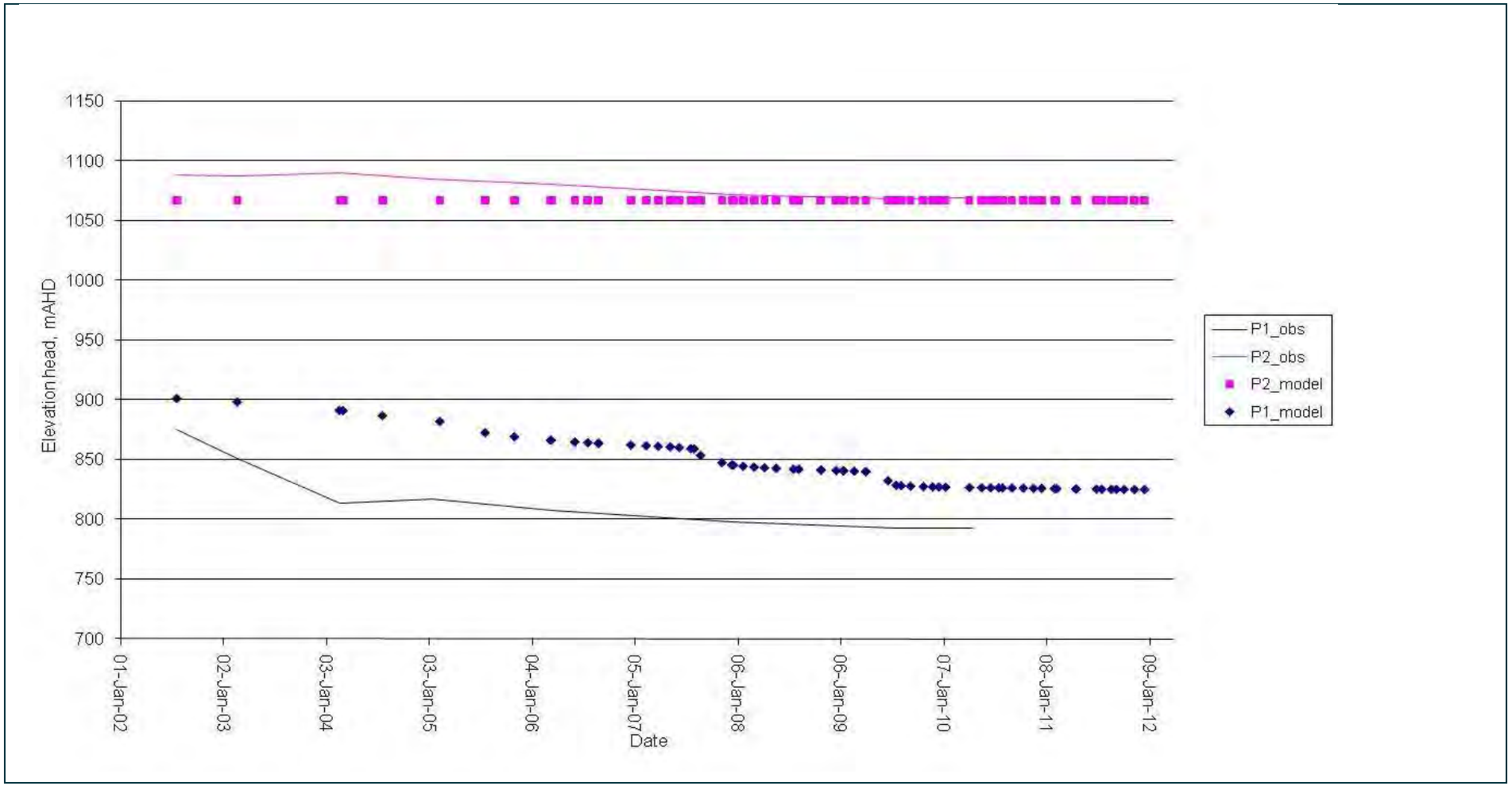

Figure B10 Comparison of observed and simulated piezometer elevation heads (Piezometer hole SPR26)

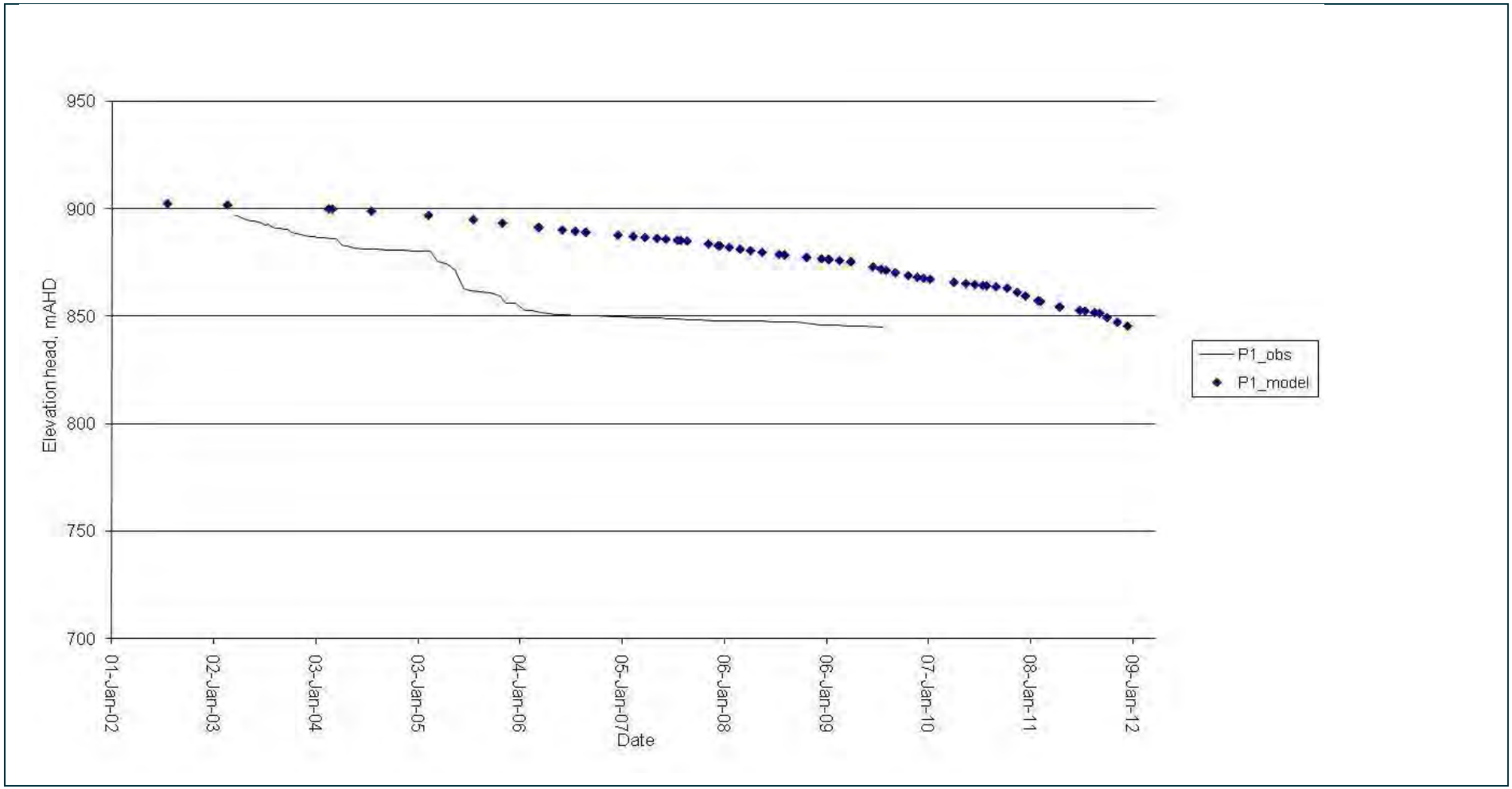

Figure B11 Comparison of observed and simulated piezometer elevation heads (Piezometer hole SPR29)

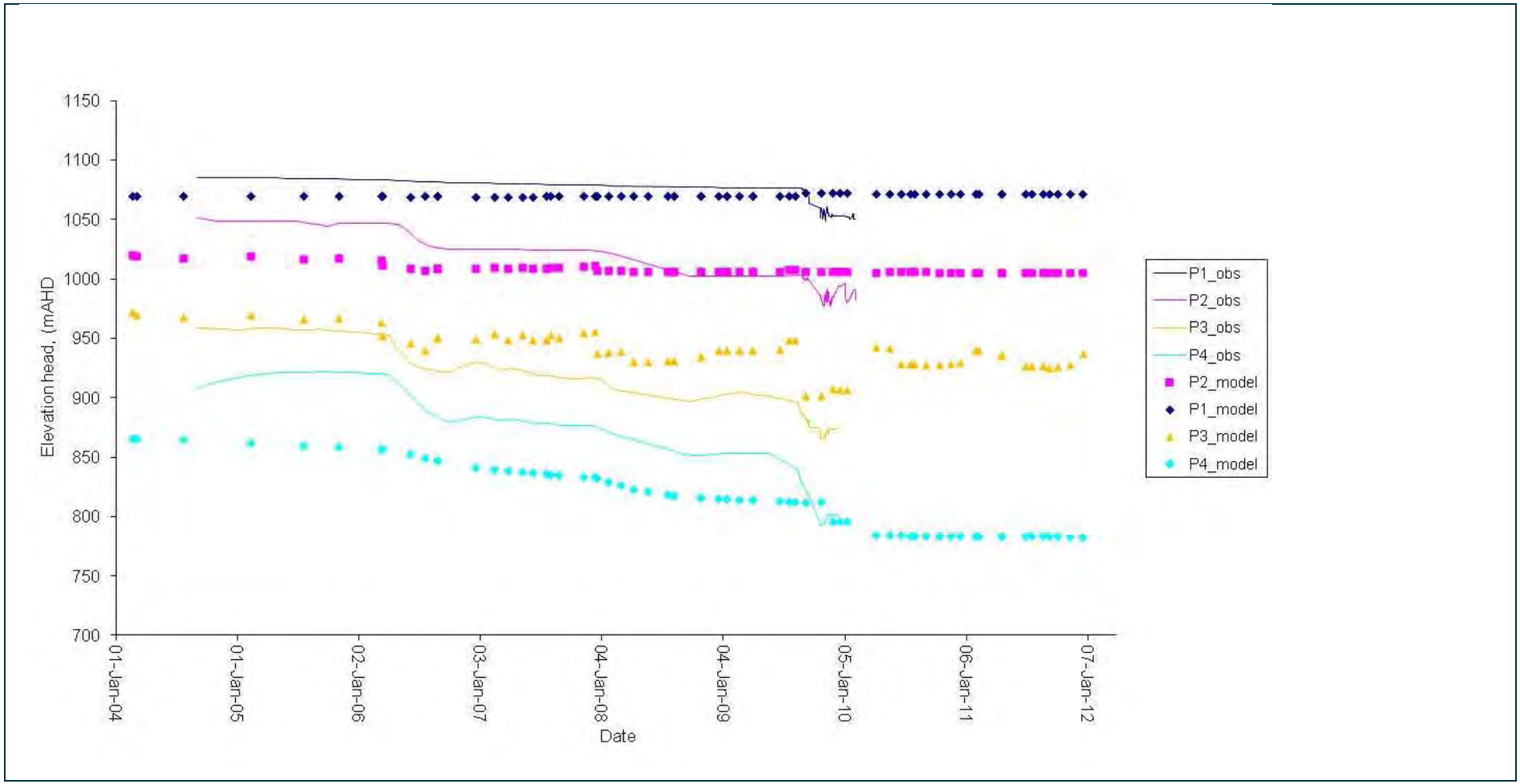

Figure B12 Comparison of observed and simulated piezometer elevation heads (Piezometer hole SPR33)

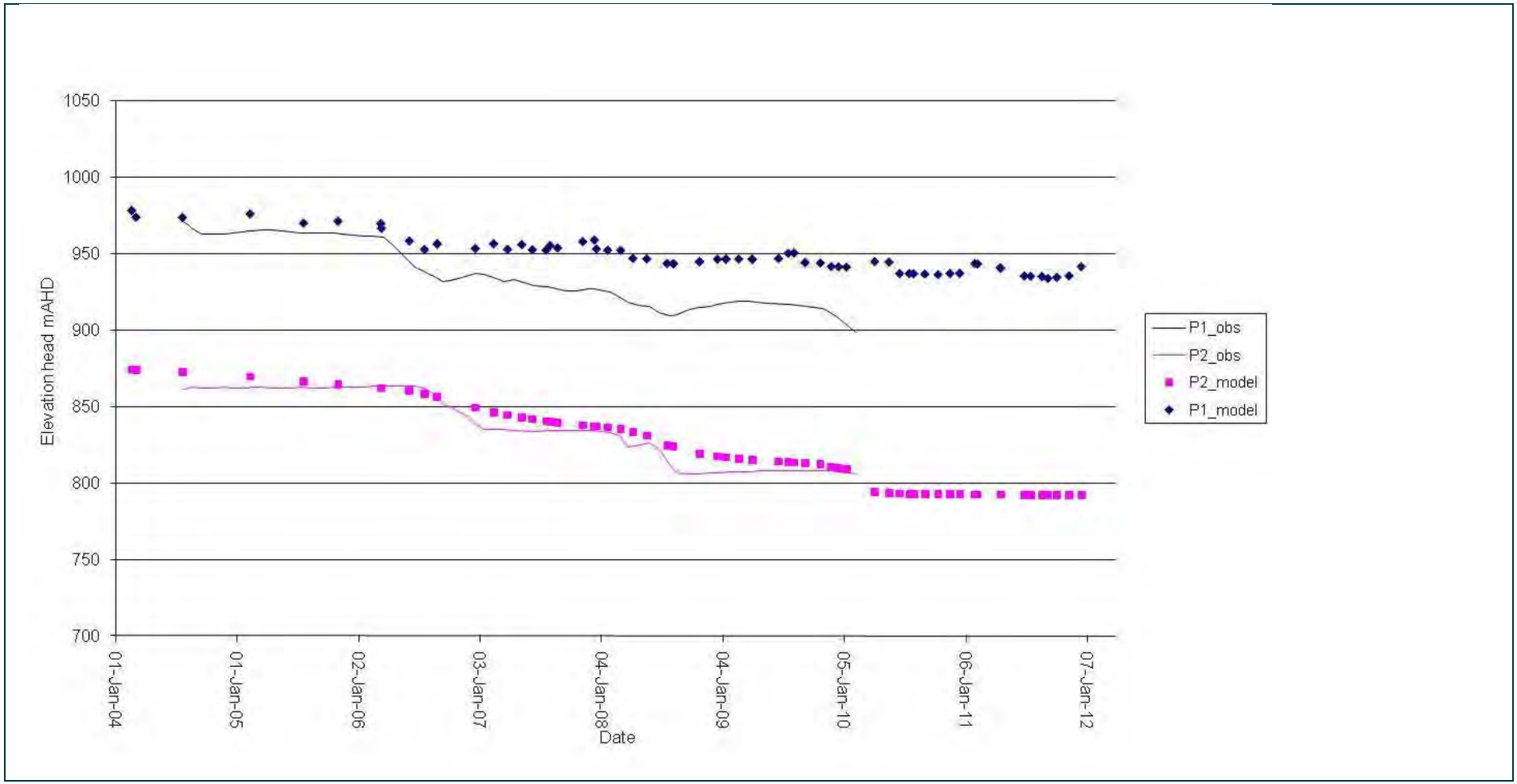

Figure B13 Comparison of observed and simulated piezometer elevation heads (Piezometer hole SPR34)

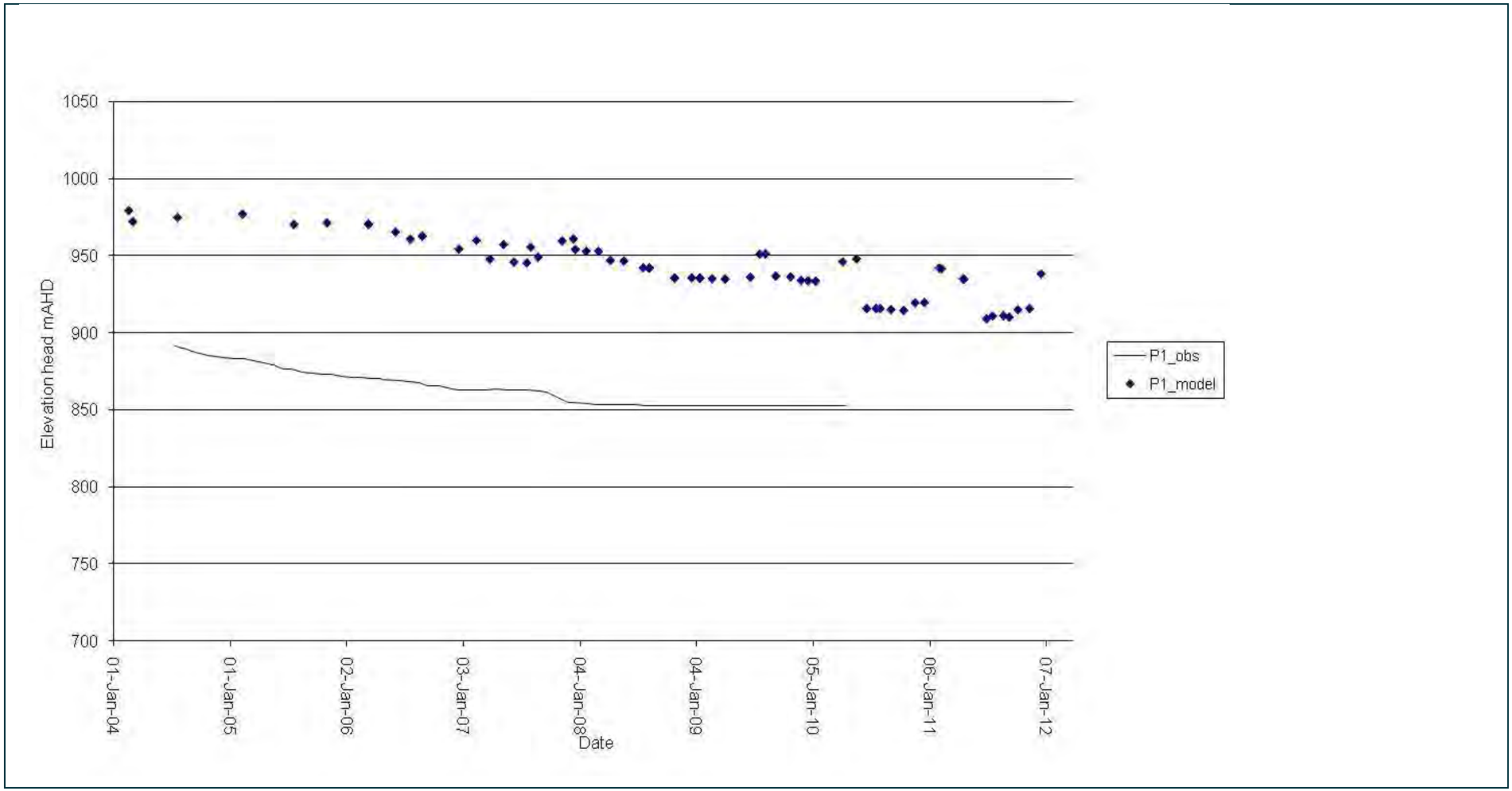

Figure B14 Comparison of observed and simulated piezometer elevation heads (Piezometer hole SPR35)

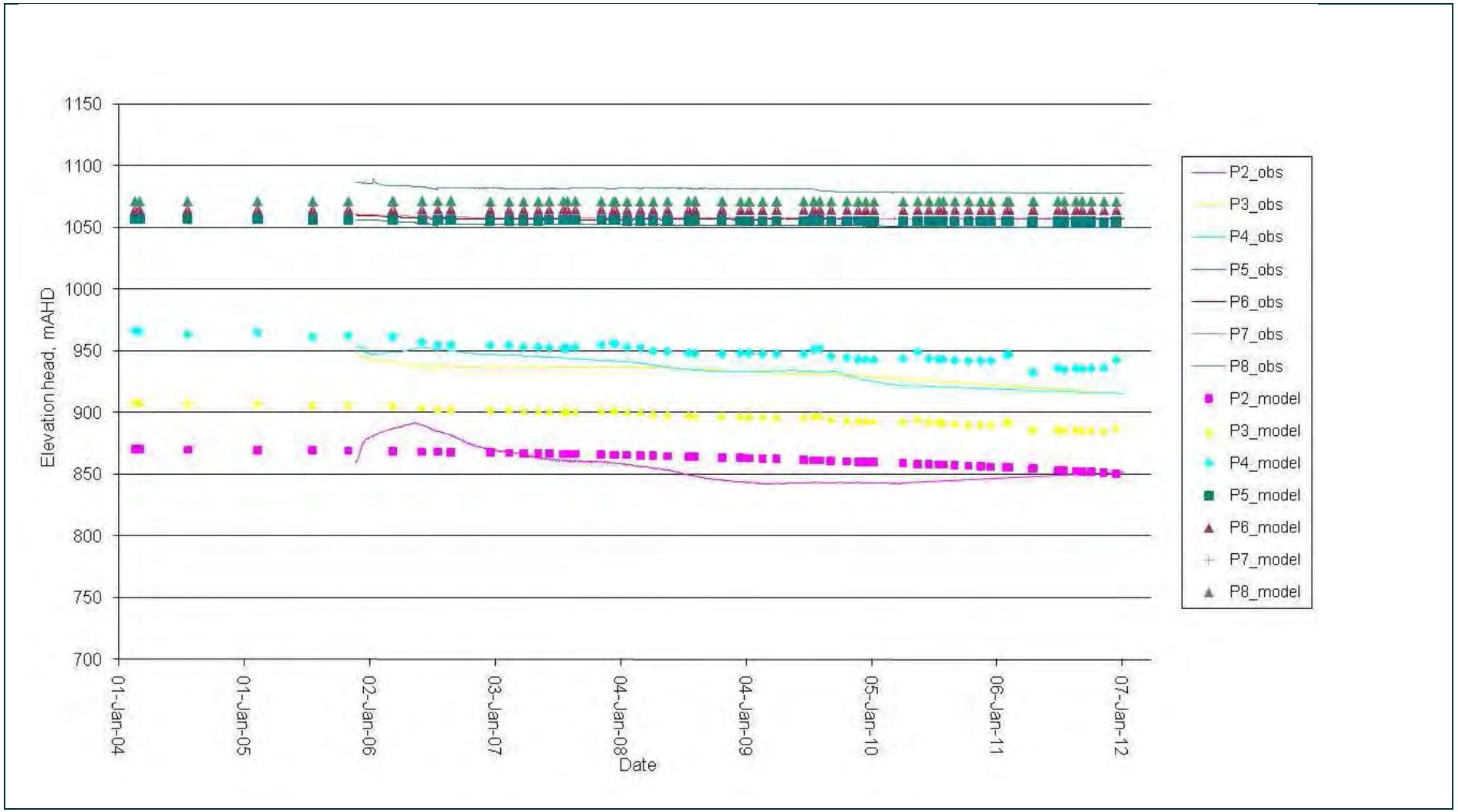

Figure B15 Comparison of observed and simulated piezometer elevation heads (Piezometer hole SPR36)

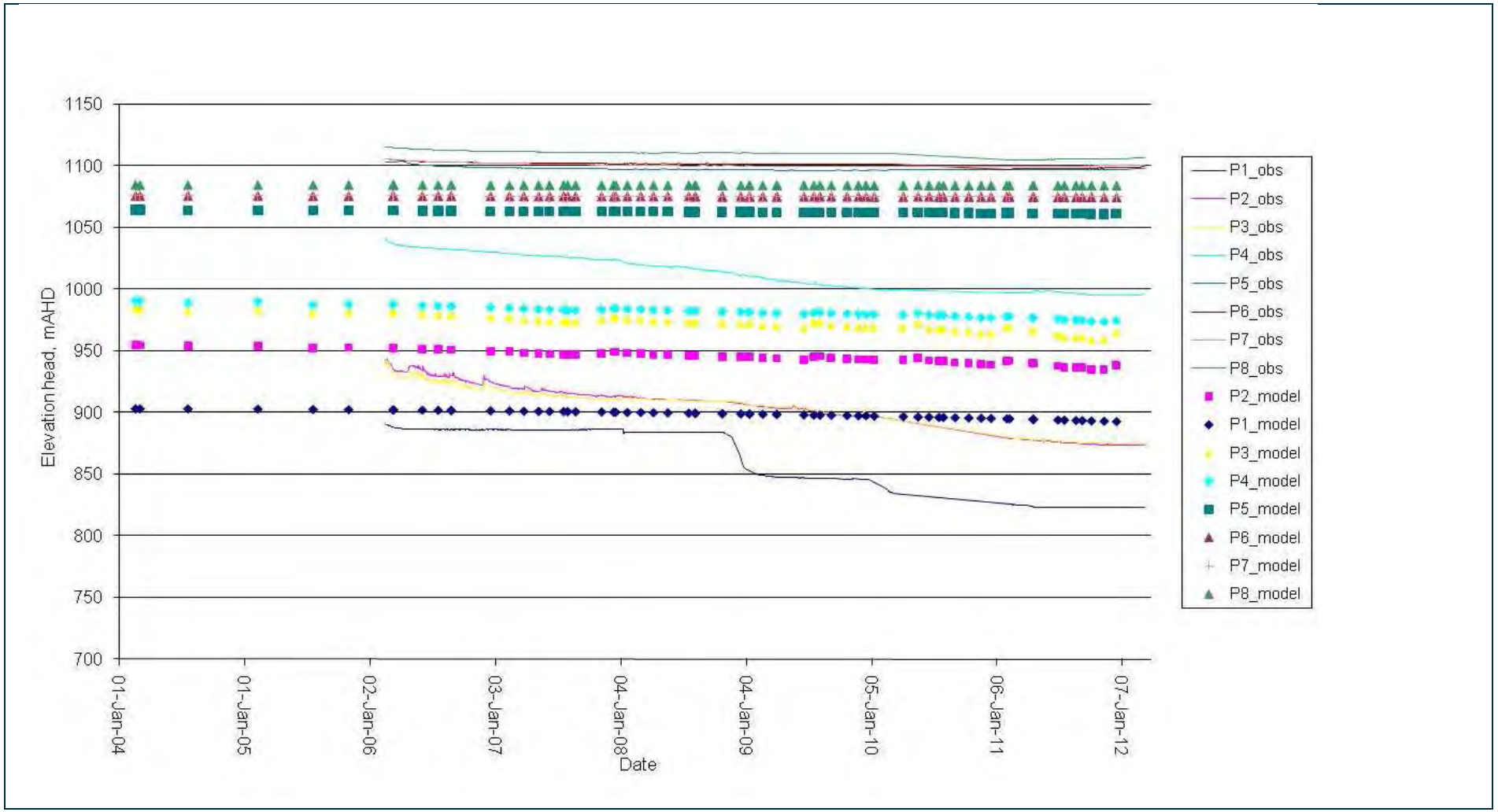

Figure B16 Comparison of observed and simulated piezometer elevation heads (Piezometer hole SPR37R)

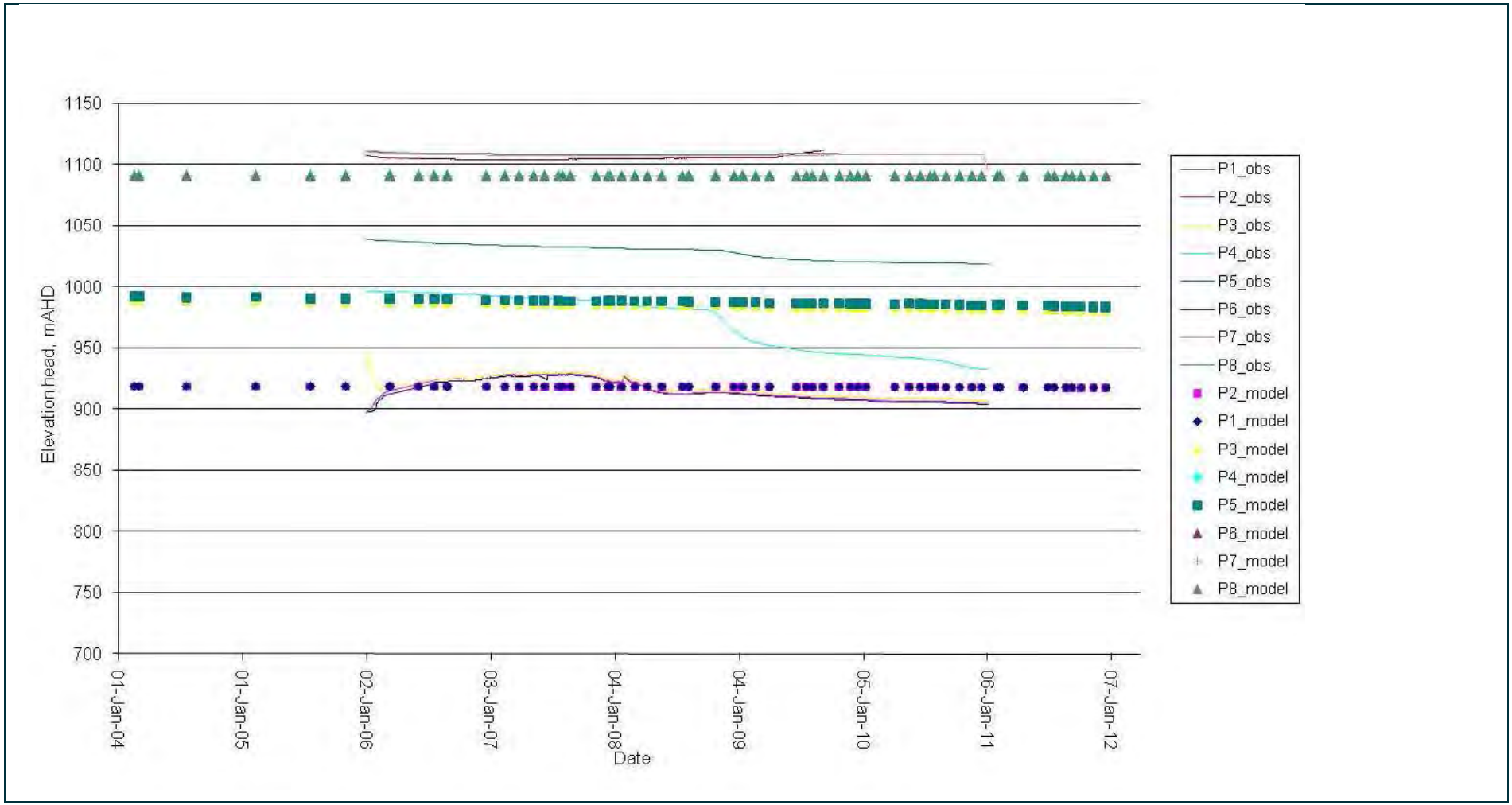

Figure B17 Comparison of observed and simulated piezometer elevation heads (Piezometer hole SPR38)

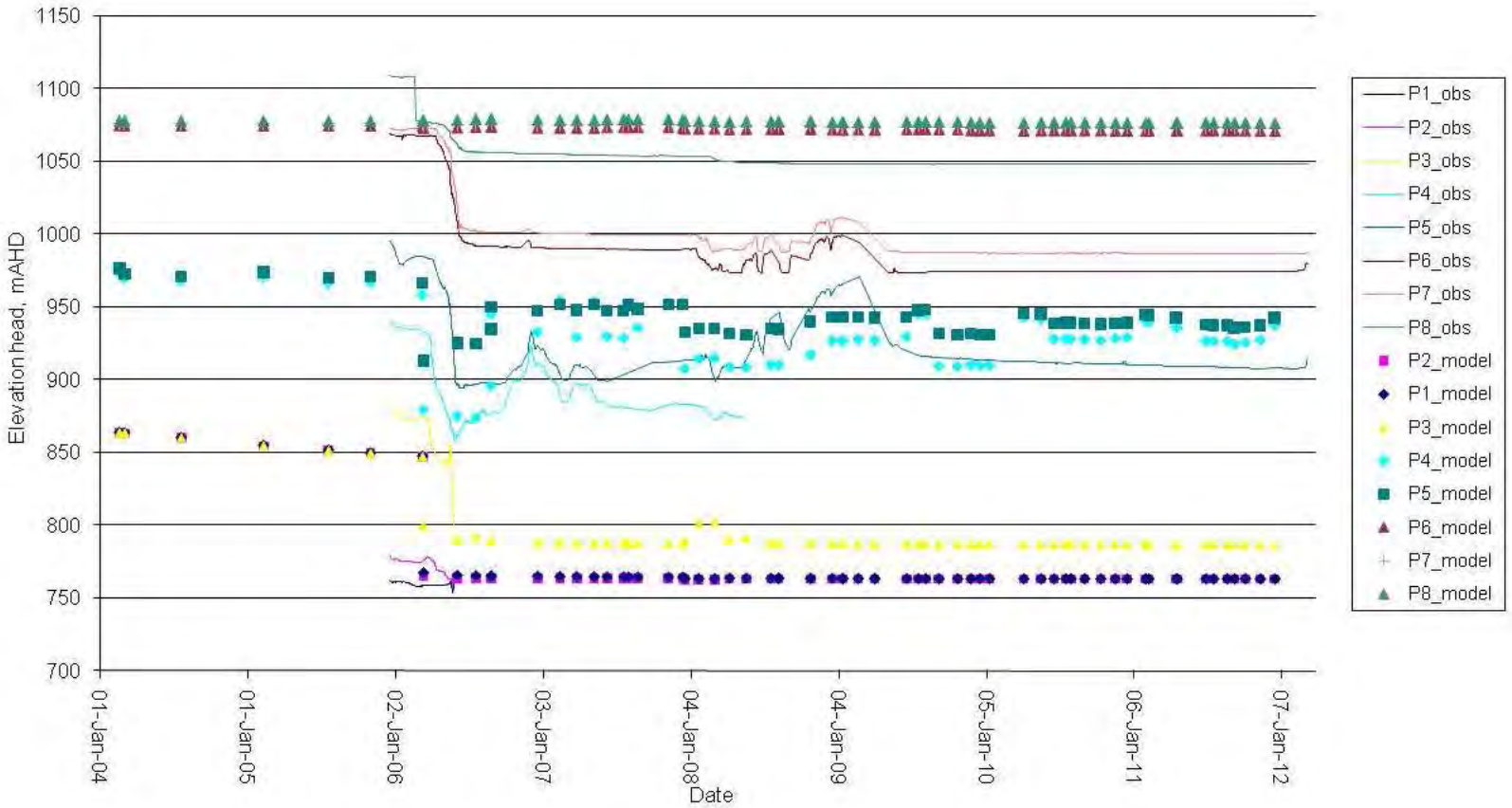

Figure B18 Comparison of observed and simulated piezometer elevation heads (Piezometer hole SPR39)

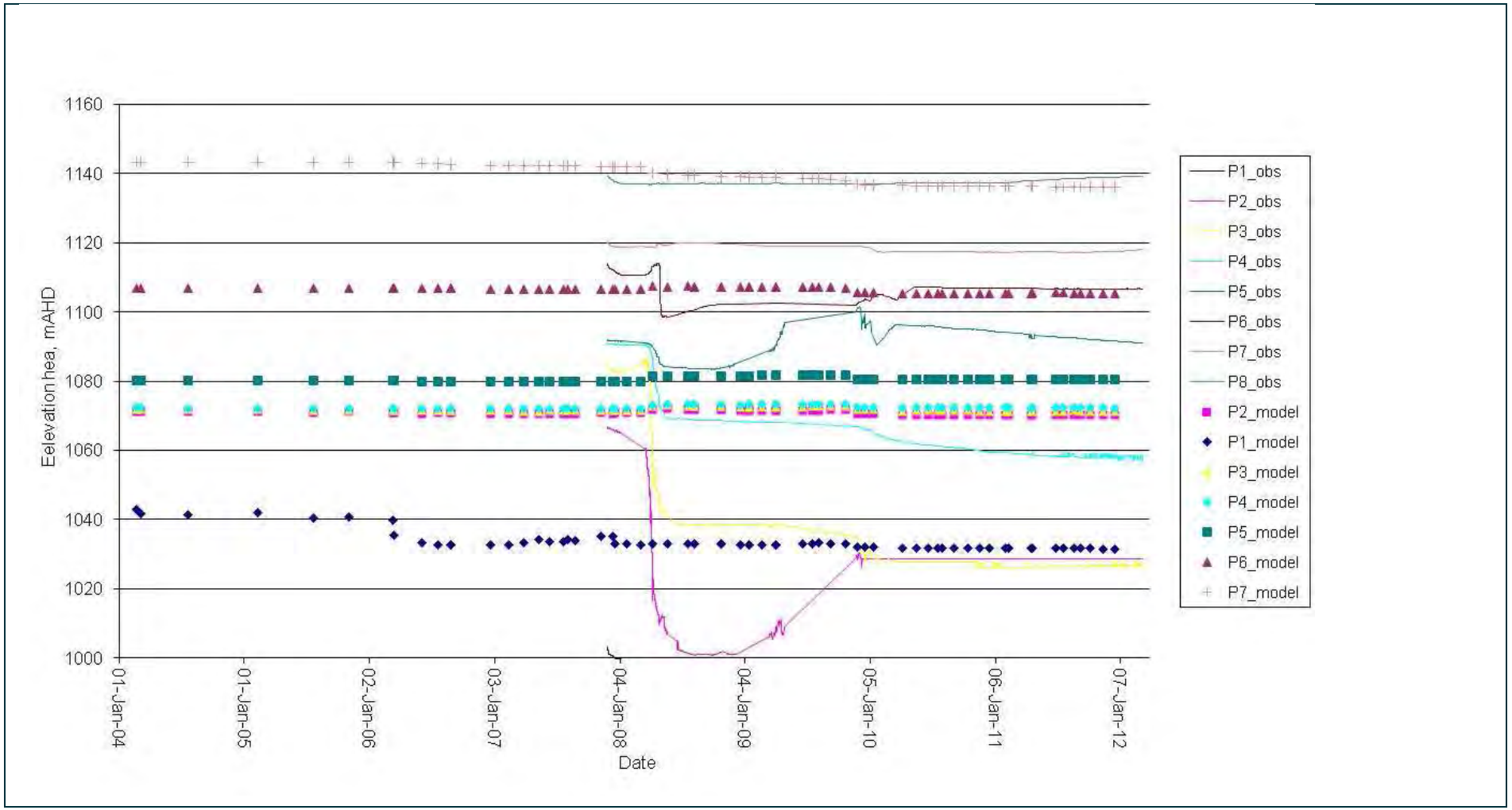

Figure B19 Comparison of observed and simulated piezometer elevation heads (Piezometer hole SPR48)

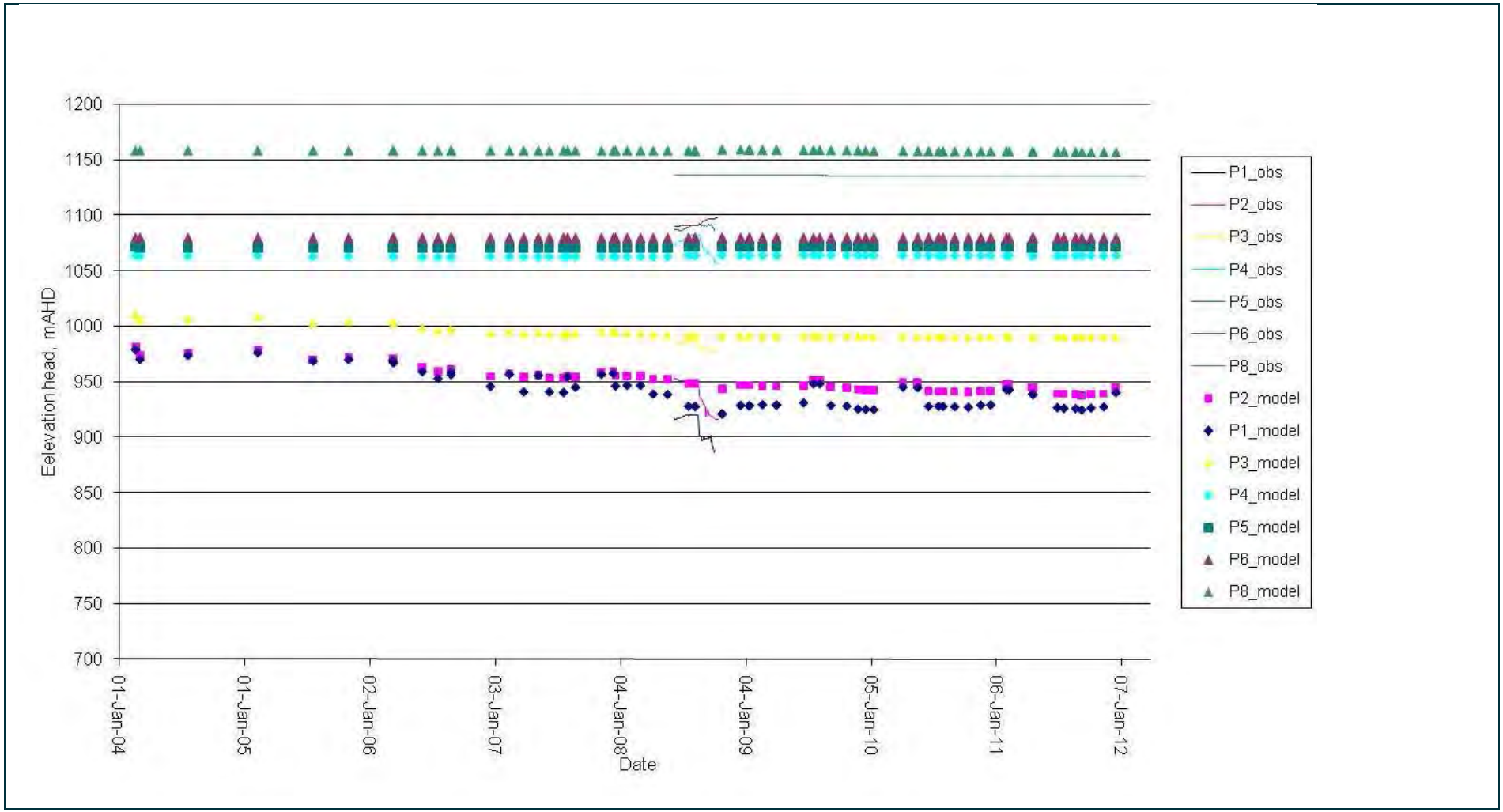

Figure B20 Comparison of observed and simulated piezometer elevation heads (Piezometer hole SPR49)

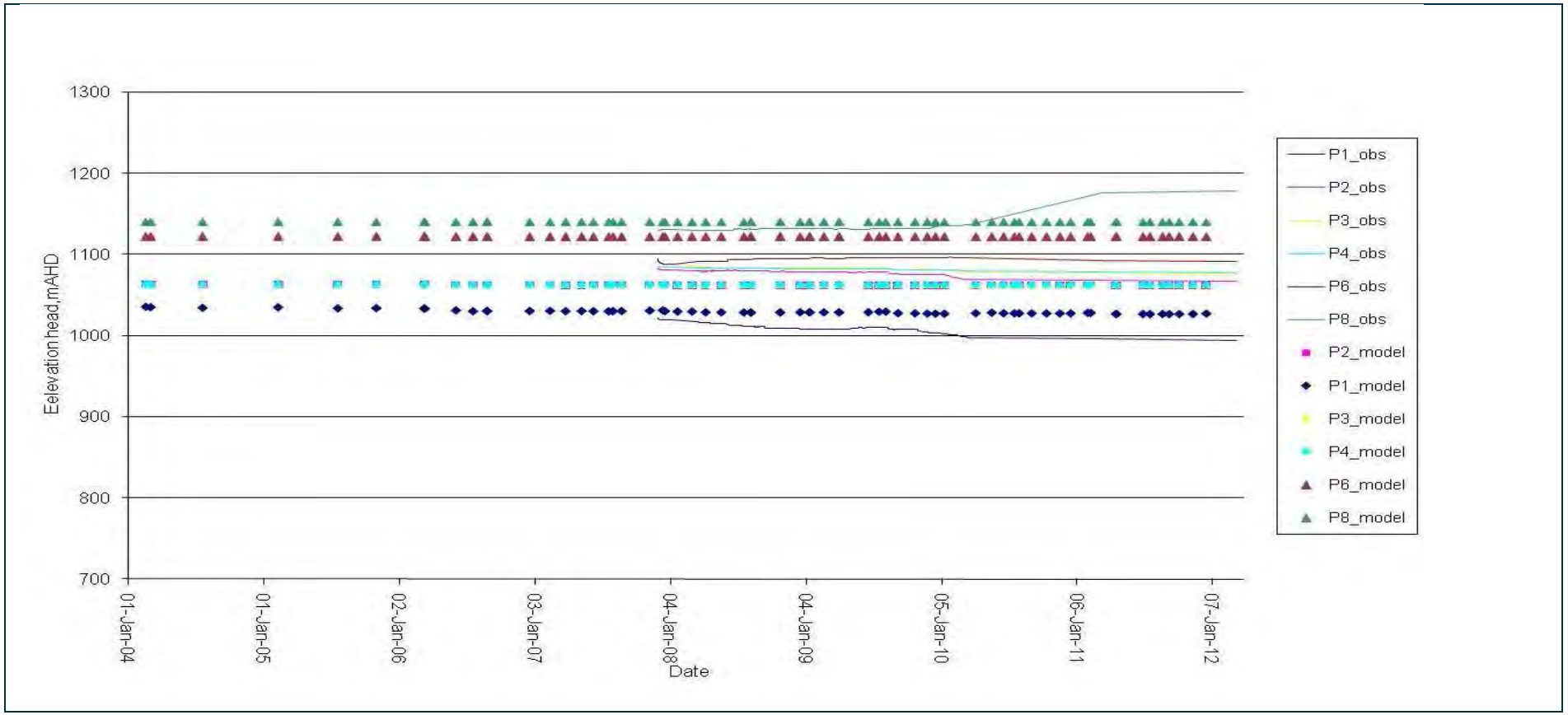

Figure B21 Comparison of observed and simulated piezometer elevation heads (Piezometer hole SPR50)

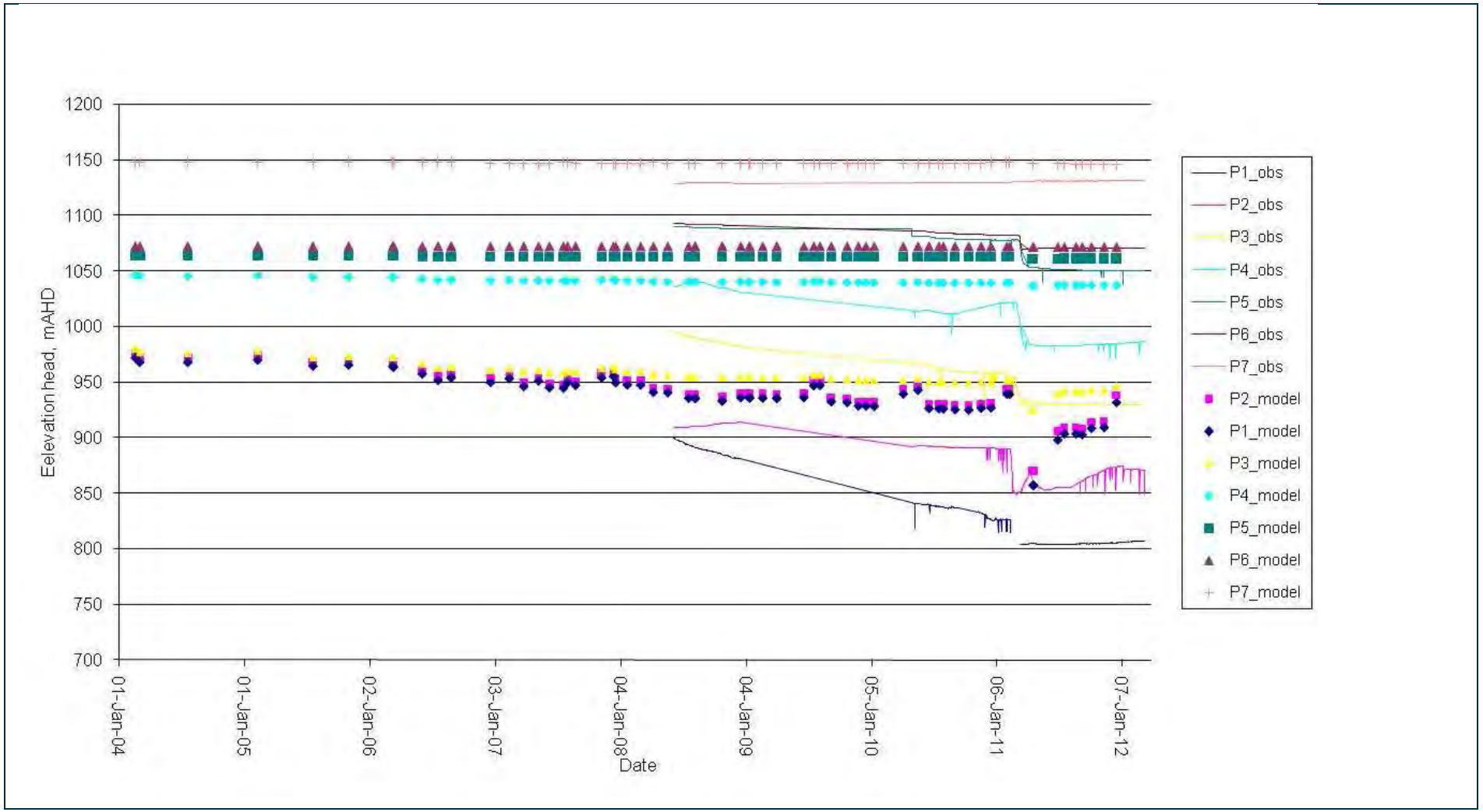

Figure B22 Comparison of observed and simulated piezometer elevation heads (Piezometer hole SPR51)

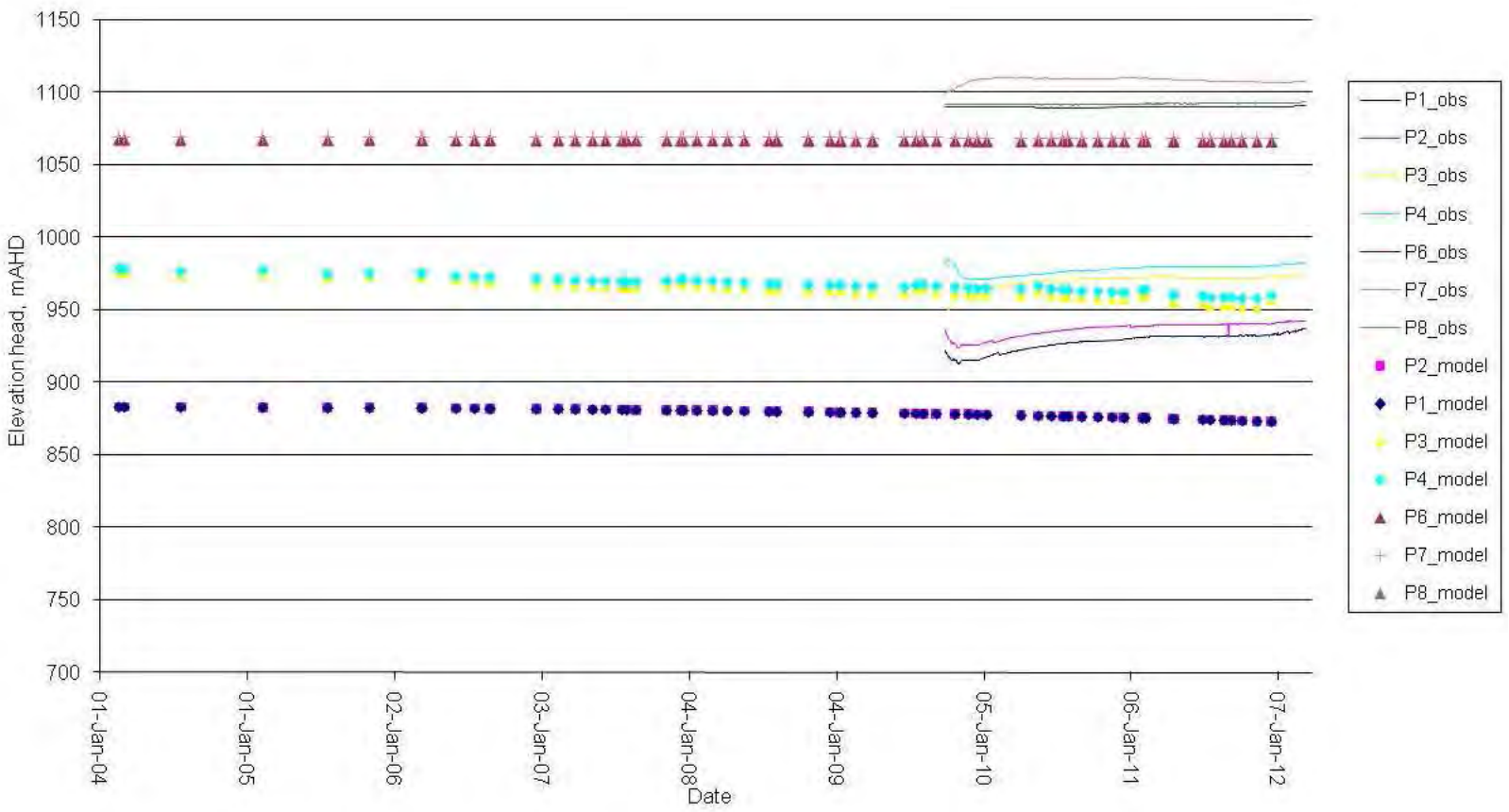

Figure B23 Comparison of observed and simulated piezometer elevation heads (Piezometer hole SPR66)

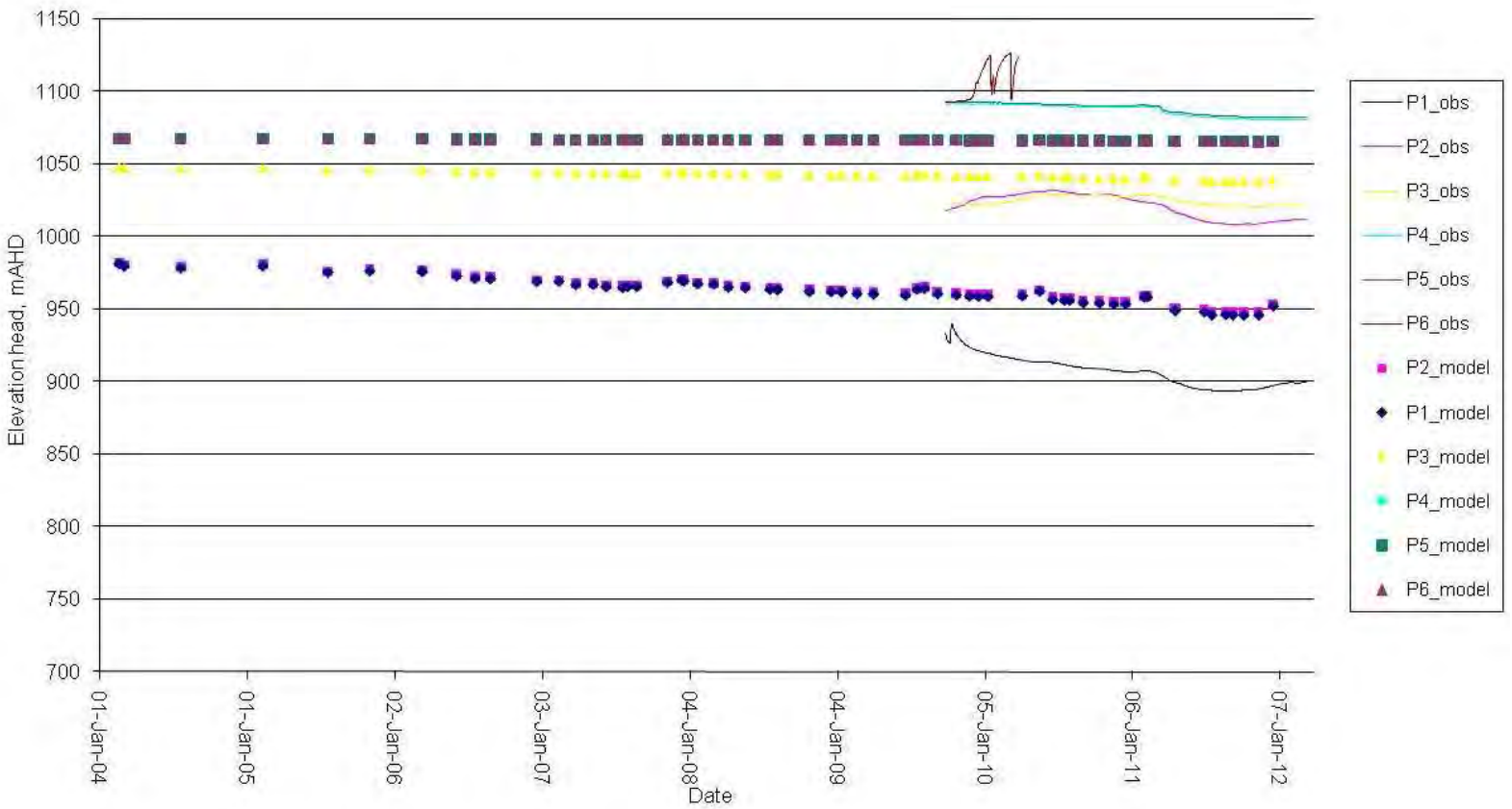

Figure B24 Comparison of observed and simulated piezometer elevation heads (Piezometer hole SPR67)

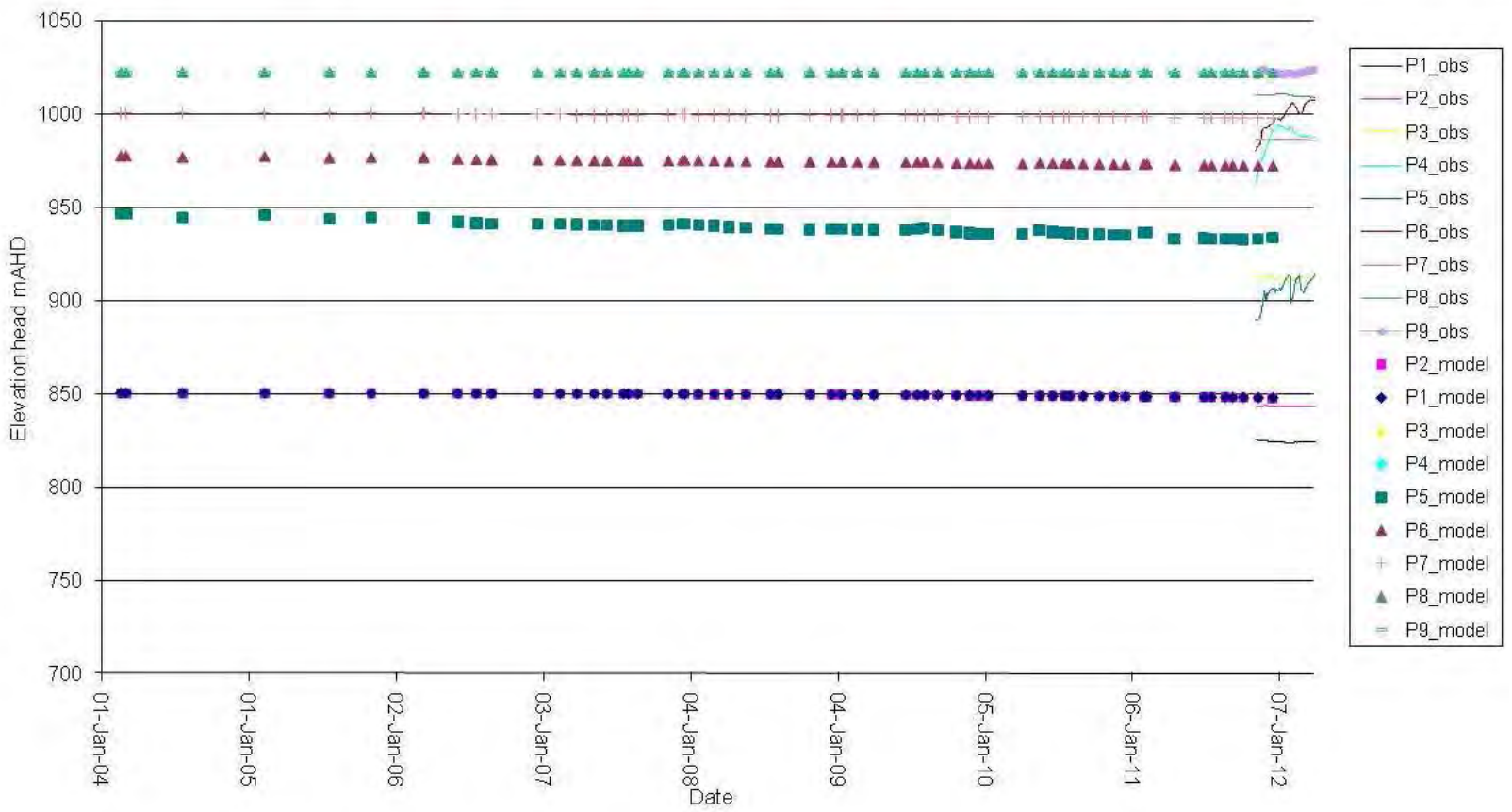

Figure B25 Comparison of observed and simulated piezometer elevation heads (Piezometer hole SPR1102)

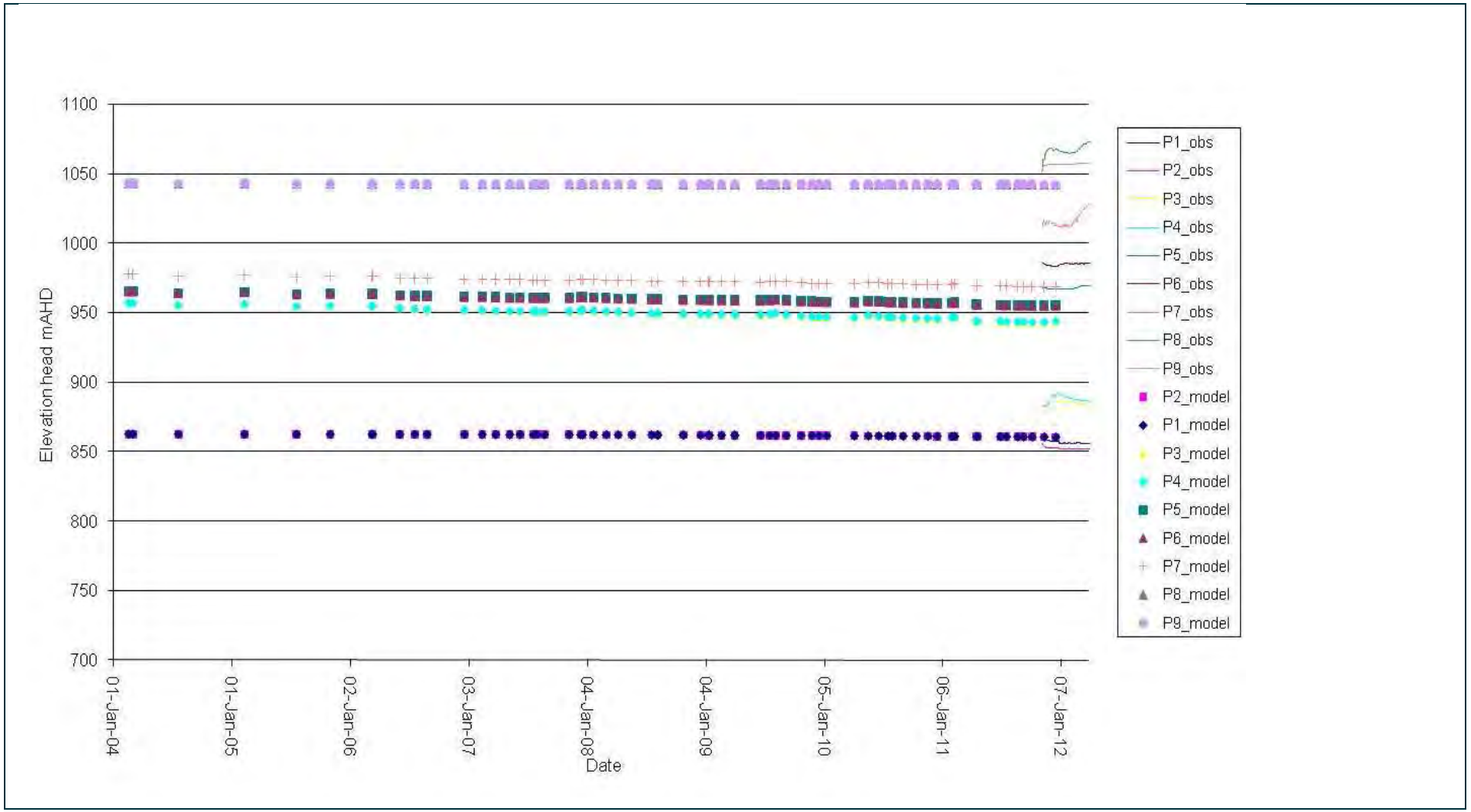

Figure B26 Comparison of observed and simulated piezometer elevation heads (Piezometer hole SPR1103)

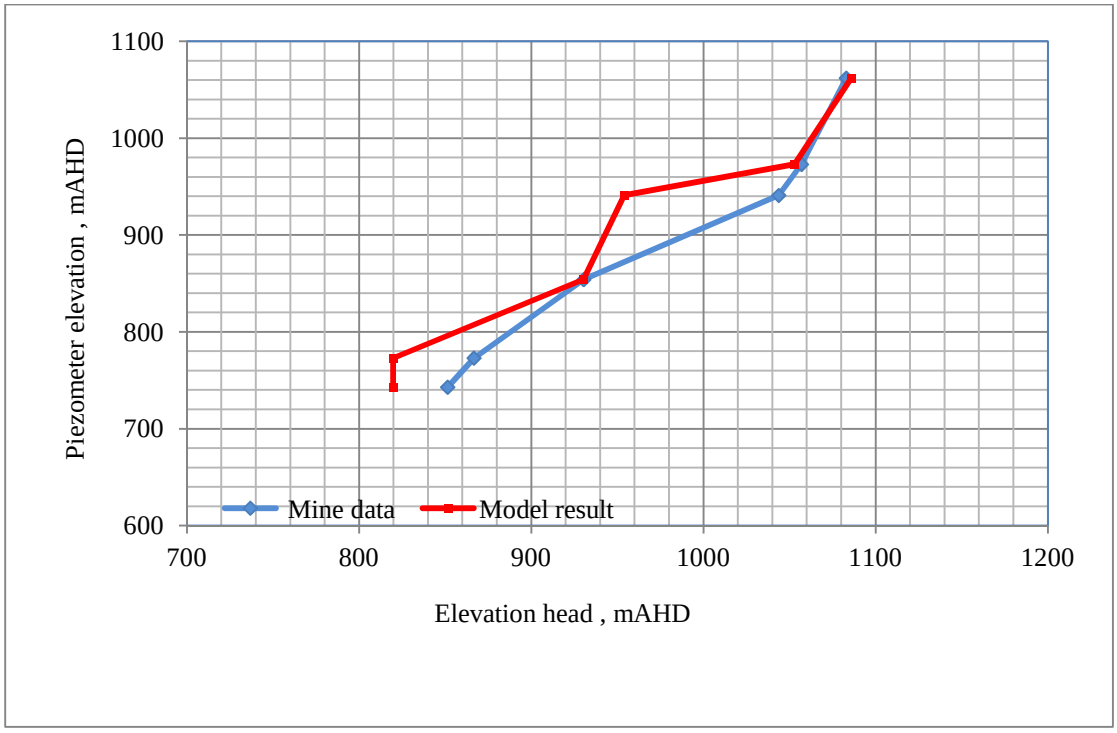

Figure B27 Comparison of observed and simulated piezometer elevation head profiles AP2PR (Date 01/01/2012)

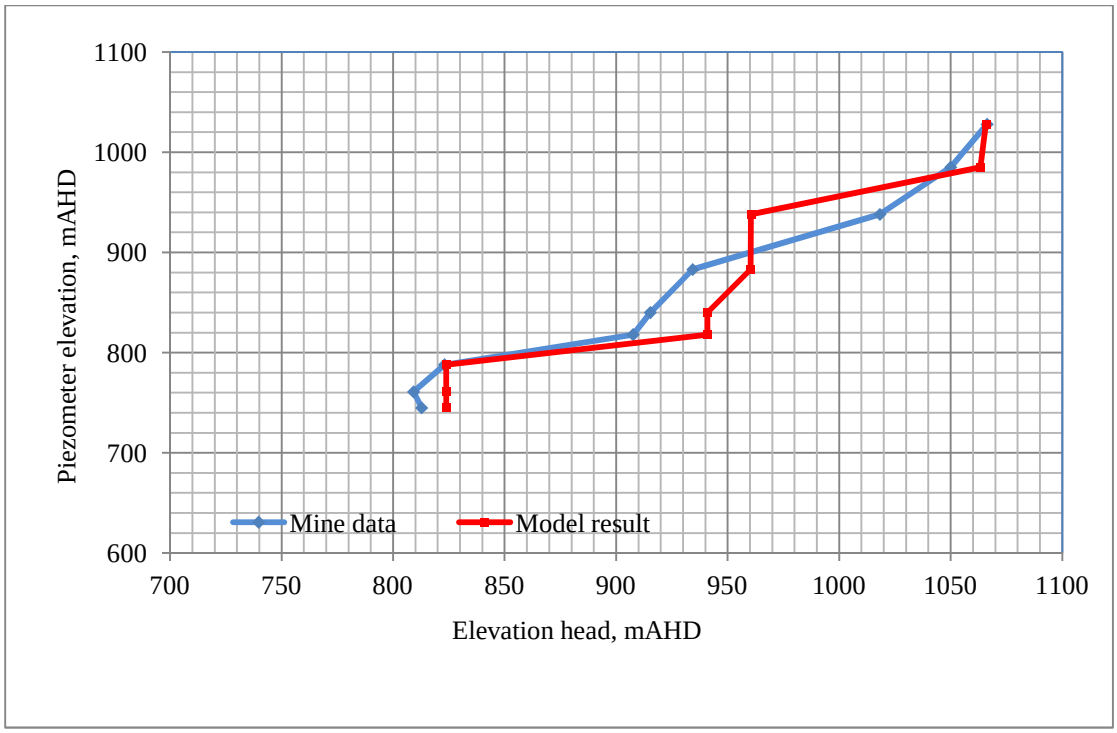

Figure B28 Comparison of observed and simulated piezometer elevation head profiles AP10PR (Date 01/01/2012)

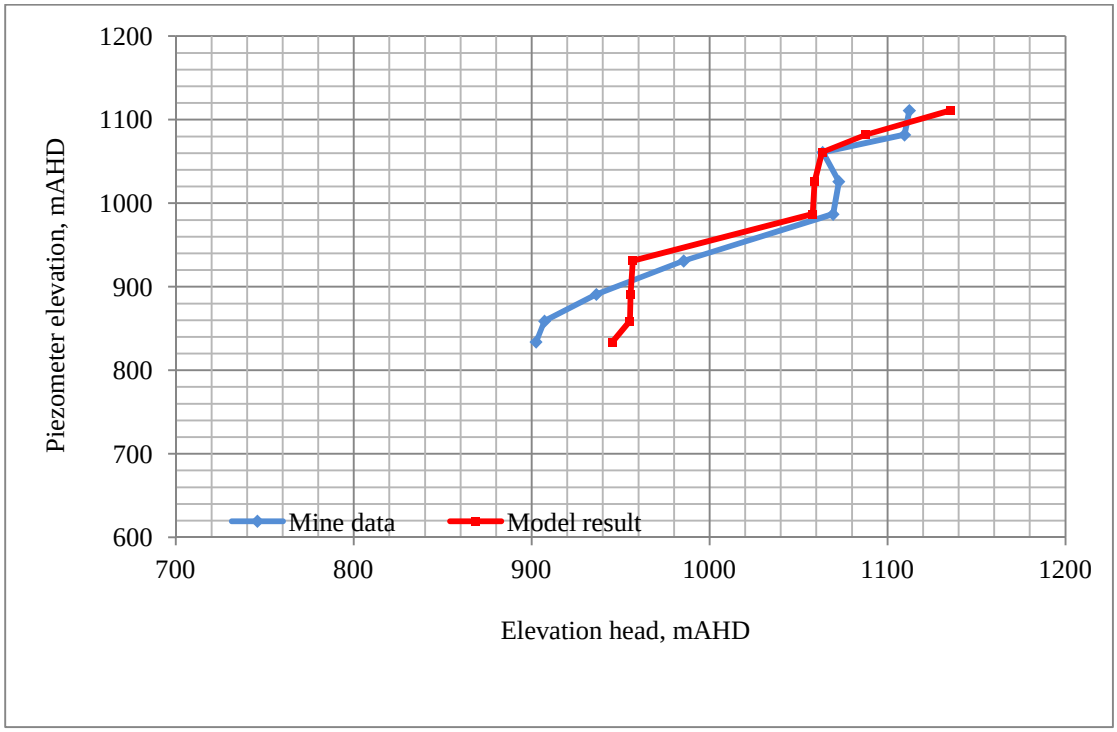

Figure B29 Comparison of observed and simulated piezometer elevation head profiles AP11PR (Date 01/01/2012)

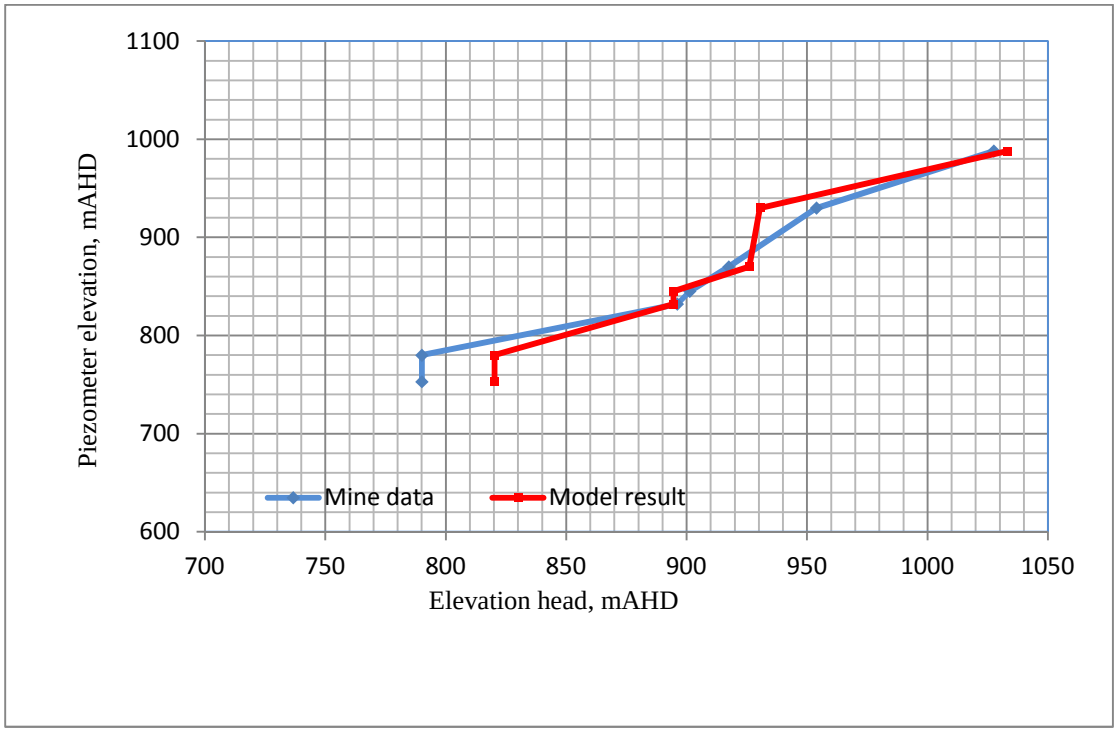

Figure B30 Comparison of observed and simulated piezometer elevation head profiles AP1101 (Date 01/04/2012)

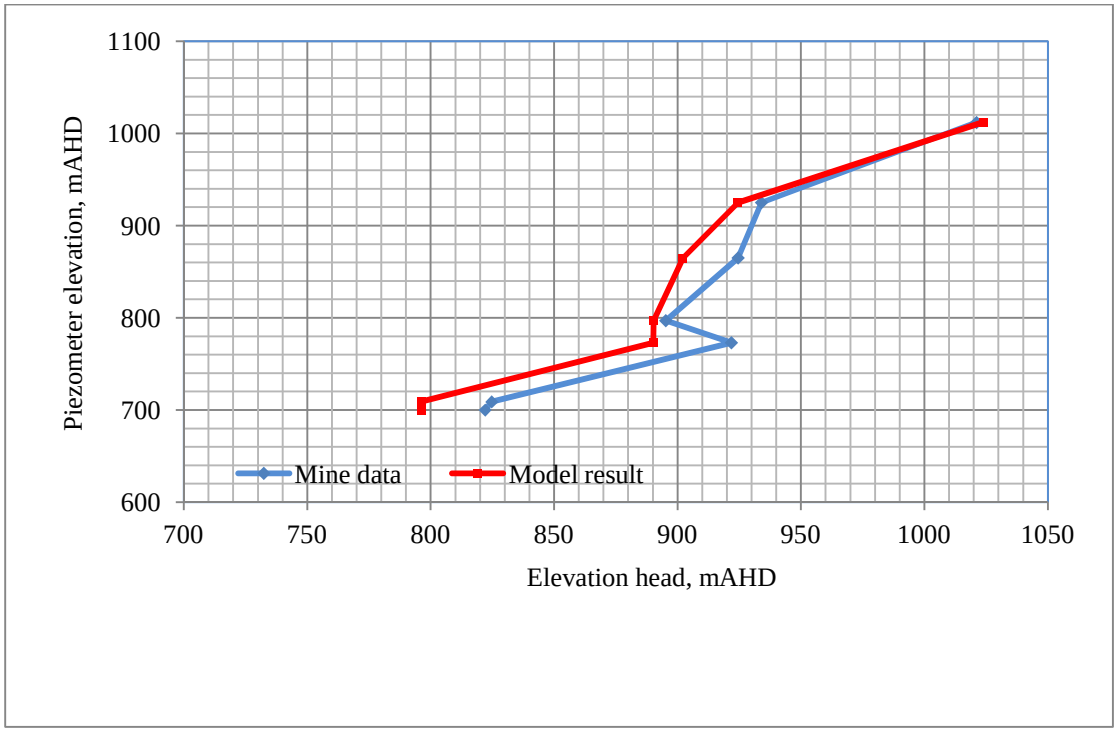

Figure B31 Comparison of observed and simulated piezometer elevation head profiles AP1102 (Date 01/04/2012)

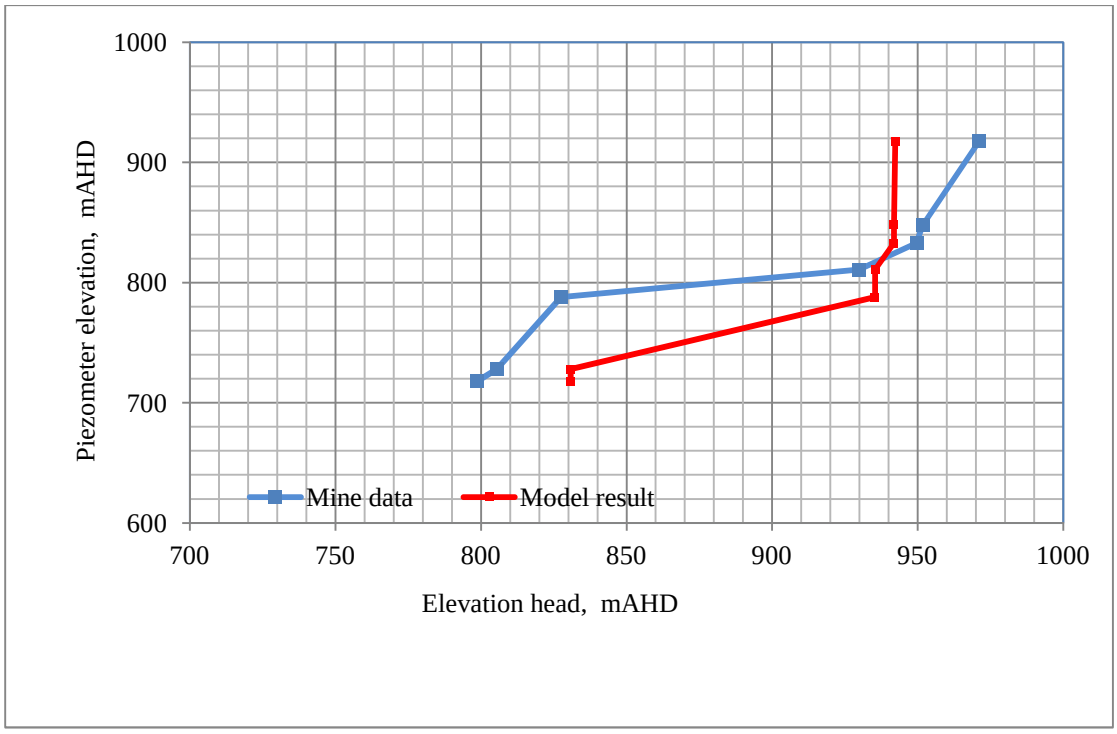

Figure B32 Comparison of observed and simulated piezometer elevation head profiles AP1104 (Date 01/01/2012)

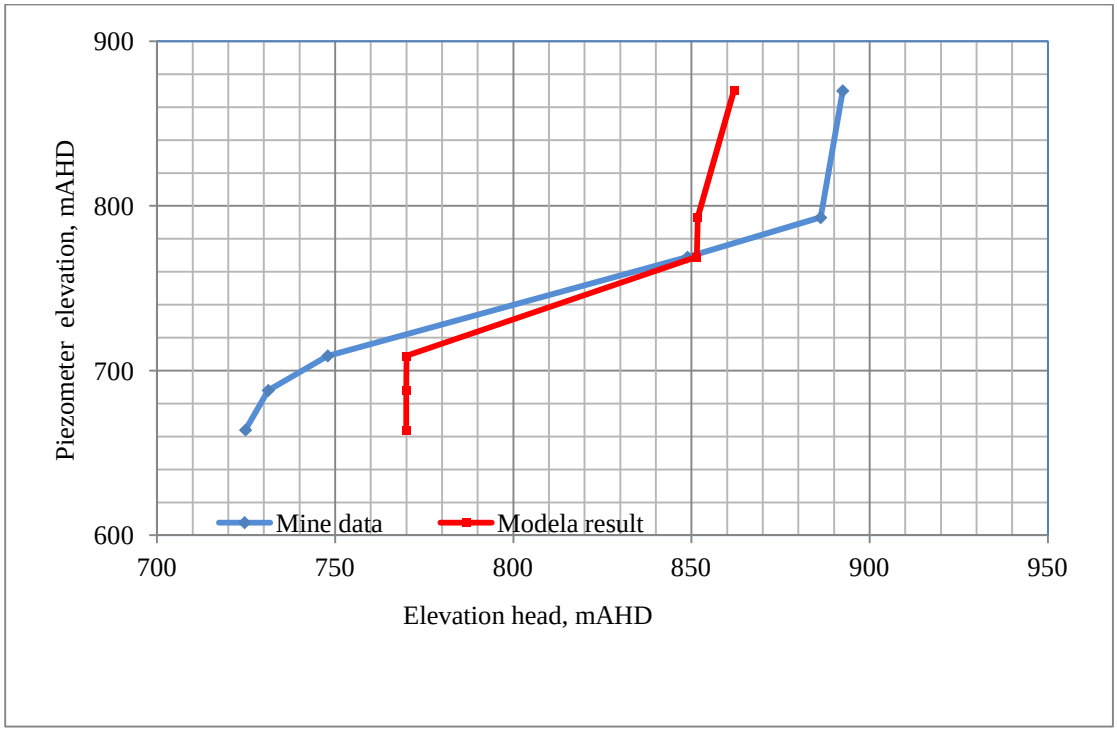

Figure B33 Comparison of observed and simulated piezometer elevation head profiles AP1106 (Date 01/04/2012)

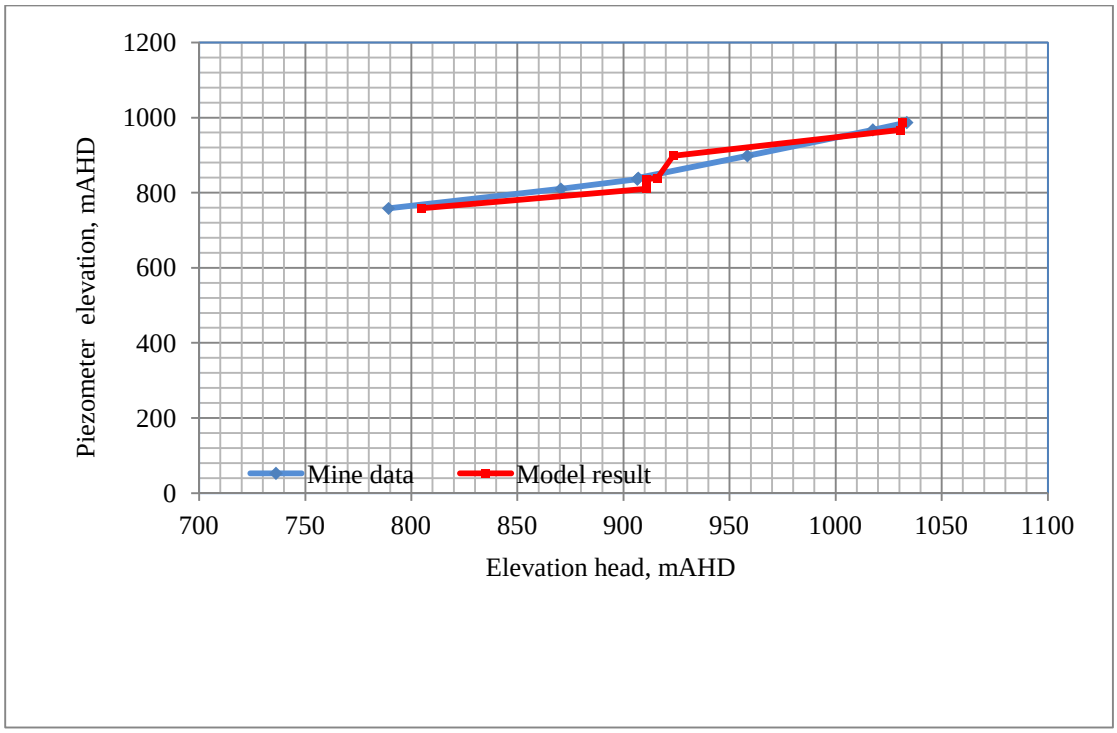

Figure B34 Comparison of observed and simulated piezometer elevation head profiles AP1107 (Date 01/01/2012)

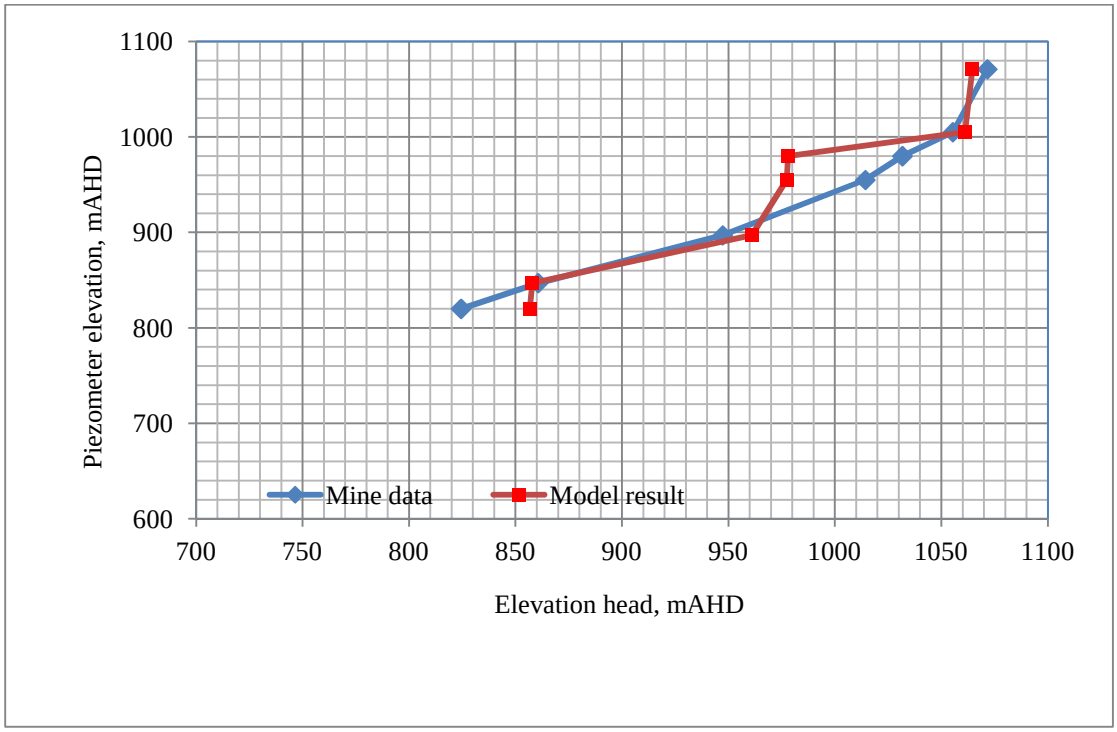

Figure B35 Comparison of observed and simulated piezometer elevation head profiles APB2 (Date 14/01/2012)

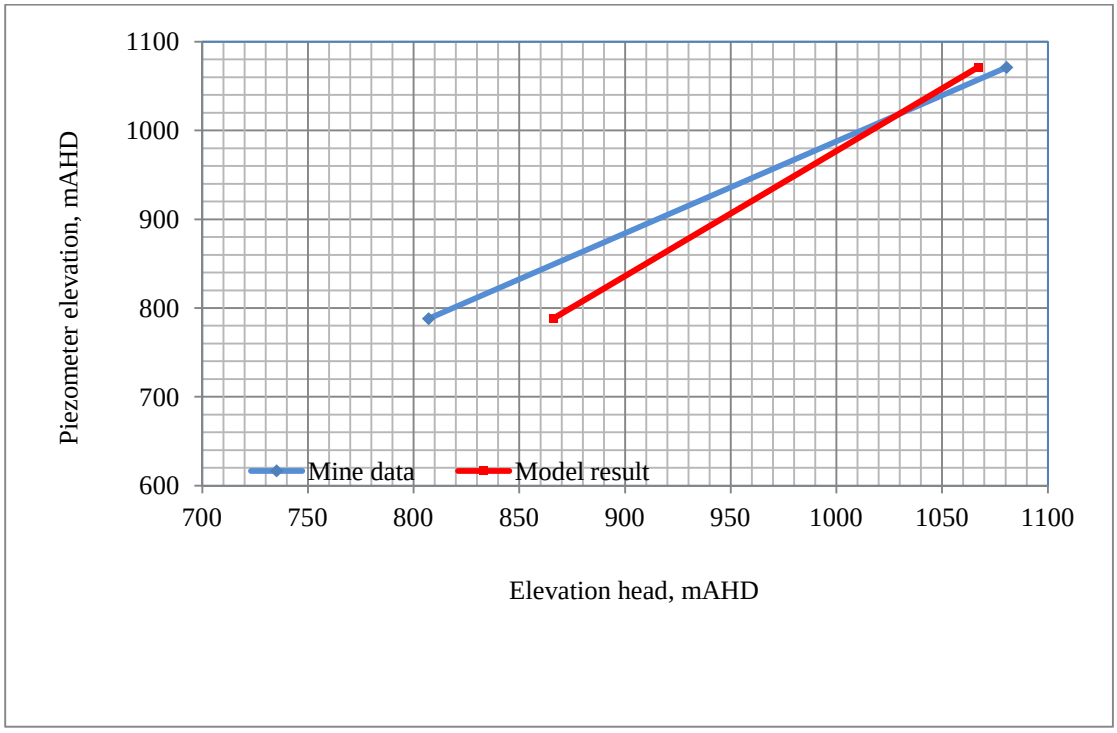

Figure B36 Comparison of observed and simulated piezometer elevation head profiles SPR26 (Date 20/03/2006)

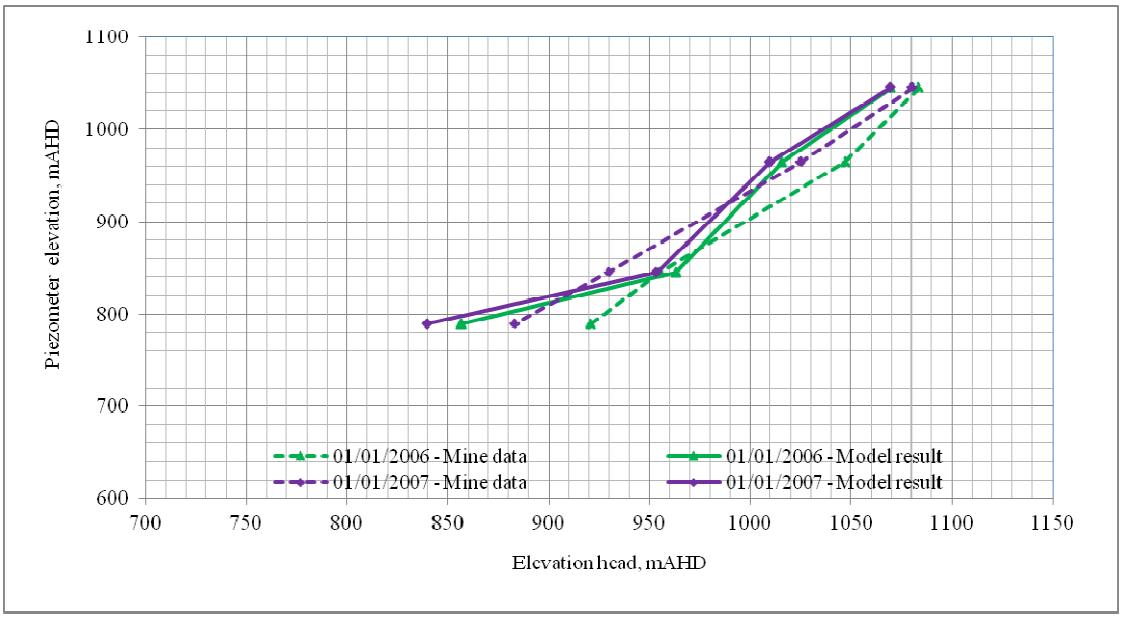

Figure B37 Comparison of observed and simulated piezometer elevation head profiles SPR33 (Date 1/01/2006)

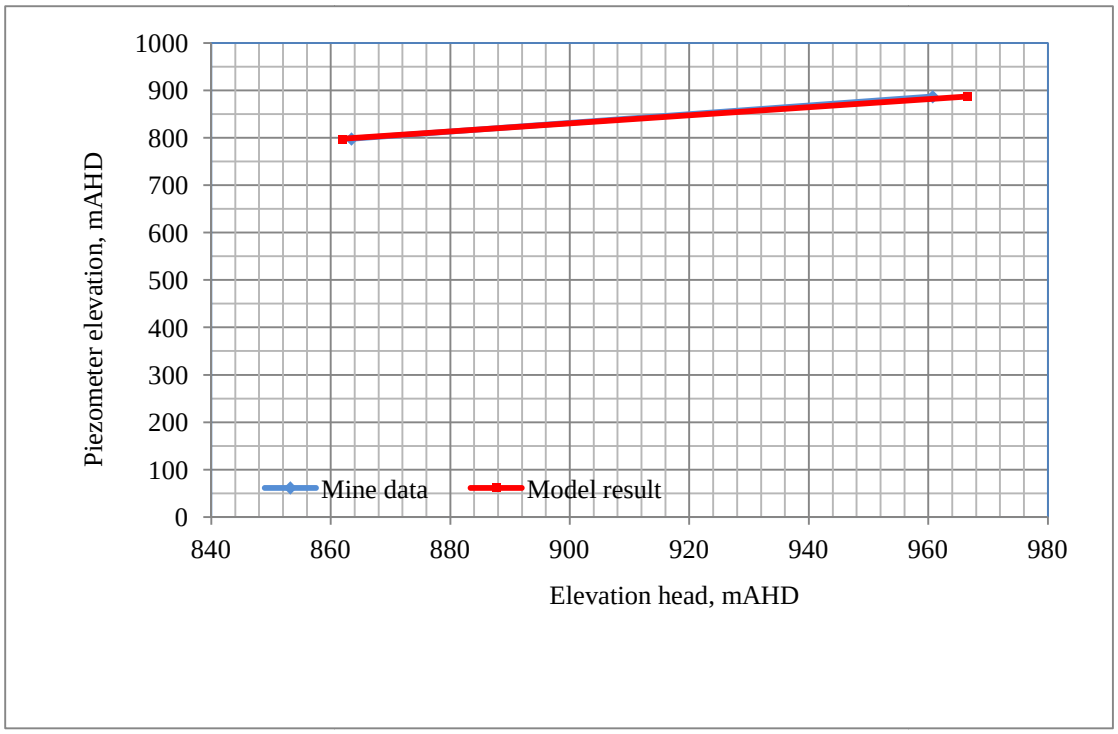

Figure B38 Comparison of observed and simulated piezometer elevation head profiles SPR34 (Date 20/03/2006)

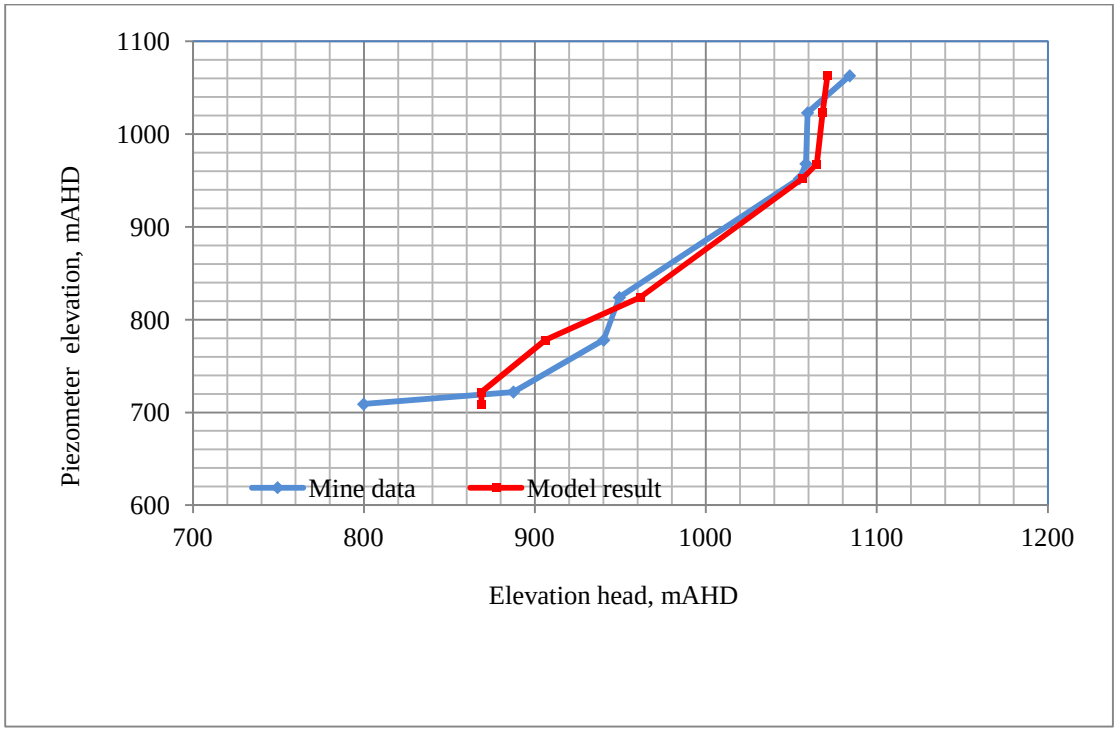

Figure B39 Comparison of observed and simulated piezometer elevation head profiles SPR36 (Date 12/03/2006)

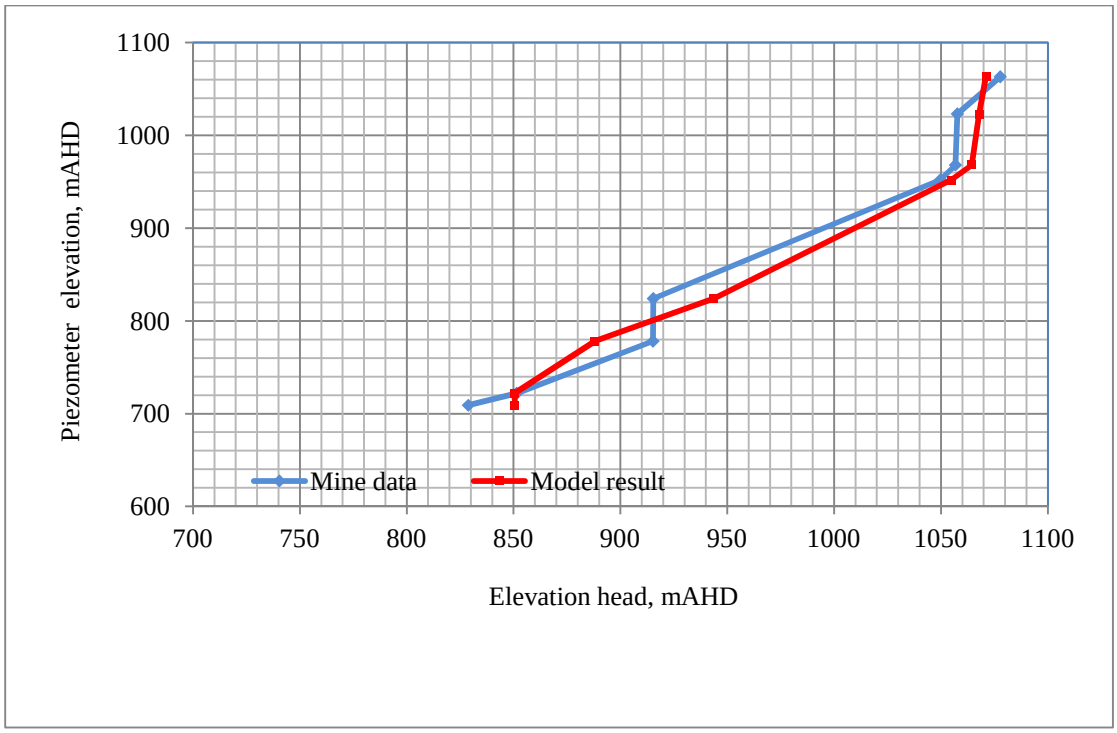

Figure B40 Comparison of observed and simulated piezometer elevation head profiles SPR36 (Date 12/01/2012)

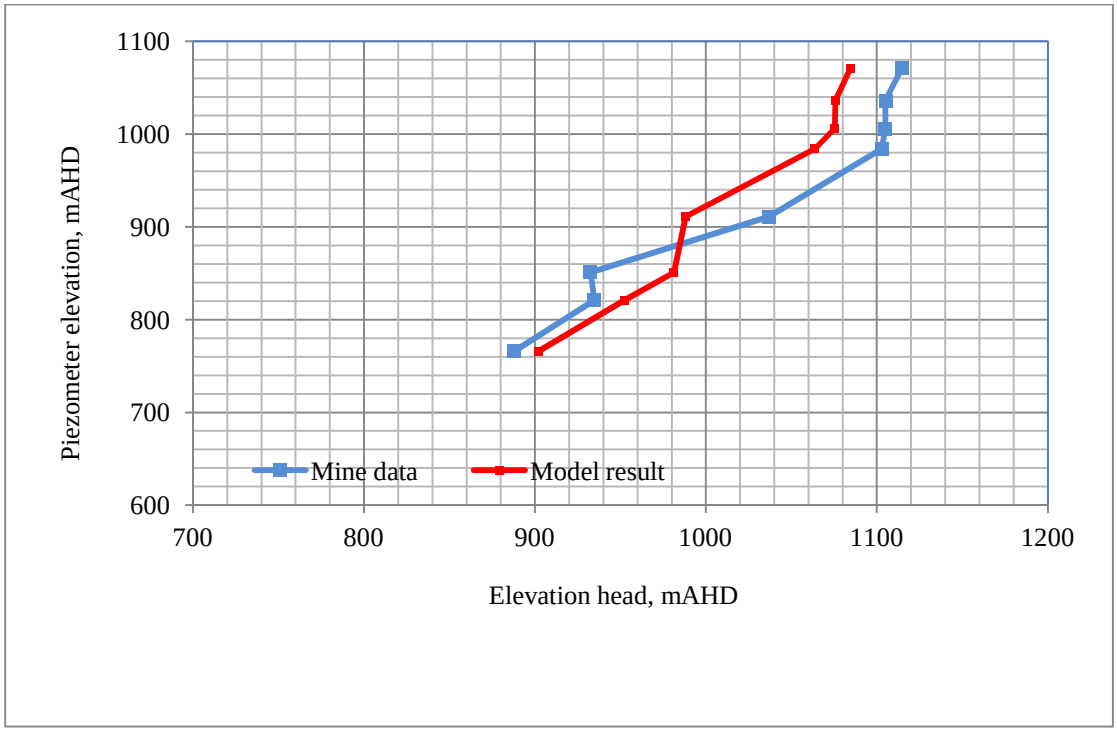

Figure B41 Comparison of observed and simulated piezometer elevation head profiles SPR37R (Date 12/03/2006)

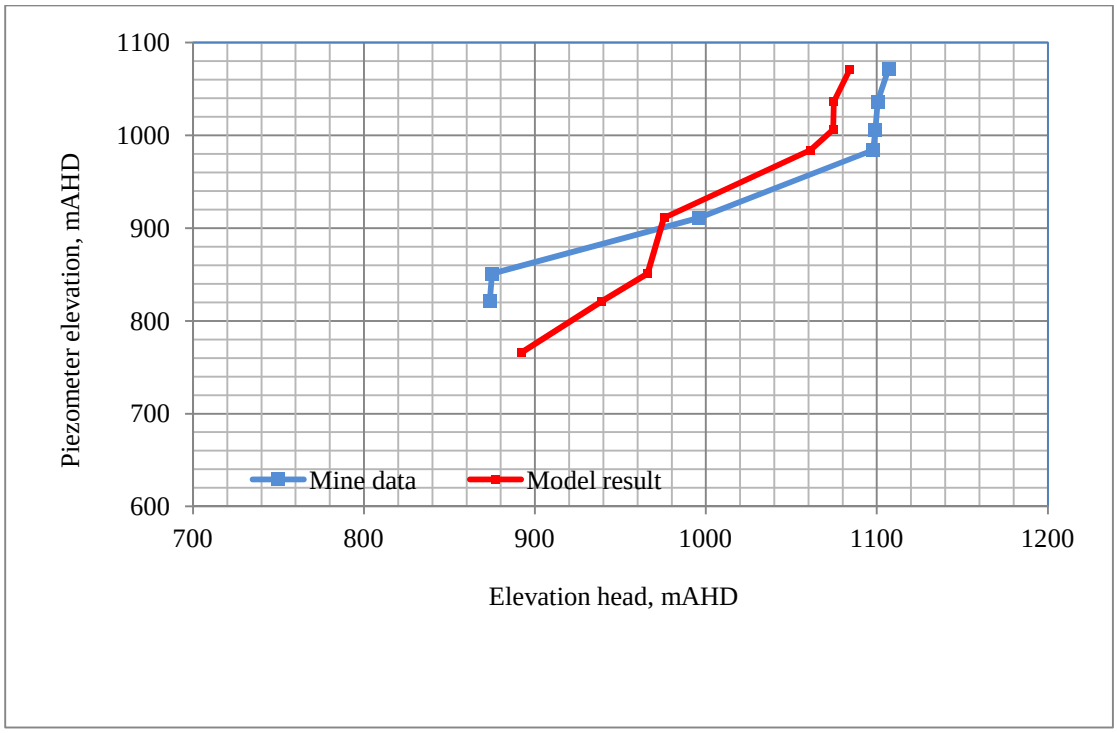

Figure B42 Comparison of observed and simulated piezometer elevation head profiles SPR37R (Date 13/03/2012)

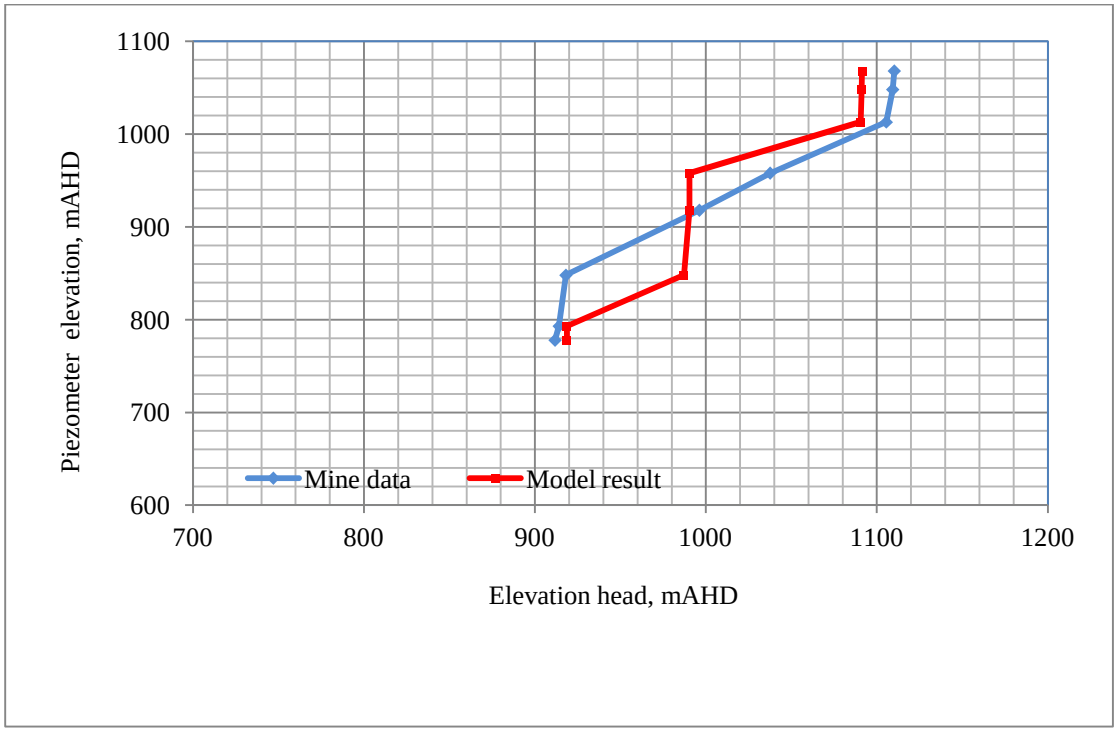

Figure B43 Comparison of observed and simulated piezometer elevation head profiles SPR38 (Date 12/03/2006)

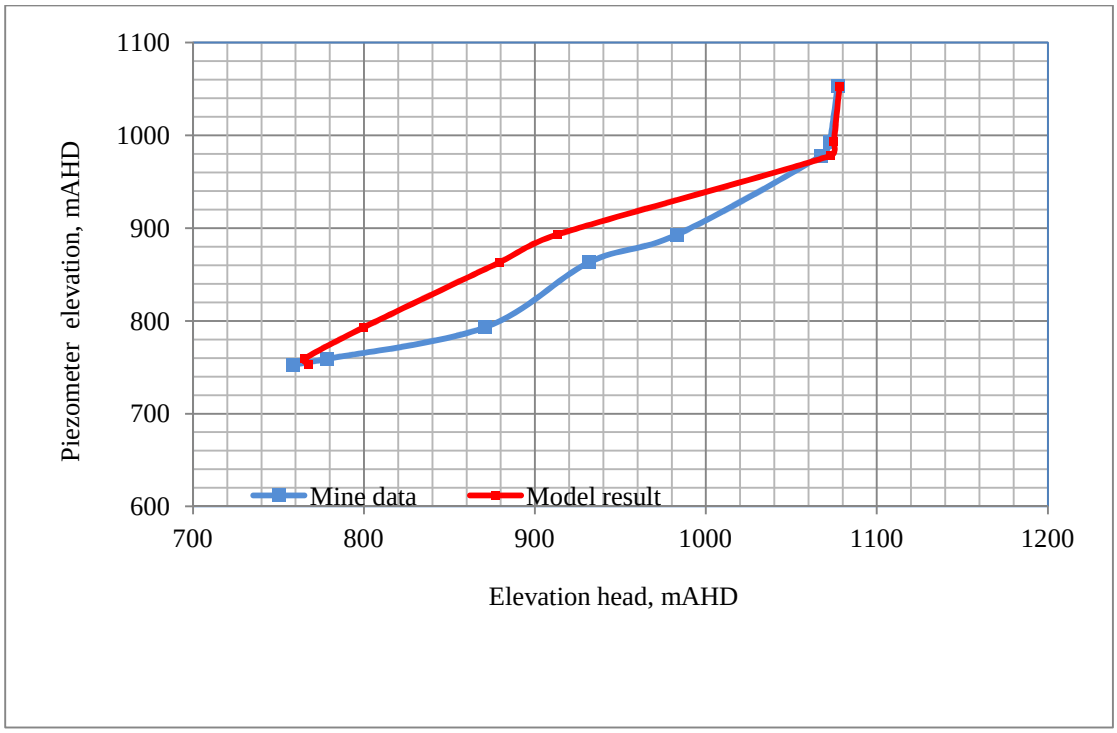

Figure B44 Comparison of observed and simulated piezometer elevation head profiles SPR39 (Date 24/03/2006)

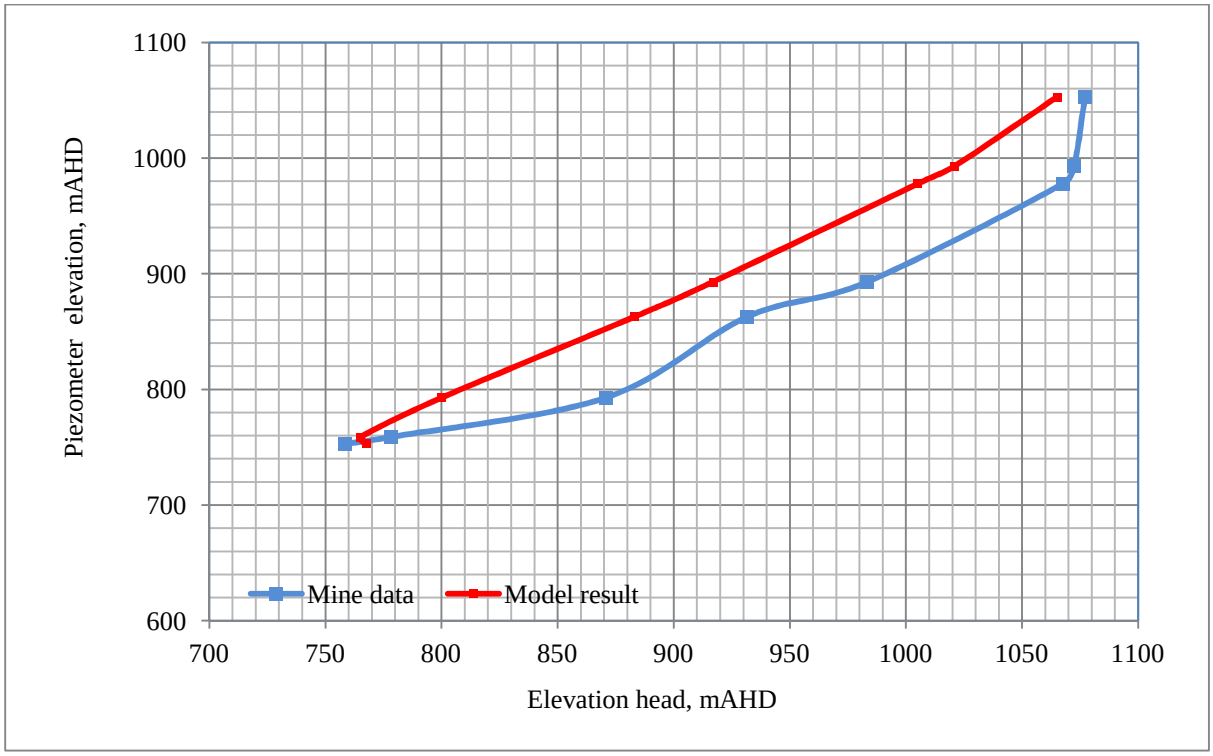

Figure B45 Comparison of observed and simulated piezometer elevation head profiles SPR39 (Date 01/01/2012)

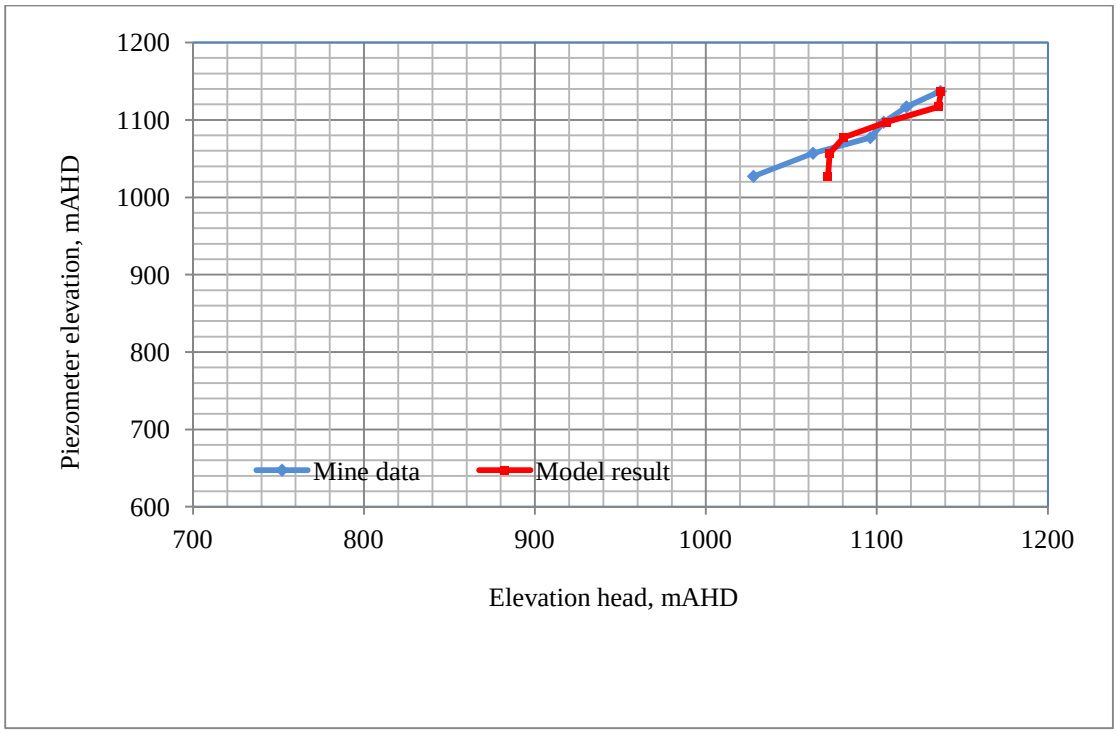

Figure B46 Comparison of observed and simulated piezometer elevation head profiles SPR48 (Date 01/01/2012)

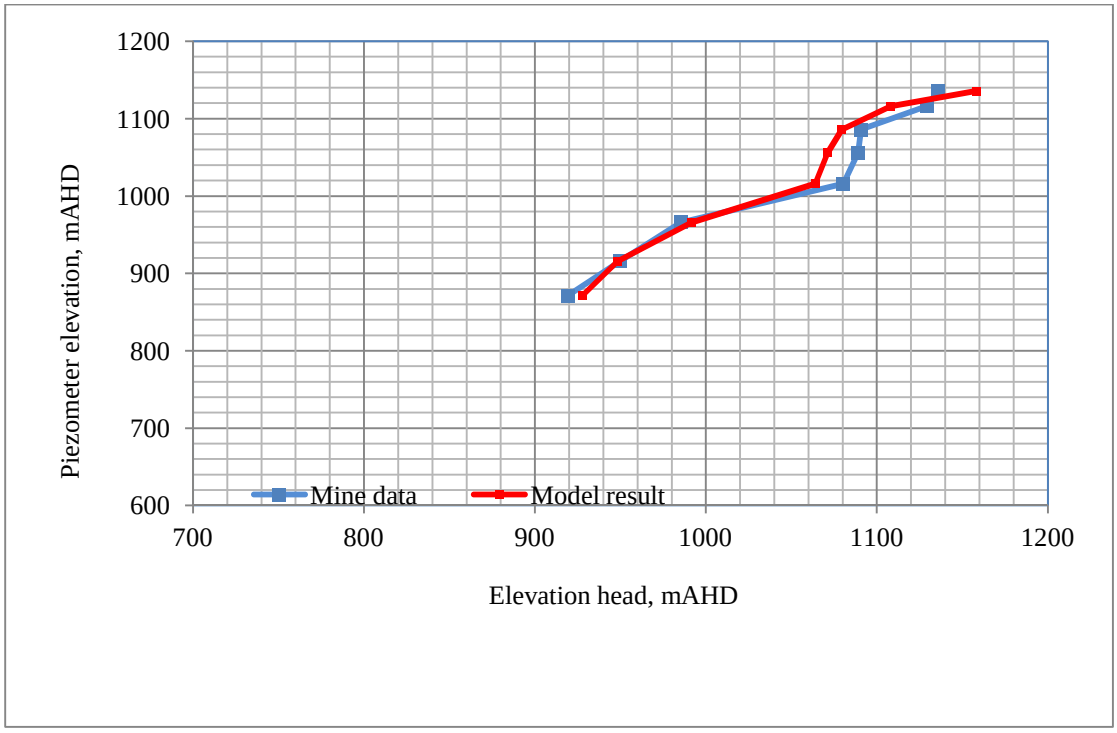

Figure B47 Comparison of observed and simulated piezometer elevation head profiles SPR49 (Date 20/07/2008)

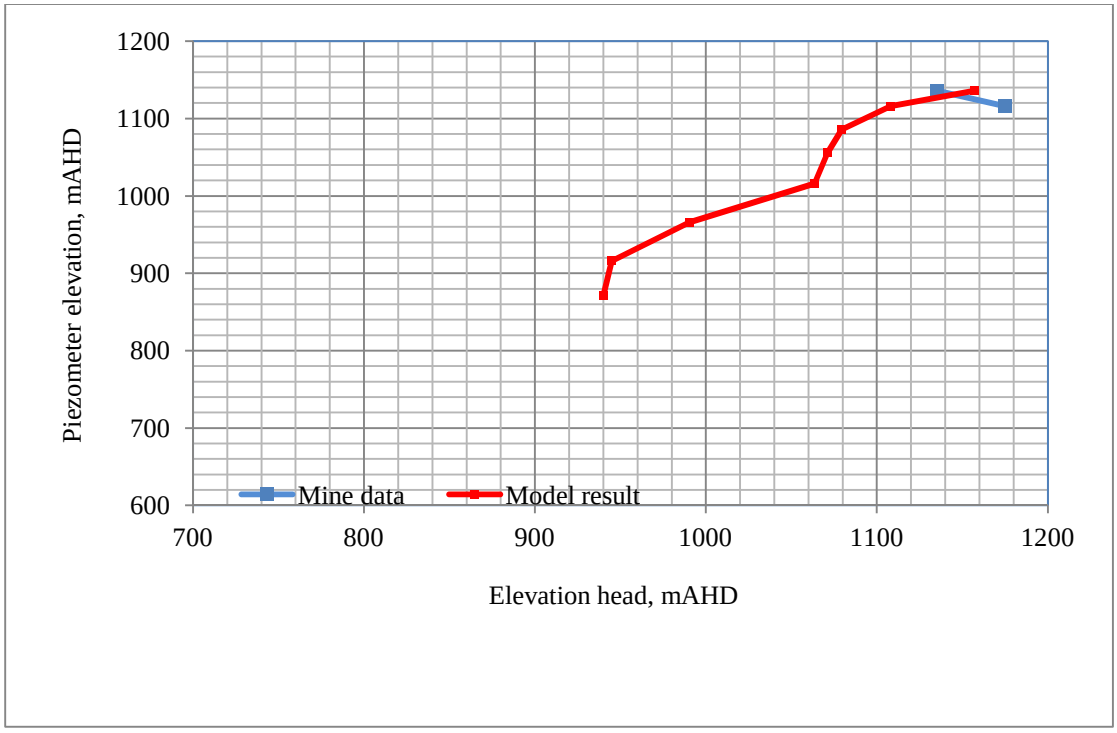

Figure B48 Comparison of observed and simulated piezometer elevation head profiles SPR49 (Date 01/01/2012, Note Piezo 1 to 6 got damaged)

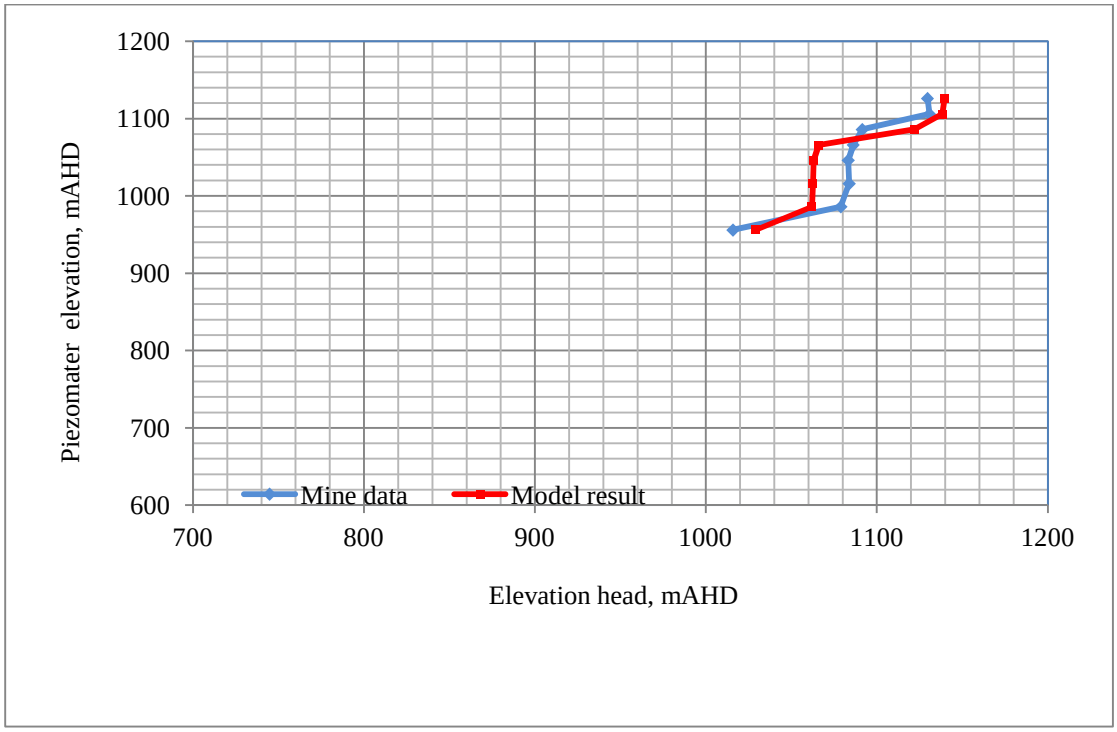

Figure B49 Comparison of observed and simulated piezometer elevation head profiles SPR50 (Date 08/04/2008)

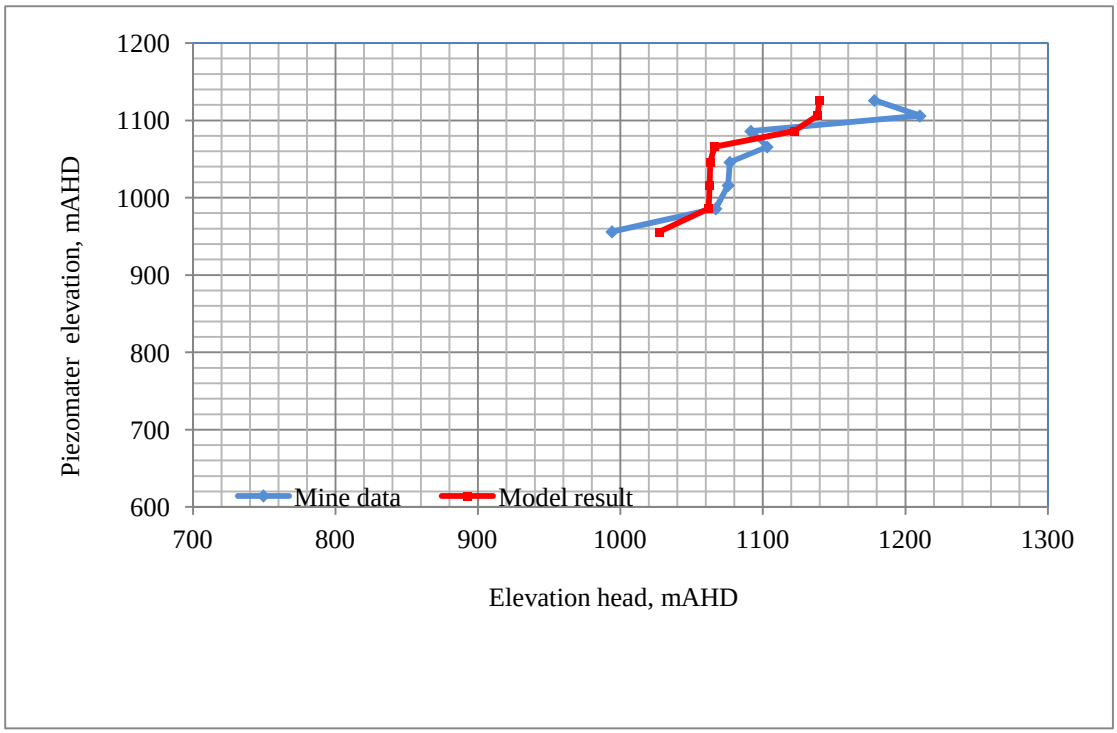

Figure B50 Comparison of observed and simulated piezometer elevation head profiles SPR50 (Date 01/01/2012)

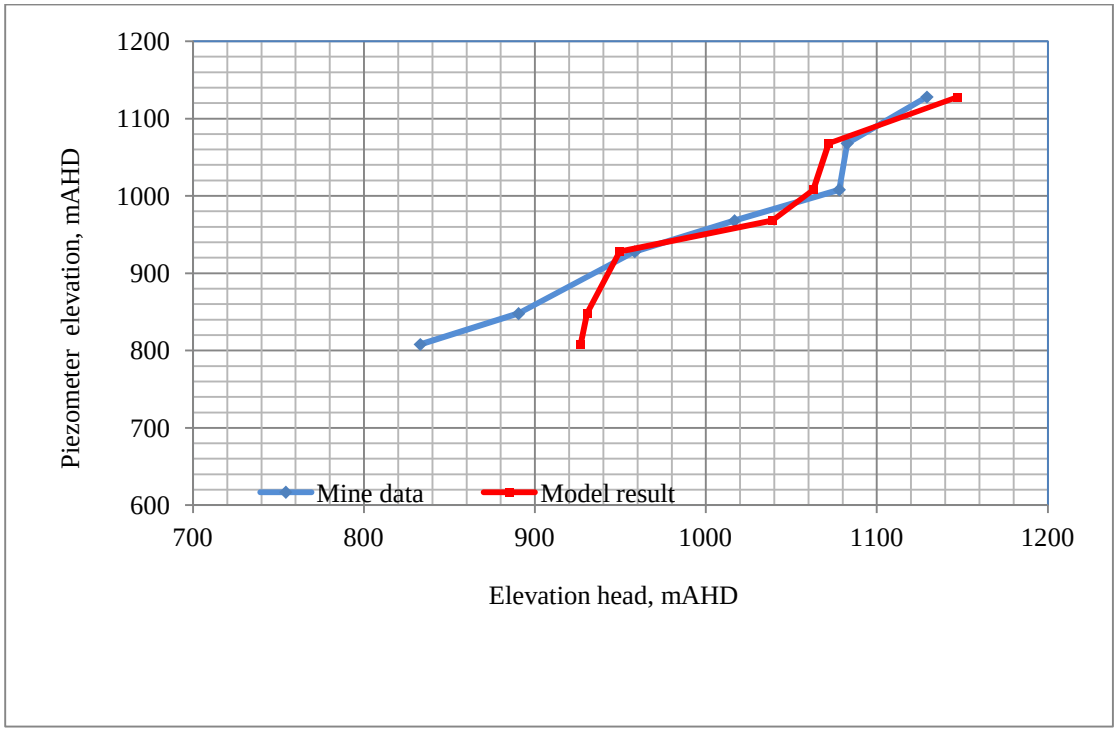

Figure B51 Comparison of observed and simulated piezometer elevation head profiles SPR51 (Date 20/01/2010)

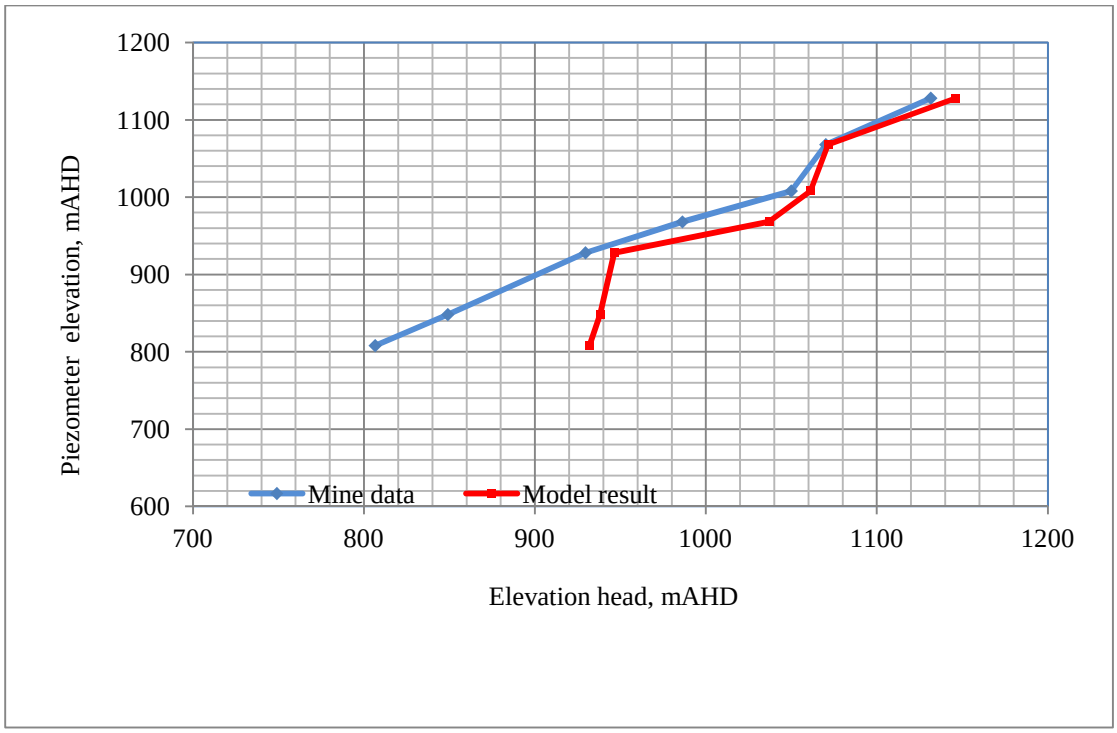

Figure B52 Comparison of observed and simulated piezometer elevation head profiles SPR51 (Date 01/01/2012)

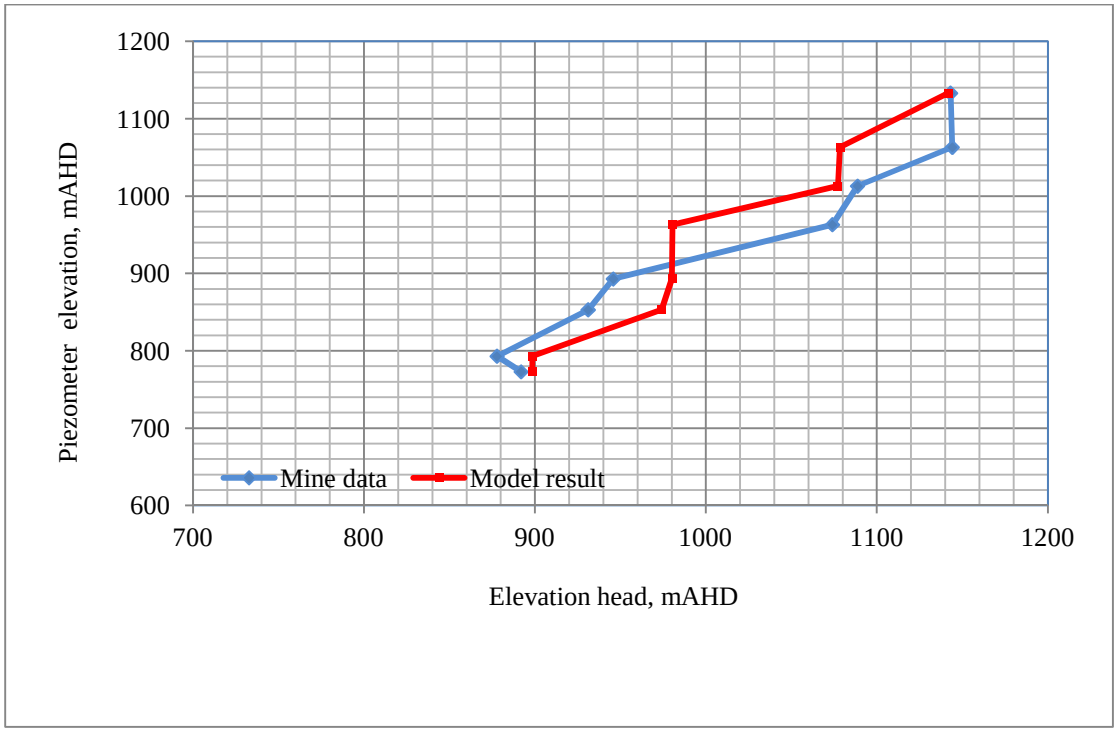

Figure B53 Comparison of observed and simulated piezometer elevation head profiles SPR64 (Date 12/10/2010)

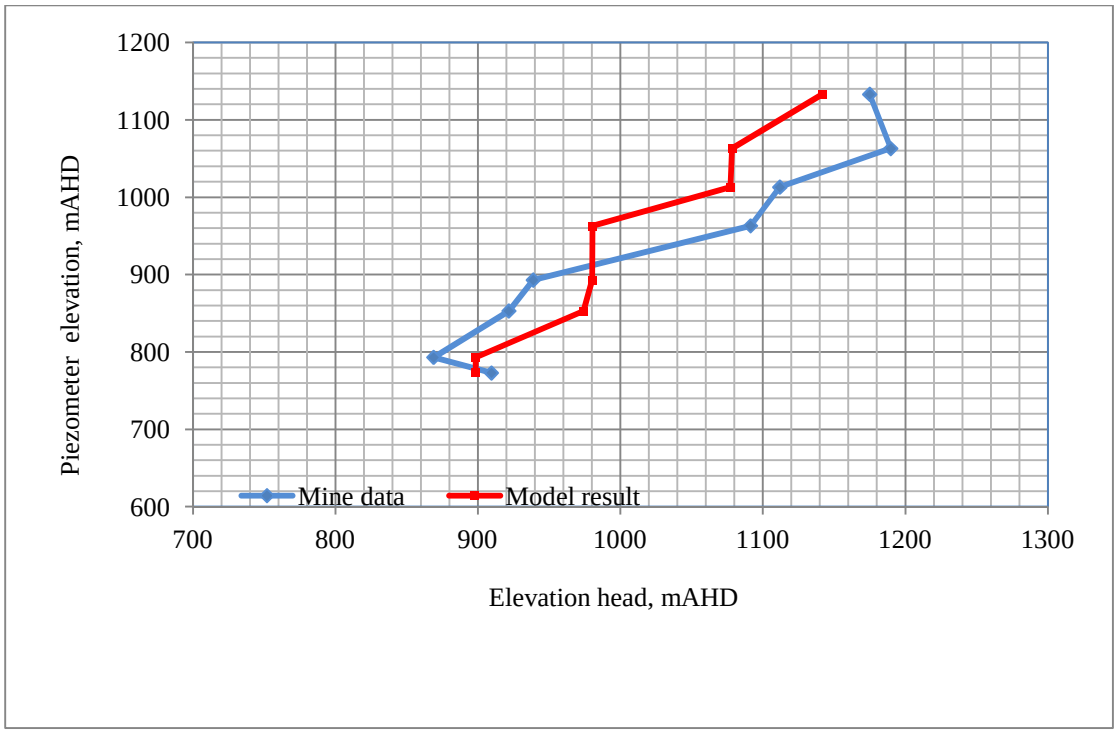

Figure B54 Comparison of observed and simulated piezometer elevation head profiles SPR64 (Date 01/01/2012)

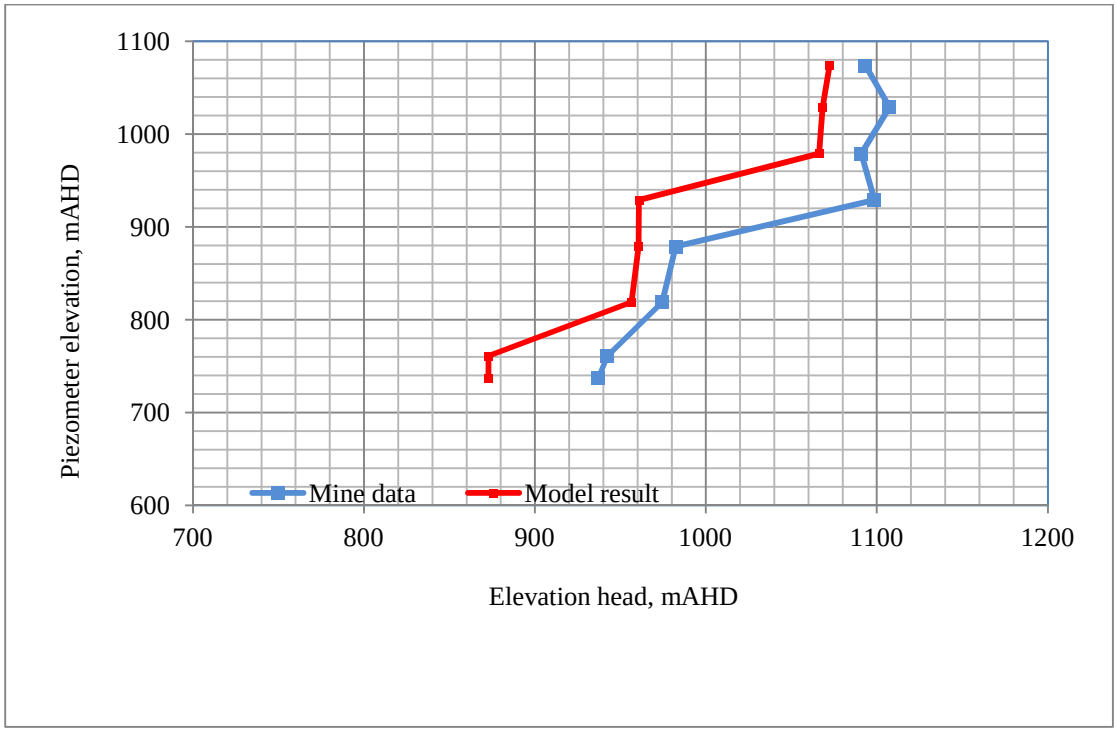

Figure B55 Comparison of observed and simulated piezometer elevation head profiles SPR66 (Date 01/01/2012)

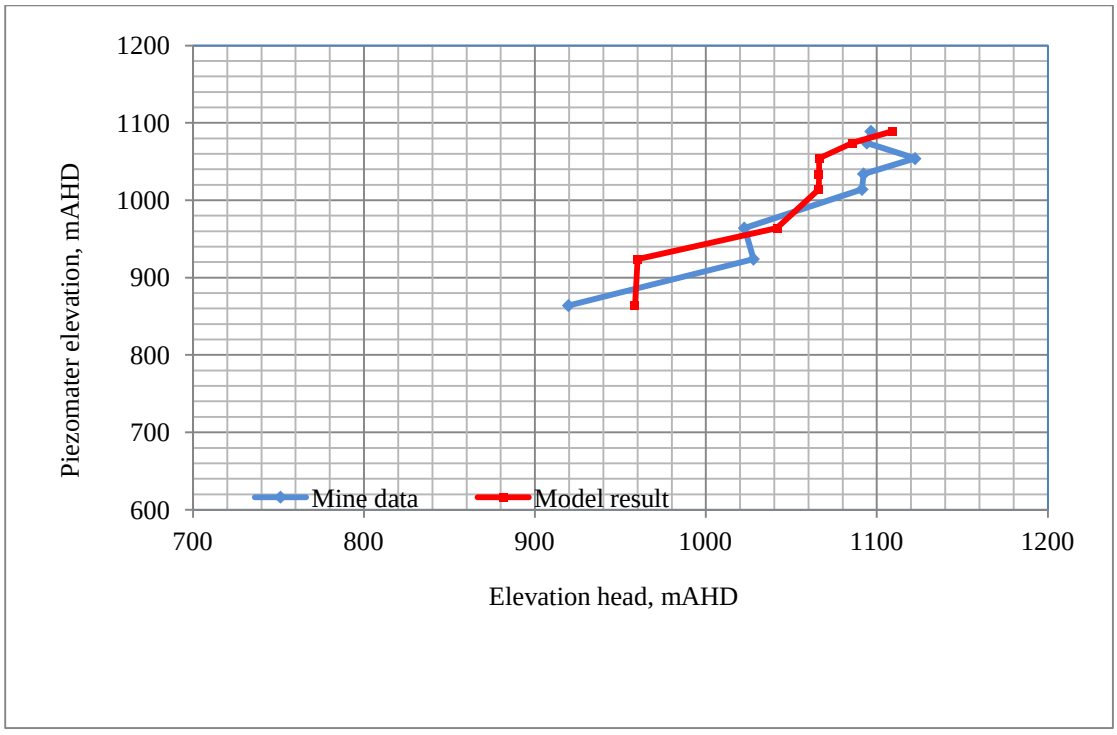

Figure B56 Comparison of observed and simulated piezometer elevation head profiles SPR67 (Date 12/01/2010)

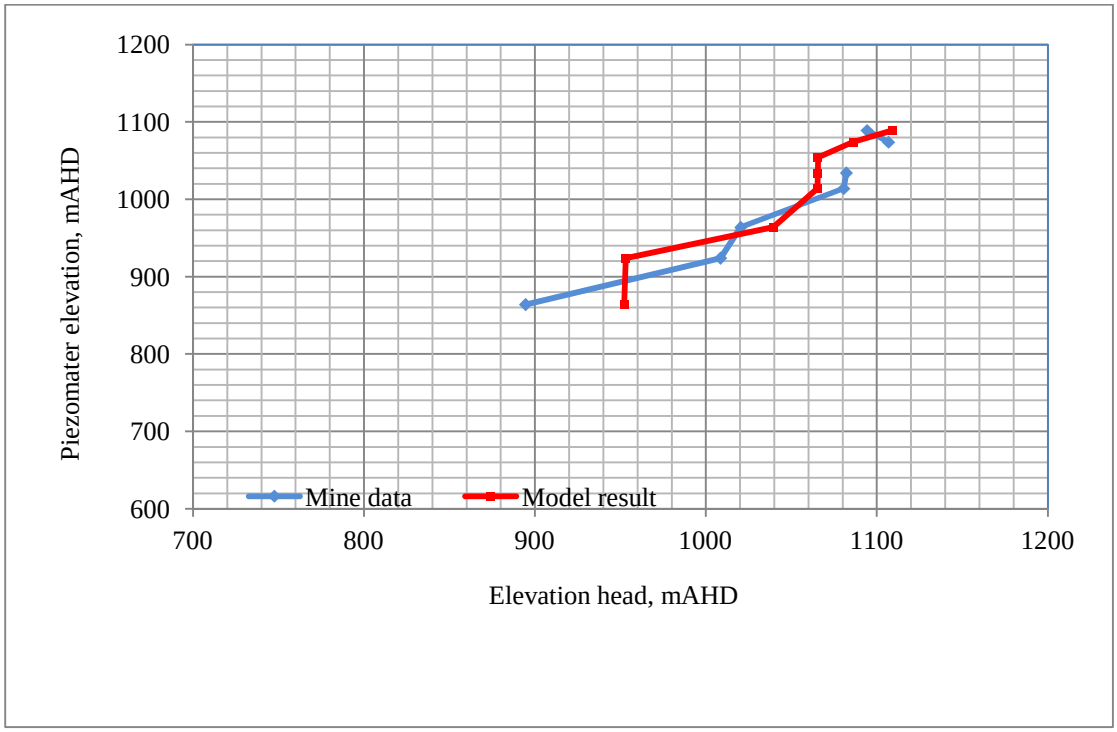

Figure B57 Comparison of observed and simulated piezometer elevation head profiles SPR67 (Date 01/01/2012)

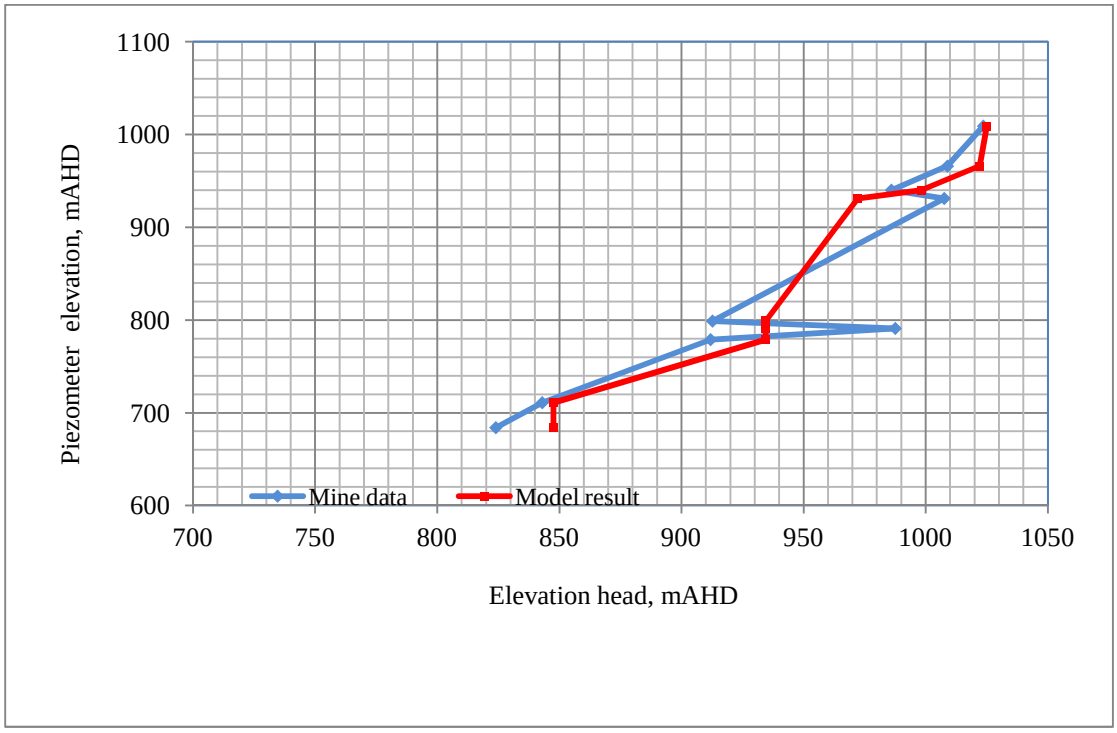

Figure B58 Comparison of observed and simulated piezometer elevation head profiles SPR1102 (Date 01/04/2012)

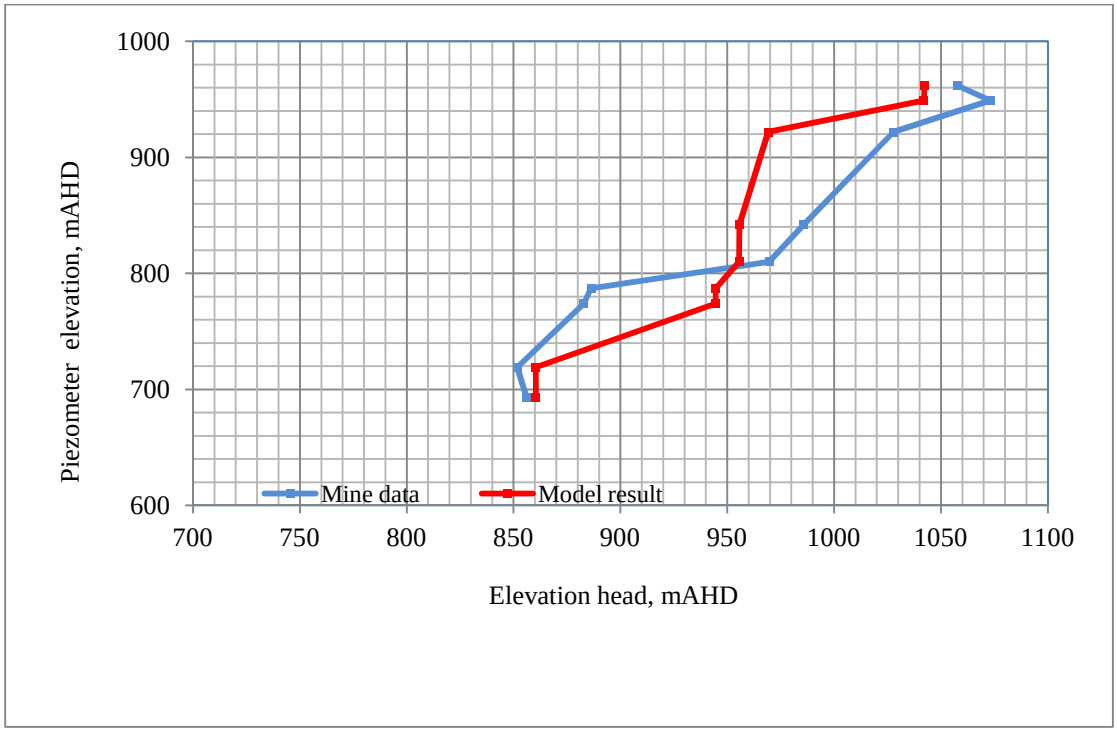

Figure B59 Comparison of observed and simulated piezometer elevation head profiles SPR1103 (Date 01/04/2012)

EARTH SCIENCE AND RESOURCE ENGINEERING
www.csiro.au

Appendix C
Baseflow to Swamps and Streams

Angus Place and Springvale Colliery Operations

Groundwater Assessment

D P Adhikary and A Wilkins
Report No EP132799
May 2013

Springvale Colliery and Angus Place Colliery

Citation

Adhikary, DP and Wilkins, A (2013) Angus Place and Springvale Colliery operations groundwater assessment. Appendix C – Baseflow to swamps and streams. Report No EP132799.

Copyright and disclaimer

Important disclaimer

Figures

Tables

Baseflow Balance

As described in Chapter 3, baseflow to swamps and streams and leakage from swamps and streams to the groundwater system were computed during calibration and validation period. Figure C2 to Figure C22 show baseflow balance in ML/day from twenty-one different swamps and streams explicitly simulated in the model (see Figure C1 and Table C1). Similar plots may be made for the "No New Mining" scenario. However, they simply show virtually no change in baseflow in any river or swamp from 2015 to the end of the simulation.

Figure C1 River reach and swamps of interest in the model

Table C1 Swamps and streams considered in the model

Notation	Rivers and swamps	Boundary conditions		Notation	Rivers and swamps	Boundary conditions
CA1	Carne Creek, main branch which flows north	Perennial		LAM	Lamb Creek	Ephemeral
CA2	Carne Creek, central branch which flows from east of LW431 and into CA1	Perennial		LOS	Long Swamp	Perennial
CA3	Carne Creek, branch which flows from GGSE and GGS to CA2	Perennial		MER	Marrangaroo Creek	Perennial
CA4	Carne Creek, branch flows from CW to CA2	Perennial		NMS	Nine-Mile Swamp	Perennial
CA5	Carne Creek, western branch which flows from above LW415 to CA2	Perennial		PDY	Paddy's Creek	Ephemeral
CW	Carne West Swamp, which flows to CA4	Ephemeral		PIS	Pine Swamp	Ephemeral
GGSE	Gang-Gang Swamp east which flows to CA3	Perennial		TRS	Tri-Star Swamp	Ephemeral
GGS	Gang-Gang Swamp south, which flows to CA3	Perennial		TWG	Twin-Gully Swamp	Ephemeral
KC1	Kangaroo Creek, downstream of KAS	Perennial		SSS	Sunnyside Swamp, which flows into WOL	Perennial
KC2	Kangaroo Creek, upstream of KAS	Ephemeral		WOL	Wolgan River	Perennial
KAS	Kangaroo Swamp	Ephemeral				

Depending upon whether a swamp/stream is permanently water logged or not, the swamp/stream node is assigned with either a constant staging height (perennial condition) or drain (ephemeral condition) as shown in Table C1. Perennial nodes will allow exchange of water in either direction between the stream and aquifer, whereas ephemeral nodes will record discharge when the groundwater pressure at the node is positive, but will allow groundwater level to drop below the node elevation without inducing leakage.

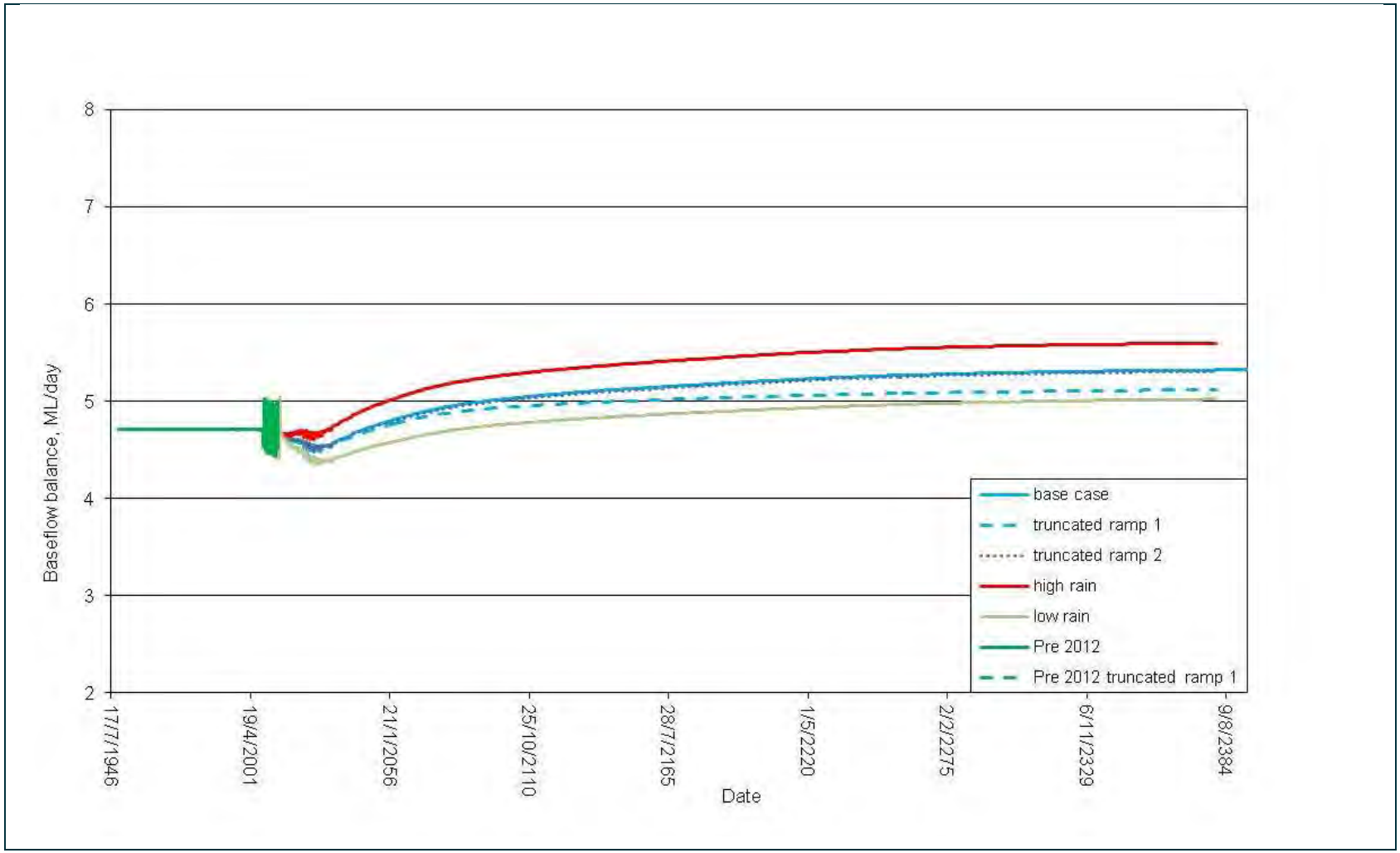

Figure C2 Estimates of baseflow balance (Carne_1)

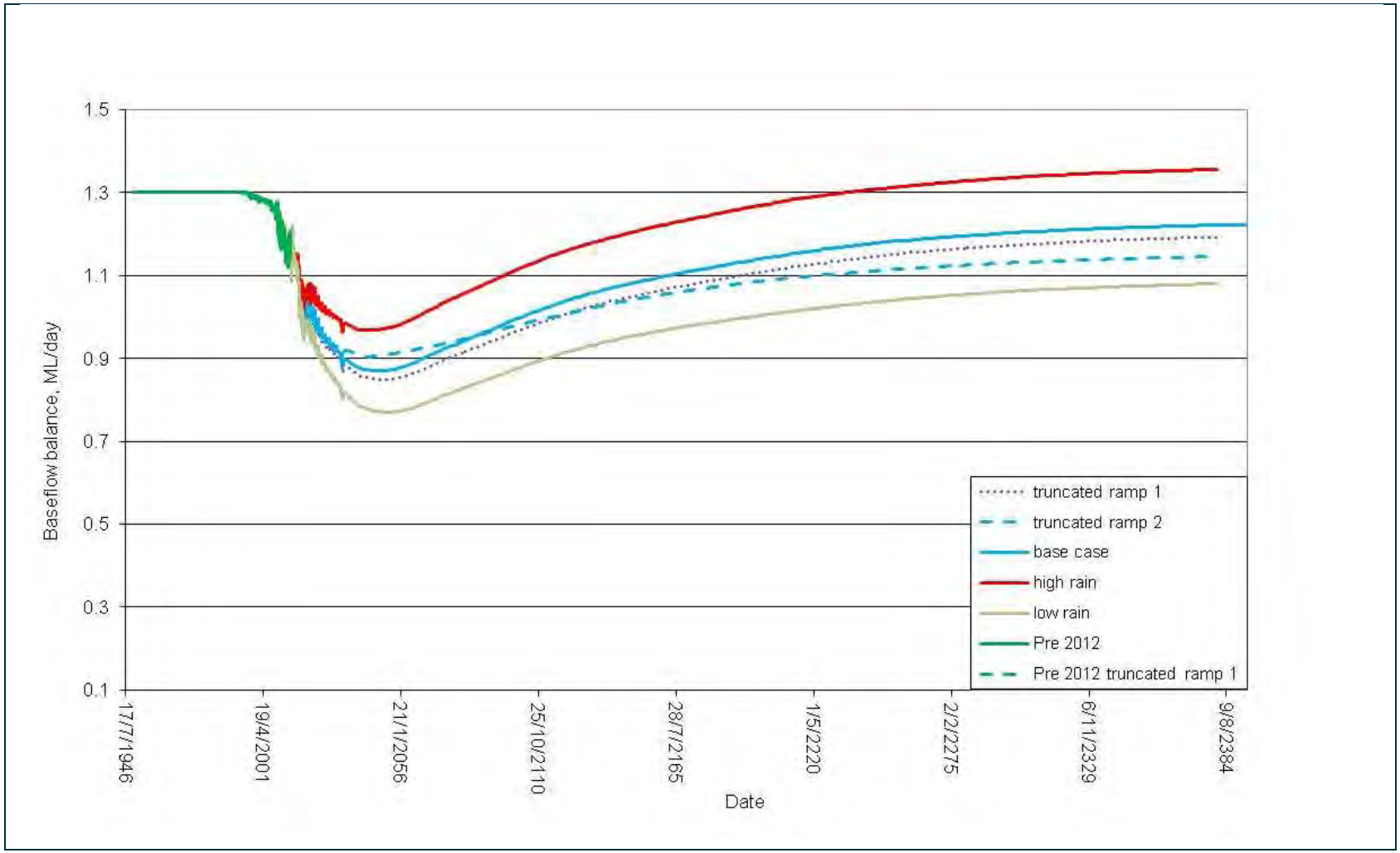

Figure C3 Estimates of baseflow balance (Carne_2)

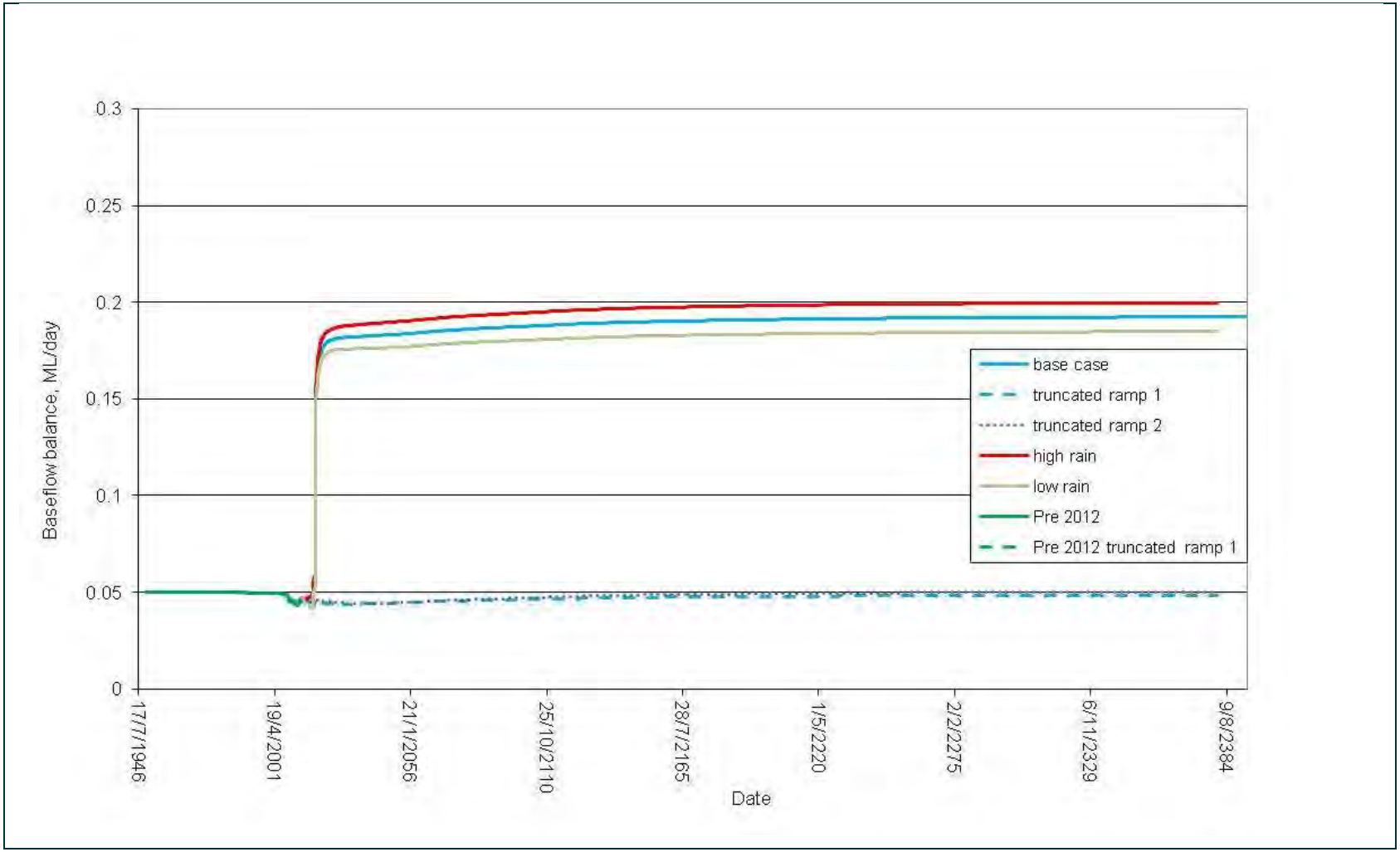

Figure C4 Estimates of baseflow balance (Carne_3)

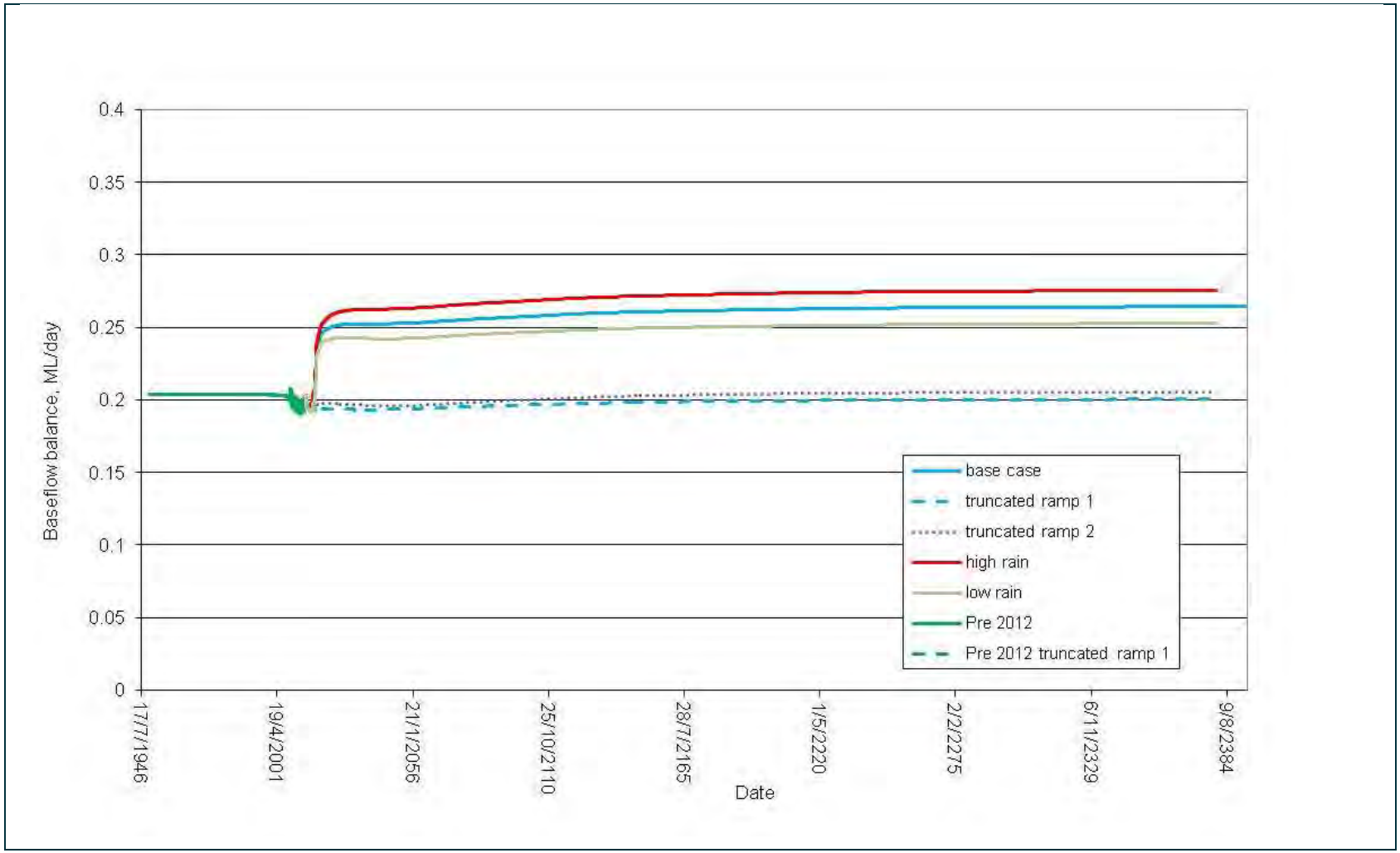

Figure C5 Estimates of baseflow balance (Carne_4)

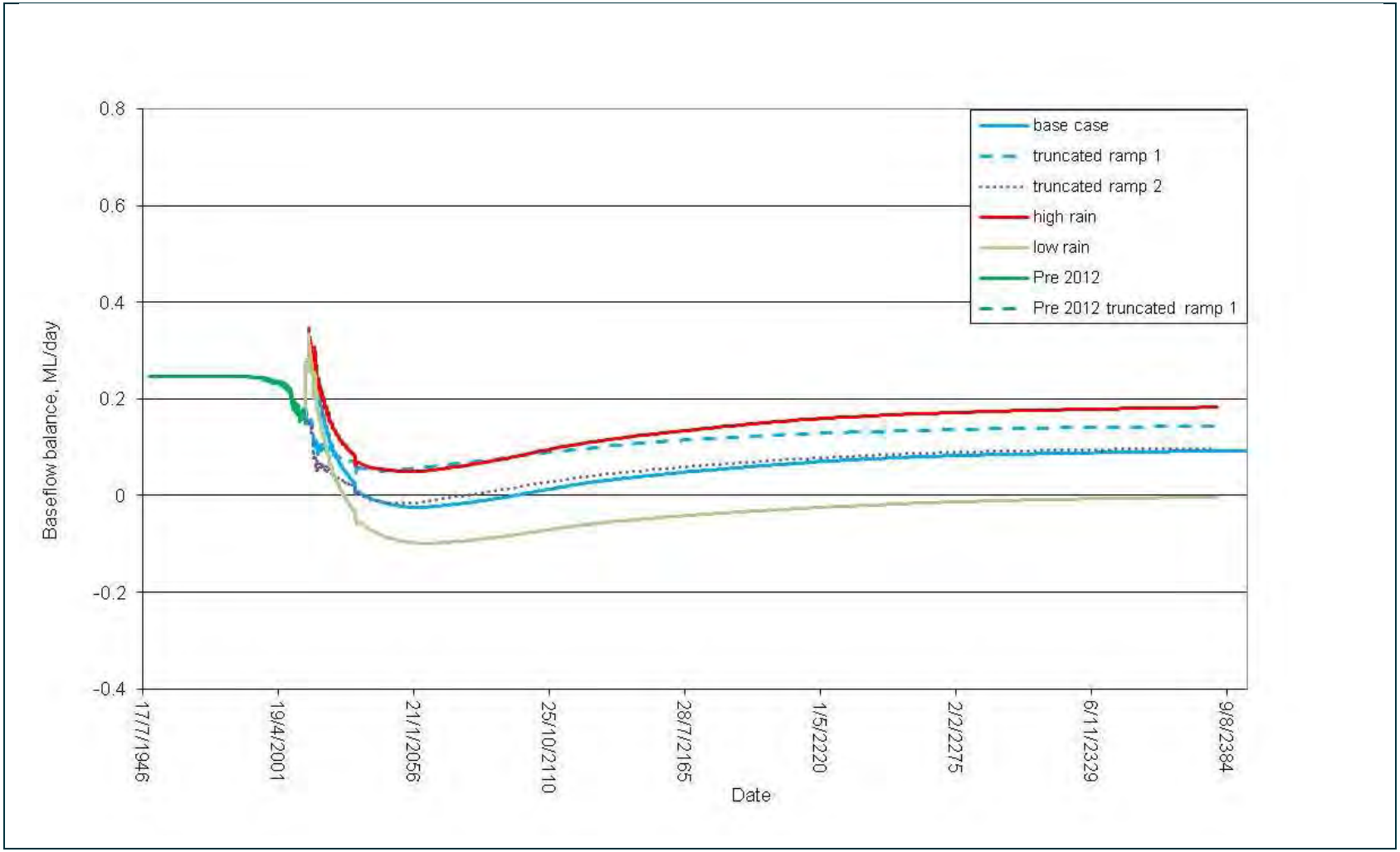

Figure C6 Estimates of baseflow balance (Carne_5)

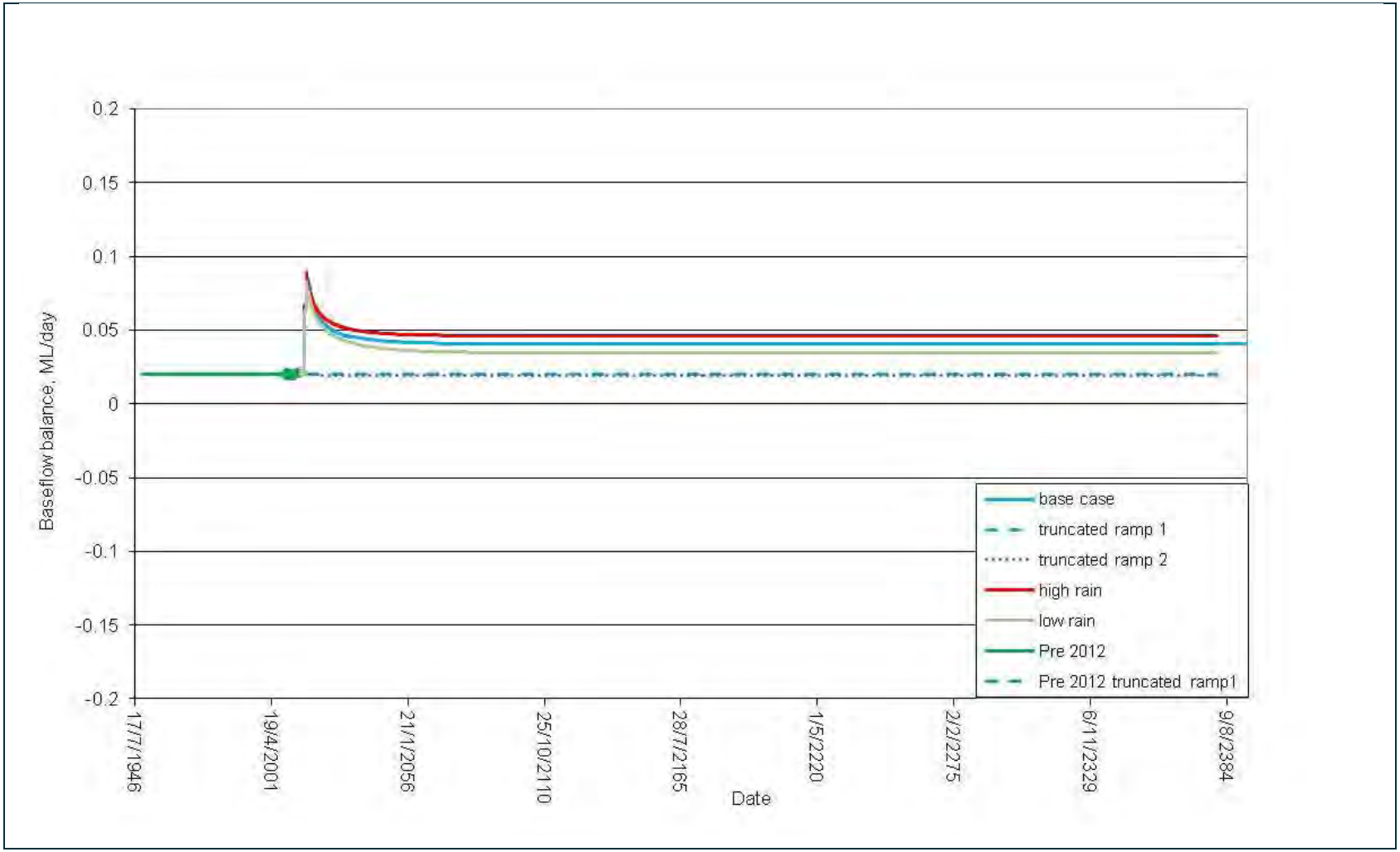

Figure C7 Estimates of baseflow balance (Carne-West Swamp)

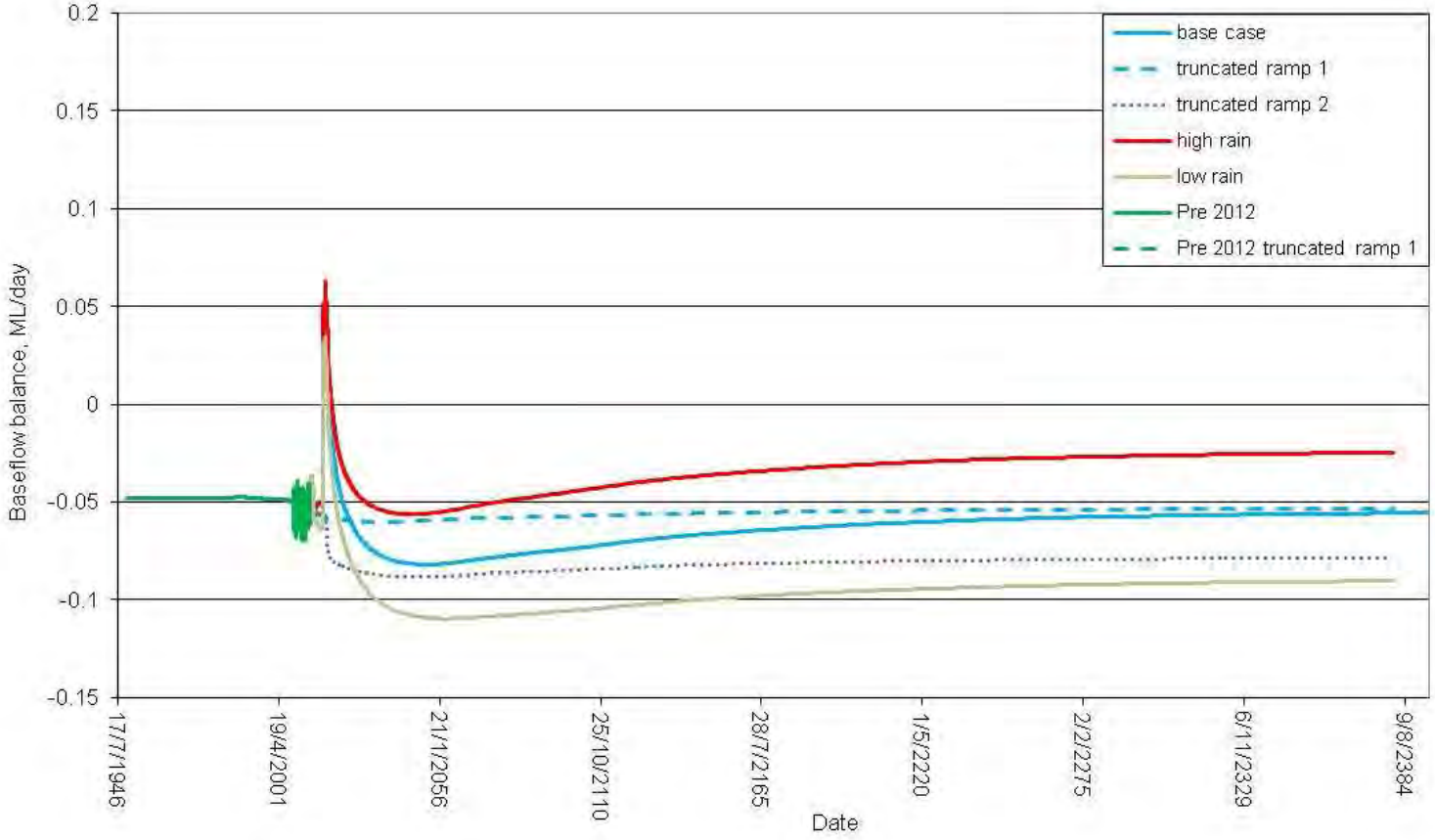

Figure C8 Estimates of baseflow balance (Gang-Gang Swamp South)

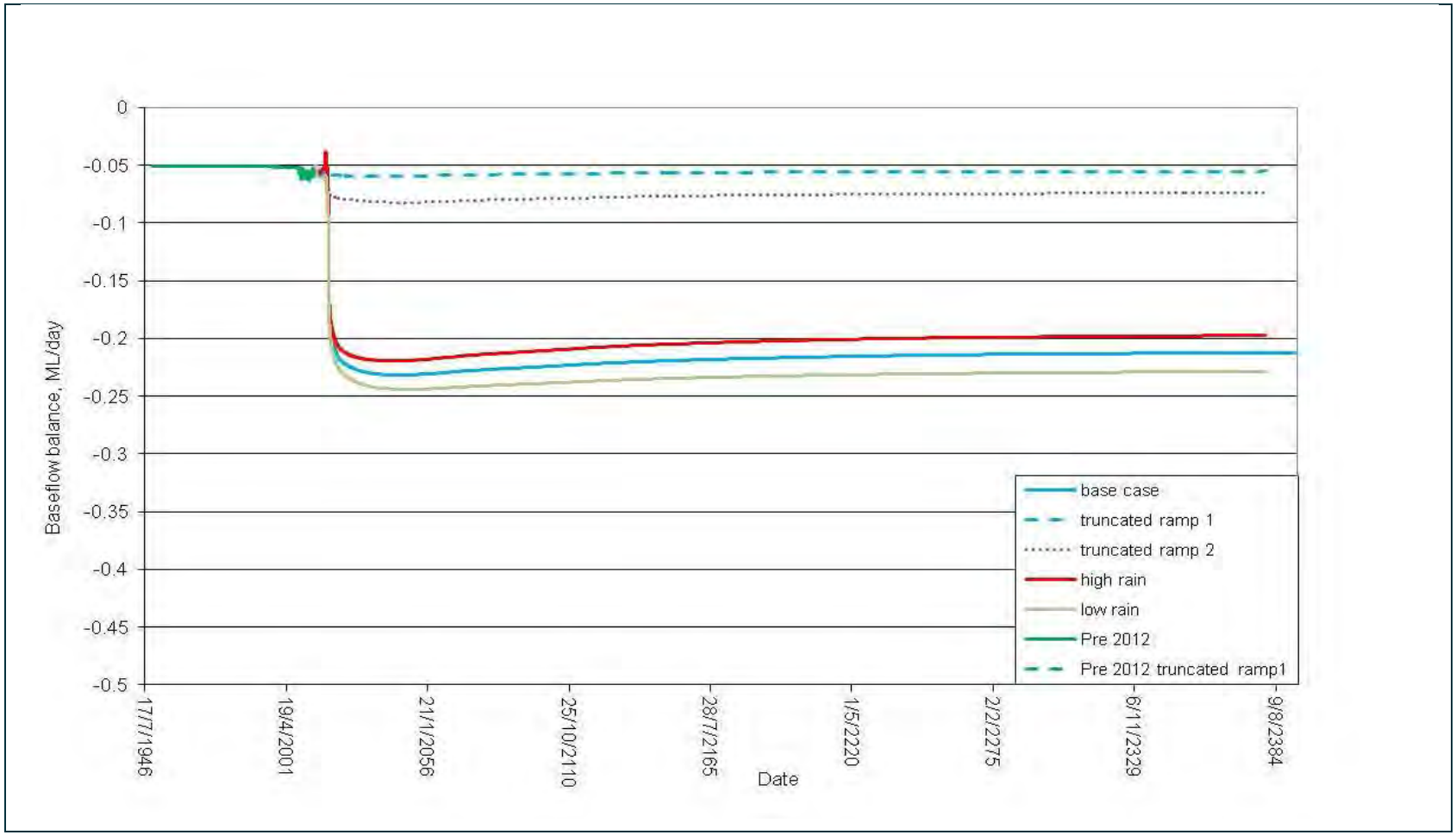

Figure C9 Estimates of baseflow balance (Gang-Gang Swamp South East)

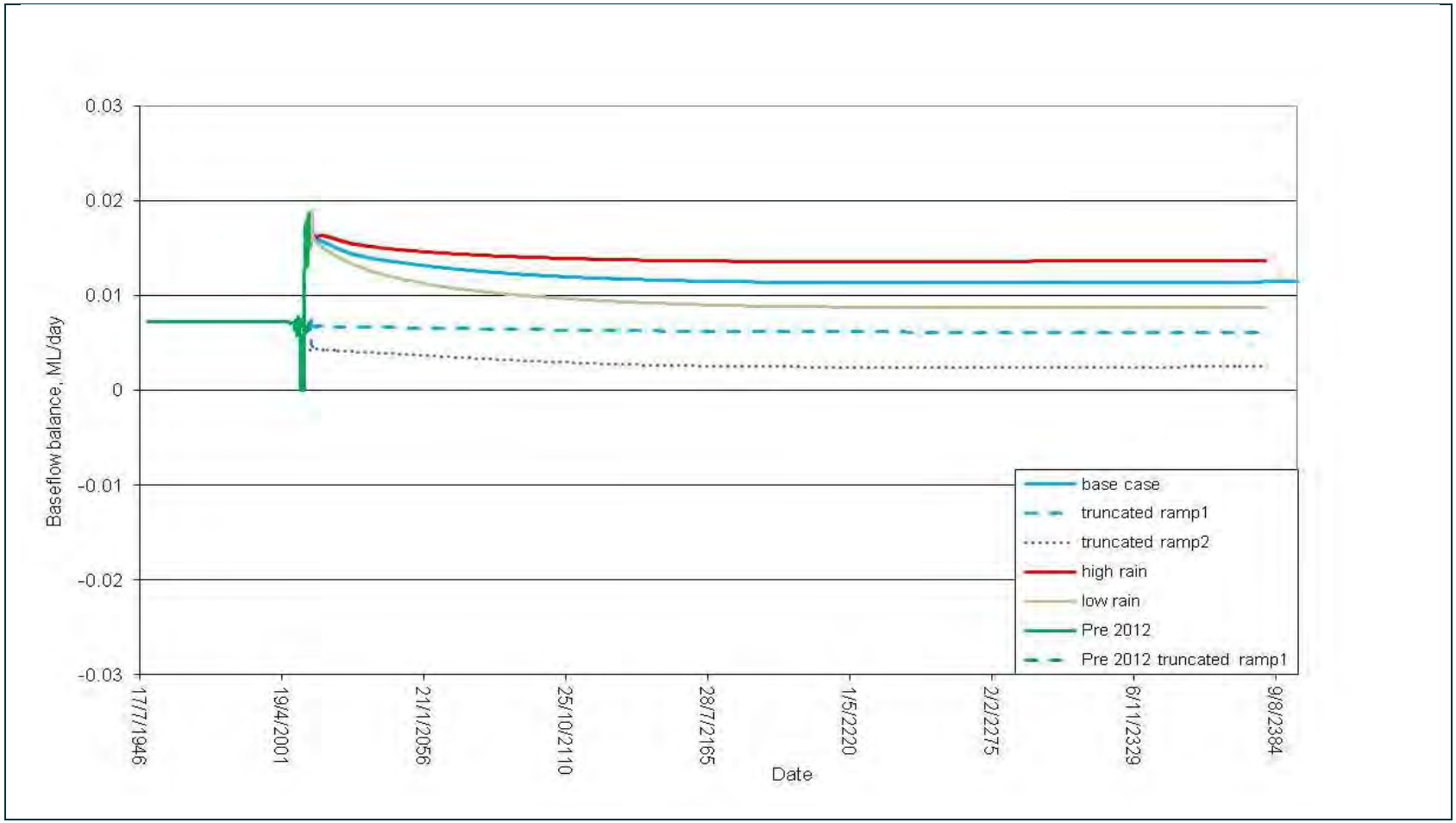

Figure C10 Estimates of baseflow balance (Kangaroo Creek Swamp). The baseflow balance reduces to zero as Angus Place LW940 passes underneath it in 2008. This agrees with piezometer data from the swamp, as described in Appendix A, Section5. As Angus Place LW950 passes underneath the swamp and upstream parts of Kangaroo Creek, the baseflow balance is restored. This is due to mining-induced permeability enhancement. The level of the waterhole near the swamp displays similar complicated behaviour, as described in Appendix A, Section 5.

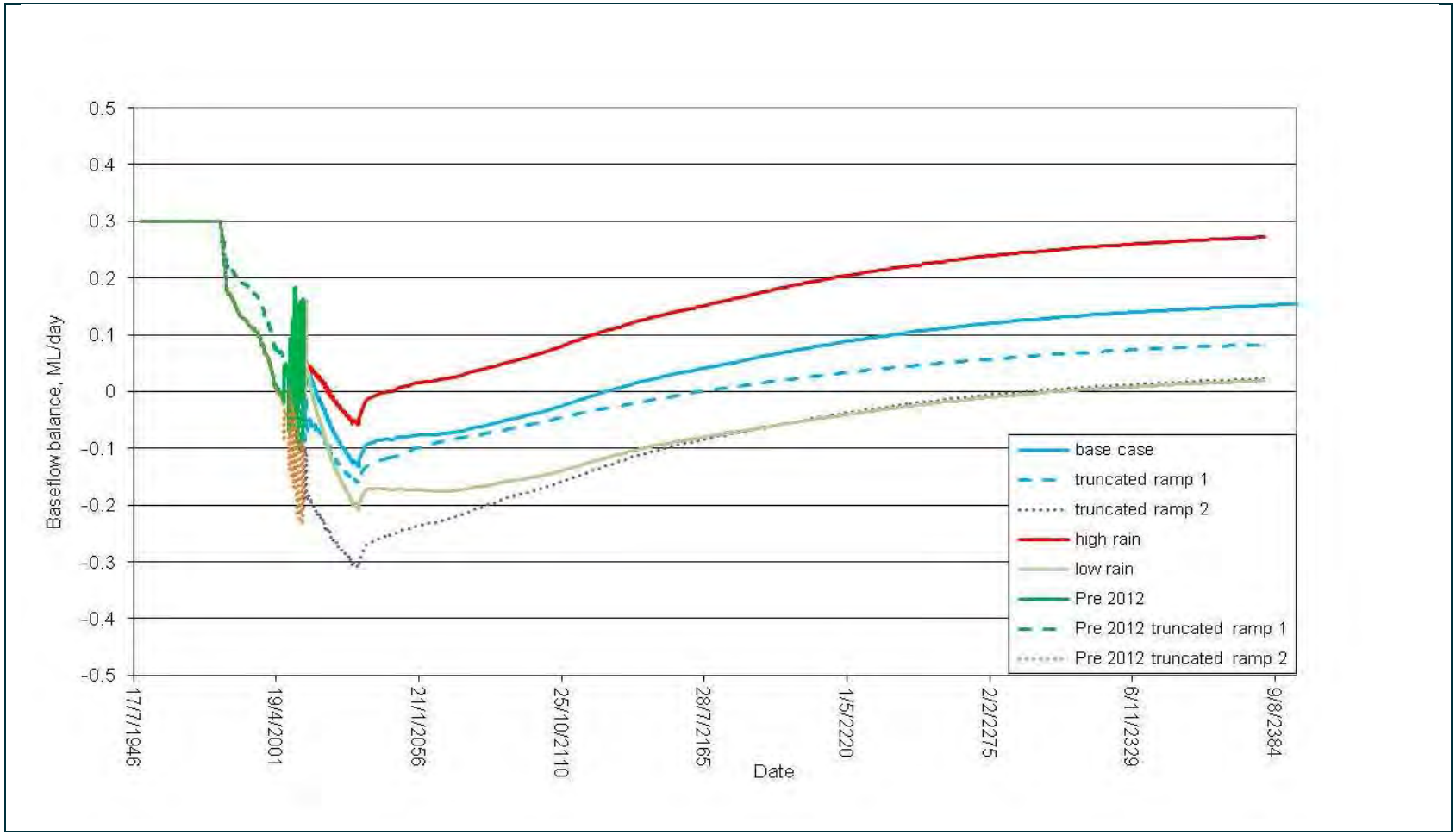

Figure C11 Estimates of baseflow balance (Kangaroo Creek_1)

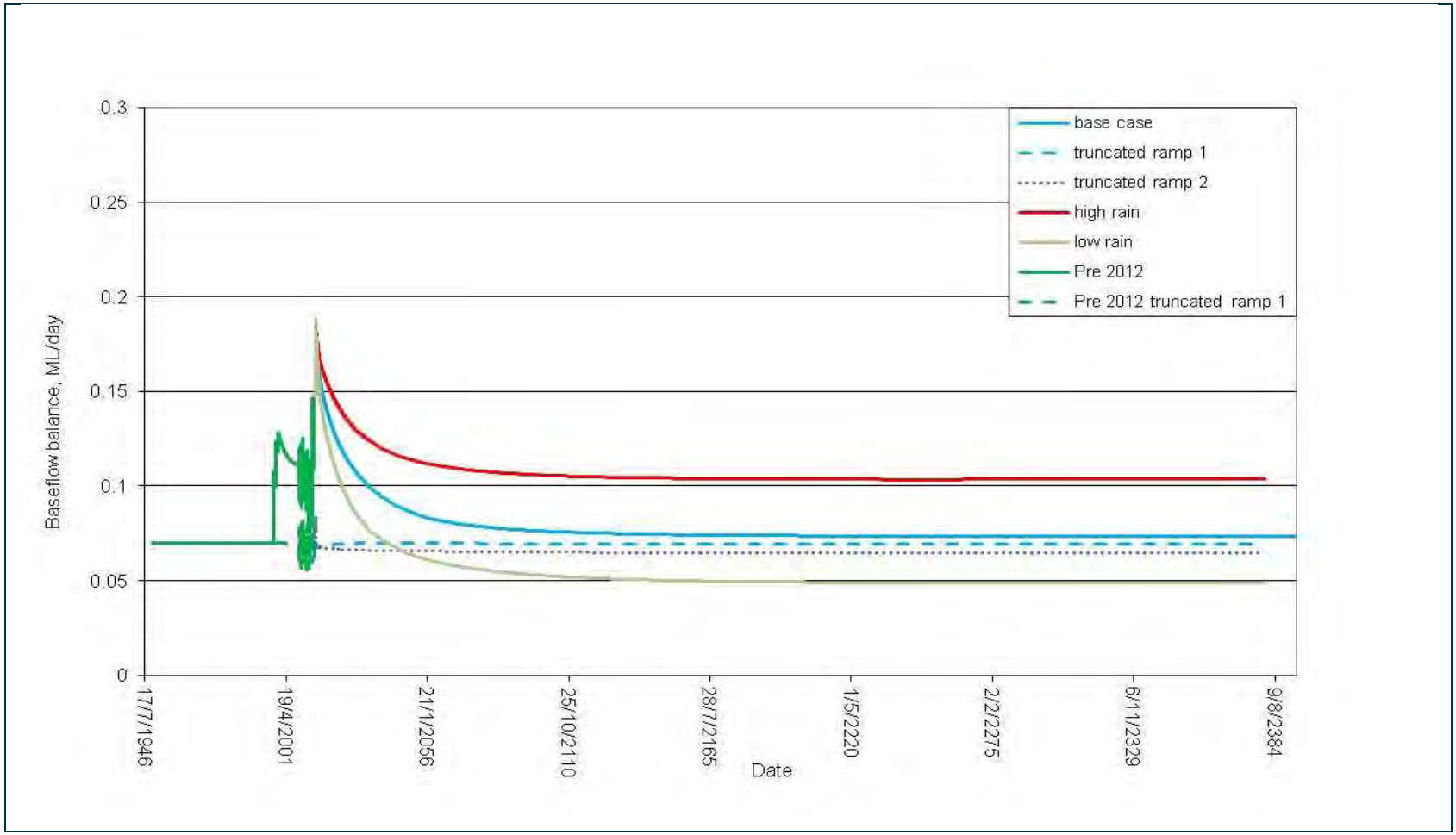

Figure C12 Estimates of baseflow balance (Kangaroo Creek_2)

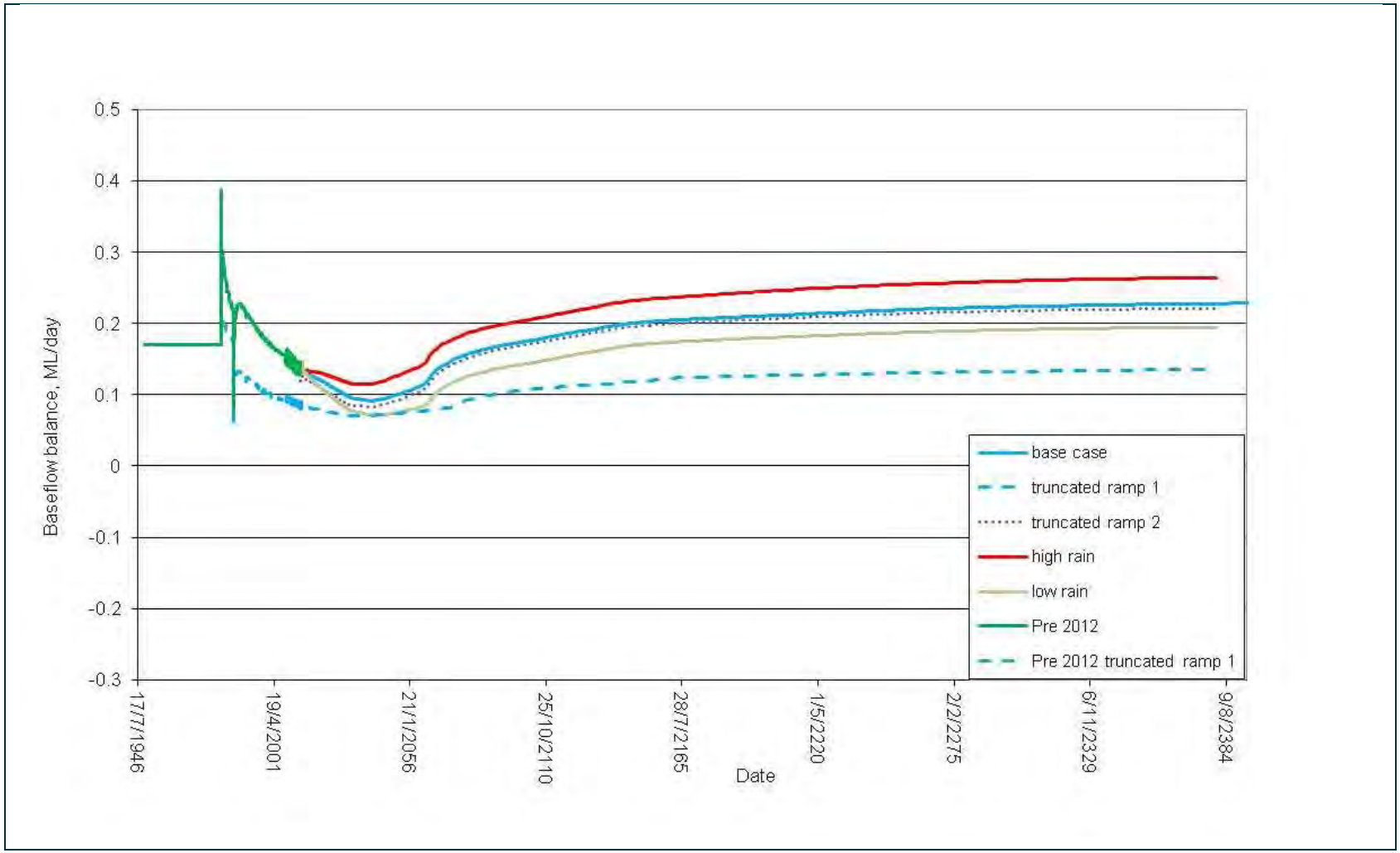

Figure C13 Estimates of baseflow balance (Lamb Creek)

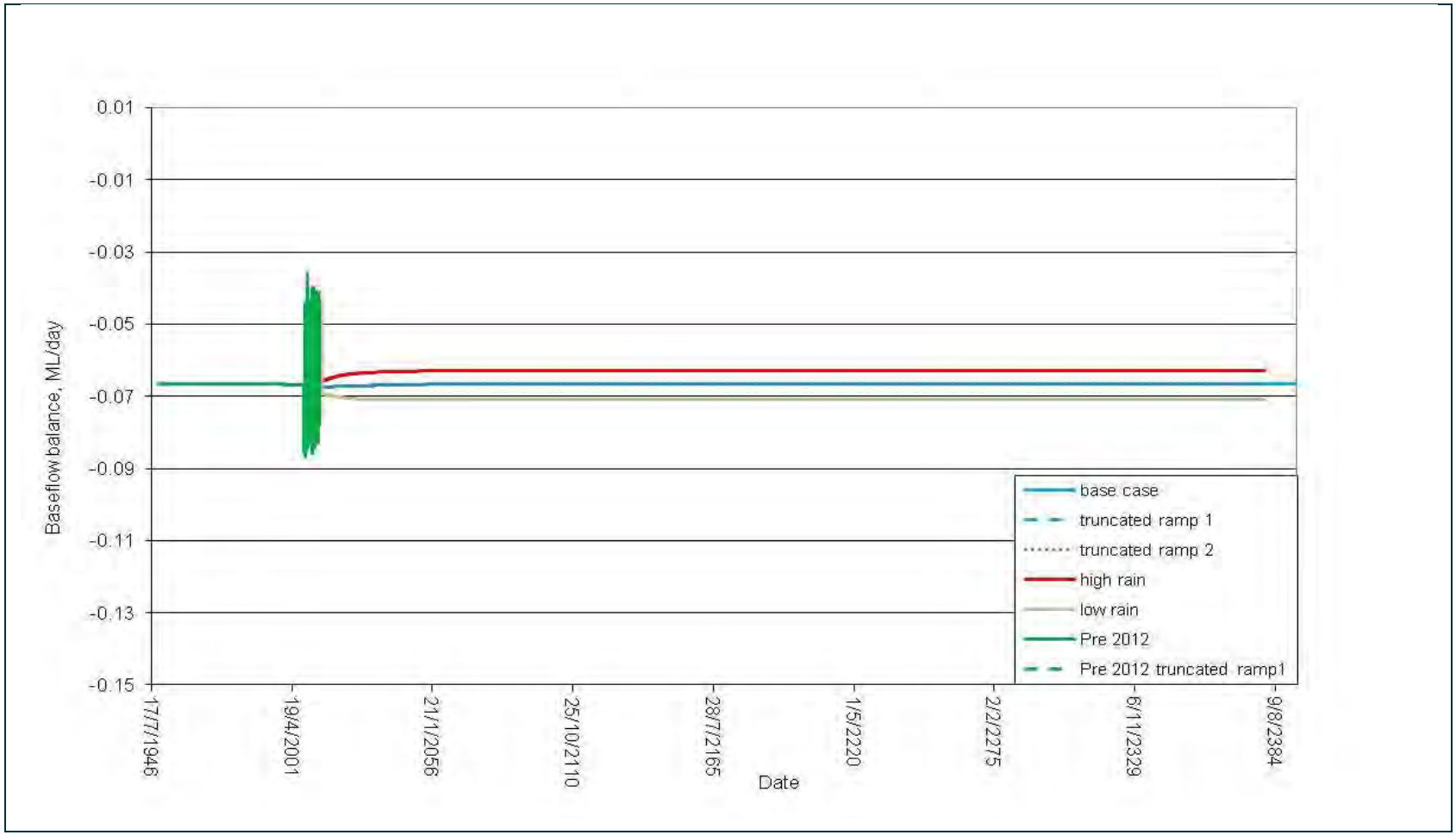

Figure C14 Estimates of baseflow balance (Long Swamp)

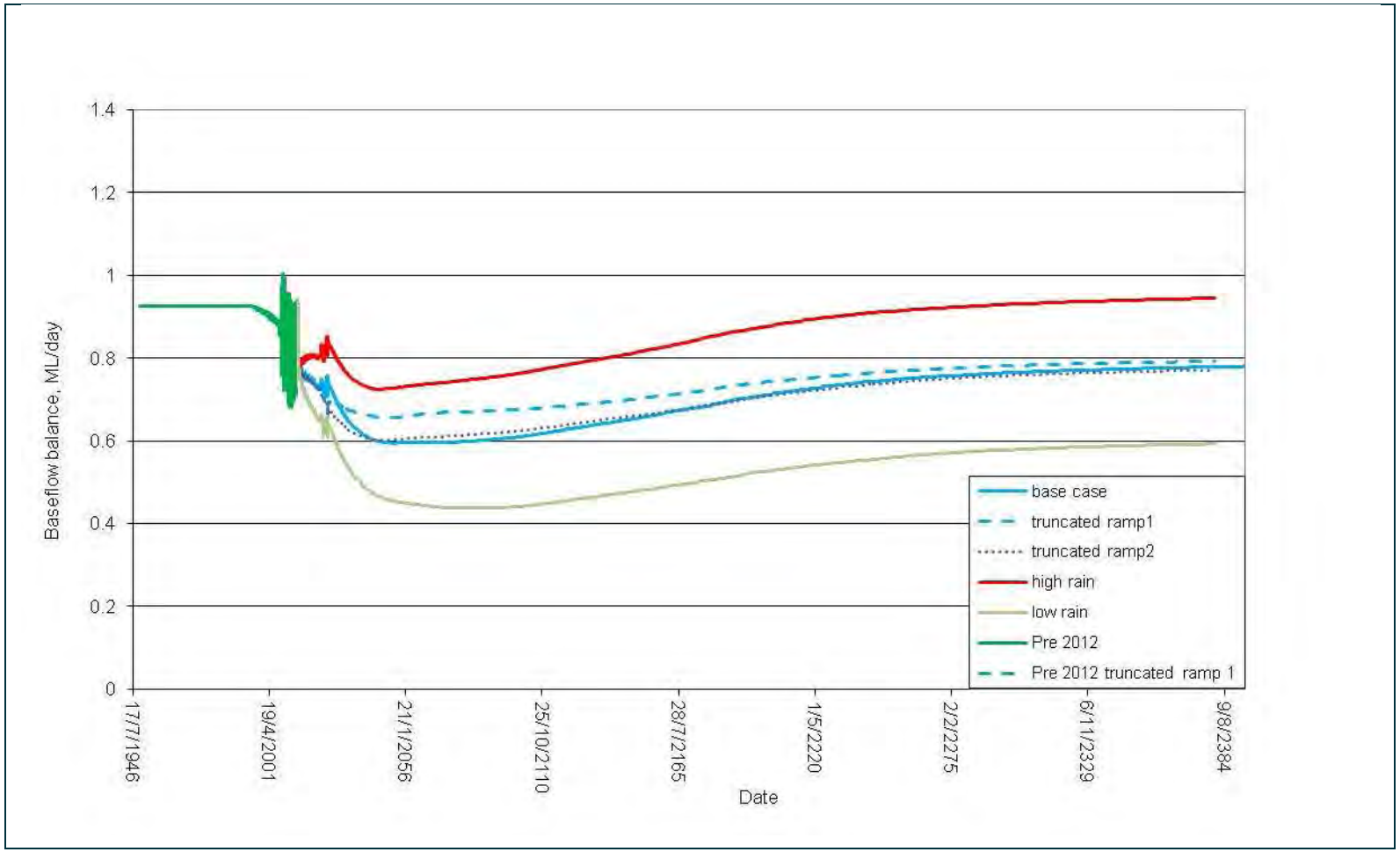

Figure C15 Estimates of baseflow balance (Marangaroo Creek)

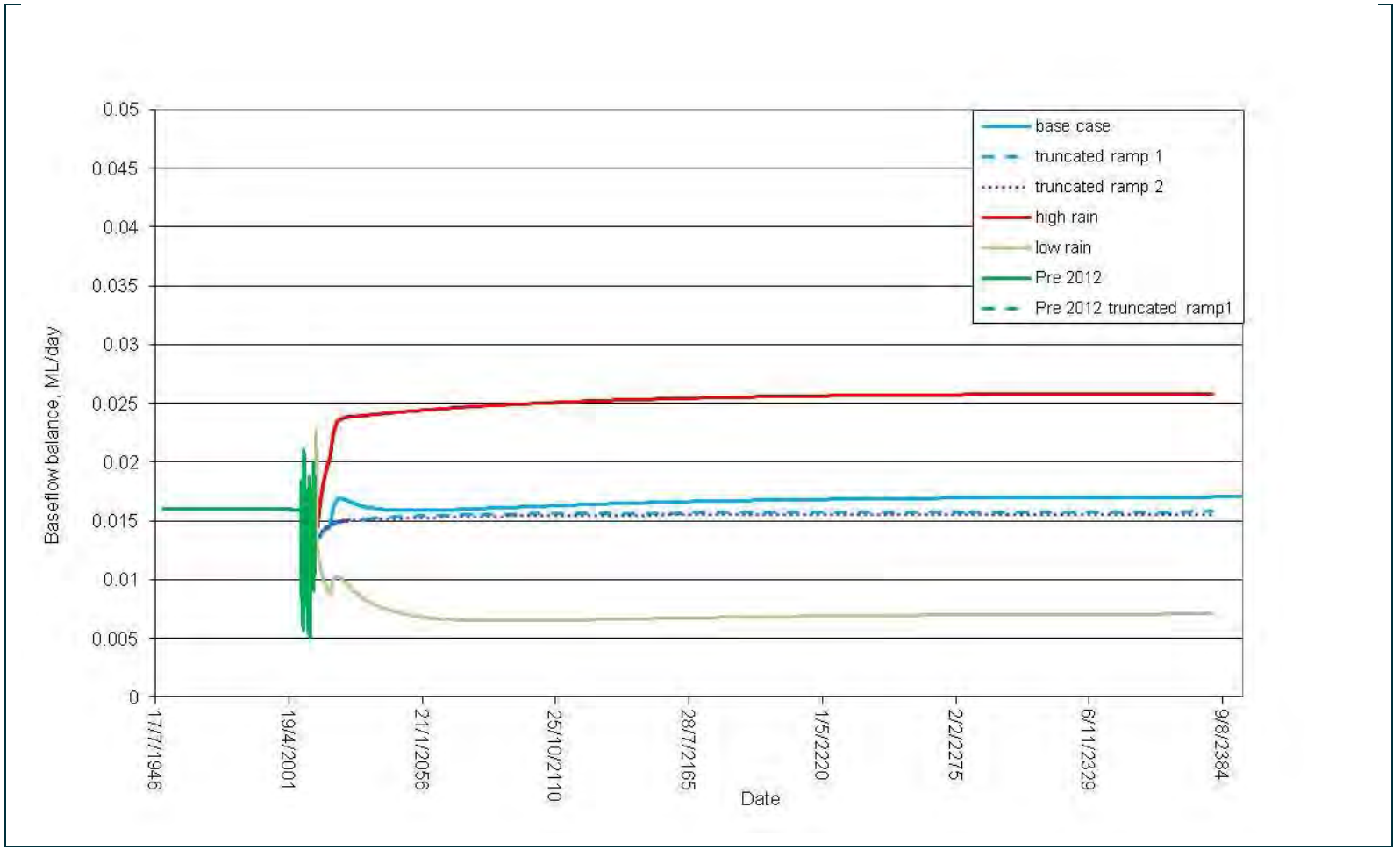

Figure C16 Estimates of baseflow balance (Nine-Mile Swamp)

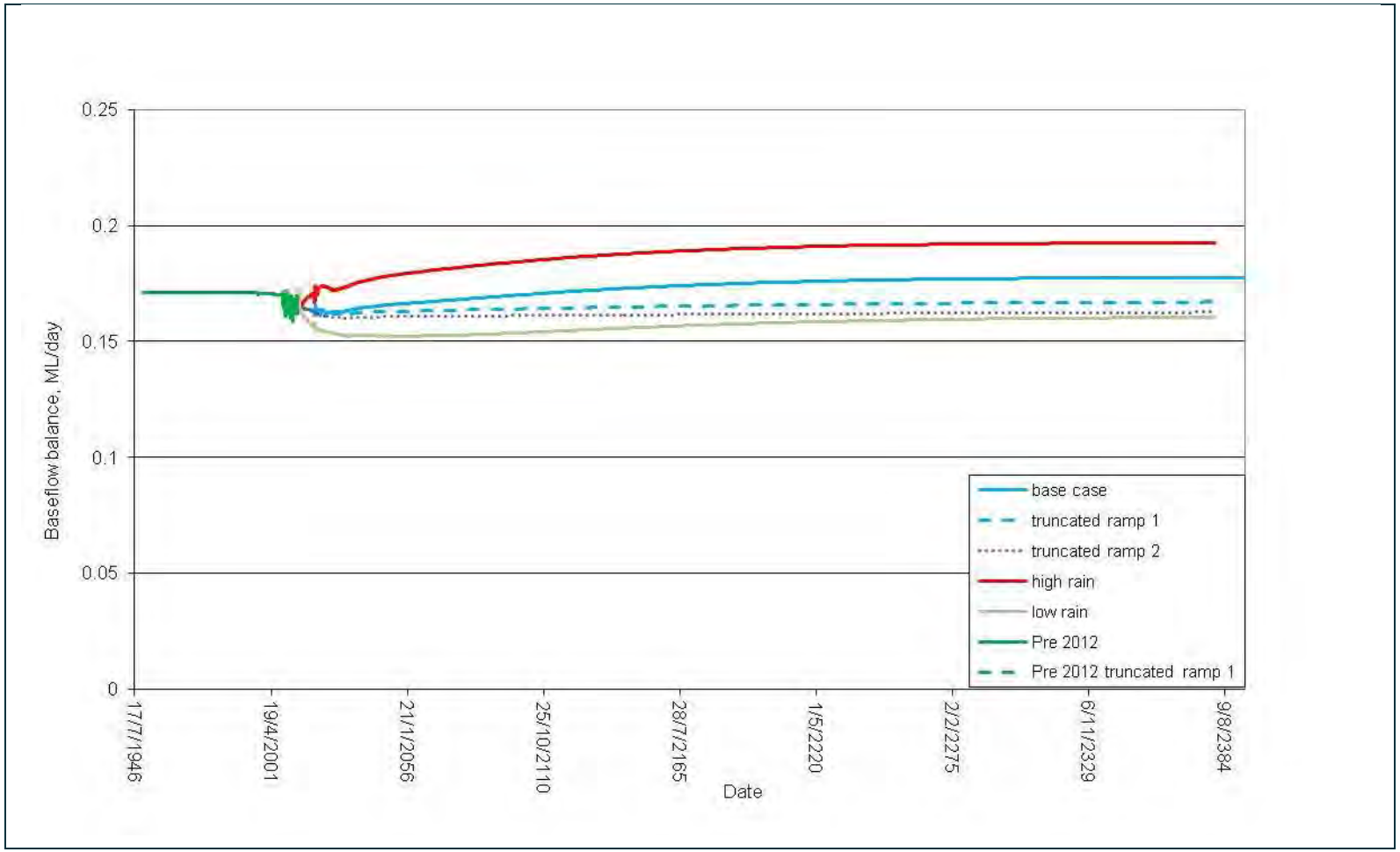

Figure C17 Estimates of baseflow balance (Paddy's Creek)

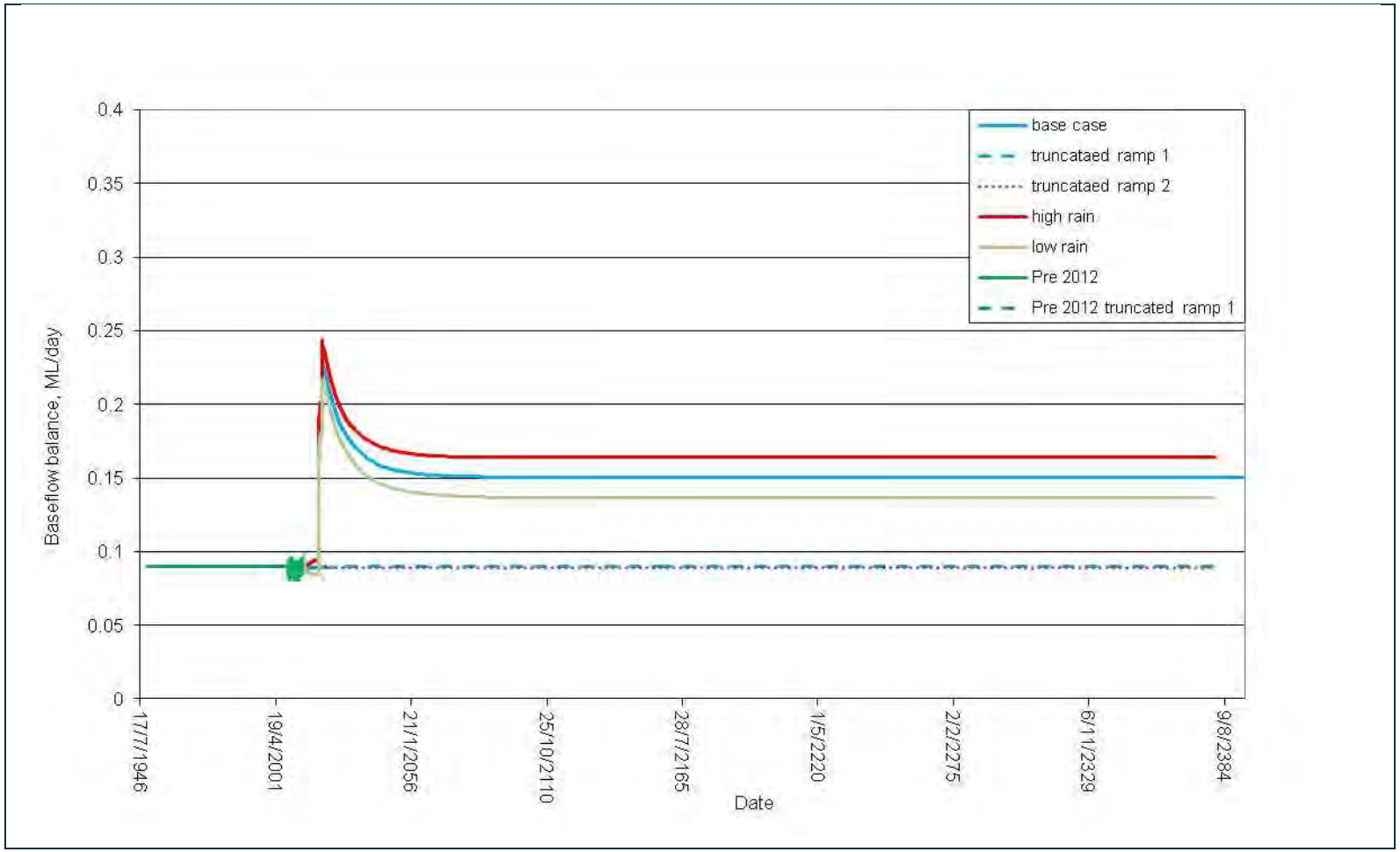

Figure C18 Estimates of baseflow balance (Pine Swamp)

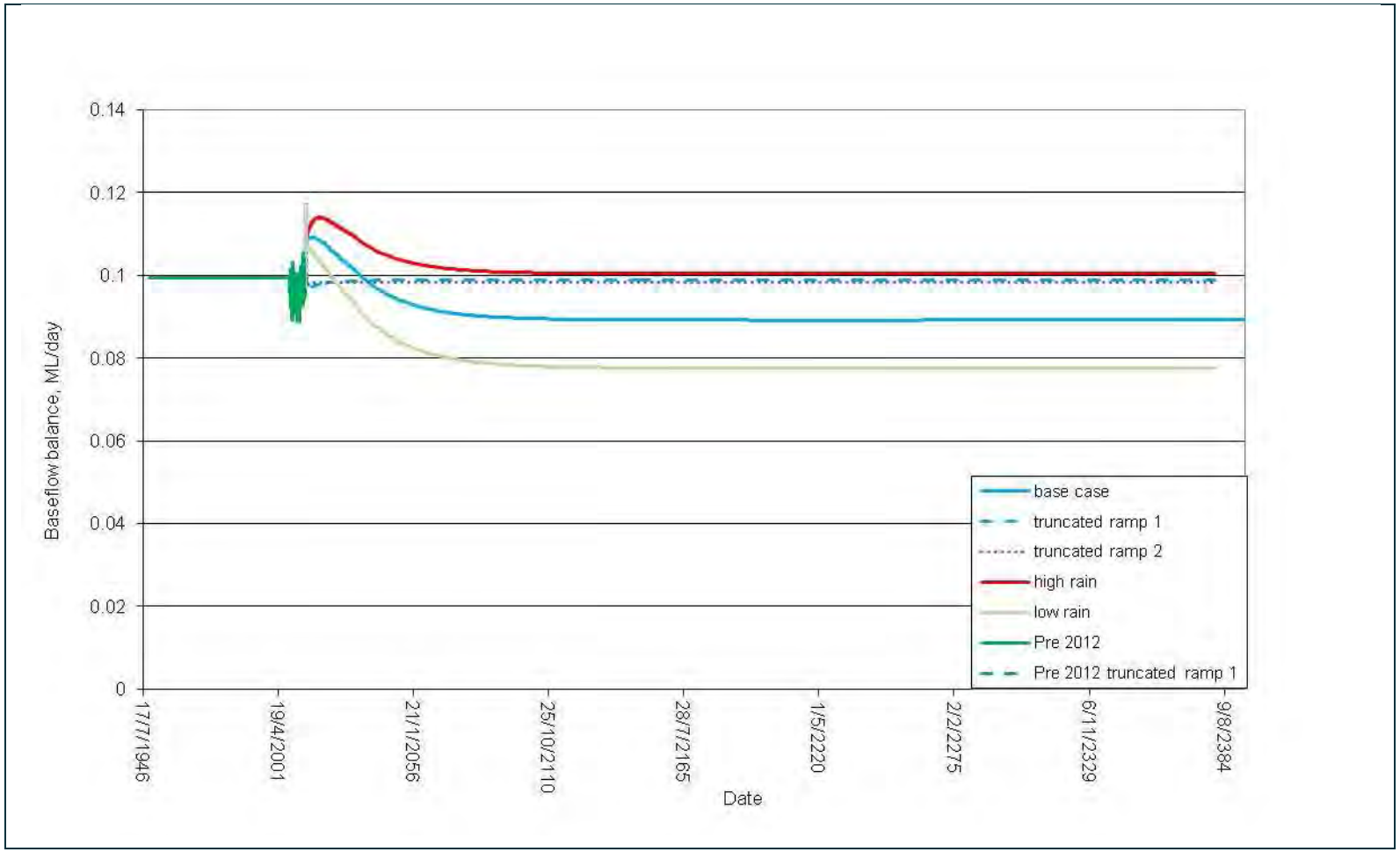

Figure C19 Estimates of baseflow balance (Sunnyside Swamp)

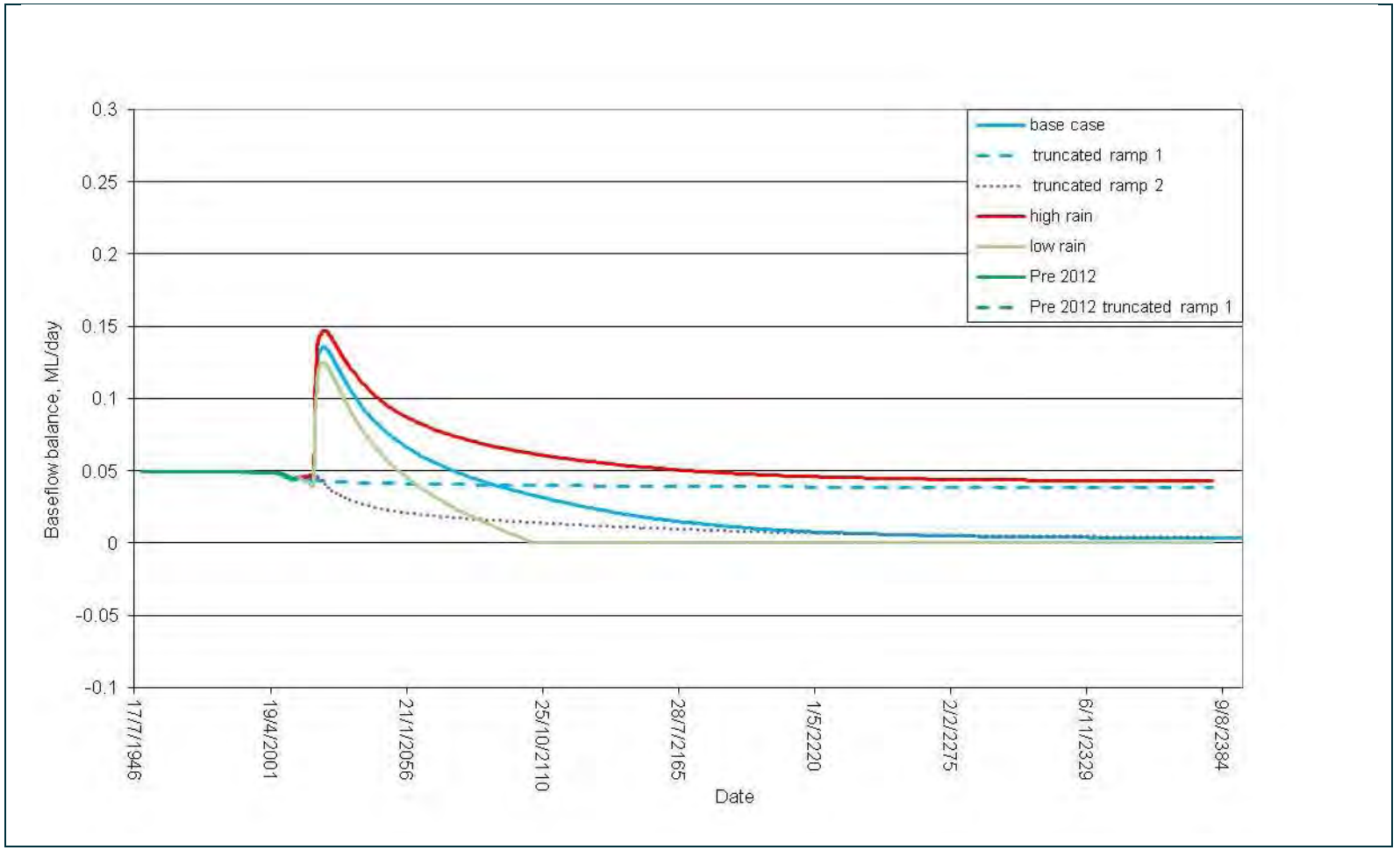

Figure C20 Estimates of baseflow balance (Tri-star Swamp)

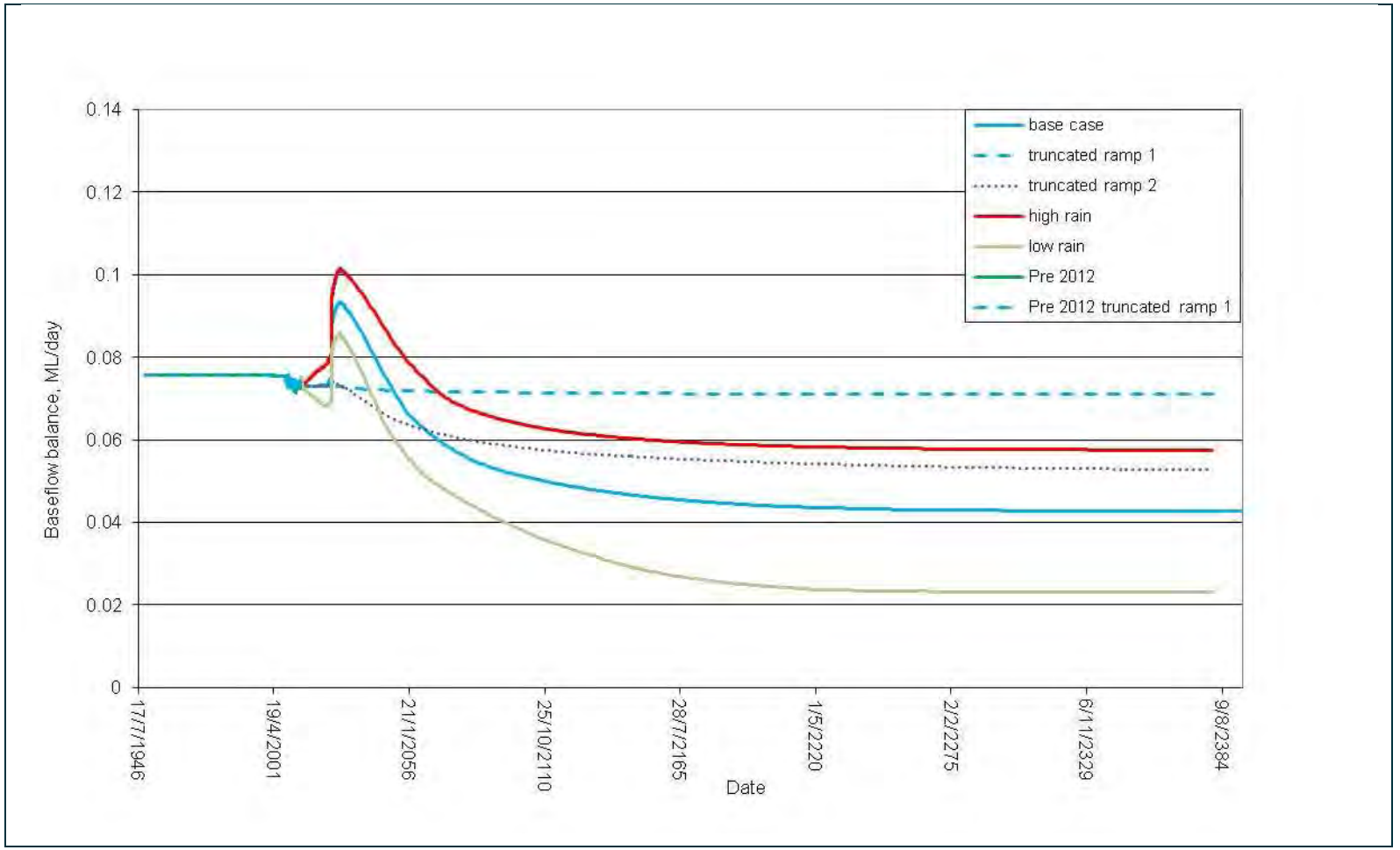

Figure C21 Estimates of baseflow balance (Twin-Gully Swamp)

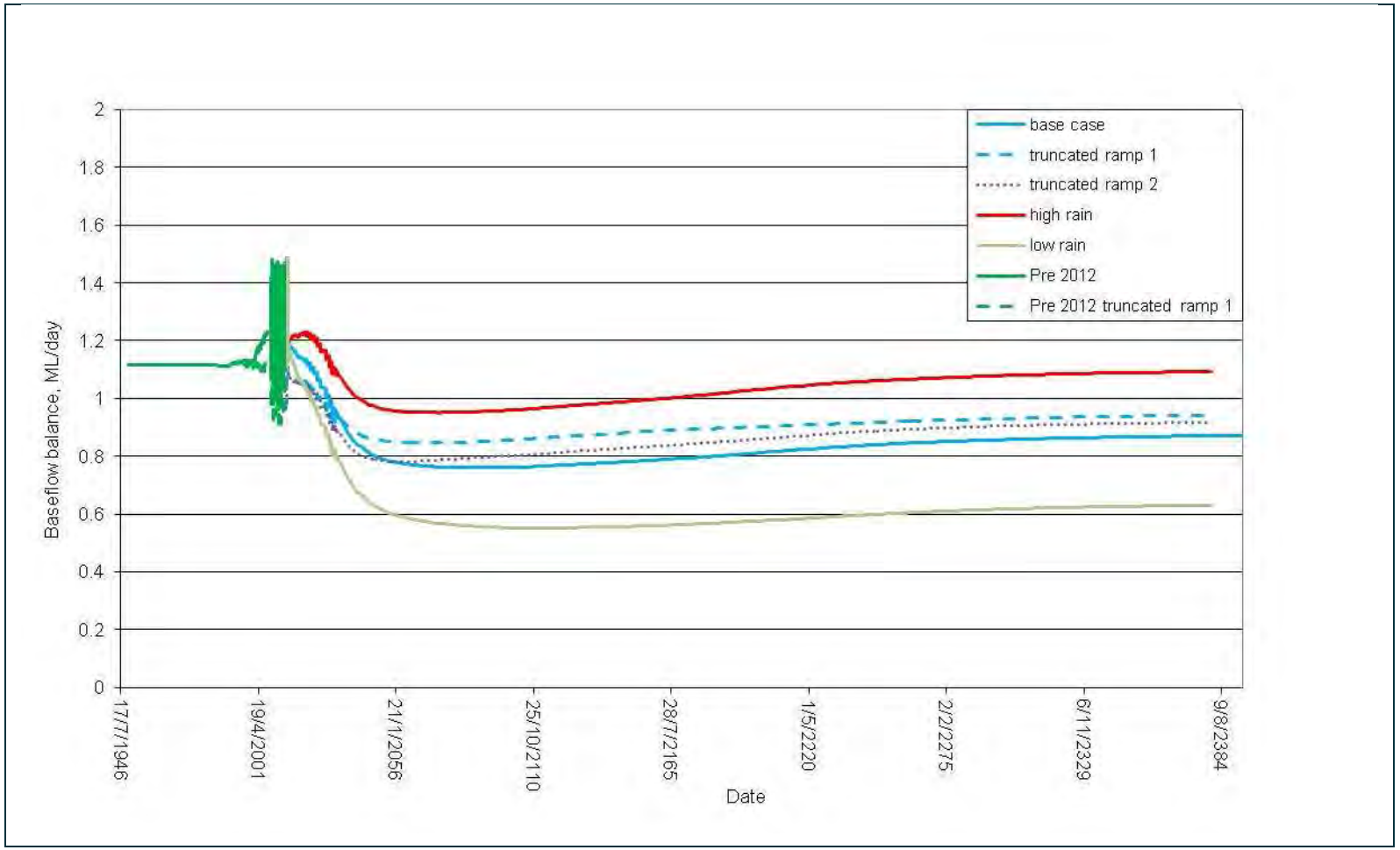

Figure C22 Estimates of baseflow balance (Wolgan River)

EARTH SCIENCE AND RESOURCE ENGINEERING
www.csiro.au

Appendix D
Drawdowns - Prediction and Recovery Periods

Angus Place and Springvale Colliery Operations

Groundwater Assessment

D P Adhikary and A Wilkins
Report No EP132799
May 2013

Springvale Colliery and Angus Place Colliery

Citation

Adhikary, DP and Wilkins, A (2013) Angus Place and Springvale Colliery operations groundwater assessment. Appendix D – Drawdowns – Prediction and Recovery Periods. Report No EP132799.

Copyright and disclaimer

Important disclaimer

Figures

Simulated Drawdowns

The simulated drawdowns for the Lithgow Seam, AQ1, AQ2, AQ3, AQ4, AQ5, AQ6 and the top of the model (i.e. the ground surface) following 5, 11 and 18 years of mining within the predictive simulation period and the recovery period at 50 and 100 years after mining are provided in this appendix.

Figure D1 to Figure D21 show the simulated drawdowns with respect to the pre-mining groundwater conditions and Figure D22 to Figure D42 show the simulated drawdowns with respect to groundwater levels at 1 January 2013.

Figure D43 to Figure D56 show the simulated drawdowns with respect to the pre-mining groundwater conditions at 50 and 100 years after mining and Figure D57 to Figure D70 show the simulated drawdowns with respect to groundwater levels at 1 January 2013.

Figure D71 to 88 show the drawdown in the Lithgow seam and at the ground surface for the "No New", "No APE" and "No New SV" mining scenarios.

Predictive Period with respect to Pre-mining Groundwater Condition

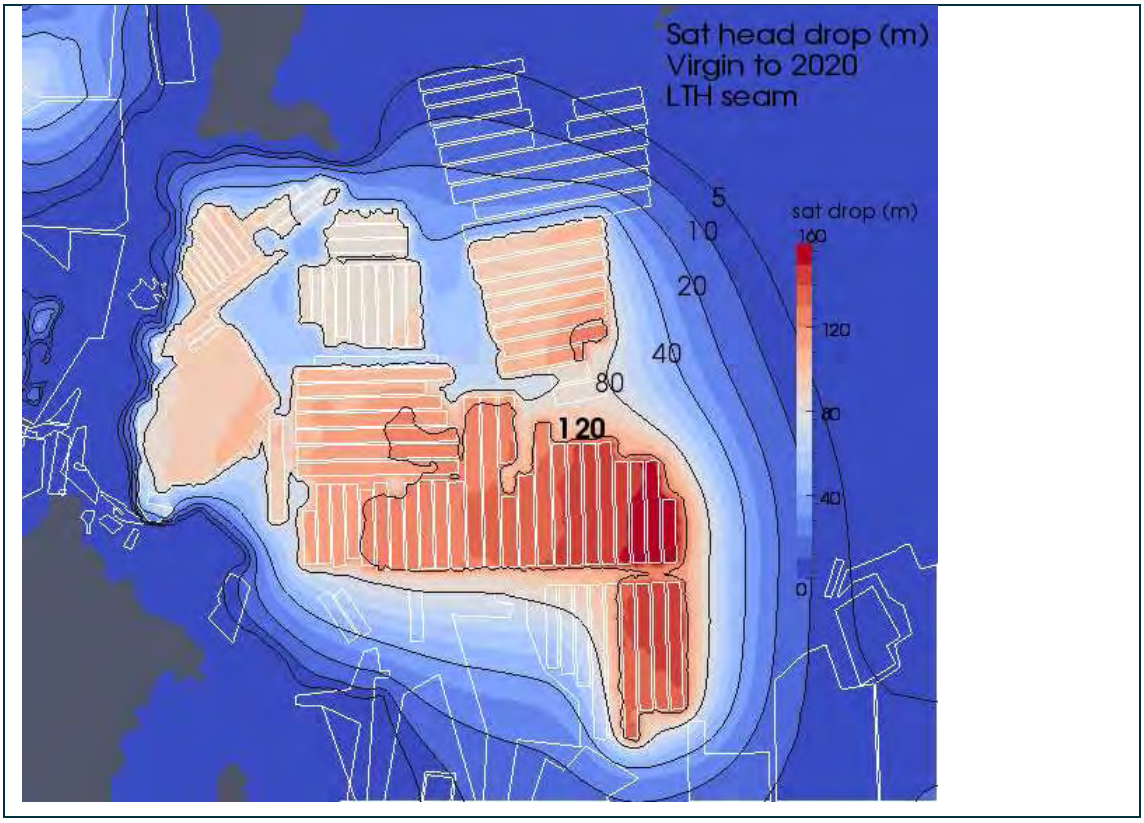

Figure D1 Distribution of drawdowns in the Lithgow Seam in 2020 with respect to pre-mining groundwater condition

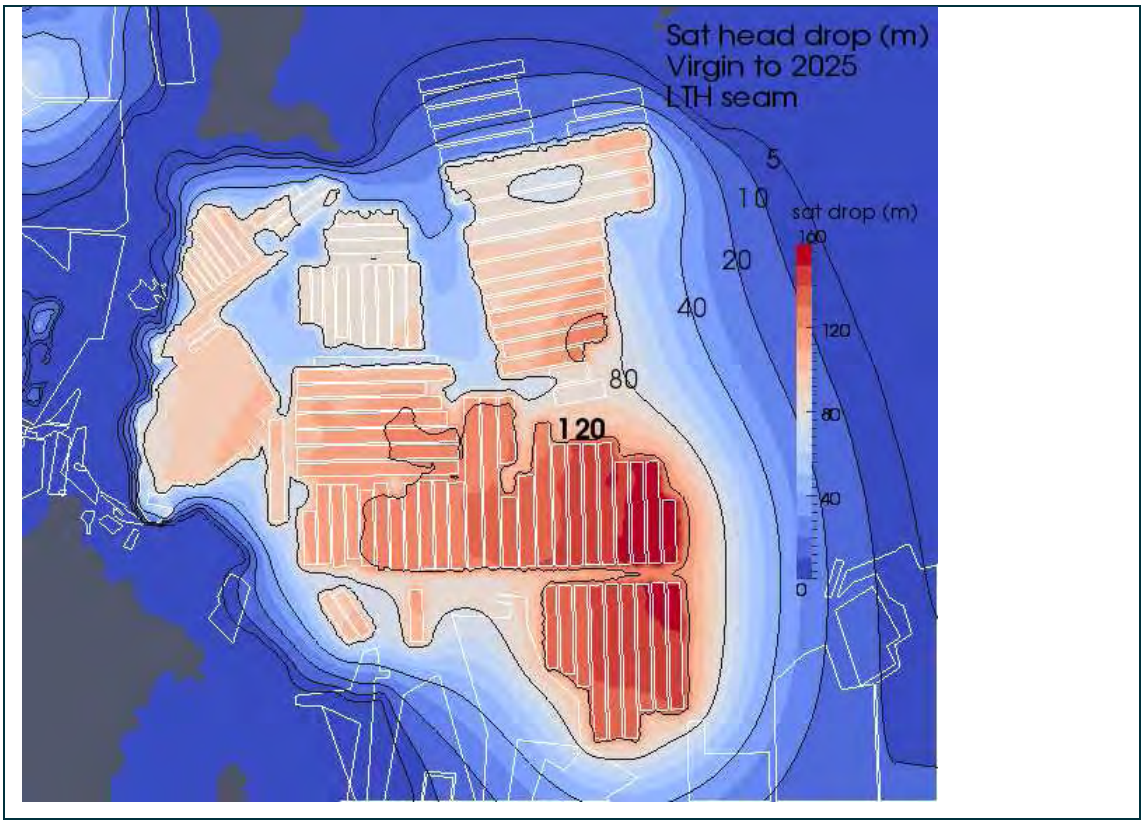

Figure D2 Distribution of drawdowns (m) in the Lithgow Seam in 2025 with respect to pre-mining groundwater condition

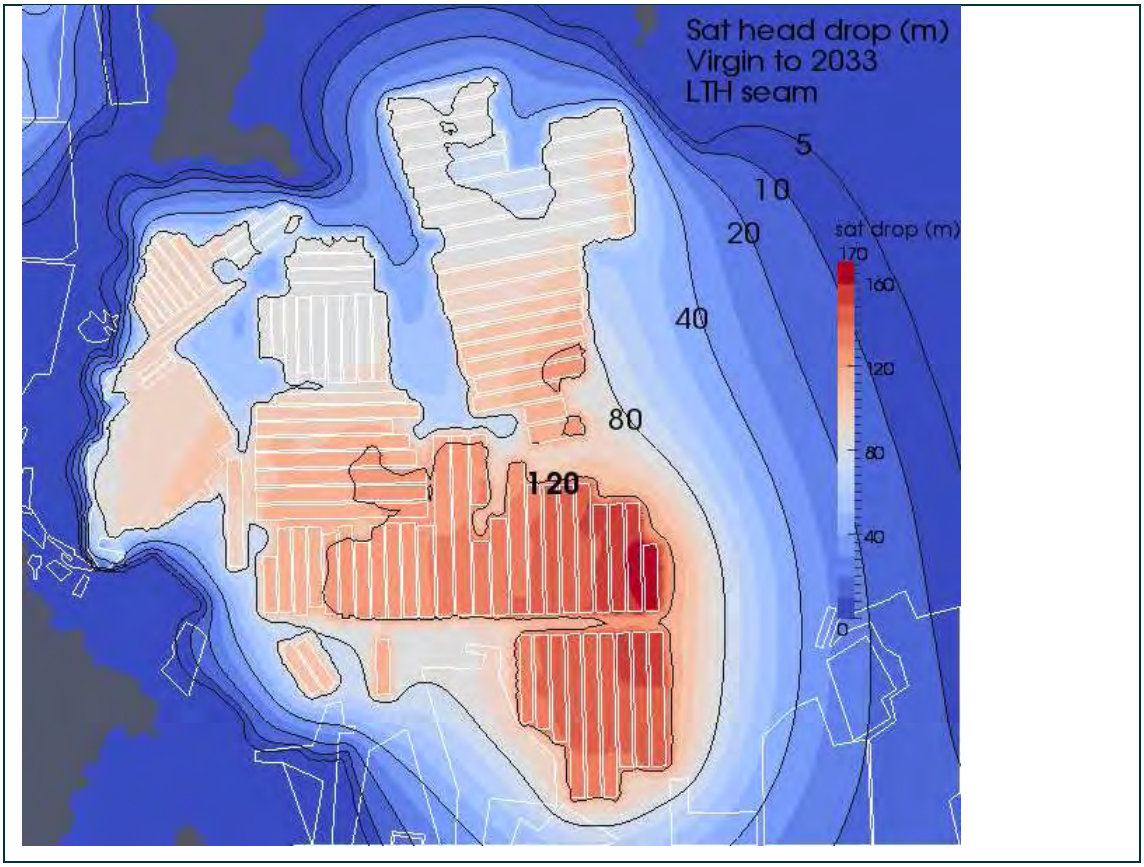

Figure D3 Distribution of drawdowns in the Lithgow Seam in 2033 with respect to pre-mining groundwater condition

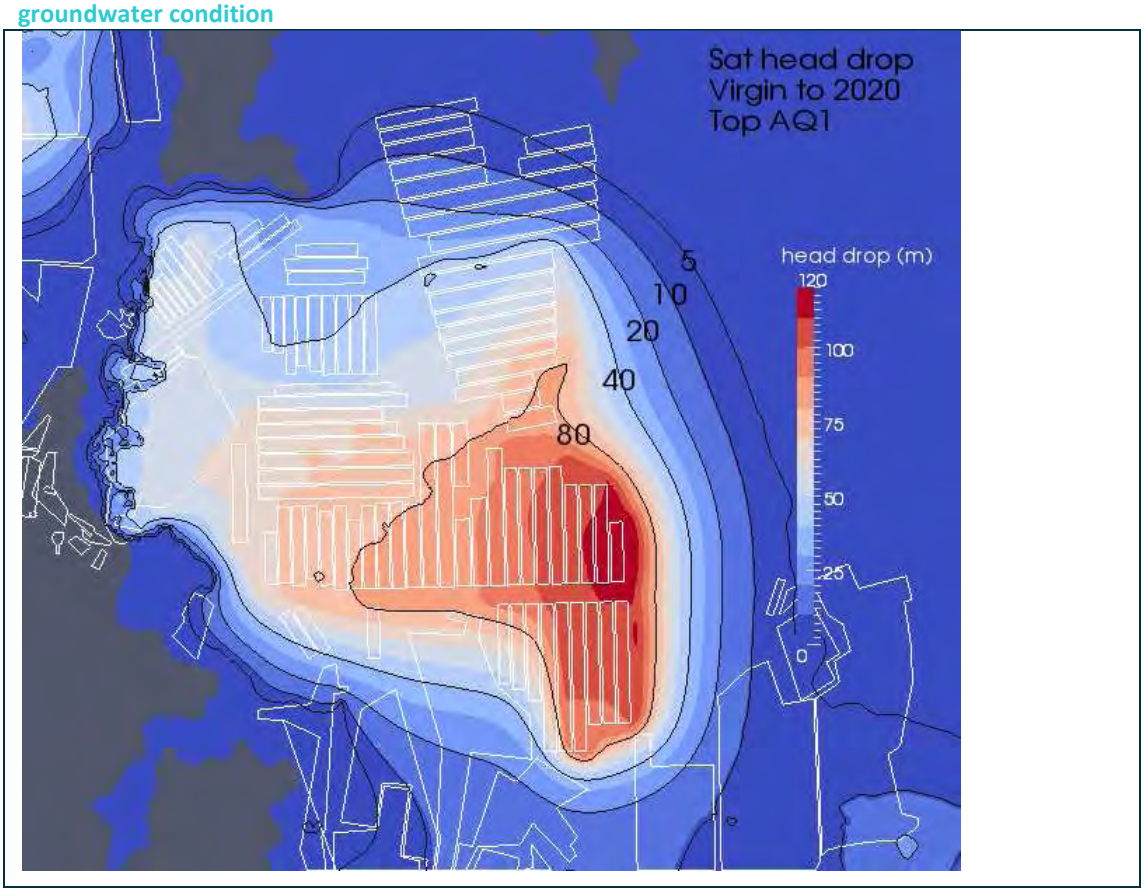

Figure D4 Distribution of drawdowns in AQ1 in 2020 with respect to pre-mining groundwater condition

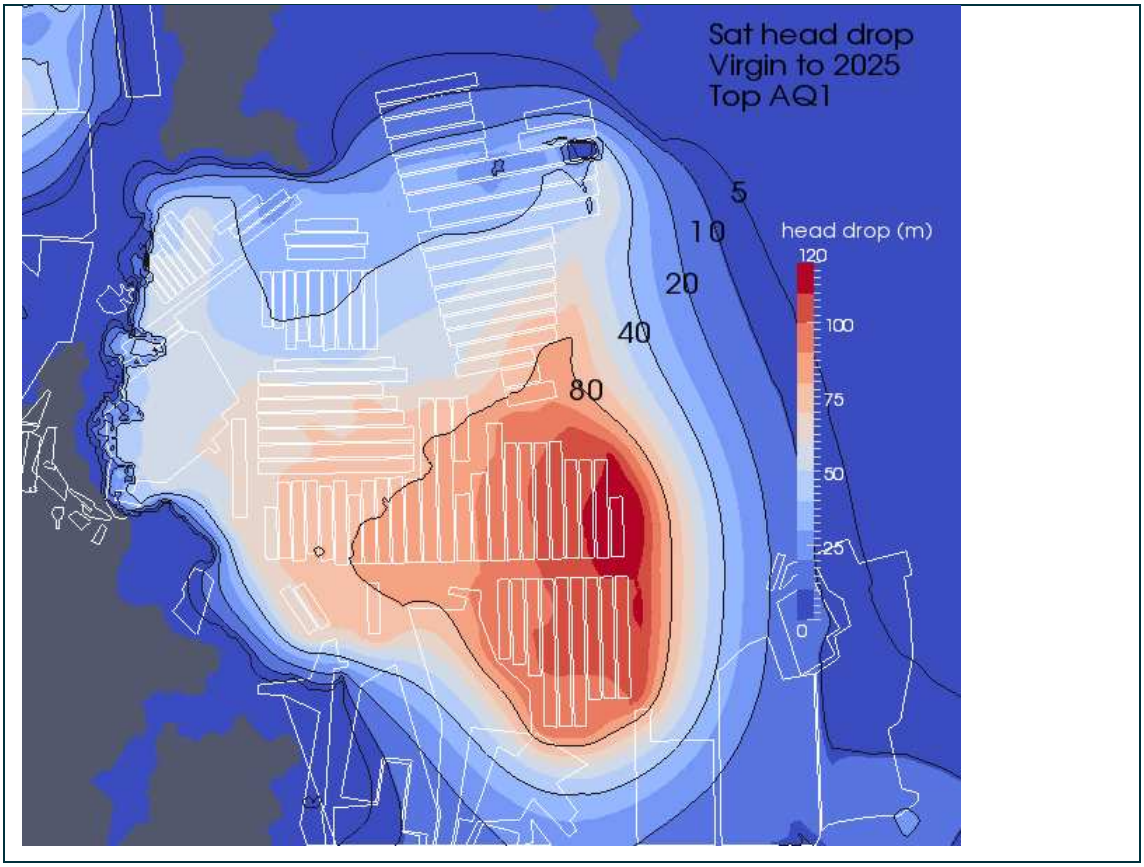

Figure D5 Distribution of drawdowns in AQ1 in 2025 with respect to pre-mining groundwater condition

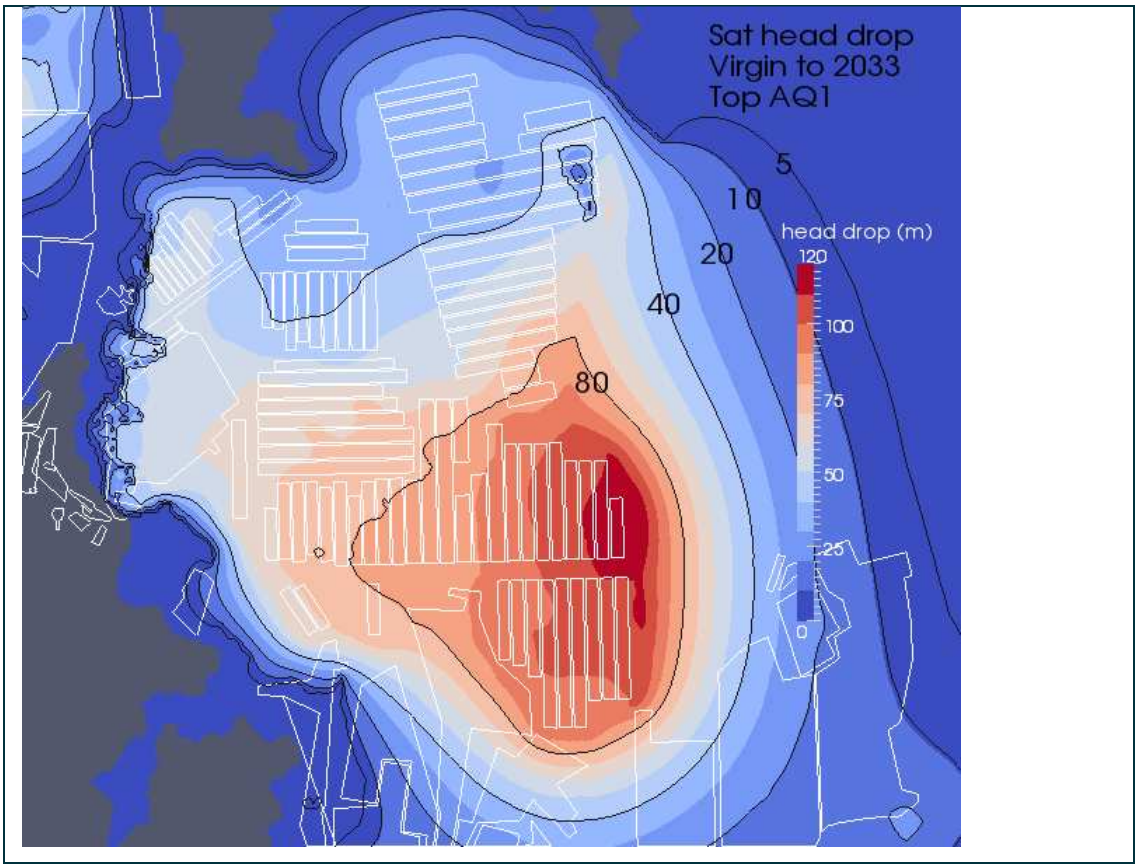

Figure D6 Distribution of drawdowns in AQ1 in 2033 with respect to pre-mining groundwater condition

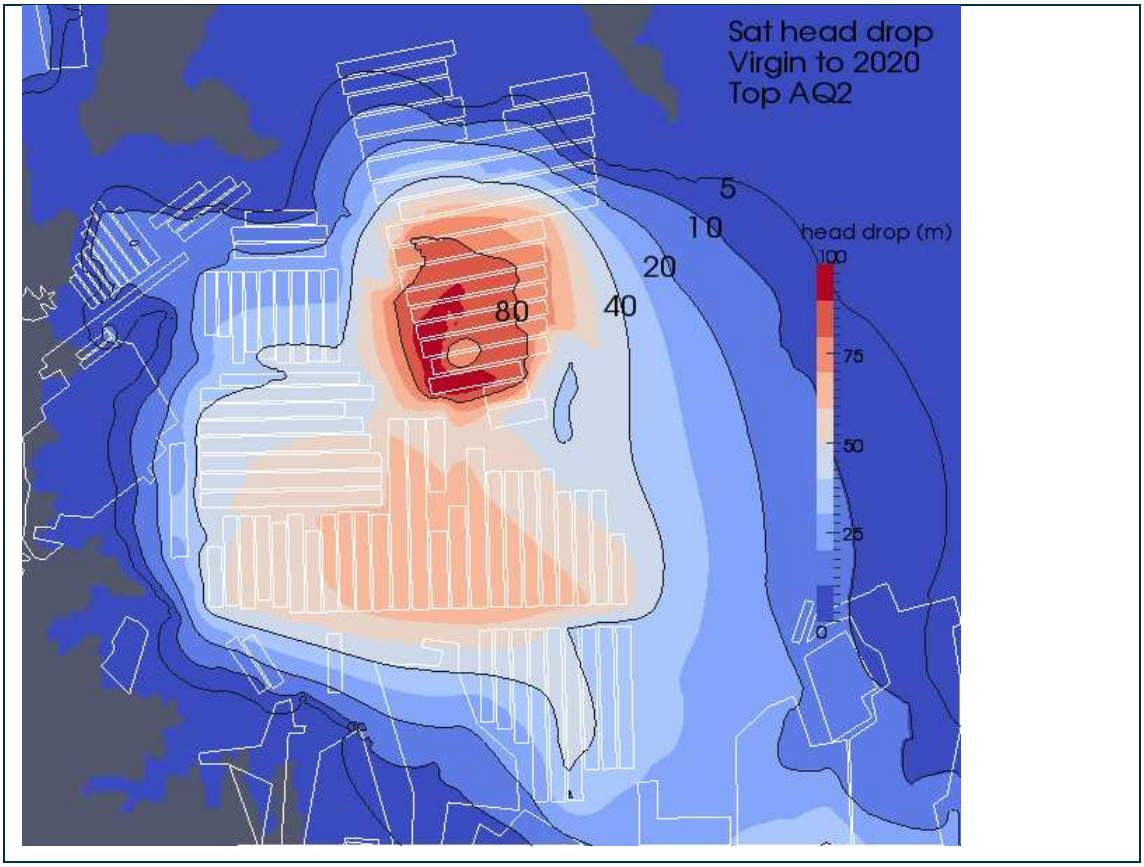

Figure D7 Distribution of drawdowns in AQ2 in 2020 with respect to pre-mining groundwater condition

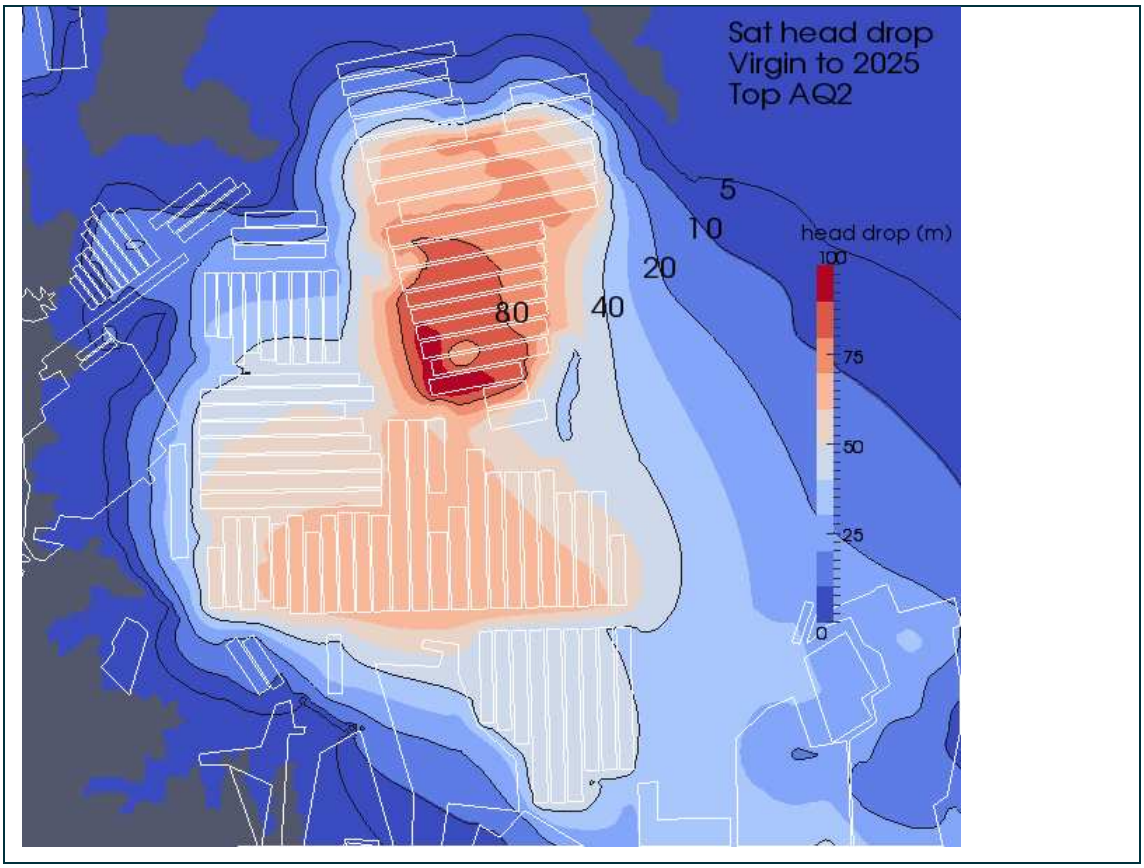

Figure D8 Distribution of drawdowns in AQ2 in 2025 with respect to pre-mining groundwater condition

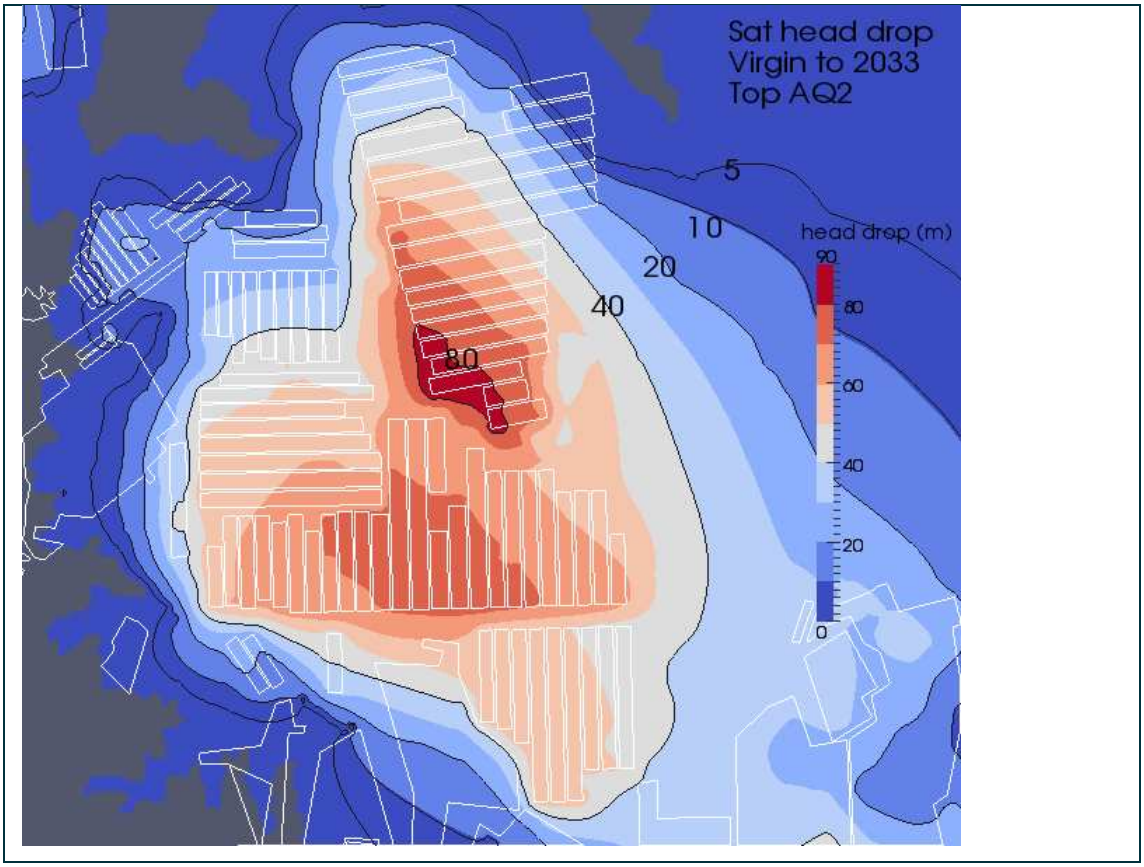

Figure D9 Distribution of drawdowns in AQ2 in 2033 with respect to pre-mining groundwater condition

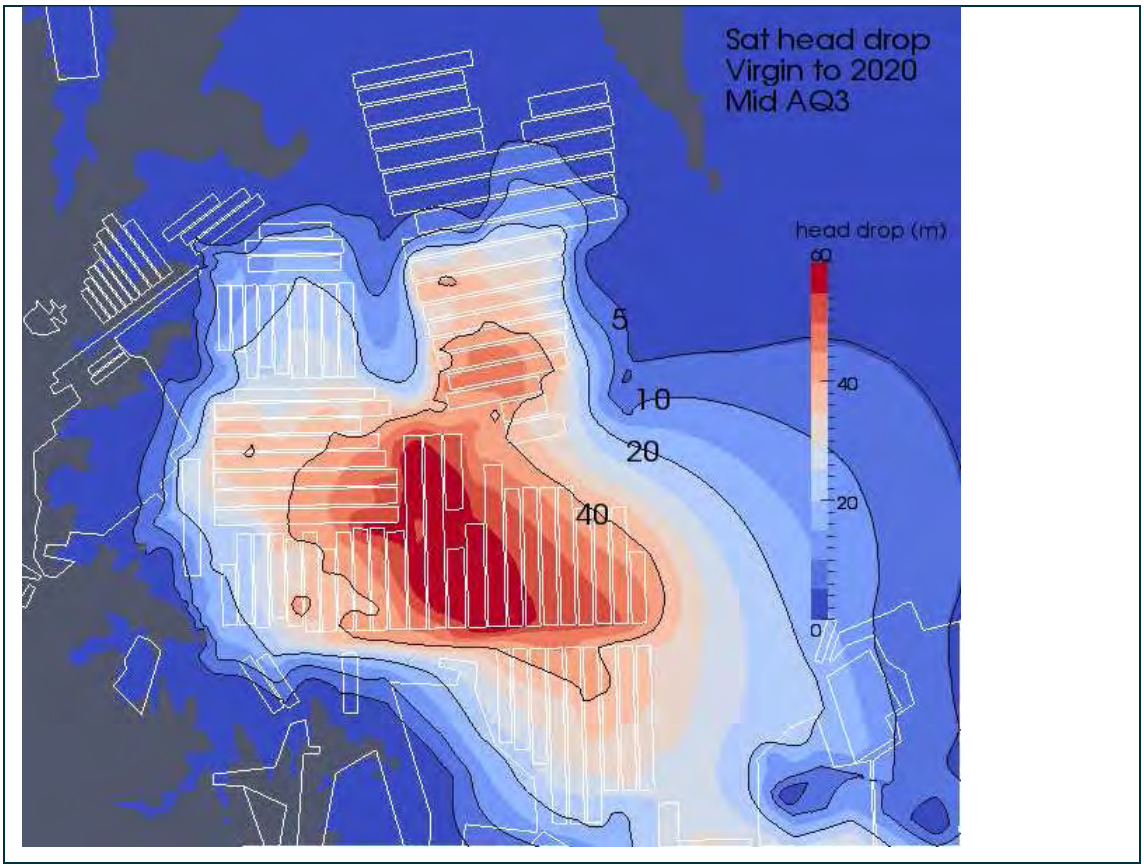

Figure D10 Distribution of drawdowns in AQ3 in 2020 with respect to pre-mining groundwater condition

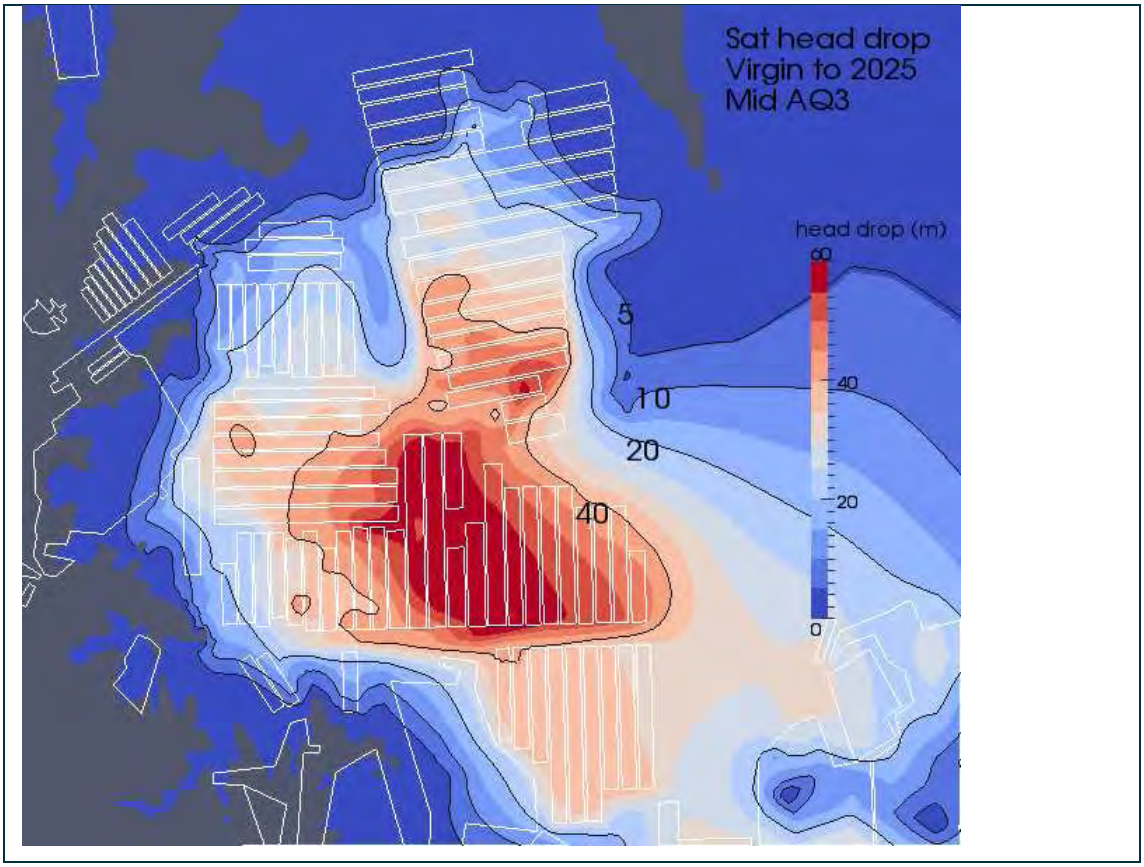

Figure D11 Distribution of drawdowns in AQ3 in 2025 with respect to pre-mining groundwater condition

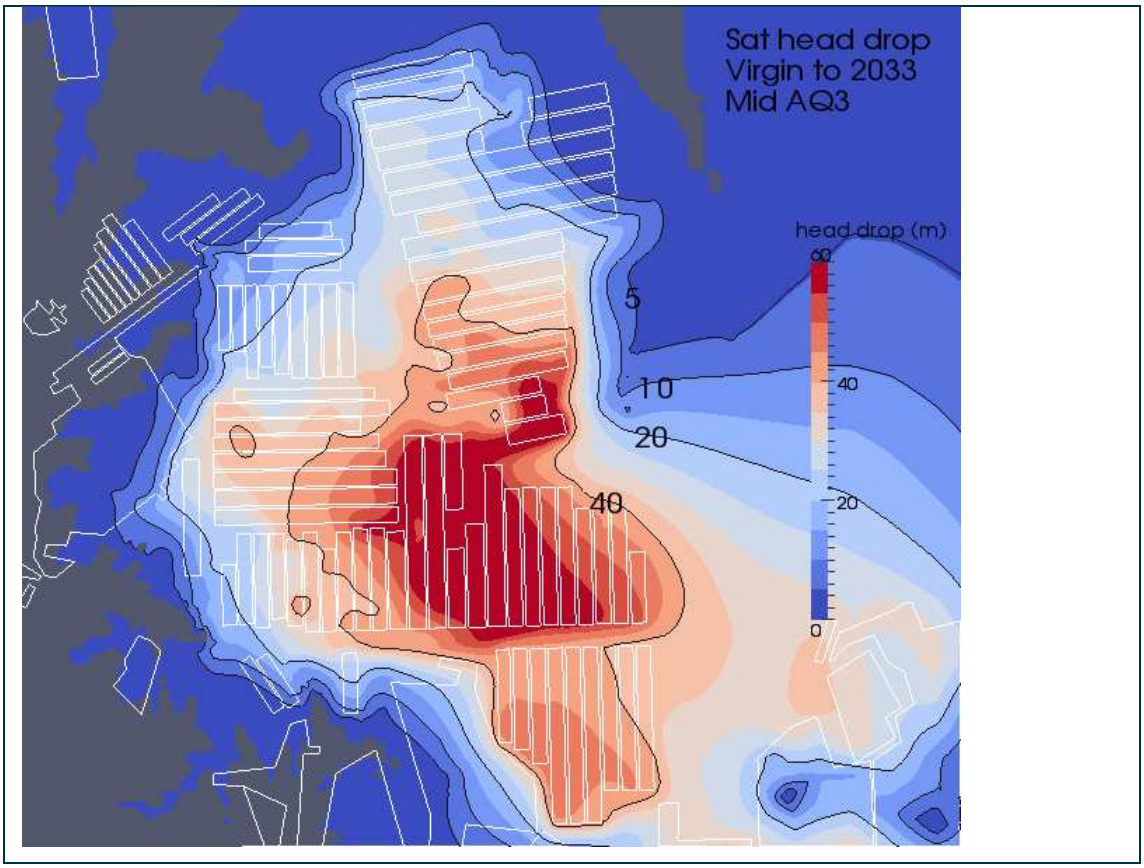

Figure D12 Distribution of drawdowns in AQ3 in 2033 with respect to pre-mining groundwater condition

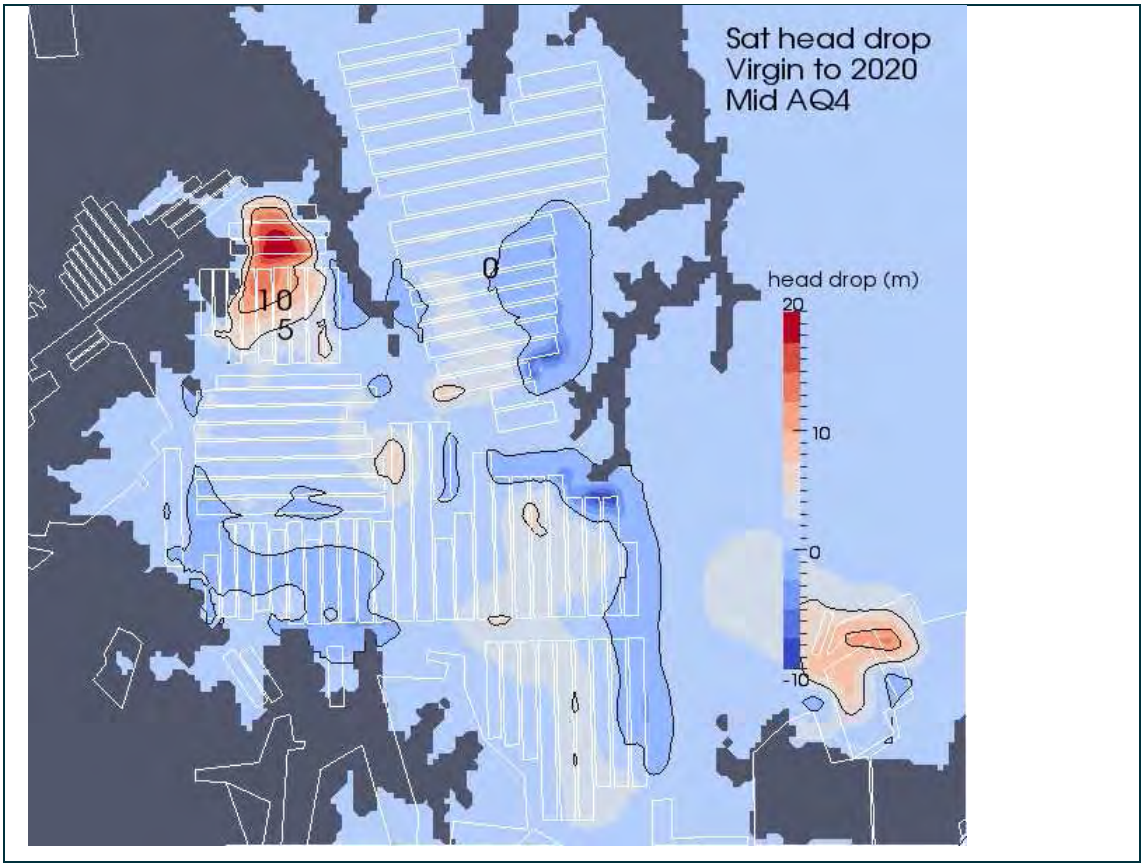

Figure D13 Distribution of drawdowns in AQ4 in 2020 with respect to pre-mining groundwater condition

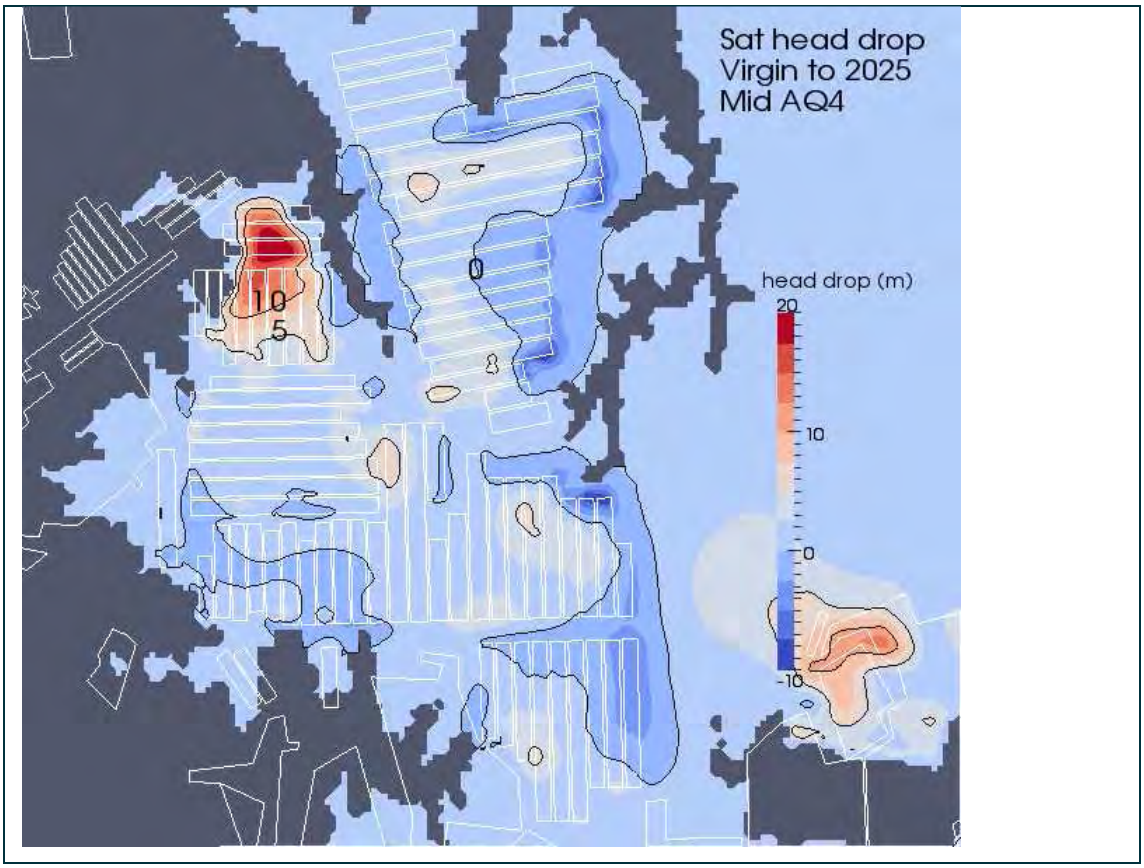

Figure D14 Distribution of drawdowns in AQ4 in 2025 with respect to pre-mining groundwater condition

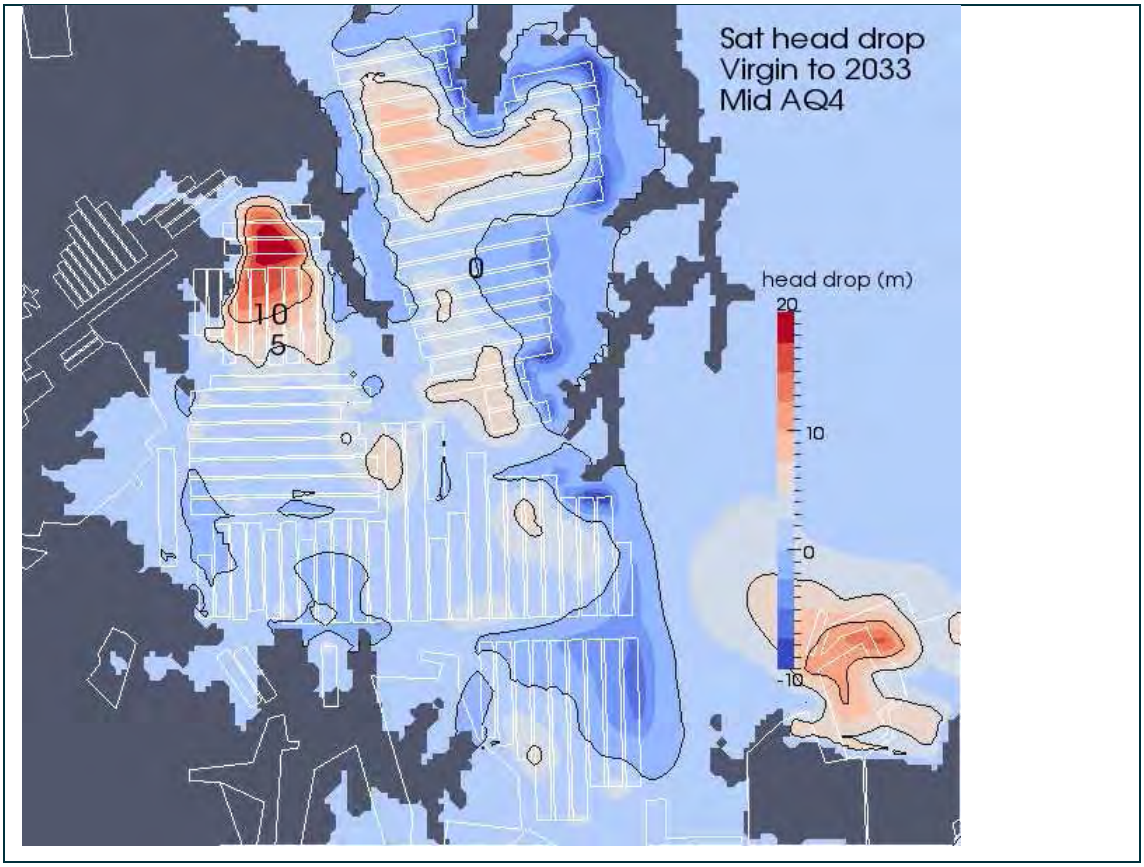

Figure D15 Distribution of drawdowns in AQ4 in 2033 with respect to pre-mining groundwater condition

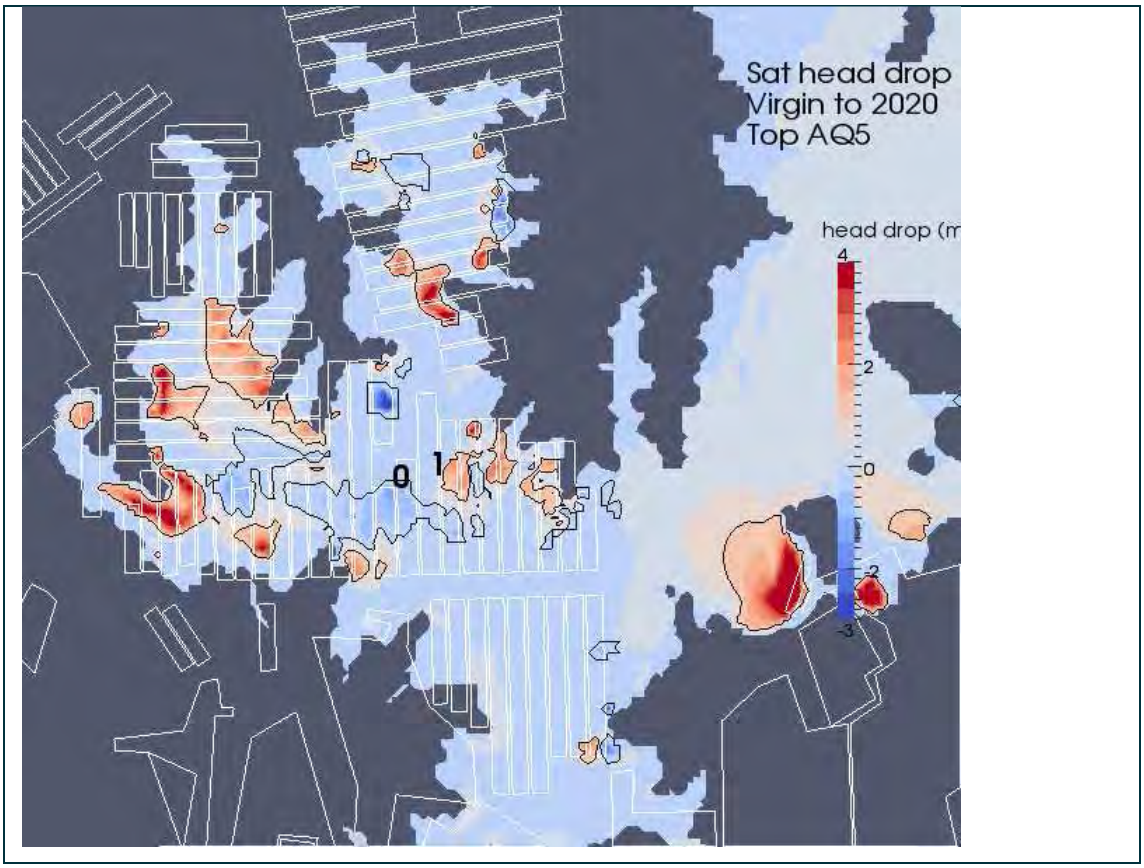

Figure D16 Distribution of drawdowns in AQ5 in 2020 with respect to pre-mining groundwater condition

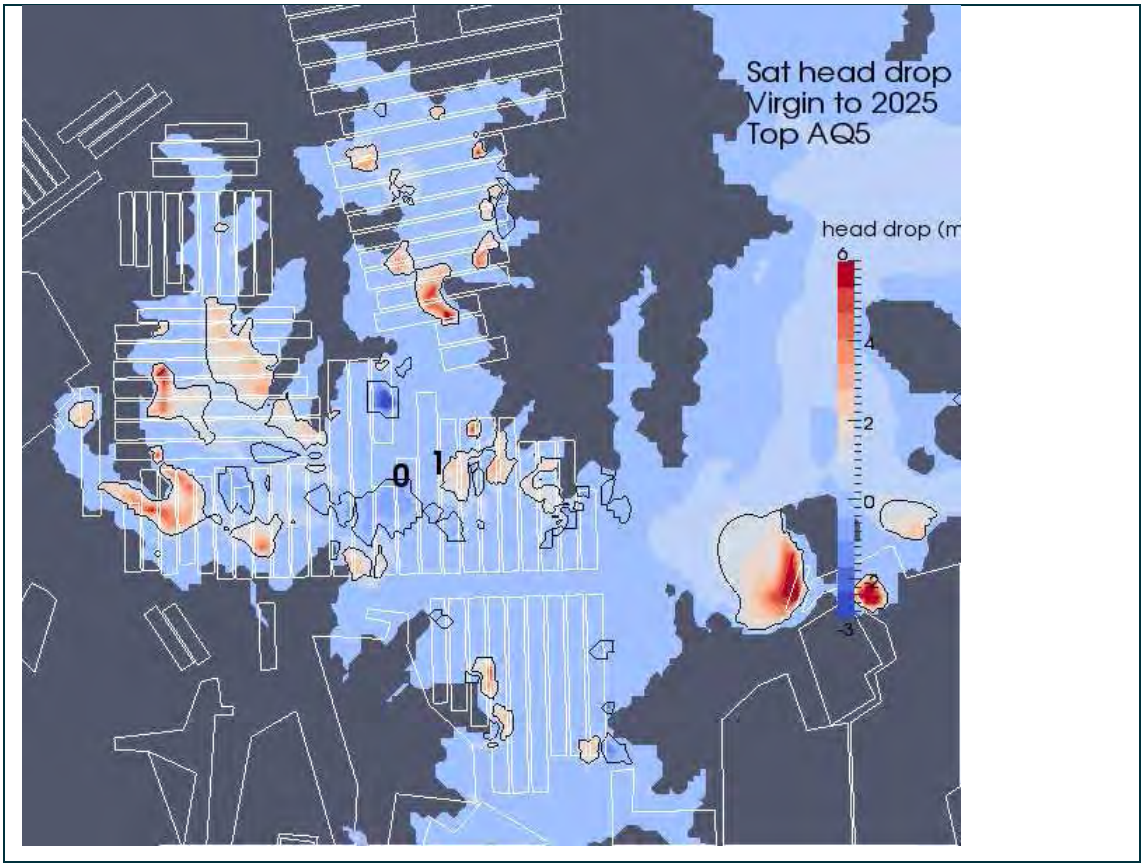

Figure D17 Distribution of drawdowns in AQ5 in 2025 with respect to pre-mining groundwater condition

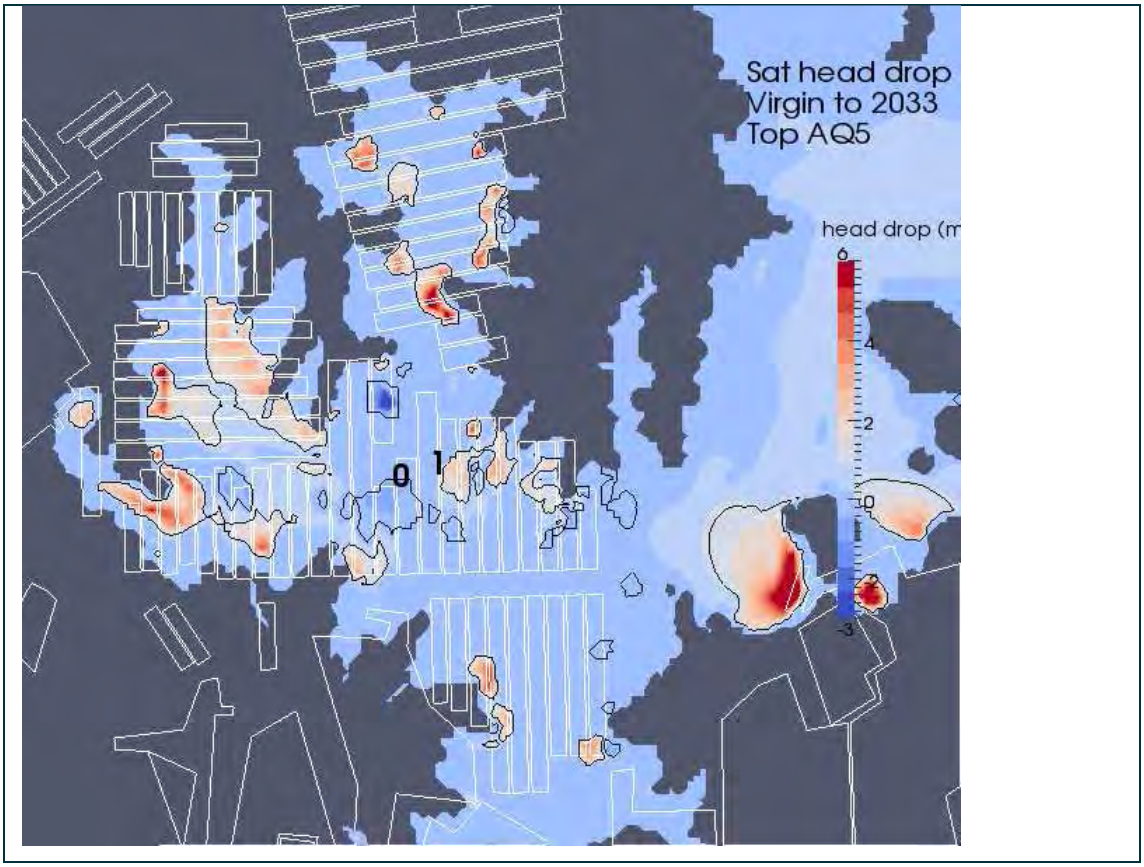

Figure D18 Distribution of drawdowns in AQ5 in 2033 with respect to pre-mining groundwater condition

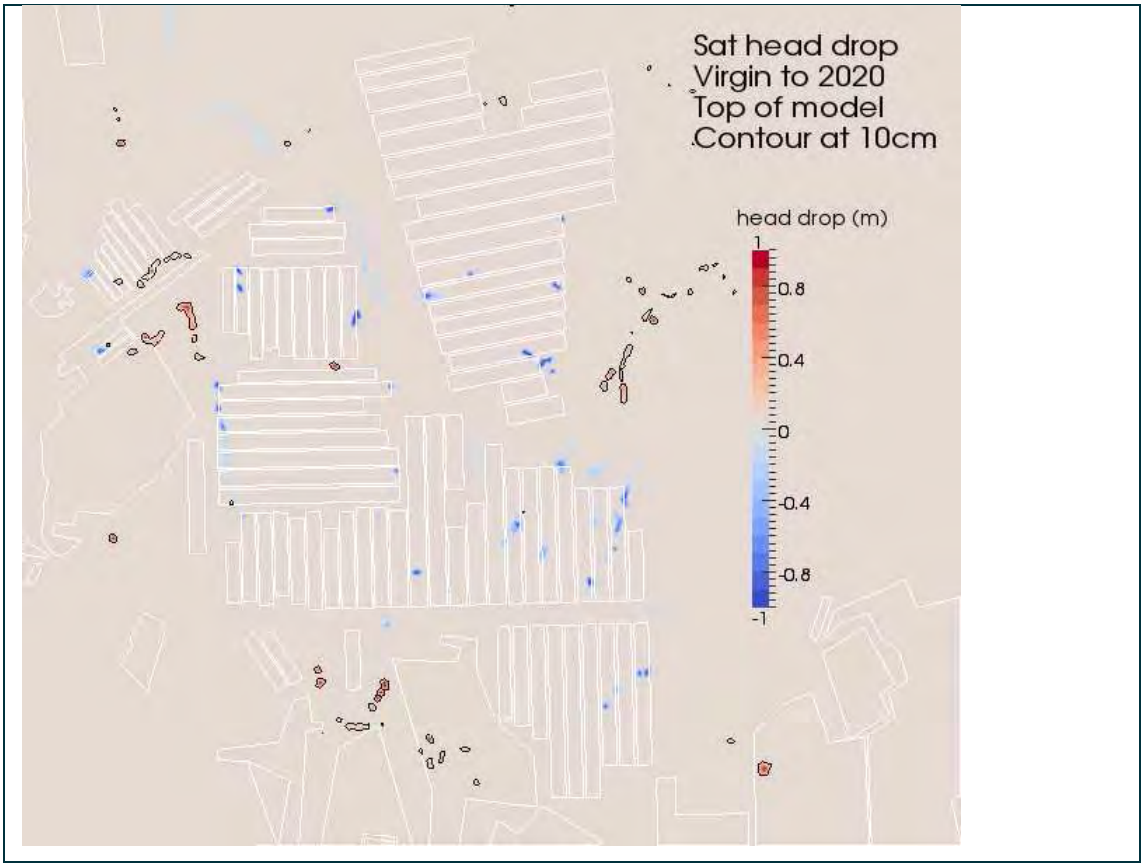

Figure D19 Distribution of head drops at the ground surface in 2020 with respect to pre-mining groundwater condition

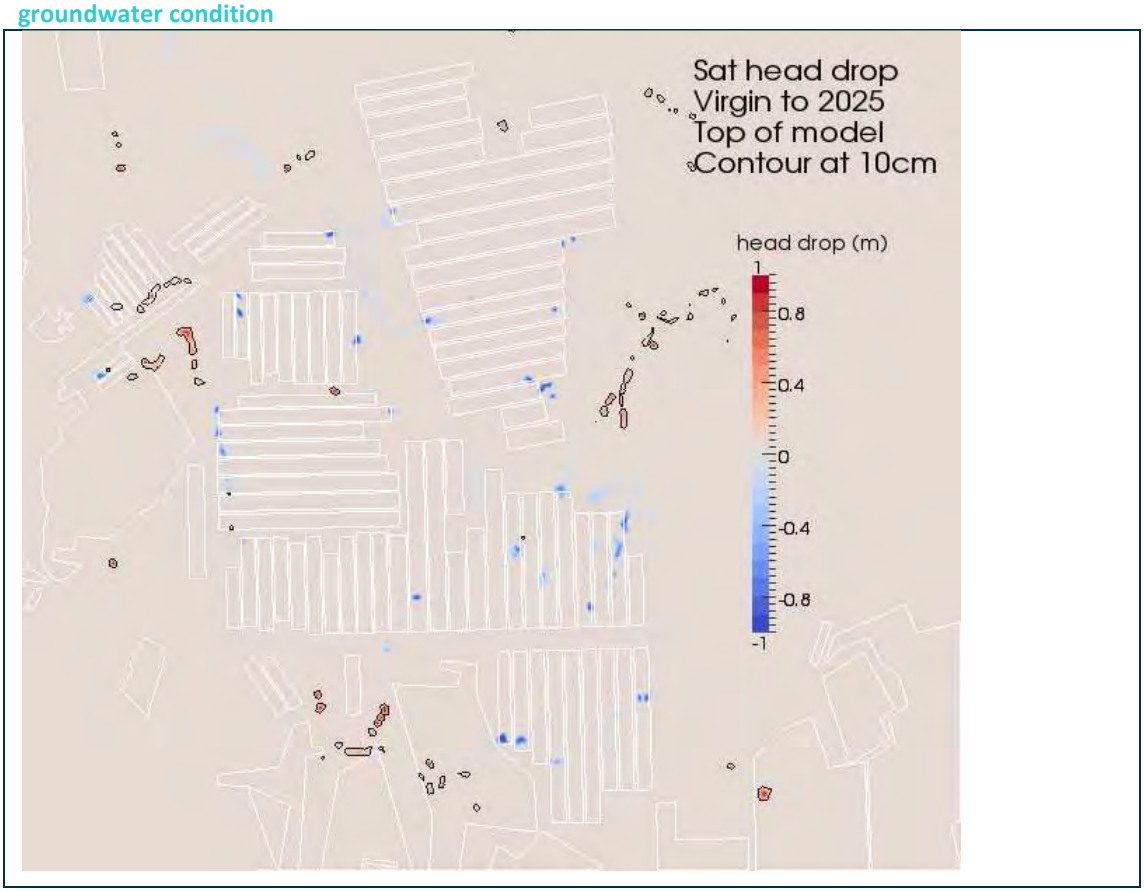

Figure D20 Distribution of head drops at the ground surface in 2025 with respect to pre-mining groundwater condition

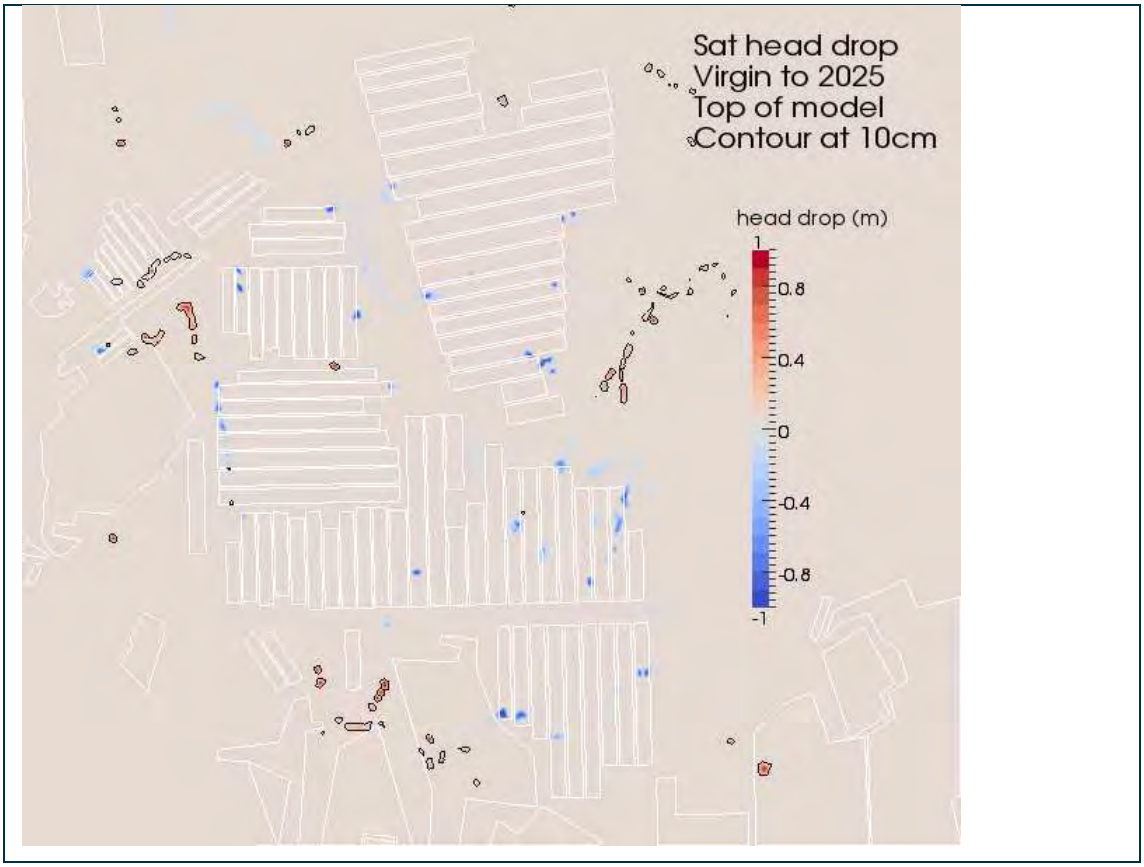

Figure D21 Distribution of head drops at the ground surface in 2033 with respect to pre-mining groundwater condition

Predictive Period with respect to Groundwater Levels in 2013

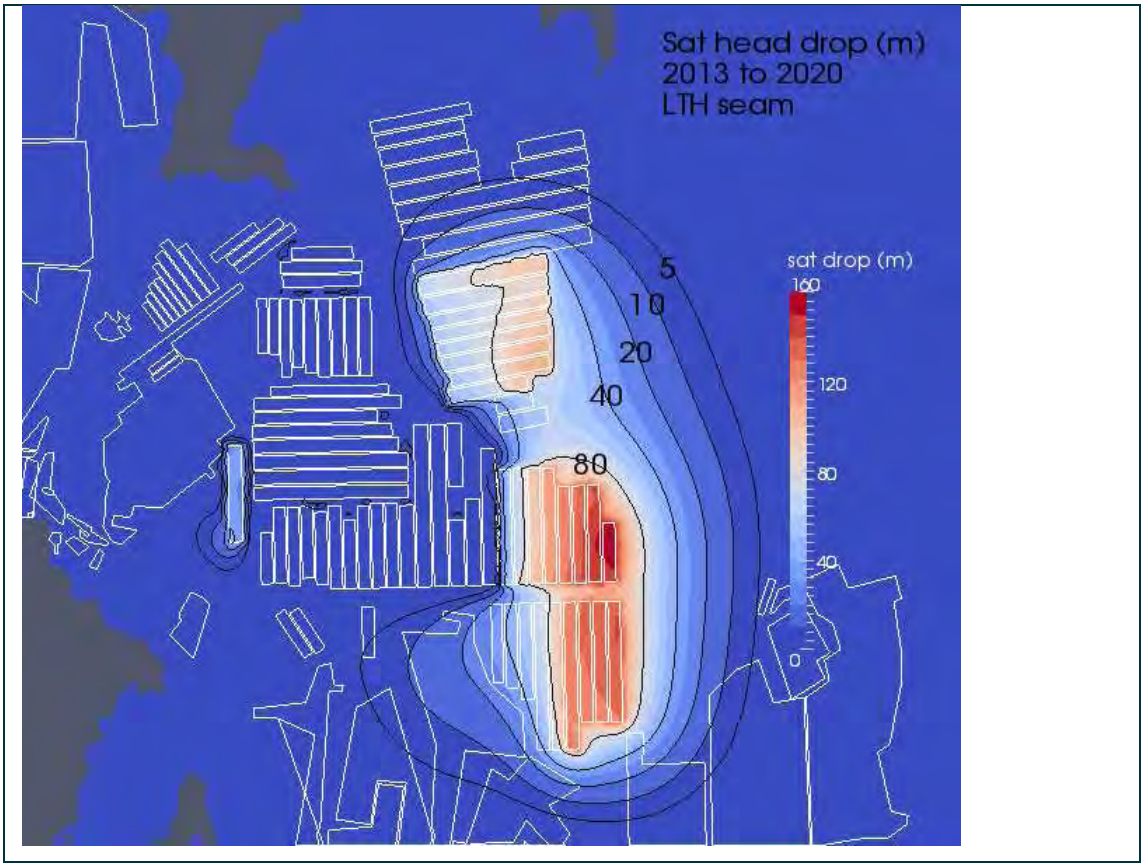

Figure D22 Distribution of drawdowns in the Lithgow Seam in 2020 with respect to groundwater levels in 2013

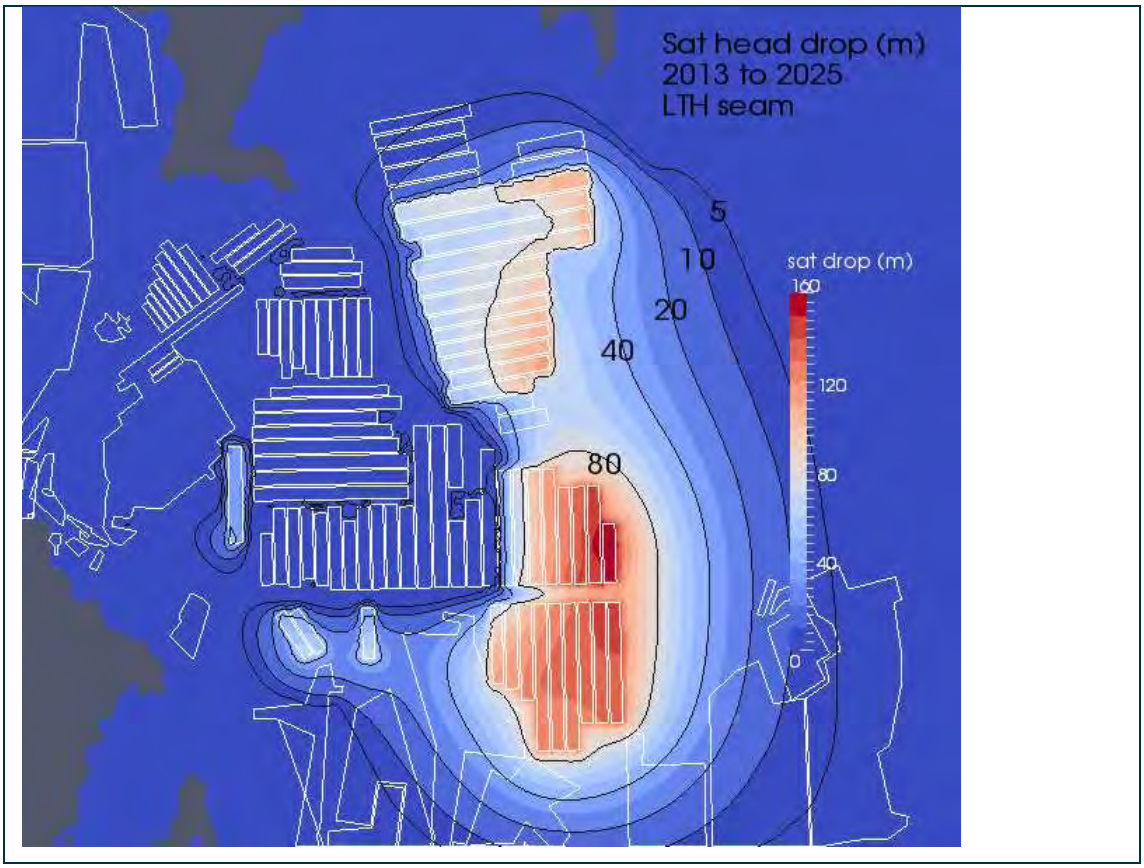

Figure D23 Distribution of drawdowns (m) in the Lithgow Seam in 2025 with respect to groundwater levels in 2013

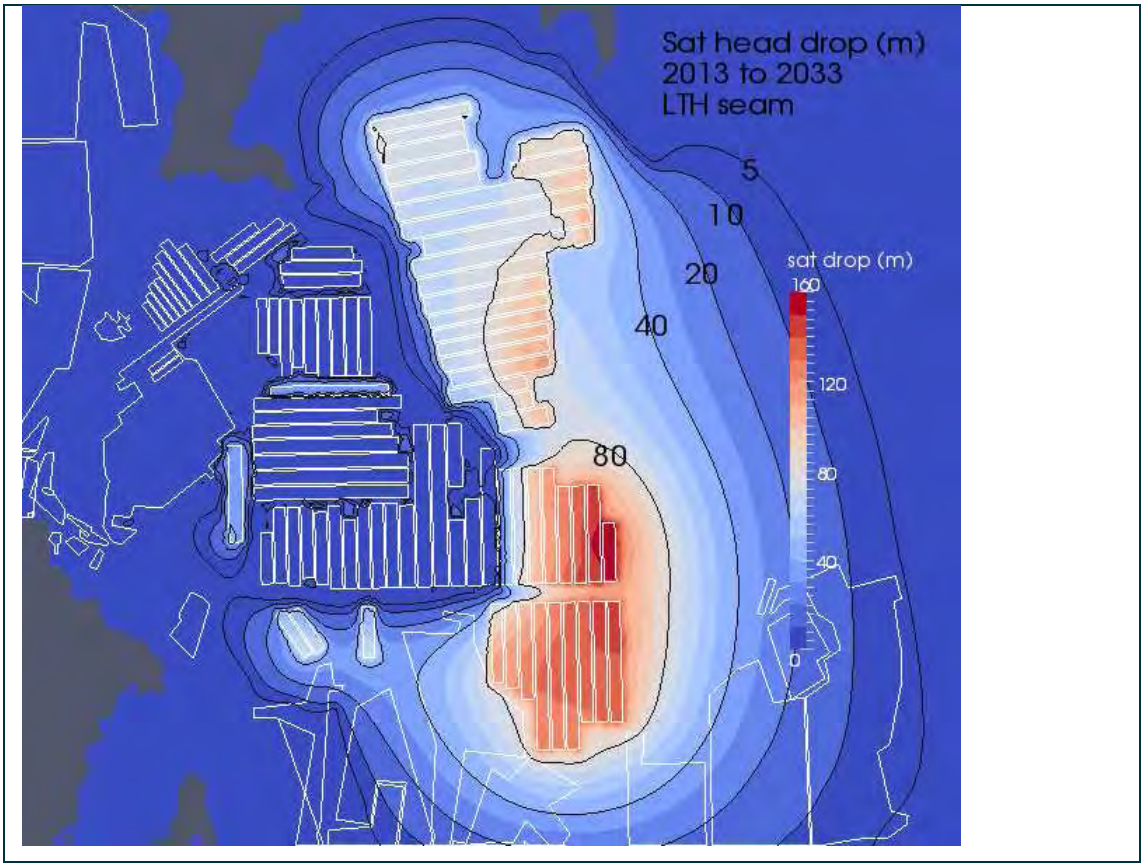

Figure D24 Distribution of drawdowns in the Lithgow Seam in 2033 with respect to groundwater levels in 2013

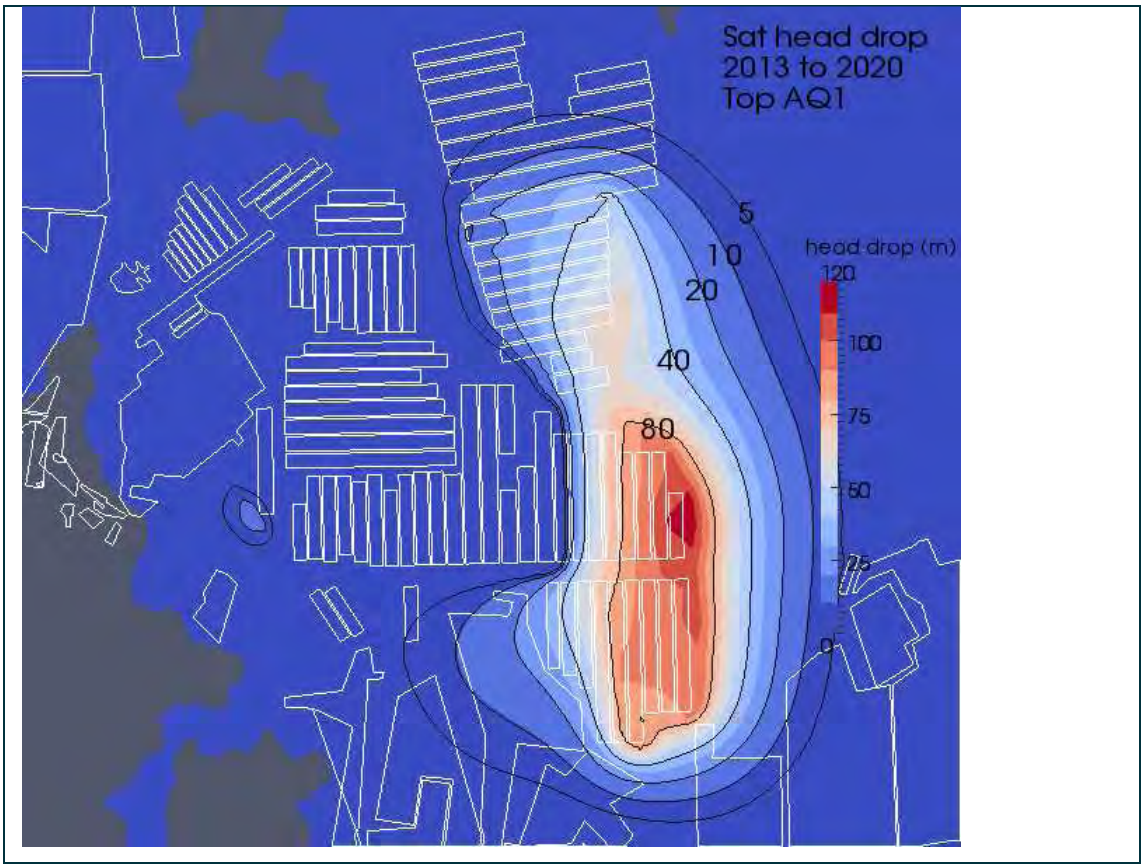

Figure D25 Distribution of drawdowns in AQ1 in 2020 with respect to groundwater levels in 2013

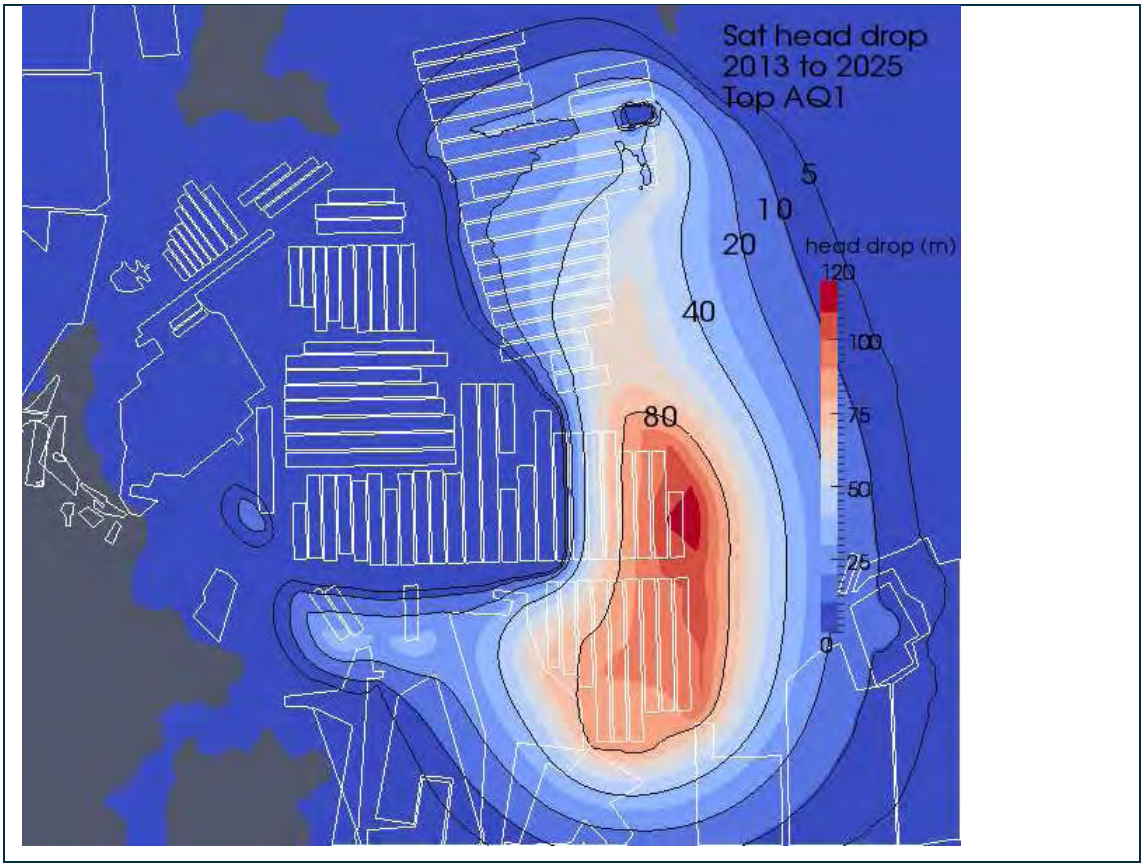

Figure D26 Distribution of drawdowns in AQ1 in 2025 with respect to groundwater levels in 2013

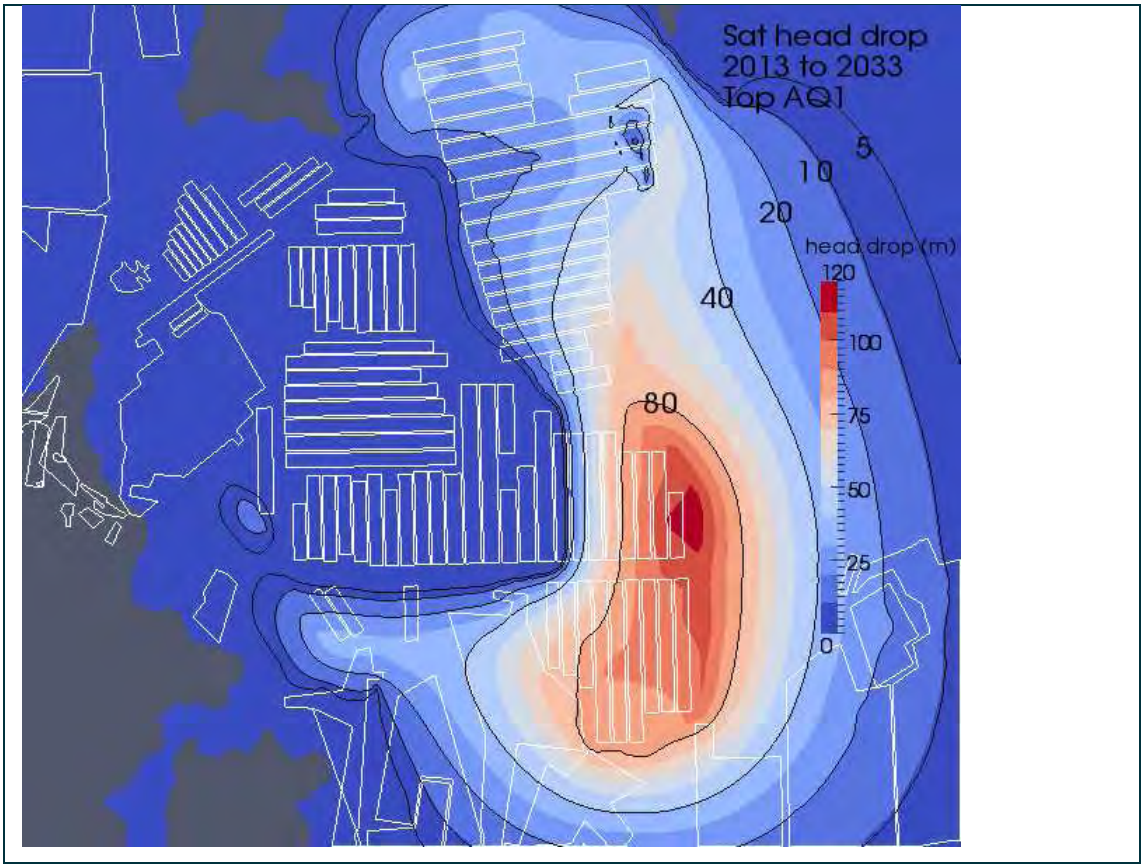

Figure D27 Distribution of drawdowns in AQ1 in 2033 with respect to groundwater levels in 2013

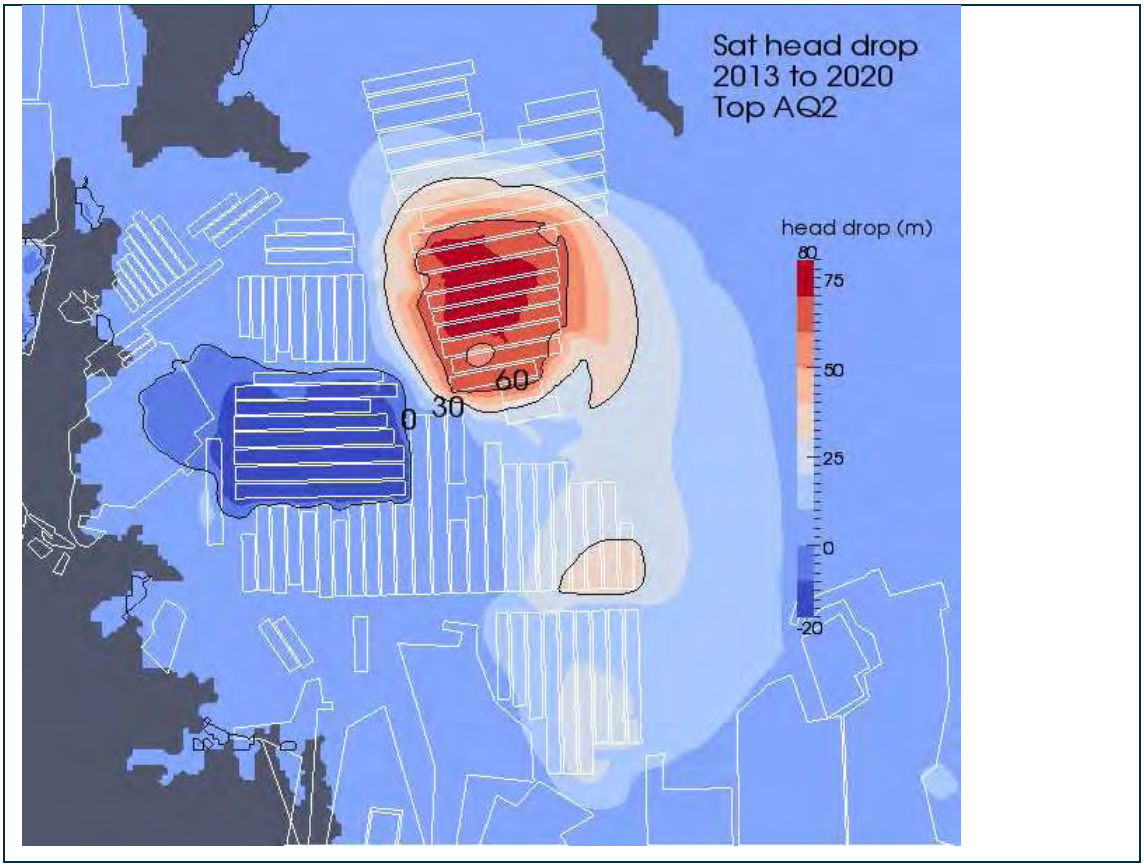

Figure D28 Distribution of drawdowns in AQ2 in 2020 with respect to groundwater levels in 2013

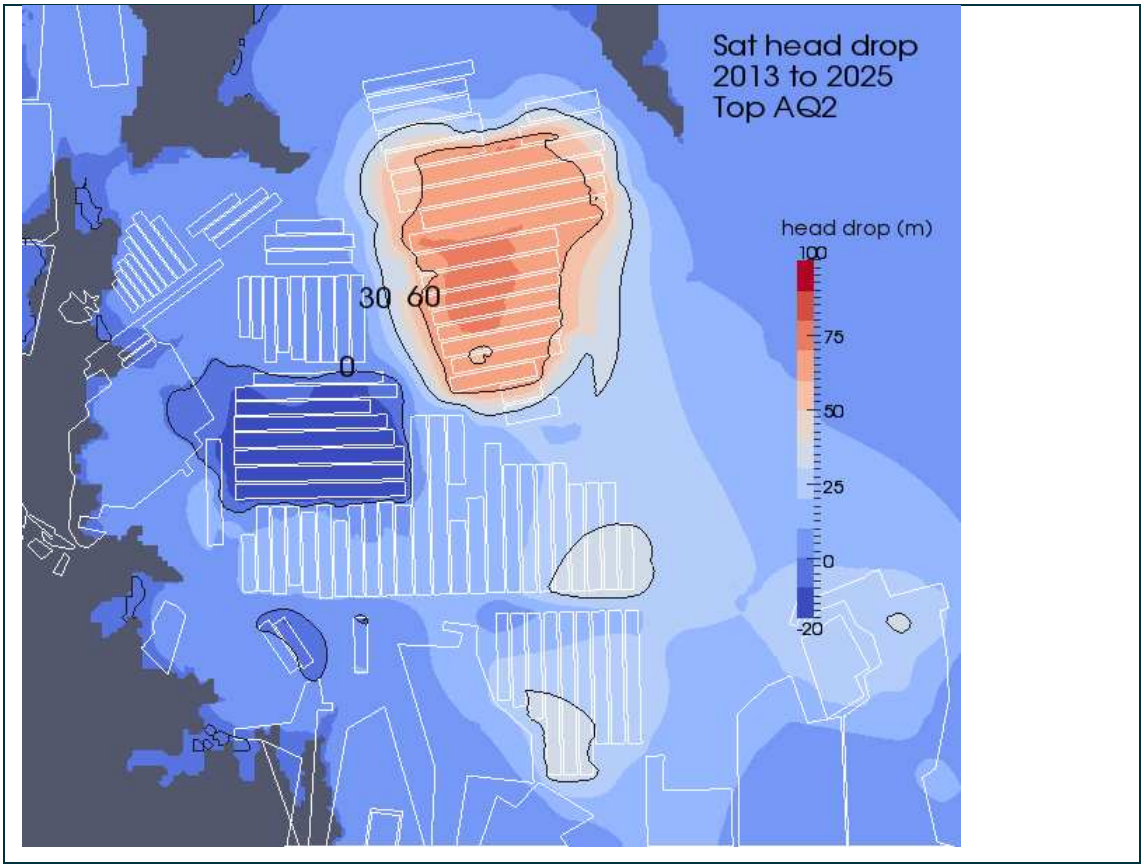

Figure D29 Distribution of drawdowns in AQ2 in 2025 with respect to groundwater levels in 2013

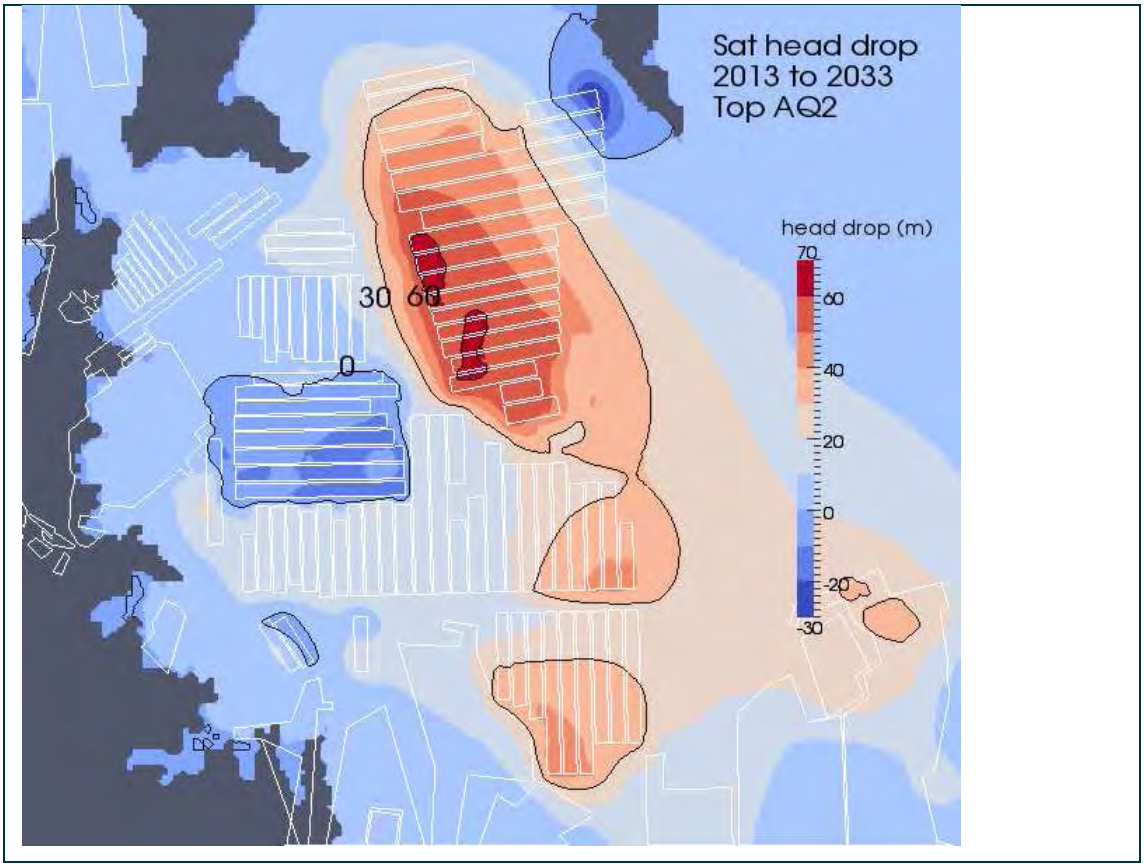

Figure D30 Distribution of drawdowns in AQ2 in 2033 with respect to groundwater levels in 2013

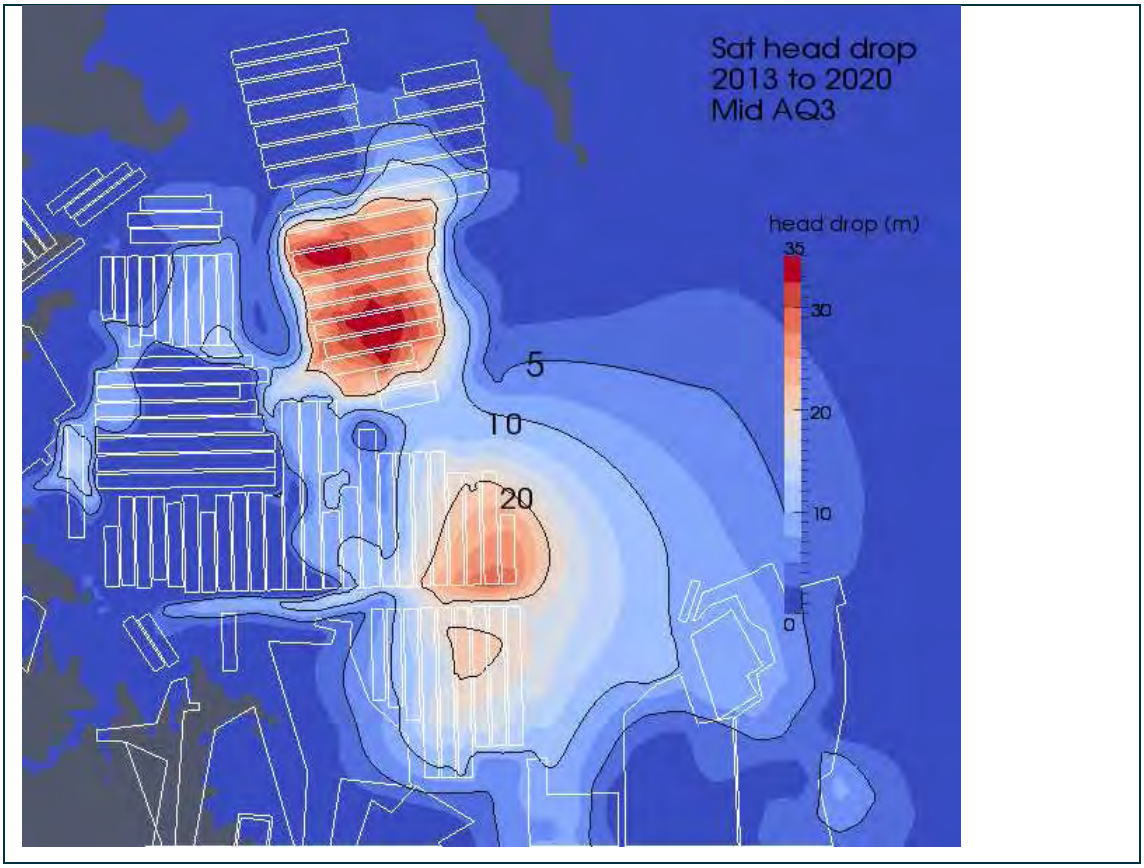

Figure D31 Distribution of drawdowns in AQ3 in 2020 with respect to groundwater levels in 2013

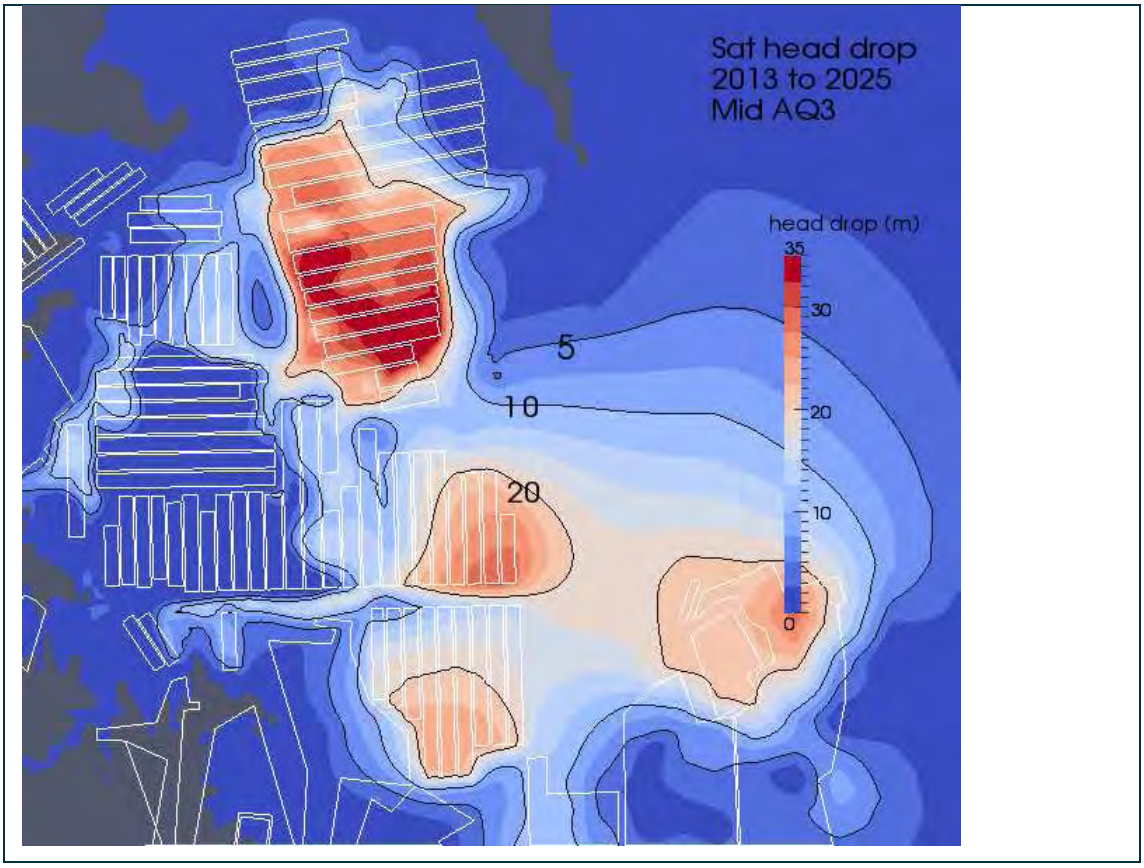

Figure D32 Distribution of drawdowns in AQ3 in 2025 with respect to groundwater levels in 2013

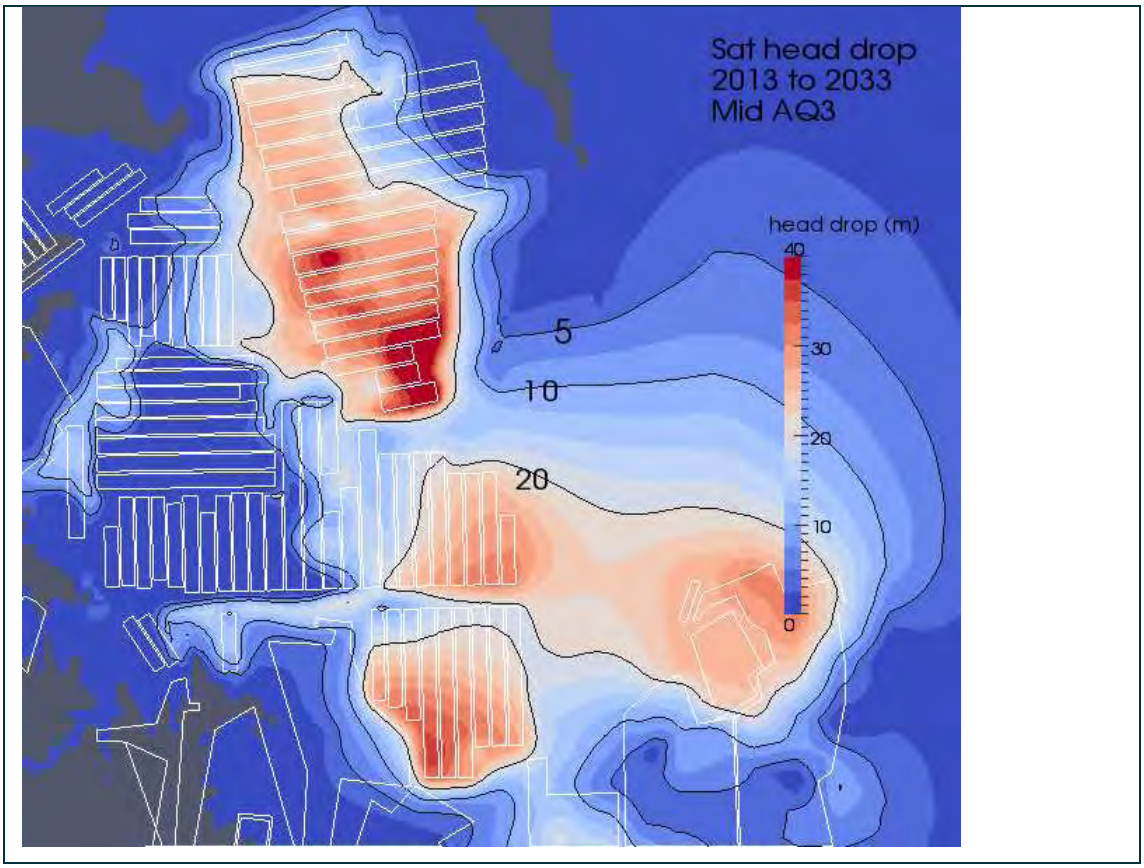

Figure D33 Distribution of drawdowns in AQ3 in 2033 with respect to groundwater levels in 2013

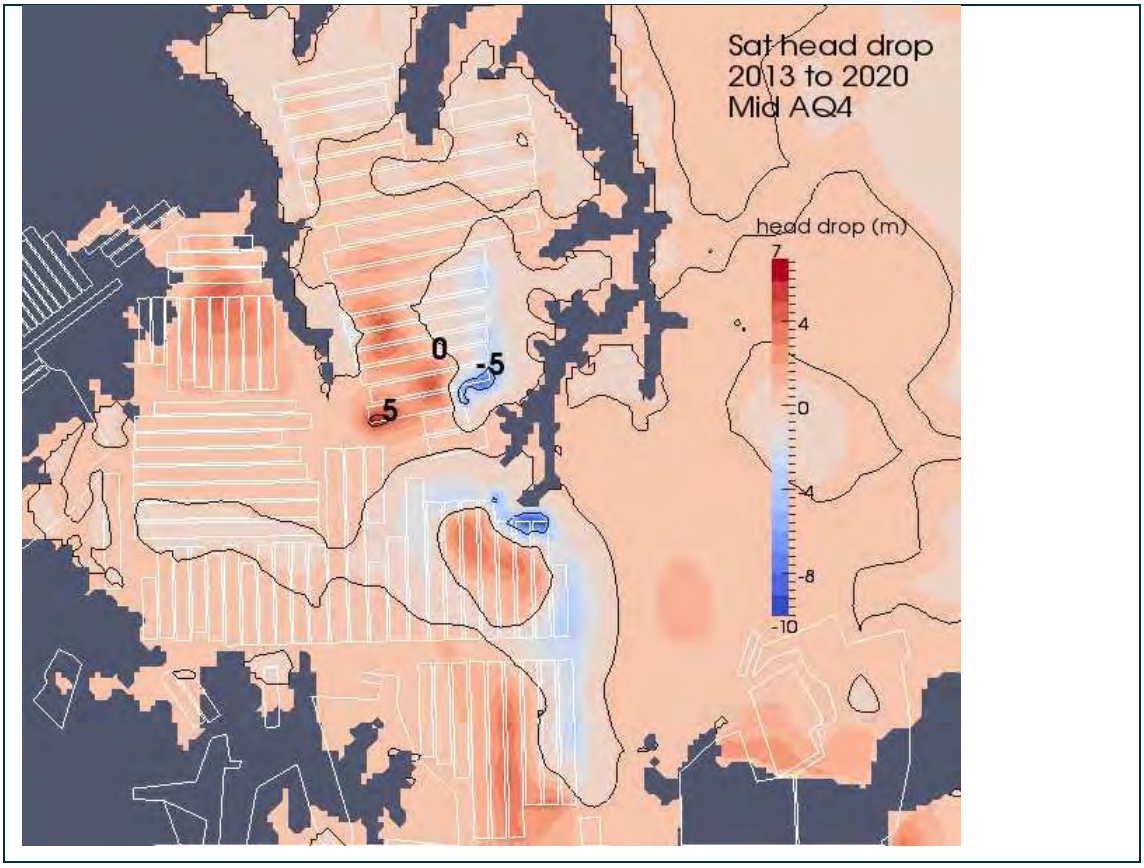

Figure D34 Distribution of drawdowns in AQ4 in 2020 with respect to groundwater levels in 2013

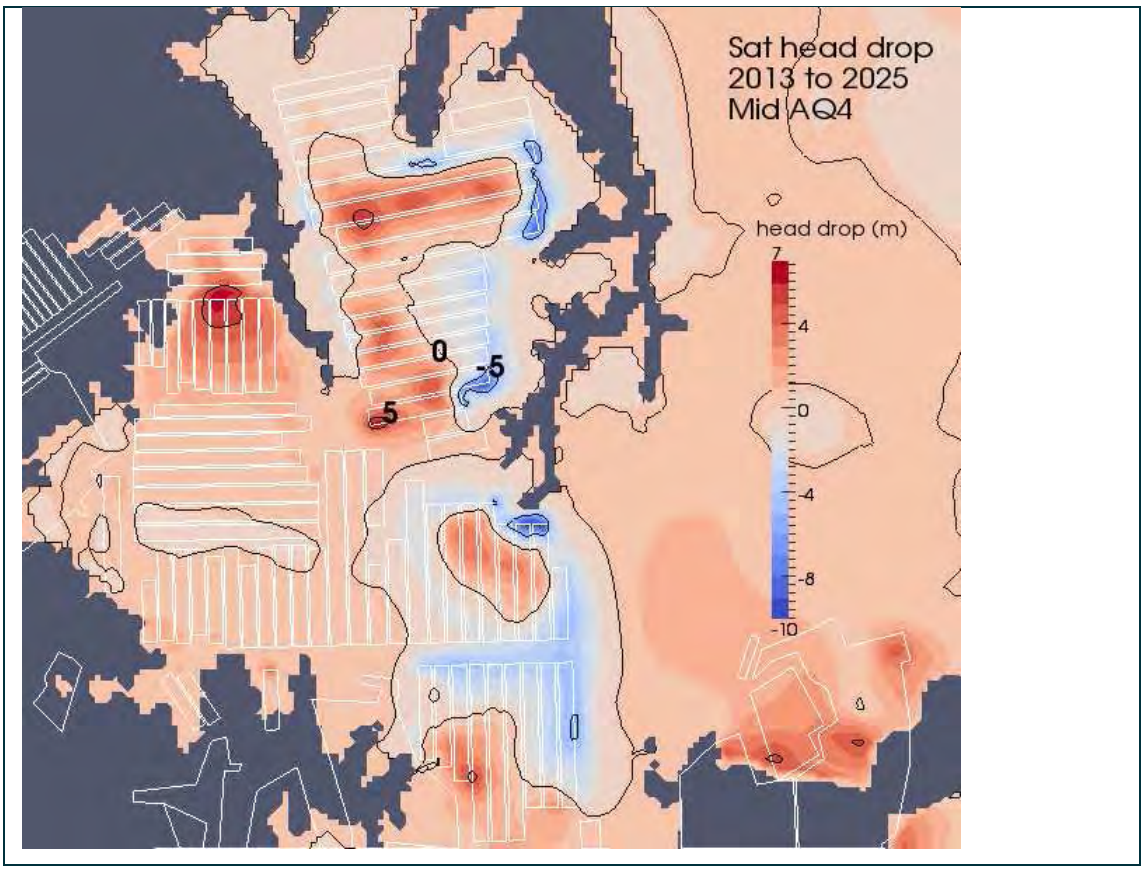

Figure D35 Distribution of drawdowns in AQ4 in 2025 with respect to groundwater levels in 2013

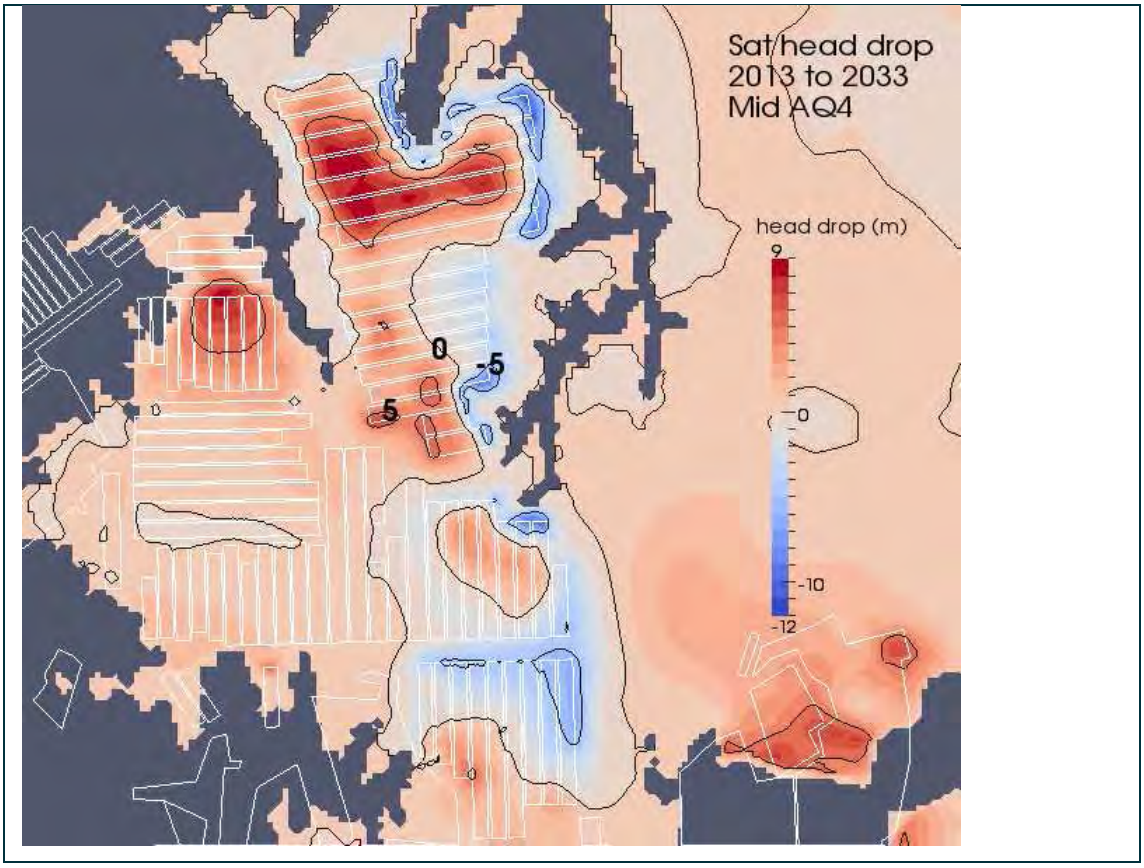

Figure D36 Distribution of drawdowns in AQ4 in 2033 with respect to groundwater levels in 2013

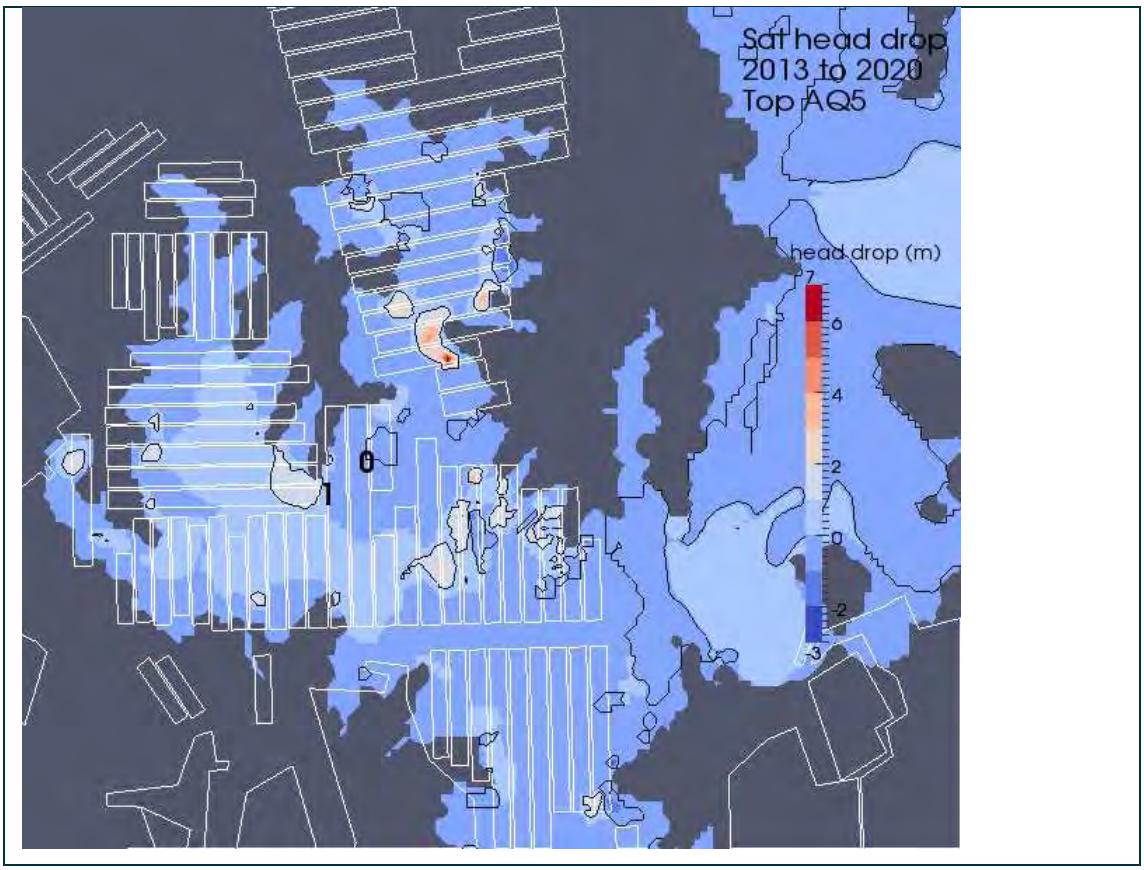

Figure D37 Distribution of drawdowns in AQ5 in 2020 with respect to groundwater levels in 2013

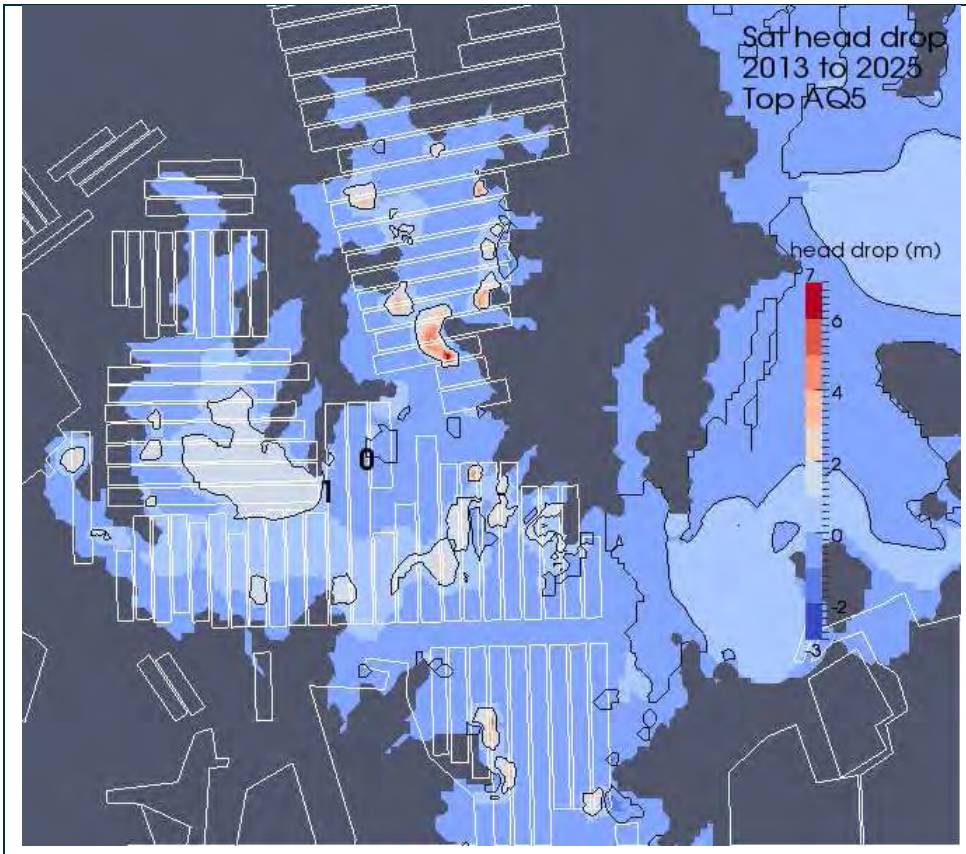

Figure D38 Distribution of drawdowns in AQ5 in 2025 with respect to groundwater levels in 2013

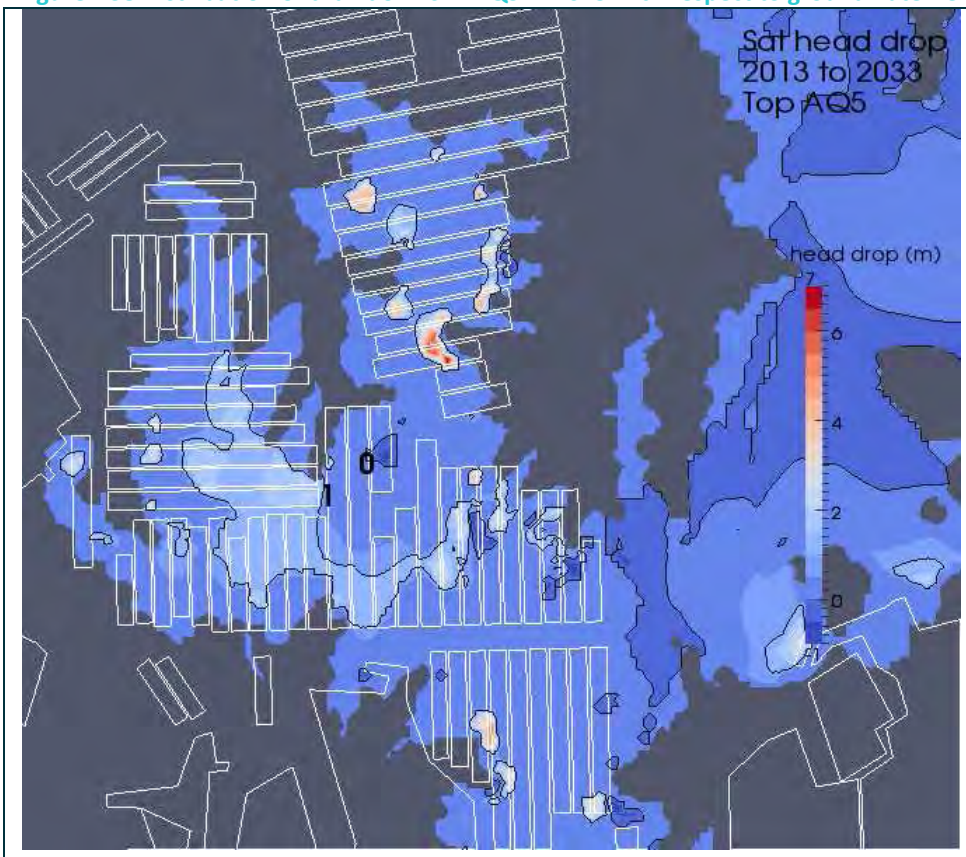

Figure D39 Distribution of drawdowns in AQ5 in 2033 with respect to groundwater levels in 2013

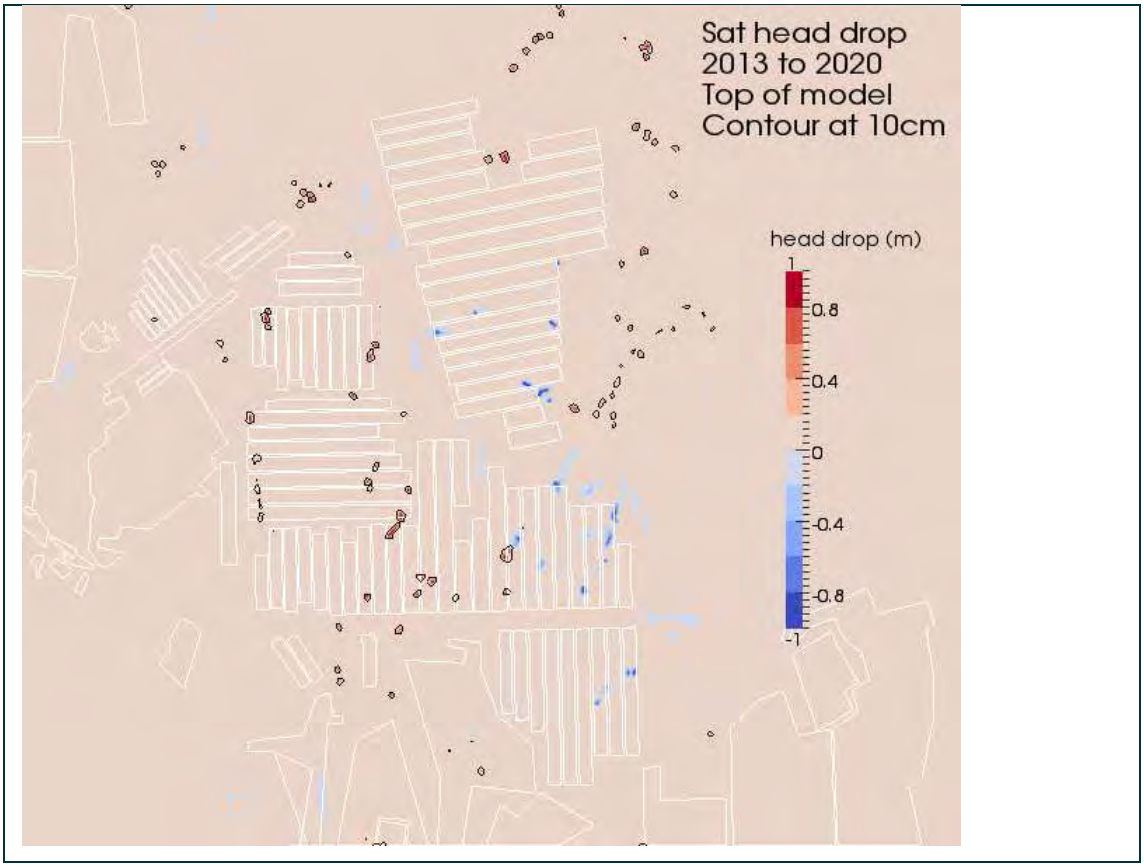

Figure D40 Distribution of head drops at the ground surface in 2020 with respect to groundwater levels in 2013

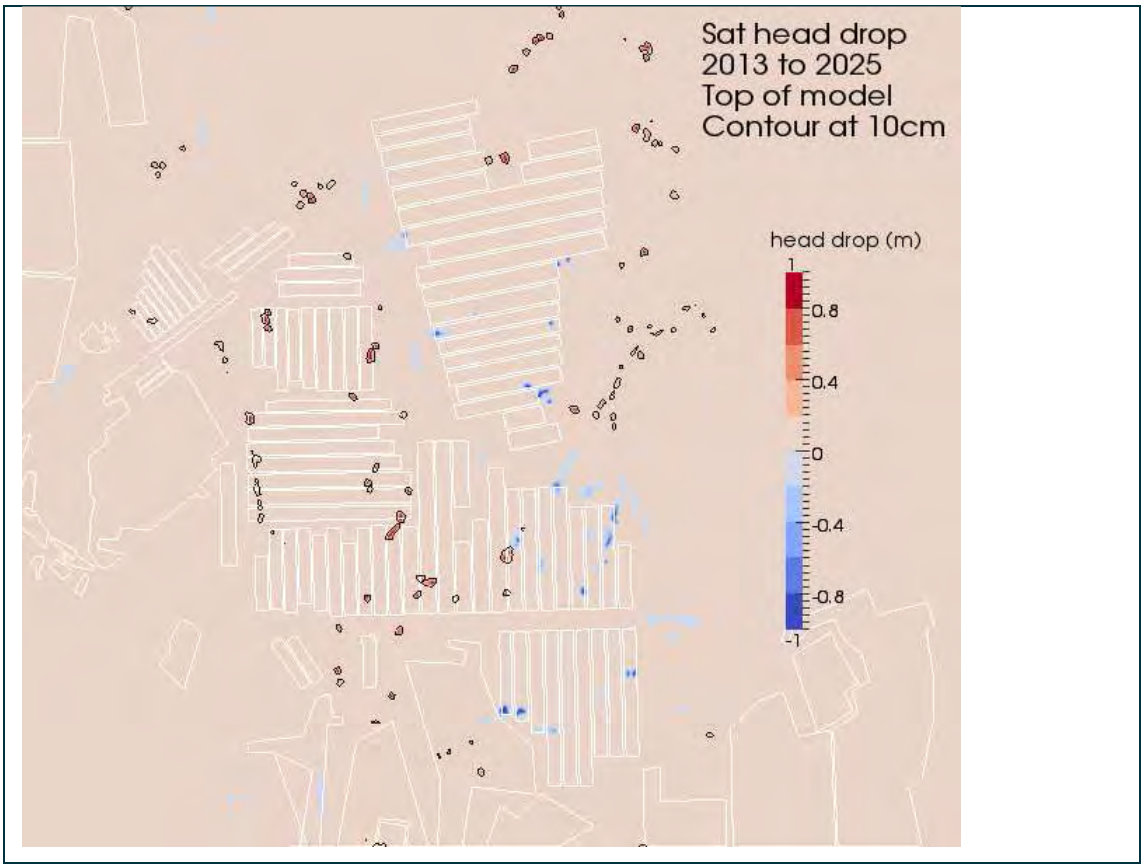

Figure D41 Distribution of head drops at the ground surface in 2025 with respect to groundwater levels in 2013

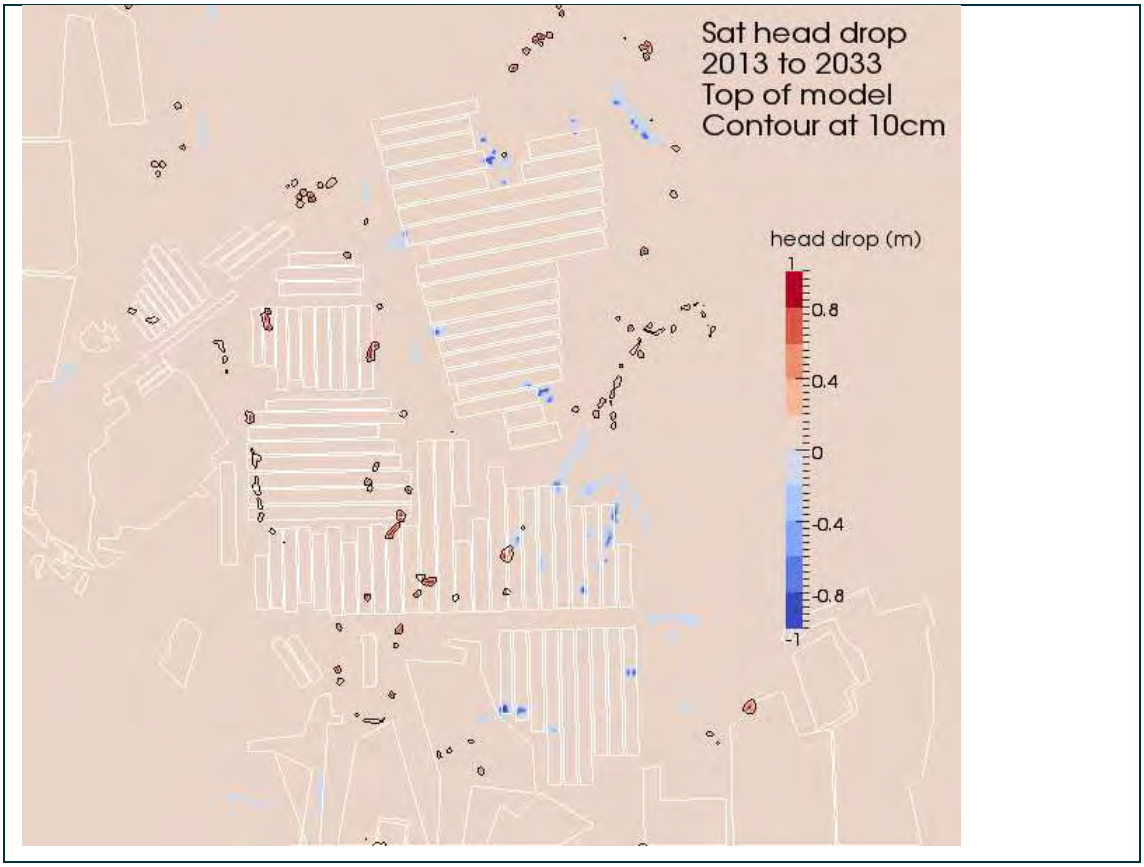

Figure D42 Distribution of head drops at the ground surface in 2033 with respect to groundwater levels in 2013

Recovery Period with respect to Pre-mining Groundwater Condition

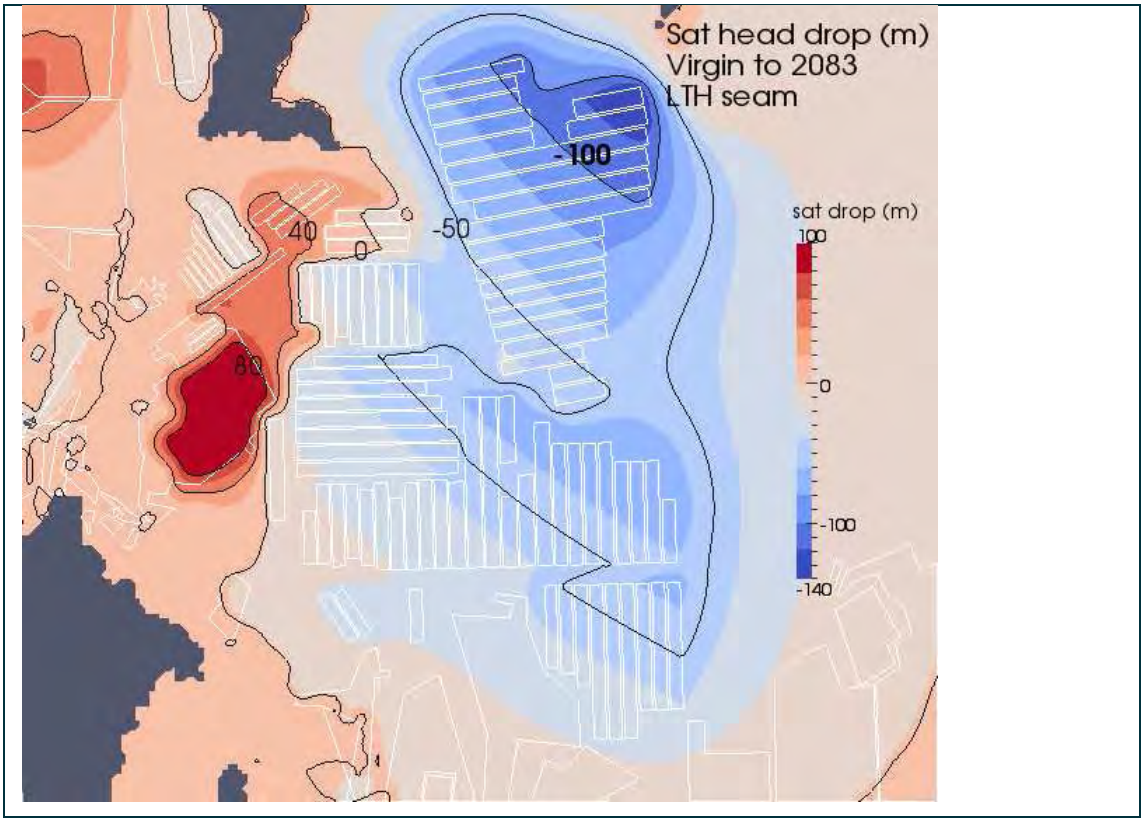

Figure D43 Distribution of head drops in the Lithgow Seam in 2083 with respect to pre-mining groundwater condition

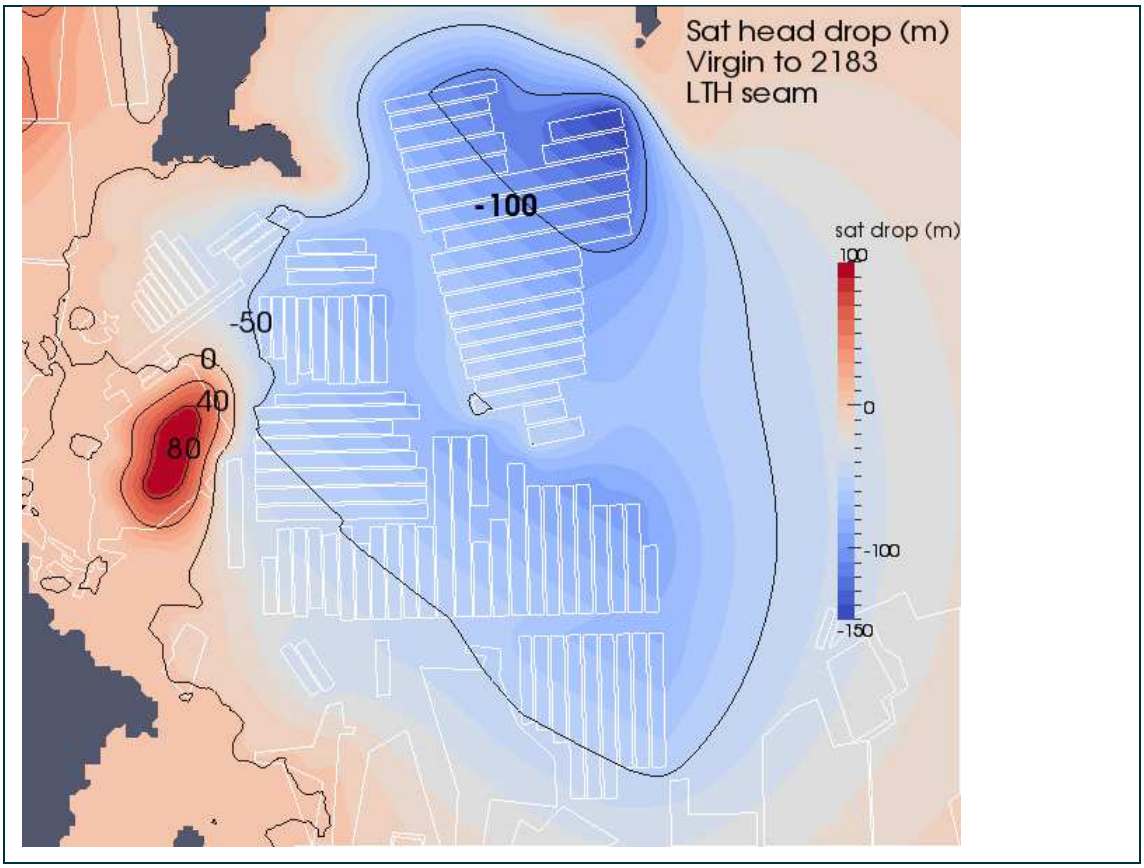

Figure D44 Distribution of head drops in the Lithgow Seam in 2183 with respect to pre-mining groundwater condition

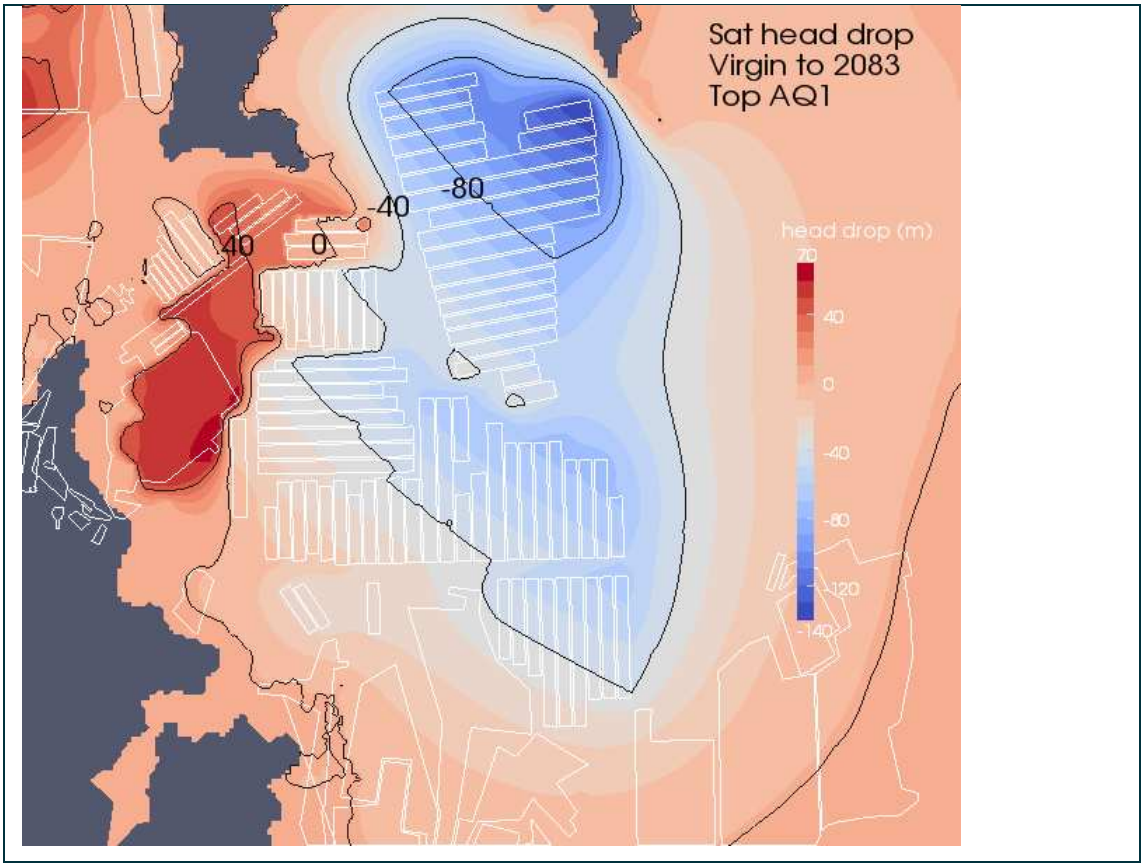

Figure D45 Distribution of head drops in AQ1 in 2083 with respect to pre-mining groundwater condition

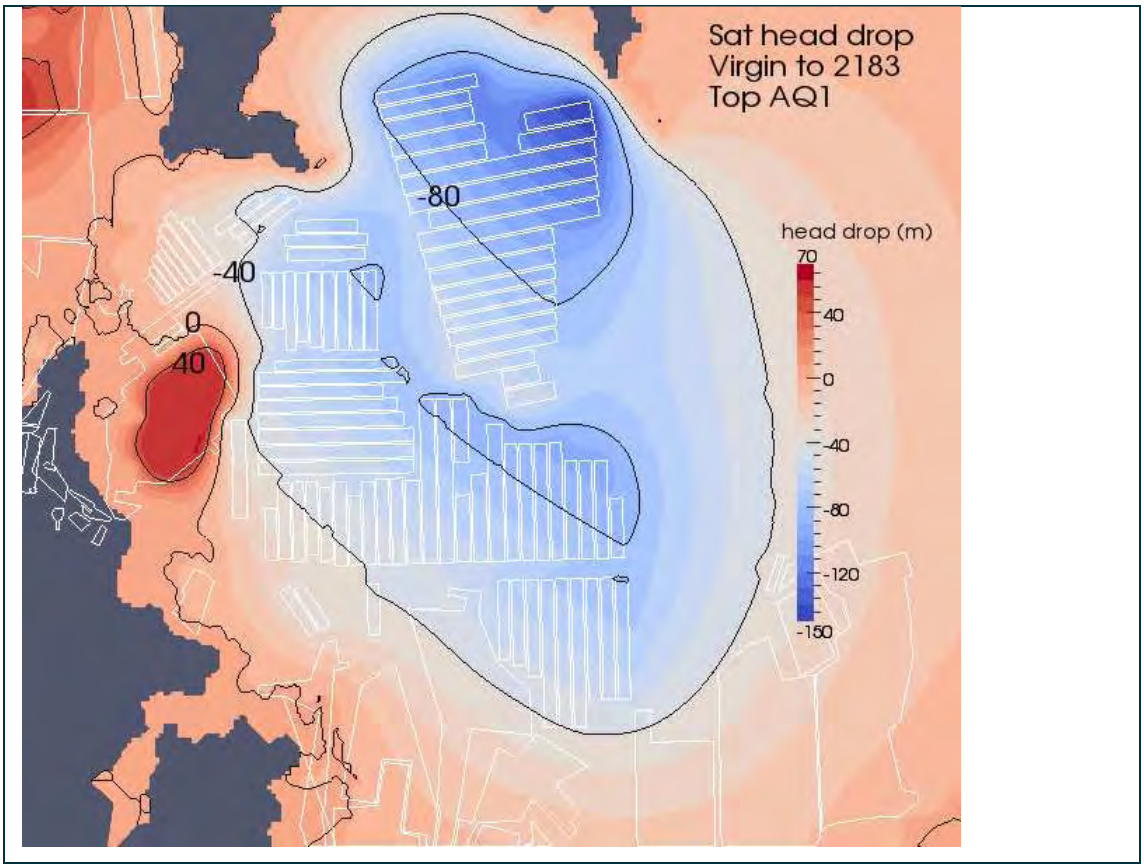

Figure D46 Distribution of head drops in AQ1 in 2183 with respect to pre-mining groundwater condition

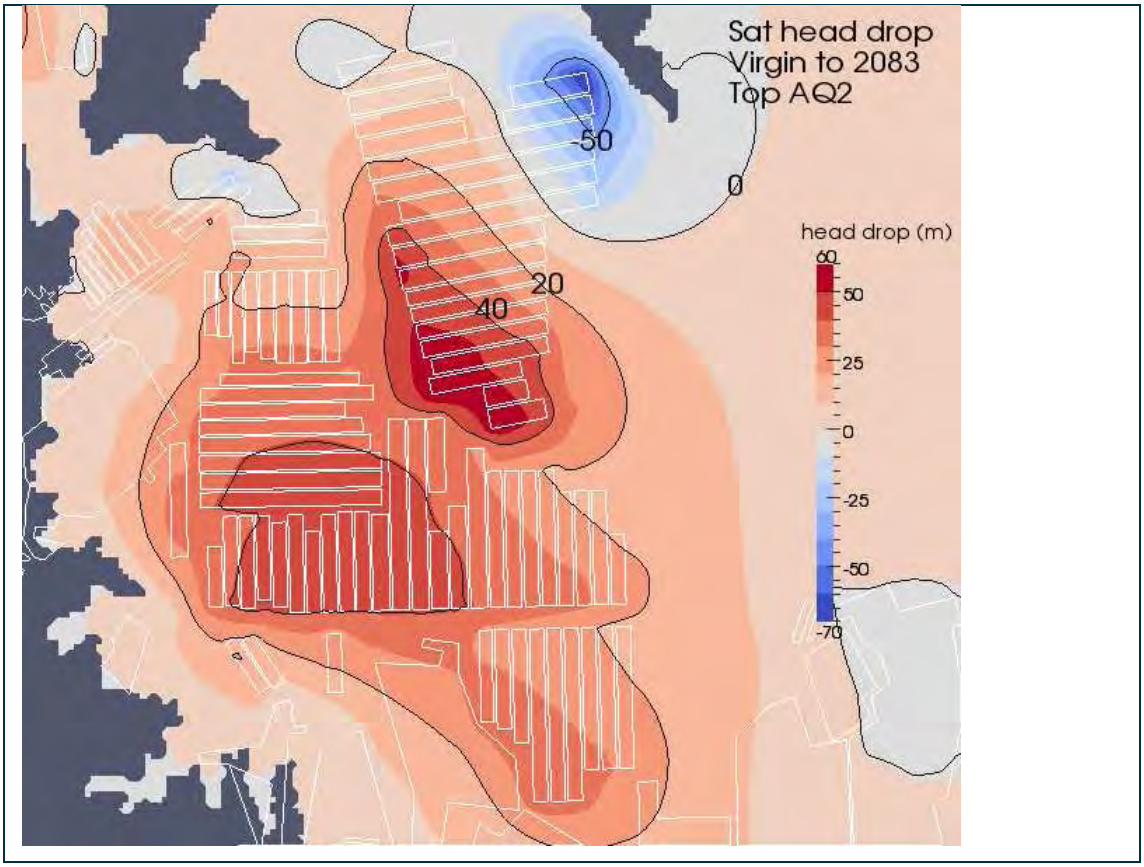

Figure D47 Distribution of head drops in AQ2 in 2083 with respect to pre-mining groundwater condition

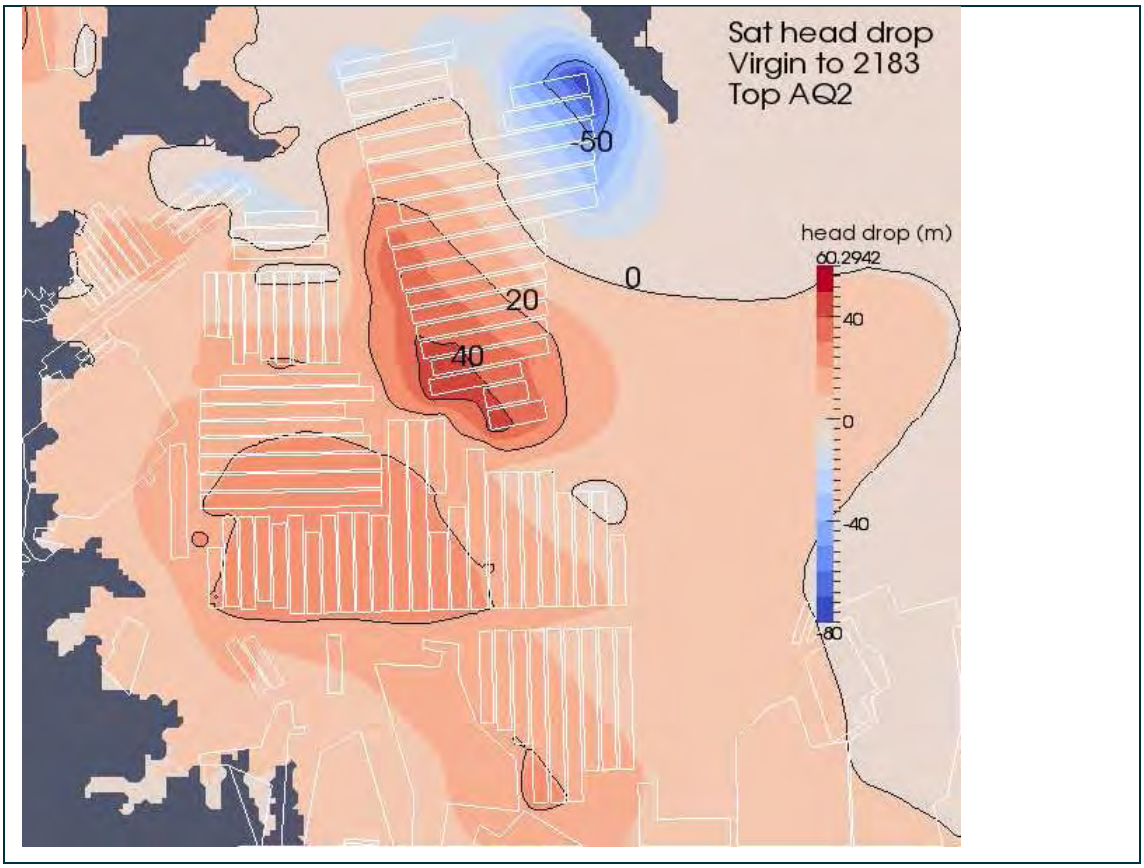

Figure D48 Distribution of head drops in AQ2 in 2183 with respect to pre-mining groundwater condition

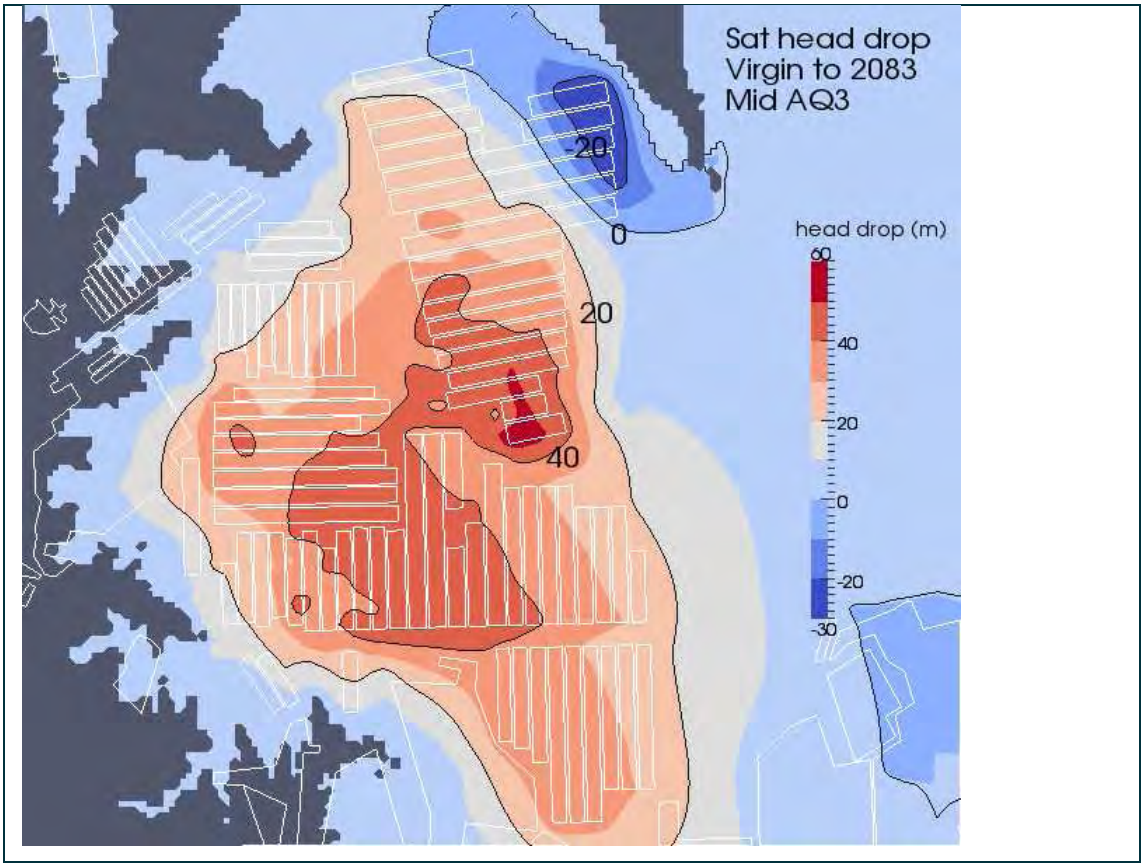

Figure D49 Distribution of head drops in AQ3 in 2083 with respect to pre-mining groundwater condition

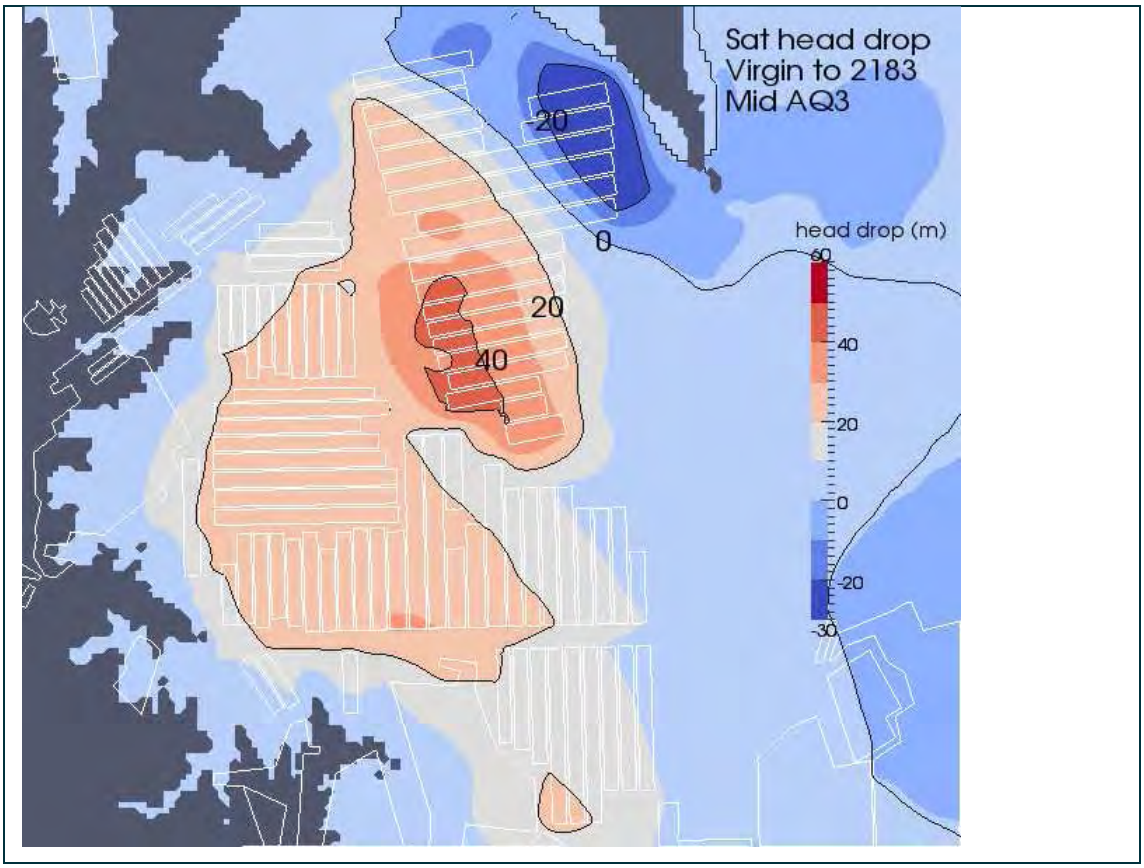

Figure D50 Distribution of head drops in AQ3 in 2183 with respect to pre-mining groundwater condition

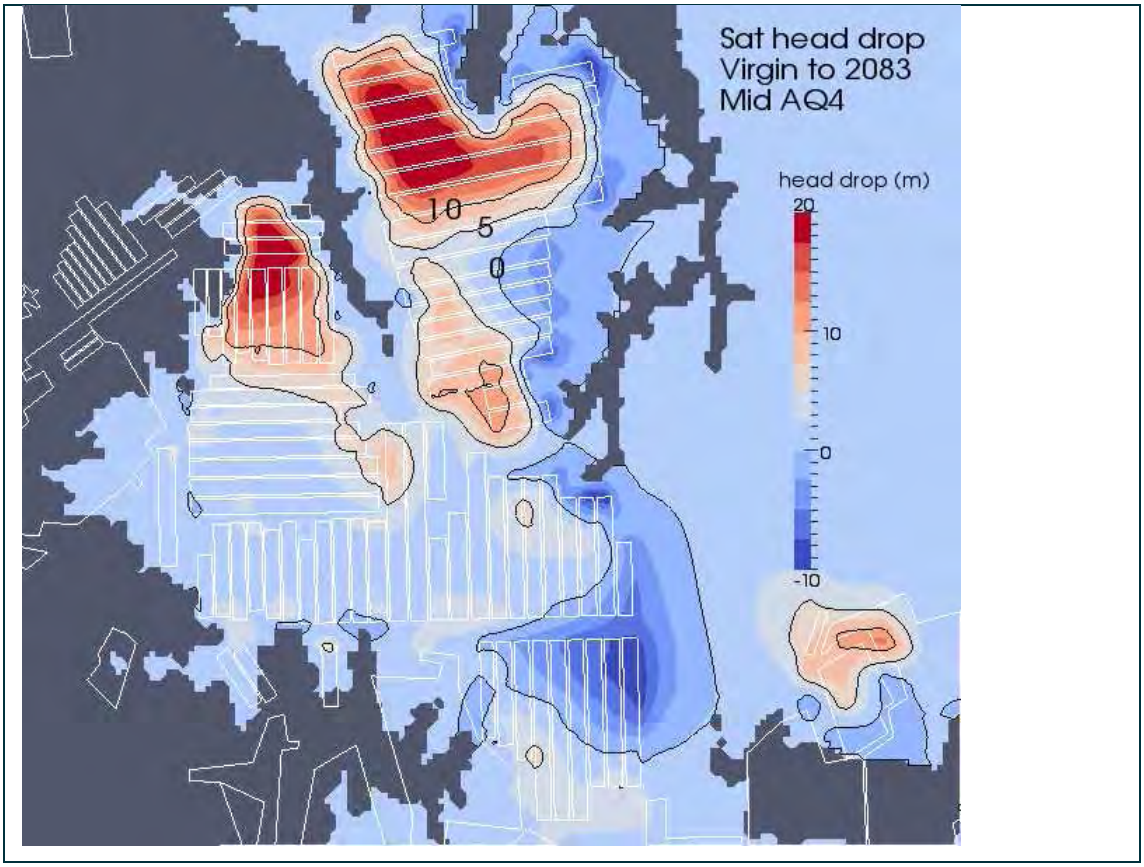

Figure D51 Distribution of head drops in AQ4 in 2083 with respect to pre-mining groundwater condition

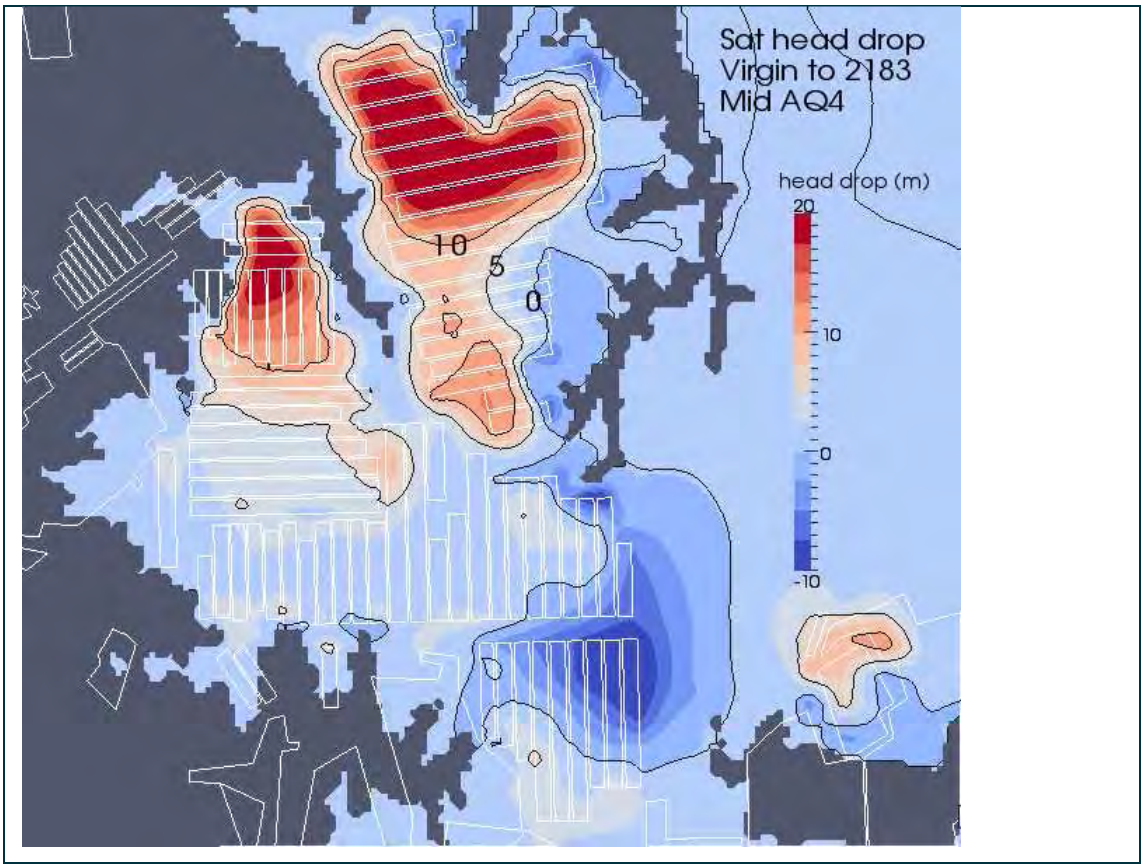

Figure D52 Distribution of head drops in AQ4 in 2183 with respect to pre-mining groundwater condition

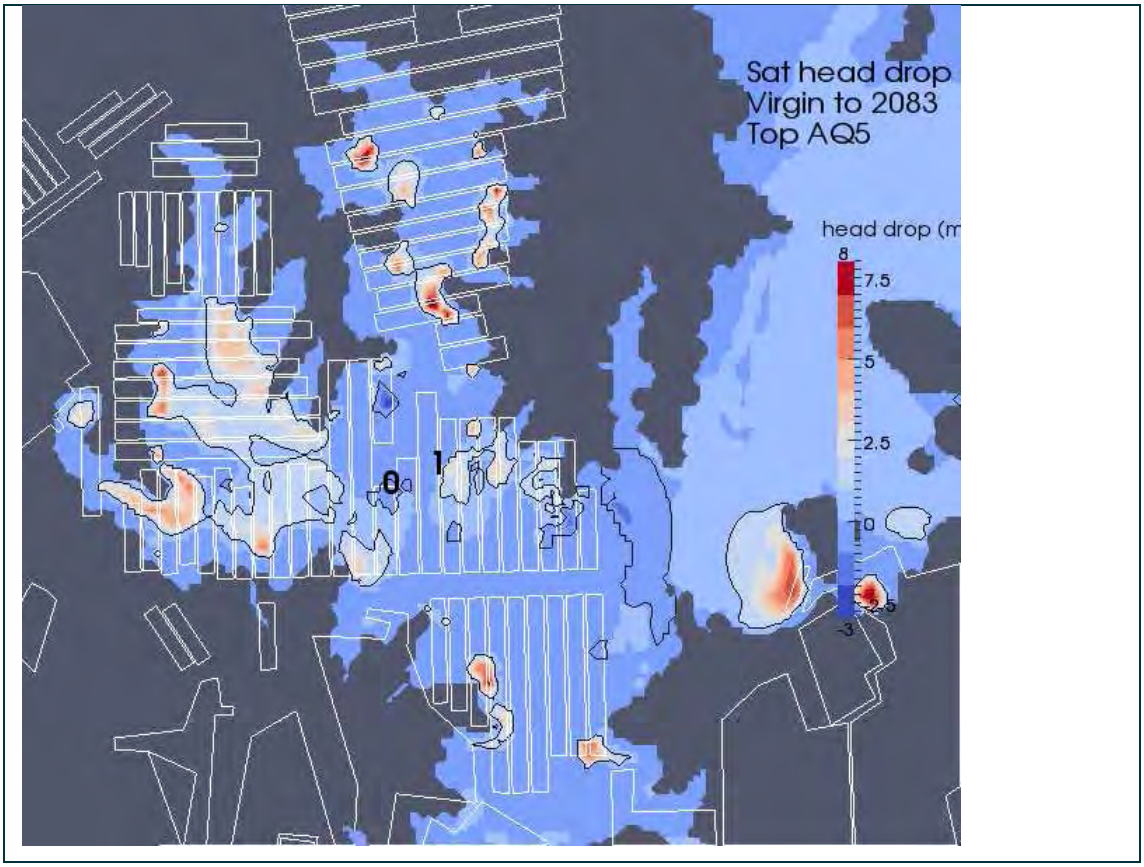

Figure D53 Distribution of head drops in AQ5 in 2083 with respect to pre-mining groundwater condition

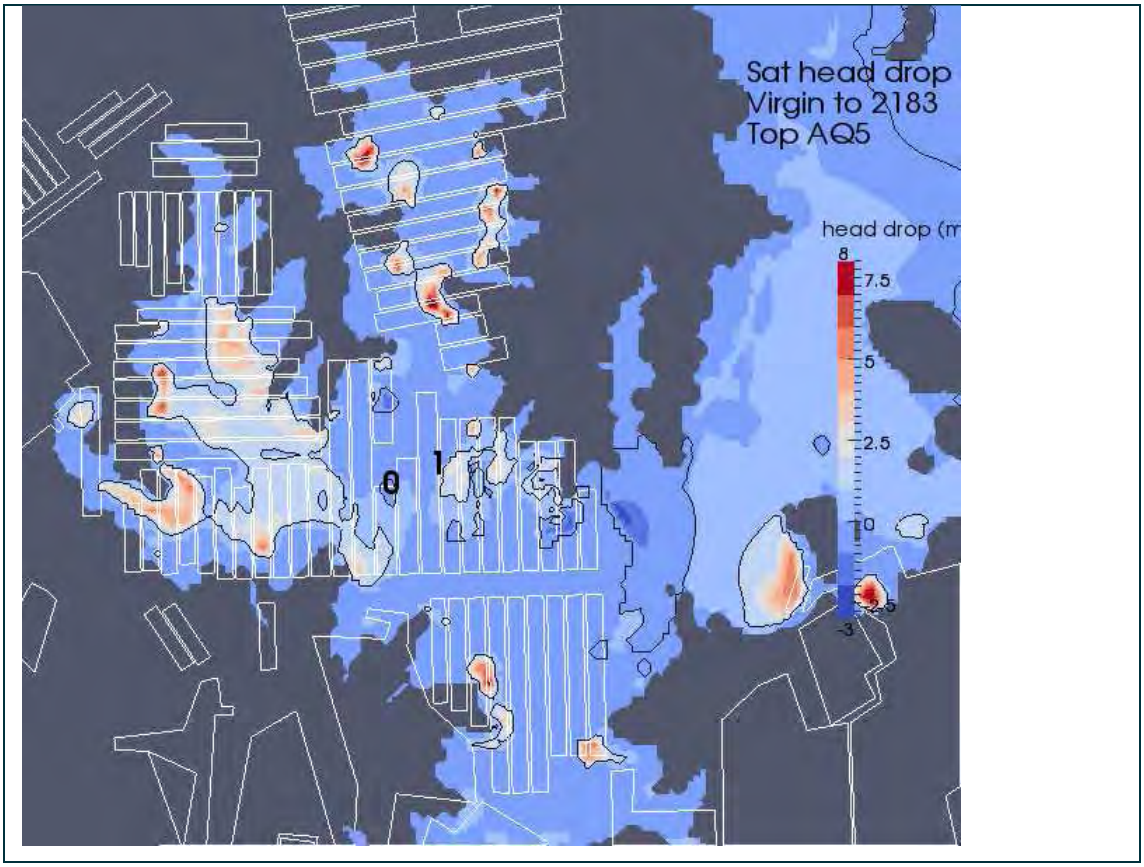

Figure D54 Distribution of head drops in AQ5 in 2183 with respect to pre-mining groundwater condition

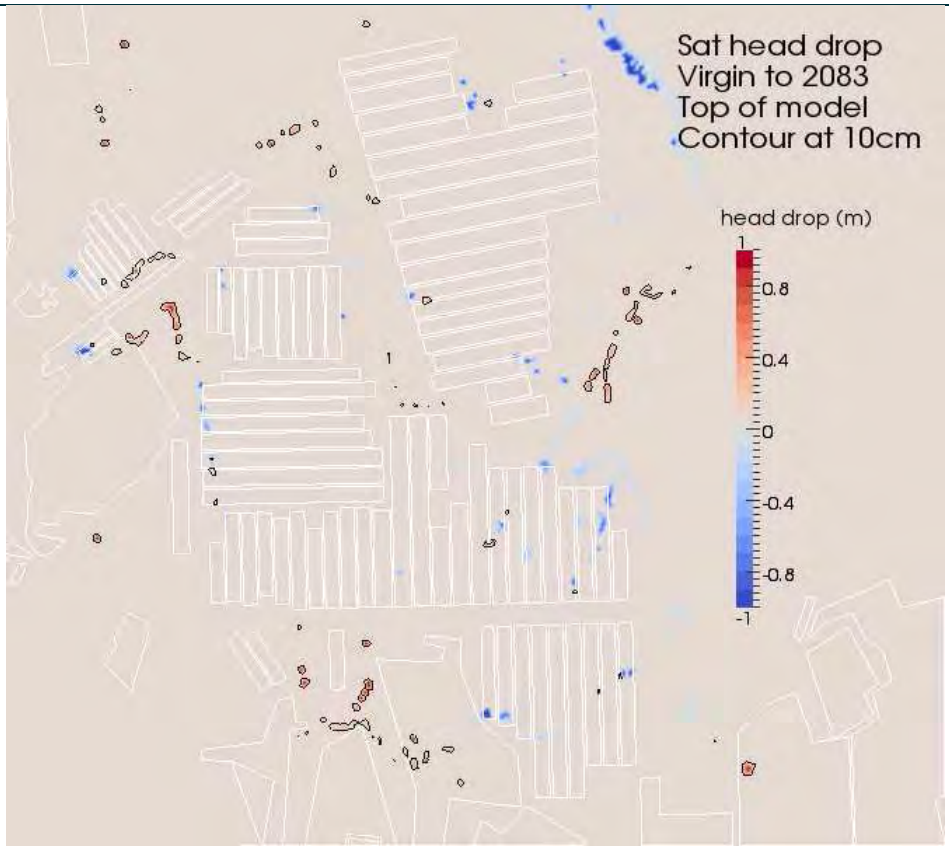

Figure D55 Distribution of head drops at the ground surface in 2083 with respect to pre-mining groundwater condition

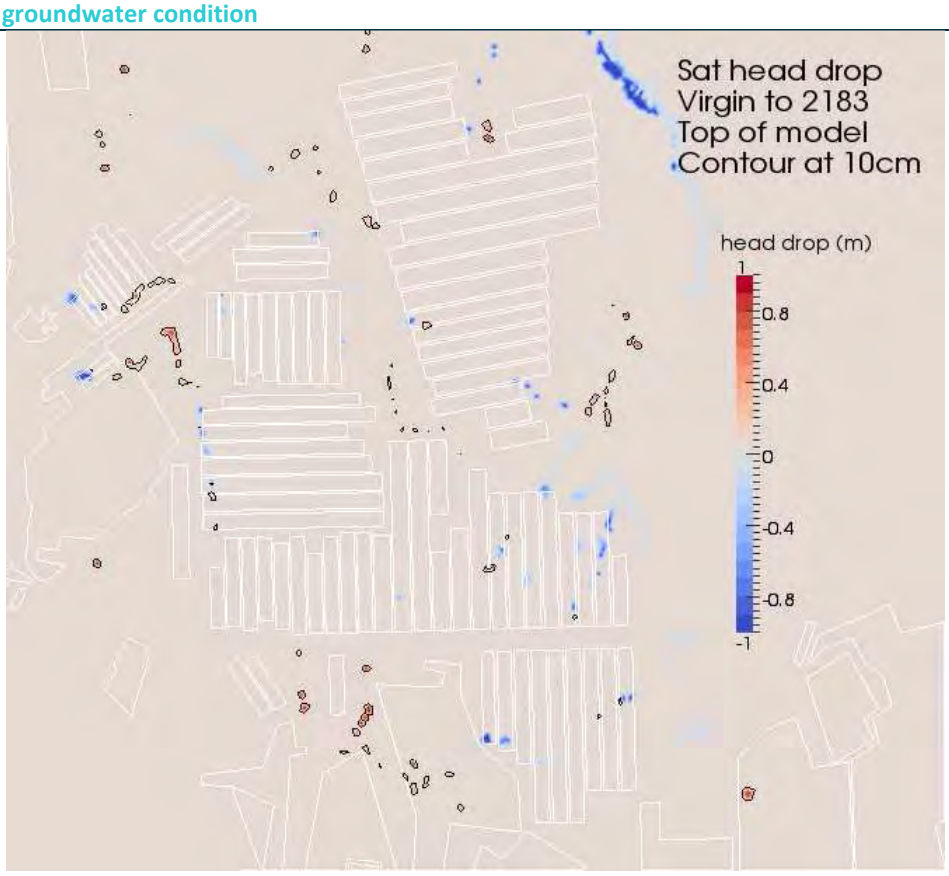

Figure D56 Distribution of head drops at the ground surface in 2183 with respect to pre-mining groundwater condition

Recovery Period with respect to Groundwater Levels in 2013

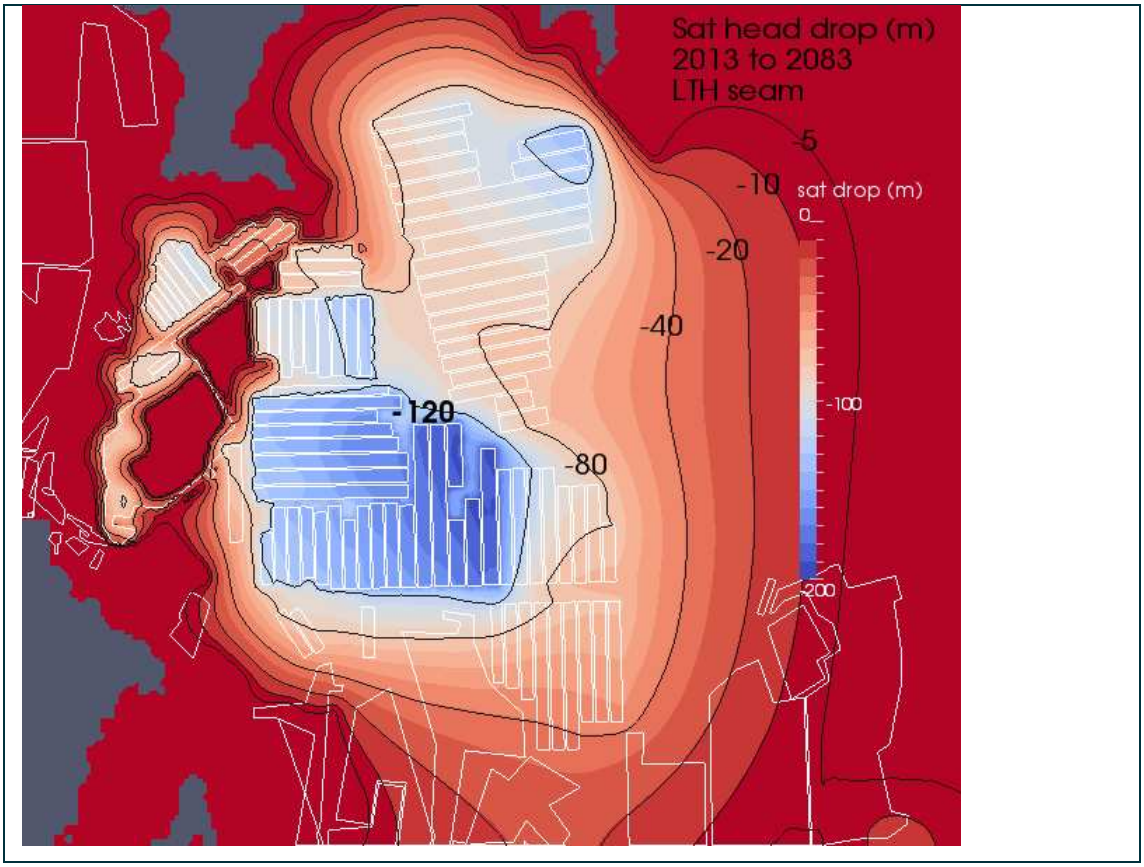

Figure D57 Distribution of head drops in the Lithgow Seam in 2083 with respect to groundwater levels in 2013

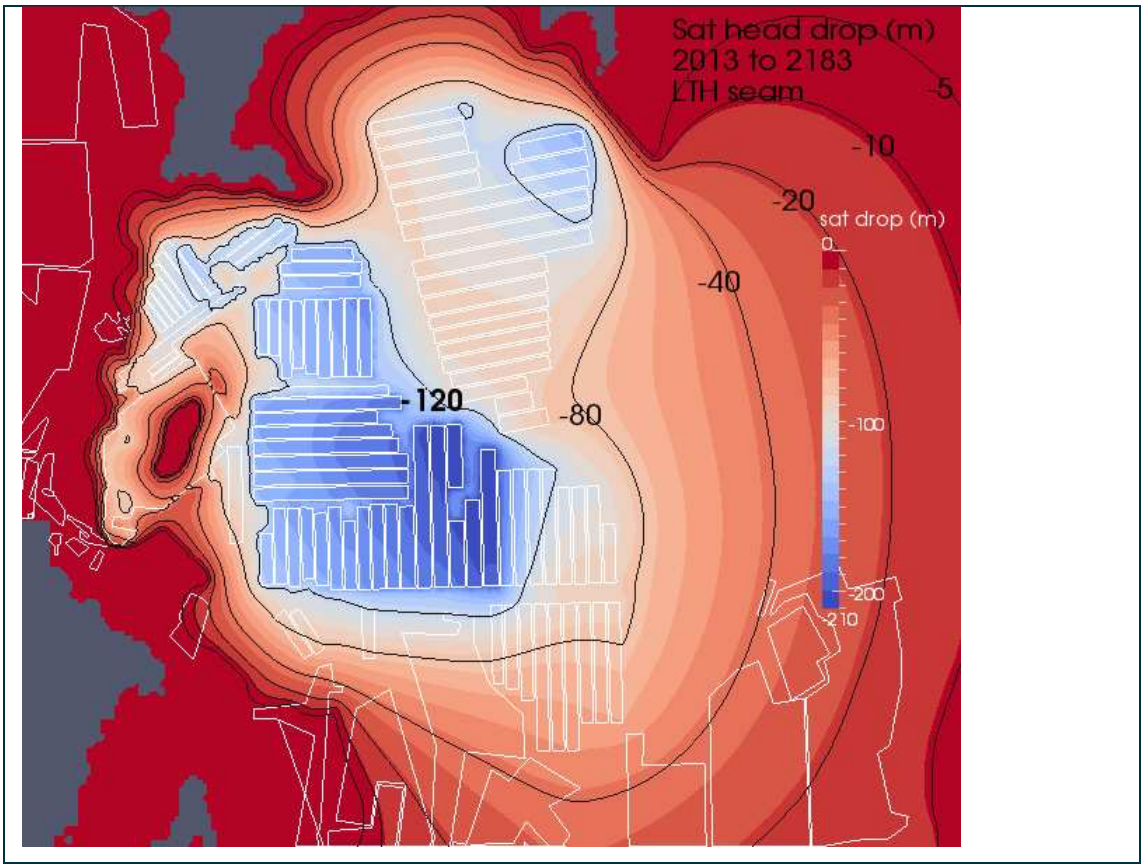

Figure D58 Distribution of head drops in the Lithgow Seam in 2183 with respect to groundwater levels in 2013

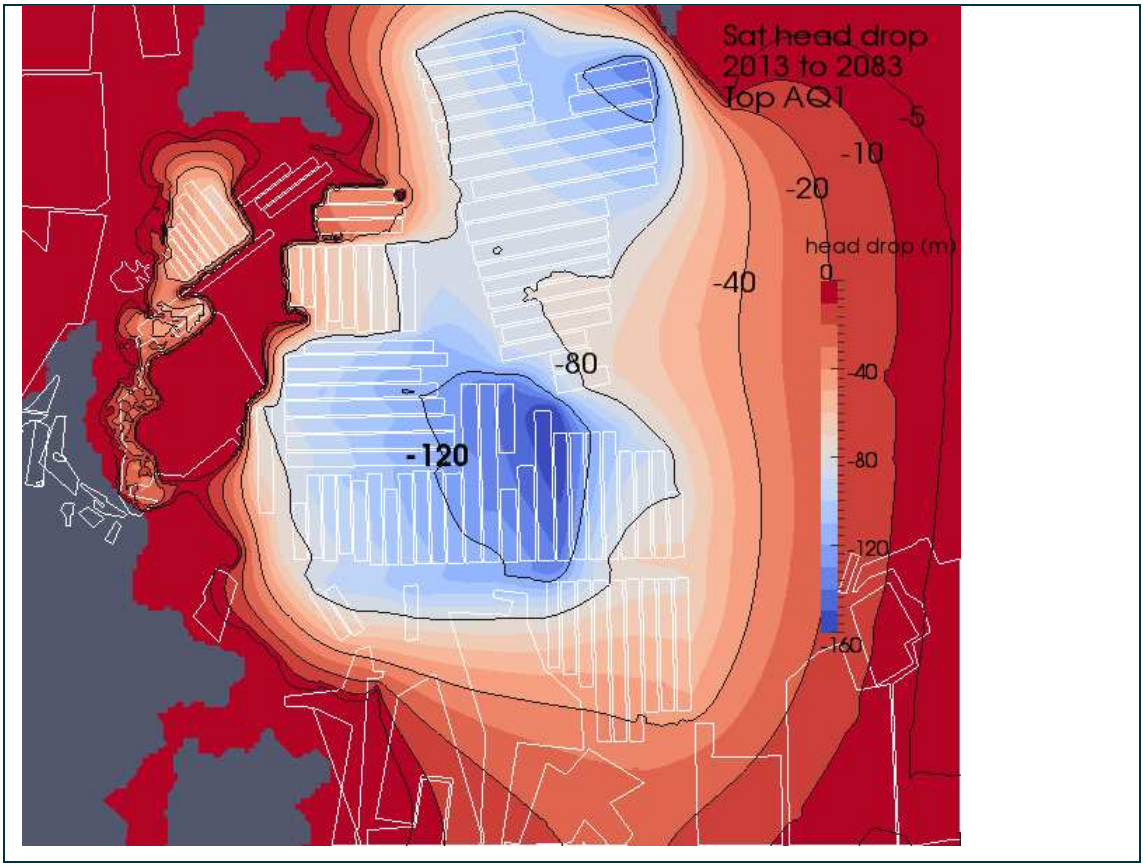

Figure D59 Distribution of head drops in AQ1 in 2083 with respect to groundwater levels in 2013

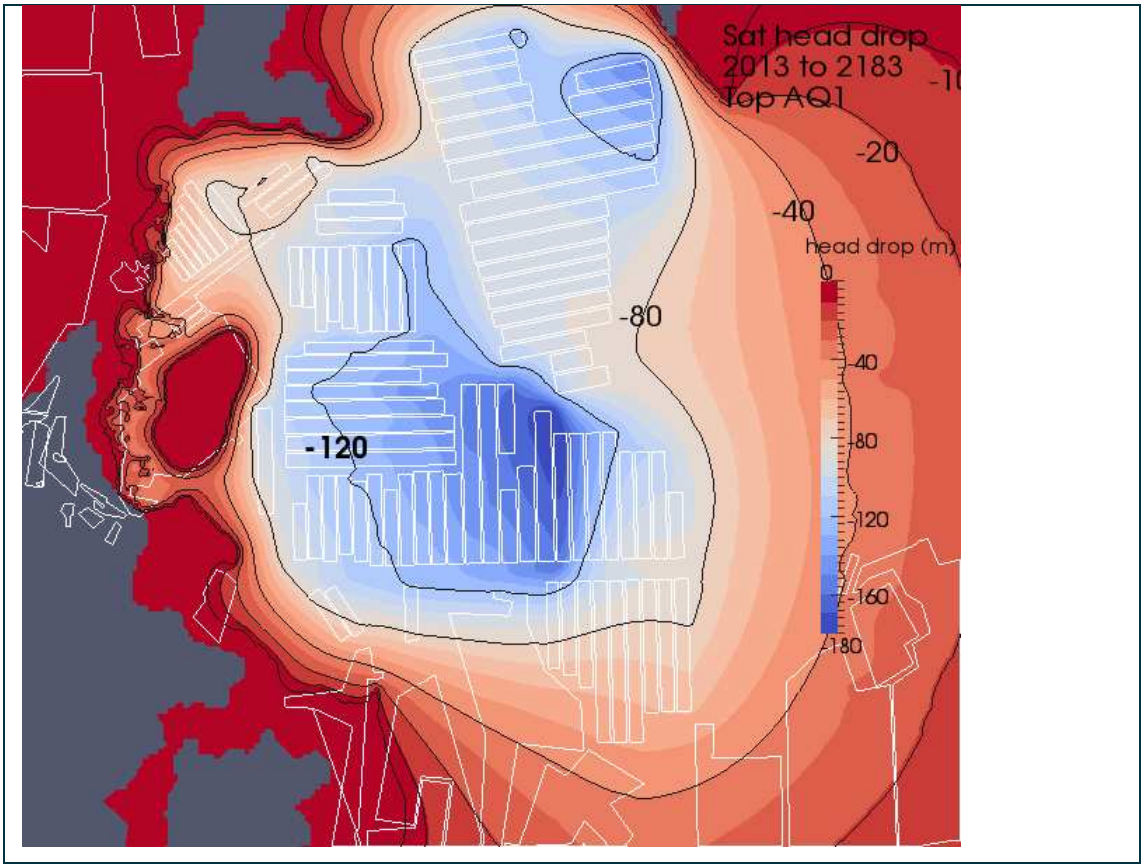

Figure D60 Distribution of head drops in AQ1 in 2183 with respect to groundwater levels in 2013

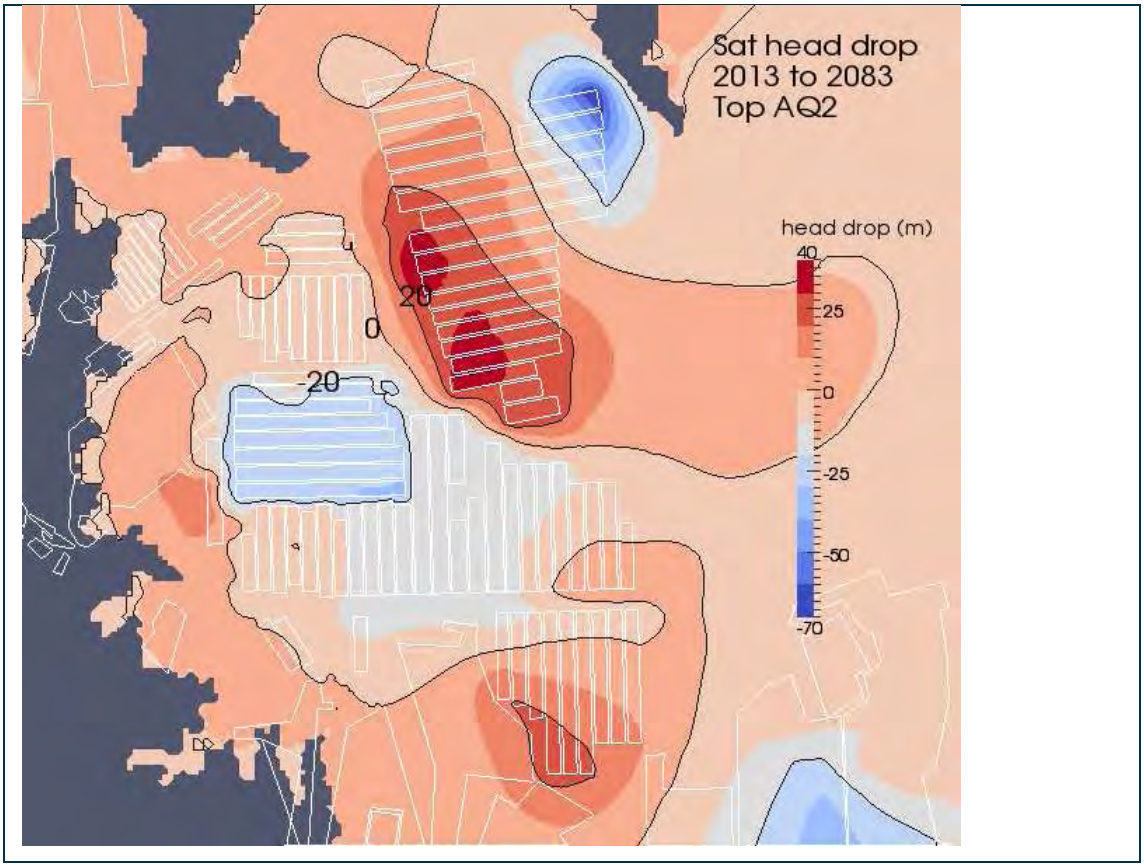

Figure D61 Distribution of head drops in AQ2 in 2083 with respect to groundwater levels in 2013

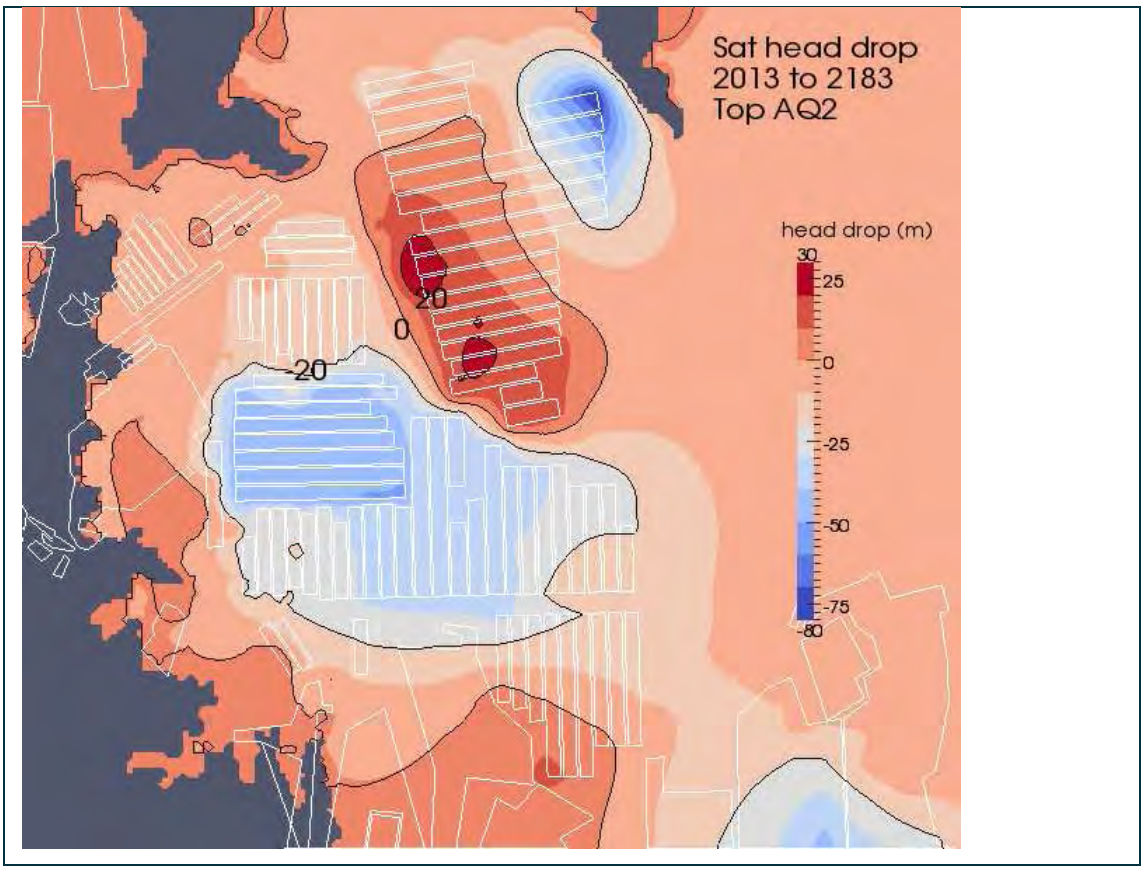

Figure D62 Distribution of head drops in AQ2 in 2183 with respect to groundwater levels in 2013

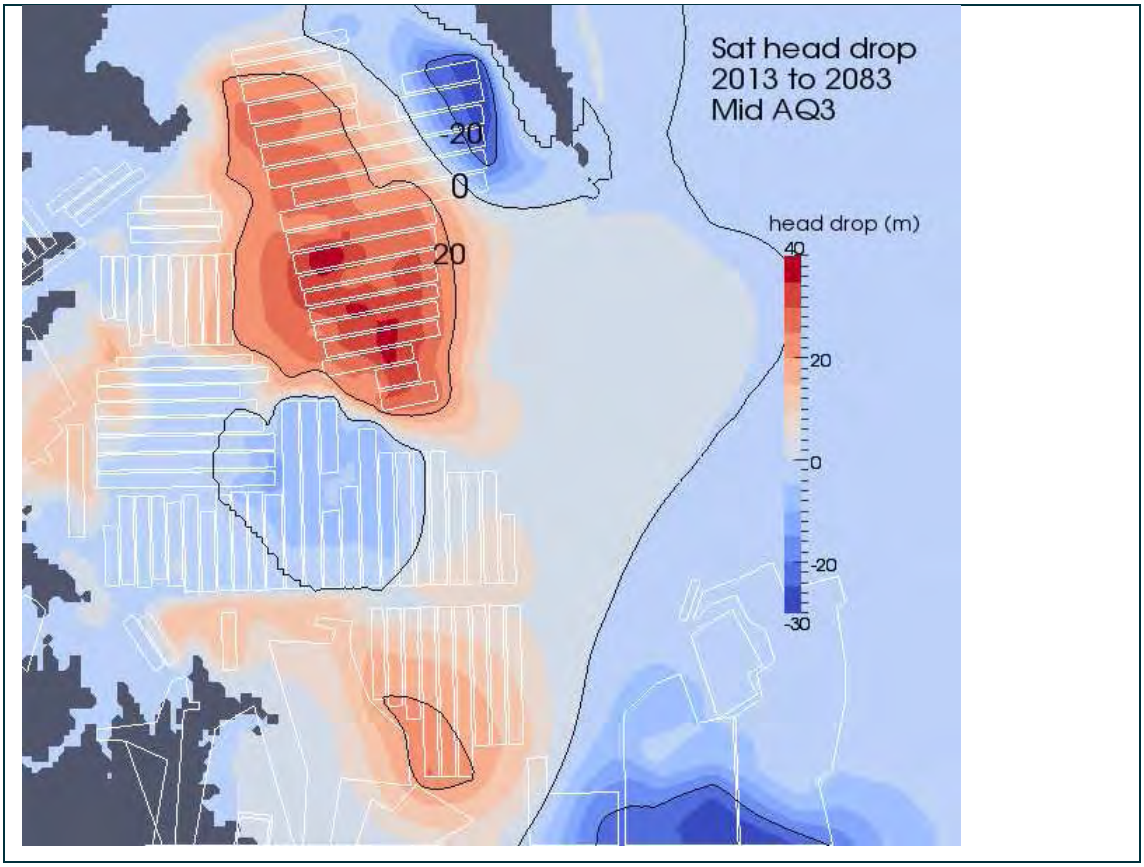

Figure D63 Distribution of head drops in AQ3 in 2083 with respect to groundwater levels in 2013

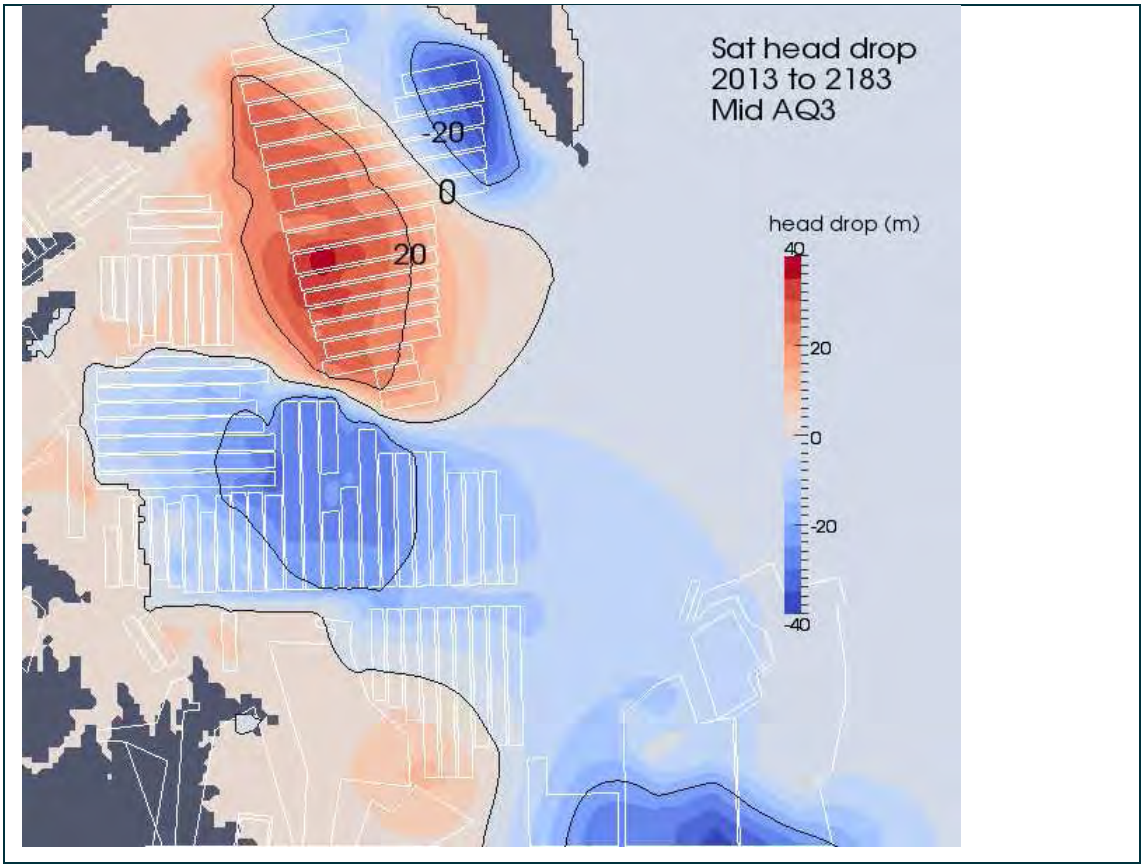

Figure D64 Distribution of head drops in AQ3 in 2183 with respect to groundwater levels in 2013

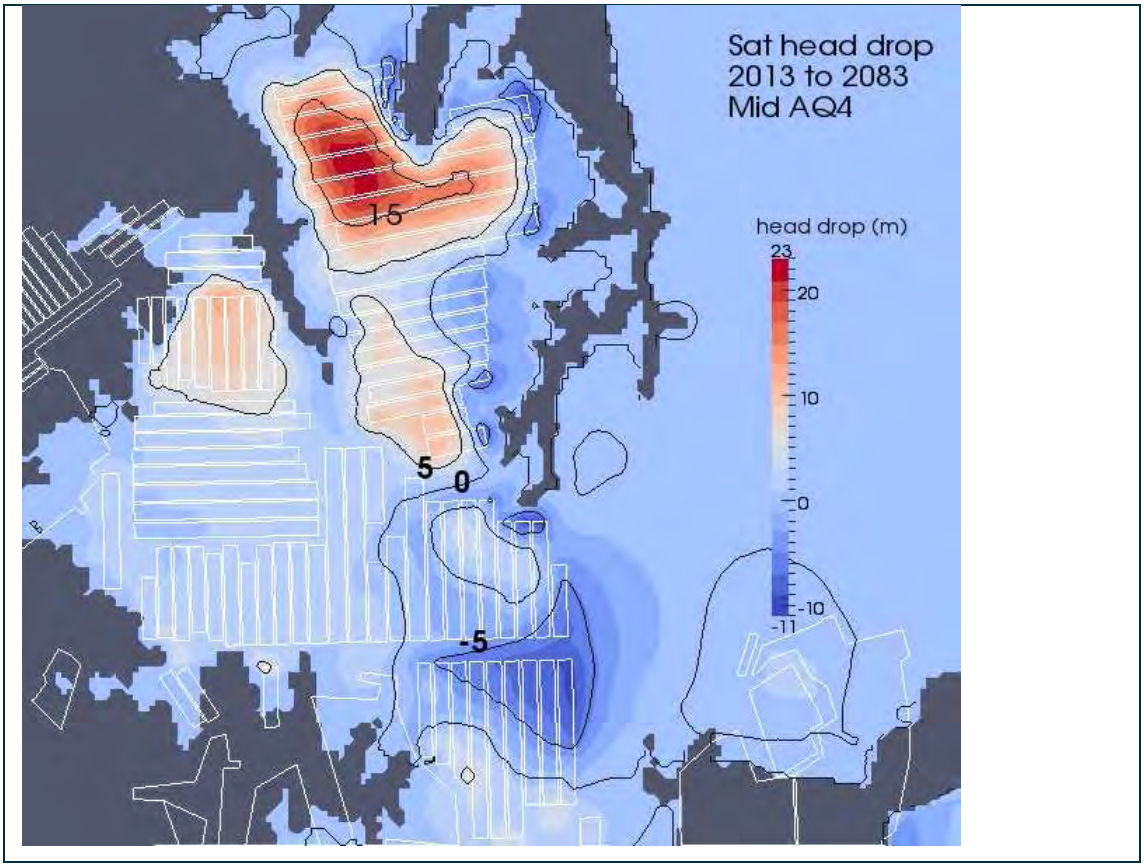

Figure D65 Distribution of head drops in AQ4 in 2083 with respect to groundwater levels in 2013

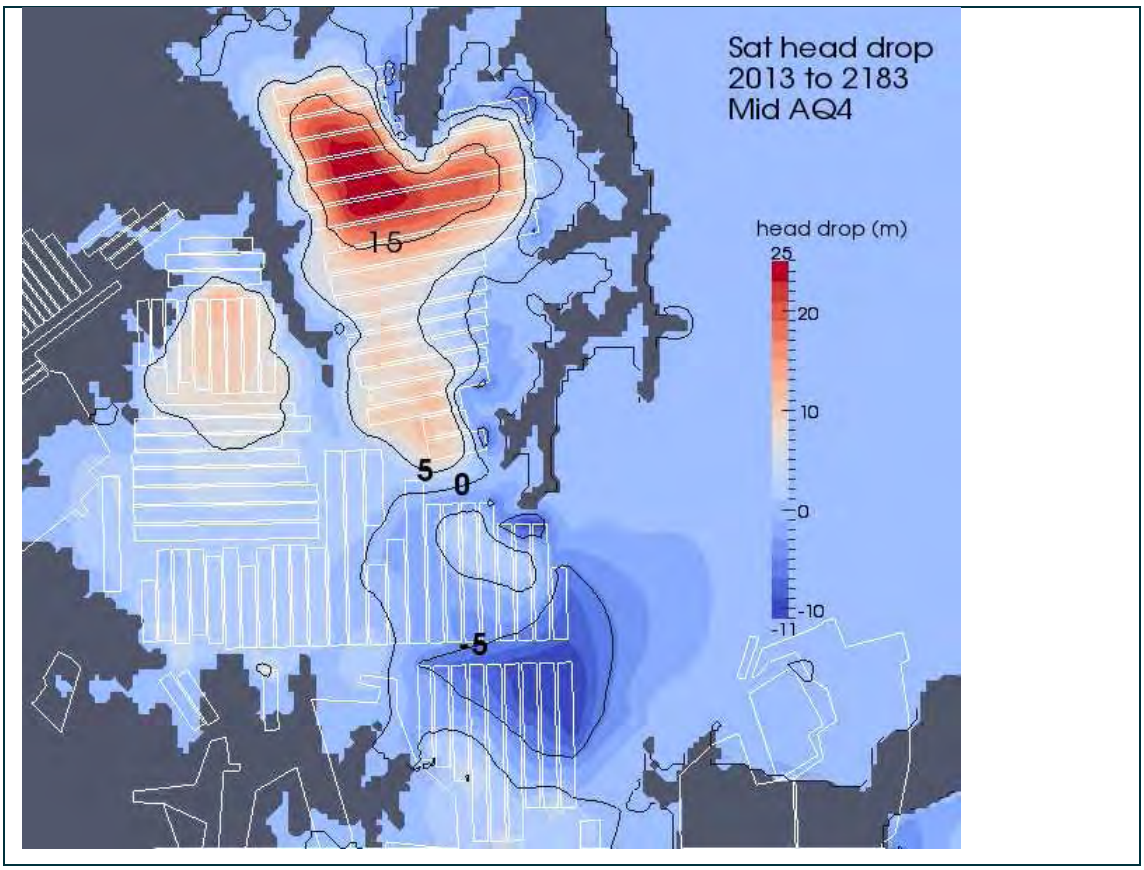

Figure D66 Distribution of head drops in AQ4 in 2183 with respect to groundwater levels in 2013

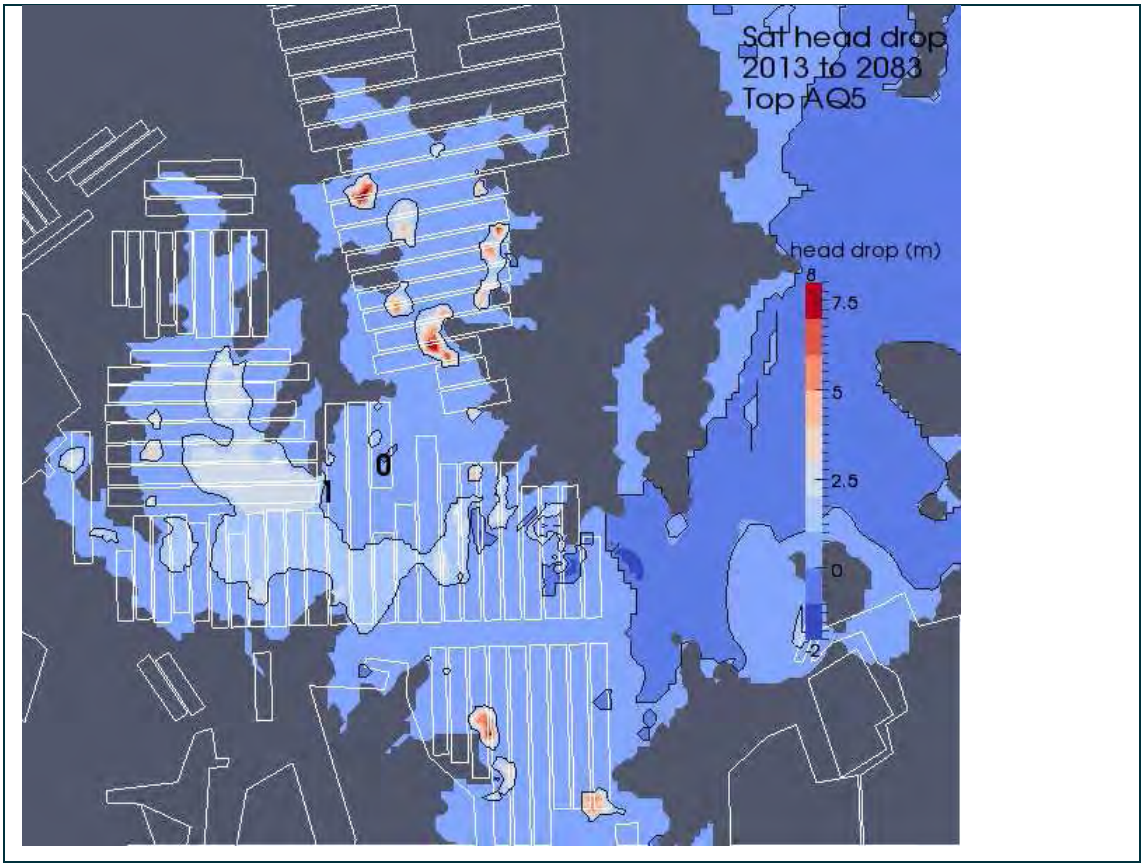

Figure D67 Distribution of head drops in AQ5 in 2083 with respect to groundwater levels in 2013

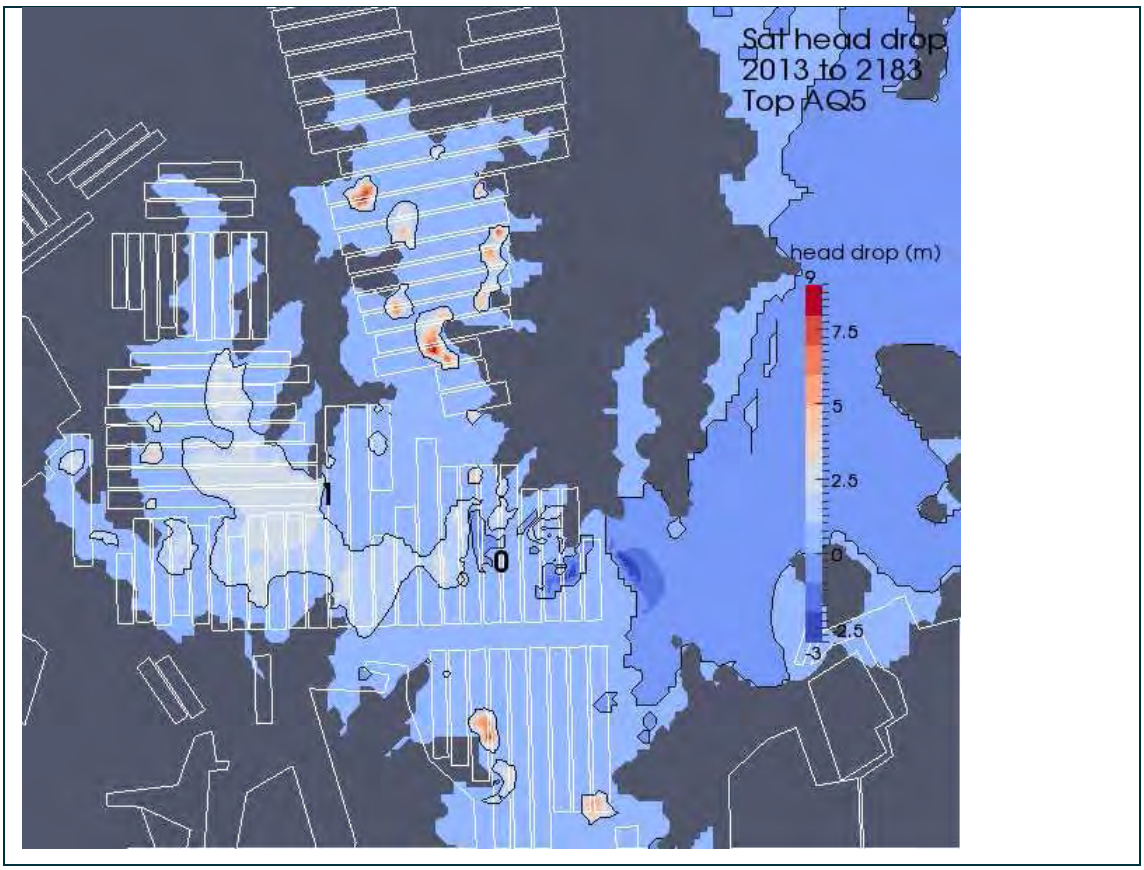

Figure D68 Distribution of head drops in AQ5 in 2183 with respect to groundwater levels in 2013

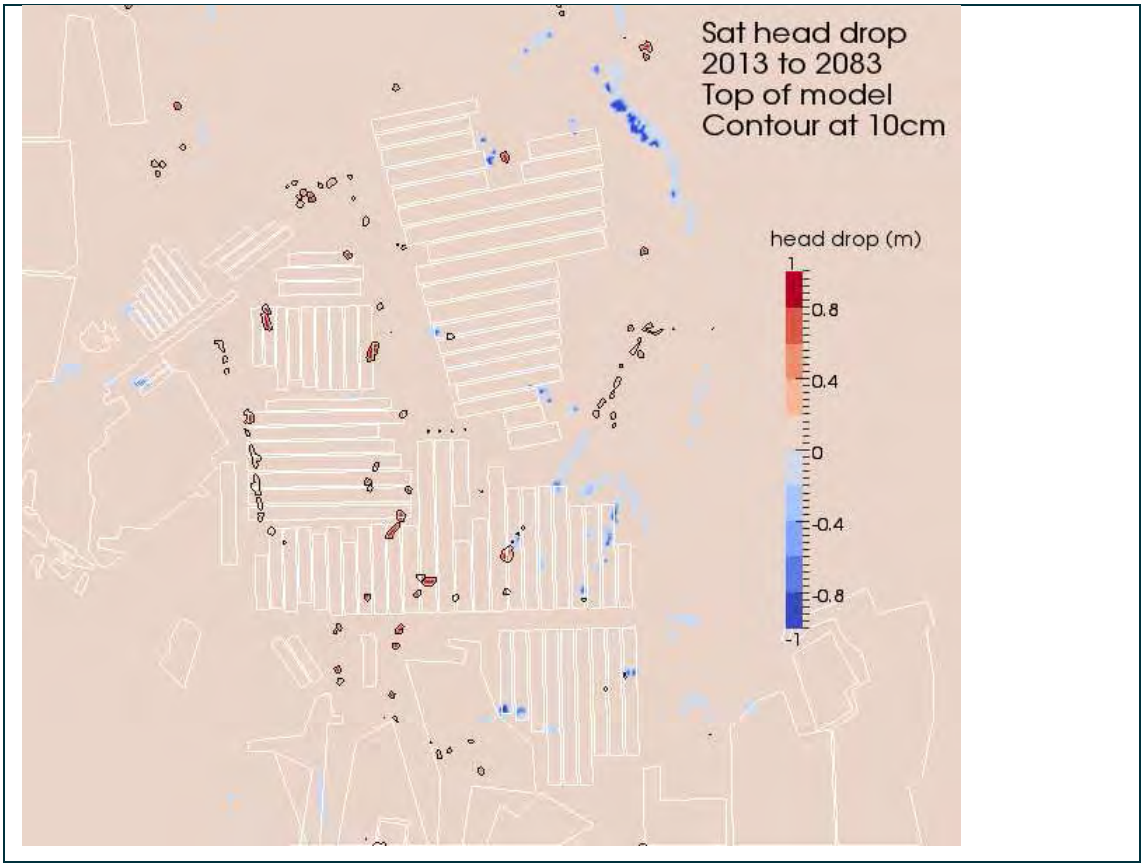

Figure D69 Distribution of head drops at the ground surface in 2083 with respect to groundwater levels in 2013

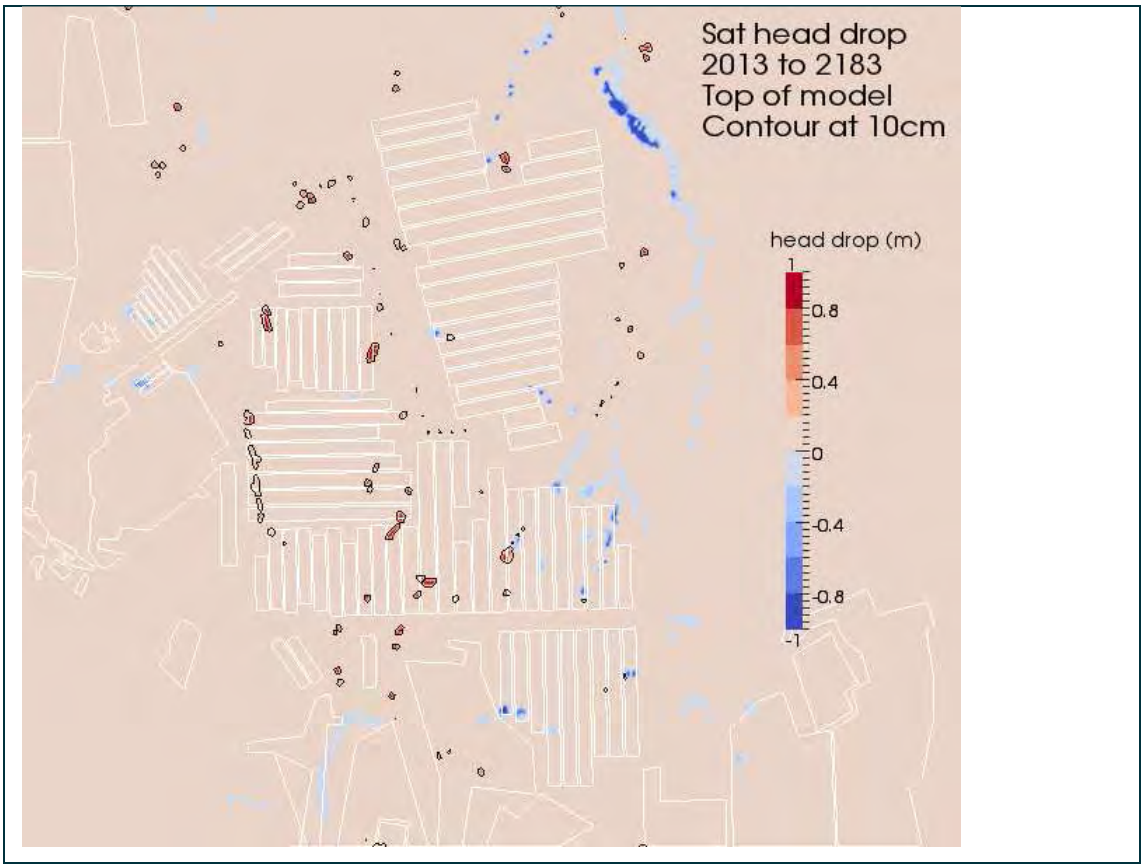

Figure D70 Distribution of head drops at the ground surface in 2183 with respect to groundwater levels in 2013

Different Mining Scenarios

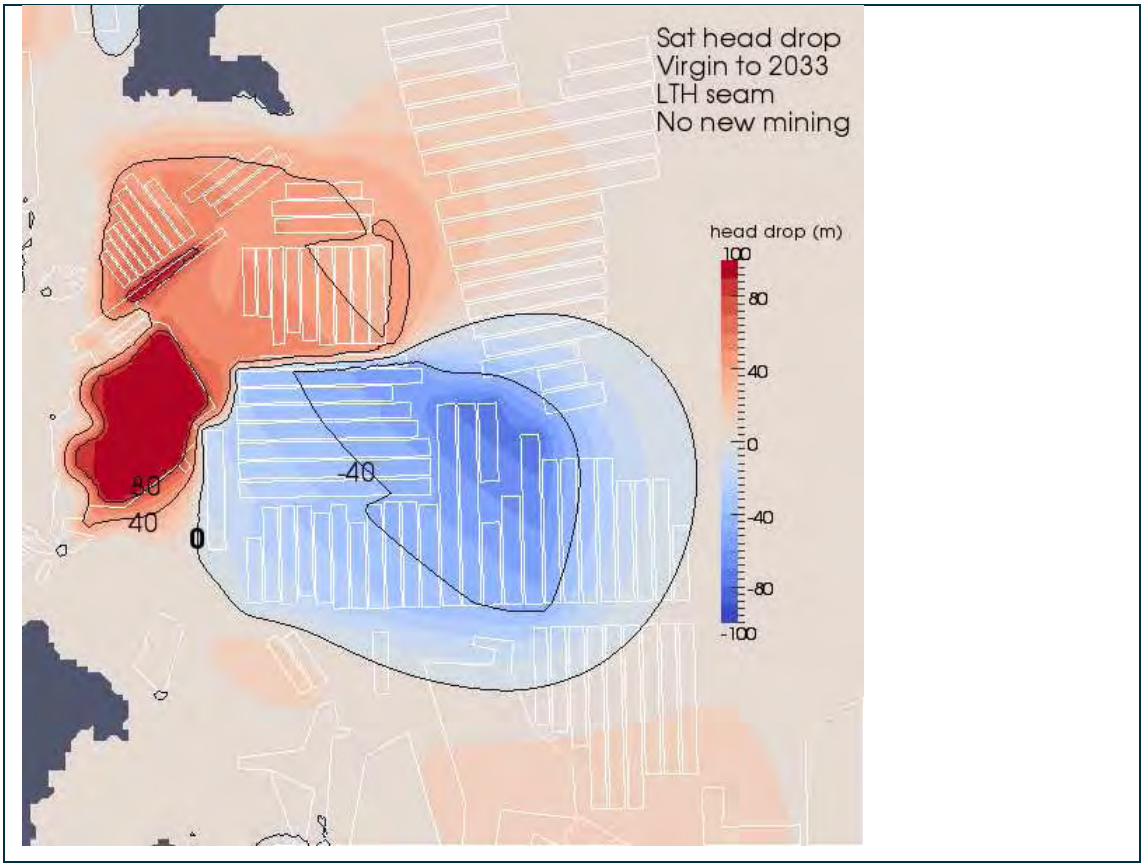

Figure D71 Distribution of head drops in the Lithgow seam at 2033 with respect to pre-mining conditions for the No New Mining scenario.

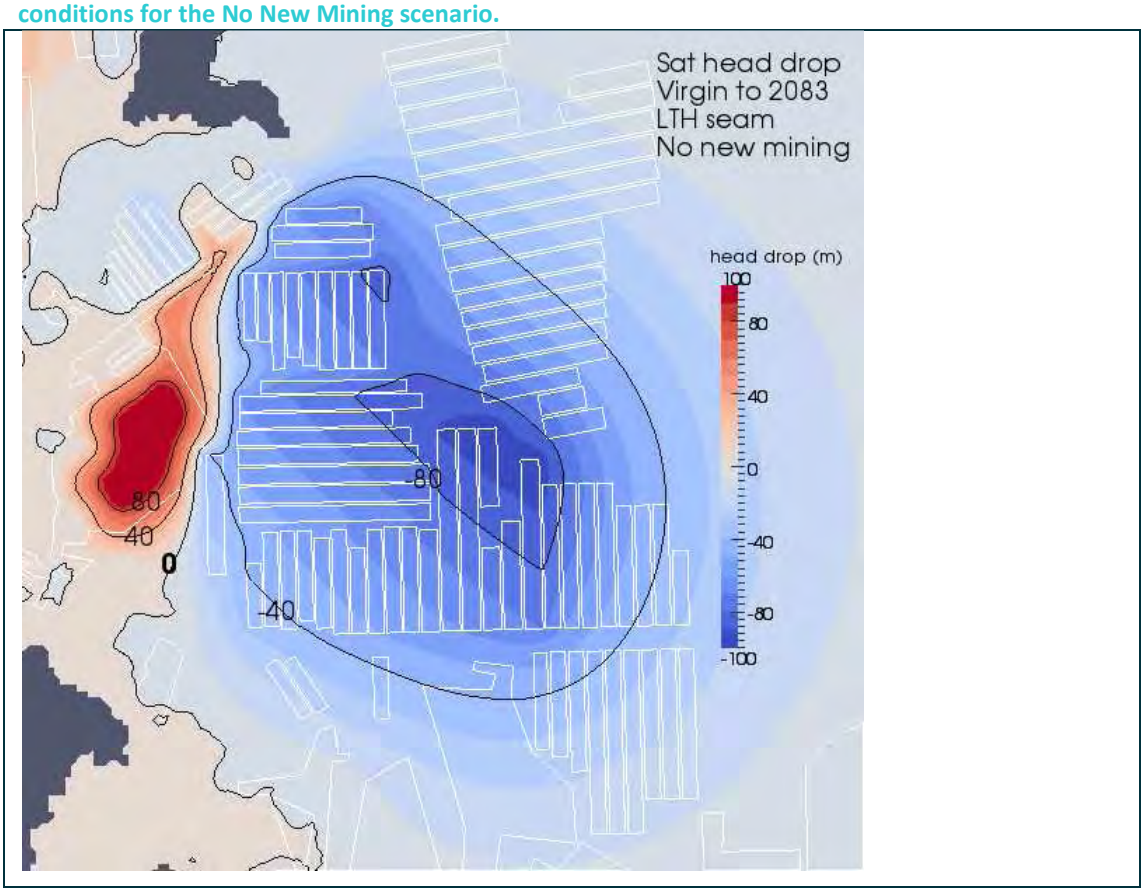

Figure D72 Distribution of head drops in the Lithgow seam at 2083 with respect to pre-mining conditions for the No New Mining scenario.

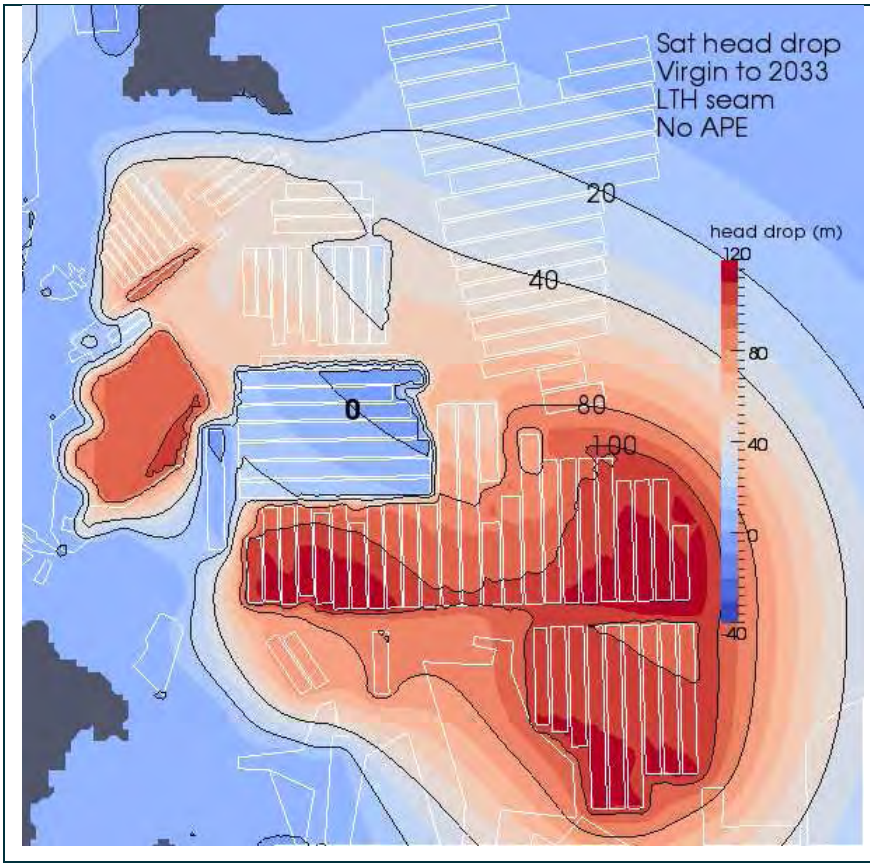

Figure D73 Distribution of head drops in the Lithgow seam at 2033 with respect to pre-mining conditions for the No APE scenario

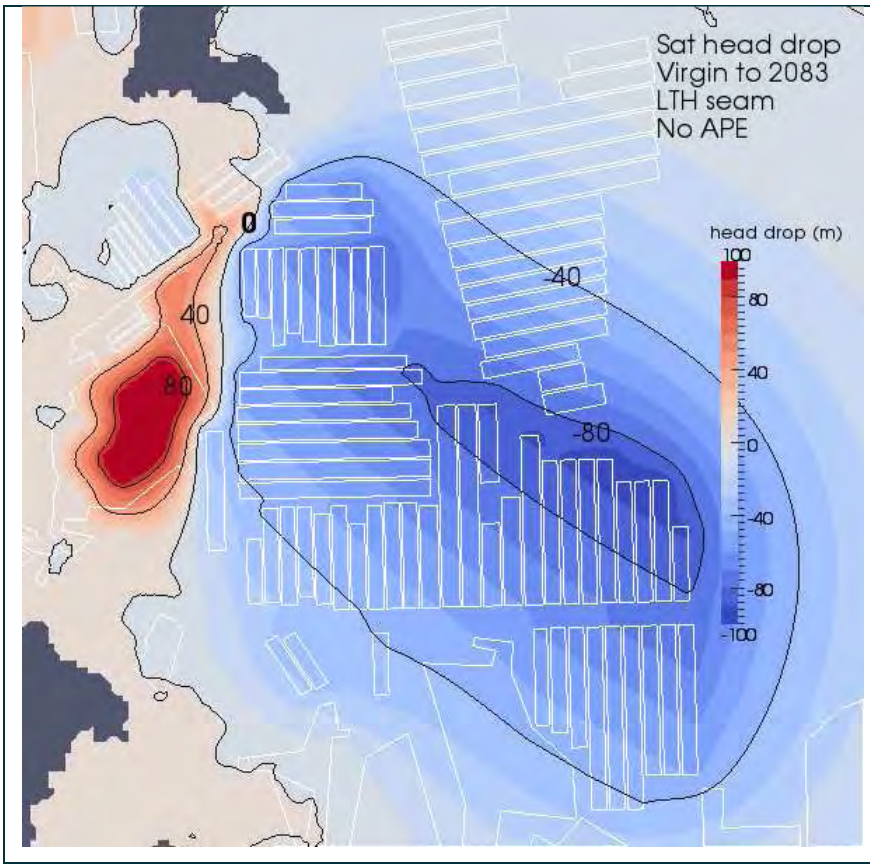

Figure D74 Distribution of head drops in the Lithgow seam at 2083 with respect to pre-mining conditions for the No APE scenario

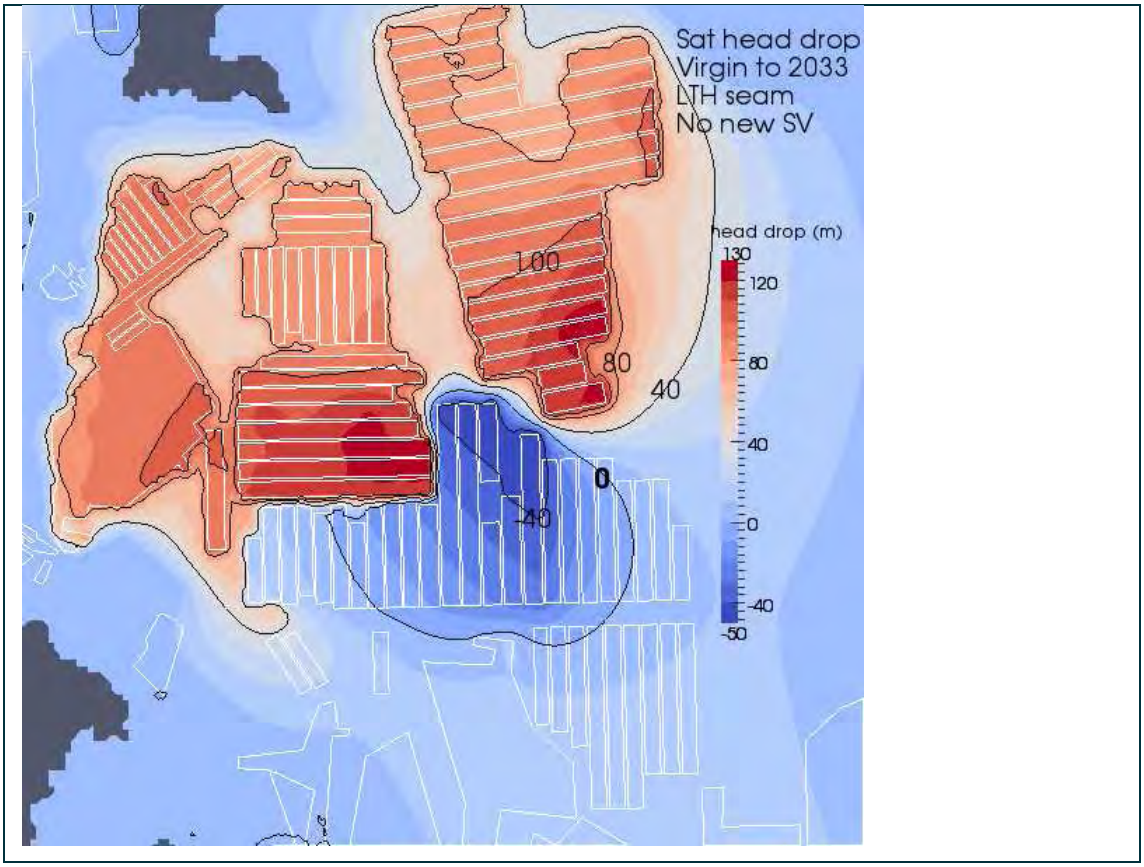

Figure D75 Distribution of head drops in the Lithgow seam at 2033 with respect to pre-mining conditions for the No New SV scenario

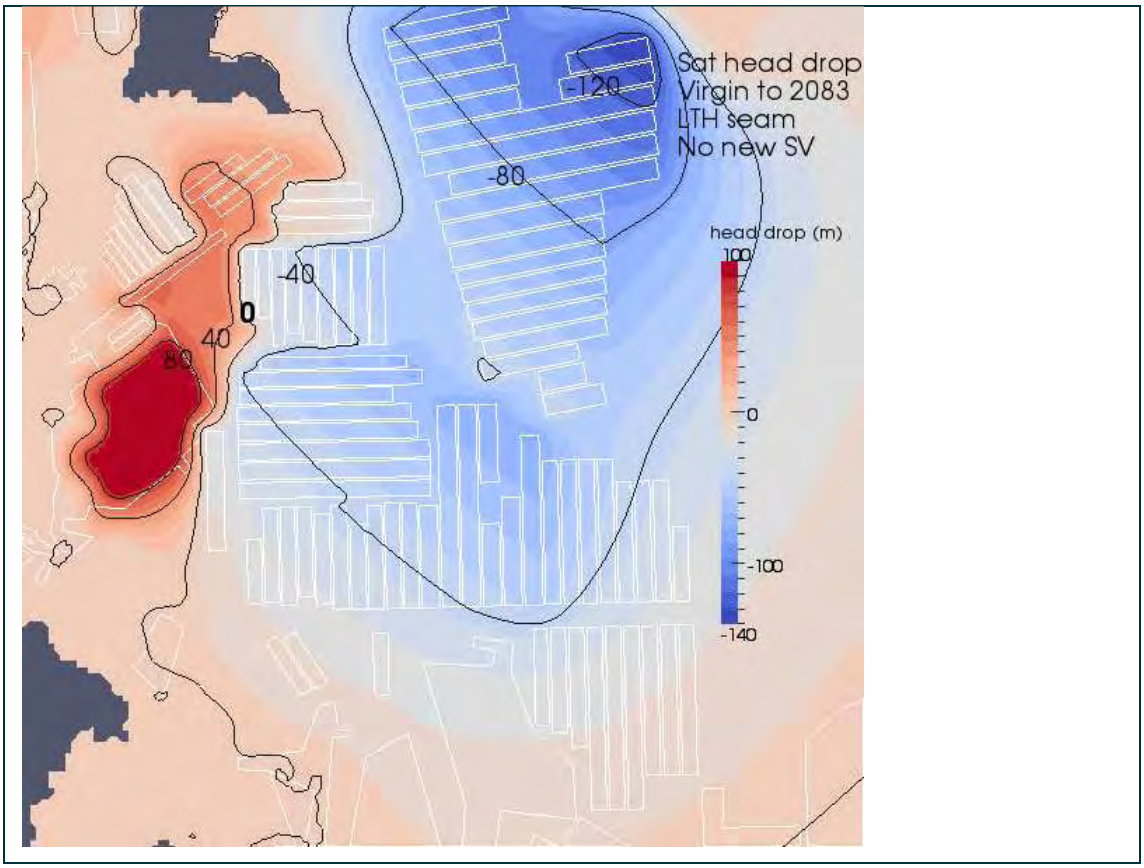

Figure D76 Distribution of head drops in the Lithgow seam at 2083 with respect to pre-mining conditions for the No New SV scenario

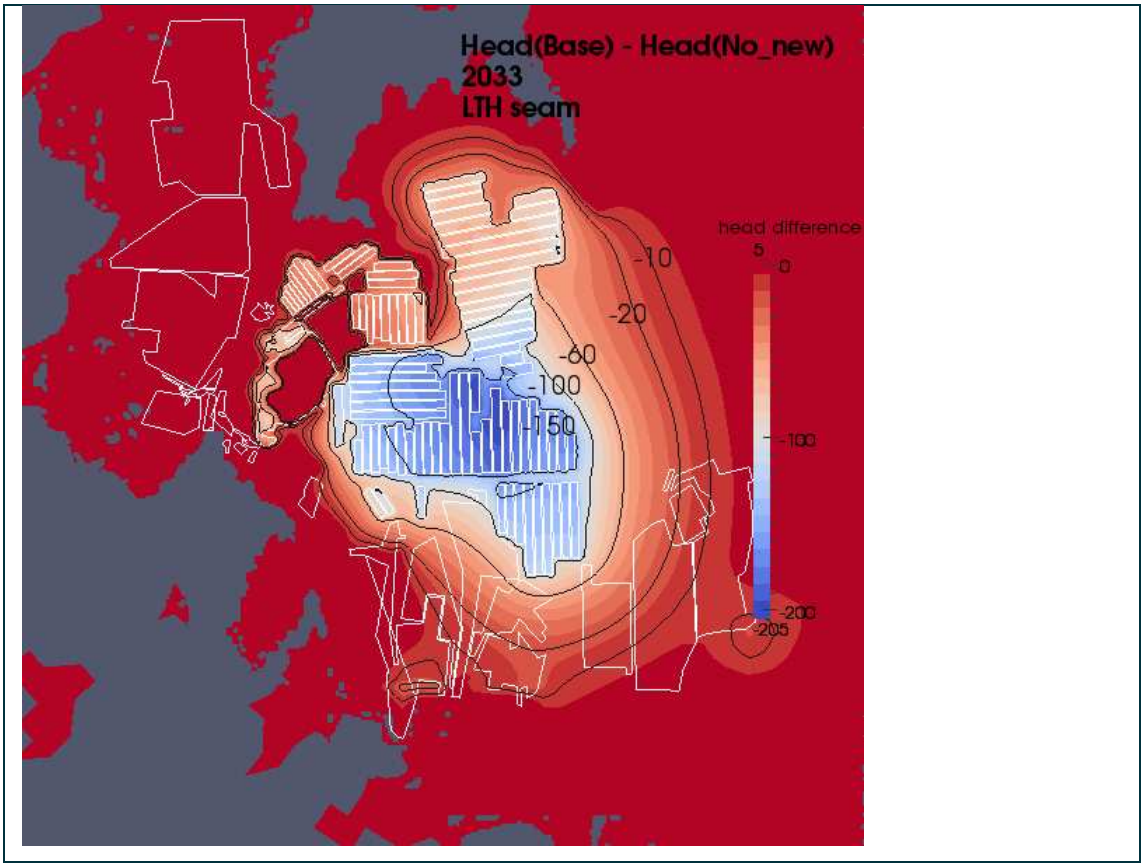

Figure D77 Head in the base model minus head in the No New scenario at year 2033 for the Lithgow seam

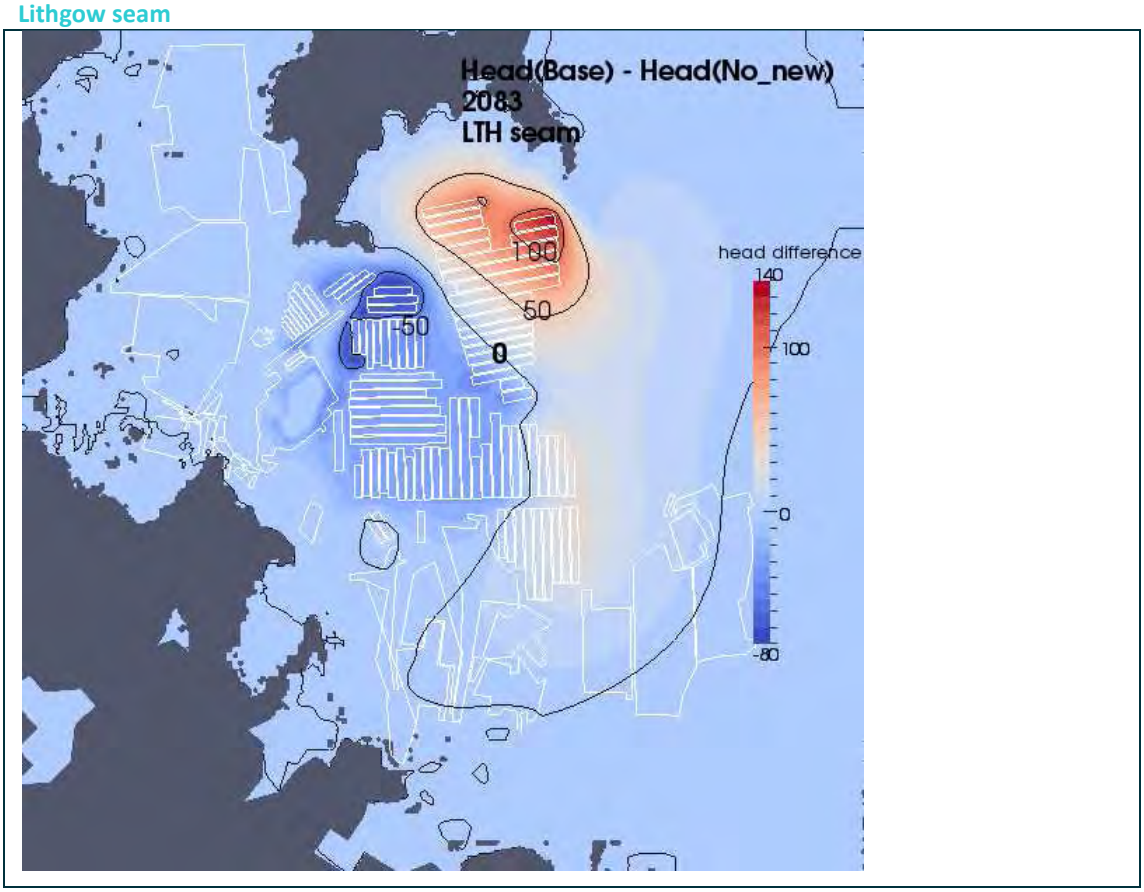

Figure D78 Head in the base model minus head in the No New scenario at year 2083 for the Lithgow seam

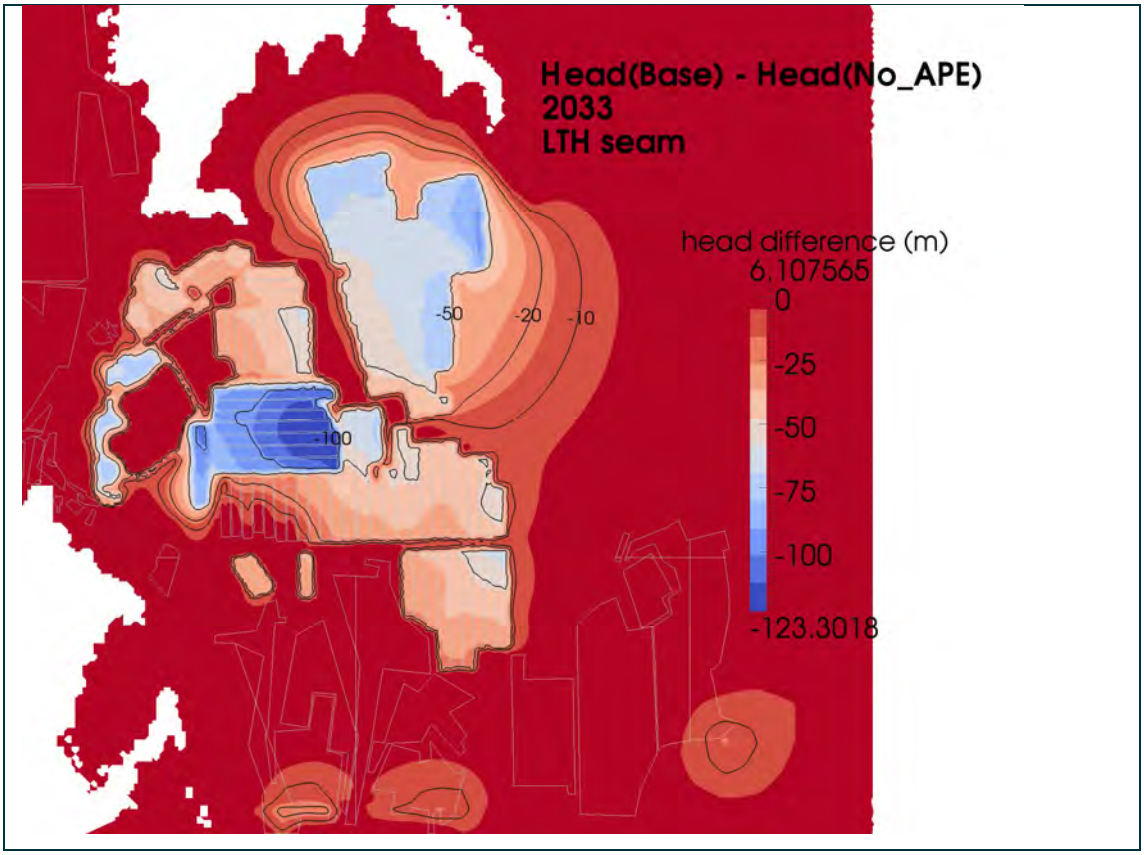

Figure D79 Head in the base model minus head in the No APE scenario at year 2033 for the Lithgow seam

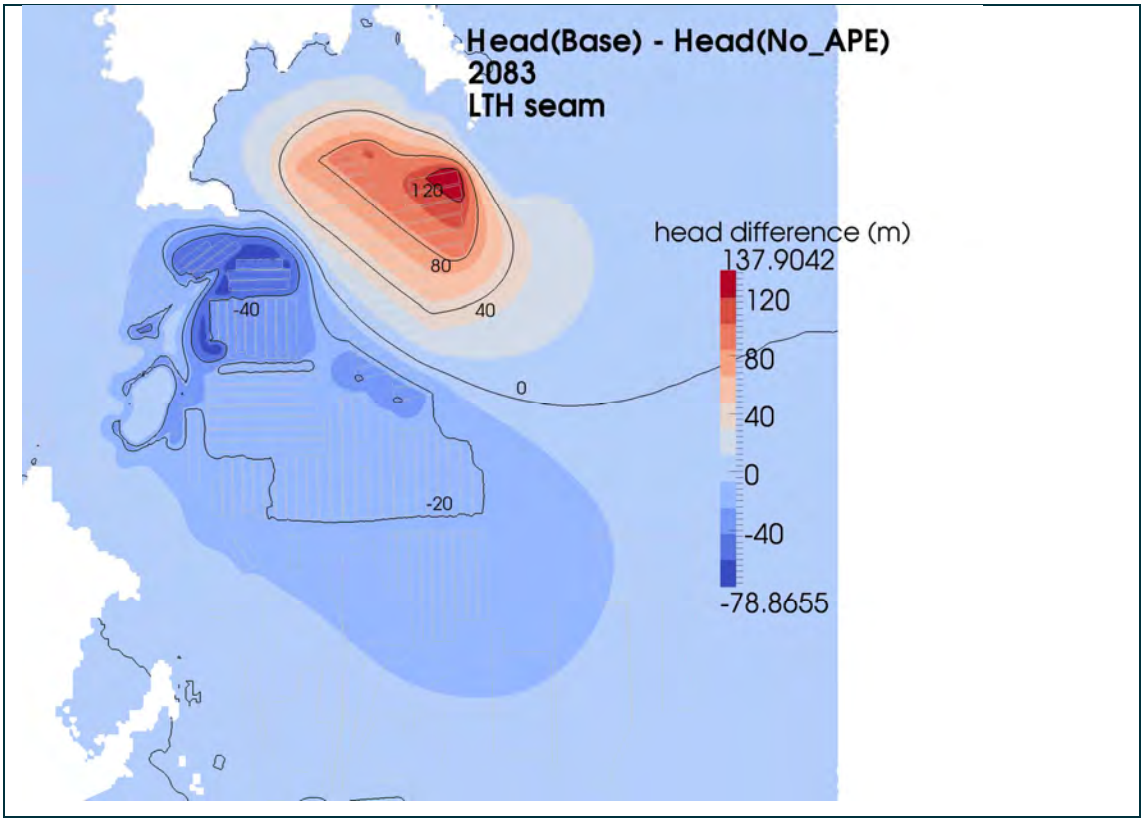

Figure D80 Head in the base model minus head in the No APE scenario at year 2083 for the Lithgow seam

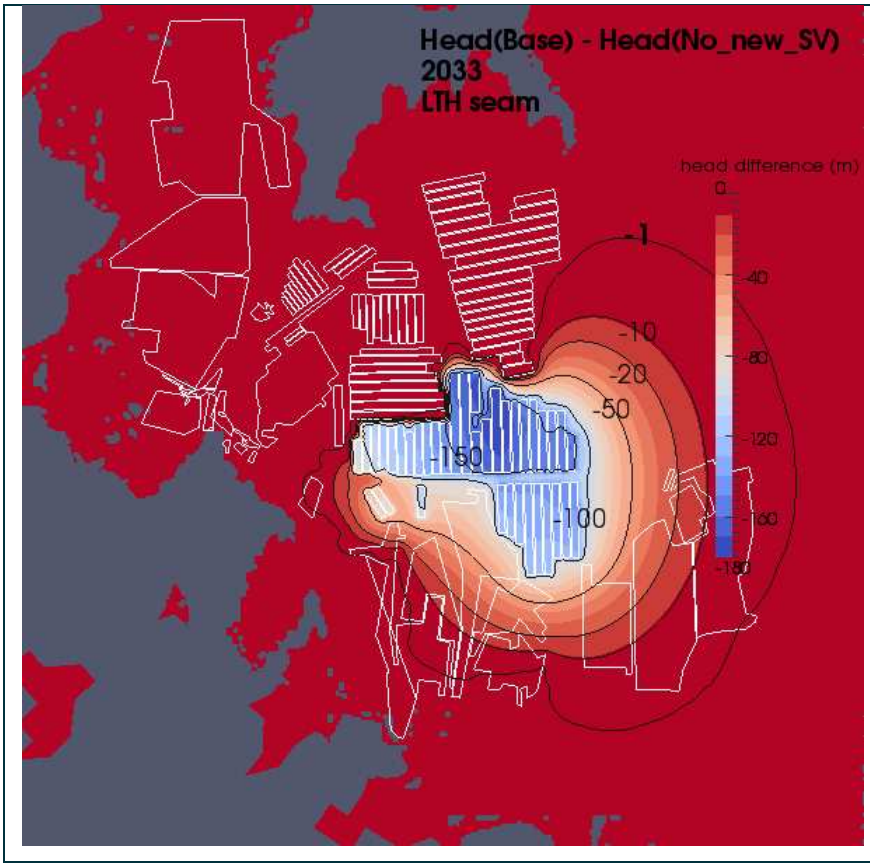

Figure D81 Head in the base model minus head in the No New SV scenario at year 2033 for the Lithgow seam

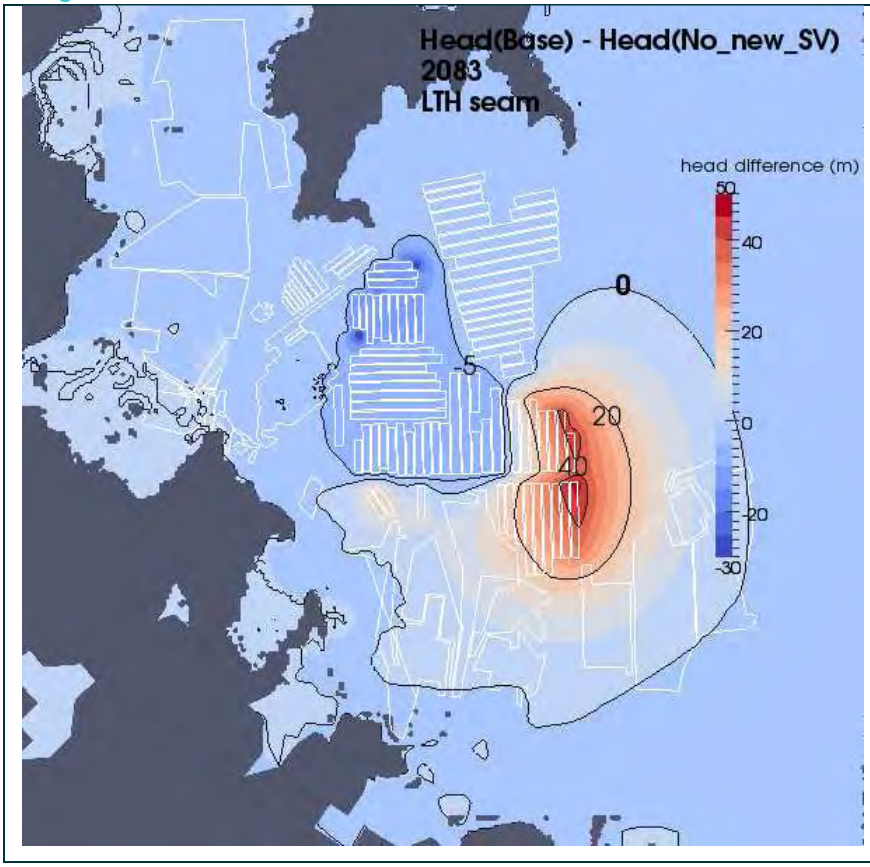

Figure D82 Head in the base model minus head in the No New SV scenario at year 2083 for the Lithgow seam

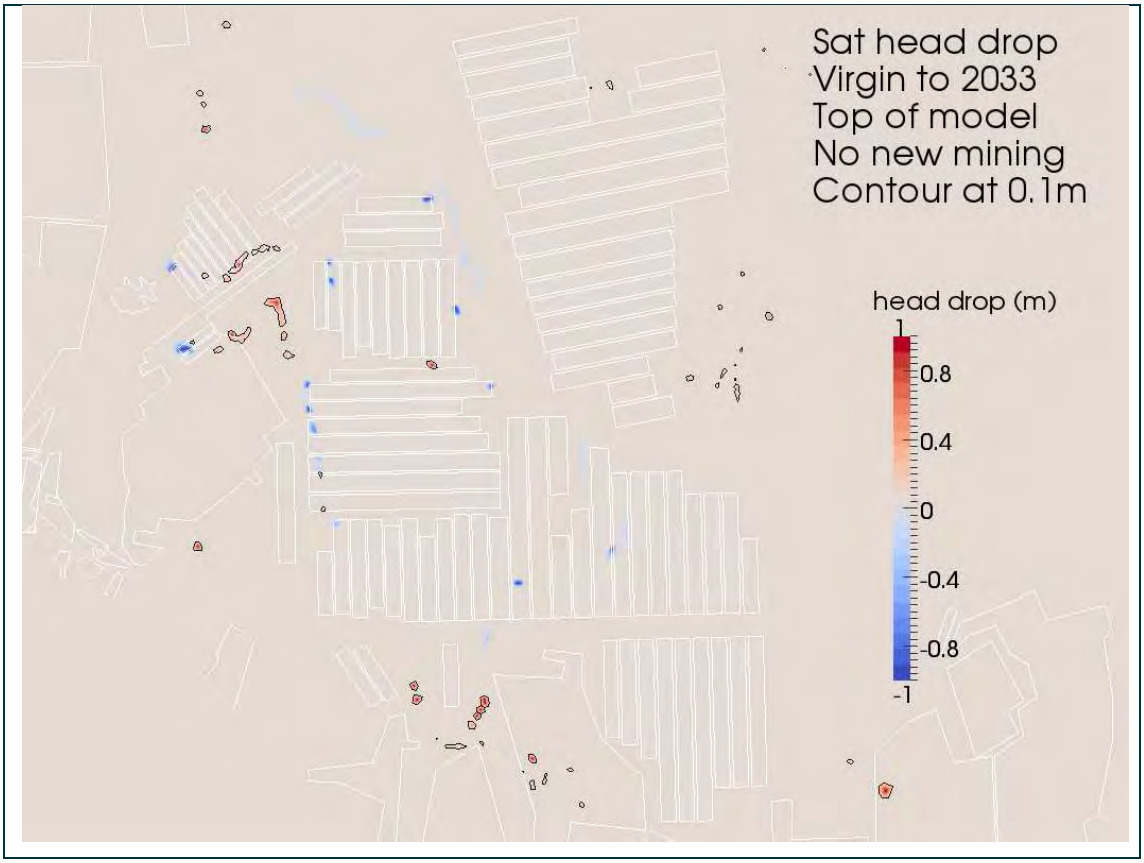

Figure D83 Distribution of head drops at the ground surface in 2033 with respect to pre-mining conditions for the No New scenario

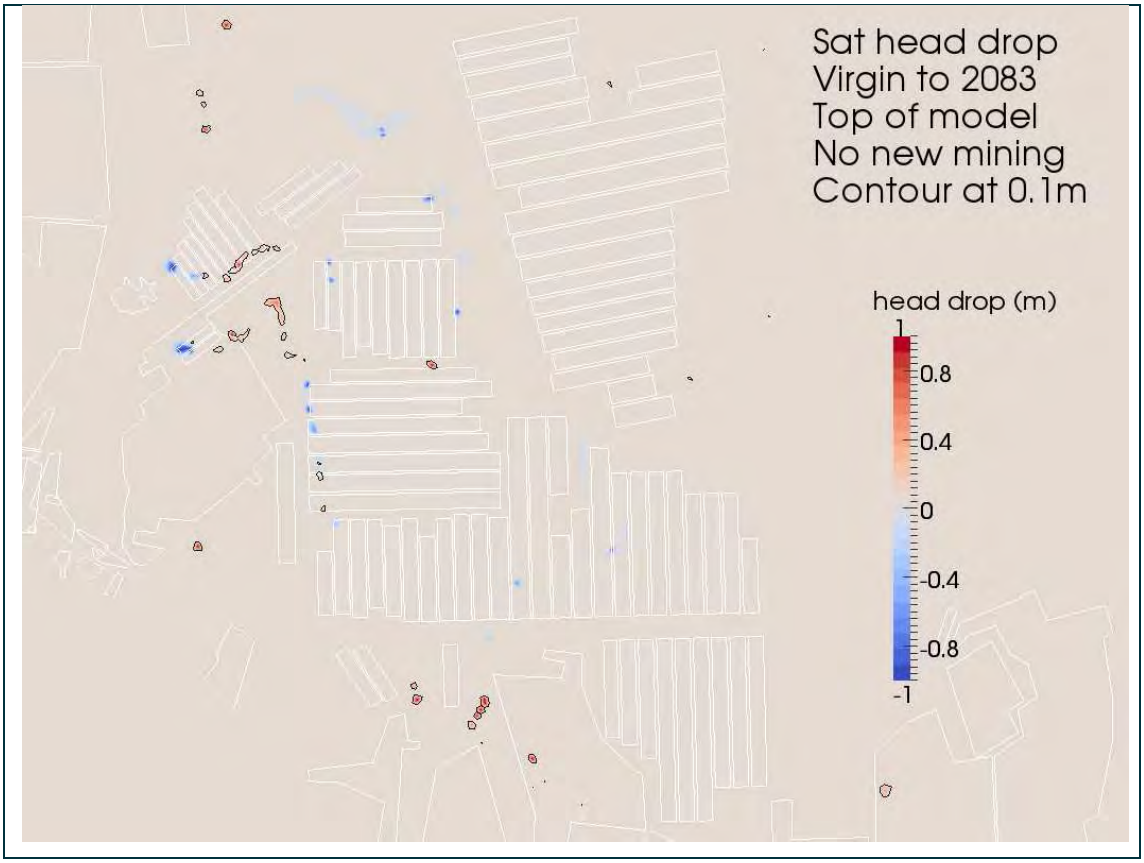

Figure D84 Distribution of head drops at the ground surface in 2083 with respect to pre-mining conditions for the No New scenario

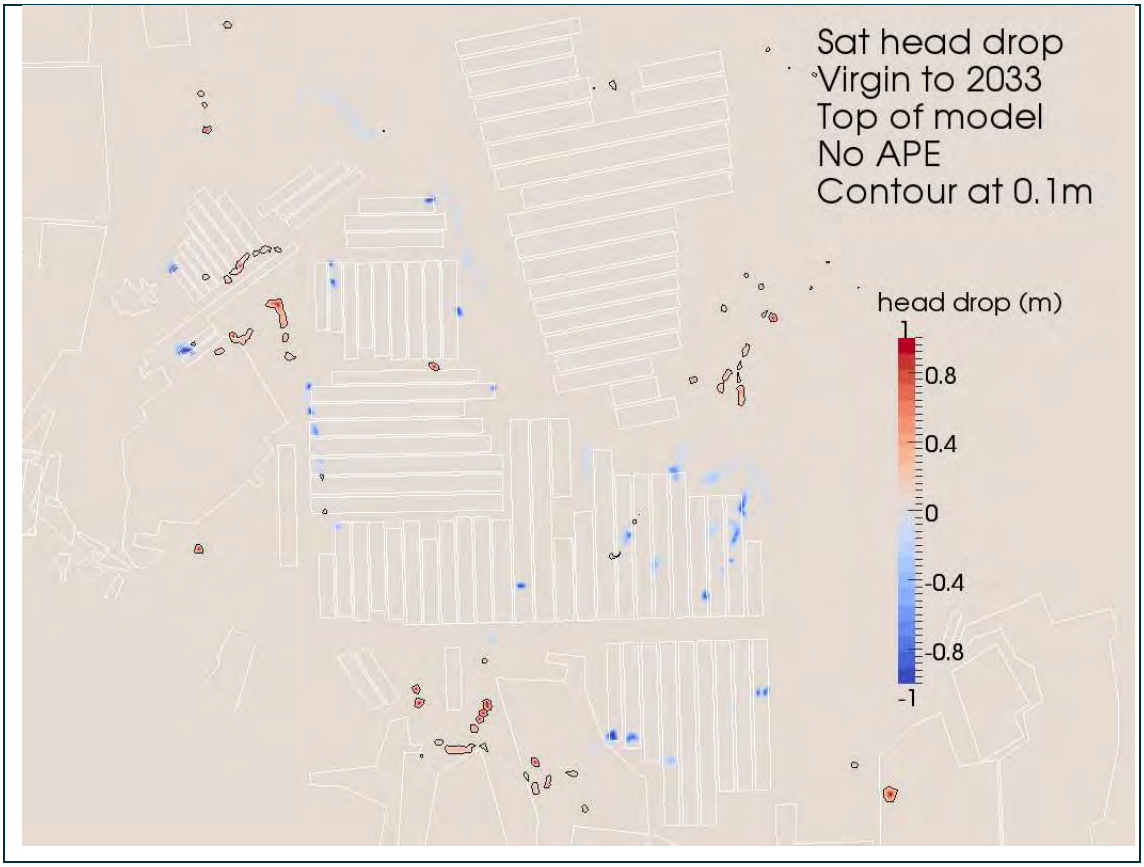

Figure D85 Distribution of head drops at the ground surface in 2033 with respect to pre-mining conditions for the No APE scenario

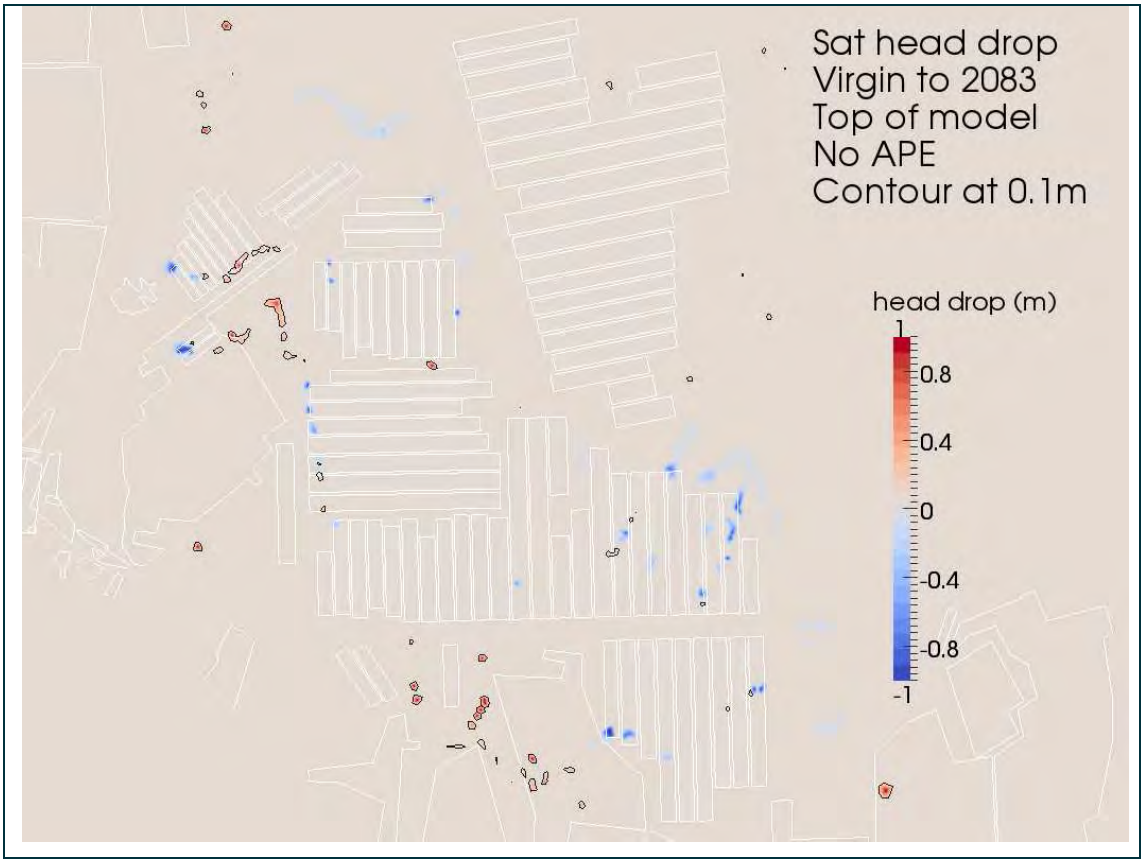

Figure D86 Distribution of head drops at the ground surface in 2083 with respect to pre-mining conditions for the No APE scenario

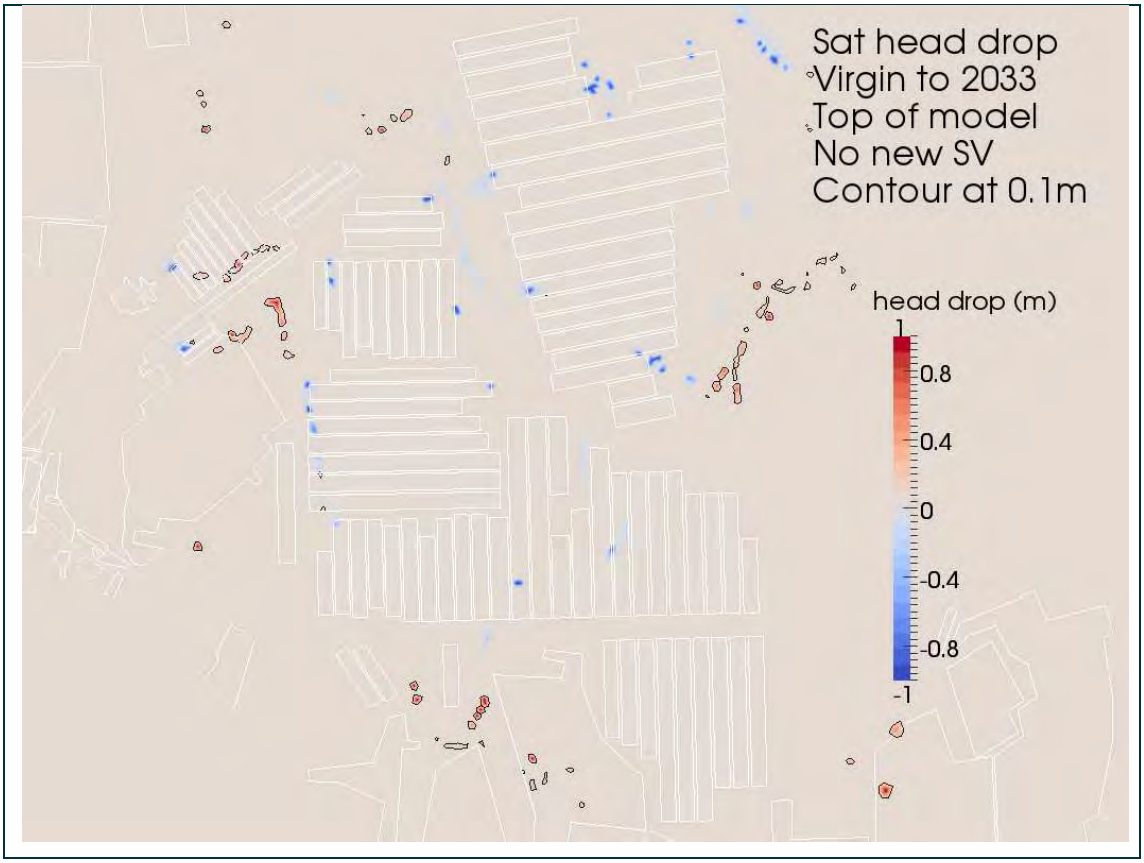

Figure D87 Distribution of head drops at the ground surface in 2033 with respect to pre-mining conditions for the No New SV scenario

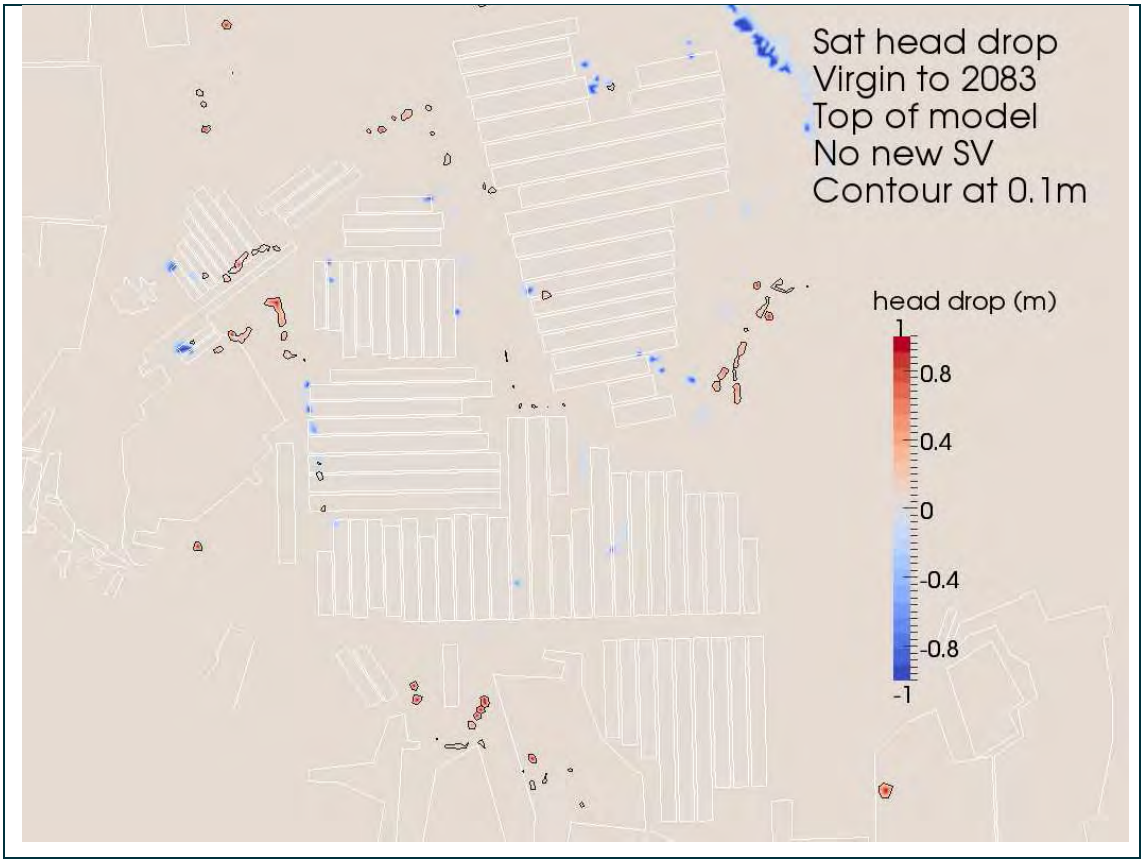

Figure D88 Distribution of head drops at the ground surface in 2083 with respect to pre-mining conditions for the No New SV scenario

EARTH SCIENCE AND RESOURCE ENGINEERING
www.csiro.au

Appendix E

Baseflow to Swamps and Streams with Seepage Boundary

Angus Place and Springvale Colliery Operations Groundwater Assessment

D P Adhikary and A Wilkins
Report No EP132799
May 2013

Springvale Colliery and Angus Place Colliery

Citation

Adhikary, DP and Wilkins, A (2013) Angus Place and Springvale Colliery operations groundwater assessment. Appendix E - Baseflow to Swamps and Streams with Seepage Boundary. Report No EP132799.

Copyright and disclaimer

Important disclaimer

Figures

Assessment of Boundary Effect on Baseflow

The 'base case' model has been prescribed mixed boundary conditions (fixed pressure and impermeable boundaries) as described in Section 2.11. In order to assess the model boundary effect on the drawdown and baseflow to swamps and streams an additional model was run with a seepage conditions prescribed on four vertical sides of the model. In that model, the pressure on the boundary is defined as $P_w \leq P_{prescribed}$, where $P_{prescribed}$ is the pressure obtained at the model boundaries from the extended model as described in Sections 2.10 and 2.11. This boundary condition will allow water to seep out from the model should pressure on the boundary node exceed $P_{prescribed}$, but will not allow any water inflow from the model boundary should pressure on the boundary node drop due to mining induced sink thus permitting unrestricted pressure drop along the model boundaries.

The boundary nodes were assigned a much higher conductance (1E-10 m/s/Pa per unit area) compared to strata permeability to ensure that any excess pressure on the boundary node dissipates quickly. This boundary condition represents another extreme compared to a fixed pressure boundary condition as it would allow unrestricted pressure drop on the model boundary. The real/natural situation would lie between the modeled seepage boundary and the fixed pressure boundary (base case).

Figure E1 to Figure E21 present comparisons between the baseflow balances obtained from the fixed pressure and the seepage boundary models. It can be seen that the baseflow values are identical, which indicates that the fixed pressure boundary condition used in the base case model has no effect on the computed baseflow values.

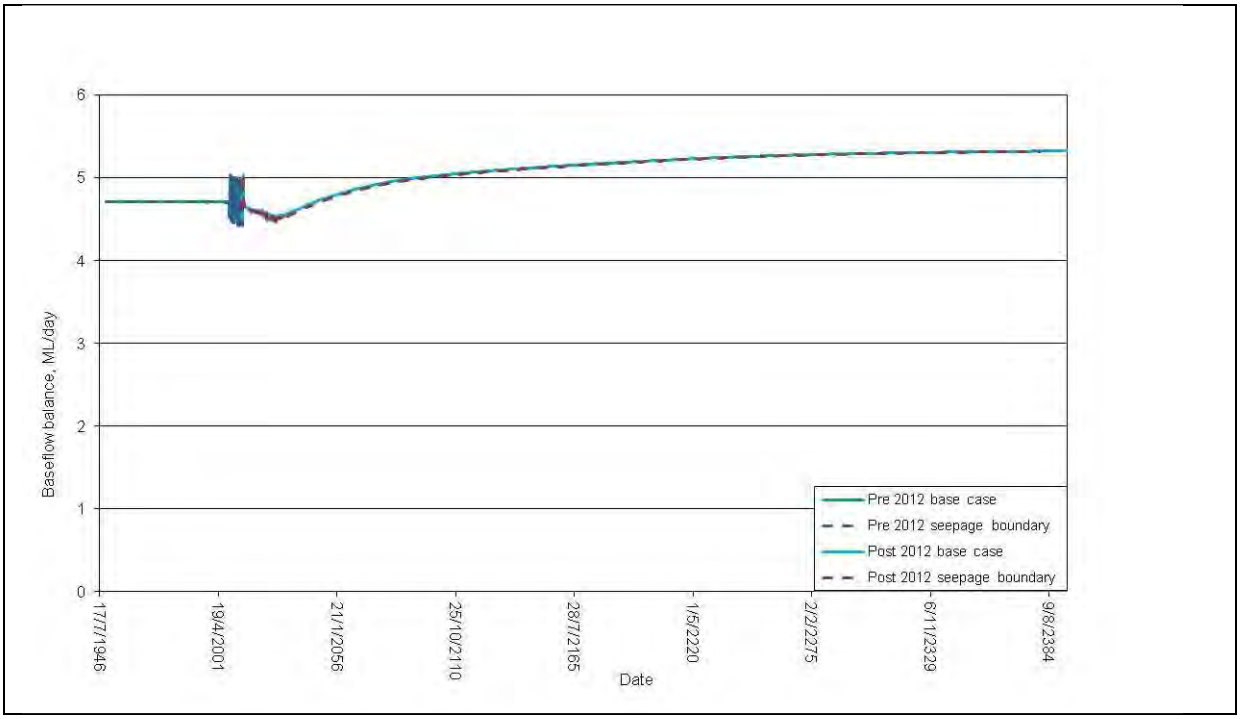

Figure E1 Estimates of baseflow balance (Carne_1) – a comparison between fixed head boundary and seepage boundary conditions

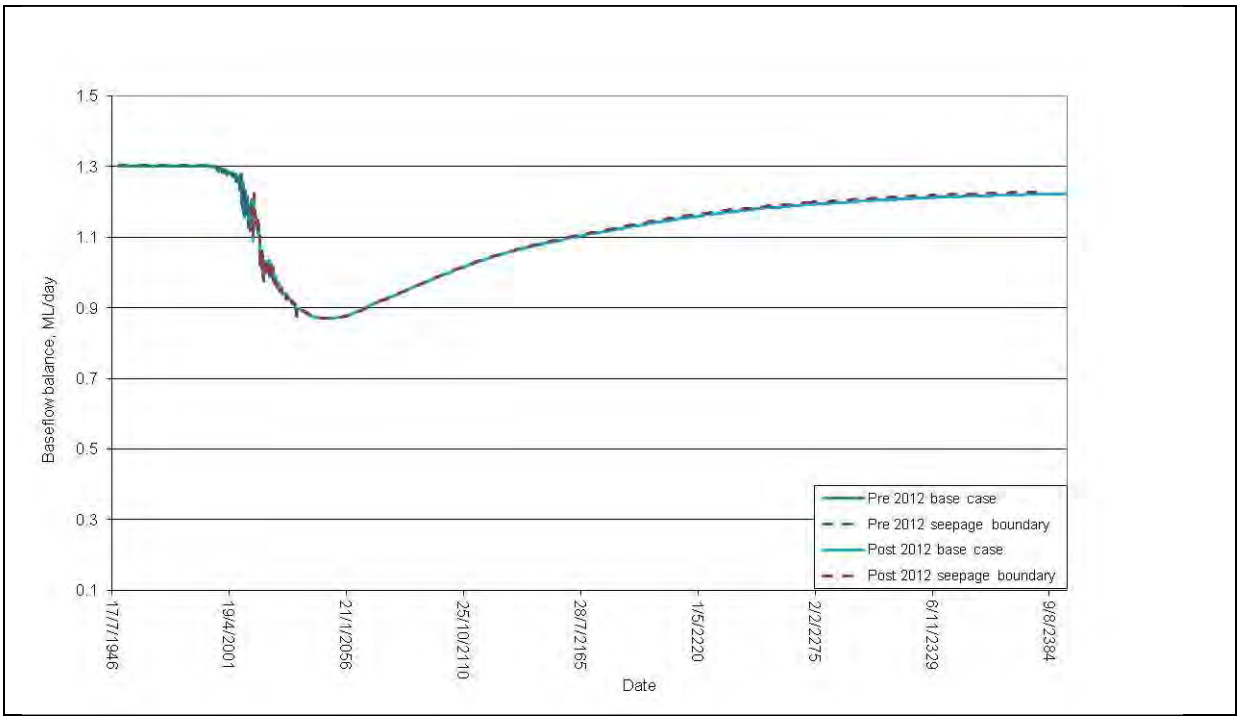

Figure E2 Estimates of baseflow balance (Carne_2) – a comparison between fixed head boundary and seepage boundary conditions

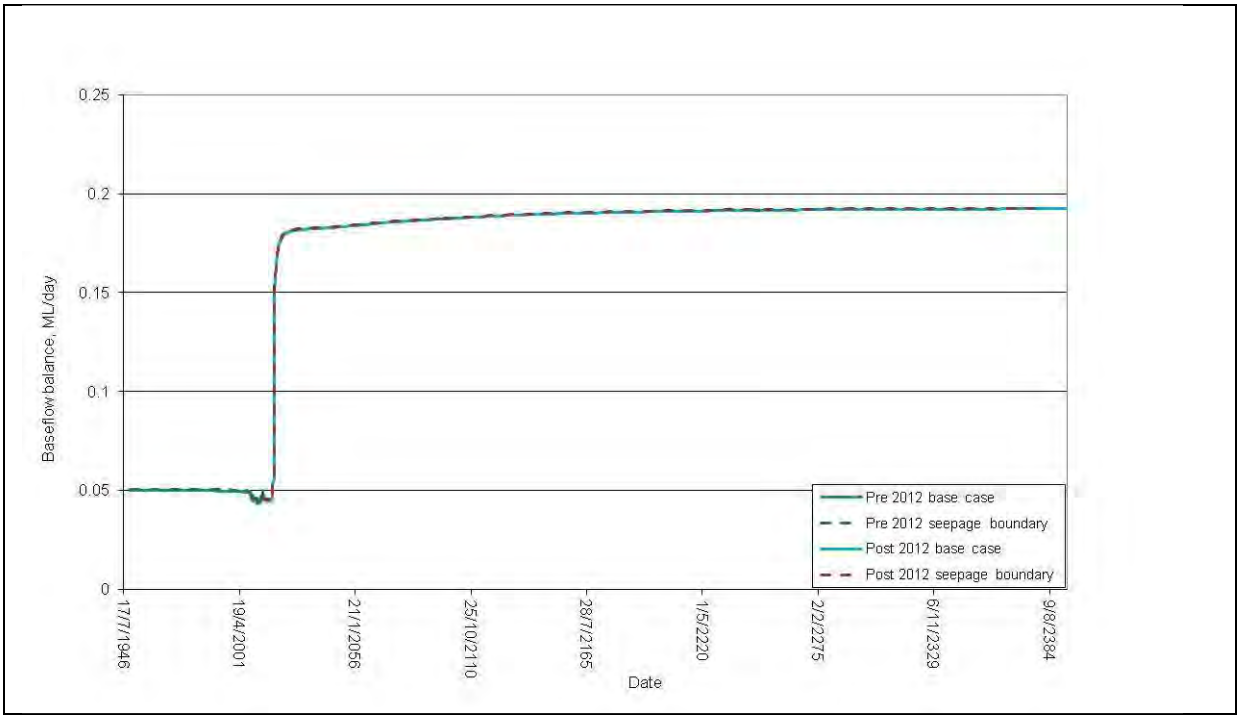

Figure E3 Estimates of baseflow balance (Carne_3) – a comparison between fixed head boundary and seepage boundary conditions

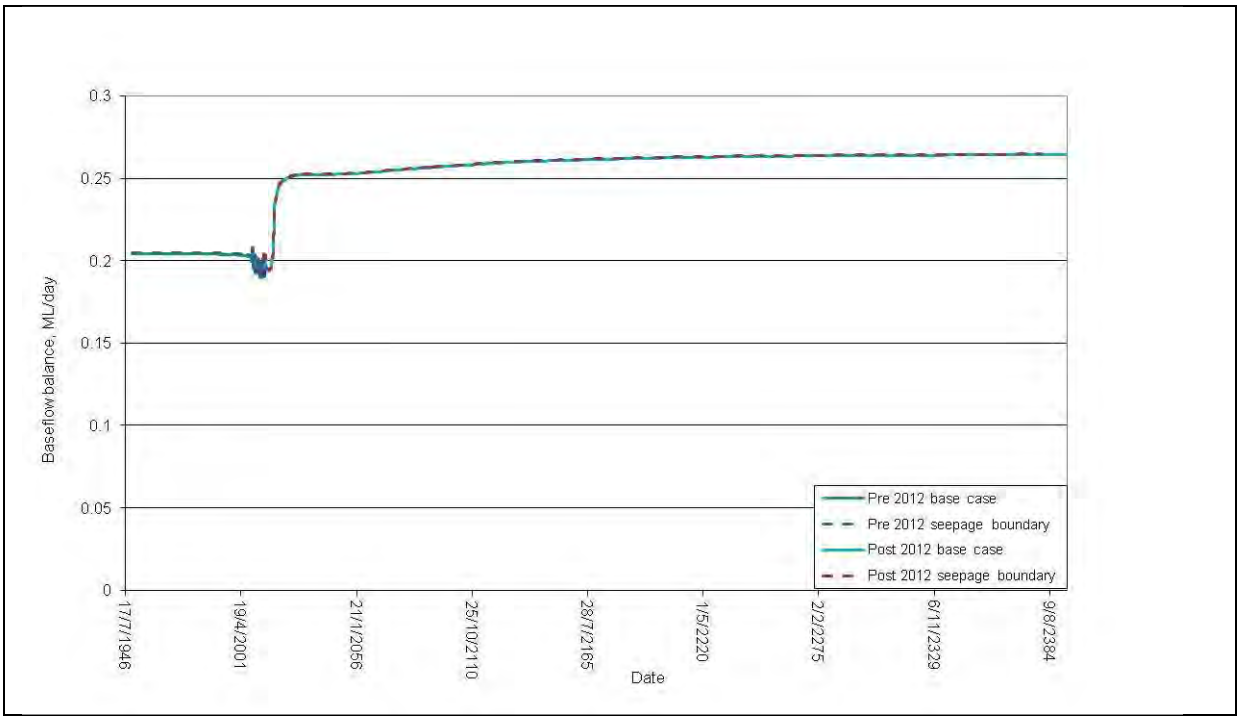

Figure E4 Estimates of baseflow balance (Carne_4) – a comparison between fixed head boundary and seepage boundary conditions

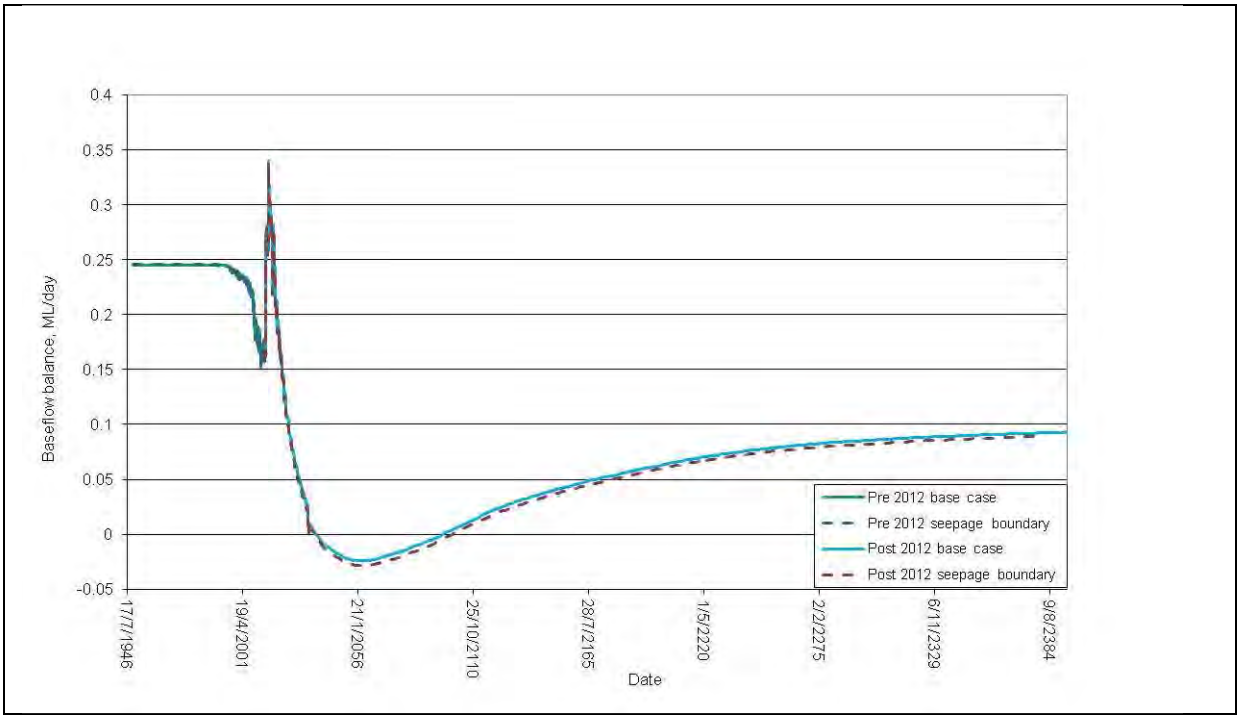

Figure E5 Estimates of baseflow balance (Carne_5) – a comparison between fixed head boundary and seepage boundary conditions

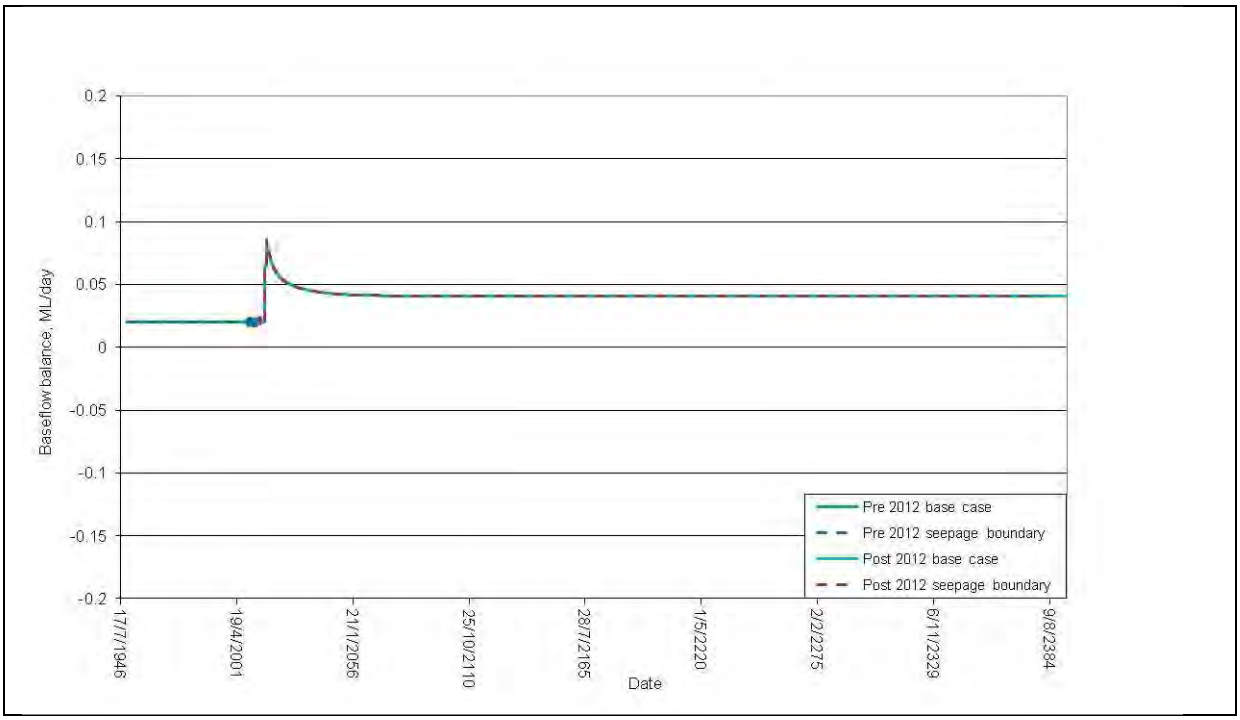

Figure E6 Estimates of baseflow balance (Carne West Swamp) – a comparison between fixed head boundary and seepage boundary conditions

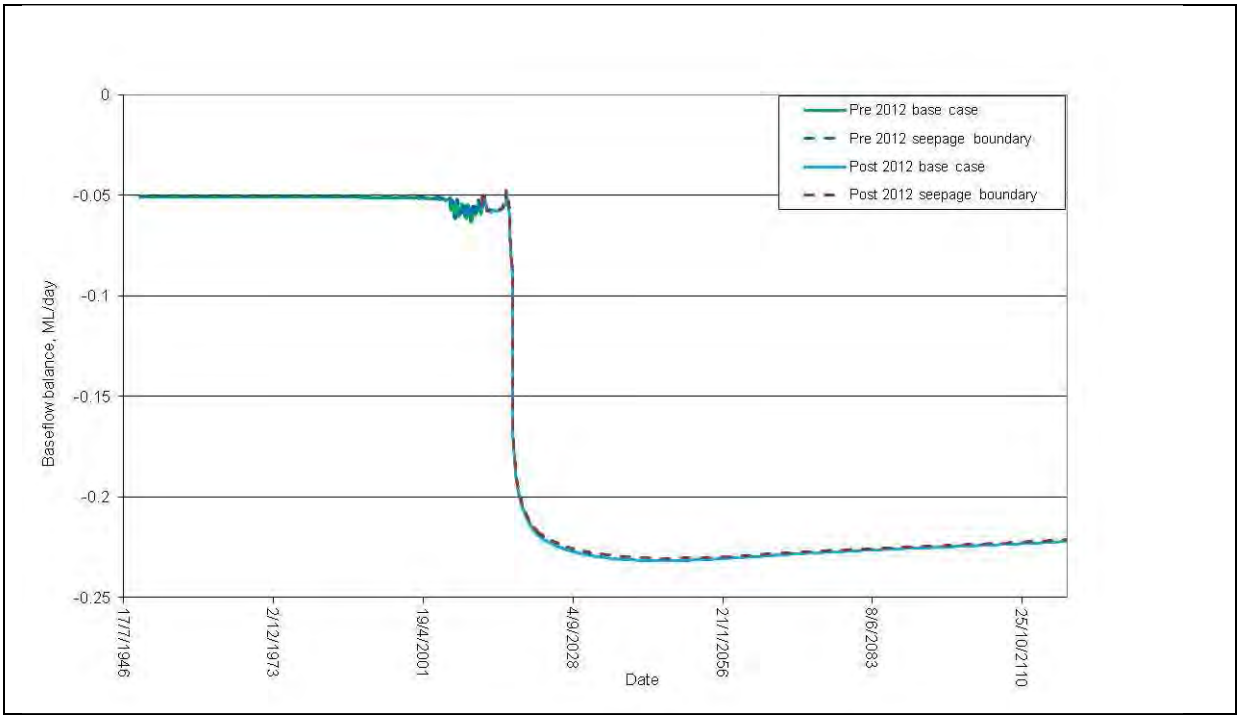

Figure E7 Estimates of baseflow balance (Gang-Gang Swamp East) – a comparison between fixed head boundary and seepage boundary conditions

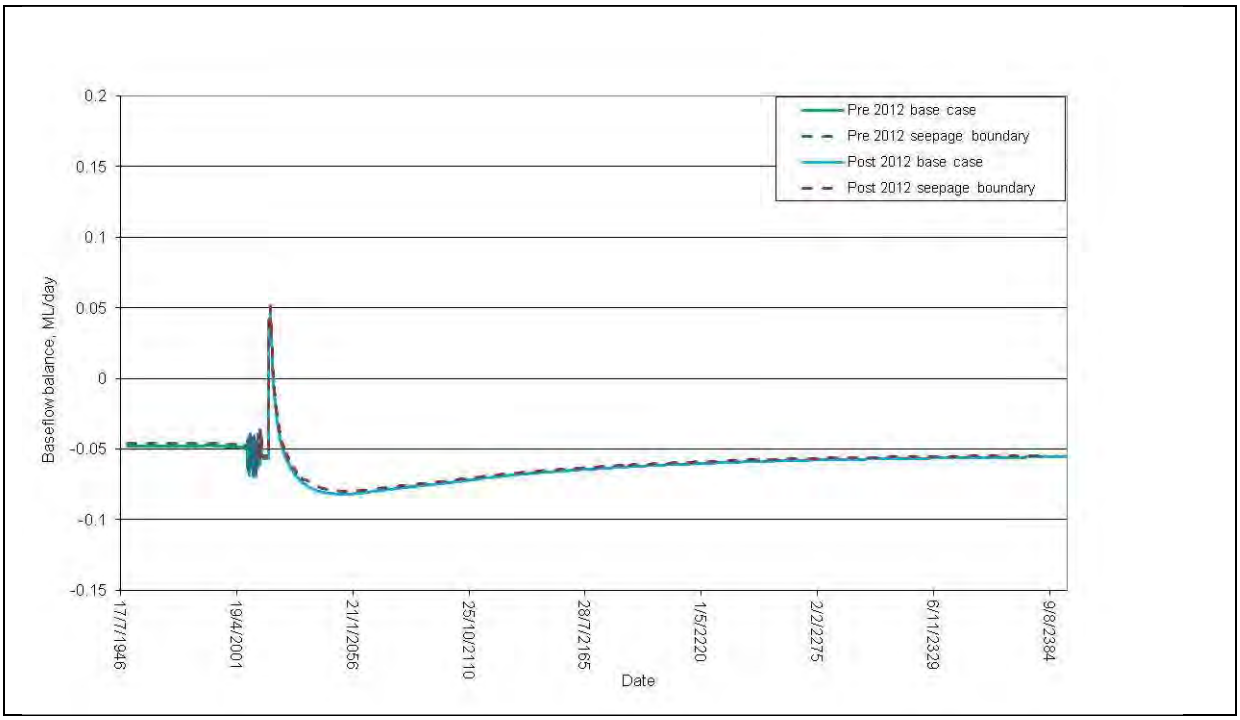

Figure E8 Estimates of baseflow balance (Gang-Gang Swamp South) – a comparison between fixed head boundary and seepage boundary conditions

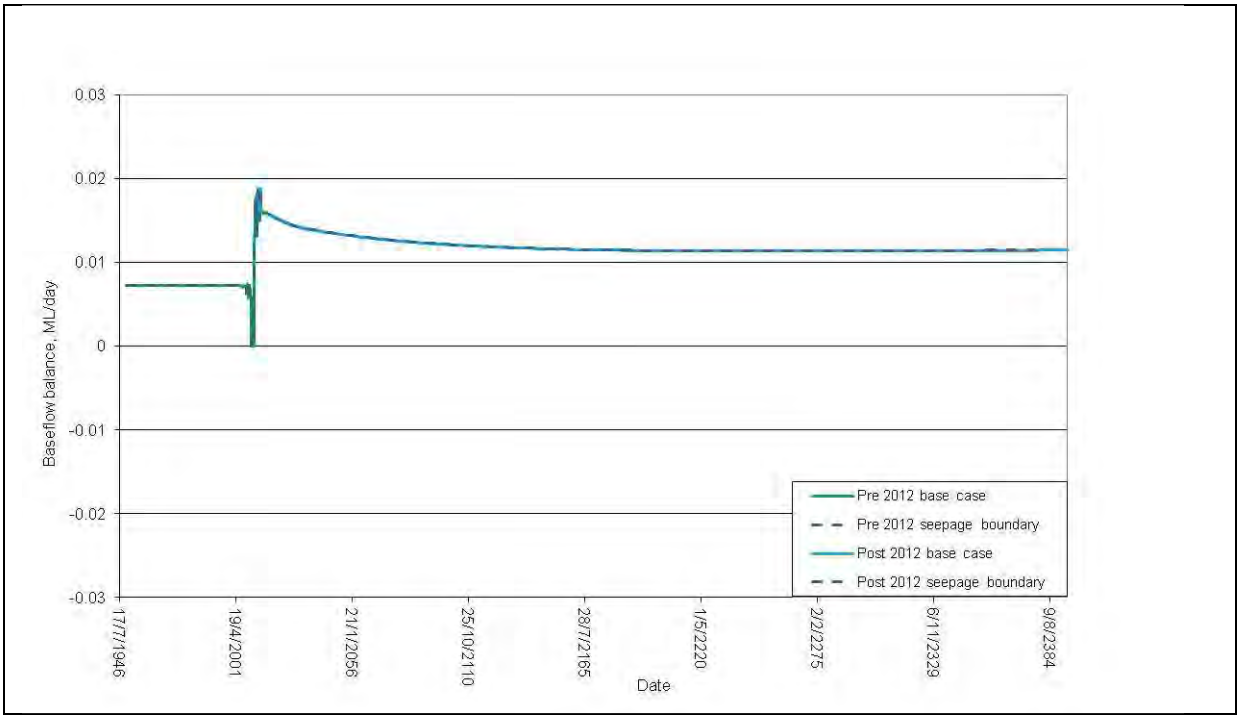

Figure E9 Estimates of baseflow balance (Kangaroo Swamp) – a comparison between fixed head boundary and seepage boundary conditions

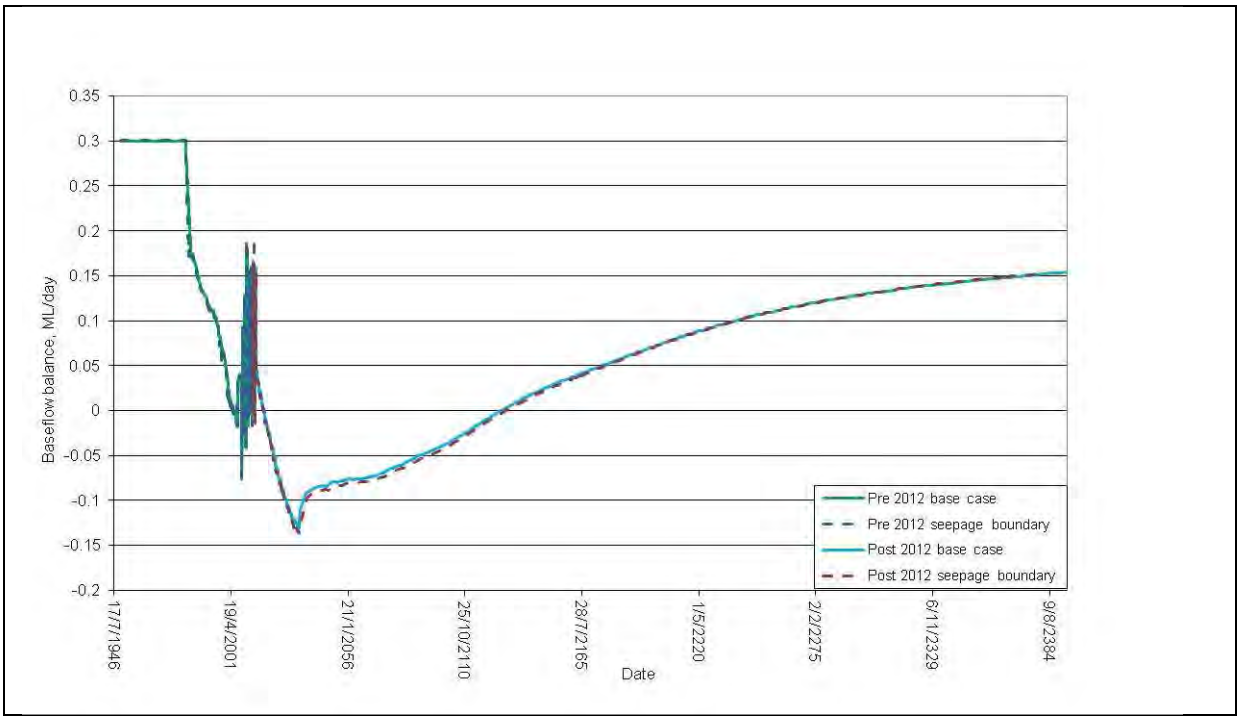

Figure E10 Estimates of baseflow balance (Kangaroo Creek_KC1) – a comparison between fixed head boundary and seepage boundary conditions

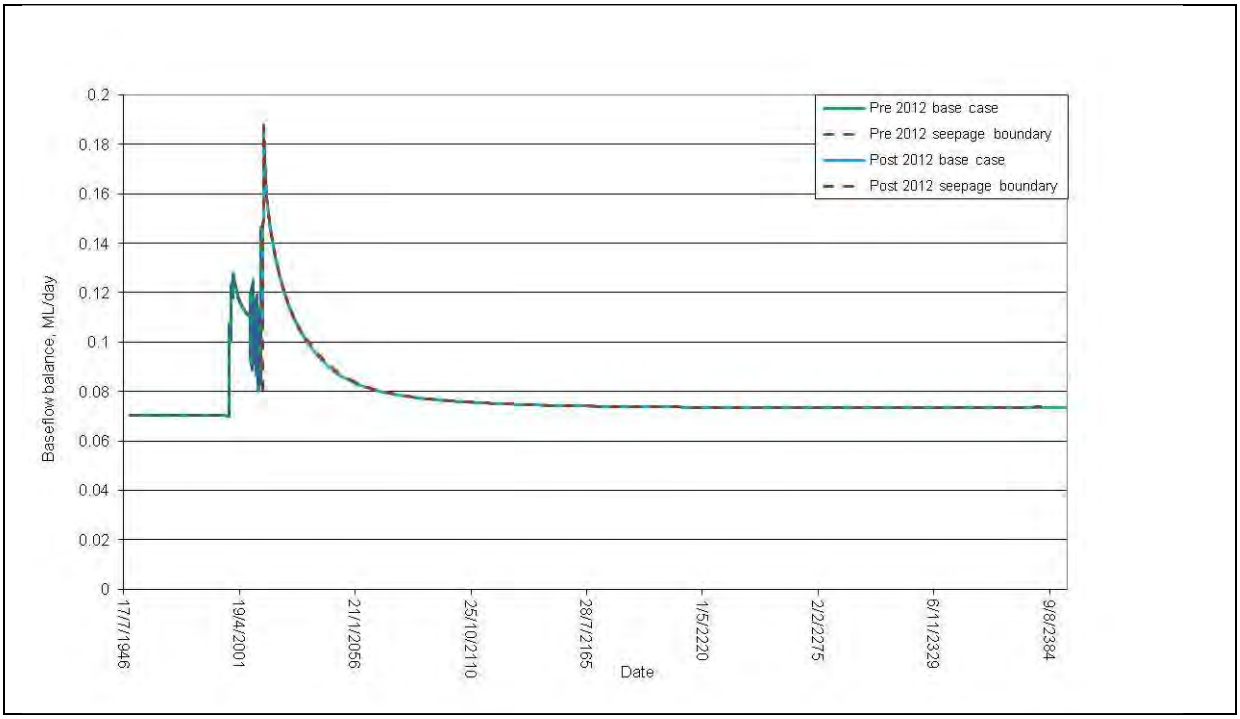

Figure E11 Estimates of baseflow balance (Kangaroo Creek_KC2) – a comparison between fixed head boundary and seepage boundary conditions

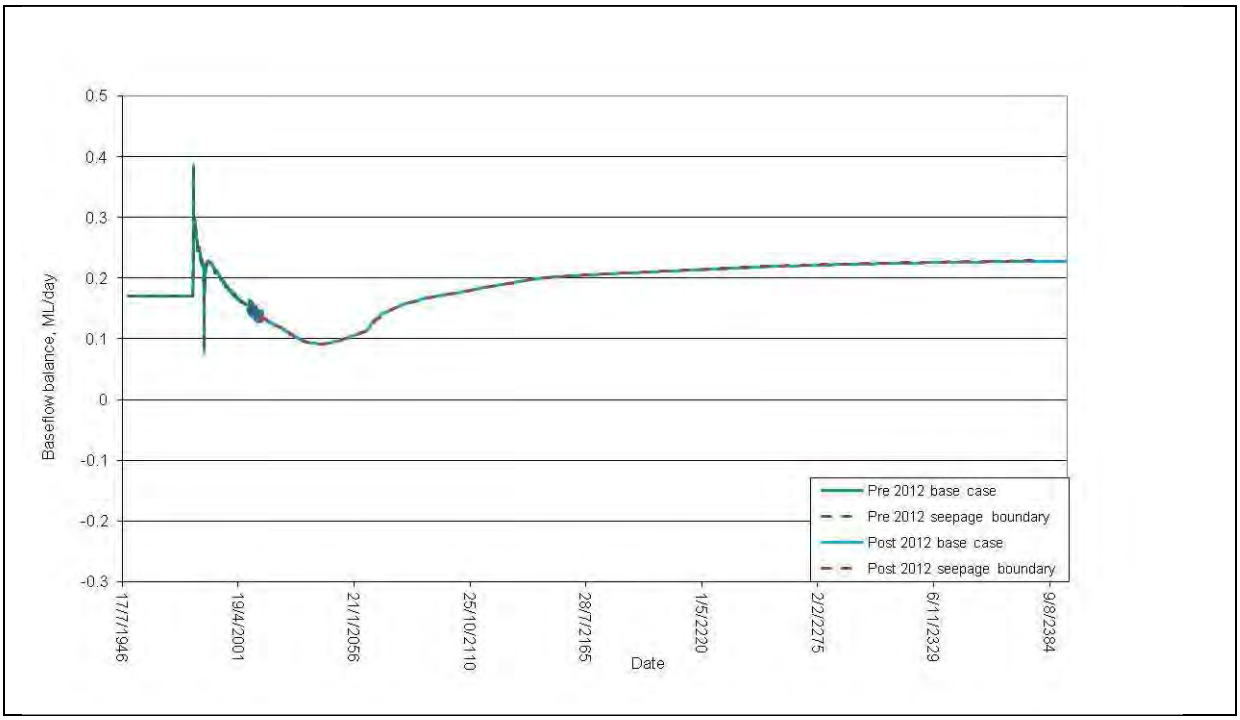

Figure E12 Estimates of baseflow balance (Lamb Creek) – a comparison between fixed head boundary and seepage boundary conditions

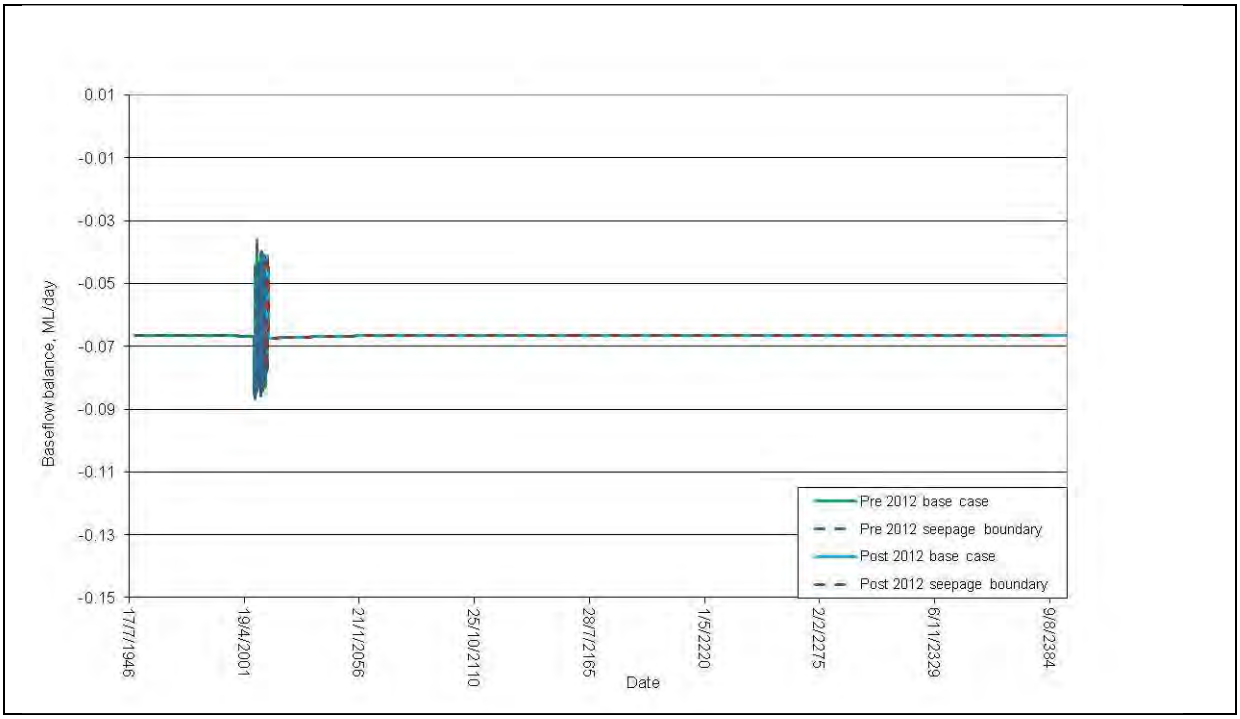

Figure E13 Estimates of baseflow balance (Long Swamp) – a comparison between fixed head boundary and seepage boundary conditions

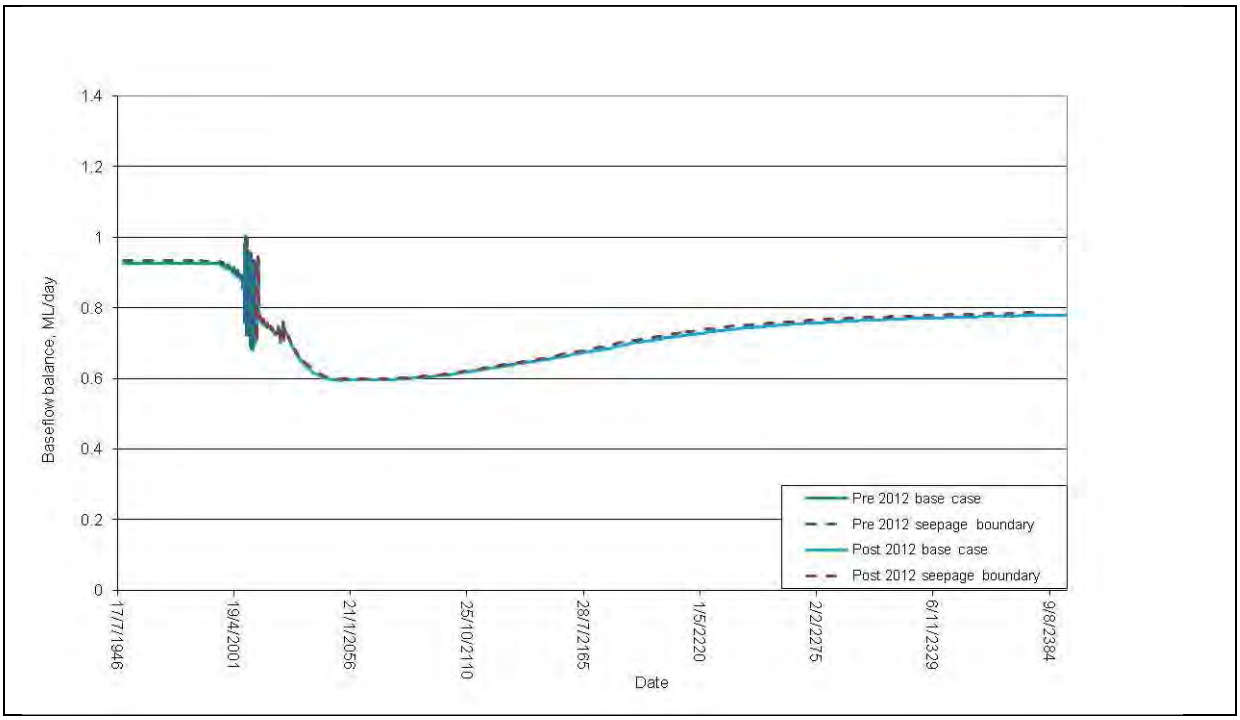

Figure E14 Estimates of baseflow balance (Marrangaroo Creek) – a comparison between fixed head boundary and seepage boundary conditions

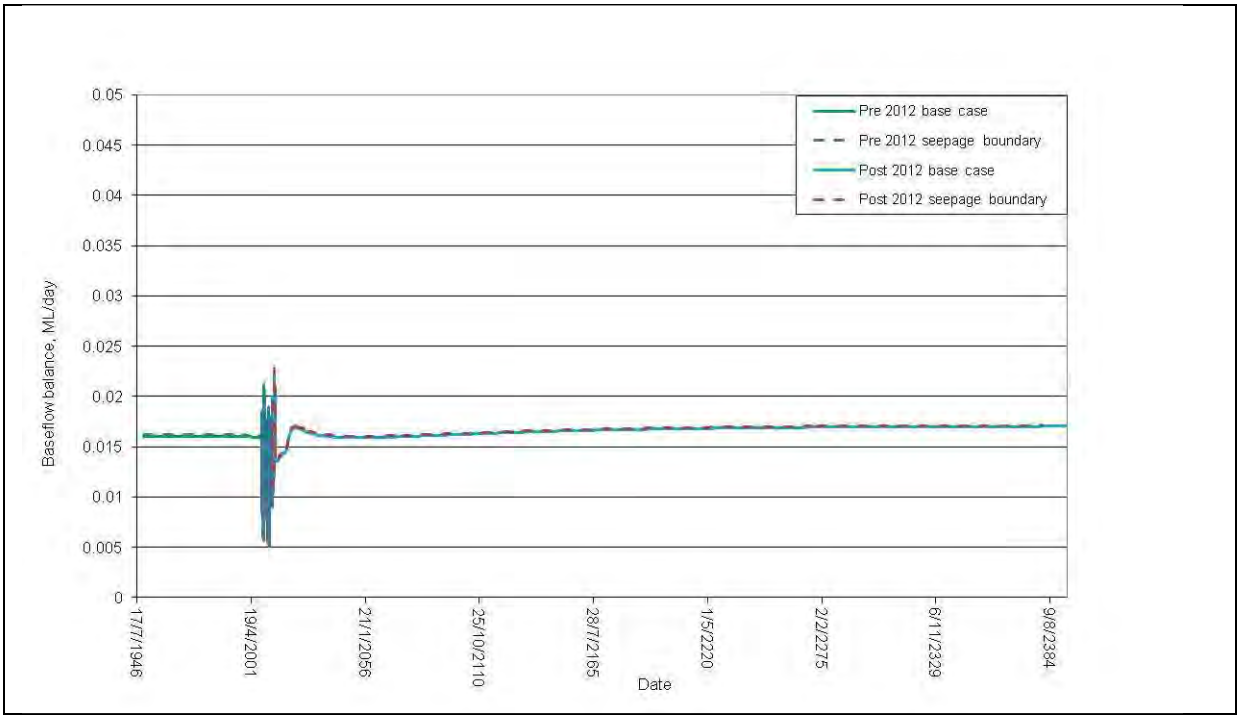

Figure E15 Estimates of baseflow balance (Nine-Mile Swamp) – a comparison between fixed head boundary and seepage boundary conditions

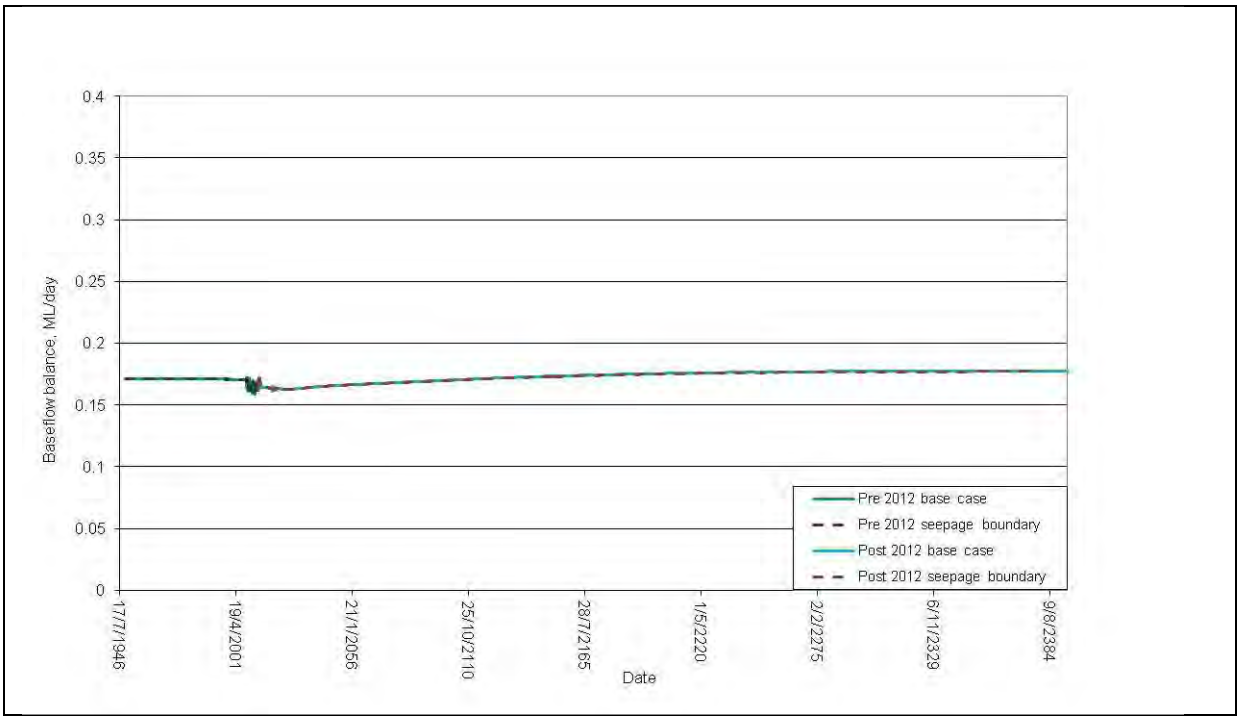

Figure E16 Estimates of baseflow balance (Paddy's Creek) – a comparison between fixed head boundary and seepage boundary conditions

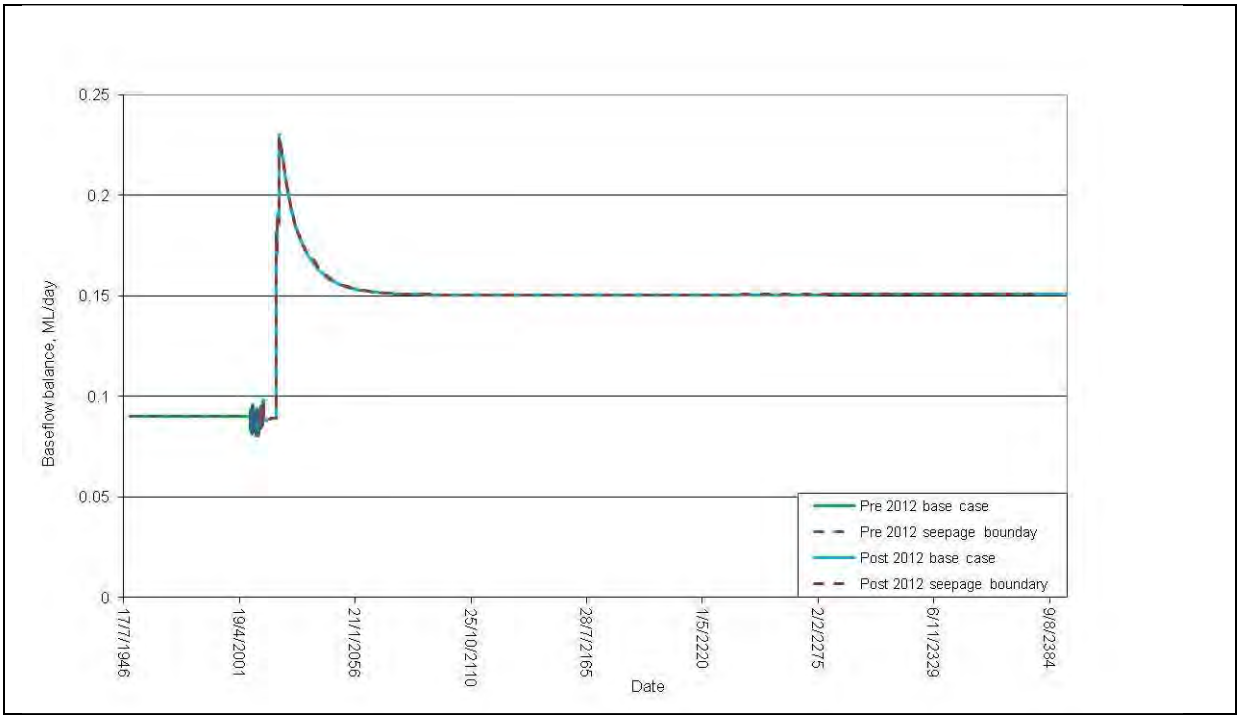

Figure E17 Estimates of baseflow balance (Pine Swamp) – a comparison between fixed head boundary and seepage boundary conditions

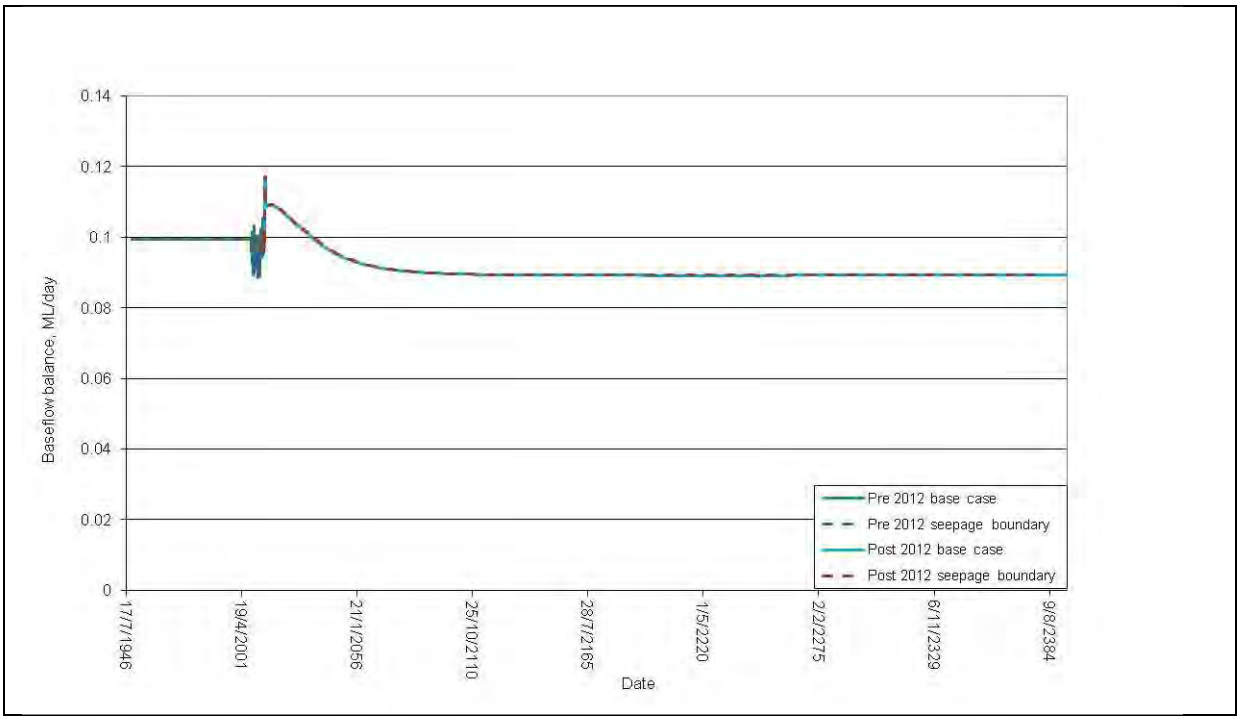

Figure E18 Estimates of baseflow balance (Sunnyside Swamp) – a comparison between fixed head boundary and seepage boundary conditions

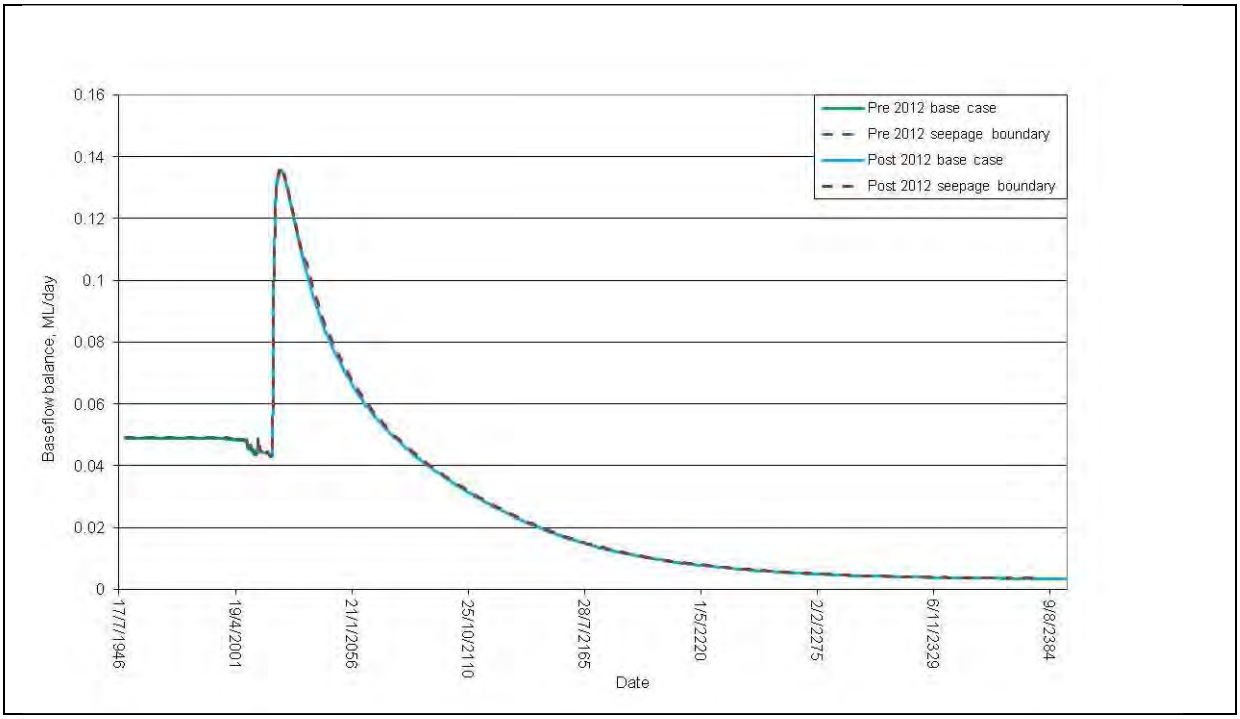

Figure E19 Estimates of baseflow balance (Tri-Star Swamp) – a comparison between fixed head boundary and seepage boundary conditions

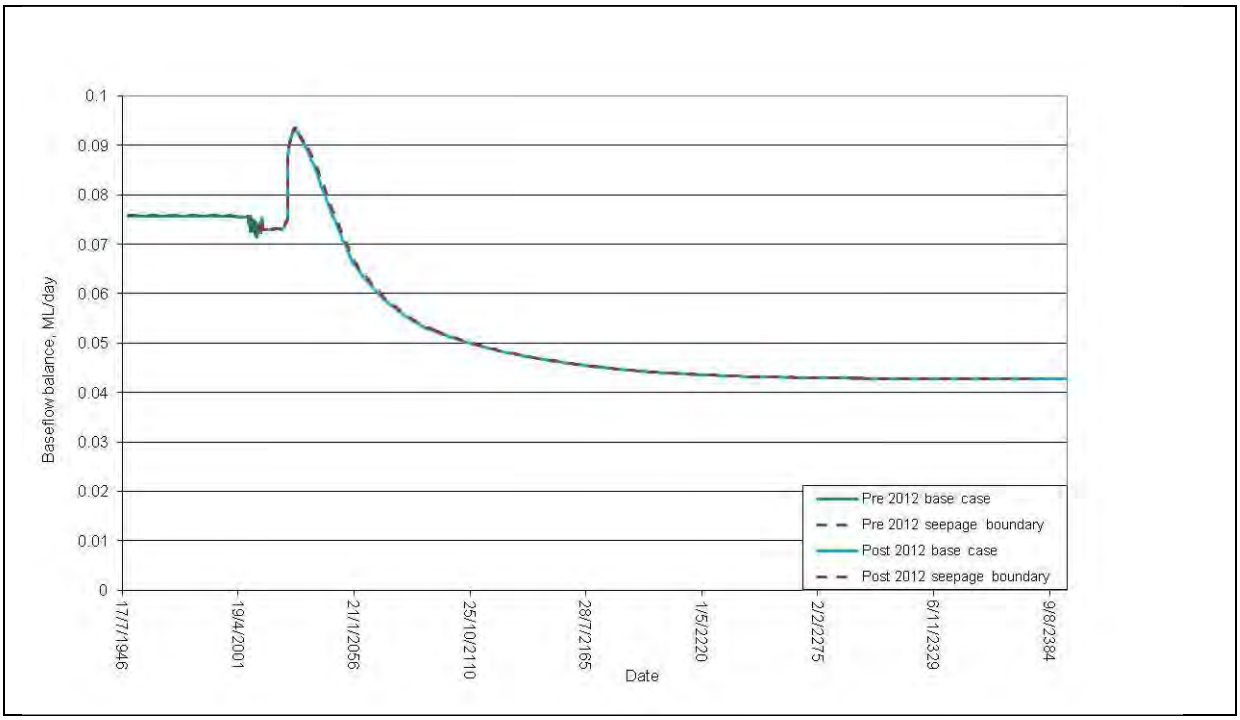

Figure E20 Estimates of baseflow balance (Twin-Gully Swamp) – a comparison between fixed head boundary and seepage boundary conditions

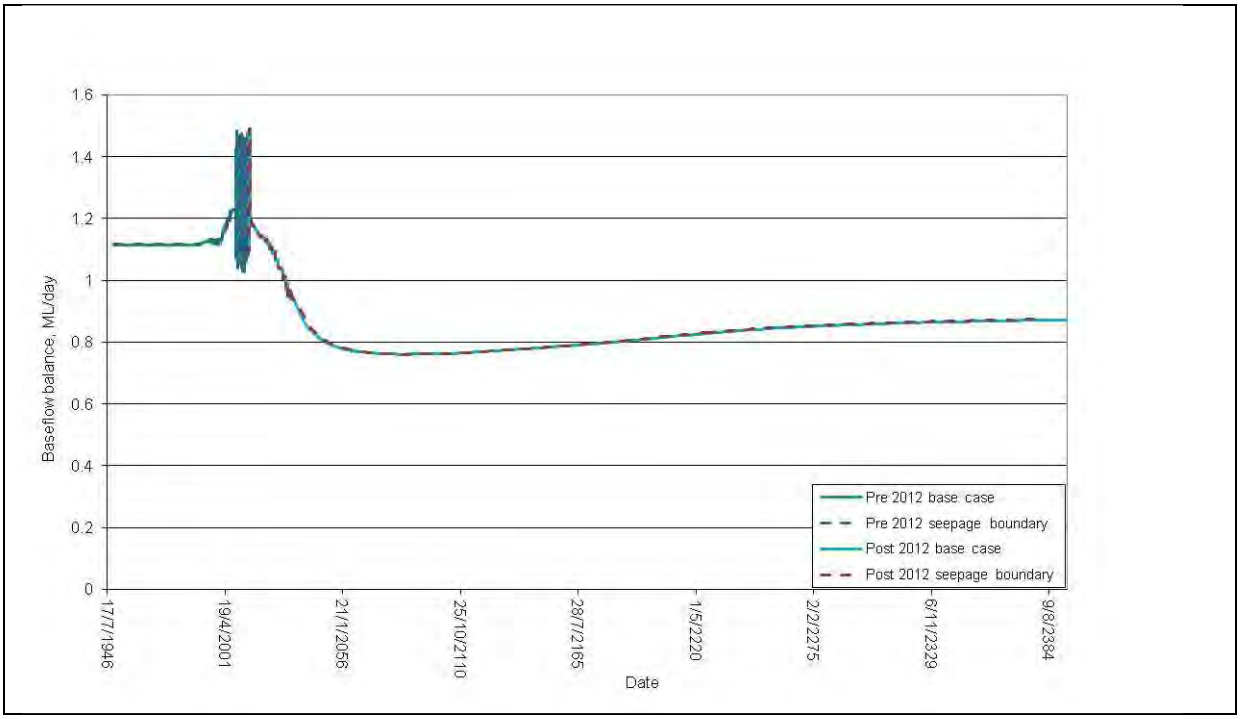

Figure E21 Estimates of baseflow balance (Wolgan river) – a comparison between fixed head boundary and seepage boundary conditions

EARTH SCIENCE AND RESOURCE ENGINEERING
www.csiro.au

Appendix F
A Brief Description of COSFLOW

Angus Place and Springvale Colliery Operations Groundwater Assessment

D P Adhikary and A Wilkins
Report No EP132799
May 2013

Springvale Colliery and Angus Place Colliery

Citation

Adhikary, DP and Wilkins, A (2013) Angus Place and Springvale Colliery operations groundwater assessment. Appendix F - A brief description of COSFLOW. CSIRO Report no EP132799.

Copyright and disclaimer

Important disclaimer

Contents

Figures

1 Mathematical Formulation and Description of Software

CSIRO's in-house software code called "COSFLOW" is used in this project. COSFLOW solves non-isothermal, multi-component, multi-phase fluid and heat flow coupled with Cosserat elasto-plasticity. For this project, COSFLOW is used with a single liquid phase – water – in isothermal conditions with no coupling with mechanical deformation. The mechanical deformations caused by mining are included by altering permeability of the rock around the mined region as described elsewhere in this report.

1.1 Differential equation and notation

The differential equation solved by COSFLOW for this project is the Darcy-Richards equation

$$\frac{\partial}{\partial t}\phi e^{P/B} S = \nabla_i \left(\kappa_{ij} \frac{e^{P/B}\kappa_{rel}}{\mu} (\nabla_j P - \rho_0 g_j) \right) + q_{\text{source}}$$

The notation is as follows:

t is time, x_i for *i=1, 2, 3* are three spatial dimensions, and $\nabla_i = \frac{\partial}{\partial x_i}$ is the gradient operator. The Einstein summation convention for indices is used.
$\emptyset = \emptyset(x_i, t)$ is the porosity. Its spatial and temporal dependence is dictated by the method described elsewhere in this report.
$P = P(x_i, t)$ is the porepressure of water. In this project *P=0* is atmospheric pressure.
S is the saturation of water. For *P>0*, *S=1*, while for negative porepressures (porepressures less than atmospheric pressure), the saturation is determined from a function similar to a van-Genuchten function with a tension cutoff of 0.38MPa which is shown in Figure F1 below.
The water density has the form

$$\rho = \rho_0 \exp(P/B)$$

where *P* is the porepressure,

$$\rho_0 = 1000 \text{kg.m}^{-3}$$

is the base density which is an assumed constant, and

$$B = 2\text{GPa}$$

is the bulk modulus which is also an assumed constant

$k_{ij} = k_{ij}(x_i, t)$ is the permeability tensor. It is assumed diagonal, and its spatial and temporal dependence is dictated by the method described elsewhere in this report.

$\kappa_{rel} = \kappa_{rel}(S_{eff})$ is the relative permeability. It is a function of the effective saturation, defined by

$$S_{eff} = \frac{S - S_{imm}}{1 - S_{imm}}$$

in which S_{imm} is the immobile saturation, assumed to be 0.1 throughout the model. In this project, the relative saturation is

$$k_{rel}(s) = 3s_{eff}^2 - 2s_{eff}^3$$

for $0 < S_{eff} < 1$, and unity for $S_{eff} > 1$, and zero for $S_{eff} < 0$.

The dynamic viscosity of water is assumed to be constant:

$$\mu = 1.1 \times 10^{-3} \text{Pa.s}$$

The acceleration of gravity is denoted by $g_j = (0,0,-10)\text{m/s}^2$

Sources are denoted by q_{source} and their various forms are described below.

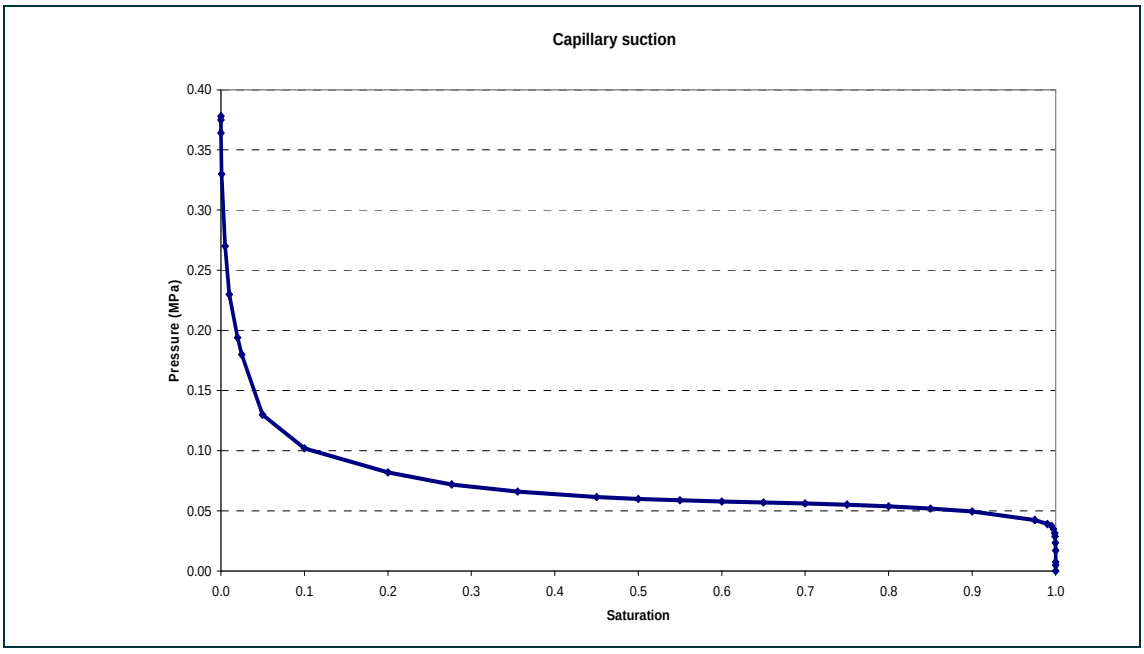

Figure F1 Capillary suction curve used in this project

1.2 Sources and sinks

In this project rainfall recharge, evapotranspiration, seepage, base-flow to rivers/swamps, river/swamp recharge to groundwater, and mine-inflow are all active. A combination of these may be active at a single point in the model. In COSFLOW, these are modelled using the source (or sink) terms in the Darcy-Richards equation. Define

$$Q = \int_V q_{\text{source}}$$

which has dimensions $m^3.s^{-1}$, and measures the rate of increase of water volume within a given rock pore volume *V*. In COSFLOW, *V* is the pore volume of a node with dimensions m^3.

1.2.1 Rainfall recharge

Here *Q= A r* if *P<0* in the node (porepressure is less than atmospheric), and *Q=0* otherwise. In this expression *A* is the area exposed on the surface of the model (m^2) and *r* is the rainfall recharge rate ($m.s^{-1}$). The rainfall recharge rate is assumed uniform over the entire topography of the model and is set to a constant fraction of the annual average rainfall during steady-state calibration, transient calibration, transient validation, prediction and recovery.

1.2.2 Evapotranspiration

Here *Q=Q(P)* is typically defined using an ET table. In this project evapotranspiration is modelled using the function

$$Q = -A\,ET_{\max}\exp\left(-(P/P_c)^2\right)$$

for *P<0* within the volume *V* (porepressure is less than atmospheric), and $Q=-A\,ET_{max}$ otherwise. In this expression *A* is the area exposed on the surface of the model (m^2), ET_{max} is the maximum evapotranspiration rate ($m.s^{-1}$), and P_c defines the pressure at effective extinction depth, chosen to be 5m in this model (Pa). The maximum evapotranspiration rate is assumed uniform over the entire topography of the model and during transient calibration and prediction is set to 3.7mm/day which is the annual average pan evaporation measured at the Bathurst weather station. .

1.2.3 Seepage through an exposed area

Here

$$Q = -AC(P - P_s)$$

for $P>P_s$, and *Q=0* otherwise. In this expression *A* is the area exposed on the surface of the model (m^2), *C* is the conductance of medium ($m.s^{-1}.Pa^{-1}$), and P_s is the seepage pressure (Pa). In this model, where seepage is active, $C=10^{-11}$ $m.s^{-1}.Pa^{-1}$, and $P_s=0$.

1.2.4 Flow to and from rivers and swamps

Here

$$Q = -AC(P - P_r)$$

In this expression *A* is the area of the river (or swamp) (m^2) in the volume *V, C* is the conductance of the riverbed ($m.s^{-1}.Pa^{-1}$), and P_r is the staging pressure (Pa). In this model, *C* is the calibration factor, and $P_r=2000$ Pa (corresponding to a staging height of 0.2m) for all rivers and $P_r=0$ Pa for all swamps in the model.

1.2.5 Mine inflow

In this project, mine water inflow is not modelled by a source/sink term in the Darcy-Richards equation. Rather, the elements lying within the mines are prescribed drain node properties, in an identical way to seepage (above) but with the conductance calculated directly from the surrounding rock permeability, and inflow to these nodes from surrounding area is recorded.

1.3 Method of solution

COSFLOW employs the finite-element technique, and runs in parallel using Message Passing Interface.. The Darcy-Richards equation is discretised spatially using the Galerkin method with linear shape functions. A fully-implicit (backwards Euler) temporal discretisation is used. A 2D finite-element mesh containing quadrilateral elements only is created using the CUBIT mesher, and this is swept in the vertical direction so that it honours the model stratigraphy using VTK routines. The result is a 3D mesh containing hexahedral elements. The mesh is partitioned using METIS, which defines the domain decomposition of the problem. The linear system resulting from the discretisation of the Darcy-Richards equation is solved using PETSc with a block-Jacobi preconditioner and a stabilised bi-conjugate gradient solver.

APPENDIX L:
CLIMATE AFFECTED BASEFLOW PLOTS

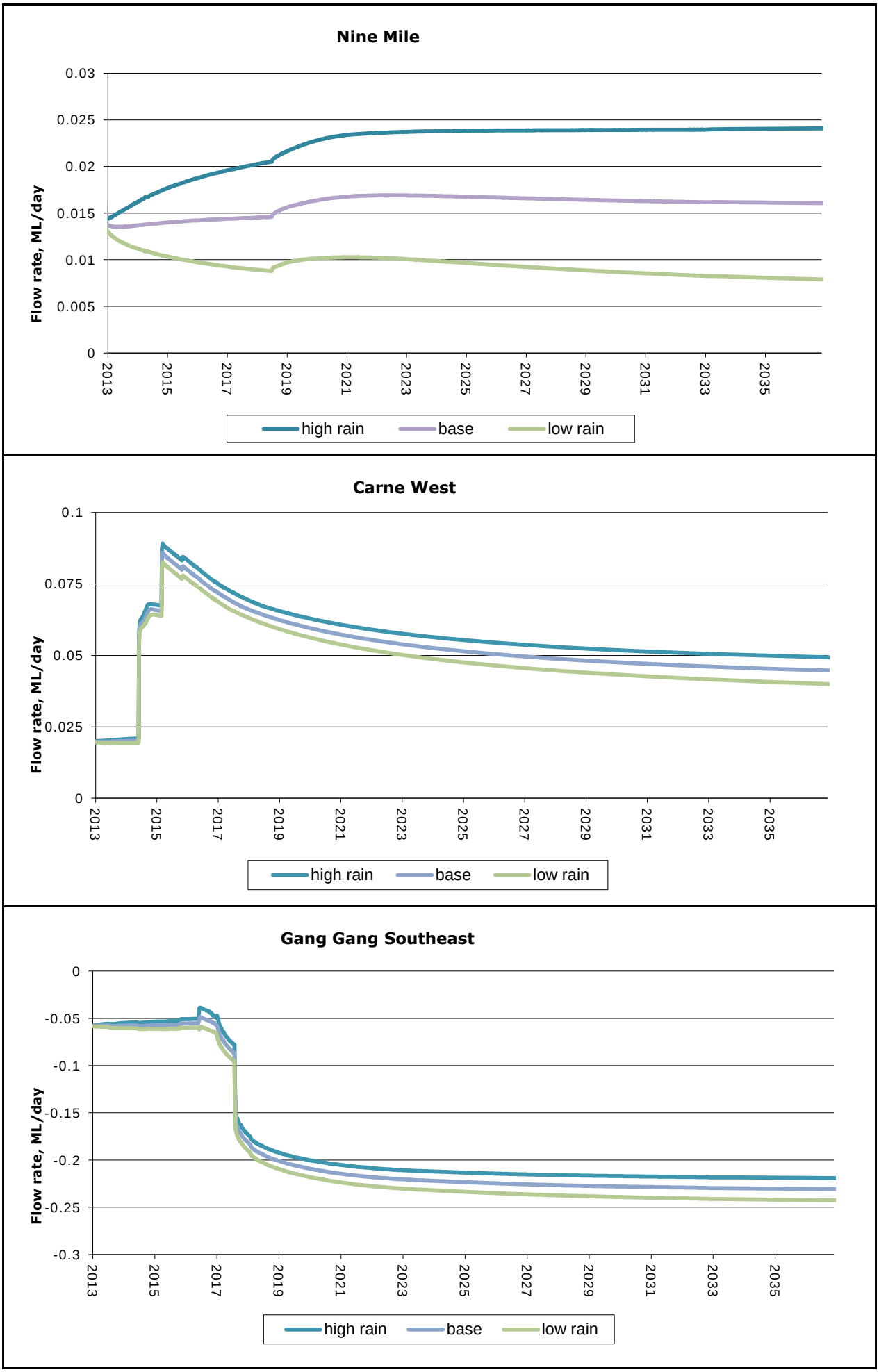
Nine Mile
Flow rate, ML/day
0.03
0.025
0.02
0.015
0.01
0.005
0
2013
2015
2017
2019
2021
2023
2025
2027
2029
2031
2033
2035
high rain
base
low rain
Carne West
Flow rate, ML/day
0.1
0.075
0.05
0.025
0
2013
2015
2017
2019
2021
2023
2025
2027
2029
2031
2033
2035
high rain
base
low rain
Gang Gang Southeast
Flow rate, ML/day
0
-0.05
-0.1
-0.15
-0.2
-0.25
-0.3
2013
2015
2017
2019
2021
2023
2025
2027
2029
2031
2033
2035
high rain
base
low rain

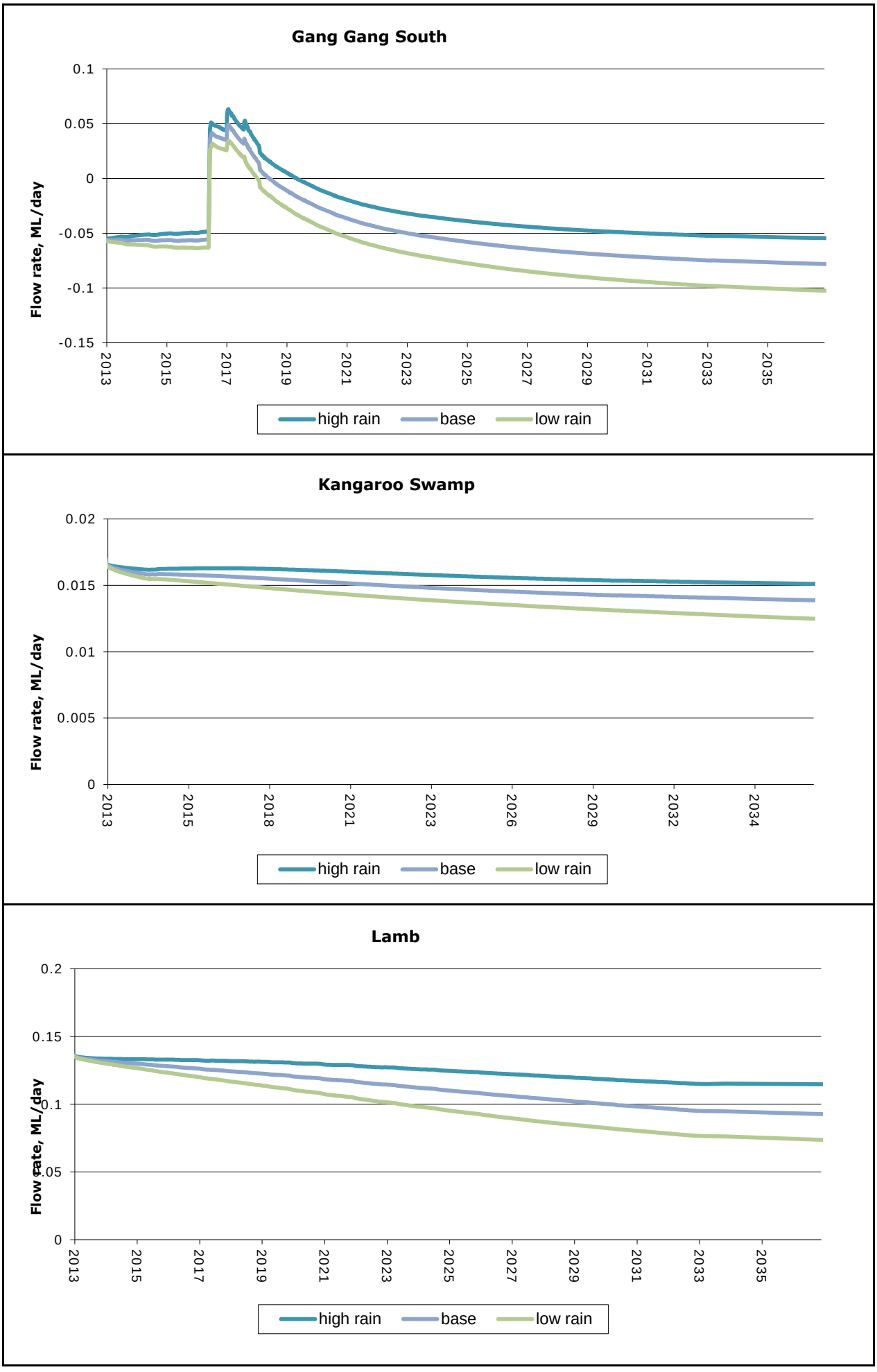
Gang Gang South
0.1
0.05
0
-0.05
-0.1
-0.15
Flow rate, ML/day
2013
2015
2017
2019
2021
2023
2025
2027
2029
2031
2033
2035
high rain
base
low rain
Kangaroo Swamp
0.02
0.015
0.01
0.005
0
Flow rate, ML/day
2013
2015
2018
2021
2023
2026
2029
2032
2034
high rain
base
low rain
Lamb
0.2
0.15
0.1
0.05
0
Flow rate, ML/day
2013
2015
2017
2019
2021
2023
2025
2027
2029
2031
2033
2035
high rain
base
low rain

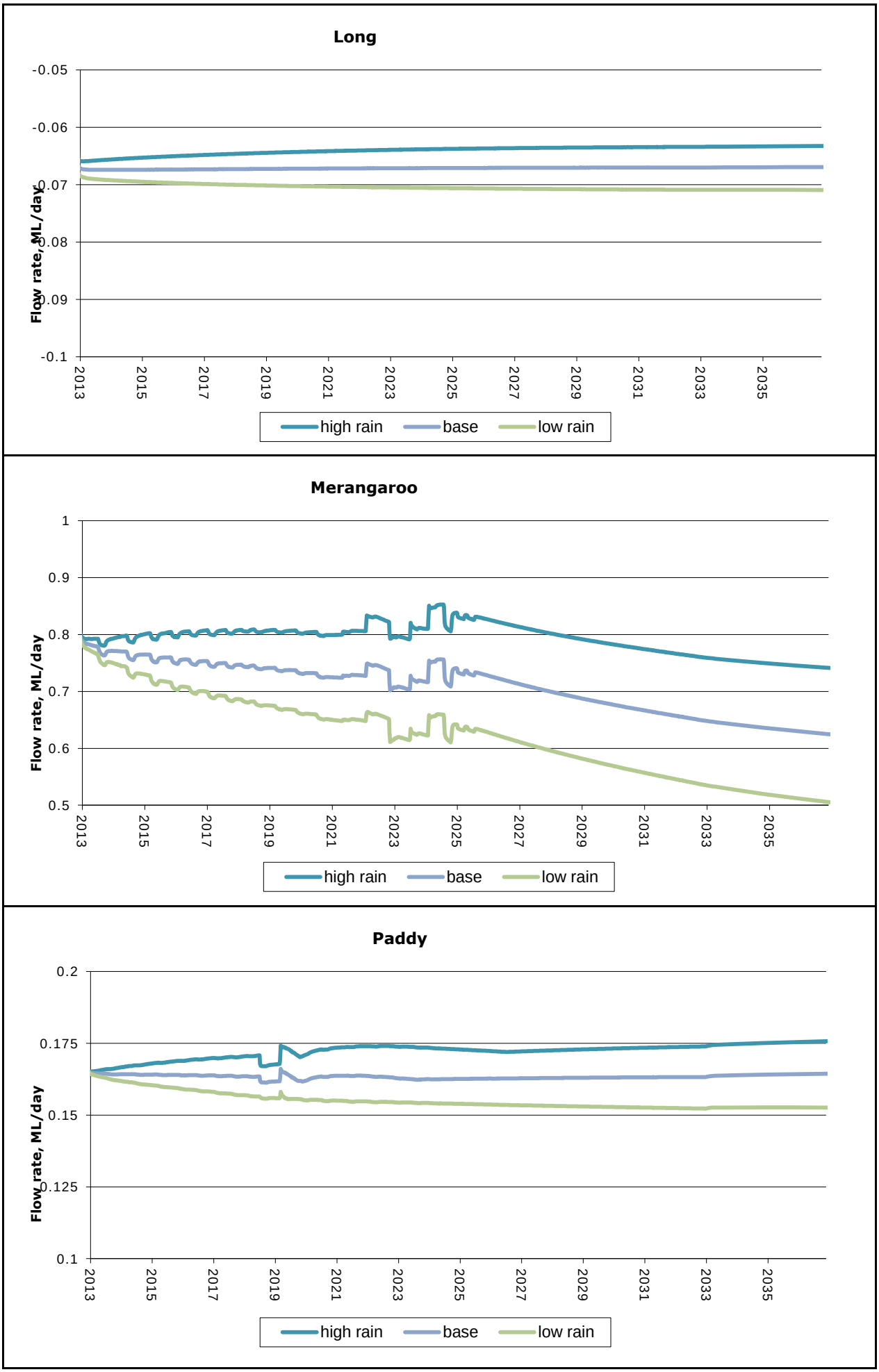
Long
-0.05
-0.06
-0.07
-0.08
-0.09
-0.1
Flow rate, ML/day
2013
2015
2017
2019
2021
2023
2025
2027
2029
2031
2033
2035
high rain
base
low rain
Merangaroo
1
0.9
0.8
0.7
0.6
0.5
Flow rate, ML/day
2013
2015
2017
2019
2021
2023
2025
2027
2029
2031
2033
2035
high rain
base
low rain
Paddy
0.2
0.175
0.15
0.125
0.1
Flow rate, ML/day
2013
2015
2017
2019
2021
2023
2025
2027
2029
2031
2033
2035
high rain
base
low rain

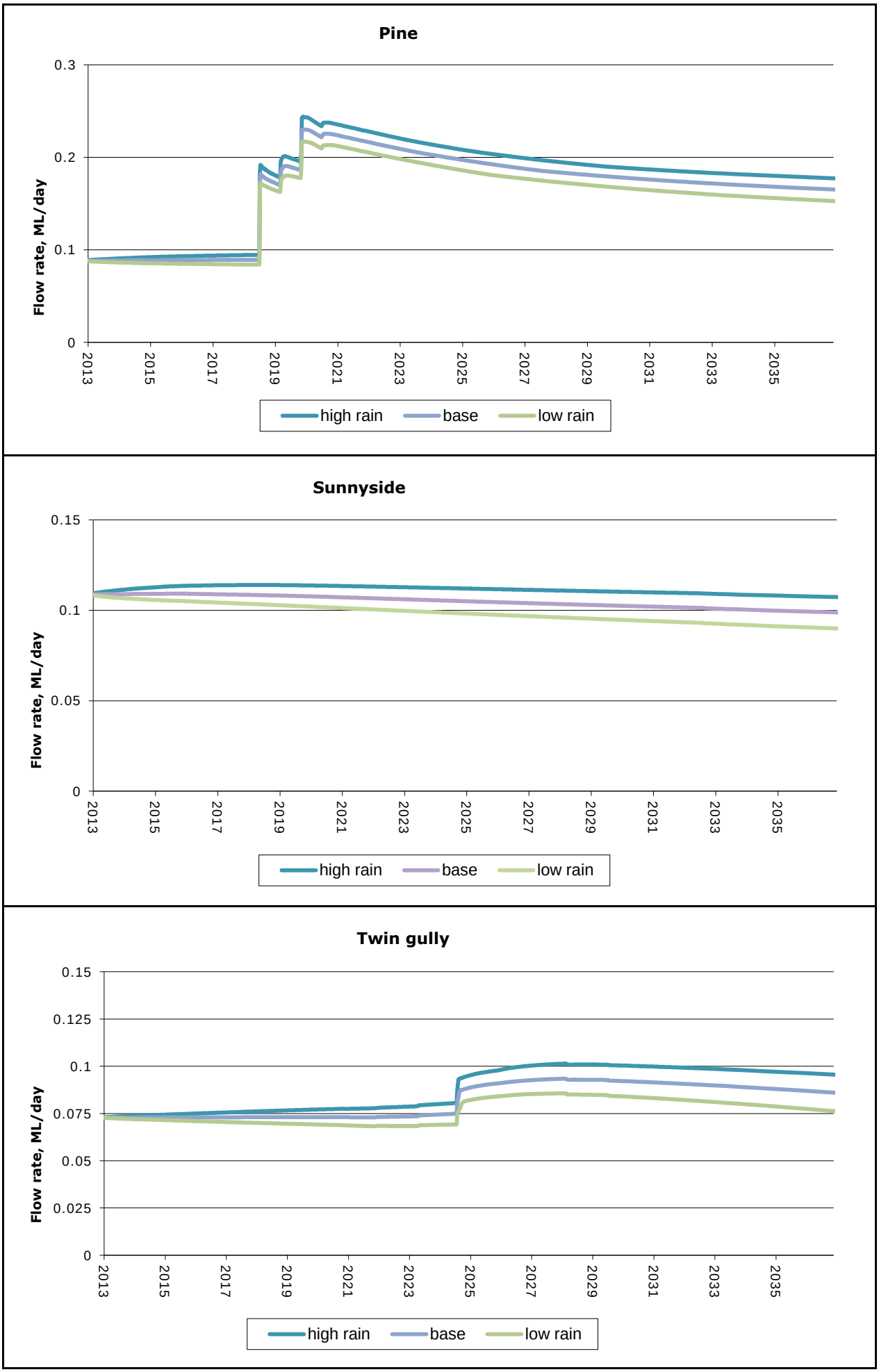
Pine
Flow rate, ML/day
0.3
0.2
0.1
0
2013
2015
2017
2019
2021
2023
2025
2027
2029
2031
2033
2035
high rain
base
low rain
Sunnyside
Flow rate, ML/day
0.15
0.1
0.05
0
2013
2015
2017
2019
2021
2023
2025
2027
2029
2031
2033
2035
high rain
base
low rain
Twin gully
Flow rate, ML/day
0.15
0.125
0.1
0.075
0.05
0.025
0
2013
2015
2017
2019
2021
2023
2025
2027
2029
2031
2033
2035
high rain
base
low rain

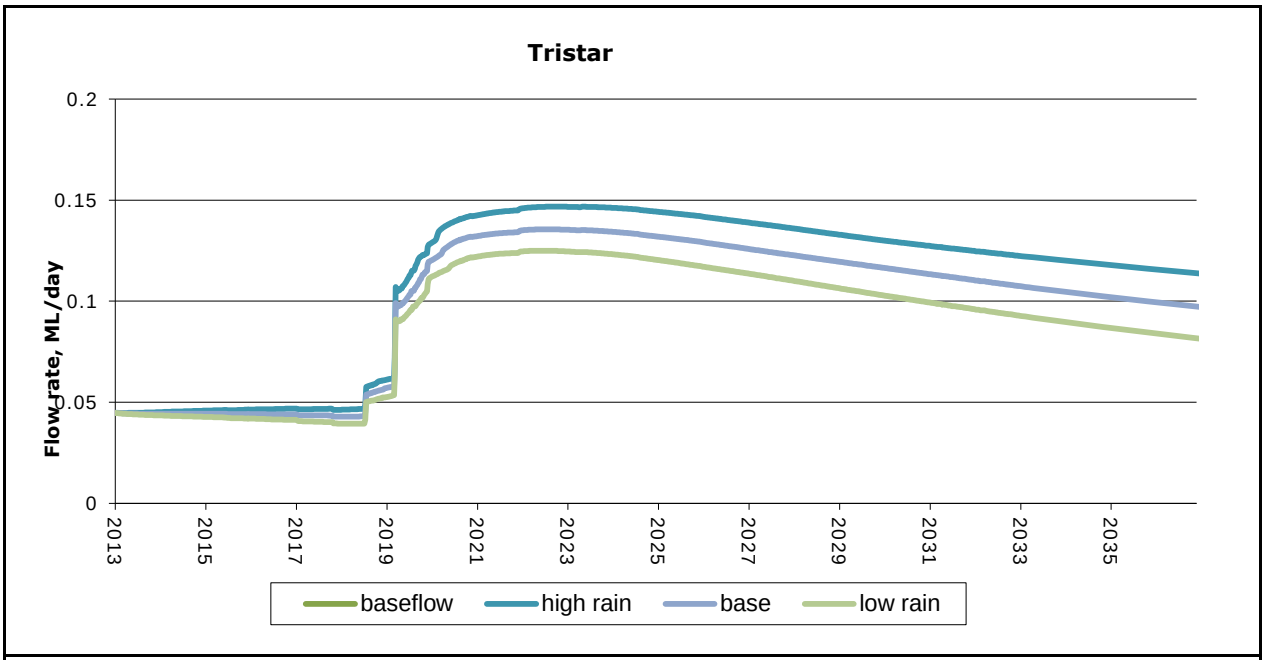
Tristar
0.2
0.15
0.1
0.05
0
Flow rate, ML/day
2013
2015
2017
2019
2021
2023
2025
2027
2029
2031
2033
2035
baseflow
high rain
base
low rain

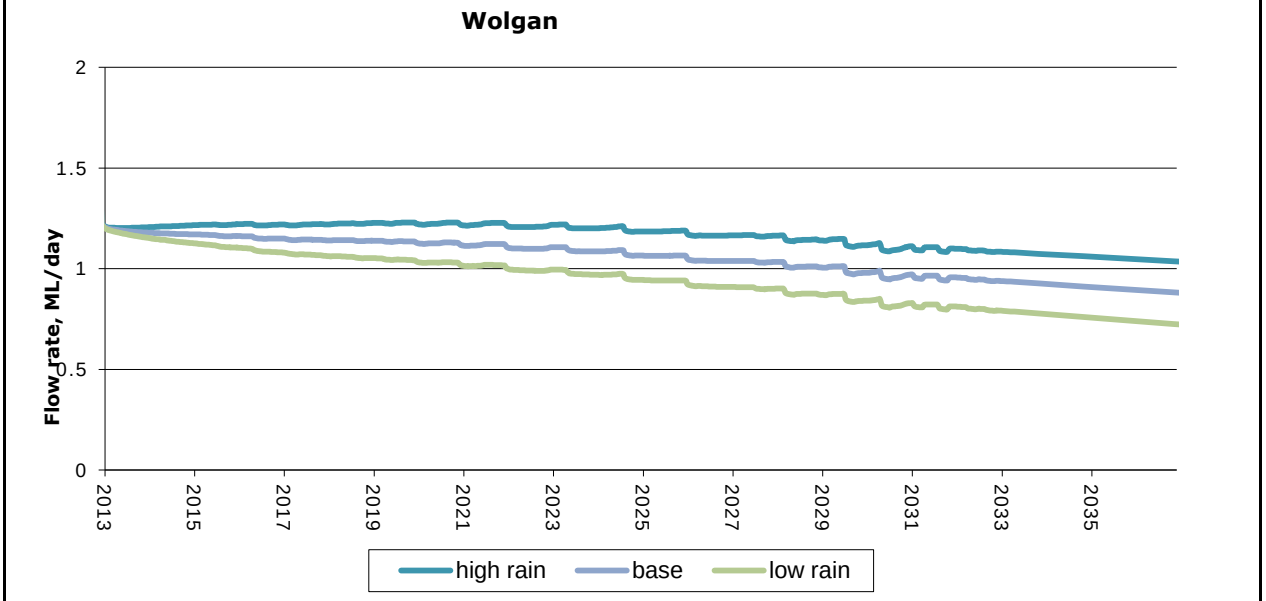
Wolgan
2
1.5
1
0.5
0
Flow rate, ML/day
2013
2015
2017
2019
2021
2023
2025
2027
2029
2031
2033
2035
high rain
base
low rain

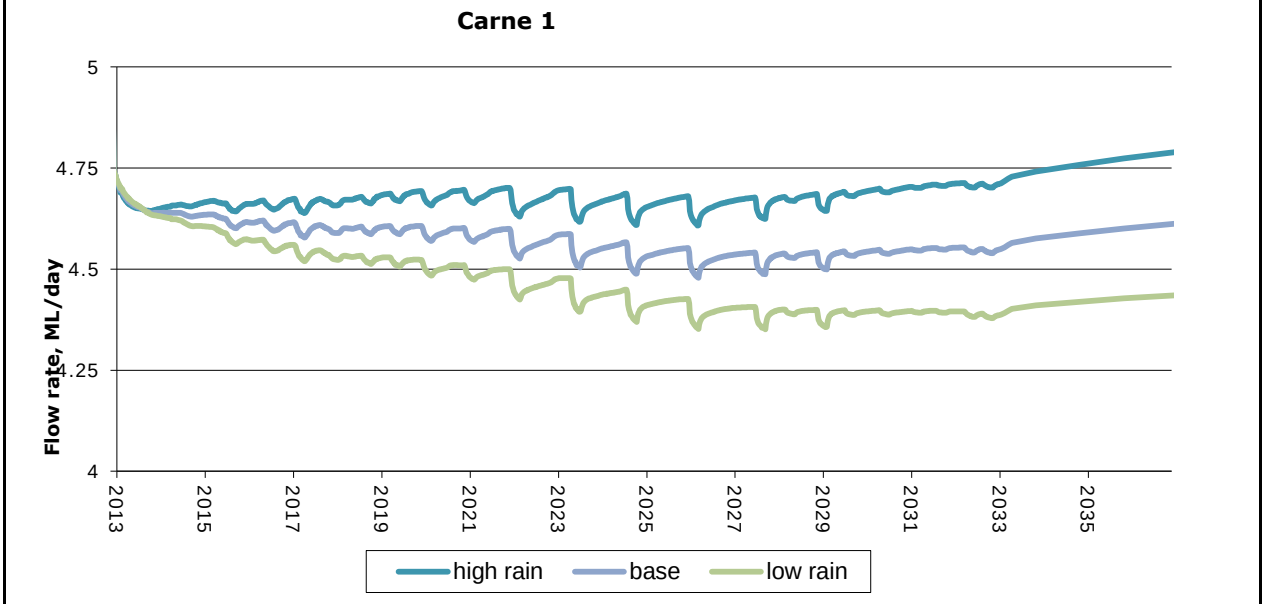
Carne 1
5
4.75
4.5
4.25
4
Flow rate, ML/day
2013
2015
2017
2019
2021
2023
2025
2027
2029
2031
2033
2035
high rain
base
low rain

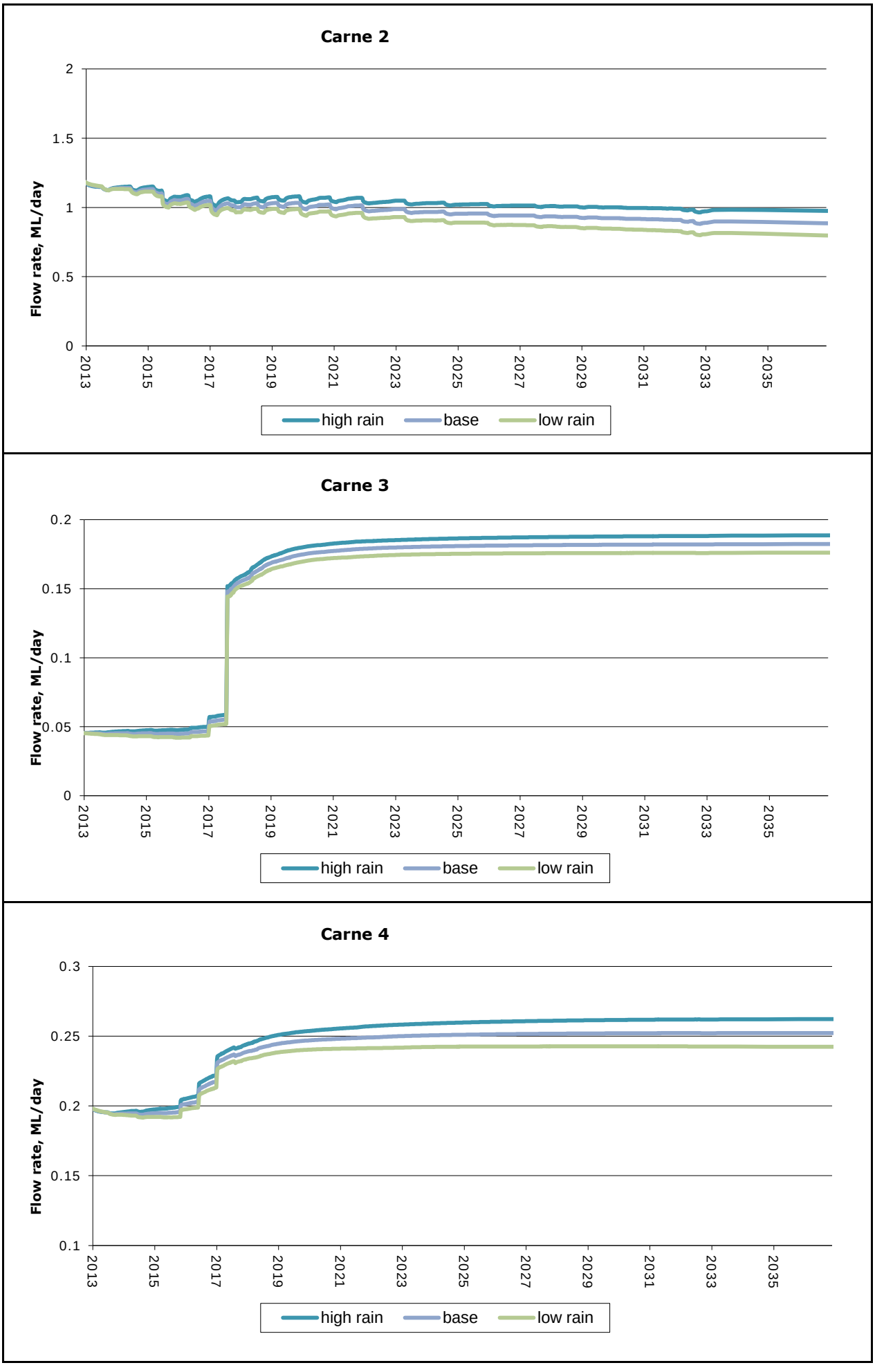
Carne 2
Flow rate, ML/day
2
1.5
1
0.5
0
2013
2015
2017
2019
2021
2023
2025
2027
2029
2031
2033
2035
high rain
base
low rain
Carne 3
Flow rate, ML/day
0.2
0.15
0.1
0.05
0
2013
2015
2017
2019
2021
2023
2025
2027
2029
2031
2033
2035
high rain
base
low rain
Carne 4
Flow rate, ML/day
0.3
0.25
0.2
0.15
0.1
2013
2015
2017
2019
2021
2023
2025
2027
2029
2031
2033
2035
high rain
base
low rain

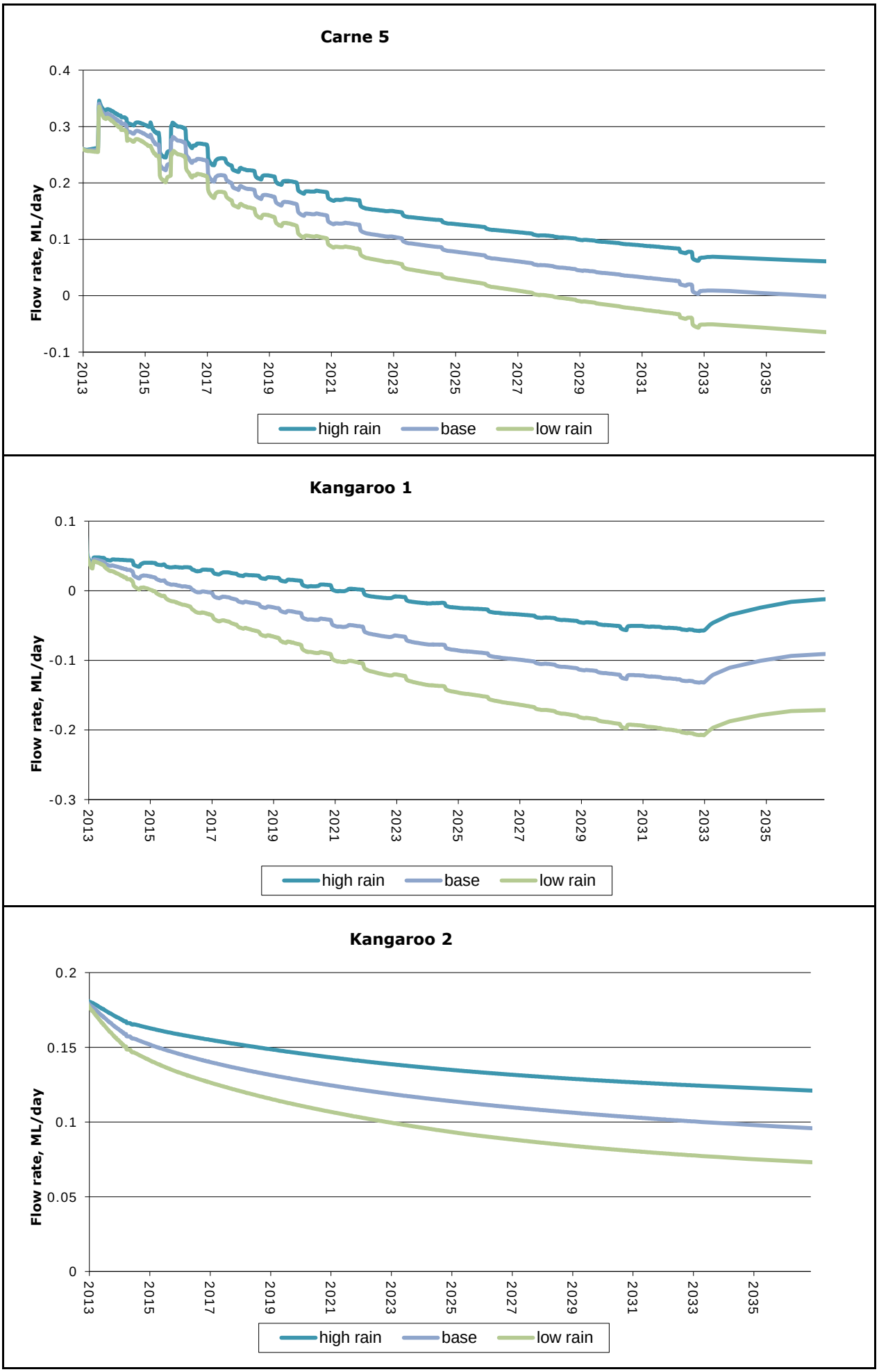
Carne 5
Flow rate, ML/day
0.4
0.3
0.2
0.1
0
-0.1
2013
2015
2017
2019
2021
2023
2025
2027
2029
2031
2033
2035
high rain
base
low rain
Kangaroo 1
Flow rate, ML/day
0.1
0
-0.1
-0.2
-0.3
2013
2015
2017
2019
2021
2023
2025
2027
2029
2031
2033
2035
high rain
base
low rain
Kangaroo 2
Flow rate, ML/day
0.2
0.15
0.1
0.05
0
2013
2015
2017
2019
2021
2023
2025
2027
2029
2031
2033
2035
high rain
base
low rain

APPENDIX M:
PREVIOUS GROUNDWATER STUDIES SUMMARY

Brief summaries of some of the historical groundwater studies which are relevant to the current Groundwater Impact Assessment are presented below:

- In November 2004, CSIRO carried out a hydrogeological analysis of ten drill holes, which were equipped with multi-level vibrating wire piezometers (VWPs). The analysis of groundwater piezometric data was used to delineate various aquifer units underlying APC. The report also provided estimates of preliminary mine water make and recommended that in-situ permeability testing be carried out and also that an integrated hydrological assessment be extended to include the Angus Place and Clarence Collieries (CSIRO, 2004).
- In May 2010, CSIRO carried out a hydrological assessment for the extension of LW414 at Springvale. The assessment comprised extensive numerical modeling simulations using COSFLOW (a coupled geotechnical and groundwater finite element model which has been developed in-house by CSIRO). The modeling and accompanying report concluded that the proposed extension to LW414 would result in predicted average inflows of up to 260 L/s;
- In March 2012, CSIRO carried out numerical modeling to estimate surface subsidence and groundwater inflow into the proposed LW417 to LW423. A detailed COSFLOW model was developed, and the results presented in the accompanying report. The report concluded that the subsidence at surface was predicted to be between 0.5 m and 0.9 m. The groundwater inflow rates were predicted to be around 180 to 240 L/s during the mining of all longwall panels including LW1 to LW414;
- In July 2012, Aurecon carried out a desktop study of the potential hydrogeological impacts associated with the construction and commissioning of the proposed dewatering Bore 8 facility comprising four boreholes installed with submersible pumps to manage mine inflows from LW416 to LW419. The report concluded that none of the activities associated with the installation or operation of Bore 8 facility posed a risk to the local or regional hydrogeological regime, or to the groundwater dependent ecosystems that rely on these groundwater resources;
- In October 2012, CSIRO presented the results of the analysis of deep piezometric data across Springvale Colliery. The report summarised groundwater piezometric data for the monitoring points across the site, and concluded that the magnitude of the impact of mining diminishes with the increase in both lateral and vertical distances from the mining activities;
- In November 2012, RPS undertook a study on four THPSS (Junction Swamp, Sunnyside Swamp, Sunnyside West Swamp and West Wolgan Swamp) which had all been previously undermined. The study looked at the long term water levels in some of the swamps in association with cumulative rainfall deviation and the progression of the underlying longwalls. In all of the swamps included in the study, none of the observed water level data fluctuations in the swamps could be attributed to the underlying longwalls
- In February 2013, RPS undertook a Swamp Delineation Study. The aim of the study was to use both hydrograph rainfall response trends and vegetation mapping to delineate the areas of swamps which are predominantly groundwater dependent, and those areas of swamps which are predominantly rainfall dependent; and
- In November 2012 to March 2013, as part of the current EIS studies, CSIRO undertook COSFLOW numerical modeling for the Project and the proposed Angus Place Mine Extension Project.

APPENDIX N:
PIEZOMETRIC PROFILES

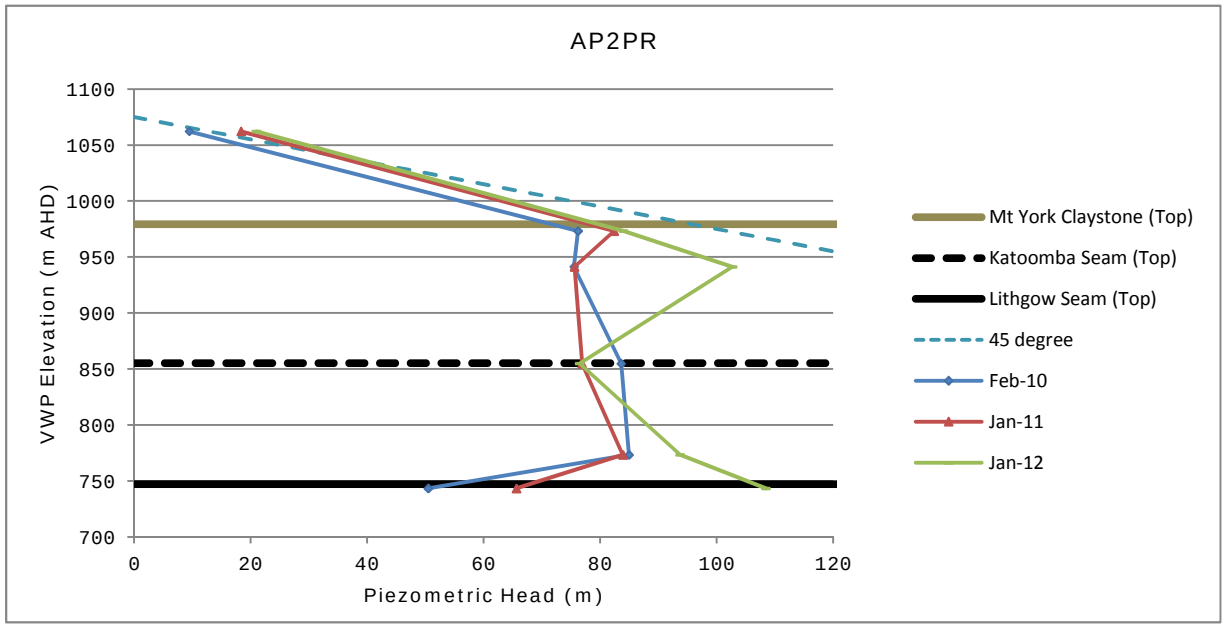

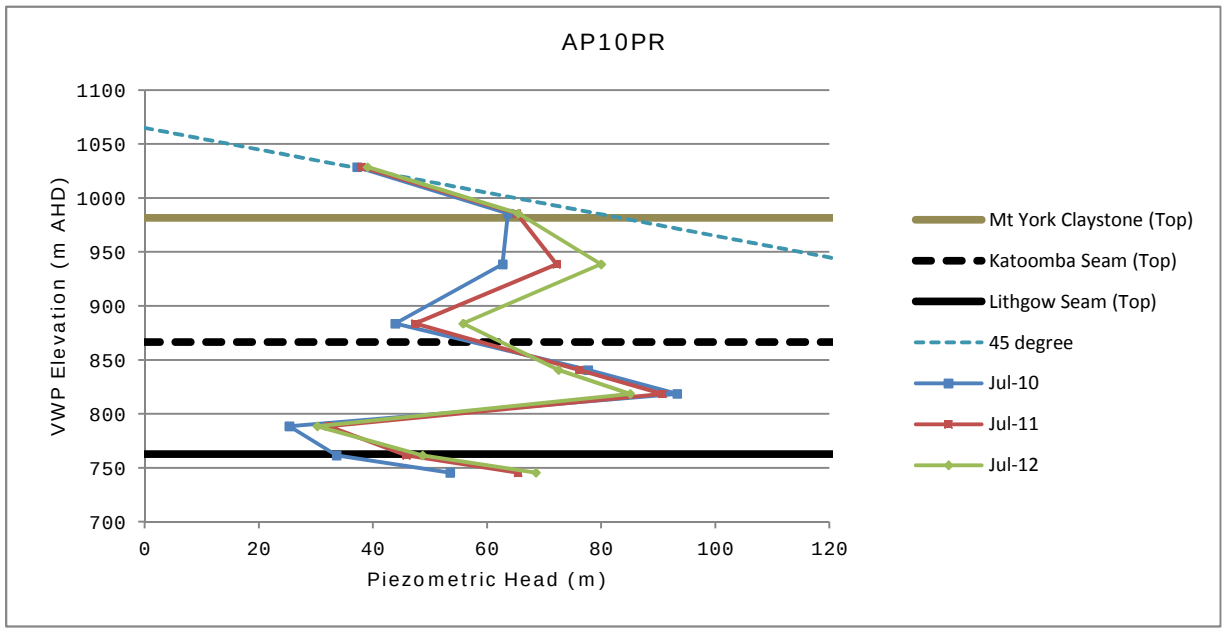

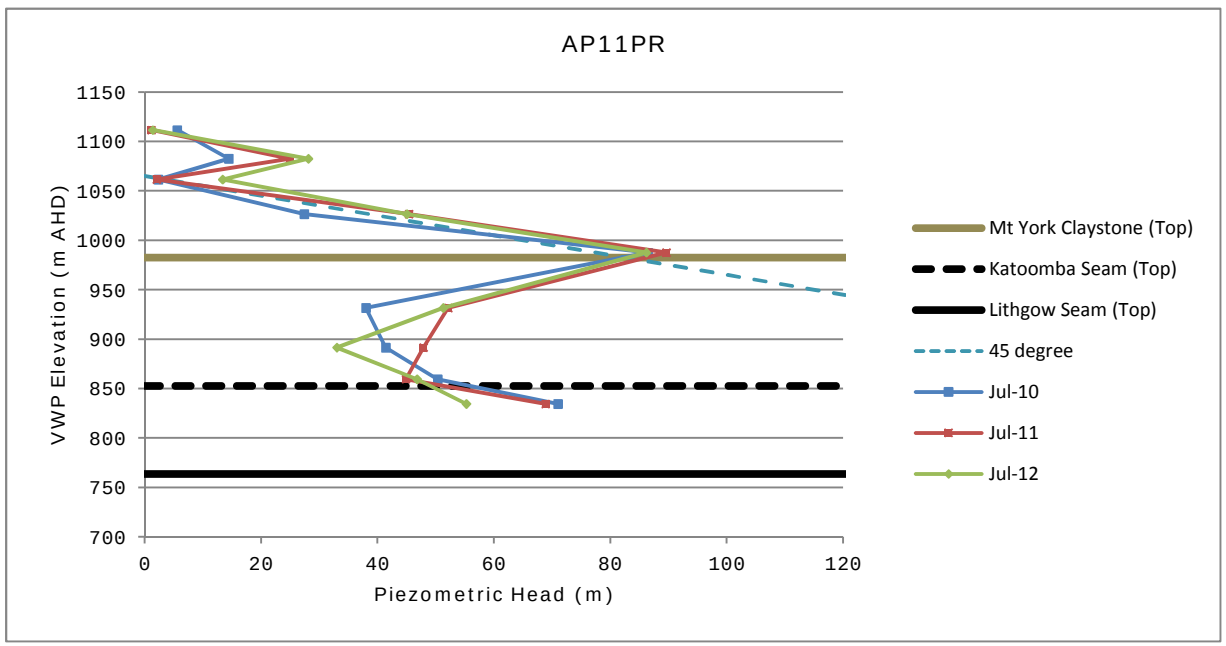

RPS

Angus Place Piezometric Profiles Figure N1

F:\Jobs\S187B\600\015b\015b Appendices\Raw Data for Appendices\[Appendix M - Piezometric Profiles.xlsx]AP

APPENDIX O:
MINIMAL IMPACT CONSIDERATIONS FOR AIP

Table O1 - Minimum Harm Criteria - Low Productivity Water Source

Less Productive Groundwater Sources							
Category	Water Source	Water Table		Water Pressure		Water Quality	
Porous and Fractured Rock water sources	Triassic Sedimentary Rocks	1) Less than or equal to a 10% cumulative variation in the water table, allowing for typical climatic "post-watersharing plan"(2) variations, 40m from any: (a) high priority groundwater dependent ecosystem; or (b) high priority culturally significant site; listed in the schedule of the relevant water sharing plan; or A maximum of a 2m decline cumulatively at any water supply work.	Consideration WT-1: The predicted drawdown in the water table (unconfined) areas of the Triassic (AQ6 aquifer) at the end of mining is presented in Figure 37. There are 3 projects (no large-scale groundwater users) in the vicinity of the project so the predicted drawdown is representative of cumulative impact. The maximum predicted WT drawdown is 15 m under the ridgelines, with no predicted drawdown of the WT along the drainage alignments inside of the Project Application Area boundary There are no water supply works in the Triassic inside of the Project Application Area boundary and as such cumulative impact on any water supply work is less than 2m.	1. A cumulative pressure head decline of not more than a 2m decline, at any water supply work.	The Triassic AQ4 aquifer system at the end of mining is not an confined aquifer inside/outside of the proposed Project Applicable Area boundary. As such, the Water Table Criterion does not apply.	1) Any change in the groundwater quality should not lower the beneficial use category of the groundwater source beyond 40m from the activity.	The Triassic Sedimentsare characterised as potable to brackish. Mining activity will not change the beneficial use of this groundwater source inside/outside of the Project Application Area boundary.
		2) If more than 10% cumulative variation in the water table, allowing for typical climatic "post-water sharing plan" variations, 40m from any: (a) high priority groundwater dependent ecosystem;or (b) high priority culturally significant site; listed in the schedule of the relevant water sharing plan then appropriate studies(5) will need to demonstrate to the Minister's satisfaction that the variation will not prevent the long-term viability of the dependent ecosystem or significant site. If more than 2m decline cumulatively at any water supply work then make good provisions should apply.	Does not apply as the activity does not trigger the requirement.	If the predicted pressure head decline is greater than requirement 1. above, then appropriate studies are required to demonstrate to the Minister's satisfaction that the decline will not prevent the long-term viability of the affected water supply works unless make good provisions apply.	Does not apply as the activities do not trigger the requirement	If condition 1 is not met then appropriate studies will need to demonstrate to the Minister's satisfaction that the change in groundwater quality will not prevent the long-term viability of the dependent ecosystem, significant site or affected water supply works	Does not apply as the activities do not trigger the requirement
Porous and Fractured Rock water sources	Permian Illawarra Coal Measures	1) Less than or equal to a 10% cumulative variation in the water table, allowing for typical climatic "post-watersharing plan"(2) variations, 40m from any: (a) high priority groundwater dependent ecosystem; or (b) high priority culturally significant site; listed in the schedule of the relevant water sharing plan; or A maximum of a 2m decline cumulatively at any water supply work.	The Illawarra Coal Measures Water Source is not unconfined (WT) inside of the Project Application Area. As such, the Water Pressure Criterion does not apply.	1. A cumulative pressure head decline of not more than a 2m decline, at any water supply work.	The predicted drawdown in the Illawarra Coal Measures Water Source at the end of mining is presented in Figure 29. There are 3 projects in the vicinity of the project so the predicted drawdown is representative of cumulative impact of these projects. The maximum predicted drawdown is 100m within the Project Application Area. There are no water supply works in the Permian except for the dedicated mine dewatering bores which supply water to the Wallerawang power station (the water is not used for potable or irrigation water supplies). Cumulative impact on any water supply works outside of the Project Application Area boundary is less than 2m.	1) Any change in the groundwater quality should not lower the beneficial use category of the groundwater source beyond 40m from the activity.	The Permian Coal Measures are characterised as brackish. Mining activity will not change the beneficial use of groundwater source outside of the Project Applivation Area boundary.
		2) If more than 10% cumulative variation in the water table, allowing for typical climatic "post-water sharing plan" variations, 40m from any: (a) high priority groundwater dependent ecosystem;or (b) high priority culturally significant site; listed in the schedule of the relevant water sharing plan then appropriate studies(5) will need to demonstrate to the Minister's satisfaction that the variation will not prevent the long-term viability of the dependent ecosystem or significant site. If more than 2m decline cumulatively at any water supply work then make good provisions should apply.	Does not apply as the activity does not trigger the requirement.	If the predicted pressure head decline is greater than requirement 1. above, then appropriate studies are required to demonstrate to the Minister's satisfaction that the decline will not prevent the long-term viability of the affected water supply works unless make good provisions apply.	Does not apply as the activity does not trigger the requirement.	If condition 1 is not met then appropriate studies will need to demonstrate to the Minister's satisfaction that the change in groundwater quality will not prevent the long-term viability of the dependent ecosystem, significant site or affected water supply works	Does not apply as the activities do not trigger the requirement